Politecnico di Torino

ScuDo
Scuola di Dottorato ~ Doctoral School
WHAT YOU ARE, TAKES YOU FAR

Doctoral Dissertation
Doctoral Program in Civil and Environmental Engineering (35^{th}cycle)

Innovative Computational Techniques and Constructability Issues for the Optimum Structural Design of Steel Structures

Algorithms and applications

By

Raffaele Cucuzza

******

Supervisor(s):
Prof. PhD. Giuseppe Carlo Marano

Doctoral Examination Committee:
Prof. PhD. Alessandra Fiore, Referee, Politecnico of Bari, Italy
Prof. PhD. Nikos Lagaros, Referee, National Technical University of Athens, Greece

Politecnico di Torino
2023

Declaration

I hereby declare that, the contents and organization of this dissertation constitute my own original work and does not compromise in any way the rights of third parties, including those relating to the security of personal data.

Raffaele Cucuzza
2023

* This dissertation is presented in partial fulfillment of the requirements for **Ph.D. degree** in the Graduate School of Politecnico di Torino (ScuDo).

A mio Padre, che ogni giorno mi indica la via

A mia Madre, che mi ha insegnato a sognare

A mia Sorella, che guardandola ricordo chi sono

Acknowledgements

Ricorderò per sempre questi anni di dottorato come i più belli della mia vita. Una vita colorata da mille emozioni e sfide. A renderli speciali hanno contributo tantissime persone dalle quali ho ricevuto più di quanto abbia dato.

Per primo, vorrei rivolgere un pensiero affettuoso al prof. **Giuseppe Marano** per avermi indicato la via quando mi sentivo perso. Credo che il giorno in cui il destino ci ha fatti incontrare, la mia vita sia cambiata inesorabilmente. La mia crescita accademica e personale è stata resa possibile solo grazie alla sua enorme pazienza e bontà d'animo. Il suo amore per la scienza è stata la più grande fonte di ispirazione e il dono più grande che potessi ricevere come giovane ricercatore. Vedere la vita con i suoi occhi mi ha fatto scoprire delle verità che altrimenti non avrei mai raggiunto. Spero di poter vivere ancora tante avventure insieme, trovandola in quell'ufficio ad aspettarmi, con quel "ciao, bidduzzo" che mi dice ogni mattina e che mi strappa sempre un sorriso.

Conosco il prof. **Giuseppe Ferro** da tanti anni e amo le nostre conversazioni. La sua visione lungimirante e strategica delle cose mi ha sempre affascinato. Durante il mio mandato come senatore accademico, ogni suo suggerimento, ogni sua parola è stata fondamentale per compiere le scelte giuste nei momenti più critici per il nostro Ateneo. Le confesso che farla arrabbiare è una delle cose che amo di più del nostro rapporto. E anche se non lo ammetterà mai...sono sicuro che piaccia anche a lei! A volte due persone trovano canali di comunicazioni anticonvenzionali e, il nostro, ne è un esempio raro. Spero che i nostri sguardi si continueranno ad incrociare e la nostra intesa continui ad essere quella di sempre.

Vorrei ringraziare anche il prof. **Marco Domaneschi**, o meglio, "lo zì" come ormai sono solito chiamarlo. La sua continua presenza (giorno ma soprattutto notte) mi ha reso più sicuro e consapevole dei miei mezzi. Sei e rimarrai per sempre il "Dorian Gray" del politecnico di Torino.

Vorrei ringraziare anche il prof. **Amedeo Manuello** con il quale ritengo di aver costruito un rapporto sincero e leale. In quest'ultimo anno, la nostra collaborazione scientifica si è trasformata in un rapporto che va aldilà di un mero rapporto lavorativo. Sono sicuro che avrà finalmente l'occasione per darmi tutte le "mazzate" che mi ha promesso e che, ne sono consapevole, merito fino all'ultima.

Infine, ringrazio te, **Eugenia**, che ispiri tutto quello che faccio, che sei nell'apice dei miei pensieri. La vita è semplicemente più bella con te al mio fianco!
Ti prometto che smetterò di fumare!

Abstract

Since the first half of the last century, the scientific community was fascinated by the potentiality of structural optimization as an efficient tool to solve hard computational problems. Moreover, the need of adopting these strategies became more evident when traditional approaches and thumb rules derived by experience appeared to be insufficient to face society's new challenges for which counter-intuitive solutions and innovative methodologies were required. In a wide variety of fields, benefits derived from the development of this branch is worth of noting. Ranging from mechanical engineering to aerospace, from civil engineering up to architecture, and again from the biomedical field to medicine the effectiveness of optimization strategies has been widely demonstrated.
Especially, civil engineering seems to be benefited the most by the growth of this branch. Bold and unusual layouts of buildings with optimal structural and economic cost-impact or new sustainable solutions represent still nowadays the main target of this subject. Therefore, soft computing techniques results to be extremely useful for the identification of optimal properties of control devices, retrofitting systems and monitoring methodology applied to existing buildings.

At first, once the goodness of the results derived by optimization processes was largely proved for simple application case studies, an increasing complexity was addressed and the main focus moved towards the identification of the most efficient and robust methods for achieving the global optimum of the problem. Different deterministic or heuristic methods appeared in literature aiming to guarantee feasible solutions with high efficiency during the exploration phase as well as accuracy during the exploitation one.

When a certain level of maturity was achieved and a deep awareness of the most promising techniques has been attained, conventional optimization strategies for the assessment of the optimal solution in terms of least structural cost (i.e. weight or

volume), highest performance rates, as well as competitive economical cost, have given way to problem statements in which constructability issues or practical design problems were accounted. The gap between theoretical approaches and practical ones represents the last obstacle to large-scale deployment in the common design of new or existing structures.

The goal of this thesis is to pursue this scope by showing how problems during industrial production processes or practical issues during the design and construction phase can be solved for a specific class of structures like steel trusses and frames. In order to deal with these problems efficiently, various already existing algorithms and novel methodologies were developed. If the first part of the thesis was dedicated to showing the improvement derived by coupling well-known optimization techniques with more efficient search strategies, the second part is focused on interesting applications where structural complexity during the assembly process or cutting pattern of steel members at the production stage become the variable parameters to be optimized.

The dissertation consists of eight chapters in total, plus the bibliography and three appendices that for clarity purposes were placed at the end of the corresponding chapter. It is organized as follows: Chapter 1 provides an overview of the optimization strategies in which all the most interesting papers were classified into sub-categories and the most significant information for each contribution was summarized in thematic tables. Chapters 2 and 3 deal with the formulation of a new machine learning approach for non-penalty constraint handling in evolutionary algorithms and the introduction of novel enhanced PSO with a Multy-Strategy Implementation, respectively. Optimal strengthening by steel truss arches in prestressed girder bridges is presented in Chapter 4 while in Chapter 5 results obtained by the size and shape optimization of a Guyed Mast Structure are illustrated. Problems related to constructability constraints for optimal sizing, geometry and topology of industrial buildings and the use of cutting stock problem in truss beam optimization are discussed in Chapters 6 and 7, respectively. Finally, Chapter 8 contains the conclusions, the original contribution of the thesis, and directions for future research.

Contents

List of Figures

List of Tables

Chapter 1

An overview of the Optimization strategies for steel structures: a critical review

1.1 Introduction

Recently, though the need for sustainable materials such as stone, masonry or new hybrid-composite represents the new goal of this century, steel remains one of the most widely used materials in the whole world thanks to the adoption of new maintenance and monitoring techniques, i.e. Structural Health Monitoring (SHM), and its incredible structural performance. The age of steel was inaugurated by the second industrial revolution with a famous structure that determined an era of unprecedented growth in history. The Eiffel Tower was built on the occasion of the first Universal Exposition in 1899 by Engineer Gustavo Eiffel. At the time it represented the world's most audacious structure thanks to both its slenderness and high structural capacity.

Taking a look at the statistics provided by the non-profit organisation *World Steel Association* (2021), the authors have pointed out a trend of the World crude steel production from 1950 up to 2021 expressed in terms of Million tonnes. As shown in Fig.1.1, at the beginning of the European Reconstruction Plan realized after World war II, the crude steel production was 189 million tonnes. 10 years later the recorded value was about double and, then, the growth kept constant until the beginning of the

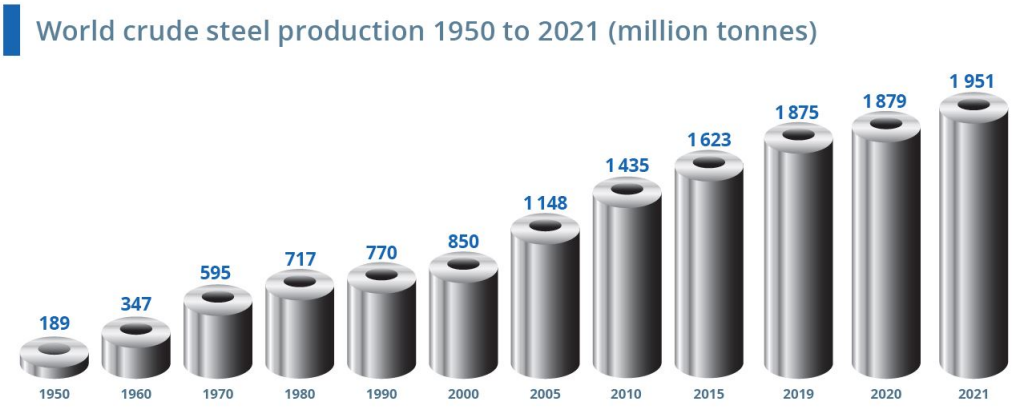

Fig. 1.1 World crude steel production from 1950 up to 2021 (million tonnes))

new century. At the end of the 19th century, in just 50 years the production of crude steel has quintupled. The highest slope was recorded between 2000 and 2005 during which the steel production passed from 850 to 1148 million tonnes respectively with an unparalleled growth ever observed. Due to the developing technologies in this field and the extensive use of this material in several engineering fields such as mechanical, aerospace and civil, the maximum crude steel production of 1951 tonnes was recognised at the end of 2021.

Several further interesting considerations have been pointed out by the authors by mapping the World-top 20 steel-producing countries at the end of 2021. In Fig. 1.2, the Circle size is proportional to the steel-producing country value. It is worth noting that the main steel-producing countries are concentrated in the Asian continent. In particular, China results still now the most steel-producing country in the world with 1032.8 million tonnes and its productivity results in being 10 times the producing value exhibited by the second country in the ranking (India). Generally, the observed trend is derived by historical or economic reasons but also practical needs. Though China and India are almost considered emerging economies with important companies in different industrial fields; Japan, for instance, which ranks third in the above-mentioned list, allocates the majority of the available steel resource to improve the seismic resistant strength of buildings and infrastructures. The geographical location of several countries, such as the presence of tectonic plates or aggressive environments, leads to requiring strict safety and structural requirements in the construction process.

Nonetheless, steel material has gained popularity for its crucial role in challenging

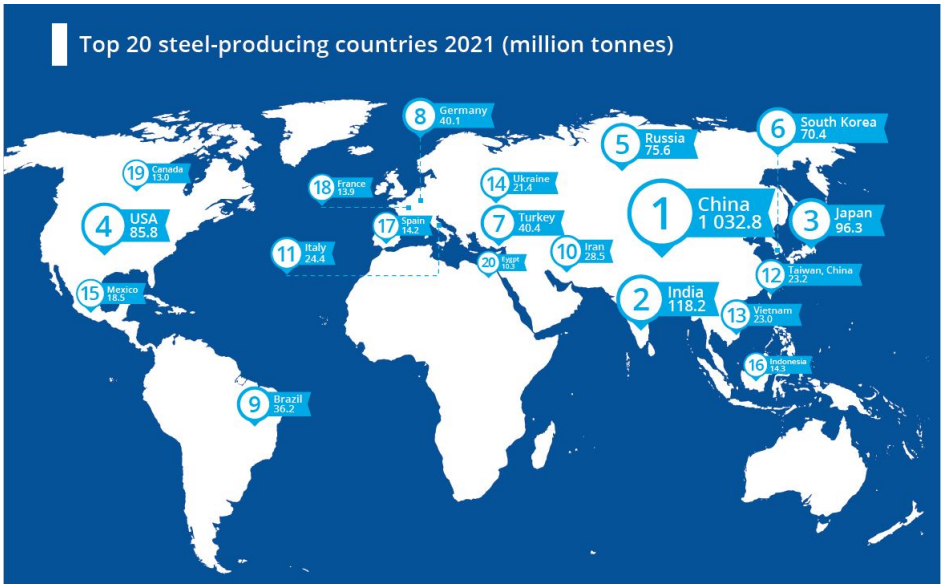

Fig. 1.2 Top 20 steel-producing countries 2021 (million tonnes)

design in which extreme and refined shapes have been requested or as a friendly environmental solution.

These preliminary considerations concerning the widespread use of steel in various structural application fields are testified by the increasing attention to steel structural optimization from the scientific community. A bibliometric investigation was conducted by the authors with the aim to compare the growth of the total number of publications in the structural optimization field, independently of the adopted optimization strategies, with those that are exclusively focused on the optimization of steel structure as generic steel frames, trusses, bridges, seismic isolation devices, etc. The underlying platform for finding the relevant works of literature was Elsevier's abstract and citation database *Scopus*. Two main keywords as "structural optimization" (SO) and "Steel structural optimization" (SSO) were utilized for our purposes. With the former, all the papers concerning optimization processes applied in any field have been involved while the latter referred solely to applications on steel structures or devices (isolation system, optimal parameters for dampers' identification, etc.).

In order to give an overview of the trends derived by the analysis paper article, conference paper, book chapter and review article published in engineering journal indexing by *Scopus* have been included and a time frame of the last 31 years, from 1990 up to 2021, was considered. In Fig. 1.3, it is evident how the increase of the

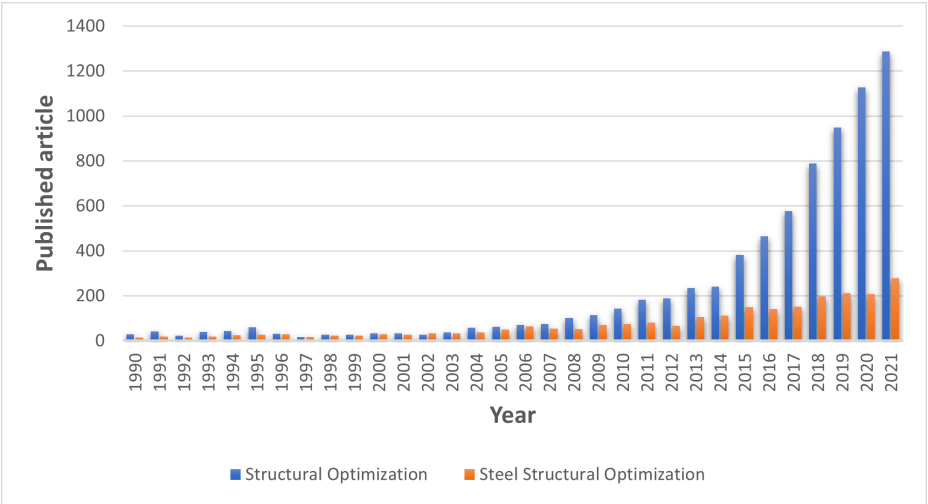

Fig. 1.3 Trend of the total number of publications by searching the keywords "Structural Optimization" and "Steel structural Optimization" within the manuscripts' title between 1990 and early 2000.

published article in the SSO sub-field is growing up faster and faster. Moreover, at the beginning of the '90s and for the further 20 years, the difference between the two trends was negligible; then, thanks to the spreading of new computational techniques in several fields of engineering, the application was extended to new frontiers of knowledge and to new case studies. However, though the gap with respect to the main field is still so marked, SS0 covers an important part of the total papers published in the SS topic still nowadays.

The main approach in SSO can be broadly classified as reported in figure 1.4 depending on the type of algorithm adopted to fulfil the scope.
At first, optimization algorithms can be classified into **Deterministic** and **stochastic** approaches. The former makes use of derivatives of the objective function and constraints in the search for the optimum solution and no random process is involved while the latter, also called the metaheuristic algorithm, relies on stochastic search paradigms inspired by different kinds of natural phenomena.

Historically, among the Deterministic solution techniques, **mathematical programming** techniques were first to be used to obtain the solution of the optimum for both linear and nonlinear programming problems (Schmit et al. 1960, Majid et al.1974, Saka et al. Saka (1980), Atrek et al. 1984, Arora et al. 2004, Kirsch et al. 2012, Belegundu et al. 2019).
There are several mathematical programming techniques available in the literature.

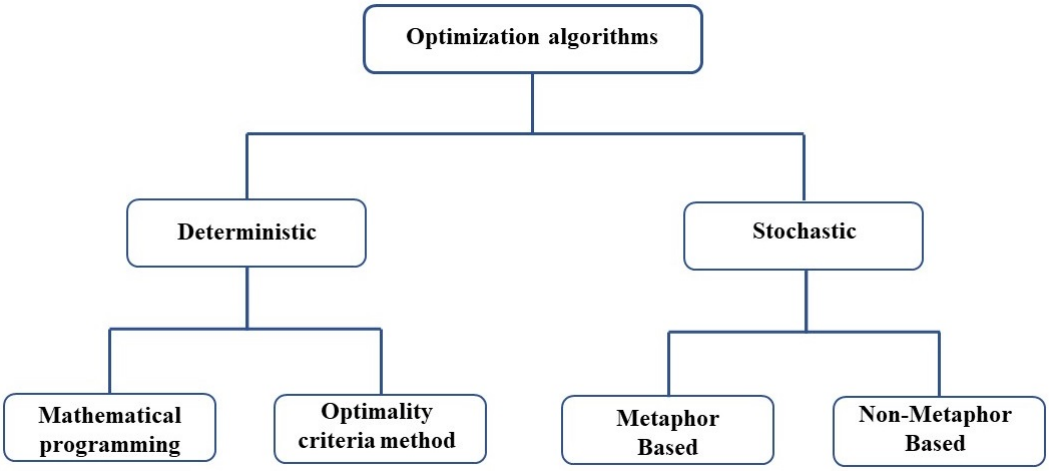

Fig. 1.4 Classification of algorithms in optimization field

The authors have selected the ones which have been applied successfully for the optimum design of steel structures.
As reported in Saka et al. (2013), three groups were recognized: in the first group, all the algorithms approximation in which the linearization concept was adopted, were collected as the **Sequential Linear Programming** method developed by Griffith and Stewart (1961), improved strategies where cross-sectional properties of members (i.e. Reinschmidt et al. 1966, Johnson et al. 1969, Arora et al. 1976) or joint displacements (i.e. Saka et al. 1980 and Schmit et al. 1976) was assumed as design variables. In the second and third groups **Penalty Function** Method through sequential unconstrained minimization techniques (i.e. Carroll et al. 1961, Fiacco et al. 1990, Kavlie et al. 1971 and Gisvold et al. 1972) and **Gradient Method** for constrained optimization problem were solved, respectively. In the latter, gradient-projection method proposed by Rosen (1960 and Zoutendijk (1960) or geometric (Morris et al. 1972) and dynamic programming (see Bellman et al. 1966 and Sheppard et al. 1972) were introduced.

Alternatively to linear programming techniques, **Optimality Criteria** Methods (Prager et al.1968) were largely used as a valid deterministic approach aiming to overcome numerical difficulties when real-size practical steel structures with more than a few dozen of design variables were taken into account. With respect to mathematical programming techniques, few structural analyses were required to achieve a near-optimum solution by deriving criteria based on intuition such as fully stressed design or based on a mathematical statement such as Kuhn-Tucker

conditions for both continuum (Venkayya et al. 1969) and discrete large-size practical structures (see Venkayya et al. 1973, 1989, Berke et al. 1987, Khot et al. 1979 and 1981a).
More in detail, different strategies were developed within the Optimality criteria field by distinguishing between the Displacement constraints-based method (Berke et al. 1970), strength constraints-based method (Tabak et al. 1981), axial and lateral stability constraints-based methods (Ulker et al. 2001) and combined stress constraints based method (Khot et al. 1981b).

If Deterministic techniques were preferred since the beginning by several researchers for solving theoretical problems or quite simple practical examples, **stochastic metaheuristic** and **heuristic** algorithms proved to be an efficient alternative to the conventional solvers for highly complex real-world problems and/or no-convex problems.
The most significant advantage of these intelligent techniques is that they do not require prior knowledge of the tackled problem. Though these do not guarantee that the best solutions can be found or whether the algorithm will work and why if it does work (Yang 2010a, 2010b), they can be an efficient way to produce acceptable solutions by trial and error aiming to find a reasonable feasible solution in an acceptable timescale.
Despite the popularity of metaheuristics, there is no agreed definition of heuristics and metaheuristics in the literature. Some researchers use 'heuristics' and 'metaheuristics' interchangeably. However, the recent trend tends to name all stochastic algorithms with randomization and global exploration as metaheuristics. Randomization provides a good way to move away from local search on a global scale. Therefore, almost all metaheuristic algorithms are usually suitable for nonlinear modelling and global optimization.
In this review, inspired by the work of Kashani et al. (2022), random strategies are classified into two main categories: **Metaphor based** and **Non-Metaphor based**.
Metaphor-based algorithms are including bio-inspired (e.g. genetic algorithm, Holland 1992) and particle swarm optimization (e.g. Kennedy and Eberhart, 1995a), art-inspired (e.g. harmony search, Geem et al.2001) and interior search algorithm (e.g. Gandomi 2014), science-inspired as the simulated annealing (e.g. Van Laarhoven and Aarts 1987) or the gravitational (Rashedi et al. 2009) and Charged System Search algorithm (e.g. Kaveh 2010), social inspired like the teaching–learning-based op-

timization (e.g. Rao et al. 2011) and school-based optimization (Farshchin et al. 2018).

The paper has the following organization. Section 2 introduces the gap of the research and the purpose of this review. Section 3 is totally focused on the organization and classification criteria adopted by the authors. Section 4 traces a historical excursus of academic research in this field selecting the main papers within a temporal range from 1968 to 2000. In section 5 the mathematical formulations of the traditional problems in structural optimization are introduced and the three main optimization strategies are defined. Section 6 explains the search method procedures and a brief description of the existing reviews realized by other authors is discussed. Section 7 is entirely dedicated to the bibliometric analysis and graphical outcomes are used for preliminary considerations. In section 8, all the papers involved in the bibliometric analysis are examined and classified into main fields and sub-categories. Finally, the conclusion is pointed out aiming to highlight the lack in the literature or propose future research areas and present some (deserved) critique of the field.

1.2 Purposes of this review

These preliminary considerations show that increasing attention to the steel material represents a crucial aspect of understanding the development of building construction trends. Several works are already available in Literature in which a list of the most efficient optimisation algorithm are collected with the aim to detect the best strategies for obtaining the optimal solution within imposed constraints (see e.g. Kashani et al. 2022).
However, few practice case studies in the Civil Engineering field have been included and, mainly, final considerations derived from these investigations are focused to prove the computational efficiency of algorithms in well-defined benchmark cases. In other words, an overview of the main structural fields in which optimization strategies have been effectively adopted to solve real design problems is missed. Hence, adopting a critical review of the most recent scientific contributions, the authors will try to answer to some interesting questions: nowadays the findings from the structural optimization fields can be assumed as efficient solutions to the most challenging design problems or they have remained, in the most of cases, only theoretical applications due to their critical application issues? What are the

main fields which have benefited the most by using these relatively young techniques?

1.3 Organization

In order to achieve the above-mentioned purposes, a critical study must be conducted and a classification in specific main areas, chosen by the authors, of the most interesting steel application case studies must be provided. The research is oriented to collect the most common structural optimization problem statements with specific regard to steel structures. The problem formulations and the corresponding case studies have been analyzed by capturing the main trends in structural design. It has been considered:

- Problem formulation: Single or multi-Objective Function (OF) considered as the target value to be maximized or minimized by respecting the various numerical tolerance and structural boundary imposed. The most efficient exploring approach to a dynamic change in the research area represents the crucial aspect of this kind of optimization process;
- type of algorithm and optimisation strategies adopted for achieving the best fitness: soft computing techniques as population-based or Nature-inspired algorithms and deterministic techniques as gradient-based approach and linear or non-linear programming;
- Practical application case studies, selected by the authors, as interesting real-world applications of optimization processes.

All the structural engineering optimization papers have been organized considering three levels of optimization identified by the authors: size, shape and topology. Moreover, in order to involve simultaneous optimization approaches, all possible combinations of the mentioned-above pure formulations have been investigated as depicted in the in-scale representation of Figure 1.5.
In future sections, we will define *pure size/shape/topology optimization* all those papers in which the optimal solution will be affected by only cross-sectional, geometrical and topology properties, respectively. Once a first classification was provided,

papers were allocated in main application fields by considering the nature of the target function as described following:

- Structural performance: all the optimization problems formulated aiming to improve the mechanical or structural efficiency of structures (self-weight, volume, surface, displacement, the natural frequency for the dynamic response, energy dissipation of isolation and/or dissipation devices, etc..);
- Cost impact: all the optimization problems in which the economical aspect is specifically considered as the main parameter affecting the design process;
- Environmental impact: all the optimization problems in which the environmental aspect is taken into account by proposing alternative solutions for sustainable purposes;

Moreover, an entire section was dedicated to the most interesting application cases in order to show what is the structural optimization field that best fits with the real-world Civil Engineering design challenges.
In the end, final remarks and deep considerations have been reported in the conclusion based on the results derived by the critical analysis conducted by the authors.

1.4 Three approaches for optimal structures: Size, Shape and Topology optimization

Each engineering problems require a specific approach which should guarantee to achieve the correct solution with the minimum effort. In this sense, practitioners and researchers focused on detecting the most promising optimization strategies for coping with single or several problems simultaneously.

For the first time, Rozvany and Prager, in some of their works (Rozvany 1995 and Prager 1974), introduced the concept of *layout* optimization as the simultaneous selection of the optimal topology (i.e. a spatial sequence of members and joints), geometry (i.e. the location of joints) and cross-sectional dimensions (sizing). Hence, the main three levels of optimization were clearly defined.
Generally, optimization problems can be formulated in different ways depending on the final scope that must be achieved and the boundary conditions to which

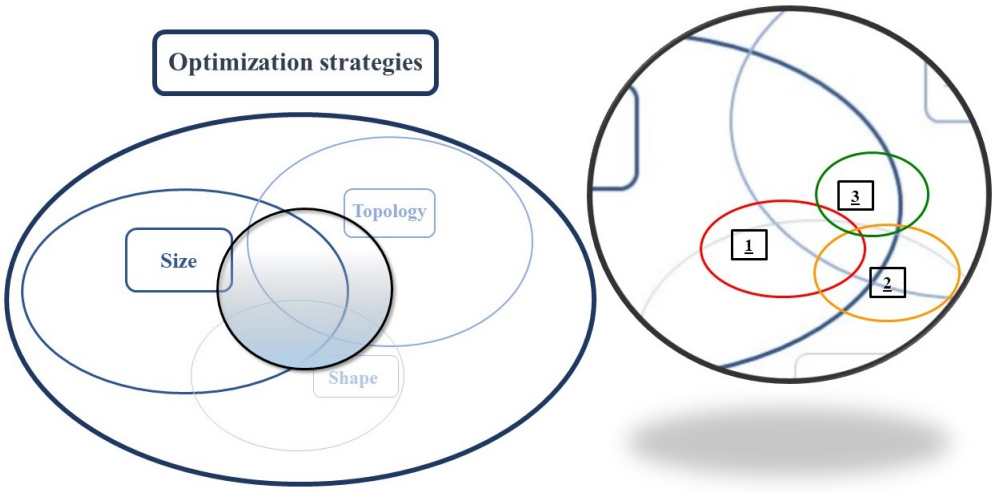

Fig. 1.5 Graphical representation of the classification criteria adopted in this review. The size of each circle is representative of the number of papers corresponding to the specific optimization level. In this sense, overlapping zone among each circle gives an idea of the frequency of combination among all three strategies. Sub-fields assumed in this review as Structural performance, cost impact, environmental impact are labelled 1,2 and 3 simultaneously.

the final solution is subjected. The formulation of structural design problems as decision-making problems has yielded a new branch in structural engineering called structural optimization (Majid 1974, Saka 1980 and Arora 2004).
The mathematical model of a decision-making problem has the following form:

$$\textbf{Minimize} \quad W = f(x_i), \quad i = 1,...,n \tag{1.1}$$

$$\textbf{Subject to} \quad h_j(x_i) = 0, \quad j = 1,...,n_e \tag{1.2}$$

$$g_j(x_i) \leq 0, \quad j = n_e + 1,...,m \tag{1.3}$$

$$x_i^l \leq x_i \leq x_i^u \tag{1.4}$$

where x_i represents the decision variable i of the design vector x. Decision variables may take continuous or discrete variables. Continuous decision variable can assume any real value within the range fixed by Eq.1.8. The design vector collects all the variables of the problem which change iteration by iteration during the optimization process. The nature of these variables depends on the optimization strategies as discussed at the end of this section. On the other hand, discrete design variables can be selected from the commercially available set of steel sections or, generally, by

adopting a database representative of the main geometrical and mechanical features of variables (moment of inertia, stiffness, etc.).
$f(x_i)$ in Eq.1.1 represents the objective function which is used as a measure of the effectiveness of the decision. Depending on the nature of the optimization process (minimization or maximization), the evaluation of $f(x_i)$, called in structural optimization *fitness*, represents the capacity, in terms of efficiency and robustness of the method, to achieve an optimal or sub-optimal solution.
The equalities, $h_j(x_i)$, and inequalities $g_j(x_i)$ conditions in Eqs.1.2 and 1.7 respectively, represent the limitations imposed on the overall structural performance of the structures.

In the last 30 years, different heuristic and metaheuristic algorithms, linear or non linear iterative approaches, have been developed aiming to detect the best approach starting from simple to hard computational class of problems. However, the scientific community agrees in recognizing three main optimization strategies with an increasing level of complexity: size, shape and topology optimization. Based on the specific purpose of the research, each one of these can be adopted individually, in pairs or by considering all three optimization levels simultaneously.

Size optimization represents one of the first processes that appeared in literature since its simplicity and applicability to a wide range of interesting industrial and technical problems. In this level of optimization, the engineer can choose the geometrical characteristic of each member while the outer shape and the arrangement of the structures remain unchanged. In other words, all the changing performing at each iteration of the process are referred to a well-defined section of the member or along the full length of itself when the hypothesis of constant sections of the structures is assumed.

The second level of optimization is represented by shape optimization in which nodes and/or joints are free to move around the starting position without varying the topology or sizes within the structures.

Finally, the third level of the optimization process is represented by the hardest computational effort procedure through which the topology of the structures is changed. This means that topology optimization is a process in which an optimal pattern of the connectivity members is explored through the decision to activate or not a specific joint placed in an exact position in the 2D or 3D dimension. Consequentially, new load paths are investigated in order to provide the optimal arrangement under

determined load and boundary conditions.
Though Eq.1.1 subjected to Eq.s1.2 and 1.7 result to be valid as a general expression of an optimization problem for both size and shape level, little differences in the formulation of a topology optimization problems occur.
In this case, the optimization problem is formulated as a minimum compliance problem in which the objective function is performance-based. The minimum compliance problem maximizes the stiffness (or minimizes the flexibility) of the entire structure under some given volume constraint by minimizing strain energy or external work done by applied loads. The entire problem formulation can be written as:

$$\textbf{Minimize} \quad \mathbf{F}^T\mathbf{d}, \tag{1.5}$$

$$\textbf{Subject to} \quad \mathbf{K}(\rho_i)\mathbf{d} = \mathbf{F} \tag{1.6}$$

$$\sum \rho_i^T L_i \leq V_{max} \tag{1.7}$$

$$\rho_{min} \leq \rho_e \leq \rho_{max} \tag{1.8}$$

where ρ is the decision variable and L_i its length, $\mathbf{F}$ and $\mathbf{d}$, whose product represents the external work, are the vector of applied force(s) and nodal displacements at free degrees of freedom respectively, $\mathbf{K}$ is the global stiffness matrix while V_{max}, ρ_{min} and ρ_{max} represent the upper and lower bound of volume and members respectively.

During the review, all the formulations introduced in this section for each size, shape and topology optimization will be treated and the adaptability to several engineering problems will be discussed.

1.5 A historical excursus: a look to the past

In this section, the authors give a look at the past in the structural optimization field by emphasizing the most promising techniques which were adopted between 1968 to 2000. The purpose of this section is that to collect the first problem formulations appeared in Literature. The authors believe that conducting an investigation of past scientific works allows a clearer understanding of recent trends.

Historically, iterative loops or parametric analysis represent the first optimization strategies that appeared in Literature. Some efforts in this direction were provided by R.M. Brach (1968) and W. Yau (1974) where maximum-minimum dynamic deflec-

tion was obtained as a function of the cross-sectional variation. A simply supported beam with varying cross-sections along the length and different types/positions of dynamic impulse was investigated. Increasing interest in these topics was demonstrated by the development of new computational approaches for structural optimization in the dynamic response regime (i.e. Fox and Kapoor 1970) and applications to more complex case studies as that one pointed out by L.J. Icerman (1969) in which structures of various type were optimized following the smallest possible amount of a given structural material criteria. Dynamic excitation was realized by harmonic vibrations variable with time.
In 1972, at the end of the first decade from the birth of this branch of research, Pierson (1972) organized a survey of optimal structural design under dynamic constraints: methods for handling constraints on natural frequencies or for treating generic dynamic constraints on quantities directly related to the dynamic response were clearly summarized.

Though, material saving represented the first issue addressed by the Scientific Community, developments related to the mathematical formulation for the minimization of economic cost were not long in coming.
Lee and Knapton (1975a) published pioneering research, in which the authors conducted investigations about the minimum cost design of a steel portal framed building aiming to evaluate the *least cost* design solution from the hyperspace of the feasible region in accordance with the relevant B.S. Codes and common industrial practice. Two years later, Jr. Thomas (1977) inspired by the concept of the *least cost*, introduced an optimization method for the elastic design of roof systems composed of rigid steel trusses, web joints and steel roof deck. In this work, cost voices achieved an important level of detail by including different grades of steel and several types of standard sections at each iterative step. Similarly, Cheng et al. (1989b) adopted the same mathematical formulation, meanwhile two-dimensional steel frameworks, with and without bracing members, subjected to both static and seismic forces were investigated. In addition, a cost-objective function of the same structures has been compared to the classical weight minimization. Regarding the cost minimization target function, the parameters considered included the cost of structural members, painting, and connections (steel plates and welding), together with the damage expense, limited to the repair of non-structural elements. The results show that the optimum solution of the minimum weight design was close to that of the minimum cost case with the exception of the column sizing.

However, though the minimization of the cost represented promising research not only for the Academy but also for the industrial field, the first 10 years of this new branch of research was characterized by the enhancement of the mechanical properties and, subsequentially, the global efficiency of the structural response under static and dynamic configuration. This goal was achieved by conducting optimization at all three optimization level introduced in the previous section: size, shape and topological.

In this direction, Al-Salloum (1995) employed an interactive approach based on the fully stressed design to find an efficient search path of the optimum design for statically indeterminate elastic frames.

One of the first works, in which a generalized steepest descent method was employed in developing a computational algorithm for the optimal design of elastic structures under dynamic loads, was introduced by T-T Feng et al. (1977a). As declared by the same authors of the manuscript "This paper deals with optimal design of elastic structures under dynamic loads, a problem that has received little attention to date". With the aim to test the performance of the developed algorithm, planar truss-frame-type structures was adopted as a structural benchmark. Minimization of the total weight of the structures subjected to dynamic loads under displacement, stress, frequency and design parameter constraints was achieved by performing a finite element model of the structural response and modal analysis techniques to solve the dynamic problem. This approach was preferred over solving purely analytical methods for dynamic analysis since its low computational cost.

After that, several works were published with the aim to test the performance of computer programs for processing both structural analysis and the optimal level of design of frame structures under proportional loadings and variable loadings (see e.g. N.D. Hung 1983 and M.G. Stewart 1989). Others like Brach (1968), M.P. Kapoor et al. (1987a) and F.Y. Cheng et al. (1989a) aimed to minimize the dynamic response for a class of specific structures, like frames, or theoretical application like a simply supported beam. The last two authors carried out deep considerations regarding the optimal configuration of multistorey and regular or irregular two-dimensional steel frames for which structural analysis including static, earthquake and wind forces were performed. Obviously, in this exploring phase of this new topic, research was focused mainly on the computational approach instead of interesting application case studies.

Until the end of '90s, majority of the most interesting applications in SSO field were related to 2D or 3D frames and trusses (Thevendran et al. 1992a, Soegiarso and Adeli 1997 and Memari et al. 1999a).
With specific regard to the beginning, applications of formers resulted in the majority of works despite the latter ones (see e.g. Stasa 1998 and Ishikawa et al. 1993) which have received more attention only after the spread of Metaheuristic algorithms (see e.g. Coello and Cristhiansen 2000a, Jakiela et al. 2000a and Erbatur et al. Erbatur et al. (2000)).
Specifically, Balling (1991a) developed a strategies for discrete optimization of 3D, six-story, unsymmetrical steel frames. The optimization was performed by treating multiple section per member and a probabilistic criterion was adopted to evaluate whether the candidate design should replace the current design or be rejected. The minimization of the weight was often adopted as Objective Function by varying elastic range of material behaviour (see e.g. Erbatur et al. 1992a), by considering linear variation of cross-section defined as the ratio of areas between both beam ends (Hayalioglu and Saka 1992a) or for achieving the least-weight of a three-dimensional tall building under multiple loading conditions, the story drifts, member strength and size constraints in accordance with Standard regulation and fabrication requirements (Chan et al. 1994, 1995a, Liew et al. 2019).
Different interesting structural case studies that respect those mentioned above were included in the Literature at the beginning of 1980. During these years, in fact, Crawford et al. (1980) introduced nonlinear programming techniques for the optimal prediction of seven different types of steel roofs based on a suitable cost model. Haque (1985a) and Scholz et al. (1986a) developed a general methodology for the optimization of skeletal rigid frames in which structural specifications provided by American Institute of Steel Construction's (AISC) was included in the optimization phase as structural constraints. More in detail, Scholz used an approximate second order for performing elastic-plastic analysis of multi-storey frames. It can be considered the first example of a micro-computer program in which a large number of variables were considered in the design method.
Other interesting case studies in which geometrically nonlinearity was provided by Saka and Hayalioglu (1992a) and (1991a) where in-plane and lateral buckling of members were included as constraints for the optimum design of elastic-plastic frames. Park and Adeli (1995) investigated the plastic design of structures using a neural dynamic model. O'Brien (1997), attempted to perform an optimal design

of pitched roof frames by using algebraic linear programming by using the Kinematic Theorem of plastic collapse as constraints of the problem. Machaly (1986b) approached the problem of the minimization of the weight of steel grid bridges. 4 Different types of bridges subjected to the same load combinations were investigated and, mainly, the truss, the plate girder, the box, the cabled system and the grid type were analyzed. Non-linear programming techniques were adopted in which behaviour constraints like strength requirements (normal and shear) or stiffness requirements (bending translation) were introduced. On the other hand, the side constraints were required to assure non-violation of the practical dimensions of cross sections. Important results are relieved by the author and optimal configurations for each typology were obtained in terms of maximum deflection admitted and height of cross-section.
Some author in (1986a) discussed the crucial problem related to the optimal percentage of rigidity in the semirigid connections which guaranteed the optimum steel weight for common types of steel frame structures such as portal and gable frames. The optimum solution to the structural design problem is expressed in the form of a solution vector whose elements represent member sizes. Simple frame test benchmarks convinced the author that the use of the semirigid connections could lead to a saving in weight of 28% in the portal frame when a rigidity ratio equal to 0.90 was fixed. Lower values were detected when gable frames were analyzed.
Other works (Xu and Grierson 1993a, L.M.C. Simões 1996, Al-Salloum and Almusallam 1995a, Xu et al. 1993b and 1994) attempted to explore the efficiency of computer-automated methods for the optimum design of steel frameworks accounting for the behaviour of semirigid connections. In all these works, the authors performed optimization processes by considering stiffness and member size as continuous or discrete value design variables. All the authors agreed on the crucial role played by the connections into the steel structures as the main parameter for achieving the most efficient and economical solution simultaneously. Few years later, a preliminary study conducted by Weynand et al. (1998) and Steenhuis et al. (1994) found that cost savings are possible with the use of semi-rigid connections.

At the beginning of the ’90s, several authors were convinced that performing optimization procedures by considering a single target function was not complying with the real engineering challenges. The minimization of a single Objective Function like the weight or the cost of structures did not guarantee the global optimum when it was dominated by several parameters. Takewaki et al. (1991) developed

a probabilistic multi-objective approach (Auto-Regressive Moving Average) for concentrically braced steel frames in order to incorporate uncertain features of design earthquakes and to provide a simplified formula for the preliminary design based on the concept of decomposed stiffness design. Then, Marks (1997a) attempted to determine the optimum dimensions of a building following the criteria of minimum building costs, including costs related to materials and construction, and minimum yearly heating costs. Others as Zhow et al. (1999) introduced a new application of multiobjective and multilevel optimization techniques for steel frames. Two objectives as maximum total structural strain energy and minimum total structural cost should be evaluated with a two-level optimization procedure: first level (system-level) in which the optimal configuration of the entire structure was achieved in terms of structural strain energy and structural weight subjected to global constraints; second level (element-level) in which the optimization was performed for each member based on the results of the system-level optimization.

Once a certain level of maturity was achieved, Literature in the structural optimization field was populated by several reviews with the aim to emphasise the main outcomes in this area.
The first review surveys on the topic of optimization of steel structures were realized by venkayya and Vipperla (1978) and Griersoni et al. (1984) in which the authors tried to classify the main adopted static and dynamic constraints as constraints on service and ultimate loading condition or structural frequency and transient dynamic response. Other authors as Topping (1983) and Yen-Liang Hu (1994a) tried to classify the best strategies for performing shape optimization mainly on skeletal structures, by considering frequency constraints (Gandhi 1992) or showing the specific difficulties in truss topology optimization with stress and local buckling constraints (Zhou 1996).
At the end of the '90s, Hernandez (1998) published an interesting work in which performance comparisons between iterative methods and mathematical programming for specific class of steel frames were faced.
Finally, only two reviews published by Osman et al. (1996) and Lin et al. (1994) appeared in Literature where an extensive bibliography related to Metaheuristics and first issues into Single-objective optimization by using genetic search were discussed, respectively.

1.6 Search method procedure

The searching method of finding the relevant papers for doing the current survey is discussed in detail in this section.

1.6.1 Search method

In this study, the relevant works of literature were collected by adopting Elsevier's abstract and citation database *Scopus*. During the searching phase, all the articles published in journals without indexing by Scopus, conference papers and book chapters have been excluded. Additionally, papers focused on reliability and/or robust optimization approach or probability-based formulations have been also excluded. Moreover, the bibliometric analysis was conducted only for scientific works published from 1990 until 2022. The time range of searching was specifically chosen by the authors in order to analyze the whole growth of the SSO field from its origins to the present.
Subsequently, the entire obtained database was automatically filtered by the platform selecting only the papers belonging to the "Engineering" sub-area. The search was conducted among all the scientific works which included the two keywords "Structural optimization" and "steel optimization "within the "article title, abstract, keywords and authors".
Finally, the collecting phase provided by the platform was completed by the authors by removing irrelevant articles or adding other ones which were considered particularly significant.
Once the database was finalised, the authors reviewed the entire database in order to place each contribution into the mentioned-above categories.

1.6.2 Other reviews

A search through *Scopus* revealed that there are numerous extensive review papers in which all aspects of relevant research papers are discussed. However, none of those review papers addressed the Structural Optimization applied to steel structures or, specifically, proposed an original clustering of the most relevant works based on the target function and design vectors involved in the optimization process for solving real-world engineering problems. All the papers collected in this section, in fact,

have the common characteristic of summarizing or comparing the most promising techniques in the SSO field without any critical discussion concerning the nature of the OF formulation adopted (structural, economical, environmental, etc.).

At the beginning of the new century, the first review papers that appeared in the literature were totally focused on summarising the first preliminary results obtained by performing structural optimization with Soft computing techniques.
Krishnamoorthy (2001) and Pezeshk et al. (2002) collected all the most promising applications of genetic algorithms. Practical design, by performing genetic modelling, of structural systems such as steel trusses, towers, bridges, reinforced concrete frames, bridge decks, shells and layout planning of buildings was largely discussed. Then, two surveys were entirely dedicated by Kicinger et al. (2005) and Coello (2002) to the potentiality of using evolutionary strategies for engineering problems.

After the first decade, metaheuristic approaches resulted to be the most common optimization strategies as demonstrated by the huge number of reviews that appeared in the literature Ramaswamy and Eekhout (2002).
Saka and Geem (2013) realized an extended survey on the most common mathematical formulations solved by either mathematical programming, optimality criteria and metaheuristic algorithms.
Kaveh (2014) and Platt et al. (2018b) collected all the most famous metaheuristic algorithms in two famous books published by Springer. Detailed descriptions, pseudo-codes of each algorithm and interesting applications of these were shown. In a work published by Yang (2010b), Nature-inspired Metaheuristic algorithms received deep attention.
Only when a certain level of seniority reached on the matter was achieved, the literature papers, considered by the Scientific Community as the most completed, were published by Gandomi et al. (2013a), and by Kashani et al. (2022). However, the usefulness of non-gradient approaches in topology optimization was discussed by Sigmund (2011). In this forum article, the author raises doubts about the practical and scientific relevance of adopting soft computing techniques that use immense computational resources for solving simple problems for which there already exist efficient solution techniques. Consistent with what was introduced before, Rozvany (2001, 2009) published a critical review of established methods of structural topology optimization where SIMP and ESO numerical topology optimization was discussed in detail.

Once the benefit of these new approaches was largely tested, several researchers focused on increasing the level of complexity within the investigated case studies. In this way, Platt et al. (2018a) in chapter 6 of their book tried to collect all the scientific papers related to interesting application cases like trusses, frames, bridges or seismic devices but several papers resulted to be excluded by the process review. Other authors provided review papers entirely dedicated to specific topics like Rahane et al. (2022) for industrial trusses or Fan et al. (2007) in which special attention was given to the optimization of large-span steel structures or high-rise buildings (see e.g. Lawson et al. 2012, Li et al. 2011 and Lacey et al. 2019). The latter realized a full review of the research on structural damage criteria in terms of material, structural members and global structures for tall buildings. Moreover, other authors as Frangopol and Maute (2003) presented a brief review of the life-cycle reliability-based optimization field with specific regard to civil and aerospace structures.

If the majority of the mentioned-above review papers were based on single-objective optimization problems, a limited number of review papers treating multi-objective optimization were identified by the authors.
Marler and Arora (2004) provided a survey of current continuous nonlinear multi-objective optimization (MOO) concepts with specific regard to their applicability to engineering problems.
Foley et al. (2007) carried out an overview of state-of-art model-code performance-based design methodology into multiple-objective optimization problems for single-story and multistory structural steel frameworks with fully and partially restrained connections.
Machairas et al. in (2014) were able to review the most used methods and tools for building design optimization in an effort to explore the reasoning behind their selection, to present their abilities and performance issues and to identify the key characteristics of their future versions.

All these review articles can be considered as comprehensive reviews and comparative studies mainly oriented to detect the optimization strategies which guarantee, as the only target function of the optimization, the highest structural efficiency related to the specific application case study.
Other relevant authors attempted to identify other crucial aspects in the formulation of the most impactful target function considered within the optimization process of a structure like the economic and environmental purposes. Sarma and Adeli (2002a)

presented a chronological review of the journal articles on the cost optimization of steel structures. It represents one of the few authoritative works on this topic in which all the economic aspects, involved within generic steel structure realizations such as material cost, fabrication cost, cost of transporting the fabricated pieces to the construction field and the erection cost including the material costs of connection elements were taken into account.
A few years ago, Lagaros in Lagaros (2018a), tried to answer the question "Is it worth performing structural optimization studies?". The author investigated, by analyzing real-world case studies as frames or high-rise buildings, how the optimization tools applied for the life-cycle assessment of structures have a drastic environmental impact and contribute to the economic development of the construction industry.

1.7 Overview on the number of publications and bibliometric analysis

In the following, the authors tried to organize available publications on different structural engineering optimization problems. To this end, the official Elsevier's abstract and citation database *Scopus* was used and, subsequently, each paper was extracted and placed in the targeted field.
In the first step, it is found a total of 2,811 publications by searching keywords such as "Steel structural optimization", "steel optimization" and "structural optimization". The official platform considered all the publications with those keywords within the "title, abstract and authors keywords" of each paper.
Once conference papers, reviews, book chapters and conference reviews were excluded by the search platform, the total number of papers dropped to 1,797. Subsequently, the research was conducted considering only scientific papers belonged to the "Engineering" subject area and published between 1975 and 2022 for a total number of 1,281 papers. In Figure 1.7, the total number of publications per year has been shown.
Finally, from a total of 1,281 papers, the authors reviewed 446 papers in three main categories as follows: Size, Shape and Topology.
For each category, further classification was realized based on the OF type adopted into the problem statement. (1) Structural performance-based, (2) cost impact-based and (3) environmental impact-based optimization problems were identified as sub-

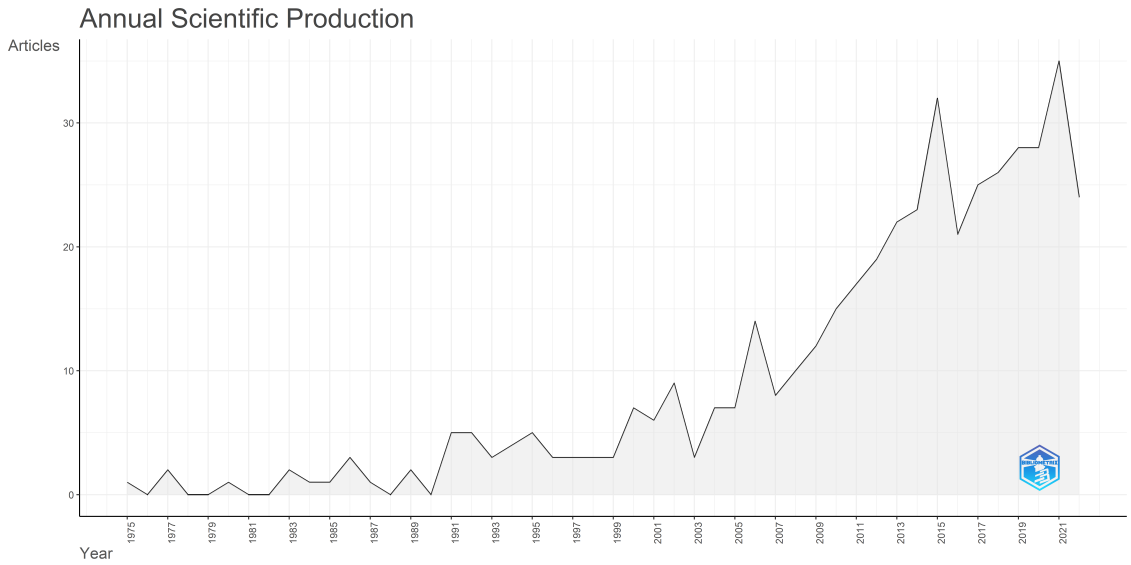

Fig. 1.6 Total number of publications obtained by reviewing 446 papers

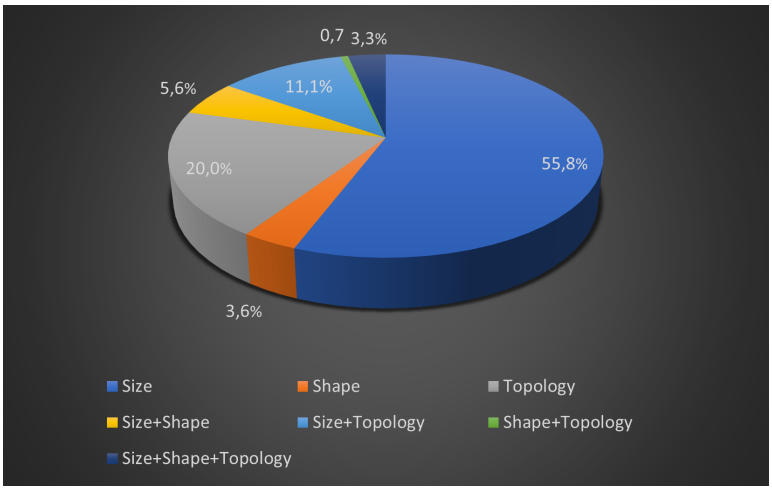

Fig. 1.7 Cake-chart rapresentation of number of publications in each sub-field identified by the authors

categories.

The observations based on the number of publications in every sub-field are demonstrated in Figure 2. Of all the revised papers, the majority focused on pure size optimization (55,8%) followed by topology only (20,0%) and coupled size+topology strategies (11,1%). The other hybrid approaches appear to have received less attention from the scientific community.

From the reviewed publication, it is obtained the statistics of publication per journal.

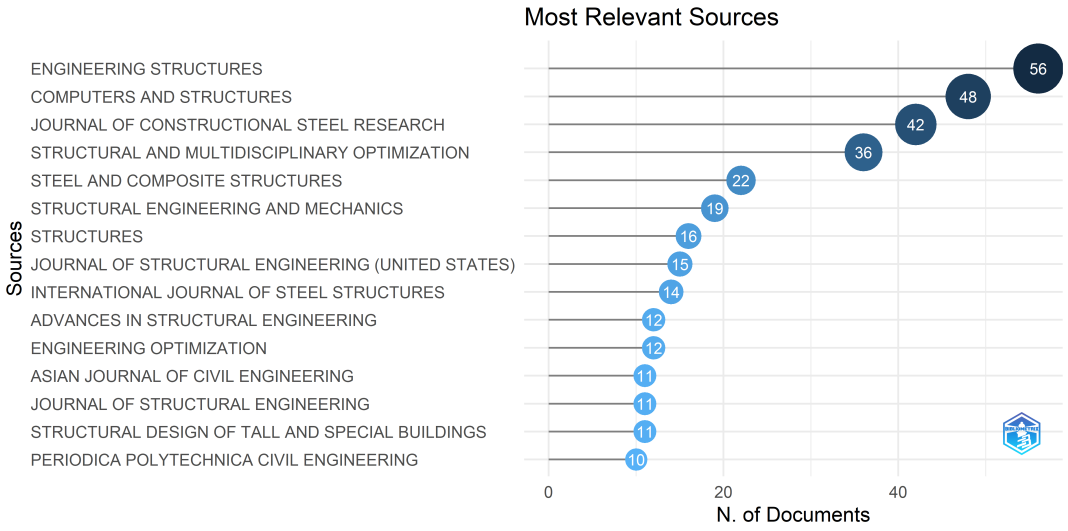

Fig. 1.8 The most relevant sources carried out from the Bibliometric analysis

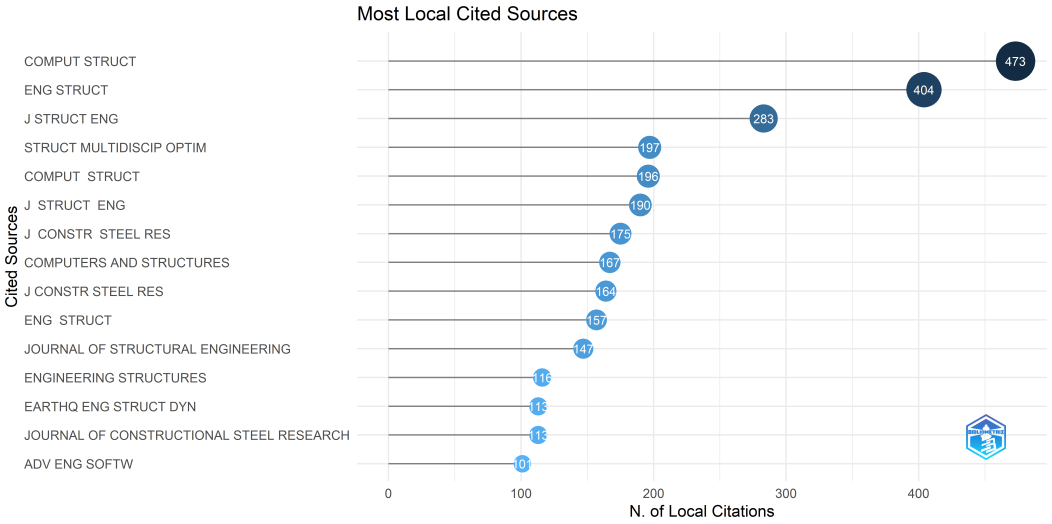

Fig. 1.9 The most local cited sources carried out from the Bibliometric analysis

In figure 1.8, the most relevant sources have been shown and the first 15 journals with at least 10 publications per journal have been plotted. The total number of publications calculated as the sum of the scientific paper published in each journal is 335 which can be considered representative of the whole database.
On the other hand, a bibliometric analysis was conducted in order to identify the most locally cited sources. A ranking of the highest cited journals has been provided in which the number of citations for each journal has been shown (figure 1.9).

With the aim to analyze the trend of the keyword in recent years, VOSviewer

software was adopted for a graphical representation of the data. It is a software tool for constructing and visualizing bibliometric networks.
Fig. 1.10 depicts network visualization co-occurrence analysis, and Fig. 1.11 shows the keyword trend in recent years. Maps created, visualized and explored using VOSviewer include *items*. The *item* that was used in Fig.s 1.10 and 1.11 are the authors' keywords.
In the network visualization (see Fig. 1.10), *items* are represented by their label and by default by a circle. The size of the label and the circle of an item is determined by the *weight* of the *item*. The higher the *weight* of an *item*, the larger the label and the circle of the *item*. Moreover, between any pair of *item* there can be only one *link*. A *link* is a connection or a relation between *items*. In this case, we are interested to detect the keywords which occur together in the reviewed documents and, hence, finding the research topics which have a sort of relationship one each other. Each *link* has a *strength*, represented by a positive numerical value. The higher this value, the stronger the *link*. Sometimes the *links* between *items* all have a strength of one. Moreover, if the *link* attribute indicates the number of *links* of an *item* with other *items*; the *Total strength* attributes indicates the total *strength* of the *links* of an item with other items.
Hence, a *network* is a set of *items* together with the *links* between the *items*.
Set of *items* can be grouped into *clusters*. *clusters* are non-overlapping in VOSviewer. In other words, an item may belong to only one *cluster*. *clusters* are represented by colours, hence, the *items* which have the some colour belong to the same *cluster*. The distance between two *items* in the visualization approximately indicates the relatedness of the journals in terms of co-citation *links*. In general, the closer two *items* are located to each other, the stronger their relatedness.
In the *network visualization* depicted in Fig. 1.10, it is quite evident that among the 1141 keywords contained within the overall reviewed documents "Structural optimization", "Optimization" and "Steel" resulted in the most popular.
In Fig. 1.11, a so-called *Overlay visualization* is shown. The *Overlay visualization* is identical to the *Network visualization* except that *items* are coloured differently. The colour of *items* is assigned depending on the *scores* of the *item*. The *score* is a specific attribute that the user wants to include during the analysis. In our case, *score* is represented by the year of appearance of each *item* (keyword).
It becomes clear how the most used keywords as "optimum design", "steel frames", "optimization" and "genetic algorithms" belong to documents which were published

between 2010 and 2014. On the contrary, other topics such as "reliability", "incremental dynamic analysis", "passive control" and "composite beam" represent the most challenging research field, considered by the Scientific Community, from approximately 2016 to nowadays. Fig.s 1.12 and 1.13 shows, respectively, the networks of a total of 839 authors among collaborating researchers and the year during which the collaboration occurs. Each *item* in the network displays an author/co-author, and the *link* between *items* illustrates the co-occurrence of the knowledge channels.
The previous analysis conducted on the co-authorship can be enriched by other considerations aiming to identify the most relevant authors in this field (see Fig. 1.14) and the most locally cited ones (see Fig. 1.15). In Fig.s 1.14 and 1.15, the ranking of the first 10 authors with the highest number of publications and citations are respectively plotted. Kaveh. A. results to be, at the same time, the most active and the most cited authors in this field.
Finally, in the last figure (fig. 1.16) a country collaboration map was carried out in order to show the countries with the highest level of scientific collaboration. The strength of the scientific collaboration corresponds to the thickness of the links between the countries. In this way, frequency and intensity, in terms of number of published papers derived by the collaboration, are crucial parameters that have been considered in the map.

1.8 Size Optimization

1.8.1 Structural performance-based optimizaton problems

In the present section, we have collected all the papers regarding size optimization problems, focused on structural performances. Due to the number of papers that appeared in the literature, a division into main topics rather than a simple chronological ordered list was proposed for clearness purposes. By means of the following chart 1.17, it is possible to appreciate the number of studies dealing with each of the 5 presented themes, i.e. non-linear behaviour of structures, optimization under seismic loadings, connection flexibility considerations of frames, soil-structure interaction investigation, large roof structures and multi-bays, multi-storeys frames.

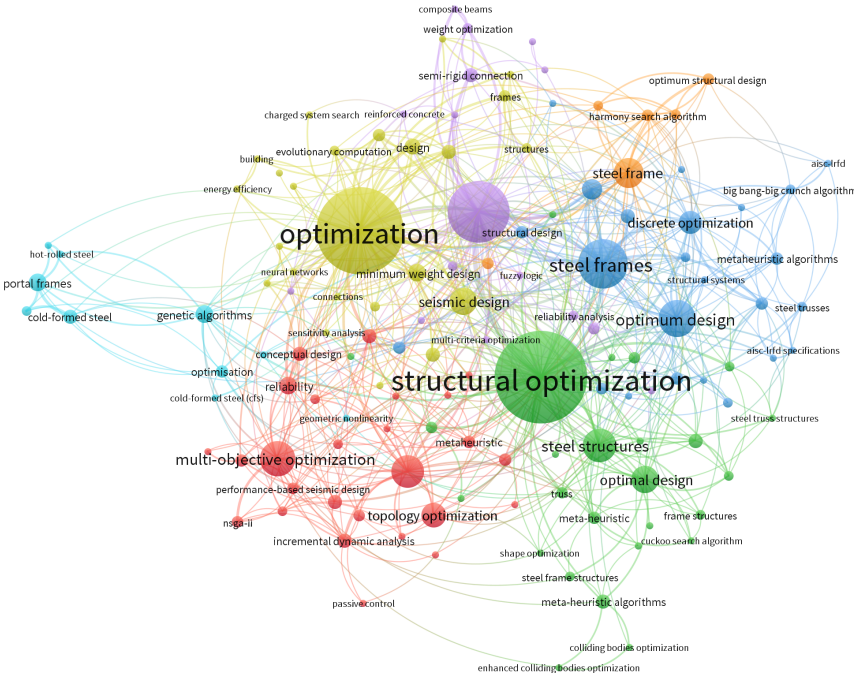

Fig. 1.10 Network visualization of the co-occurrence author's keywords

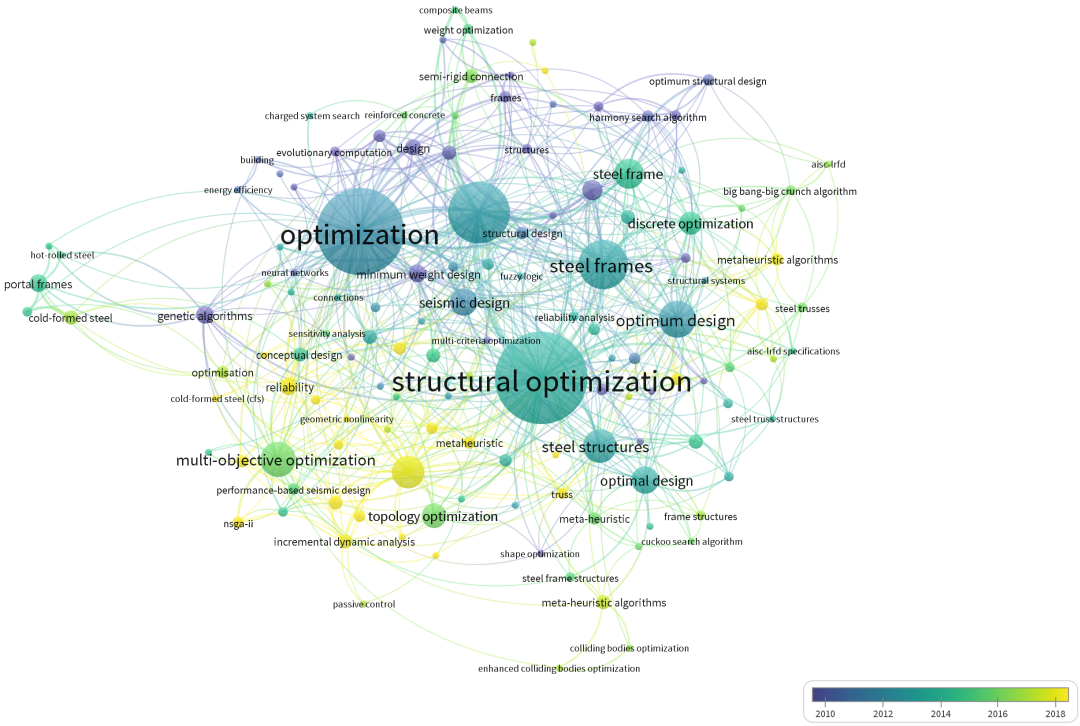

Fig. 1.11 Overlay visualization of the co-occurrence author's keywords in the last years

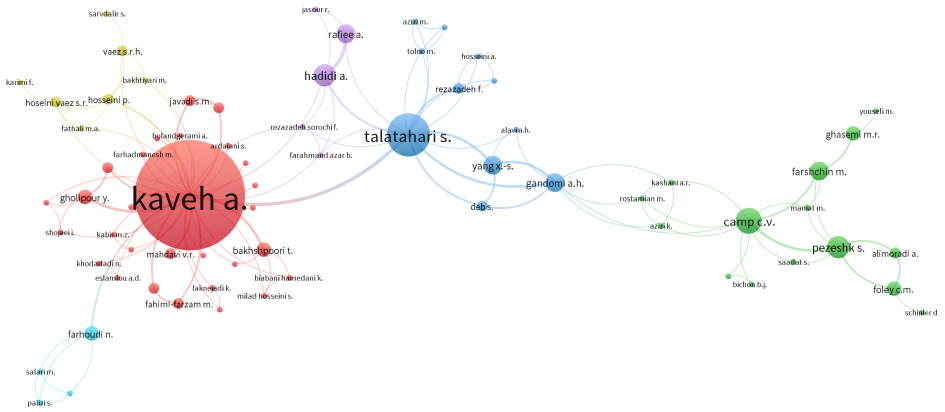

Fig. 1.12 Network visualization of the co-authorship and collaborations within the SSO Scientific Community

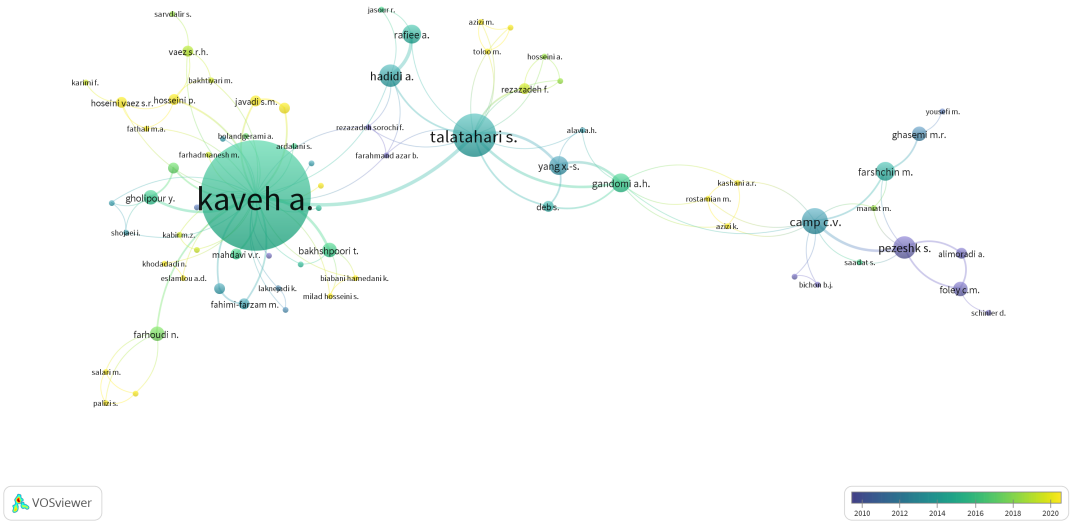

Fig. 1.13 Overlay visualization of the co-authorship and collaborations within the SSO Scientific Community in the last 10 years

Non-linear behaviour of structures Many researchers on frames or truss structures have primarily concentrated on their linear-elastic behaviour, entirely neglecting their resistance capacity to loads outside the elastic domain. However, geometrical and material non-linearity play a crucial role in the realistic modelling of structural behaviour and the influence on the minimum weight search was investigated.
For instance, in Saka et al. (1991), a minimum weight design of a non-linear elastic-plastic frame with displacement limitations has been investigated such that large deformations were admitted. By employing the Newton-Raphson-type iteration technique, small load increments are imposed and plastic hinges appear when members,

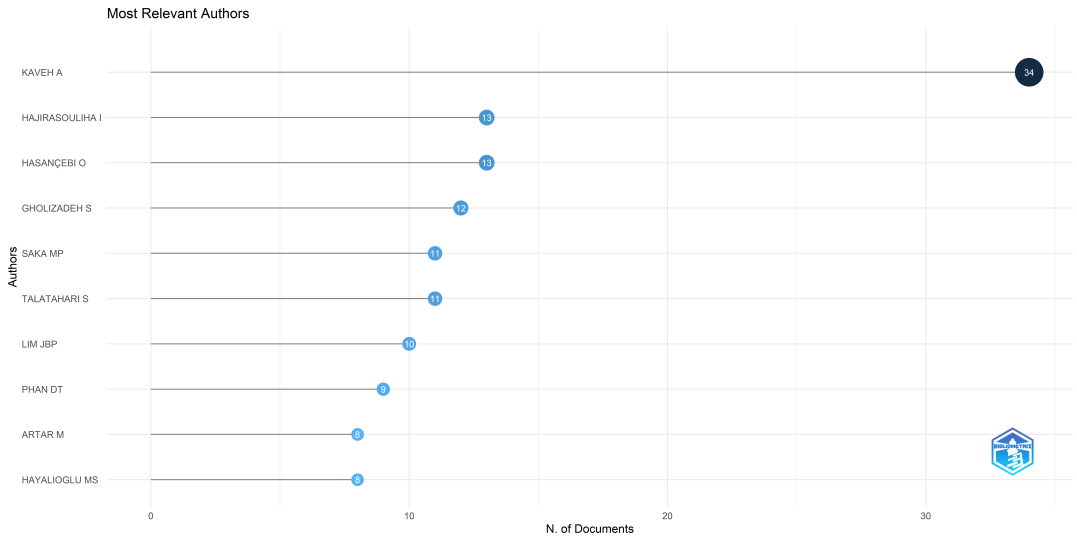

Fig. 1.14 The most relevant authors in the SSO field

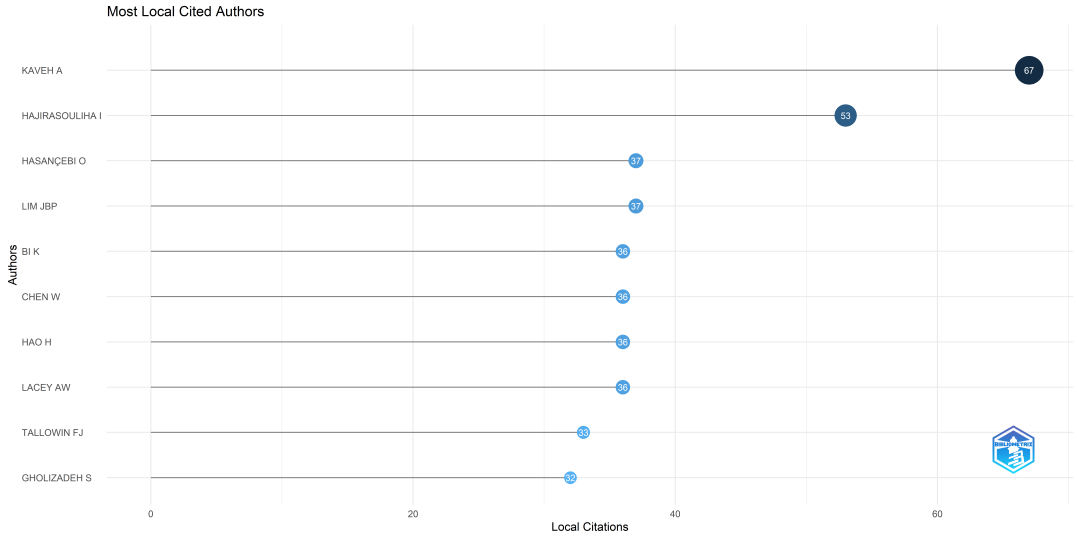

Fig. 1.15 The most cited authors in the SSO field

with variable geometrical properties at each iteration, reach yielding. By comparing the results obtained from a multi-storey and multi-bay elastic frame with that one in which non-linearity was included, optimal design with lighter frames was provided by the latter at the cost of a higher computational time.

The same author in Hayalioglu and Saka (1992b), extended the design of geometrically non-linear elastic-plastic steel frames including tapered members. Two variables were involved in the design problem: the cross-sectional area at one end

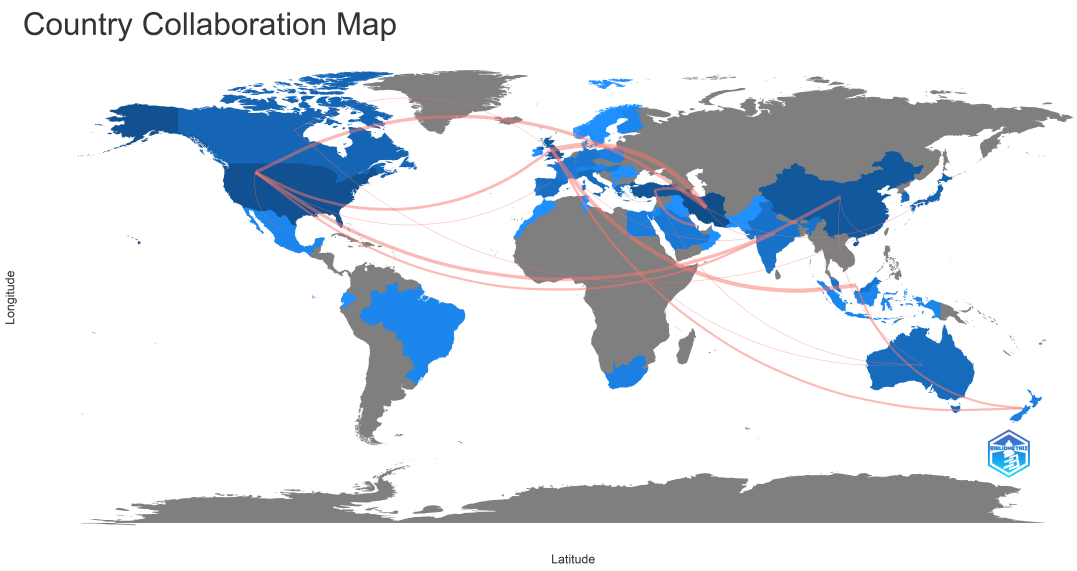

Fig. 1.16 Country collaboration map

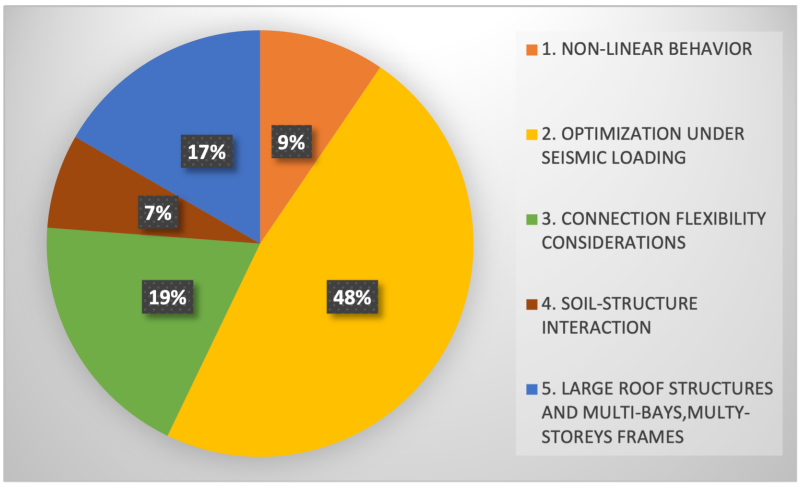

Fig. 1.17 Collected papers with size optimization approach

of the beam and the area ratio of each edge member resulting in a well-defined linear reduction function. A minimum weight solution was performed for three elastic-plastic steel structures in which large deformation was considered during the analysis. As in the previous study, a greater saving in the mass of structures with respect to the traditional linear-elastic modelling was recognized.

At the beginning of the century, Choi et al. (2002) proposed a non-linear inelastic analysis for an optimal design of steel frames. The optimization framework was realized by substituting at each iteration all the unfeasible cross-section elements

(structural verification not satisfied) with stiffener flange sections (i.e. *W-section*) taken from the AISC-LRFD (American Institute of Steel Construction) database. This routine was repeated until the serviceability, strength verifications and ductility requirements were satisfied. Results showed that the weights can be reduced by 8.0% and 3.7% for the planar portal frame and for the space two-story frame respectively, if compared with those of the conventional design using LRFD specifications.
The latest research was focused on reducing the computational time due to the non-linear analysis calculation. Conventionally, Non-linear static analysis (Pushover) is preferred for its effectiveness in the prediction of the structural behaviour as well as its competitive computational effort (e.g. Izadpanah and Habibi 2015 and 2018, Ozgenoglu et al. 2017, Costa et al. 2017 and Tiana et al. 2018). Robustness of this approach is strongly related to the shape of the lateral load pattern (Gupta et al. 2000 and Jan et al. 2004). However, researchers agreed to consider Non-linear dynamic analysis (Time-history) analysis as the most accurate method for the evaluation of the inelastic behaviour of structures (Antoniou and Pinho 2004 and 2004). In this sense, minimising the difference between the results obtained by the former and the latter result in an appropriate prediction of the responses with a low computational cost.
An attempt in this way was provided by Habibiet al (2019) in which a novel optimization technique was developed aimed to evaluate the optimal shape of lateral action for the minimum disparity between the floor displacements calculated adopting pushover analysis and that one derived by Non-linear Dynamic Analyses (NDA). Once the lateral floor displacements obtained by benchmark NDA analysis are calculated, the lateral load pattern that produced the least difference between the lateral floor displacements of the NDA and those of the pushover analysis was identified. The adopted OF was simply the ratio between the difference of floor lateral displacements resulting from non-linear time history and pushover analysis, normalized with respect to the floor lateral displacement from the non-linear time history analysis. 5 story- 2 bay, 10 story-3 bay and 15 story-3 bay special moment resisting steel frames were analysed to validate the applicability of the recommended method and a final comparison with well-known lateral shape action modelling as uniform, linear and parabolic was pointed out.

Optimization under seismic loading Undoubtedly, a crucial topic for academicians and practitioners regards the dynamic behaviour of structures under seismic

actions. Though first approaches appeared in Literature regarded mainly deterministic approaches as state space steepest descend method developed by Feng et al. (1977b) or traditional gradient method as in Memari et al. (1999b) or, generally, iterative procedures (Hall et al. 1989) for the optimum seismic design of different types of braced, unbraced, regular and irregular frames; at the beginning of the century, authors experienced soft computing techniques for the reduction of the effectiveness during the exploration phase and limited computational effort (pezeshk et al. 2000, CHen et al. 1997).

More in detail, Feng et al. (1977b) presented a state space steepest descend method for the weight minimization of elastic structures subjected to dynamic loads, where the elements' cross-sections were taken as continuous design variables. The adopted constraints were applied to the dynamic response, i.e. displacements and stresses, at critical points of the structure. In addition, upper and lower bounds on natural frequencies were imposed, as well as a design parameters boundary.
A step forward in the application of weight minimizations was proposed by Memari et al. (1999b). A comparative study of different types of braced, unbraced, regular and irregular frames, subjected to combined gravity loads and seismic lateral forces, has been carried out by the authors. Thought cross-sectional areas were chosen as design variables in a continuous range, round-off strategies were applied and the closest section properties from the German standard database were assigned. the design had to satisfy combined bending and axial stresses, shear stress, compression buckling and tension slenderness criteria, according to the AISC.
Similar approaches were experienced by Rosso et al. (2021c) and Cucuzza et al. (2022) for trussed structures in which issues related to discrete design variables have been overcome by realizing round-off strategies at the end of the optimization.
In Palizzolo et al. (2015), minimum volume optimization was achieved for 4-storeys elastic-plastic frames. In the static condition, the structure had to remain in the elastic field when subjected to fixed loads, while, for seismic excitations, the elastic shakedown limit could not be violated by the plastic frame. Specifically, the thickness of the box-shaped cross-sections was allowed to vary within a specified range. As expected, the structural volume related to the discrete variable design was higher than the continuous variable one.

In the context of structural optimizations under seismic loading conditions, many studies agreed on considering uniform distribution theory (UDT) as an efficient goal for optimal design. In other words, following this approach, an optimal design under

seismic loads must require that all the strength and serviceability performance of each member are maximized (see Lv et al. 2015)

The first outcome was carried out by Kapoor et al. (1987b), in which the best stiffness distribution of a multi-storey frame was investigated. The objective function of the optimization was tackled as the minimum structural weight evaluated by means of a nonlinear programming technique. In the probabilistic procedure presented, the multi-storey frame has been idealized as a multi-degree "shear beam" subjected to earthquake ground motion treated as a random process. The design variables were chosen as the moments of inertia of the columns of different storeys, expressed as a function of the areas, section dimensions and modulus of all the available I-sections listed in the Indian Standard Institution (ISI) specifications. From the comparison between the probabilistic and deterministic formulations (spectrum analysis), it has been demonstrated that the first one provided more realistic results.

Later on, Moghaddamet al. 2005, proposed a strategy for enhancing the dynamic response of concentrically braced steel frames, subjected to seismic excitation, based on the concept of uniform distribution of deformation. As demonstrated in previous studies, during strong earthquakes the deformation demand in structures does not vary uniformly, but there are some stiffer elements that do not fully exploit their seismic capacity. Therefore, the goal of the proposed iterative optimization technique was to gradually shift inefficient material from strong to weak areas of a structure, by changing its structural features. At first, the optimizer attempts to size columns and beams according to the code drift requirements. Finally, optimal bracing systems were assigned in order to reach the uniform deformation state. From the analysis, it has been demonstrated that generally there is a unique optimum distribution of structural properties, independent of the seismic load pattern used for the initial design.

The effects of strength distribution pattern on the seismic response of tall buildings have been examined by Moghaddam, H., et al. (2008), which proposed an efficient optimum performance-based seismic design aimed to identify the optimum pattern for distribution of seismic lateral loads. A lumped mass model of the tall building was realized by placing perfect elastic–plastic shear springs at each joint. The total mass of the structure is distributed uniformly over its height. The optimal loading pattern is derived when the minimum required structural weight would is achieved. To accomplish this, the total weight of the seismic resistant system has been calculated for shear building models with various fundamental periods, ranging

from 1 to 3 s, and different target ductility demands. Fifteen selected strong ground motion records have been considered and modal analysis has been performed at each iteration to retrieve the building's seismic response. It is shown that having the same story ductility demand, models designed according to the average of optimum load patterns have relatively less structural weight in comparison with those designed conventionally.

Interesting outcomes were pointed out by coupling the uniform deformation theory with a novel Performance-Based Design (PBD) approach (i.e Mohammadi et al. 2014) and for the optimal design of eccentrically braced frames (EBF) (see Mohammadi et al. 2004)). Hence, the uniform distribution of shear deformation in the link beams resulted in a less damage level in the EBF system. In PBD frameworks (see Moghaddam et al. 2005 and 2004), performance objective is usually defined as a given level of performance for a specific hazard level. More in detail, a performance level is representative of the level of expected loss, while the hazard level of the seismic intensity. In the considered paper, the authors focused the attention on the optimization of 3, 5 and 10 storeys eccentrically braced steel frames (EBF), subjected to 12 earthquake ground motions. Once again, the weight minimization has been defined as OF, while design variables of the problem were mainly dependent on the properties of the link beams that basically govern the seismic behaviour of EBF.

Due to the improvement in strength capacity and dissipation energy guaranteed by EBF systems, they represent interesting application case studies for several authors (see Brognoli et al. 1998, Fathali et al. 2020, Balling et al. 2009 and Abedini et al. 2020). For instance, in Ohsaki et al. (2012) locations and thickness of Link members between the connections of beams and braced of EBF were adopted as Design Variable while plastic dissipated energy before failure was assumed as the Objective function of the Tabu search algorithm. Others, focused mainly on the weight optimization of EBT or its performance-based optimum seismic design (Gholizadeh et al. 2022, Stromberg et al. 2012a and 2016a) via dissipation energy maximization (i.e. Kaveh et al. 2020b) and, generally, plastic analysis of braced frames (i.e. Palizi et al. 2020, 2020).

The benefits of adopting UDT were also recognized by Moghaddam et al. (2021) for the optimal design of steel moment-resistant frames (MRFs). In the minimum-weight optimization, the design variables were always the members' cross-sections, while constraints were applied to maximum plastic rotations for the monitoring of the deformation of the frame and strength-based demand to capacity ratios for the

acting forces verifications. The efficiency of the proposed optimization has been demonstrated considering 3, 5, 7, 10 and 15-storey steel MRFs and a set of five strong earthquake records from the Pacific Earthquake Engineering Research Center (PEER) database.
Moreover, The optimization process of MRFs for multiple performances and multiple hazard levels under various performance objectives was deeply investigated by Qimao et al. (2015). In this work, authors compared minimum weight solutions obtained for each hazard and performance level by varying geometric characteristics of all the beams and columns at each story.
The potentiality of the PBD was also appreciated by adopting different soft computing techniques such as the well-known population-based algorithms PSO, DEO, ECBO (e.g. Gholizadeh et al. 2016), or in combination with metaphor-based algorithms (Kaveh et al. 2021) and novel optimization approaches as the Constraint Control Method (CCM) developed by Mansouri et al. (2019). This approach requires that the most conservative member sections are first chosen for each member and then, iteration by iteration, lighter solutions are progressively assigned toward the global optimum design, meanwhile, problem limitations and constraints are respected. Three-storey four-bay frame and nine-storey five-bay frame steel sway frames were analyzed, and the efficiency of the proposed method was demonstrated by a drastic reduction in the number of structural analyses when compared to other well-known metaheuristic algorithms.

As noted by some authors, parameters which affect the structural performance during a seismic event can assume opposite trends or the optimum can not be achieved by simply minimizing a single target function. As briefly mentioned in this section, multi-objective optimization procedures are quite challenging if compared to single-objective problems. The main issue is that they work with competing goals, meaning that the design accounting for one target may lead to a decrease in the performance of the other objectives. As a result, rather than a single global optimum solution, that maximizes or minimizes more than one objective function simultaneously, there is a set of incomparable optimal solutions, each of which is superior to the others for the target function of competence. Decision-makers can choose from a variety of options in this collection of non-dominated or Pareto optimal solutions, in order to best meet the needs of a given project.
In order to fulfil different goals simultaneously during the optimization, the first studies were focused on coupling minimum construction cost in terms of sections weight,

minimum structural damage using a damage index, and minimum non-structural damage under the applied ground motions (see Xu et al. 2018 and Hong et al. 2020). More in detail, Kaveh et al. (2013) experienced the minimization of some seismic eccentric braced frame (EBF) features as cross-sectional area, inter-story drift and level of damage expressed in terms of inter-story drift or dissipation energy. While for the first objective function, they have been simply varied to meet the minimum weight of the structure, for the other two objectives a balance needed to be found on the strength of the material. In fact, high yield strengths could not ensure decreasing damages, especially for non-structural elements. Essentially, when subjected to high strength, the structure will experience high accelerations even during mild excitations that could lead to local failure due to non-structural damages. Results have revealed, as expected, that an increase in volume, led to a decrease in the inter-story drift but also to a damage index larger than a given threshold. Thus, high computation time was required to find a good balance between the three OF, even though neural networks helped in the decrease of the number of calculations.
In the same year et al. (2013) performed the multi-objective seismic design of special moment resisting frames (SMRF) taking into account hierarchical design in order to obtain a concentration of plastic hinges in the beams before then in columns. Consequently, the scope of the work was to minimize not only the structural weight but also the column-to-beam strength ratio which ruled the activation of hinge mechanism. Constraints were imposed to control member strengths, inter-story drift ratio, prevention of formation of the plastic hinge at columns connected at joints, and cross-sectional areas of vertically continuous columns. In particular, the multi-objective optimization was performed through Non-dominated Sorting Genetic Algorithm-II (NSGA-II), based on multiple Pareto-optimal solutions. Predictably, the results on both three-story and nine-story steel moment frames presented decreasing optimal strength ratios for increased structural weights.
The crucial role of an optimal capacity design was investigated by Karimi et al. (2019) and Kaveh et al. (2019) where a performance-based seismic design was proposed for frames and steel plate shear wall (SPW) systems, respectively. In these studies, the goals were weight minimization and a uniform distribution of inter-story drift along the structure's height avoiding soft-story mechanics during seismic excitation. The optimization has been carried out considering not only the performance-based design (PBD) method at the Collapse Prevention performance level, but at first accounting for the load and resistance factor design (LRFD) method.

Uniform Damage Distribution (UDD) theory was also widely adopted for multi-objective optimization problems.
Ghasemof et al. (2021) developed the so-called multi-objective uniform damage optimization (MUDO) method in which structural weight and maximum inter-story drift ratio (IDR) have been treated as two conflicting objectives, representing economy and safety measures, respectively. Not only constructability constraints were included but also the flexural behaviour of beams and columns was controlled, in order to avoid strong columns and weak beams effects. To demonstrate the efficiency and robustness of the proposed algorithm, 3-, 6- and 9-story steel moment frames have been compared with those of two well-known NSGA-II and MOPSO optimization metaheuristic algorithms. A similar approach was adopted by Liu et al. (2013) in which optimal robust design of steel frames structure was achieved by considering three objective functions: the weight of the structure, the mean value and standard deviation of the maximum inter-story drift for the assessment of the global robustness of the structure.
In the multi-objective seismic design framework, it is worth mentioning other two studies that in different ways addressed the importance of the connections' role in frames under seismic loads. If in the first work (see Mojtabaei et al. 2021) thin-walled cold-formed steel (CFS) components and connections used in portal frames were investigated with the aim to maximize the seismic resistance in terms of ductility and energy dissipation; the second approach (e.g. Moradi et al. 2017) is entirely focused on the post-tensioned (PT) steel beam-column connections in frame structures, able to significantly reduce long-term seismic damages and the corresponding post-earthquake maintenance costs. The goal was to increase the PT connection's initial stiffness, load capacity and final drift. In particular, it was desired to produce a ductile behaviour for a PT steel beam-column connection by maximizing the ultimate drift meanwhile, the cost minimization has been accounted, for in terms of the amount of material.

Connection flexibility of frames Historically, many authors are interested to investigate the role of connection flexibility in structural optimization (see Xu et al. 2001 and Simoes et al. 1996).

In fact, most of the time, in the analysis and design of steel frames, beam-to-column connections are generally assumed to be either fully rigid or perfectly pinned (see Chen et al. 1995, 2018). In the former case, bending moment, as well as

shear and axial forces are transmitted from one element to another and no relative rotation of the connection is allowed; in the latter, only shear and axial forces can be transmitted between the joined elements. Since experiments have revealed that the real behaviour of the frame's joints can be modelled with semi-rigid connection in order to allow comparison of different connections' rigidity through the variation of their stiffness (e.g. Da Silva et al. 2008, Wang et al. 1999 and Gorgun et al. 2012). Moreover, Researches have shown that the assumption of a constant value for the stiffness of a connection is not realistic because it changes as the load as demonstrated by Nethercot et al. (1985) and Ballad and Chen (1995). Specifically, two modelling strategy of semi-rigid connections was investigated consisting in adopting new elements with a specific constitutive law (hsieh et al. 1991 and Dhillon et al. 1999) or by using lumped rotational springs with negligible lengths (Kaveh et al. 2008, Chen et al. 1989). In literature, considering semi-rigid connections' effect on size optimization processes led to contrasting results.

For example, one of the earliest studies herein examined was published by Machaly et al. (1986c). They demonstrated the advantages of using semi-rigid connections modelling in several weight optimizations. Gables, portal frames and multi-bay three-storey frames have been optimized, using a nonlinear programming technique. During the process, I-shaped cross-sections were assumed for the columns and girders and their geometrical properties were chosen as design variables (i.e. breath of flange and height of web). In addition to strength requirements, side constraints regarding physical limitations of the cross-sections and buckling considerations were applied too. Results show that a semi-rigid connection is able to provide a weight saving from 10% to almost 30%, depending on the structure considered. In particular, such material reduction can be mainly addressed to girders rather than columns.

In agreement with such results, Csébfalvi et al. (2007) presented a study focused on discrete minimal weight design of steel planar frames with semi-rigid beam-to-column connections through the use of a Genetic Algorithm (GA). During the procedure, the connection spring's characteristics had been allowed to vary within a defined range of spring rotational stiffness. Then, semi-rigid joints were adjusted in order to account for both displacements and internal forces distribution. By means of two examples, a simple-bay frame and a two-bay frame, it has been shown how semi-rigid connections modelling improves the design, if compared to the case of rigid or pinned connected frames. However, it is worth of noting that the optimal solution highly depended on the loading condition and geometry of the structure.

The effectiveness of the genetic method was also proved for discrete optimum design problems where semi-rigid connections were considered as in Kameshki et al. (2001), (2003) and Hayalioglu et al. (2004a, 2004b).
The beneficial effect of semi-rigid connection in the optimal design of steel frames was also demonstrated by adopting other metaheuristic algorithms such as the harmony search method (HS) (Degertekin et al. 2009) or the improved HS-PSO Hadidi et al. (2014). In both works, a computer code is developed for the optimal sizing design of non-linear steel frames with various semi-rigid and rigid beam-to-column connections
Also Korkmaz and El-Gafy (2018) demonstrated that neglecting the effects of beam-to-column connection flexibility in the design would lead to unrealistic predictions of the overall stiffness of the structures and to heavier designs. More in detail, in the proposed analysis, the target function of the optimization was the weight minimization of structures considering geometric non-linear behaviour (Pushover analysis). The constraints were applied to the stresses and displacements, while the design variables were representative of the members' cross-sections, taken from a list of available sections. Optimal design examples of 3,10 and 20-story rigid and semi-rigid connected frames were investigated and designs with rigid connections not only exhibited over-stressed members and lower accuracy in the drift predictions higher value of the total weight.
So far, all the authors agreed to consider optimal design including semi-rigid connection as the most promising one. However, some exception was identified and interesting application cases demonstrated an opposite trend. The principle of virtual work was largely used for the investigation of semi-rigid connections' behaviour as reported in Elvin and Strydom (2021) and (2018). In another study, Al-Salloum and Almusallam (1995b) developed a novel approach called the virtual work optimization method (VWOW) based on the principle of internal virtual work. VWOM is an automated method that aims to minimize the weight of the structure while remaining consistent with building code standards for a particular geometry, deflection criteria, and load scenarios. A section adjustment was considered efficient if it caused a significant decrease in deflection at all critical points for a small increase in mass. To illustrate the method, four case studies of tall buildings were presented. Results showed that buildings with semi-rigid connection stiffness lead to optimal solutions with heavier (6% of mass increase) or almost the same weight as the same structures with rigid connections. In some scenarios, It seems that the connection flexibility

lead to stiffer and, hence, heavier members. However, based on economic considerations, the authors' outcome is that the semi-rigid connection leads to cheaper design. A well-detailed analysis concerning the connection flexibility topic has been illustrated by Oskouei et al. (2012). A genetic algorithm has been employed for the minimum weight optimization, in which the variation of the degree of rigidity of the structure has been carried out by changing the cross-sections of beams and columns. To demonstrate the main differences between using rigid or semi-rigid connections, nine frames were analyzed. If the first group of investigated structures, results showed a simultaneously increasing in the natural period and overall weight of the structure; in the second and third groups, the trend was exactly the opposite. Solutions seem to be critically affected by the natural period of the structure: in the case of low-rise frames with low periods, the weight obtained for semi-rigid connection frames increased; meanwhile, medium-high-rise frames with higher periods experienced a weight reduction of the structure.
A comparison between fully restrained and semi-rigid connected steel frames has been reported also by Doğanet al. (2018). In particular, this study presented a Hunting Search method-based optimum design algorithm for unbraced steel frames. The non-linear problem, aimed at the weight minimization, was formulated as a size optimization in which wide-flange shape sections were assumed as design variables. According to the previous observations, since a great amount of horizontal displacement exists in the flexible connections, displacement constraints became dominant in the design, hence, stronger sections has been selected. As a result, the weight of the whole structure was greater than the one designed with fully restrained connections. Another interesting research has been illustrated by Artar et al (2015b and 2015c) in which the benefic effect of the concrete slab effects in steel frames with both semi-rigid beam-to-column and column bases connections was introduced. Three different plane frames with semi-rigid beam-to-column and column-to-base plate connections were carried out, at first considering only plain steel beams in the finite element analyses. The same optimization procedures were then repeated for the case of frames with composite beams. From the results, it can be noticed that by adopting rotational spring stiffness of frames at the level of joints, an increase of the structural weight is recognized due to the effective length factor K related to the buckling verification. However, optimum weight is decreased by about 5-8% when the effect of concrete slab on the behaviour of beams is considered.

Soil-Structure Interaction and geotechnics Another factor, influencing size optimizations of steel frames, that has raised the interest of some researchers is related to the soil-structure interaction effects. Most of the investigated papers adopt soft computing techniques for counterbalancing the huge computational cost due to the soil-structure interaction analysis (see Bybordiani et al. 2019).
Daloglu, Ayse, et al. (2016), have investigated such a topic using metaheuristic algorithms. Three-parameter foundation model has been adopted to incorporate the effect of soil foundation on the behaviour of the frames in the optimum design process. The moduli of subgrade reaction and soil shear parameter have been calculated in terms of vertical deformation profile. A computer program was coded in MATLAB (2009) for the optimization processes and connected to SAP2000 (2008) to perform the dedicated analysis of the frames. Both Genetic Algorithm (GA) and Harmony Search (HS) algorithm were used for the minimum weight optimization process and appropriate cross-sections, chosen as design variables, were selected from a predefined list of W-shaped sections. Results have shown that consideration of soil effects increased the steel design weight of the frames.
Later on, Fathizadeh et al. (2021) introduced a Performance-based design (PBD) optimization of two-dimensional moment-resisting steel frames (MRSF) that accounted for the effects of the soil-structure interaction (SSI). In particular, an engineering cluster-based genetic algorithm (ECGA) has been employed to run the optimization problem. The minimum weight of structural elements of the frame was tackled as the objective function and cross-sectional elements profiles, taken from the W-shaped American profiles, were assumed as design variables. In the connection between beam and column, weak beam–strong column constraint was assumed, regulating the amount of plastic moment in the node. In addition, strength and drift constraints were imposed, together with checks on displacements and rotation of the foundations, to control their uplift and settlement. Results obtained by practical applications of the proposed methods to investigate Soil Structure Interaction (SSI) effects on the PBD Optimizations show that with decreasing soil stiffness, stronger cross-sections are selected. For a frame on a type IV soil (loose soil) an increase of weight equal to 12.94%, in comparison to a frame with a fixed foundation, was detected.
Soil-structure interaction was also taken into account for solving multi-objective problems as shown in the study of Dehghani et al. (2019). A cluster-based non-dominated sorting genetic algorithm (NSGA II) was introduced to study the effects of the rehabilitation objectives on multi-objective design optimization of two-dimensional

steel X-braced frames. The target functions taken into consideration were weight minimization and maximum storey drift minimization. Geometric and strength constraints were applied and rotations and displacements at the level of the foundation were checked for three different performance levels. The efficiency and accuracy of the proposed method have been demonstrated by way of different examples of frame structures. It is worth noting that, in agreement with the previous studies, soft soils lead to an increase in the structural weight of the structure.

Finally, metaheuristic algorithms were also widely employed to face specific topics in the geotechnical field as the slope stability problem (1980) solved by using PSO algorithm (Gandomi et al. 2015), ACO algorithm (Baker et al. 1980), SA (Cheng et al. 2007). The same problem was faced by Cheng et al. (2007) where performance studies on six heuristic methods (SA, GA, PSO, simple HS, modified HS and Tabu search) were performed.
However, deterministic approaches were adopted by Basha and Bubu (2008) and Leung et al. (2010) for the optimum design of an anchored cantilever sheet pile wall and lenght optimization of pile groups, respectively.

Large roof structures and multi-bays, multi-storey frames In this last section, we have collected all the articles concerning the application of size optimization on large span structures, large multi-storeys and multi-bay frames.
Interesting research has been proposed by Scholz et al. (1986b). It has been described as the computerization of the interaction method, developed by Scholz, applied on a storey-by-storey basis, from top to base, of large multi-storey frames. The goal of the optimization was to obtain a value of the storey failure load factor within a specified range. In the procedure, at first, a simplified method has been used to obtain trial member sizes for the whole structure. Then the structure has been analysed using the programmed interaction method. This analysis was carried out in order to obtain the elastic-plastic failure load of each storey, whose members later have been adjusted if the failure load was not within its acceptable threshold limits. In the examples reported to demonstrate the validity of the proposed method, the frame's members were chosen among the American standard sections and the loads applied on the structure were simply the gravity ones, multiplied by given design load factors. Results have shown a good agreement between the proposed method and the rigorous elastic-plastic second-order analysis. It has been argued that the technique can greatly reduce analysis time as well as simplify the optimization of

members in the design of such frames.
Later on, multi-bay and multi-storey steel frames have been optimized, in a three-step numerical procedure, by Thevendran et al. (1992b). Volume minimization has been developed in the optimization, where I-shaped sections have been chosen as design variables, taken from a list of available steel sections. The peculiarity of such analysis was that at the beginning the design variables were considered continuous and then, from the obtained results, the members' cross sections were selected from the database. In fact, in the first stage, both columns and beams have been treated as continuous variables, in the second stage only columns have been approximated with the available sections and finally, in the third stage, also beams sections have been converted into the real ones. The frame was finally re-analysed to check whether any design criteria have been violated. In particular, the frame structure, subjected to dead, live and wind loads, have been designed considering beams' maximum deflection and both shear and moment capacities requirements, as well as stresses and buckling verifications for columns. Moreover, the horizontal deflection of the structure has been checked, along with geometric constraints referred to limiting bounds of the cross-sectional areas and to the variation of column sizes with levels. The simplicity of the procedure has been shown in a number of examples of such structures.
For industrial, commercial, and leisure buildings, single-story frame structures, also known as large-span portal frames, are frequently employed. Such buildings require the design of a structural system that can cover wide regions without requiring intermediary columns. Moreover, since steel offers a cost-effective alternative, the majority of these buildings are made of it. Pitched roof steel frames belong to that category of the single-story frame and their design has been the subject of Saka's studies (2003).
Although the design of pitched roof steel frames has been compared to simple one-story buildings, it nevertheless had to take into account several difficult issues. Design variables, considered to proceed with the optimization, were rafters and columns sections, chosen from the standard universal beam sections set, and the depth and length of the haunches. Regarding the design variables, it is important to underline that it is standard practice to use the same universal beam section for both rafters and use other cross sections for stanchions when designing steel portal frames. Additionally, for economic reasons, the haunches were made from the same section as the rafters. The minimum weight design of the frame was taken as the Objective

Function of the problem and different constraints were considered. First, due to serviceability requirements, the horizontal displacement of a column due to unfactored imposed and wind loads was limited to a height of the column/300. Similarly, the constraints have restricted the deflection of a beam to its span/360 if it has been carried plaster or other brittle finish. In addition, local capacity check for beams and columns with semi-compact or slender cross-section needed to be properly verified against bending and compression(buckling). A genetic algorithm was exploited to find the optimum design and an exterior penalty function was considered during the iterations. To illustrate the procedure, a practical example was reported regarding a frame with 20 meters span and 5 meters in height. Results have revealed that while the displacement and strength constraints didn't approach their upper bounds in the final design, the lateral torsional buckling has reached the allowable value. This had an impact on the ideal depth and length of the haunch among the iterations.
McKinstry et al. (2015), focused their attention on the design of large-span portal frames with fabricated beams. Fabricated beams were used, in contrast with the most common hot-rolled steel sections for column and rafter members, for weight reduction purposes. In particular, the advantage of employing fabricated steel beams, over the hot-rolled steel section, relies mainly on the maximum span achievable. Using the latter, spans can reach only 50 m, while 100m can be achieved by employing the former. Fabricated beams were built-up through the welding of steel plates. The dimensions of steel plates were the considered design variables of the optimization. With more details, discrete design variables were adopted for the thickness of the steel plate used for the web and flange, while continuous design variables for the breadth and depth of the section. The overall design optimization goal was to find the portal frame with the least amount of material for the main members while satisfying the design specifications. Columns, rafters and haunches were considered primary members of the structure and their weight was used to define the objective function. Both ultimate and serviceability limit states were included in the optimization, adopting deflection limits, recommended by the Steel Construction Institute (SCI), and accounting also for the buckling stability of the sections. To optimize the size of the plates used for the columns, rafters, and haunches, a genetic algorithm (GA) was used. For practical purposes, three different frames have been considered with different spans (40 to 60 meters) and different heights (10 to 12 meters). To make a comparison, each of the previously introduced frames was designed and analyzed with both universal beams (UB) and fabricated beams. Four types of UB

have been examined, each of which with a different number of design variables, concerning column, rafter and haunch sections, as well as haunch length. Instead, for the fabricated beams cases, the design variables were chosen between height, breadth and thickness of the column, haunch, web, flange and rafter. Moreover, in this case, they could vary according to geometric constraints. Interesting considerations can be drawn from the results, beginning with an achievable weight saving of 15% in frame weight for large-span frames (> 40 m). Instead, fabricated beams will be ill-advised for small frames where savings were minimum.

In the design of large-span portal-frames, the large span and elements' slenderness make them very sensitive to applied loads, especially wind loading. Regarding this last aspect, an interesting approach is given by Fu et al. (2019). In this research, long-span portal frames with inclined roofs were designed when subjected to dynamic loads, particularly wind loading. The evaluation of the wind loading on the inclined roof was more complex than ordinary rectangular buildings. To overcome these limitations, the load imposed by the wind was evaluated as an Equivalent Wind static Loading (EWSL) by means of Gust Loading Factor (GLF), Load Response Correlation (LRC) and Proper Orthogonal Decomposition (POD) method. Basically, those methods allowed us to transform the dynamic loading induced by the wind into a linear static pressure. The objective function was the minimization of the structural weight of all the elements in the portal steel frame, while the design variables were the tapered sections. Sizes need to be determined for several components of the tapered section, including the web's thickness and height as well as the flanges' width and thickness. Constraints of the optimization problem were based on the drift induced by wind pressure, with particular attention to displacements at the top of columns and vertical displacement at the mid-span of the rafters. In the examples reported, the main focus was on the effects of different combinations of EWSL, on the stiffness of elastic rotational restraints at supports and on the stiffness of semi-rigid connections between rafters and columns. It has been demonstrated that the optimized weight was generally reduced with an increase in the stiffness of both column support and the semi-rigid raft-column connection. The GLF technique yielded the highest optimal weight for ESWLs.

The same type of structure has been analysed also by Kavehet al. (2019). In particular, a comparison of different metaheuristic algorithms has been proposed for two different multi-span pitched roof frames with tapered members. Moreover, in the analysis, the apex height of the structures has been investigated, in order to find

the best design with minimum weight. The I-shape of the cross-sections of beams and columns was assumed, and specifically, the height and the thickness of the web together with the tapered length ratio have been chosen as design variables in the optimization. Their values were allowed to vary between feasible discrete ranges, as reported in the paper.

The structures under study have been subjected to the load combinations specified in the ASCE7 code (Minimum Design Loads and Associated Criteria for Buildings and Other Structures), in which dead, earthquake, wind, snow and roof live loads were considered. The constraints were applied to the strength of structural members, subjected to compression axial forces and bending. Moreover, displacement limits were imposed, depending on the loading cases, and construction criteria were applied to horizontal and vertical elements of the structure. The optimization algorithms used in the analysis were the following ones: Teaching-Learning Based Optimization, Colliding Bodies Optimization, Enhanced Colliding Bodies Optimization, Vibrating Particles System and Harmony Search. MATLAB software has been used for the algorithm implementation, while SAP200 for the modelling, structural analysis and design of the structures. From the optimization of the two-spans roof frame, the performance of all algorithms resulted to be appropriate, while for the three-span roof frame, ECBO algorithm has been demonstrated to be the best one. In both examples, the diagram representing the optimized weight as a function of the roof angle has shown that the best weight can be achieved by employing the minimum angle.

Another comparison between metaheuristic algorithms has been depicted by Kaveh et al. (2020a) for multi-storeys and multi-bays structures. Seven population-based meta-heuristic algorithms have been used to optimize the size of two-dimensional steel frame structures. The optimization was aimed at minimizing the weight of rigid-jointed steel frame structures while satisfying some requirements on stress and displacements, according to AISC and Load Resistance Factor (LRFD). Minimum weight design has been obtained by selecting an appropriate cross-section from a catalogue containing 267 W-shaped sections. The well-known penalty approach has been used to handle the constraints of the optimization problem. Specifically, the parameters considered in the penalty were related to the total amount of the constraint that was violated and two constant parameters that had to be properly set in order to achieve a good balance between the intensification and diversification of the algorithm. Three benchmark frame structures have been analyzed, which

have a number of stories varying from 10 to 24 and 1 or 3 bays. Optimized frames have been examined considering Artificial Bee Colony (ABC), Big-Bang Crunch (BBC), Cyclical Parthenogenesis Algorithm (CPA), Cuckoo Search (CS), Thermal Exchange Optimization (TEO), Teaching-Learning-Based Optimization (TLBO), and Water Evaporation Optimization (WEO) metaheuristics techniques. The results of the optimization showed that WEO, CS, and TEO algorithms performed better in terms of the best weight, average weight, and standard deviation on average weight, according to a close examination of the optimization results. In addition, TEO, TLBO, and WEO have exhibited faster convergence rates than other examined algorithms, as shown by convergence curves.

1.8.2 Cost impact-based optimization problems

At the beginning, several authors believed that by performing a structural optimization aiming to obtain the smallest solution meant to obtain the most economical design. In other words, optimization guided by saving material criteria was confused with the optimal economical cost.
In the first applications, the economic cost is indirectly evaluated as the amount of steel employed for the construction (e.g. Van Mellaert et al. 2016, Kaveh et al. 2013). Other authors as Foley et al. (2003) adopted an Evolutionary Algorithm for the minimum weight building frame components. The cost of the connections was expressed as an increment in steel weight by adopting a suitable amplification factor. Further considerations related to the connections cost of shrunken segments in bridge Warren trusses were pointed out by Cheng et al. (2013). As reported by the same author " the cost rise due to steel strength enhancement of shrunken segments is taken into account in the nominal weight of the whole truss". In some works (e.g. Cucuzza et al. 2021a, Lagaros et al. 2020), economical aspects related to optimal steel retrofitting system were pointed out aiming to demonstrate the optimal solution performed by minimum weight results into cheapest design when compared with the traditional approach as external prestressing.

The weight optimization correlated with cost was used also as a way to take into account the cost in a more wide structural performance optimization. For instance, this kind of resolution was implemented for coupling the material minimization with the improvement of seismic performances. Xu et al. (2006) and Gong et al. (1989) conducted an optimization in which seismic performances were taken into

consideration in terms of uniform ductility demand at the inter-story drift level. As reported by the same authors in their works "Minimizing structural cost (interpreted as structural weight) is taken as one objective".

After that, other components were directly implemented in the cost objective function as connection, fabrication, transportation and erection costs Pavlovvcivc et al. (2004). The new cost function called *total initial cost*, Ali et al. (2009), results to be more representative of the effective price of the entire structure and an increasing level of accuracy in the evaluation of each detailed cost item can be obtained. Further developments in cost optimization were to evaluate the cost along the entire service life of the structure by including the maintenance, demolition and disposal *Life Cycle Cost* (LCC) (e.g. Fragiadakis et al. (2006), Lagaros and Magoula (2013), Lagaros and Karlaftis (2016)). The procedure called *Life Cycle Assessment* (LCA) was used to evaluate not only the cost but also the structure's environmental impact for the entire duration of the construction service (see Sarma et al. 2000).

As demonstrated by several authors, cost optimization should take into account different aspects involved in the realization phase as erection, fabrication, transportation and labour cost. Moreover, while the weight of a steel building is a crucial component of the total cost, cost reduction should be the ultimate goal to guarantee the best use of available resources.
The first approach experienced by researchers consists in multiply the weight or the volume of each member by the unitary cost of material such that an actual cost function expressed in monetary terms can be derived. Undoubtedly, the outcomes obtained by this simplified approach represent a crucial part of the overall cost of construction and they can be adopted in a preliminary estimation phase. However, it is not sufficient when a real estimation is required. Specific production procedures or activities realized on the construction site may represent up to 30% of the total cost (Jamai et al. 1999).
In this sense, a very detailed cost function was developed by Pavlovcic et al. in Pavlovčič et al. (2004) that considers both manufacturing and material costs. The cost function was a sum of the prices due to steel elements, welding, cutting, painting, surface preparation, flange aligning, joints, transportation and erection based on the Slovenian market. The discrete design variables of the problem were related to the geometrical properties of the cross-section (i.e. section shape, the height of the section, length of the flange, the web and flange thickness).
In particular, an approach to consider the welding cost in the objective function

was developed in Jin et al. (2017) where the welding cost was the sum of the factory welding cost (welding that was done in the factory before the installation on site) and the site welding cost (welding that was done directly in construction site). Specifically, each welding cost is computed by multiplying the unit length price of a 6 mm fillet weld by each length member. For allowing a correct design of the welding joint constructability, constraints were added to guarantee the feasibility of the connection.
Another interesting application was provided by Gatheeshgar et al. (2020) in which size optimization was performed for a predefined Modular building system (MSB). The paper performs a comparative study between three types of cross-sections: lipped channel, folded flange and super-sigma. During the optimization process, an optimal sizing for each member typology is performed by choosing the most feasible solution among the available ones.

The main problem associated with using a unit cost for materials, fabrication, assembly and erection is that the various procedures are closely related to local market prices. That issue entails the difficulty to translate these methods into different geographical and economic regions.
To overcome this problem Jamai et al. in (1999) proposed a solution for considering the fabrication cost, with specific regard to the role of welding as a percentage of the material cost. This method computes the fabrication cost as a specific cost ratio of k_f/k_m, in a range between 0 and 2kg/min, where k_f and k_m represent the fabrication and the material cost respectively. In this way, it is possible to adapt the minimization of the cost function as directly dependent on the time needed to accomplish that specific work in different economic conditions. The paper advances some extension of this method for other fabrication costs like flattening plates, surface preparation, cutting and edge grinding.

Even if the considerations of the fabrication and erection cost improved the accuracy of the final cost evaluation, it did not take into account other important factors which were introduced by Sarma et al. (2002b), in which the concept of life cycle cost (LCC) was suitable used for the calculation of the maintenance cost. This optimization was based on four criteria: **a)** selection of the discrete commercially available sections with the lowest cost; **b)** recognition of the standard section with the lightest weight, **c)** search for the minimum number of different types of commercially available sections and **d)** identification of the section with the minimum total perimeter length. Those four criteria guarantee not only a low initial cost but

also a low maintenance cost since, for instance, the least perimeter of the element cross-section assures a low painting cost during the building life.
LCC analysis was also widely used to evaluate the cheapest solution when structures are subjected to seismic actions. Specifically, the seismic damage cost and repair cost has been evaluated in different manners with the expression of the total cost as a single-objective function or through a multi-objective function where conflicting target functions have been simultaneously optimized.
To achieve this goal, the single-objective function is generally formulated as the sum of the initial cost function and new contributions related to the seismic risk. Li, Jiang et al. (2012) developed an objective cost function as the summation of the initial material cost and the future expected damage loss. In this paper, the initial cost was simply computed as the addition of the column and beam cost. Meanwhile, the damage loss was calculated as a function of the inter-story index evaluated by pushover analysis according to Chinese regulation.
On the other hand, Sarcheshmehpou et al. (2021) substituted the future expected loss with an LCC analysis. To achieve this goal three different approaches were performed: code-based design, cost-based design and fixed-weight design. The code-based approach aims at minimizing the construction cost of the building while two other approaches result in a design with the least cost in the lifetime of the building. Finally, the fixed weight approach redistributes the total structural material of the code-based design to attain a new design with less LCC. For the dynamic analysis and the computation life cycle, the Endurance Time (ET) method was performed.
Moreover, for the computation of the LCC, Ghaderi (2021) proposed the use of Wen and Kang's formulation applied to multiple damage states. For each damage state, the exceedance cost is determined as a percentage of the initial cost.
As mentioned above, there are also multi-objective approaches to solving the LCC optimization. Liu et al. (2004), for instance, adopted, as objective functions, the initial construction cost and the degree of complexity of the structure expressed in terms of the number of different standard steel section types and the lifetime seismic damage cost. While the initial cost was simply the weight of the structure multiplied by the unitary cost, the damage cost function, for each damage state, was formulated as the sum between the direct structural and non-structural damage and repairing cost due to loss of contents, relocation cost, direct and indirect economic loss, human injury cost and human fatality cost.
Conversely, Saadat et al. (2016) implemented a multi-objective optimization problem

where the two objective functions were the initial construction cost associated with the weight of the building and the expected annual loss (EAL) considering direct economic losses. Seismic performance and loss estimation of a structure can be organized into four steps: **(1)** probabilistic seismic hazard analysis (PSHA), **(2)** probabilistic seismic demand analysis (structural analysis), **(3)** probabilistic capacity analysis and **(4)** probabilistic loss analysis. PSHA's purpose is to quantify the uncertainties in the location, magnitude, and resultant shaking intensity of a hypothetical future earthquake at a specific site. The second and third phase in a structure's loss assessment procedure is to find the optimal engineering demand parameters (EDPs) and evaluate fragility curves from probabilistic capacity analysis, respectively. Finally, the probabilistic loss analysis aimed to convert the damage estimate in the previous point into direct dollar losses, downtime (or restoration time) and deaths.
Others as Gholizade and Fattahi (2021), Rezazadeh et al. (2018 and Farhat et al. 2009, 2020) focused on performing multi-objective optimization where the structural cost (weight corresponding to each element) and overall damage index (ODI) for the assessment of the structural damage during seismic events were included into dedicated target functions.
These approaches require a huge computational effort due to the complexity of the seismic analysis like a pushover, time-history analysis end direct dynamic integration of ground motion. To achieve time competitive techniques, Kaveh et al. (2012) developed a multi-objective problem where the two objective functions were the initial cost of the structure simply computed as the weight function (linked with the unit initial cost of the building) and the life cycle cost computed with the Wen and Kang's formula as a percentage of the initial cost. The importance of this research lies in the advances implemented into the optimization algorithm that was based on a non-dominated sorting genetic algorithm (NSGA-II) with the aid of a specific meta-model utilized for reducing the number of fitness function evaluations.
When the buildings are subjected to horizontal loads, the traditional approach developed by researchers aimed to estimate the fitness of the objective function by evaluating the violation of seismic constraints according to the various technical regulations. However, several authors demonstrated that hybrid optimization techniques for cost and seismic performance evaluation must be preferred in order to improve the accuracy of the optimal solution and the computational time too.
Following this trail, Tu et al. in (2020) created a multi-objective collaborative optimal design procedure for steel frames equipped with buckling tension bracing (BRB)

to minimize seismic damage and material cost. For this purpose, two objective functions were built in order to create a Pareto front. The first one was simply the material cost, while the second objective function taken the maximum energy dissipation ratio referred to a story among all stories, where the dissipation coefficient was evaluated as the ratio of the hysteretic energy dissipated by the BRB at the level of the retrofitted story and the hysteretic energy dissipated by the entire frame (columns, beams and BRB system) at the level of the same story.
Moreover, in 2020 Barg et al. in (2020), for the evaluation of the inter-story drift limitation and the optimum seismic design, used a multi-objective solution where in addition to a material cost function they added the displacement participation factor (DPF) as a second objective function. The DPF can be derived by the virtual internal work where all stresses and strains are assumed to be constant throughout the length of the element. As a result, without analyzing again the structure, we can compute the influence on any global drift for all scaled scenarios by managing DPF.
Moreover, regarding the performance optimization coupled with an economic design, Xu et al. in (2020) performed a size optimization for a supertall structure subjected to wind load. This study first addresses the optimization formulation of a complex structure system which includes concrete-filled steel tube (CFST) frame members and shear wall members. The adopted cost function was simply the volume of the structural elements multiplied by the unit volume material cost of concrete and steel. The objective function was expressed in terms of the problem design variables dependent on the size of the elements (thickness of the shear wall and external diameter and thickness of the CFST element). The optimization method was tested on the Guangzhou West Tower and results revealed that a significant decrease of 20.56% from 136.8 to 108.7 million yuan was obtained. Meanwhile, wind-induced reactions such as displacement response at the top of the structure, inter-story drift response, and acceleration response drastically decreased.

1.8.3 Enviromental impact-based optimization problems

This Chapter presents an overview of the most potent methods used for environmental optimization.

It is essential to note that in the context of energy optimizations, the prior categories have been interpreted differently. Size optimization typically involves the sizing, and thus the choice of typology, of HVAC systems according to the amount

of energy consumption and the degree of thermal comfort that is desired and needed; this achievement of indoor thermal equilibrium is frequently combined with the need to design openings (*envelope* optimization) of favourable size and with convenient thermal properties to balance heat gains and losses. The latter ones include losses through external walls and the ones resulting from ventilation. On the other hand, heat gains are due to solar radiation through the windows. The difference between losses and gains represents the amount of energy that must be provided by the installed heating system.
Clearly, the issue of window sizing is insufficient to yield an optimum solution. As a result, shape optimization, often in conjunction with size optimization, employs the orientation of the building as a design variable in order to maximize the structure's exposure to sunlight during the day and during the cold and temperate seasons.
Azimuth and *Window-to-Wall Ratio* are the parameters that show the most commonly in literature. The azimuth is defined as the angle formed by true North and a line is drawn from one location to the Sun. This angle changes as the Sun moves across the sky during the day, making it critical to properly orient, for example, solar panels and optimize their performance. The window-to-wall ratio, on the other hand, is a measure of the amount of window area on a building in relation to the total amount of exterior wall area and it can be differentiated for exposure.
Finally, similar considerations made for shape optimization are worthwhile in terms of topology optimization. Topological environmental optimizations have been discussed in the literature as a strategy to attain a certain architectural appeal of the optimal structure (Coley et al. 2002b).

It has been noted that most of the research in the literature focuses on case studies of composite or reinforced concrete structures, with little focus on pure steel ones. In order to find a strategy that is also applicable to the latter, it has been discovered that in optimizations that use CO_2 equivalent emissions (or the Global Warming Potential, GWP) as an environmental indicator, the Objective Function is frequently presented as the sum of the product between construction and emission units. Quite often, instead of emission units, the cost of greenhouse gas emissions is found, which represents the monetary value of environmental damage caused by greenhouse gas emissions linked to the building. Typically, these data are acquired either from discrete national or regional databases or product-specific data sets with the support of professional LCA software. Most of the papers identified in the literature belong to the size optimization category. In particular, numerous studies regard multi-objective

optimizations that minimize costs and environmental indicators simultaneously.
The environmental effects of buildings are measured in terms of CO_2 equivalent emissions and energy use, which, as a matter of fact, correspond to the first groups of papers reported afterwards.
Moreover, among size optimization, LCA-implemented strategies have been highlighted.

CO_2 emissions and embodied energy Over a 50-year period, the structural frame of a building accounts for 20–30% of the total whole lifecycle GHG emissions. In addition to financial benefits, the employment of optimization techniques in the creation of a structural design can lower the consumption of materials whose extraction, fabrication, and transportation cause significant environmental harm.

As cross-section optimization is the most feasible type of optimization, several studies look either at the frame structures or at column/beam elements to evaluate the carbon and cost savings that may be obtained without modifying the floor system and the beam arrangement. Indeed, according to Drewniok et al. (2020), for an assumed 60-year lifespan, mass reductions of 35% in the steel structure can result in up to 5% total-life carbon savings. The authors developed a tool called The Lightest Beam Method (LBM), which selects the lightest beam from a concrete catalogue of Universal Beams (UB) in line with European design regulations. According to each design constraint, the tool minimizes the needed section mass and then indicates which constraint is influencing the member. The reductions from steel floor beam optimization can range between 17% and 35% of the frame's initial embodied carbon. The research of Paya-Zaforteza et al. (2009), instead, outlines an approach for designing reinforced concrete (RC) building frames with a minimum amount of costs and of embedded CO_2 emissions, incorporating two single-objective functions optimized by a Simulated Annealing (SA) algorithm. The emissions of the building frame materials and costs are computed similarly by multiplying unit values and measurements of the materials. The Institute of Construction Technology of Catalonia's 2007 database was utilized to get the unit emissions for the study's concrete, steel, and formwork materials. When cost rather than emissions were the goal, the comparison of the solutions revealed a maximum 3.38% increase in CO_2 emissions. On the other hand, CO_2 solutions might raise the price by a maximum of 2.77%. These results support the hypothesis that both objectives were quite coincident and provide comparable results. Since prices

are more susceptible to changes in market values than emissions, which depend on industrial processes, the CO_2 target function looks to be also more robust and environmentally favourable. In a similar way, other authors (e.g. Kaveh et al. 2017, Arpini et al. 2021, Camp et al. 2013, Park et al. 2014 and Santoro et al. 2020) performed optimizations using discrete national databases for unit emissions and costs applied both to materials and construction units. In particular, Guimarães et al. (2022) formulated a design problem of concrete-filled composite columns with different types of sections. Steel was shown to be the most expensive and least eco-friendly material across all scenarios, accounting for more than 80% of the cost and emissions in columns without reinforcement and more than 70% in all other cases. Furthermore, longitudinally reinforced columns had reinforcing steel as the second most costly material, while concrete had the greatest CO_2 effect. Comparably, Yeo et al. (2015) and De Medeiros et al. (2014) performed a design optimization based on the CO_2 footprint of reinforced concrete (RC) structures and made an economic comparison with basic cost optimization. In the research of Yeo et al., the two single-objective functions were computed as the homogenized volume of the structure, obtained by using cost and CO_2 footprint ratio coefficients, which were simply the ratios of the cost/CO_2 footprint of steel and the one of concrete per cubic meter, multiplied by the cost and CO_2 footprint of concrete per cubic meter. The CO_2 footprint is reduced by 5% to 15% by optimizing the design to achieve the lowest possible carbon emissions. On the other hand, De Medeiros et al. suggested ways to reduce the environmental costs associated with the section of rectangular reinforced concrete columns utilizing the Harmony Search heuristic approach. The following environmental costs associated with reinforced concrete inputs are taken into account: carbon dioxide (CO_2), equivalent carbon dioxide (CO_2e), or global warming potential (GWP), energy consumption, and environmental scoring units, also known as Eco indicator. The optimized monetary solutions were likewise more favourable in terms of the environment, leading to the overall conclusion that the reduction of environmental costs is directly tied to the optimization of monetary costs.

An interesting and peculiar application on modular building systems (MSBs) was developed by Gatheeshgar et al. (2020). This type of system offers the benefits of high productivity, improved structural performance, and quicker construction times, and it is a practical answer for areas with rising housing demand. MBS may minimize the operating energy required in buildings due to its highly insulating

and airtight design, helping to fulfil the rising need for environmentally friendly structures.

In the matter of tall buildings, parametric research on environmental assessment was conducted by Mavrokapnidis et al. (2019) to compare five distinct cost-optimized tall building typologies. The cross-sectional dimensions of structural elements serve as the design variables in the optimization problem. Then, a Life Cycle Assessment (LCA), also referred to "cradle to grave", was conducted on the five cost-optimized outcomes to compare the various environmental profiles across tall structure typologies. The LCA computes the environmental effect from the acquisition of each material to the disposal and recycling. When comparing structural systems made of concrete and steel, it can be relieved that the latter need approximately twice as much energy and produce twice as much CO_2 as concrete-based systems. However, steel constructions are most widely employed due to structural efficiency even if it has been demonstrated, through this study, that concrete works well for tall buildings, up to 60 stories.
The embodied energy content of buildings has drawn the attention of researchers, as well as the embodied carbon emissions, derived from industrial processes of building materials. In the study of Lagaros (2018b) two actual test cases are illustrated, a high-rise building and an athletic stadium. For the high-rise structure, an environmental benefit of 11.2% and 12.7% in terms of energy consumption and Greenhouse gas (GHG CO_2 equivalent) emissions was achieved. The embodied energy is calculated as the sum of the initial embodied energy of design, which is a function of the quantity of building material and its unit energy content, and the recurring embodied energy, which is likewise a function of the structure's and material's life span.
Consequently, the realization of sustainable future designs relies heavily on reducing the embodied energy of building materials. In the work of Whitworth et al. (2020) a Matlab algorithm is presented to optimize a composite beam for tall structures for five different objective functions. The amount of material multiplied by the cradle-to-gate energy content of the material per unity quantity added to the energy utilized on-site for construction will be used to quantify only the initial embodied energy of the structure, which results to be a reduction for each of the OFs.

The attention of various authors has been drawn to bridges, one of the most important civil engineering structures. However, because of the numerous design variables that characterized the structural problem, building a sustainable bridge is challenging.

To cover these difficulties, the study of Penadés-Plà et al. (2019) proposed the use of metamodels, in particular the Kriging one, and of a simulated annealing (SA) algorithm. The structure under examination was a concrete box-girder pedestrian bridge and its design variables were the depth of the cross-section, the bottom slab and web inclination width, the top slab and external cantilever thickness, and the bottom slab and webs slab thickness. This problem involves a single-objective optimization of the embodied energy of the structure, used as a representative criterion of its environmental impact. The embodied energy is computed as the summation of each unit of energy, obtained from the BEDEC ITEC database of the Construction Technology Institute of Catalonia, multiplied by the measured values of each element. Simple and combined solicitations, cracking, compression and tension stresses, and vibration are all structural constraints to check the serviceability and ultimate limit states (SLS and ULS). In terms of the best solution, the comparison demonstrates that Kriging raises the optimal energy by 2.54%.

Several multi-objective optimizations were proposed to demonstrate the strict relation between costs and CO_2 emissions in bridges' case studies. The objective functions were computed similarly for emissions and for costs, as unit emissions/prices multiplied by construction units. The values of CO_2 emissions for materials were taken from the same database of the previous single-objective problem also for Yepes et al. (2015) and Garcìa-Segura et al. (2016). In the case of Martínez-Muñoz (2022), a cradle-to-gate analysis for each unit of the material multiplied by the amount of material used is performed for emissions' computation.
Also costs are acquired from discrete databases, such as the BEDEC ITEC one, or from surveys of precast structure constructors and subcontractors and updated to current values.
Metaheuristic methods, in particular, have done well in handling complex Steel–Concrete Composite Bridges (SCCBs) optimization. For example, in Yepes et al. (2015) a hybrid glow-worm swarm optimization (SAGSO) method is employed to combine the synergy effect of local search with simulated annealing (SA) and global search with glow-worm swarm optimization (GSO); while, in Martínez-Muñoz (2022), a hybrid k-means discrete (KMDA) approach that combines the Sine Cosine Algorithm (SCA), the Cuckoo search algorithm (CS), and the k-means unsupervised learning methodology were adopted.
Structural and safety (ULS and SLS) constraints imposed by advice from experts and standards (CEN Eurocodes) are placed on the bridge design process as well as

the problem's geometry and constructability criteria.
From these three studies, similar results has been obtained. In particular, it turned out that CO_2 emissions and cost are tightly associated. Specifically, a euro decrease in cost translates into a 1.75 kg reduction in CO2 emissions (2015). As long as cost and CO_2 emission criteria result in a decrease in material consumption, the results demonstrate that cost optimization is a solid strategy for achieving an environmentally friendly design.; when emissions are decreased, however, it does not always follow that costs are also optimized. This has to do with the fact that whereas material types vary in price, emissions are the same.

LCA implementation Implementing LCA as a method for planning environmentally acceptable buildings, and retrofitting that use less energy are commonly recognized as the most economical approach to reducing the environmental impact of buildings. They are also seen as a possible opportunity to make a substantial contribution to this cause. As a result, enhancing the energy efficiency of existing structures while limiting extra CO_2 emissions and costs has emerged as a critical issue and challenge in minimizing the life cycle effect of buildings. The case study building examined in Schwartz et al. (2016) is a recently refurbished council housing complex in Sheffield (UK). Two objective functions were minimized: the life cycle carbon footprint (LCCF) and the life cycle cost (LCC). The LCCF (kgCO_2) was computed as the summation of embodied carbon per material and the operational energy-related carbon (OERC), which is obtained by multiplying the predicted energy consumption values by the CO_2 emissions of the fuel. Similarly, LCC was calculated. The findings suggest that the best models have envelope components that reduce OERC or operating costs more than they do. For instance, the best models avoided using brick as an insulating layer and had the fewest windows possible because these materials cost more than the OERC or the money they save.
Similarly, the goal of the study of Mostavi et al. (2017) was to create a multi-objective design optimization model that would reduce life cycle costs and emissions (Global Warming Potential, GWP) while maximizing occupant satisfaction (thermal comfort) in a typical small office building in Pennsylvania (USA). This study revealed that making wise choices early in the design process might help designers produce the best sustainable designs.
In the research of Van Cauteren et al. (2022), instead, the environmental life cycle assessment (E-LCC) and life cycle cost analysis are combined in two case studies of

hybrid (steel/timber) truss structures. The findings demonstrate that any intermediate Pareto optimum design is a hybrid steel/timber structure in each situation. According to this, a hybrid steel/timber structure seems to be the best option for a designer who is focused on a sustainable building but constrained by the available financial means. Other problems' formulations based on a combination of LCA and discrete structural optimization were given by Brütting et al. (2018, 2020a and 2020b). The author suggested looking into truss structures that were planned and built using reused materials that were selected from stocks of pre-existing supplies in order to significantly minimize material consumption and waste created by the construction industry.

Energy consumption Building design must balance two basic yet opposing goals: energy usage and indoor climate. Even for highly experienced engineers, finding a design that fully exploits a situation while fulfilling both of these goals is difficult because of the enormous amount of factors and techniques involved. Global optimization methods, like genetic algorithms, can be used to greatly reduce energy usage while keeping a comfortable indoor environment (2010). Building envelopes make up the barrier separating a structure from the outside world, and their construction really determines the building's future energy needs for heating and cooling, which has a significant impact on how the structure behaves thermally. A multi-objective decision model proposed by Diakaki et al. (2010) enables the examination of a potentially infinite number of alternative measures and evaluates them in accordance with a set of criteria, such as the building's annual primary energy consumption, its annual carbon dioxide emissions, and the initial investment cost. Choices are made about space heating, cooling, and hot water distribution systems based less on their generating efficiency and more on the release of CO_2 emissions. The categories of systems with fewer CO_2 emissions are therefore favoured, and from these categories, the systems with the highest generating efficiencies are chosen.
On the other hand, for retrofitting buildings, the research of Antipova et al. (2014) is based on the combined application of multi-objective optimization and LCA concepts. It considers two objective functions: an environmental one, expressed as the total environmental impact associated with the quantity of natural gas and electricity used for space heating and cooling and water heating; and an economic indicator quantified by the total cost which includes the retrofit and operation (energy) cost. The retrofit measures contribute to a 10.7% decrease in the overall effect of the minimal environmental impact solution. This reduction is made possible by a 4%

reduction in the impact of electricity and a 68% reduction in the impact of natural gas.
A process for applying sustainable design principles to both new construction and building retrofits has been outlined by Brunelli et al. (2016), in which five objectives have been identified: minimization of thermal energy consumption, electric energy consumption, Net Present Value (NPV) of the investment, emissions of CO_2, and maximization of comfort level.

Frequently, researches in literature face the particular problem of optimal sizing of windows in a building to optimize lighting, heating and cooling performances. This issue is typically dependent on climate, as in the single-objective optimization of Caldas and Norford (2002). The structure is investigated under two different locations, Phoenix and Chicago, and the problem was dependent also on the glazing used, the orientation of windows and the type of use of the building. The objective function was expressed as annual energy consumption, which was computed as the sum of the energy spent in heating and cooling and the lighting energy. Suga et al. (2010), instead, proposed multi-objective research for a window format that optimizes the lighting environment, energy consumption, initial cost, and draft (natural ventilation) performance, while maintaining a constant thermal environment.

Few studies have been recorded that compare the ideal envelope design with those specified in standards and regulations, taking into account the three Es: energy, economics, and environment. The study of Al-Saadi and Al-Jabri (2020) uses a life cycle cost (LCC) analysis in conjunction with the EnergyPlus simulation tool to optimize envelope design for houses in hot regions of Oman. This research also recommended solutions derived from regional thermal codes. As expected, design scenarios based on tight code requirements have a lower environmental effect.
A new multi-stage framework, instead, is proposed by Ascione et al. (2017), called CASA. The recommended packages of energy retrofit measures (ERMs) are chosen using a multi-objective genetic algorithm (MOGA), which minimizes primary energy consumption (PEC), thermal discomfort hours (DH) and global cost for energy uses during building lifetime (GC). Clearly, this approach provides significant benefits for both the private, as building lifespan expenses are reduced, and the public, as energy consumption and building environmental effects, may be drastically reduced. For example, a decrease of around 14.3 tCO2-eq/a is achieved. On the other hand, Flager et al. (2009) evaluated the potential of Process Integration Design Optimization (PIDO) technologies to support more successful Multidisciplinary Design Optimiza-

tion (MDO) processes in the Architecture, Engineering, and Construction (AEC) industry. Using MDO techniques integrated into PIDO software, some civil engineering sectors have surmounted comparable constraints, resulting in a shortened design cycle and better product performance.
Another interactive optimization framework built on MATLAB is created by Li et al. (2017) to make it easier to create performance optimization solutions. Using computer simulations and a basic building energy model, a performance comparison of three optimization strategies has been done. Three functions are chosen as the optimization application's objectives of a typical residential building in China: the total percentage of cumulative time with discomfort (TPMVD) over the course of the whole year, the life cycle cost (LCC) corresponding to the total amount of costs during the building's lifespan and, the total carbon dioxide equivalent (CO_2-eq) which is the summation of the CO_2-eq emissions of each material and the electricity CO_2-eq emissions.

In the academic and professional worlds, interest in low-energy and zero-energy buildings is also growing. The EPBD defines two particular categories of Zero-Energy Buildings (ZEB), called "nearly-Zero Energy Buildings" (nZEB) and "Net-Zero Energy Buildings" (NZEB). In a ZEB, the actual yearly supplied energy is less than or equivalent to the on-site renewable exported energy, measured on a source energy basis. These structures are intended to work with less overall greenhouse gas impact on the environment than traditional structures.

It is feasible to see how literary studies differ based on the type of developed method (one article examines both single and multi-objective algorithms) (2015). The collection of works that uses multi-objective optimization, which is frequently favoured over single-objective algorithms, is unquestionably the most prevalent. The intricacy of a building's energy optimization is brought to light by this orientation.

When it comes to multi-objective optimizations, heuristic algorithms are used the most frequently, with the Non-dominated Sorting Genetic Algorithm predominating (NSGA II).

Another insightful analysis focuses on the following variables for the building's optimization:

- the building envelope (including the use of PCMs, the form and direction of the structure, and the walls, roofs, and layers' thermophysical characteristics) (e.g. Gilles et al. 2017, Ascione et al. 2016);
- Fixtures (window and door thermal characteristics, glass emissivity) (e.g. Ascione et al. 2016);
- HVAC and equipment (air conditioning systems, energy storage);
- Renewable Energy Sources (RES) plants (solar collectors, PV, wind turbines, bio-diesel generators) (e.g. Lu et al. 2015).

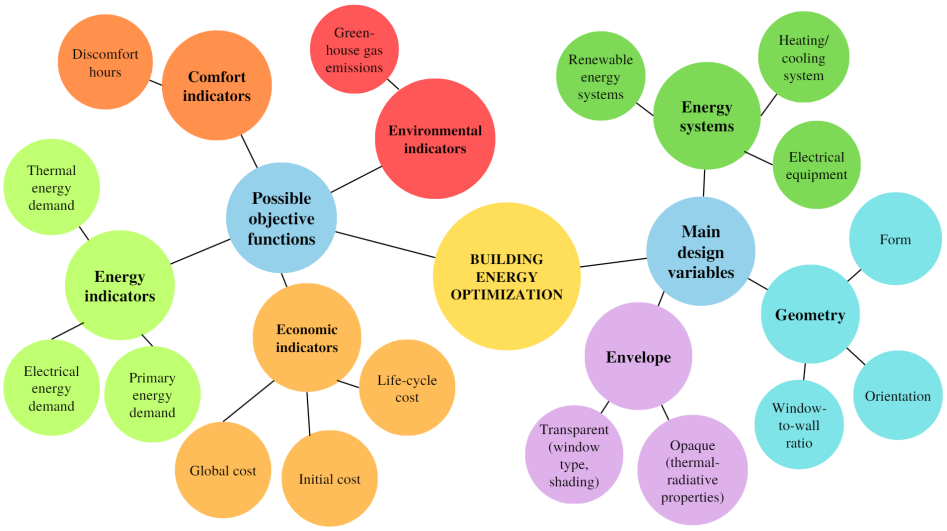

Fig. 1.18 Building energy optimization: possible objective functions and main design variables.

Moreover, regarding the need for a global approach for ZEB, many performance indicators should be taken into account, including cost (Life cycle cost, LCC), thermal comfort, embodied energy, CO_2 emissions, energy usage, the output of renewable energy sources, and durability (as in Gilles et al. 2017, where these main classes of objective functions were simultaneously analyzed).

Therefore, it is likely that the building industry is evolving toward sophisticated, robust optimization techniques that use a variety of criteria, many disciplines, and meta-models established through the appropriate adaptive design of trials. Life cycle approaches emerge logically as a result of the decrease in yearly consumption, which has underlined the importance of taking into account the embodied energy related to

building. When optimizing the design of ZEBs under these circumstances, the life cycle should be taken into consideration.

1.9 Shape optimization

1.9.1 Structural performance-based optimization problems

Shape optimization attempts to integrate geometric modelling, structural analysis and optimization into one complete automated computer-aided design (Hsu 1994b). During the entire shape design optimization process, the design domain keeps on changing through design variables updating and subsequent internal and/or external boundary variations. The design variables that characterize a shape optimization are the nodal coordinates of the structure under study, while constraints on the geometry and structural responses such as stress, displacements and natural frequencies are generally considered. Throughout a shape optimization process, a change in the coordinates of the elements will lead inevitably to a change in the state of stress. Due to that, a Finite Element Analysis and mesh refinement are always required at each iteration of the optimization process. Moreover, it is worth mentioning that in most of the studies, shape optimization is generally coupled with size or topology techniques, seldom implemented alone.

Size and Shape Optimization An early coupled optimization of size and shape techniques has been reported by Haque, M.I. in (1985b). The design of skeletal geometry of plane rigid frames has been tacked as the paper's aim, by using a gradient-based method called the complex method of box. The design variables considered in order to obtain a minimum weight of the optimized skeletal structure are simultaneously the cross-section of the structural members and joint coordinates. A plane symmetrical frame has been considered and weight saving with low computational effort was proved for symmetrical plane frames.
Later on, another study conducted by Gil and Andreu 2001 developed a method for the identification of the optimum shape and cross-sections of a plane steel trussed bridge under stress and geometrical constraints. The novel full stress-gradient-based approach was adopted in order to overcome the difficulties related to the different nature of the design variables (discrete for sizing vs continuum for geometry). In

the last decade, Kazemzadeh et al. 2018 proposed an application of size and shape optimization on steel truss structures subjected to dynamic excitations. By adopting the big bang-big crunch algorithm, the minimum-weight design has been pursued a 22-member cantilever truss, optimized under sinusoidal excitations, as well as for a 44-member truss, designed under rectangular periodic excitations, and a 37-member truss, subjected to step forces with different finite rise time values. The same statement of the optimization problem showed in the previous paper was adopted and the effect in minimum weight obtained for different excitations was discussed.
In the last year, several authors ventured into evaluating optimal designs of very challenging shape structure as curved beams, domes or, simply, 3D frames Kaveh et al. 2020a proposed a design procedure for curved steel roof frames via Enhanced Vibrating Particles System (EVPS) Algorithm. A combination of size and shape optimization was employed to find respectively the minimum weight design and the slope angle of the curved roof frames. In particular, for an assigned slope angle of the roof, the amount of load carried by the frame is evaluated. The results have shown optimal roof slope angle values were obtained in a range between 9 to 22 degrees and buckling or displacement limitations were proved to be the most critical verifications. In this way, a practical recommendation for the optimal design of steel curved roof frames was derived.
Kameshki et al. (2007) adopted genetic strategies for the optimum geometry design of nonlinear braced domes. The optimal value of the height of the crown and cross-section of members were obtained according to instability check serviceability requirements as well as serviceability requirements, combined strength limitations set by BS 5950. Promising outcomes were obtained by Phan et al. (2020). In this research, the optimization of cold-formed steel (CFS) structures has been addressed, giving a deeper look at the design of thin-walled CFS sections which are generally affected by various buckling modes. Cold-formed steel sections are employed in construction because of their great benefits, including a relatively high strength-to-weight ratio, better production flexibility and simplicity in handling, shipping, and installation. Size and geometry optimization was carried out considering discrete cross-section features and layout properties such as the roof pitch, frame spacing and knee brace configuration (i.e. knee depth and knee angle) as design variables. Finally, a cost-saving equal to 20% was recognized. Differently from all the works mentioned above in which steel frames were analyzed, Mam et al. (2020) investigated the influence of semi-rigid dowel-type connections in timber structures. The

authors developed an iterative process for the minimum number of dowels for a given load-bearing capacity according to EC2 verifications. Moreover, the benefit obtained by adopting semi-rigid connections was proved when changes in the shape of the single module frame were performed for minimal tip deflection.

1.9.2 Cost impact-based optimization problems

The goal of shape or geometry optimization is to obtain an ideal shape by defining certain critical points whose motions condition the structure's overall shape with a given size, topology and/or some set boundary conditions. In the case of a truss or generic skeleton frame structures, for example, the key points are the nodes where the members converge. When a node is moved, all the linked elements must change their length and inclination, affecting the overall geometry of the structure. In the literature, no interesting applications of pure shape optimization, fitting with the purpose of the current work, were recognized. Indeed, it is often implemented as an aid to cross-sectional size optimization (which is more efficient for the minimization of the material cost) and topological optimization.

Size and Shape optimization As mentioned above shape optimization is mostly used as an improvement of the already efficient size optimization.
Due to the higher material cost of raw steel materials with respect to reinforced concrete, reducing the former results in the cheapest design. In this sense, two studies were developed by Aydin et al. (2015, 2022) where combined shape and size optimization was performed on prestressed steel trusses in order to reduce the total amount of employed steel. While the first paper referred only to Warren's prestressed truss, the second investigated a more generic problem in which the objective function was a cost function that summed up the price contribution of steel elements and tendons by multiplying the weight with the unitary cost of the steel and prestressed tendons, respectively. Design variables involved in the process are the cross-sections of the truss system's bars and deviators' position, while shape variables are the height of the beam and the eccentricity of the prestressing tendon.
Results shew that prestressing leads to a cutting of the overall cost of steel truss beams by up to 25% when feasibility conditions such as strength, stability, and displacement limits are considered.
Concerning truss optimization, another relevant work was done by Tiainen et al.

(2017), in which different size-shape Warren truss configurations were investigated by varying steel grades and geometrical properties as truss height, the locations of joints, the gap width at the joints (continuous variables) and the member sections (taken from a catalogue of cold-formed square tubes). Minimum weight and minimum cost were obtained separately by using the PSO algorithm. Cost calculations were performed by means of a general feature-based costing method (Haapio 2012). The constraints were derived from the Eurocodes and consisted of strength, buckling, serviceability and geometrical limitations. The results analysis indicate considerable weight savings when high-strength steel (HSS) was considered. With respect to this one, cost reduction was smaller but still around 20 % for the scenario in which structure was the most stressed

One of the most comprehensive and complex size-shape optimizations was advanced by De Santana Gomez et al. (2013). This article covers the difficulties of addressing real-world structural optimization issues while considering the effect of the failure risk. The optimization consists of a risk optimization problem that was implemented by adding the expected cost of failure to the other terms that constitute the total life-cycle expected to cost. The total cost function was formulated in terms of the manufacturing cost, the operation cost, the inspection and maintenance cost, the disposal cost and finally the expected cost of failure. The expected cost of failure was computed as the sum of the expected cost for each failure mode. For each failure mode, the expected cost of failure was given as the product of failure cost by the failure probability.

Shape optimization can be also performed by considering perforated beams with optimal web openings in order to reduce the mass of the members. This strategy was experienced by Kaveh et al. (2021) who adopted the vibrating particle system (VPS) meta-heuristic algorithm for the optimal cost of supported castellated beams (CBs). The evaluation of the fabrication cost in representing a floor system composed of concrete slab and CBs resulted to be dependent on the cutting, welding and, generally, assembly procedures. Moreover, the entire process considered 25 design variables including geometrical properties related to both composite deck-slab system and web openings (angle of inclination of the hexagonal castellation, height of the hole, etc).

1.9.3 Enviromental impact-based optimization problems

It has been observed that shape optimization study tends to focus primarily on the issue of energy usage. Many studies have been hybridized by coupling size and shape optimization in order to best combine the energy, aesthetic, and functional requirements of buildings.

Shape Optimization Because the building shape controls the size and orientation of the external envelope exposed to the outside environment, it may impact building performance in a variety of ways, including energy efficiency, cost, and aesthetics.

As the environmental implications of buildings are recognized, it becomes increasingly important to include environmental performance in building design. Green construction is a new design concept that demands the consideration of resource depletion and waste emissions over its whole life cycle. The building life's phases investigated are natural resource extraction, building material production, on-site construction, operation, and transportation associated with the aforementioned phases. Two studies by Wang et al. (2005a) and (2006) employed exergy as an environmental parameter to overcome common issues in the optimization process. The amount of work that a system can accomplish when brought into thermodynamic equilibrium with its surrounding environment is known as *exergy*. The evaluation of exergy is dependent on both the status of the system under study and the circumstances of the reference environment, and it may be included in Life Cycle Assessment (LCA) to solve natural resource depletion characterization and valuation difficulties. The optimization models were set to minimize both life cycle cost (LCC) and life cycle environmental impact (LCEI). Using LCEI as an indicator for life cycle environmental performance, the optimization issue may be simplified by combining all examined impact categories into a single objective function. In particular, in the study of Wang, Rivard, and Zmeureanu, the study's variables were divided into four categories: shape (orientation, edge length and bearing), structure (building structural system), envelope configuration (wall and roof types and layers) and overhang, which is a passive solar architectural feature put over windows to prevent direct solar radiation through the windows in the summer.
An alternative solution is proposed by Tuhus et al. (2010) to find a minimum optimized solution for four different cost functions (annual electricity use, annual gas use, annual total energy cost and life-cycle cost) to the problem of residential

buildings envelope energy efficiency. Different building shapes were considered, including the rectangle, L-shape, T-shape, H-shape, U-shape, cross and trapezoid. The functions were optimized using the aspect ratio (ratio between width and height), the orientation and two characteristic shape parameters (normalized concerning width or height) for each configuration through a genetic algorithm (GA). It was found that the trapezoid and rectangle were consistently the best shapes. However, the reference square design offers the lowest life-cycle costs across all climates when all building envelope parameters are permitted to vary.

A high-performance, sustainable structure has been defined in modern buildings as one that uses the least amount of energy during each of the four major phases of a building's lifetime: material manufacture, construction, usage and maintenance, and end-of-life. Since many classic optimization approaches have only found limited application, the research of Brown et al. (2016) focuses on multi-objective optimization (MOO), which prioritizes structural efficiency and operational energy efficiency applied on three case studies of structures with long-span roofs (the enclosed arch of the Montreal Olympic stadium, the "PI" cantilever overhang of Suvarnabhumi Airport and the "x-brace" cantilever overhang of Qingdaobei Station). The goal of structural optimization was to reduce the amount of steel necessary; while, energy optimization aimed to reduce the yearly operational energy of the building, which includes needs for lighting, heating, and cooling. Similarly, an intriguing multi-objective optimization was proposed by Quaglia et al. (2014) to minimize both structural performances and energy efficiency of an origami-inspired deployable shelter for military and disaster relief housing use. In particular, the Lever Shelter Module (LSM) was analyzed, which is made up of sandwich panels constituted by two fiber-reinforced polymer (FRP) rigid faces and a foam lightweight core. Two objective functions were formulated: the structural one was a deflection function computed as the maximum between the deflection in any direction of the two modules under self-weight, wind and snow; the energetic one, instead, was the total thermal energy load for the modules obtained as the sum of heating and cooling loads. The design variables were constrained by demanding that the shelter can be packaged on a 463L pallet interfacing with Tricon containers. When compared to the minimal deflection result, the multi-objective optimization demonstrates a 12% reduction in thermal energy load while only marginally increasing deflections. It also demonstrates a considerable reduction in deflections when only increasing the thermal energy load by 12% compared to the minimal thermal energy load result.

A novel technique, called agent-based, was also explored by Yi and Malkawi (2009) to control building shapes by creating hierarchical relationships between geometry points. The agent-based representation begins with the establishment of hierarchical relationships between points (nodes) that represent and regulate the geometry. Three distinct major points are required: the centre point, the agent point, and the child point. The centre point acts as a pivot between agent and child points, while the agent point defines the position of the child ones. Lastly, child points are the points that control a surface, which construct the building form. The objective function minimized the heat flow between indoor and outdoor spaces, including targets, surface heat flow, heat gain, heat loss and volume.

Size and Shape Massive energy savings may be realized throughout the operational stages by implementing passive and active tactics. According to certain research, increased operational energy savings led to exponential increases in embodied energy. Over 45% of the lifespan energy in low-energy buildings might be attributed to embedded energy usage, therefore from a lifecycle viewpoint, the embodied energy could outweigh the operating energy savings. It is consequently essential to reduce operational energy consumption while maintaining embodied energy performance. The optimal design of several building envelopes with local materials typical of climatic conditions in Africa's Sub-Saharan area was investigated in the study of Ansah et al. (2021). In the first step, the building geometry and renewable energy are optimized and used as the foundation to design the building model for assessing the trade-off between embodied and operational energy with different façades in the second stage. Similarly, depending on climate, Echenagucia et al. (2015) proposed an integrated strategy for the first phases of building design. The energy required to heat, cool, and light a case study was minimized by varying the number, position, shape and type of windows and the thickness of the masonry walls. The results of the search process can give designers important information that will help them make better-informed decisions. For instance, designers can choose the objective function they want based on the environment and the HVAC system they have chosen.
Several papers discuss multi-objective optimizations exploited in three sectors: the optimization of the building envelope to reduce Heating, ventilation and air conditioning (HVAC) usage as well as construction costs, the optimization of building form (windows sizing and positioning), and the optimization of HVAC system design

and operation (e.g. Caldas and Norford (2003), Negendhal and Nielsen 2015, Wang et al. 2005b and Raphael 2011). In particular, the study of Marks 1997b aimed to optimize the dimensions of a structure with known volume and height in order to minimize building and annual heating costs. The problem is formulated in two ways, by making as first an optimization of a building of an arbitrary shape and secondly of a building on polygonal plans, both solved numerically by a computer system, called CAMOS. As a consequence of optimizing the design of the structure, construction and heating costs over the N-year period can be reduced by several to several dozen per cent. Likewise, due to the enormous number of interactions between the elements that contribute to the overall behaviour of a structural solution, also the research of Caldas et al. (2003) benefits from the use of computer simulations (DOE-2.1E) for the case study of the Alvaro Siza's School of Architecture. The use of this new generative system (GS) that combines a search technique (GA) and DOE-2.1E showed that it may be used to change building geometry to make it better suited to its environment. Although the GS made several adjustments to each façade of the building, which may have resulted in a better-balanced use of daylighting, the building's overall artificial lighting usage did not decrease significantly. However, a significant gain in terms of heating and natural lighting is recognized due to the crucial role played by the overhangs: decreasing its depth results in greater beneficial south sun absorption in the winter and reduces heat loss sources simultaneously. An innovative comprehensive framework for building energy design, called Harlequin, has been suggested by Ascione et al. (2019). Because each façade can have a variable composition and thermal-radiative qualities depending on the exposure, the obtained solutions are called "Harlequin buildings". As a result, the proposed architectural solutions are referred to as "Harlequin" buildings because of how irregular their colour and composition are, which is evocative of the well-known figure "Harlequin". The three objective functions to be minimized are: the annual percentage of discomfort hours over occupied hours (DH), the annual electrical energy demand for artificial lighting (EEDL), and the annual thermal energy demand for space conditioning (TEDSC). Depending on the chosen solution, considerable decreases in primary energy consumption (PEC), global cost (GC), and CO2-eq emissions can be made in comparison to a reference design. The maximum reductions are 12.3 kg/m^2 for CO_2-eq, 43.9 $kWhp/m^2$ for PEC, and 63.9 $/m^2$ for GC.

1.10 Topology optimization

Topology optimization not only seeks the optimal spatial arrangement of structural elements within a given domain that affects structural layout, but it also examines how the available material might be structured to achieve the greatest structural performance. For instance, the purpose of topology optimization for a fixed span is to specify the type of truss to utilize for the specified loads and boundary conditions. Another way to perform topology optimization in continuous design space is to remove the less stressed material while adding material in the more strained locations. Actually, topology optimization is not simply the change in the arrangement of the elements but also every modification that varies the internal load path in the structure. Therefore, the change in the connection typology (pinned or fixed joint) and stiffness (semi-rigid connection) should be considered as a specific case of topology optimization since variations of the stress distribution occur in the structures. As demonstrated by the research reported in the future section, topology optimization results in a refined optimal strategy in which novel efficient load paths can be recognized. Subsequently, though size optimization brings a simple reduction of the overall weight, changing the topology of the structures permits to the achievement of innovative arrangements with a higher cost-saving impact. For these reasons, once a preliminary weight cutting is performed by using size optimization, topology can be adopted as a second-level strategy to achieve a more refined solution. This aspect is demonstrated by the fact that any pure topology optimization has been recognized in the literature. Most frequently, authors preferred a hybrid optimization by coupling size and topology or size, shape and topology.

1.10.1 Structural performance-based optimization problems

Topology Topology optimization is generally employed in the conceptual design phase of a high-rise building, in which the main focus is related to the overall stiffness/drift requirements under lateral loads. Therefore, many of the decisions made during this process are related to defining the lateral system that allow to reach an optimal structural design to satisfy certain conditions. The balance between engineering and architecture is another issue that frequently affects the topology optimization industry today. Traditionally, an architect's focus is more on the aesthetics, or "form," of a structure, whereas an engineer's target concerns stability and

efficiency, or "function", of the structure Beghini et al. (2014). To overcome those conflicting goals, for example, we can think to add some architectural constraints during the optimization process.
Mark et al. in (2000b) presented the Genetic Algorithm(GA) for structural topology optimization, through the use of examples and reviews. By applying this algorithm, the design domain has been discretized into small rectangular elements, as said before, representative of the presence of material or void by means of a specific code number (respectively number 1 and 0). In this way, the topology has been defined, so the next step was its structural verification through a finite element analysis. Then the fitness of each chromosome, thus of each topology, was computed as a function of the stiffness value, determined as the inverse of the displacement. In fact, the Objective Function was aimed at the minimization of the structure's compliance, by finding the optimal configuration of material and voids within the design, while stress and displacement constraints were applied. An example related to a cantilever plate subjected to vertical load has been provided and discussed.
A classical approach to topology optimization was provided also by Pan et al. (2006) in which truss structures with 12, 20 and 72 bars were analyzed using Adaptative Genetic Algorithm(AGA). The objective function of the optimization problem was a minimization of the truss structural weight when subjected to frequency domain excitations. Minimum weight was achieved by removing extra bars and nodes, classified as removable and non-removable. The analyzed truss structure was subjected to three kinds of constraints: fundamental frequency, displacement responses and acceleration responses in the frequency domain. The maximum amplitude of displacements and frequency acceleration response had to be lower with respect to an upper bound limit. Those types of constraints have been evaluated from the structural vibration equation, based on the finite element method, in which the mass, damping and stiffness matrix of the structure needed to be known. Moreover, to obtain accurate natural frequencies and dynamic responses, it was necessary to renumber every bar and node in the structure and rebuilt the stiffness and mass matrices when some bars or nodes were removed.

Another important topic addressed in topology optimization techniques deals with the design of conventional moment-resisting steel frames. This type of structure as is well-known, exhibits good behavior under gravity-induced forces. However, the structure is likely to be ineffective in self-resisting lateral forces promoted by wind and/or earthquake actions. The use of a hybrid system that integrates cross

braces to the moment-resisting frames is widely accepted for its cost-efficient and safe performance. Due to that, founding optimal bracing positions and their sizing is one of the most treated issues in this field. Cross bracings designs, especially when the braces are added afterwards as part of a retrofitting scheme, traditionally use a simple trial-and-error procedure, with the overall goal of minimizing the distance between the floor's mass and stiffness centres and ensuring that the lateral resisting system has a workable load path. A more systematic approach is to set up and solve an optimization problem that automatically computes optimal brace layouts and sizes while satisfying the safety of the targeted structural performance.

In the research Safari and Maheri (2006) proposed a straightforward Genetic Algorithm was used to perform topology optimization of steel braces in 2D steel frames. In this paper, the optimal position of X-braces was explored, with the objective to reduce the weight of steel used in the 2D frame-brace system. The constraints related to the problem included: total drift of the frame, column uplift force, number of braced panel and architectural limitations. Focusing on the latter, it involved limits on the allowable bracing, restricted to some bays only. For example, in the case of the three-bays structure, bracing was first allowed in the two right hand bays and then only in the outer bays. Different examples related to 2D frames, having different numbers of storeys and bays, have shown the efficiency of the proposed algorithm. In fact, over 5% reduction in weight and 8% reduction in drift was achieved by GA topology optimization when compared with conventional frames, in which brace location was admissible horizontally along the same bay or in vertically along the same storey.

Always in the topology optimization environment, since in recent years, seismic rehabilitation for existing buildings has been an increasingly important issue, studies on brace systems have been emphasized due to their applicability and effectiveness as reinforcing structure techniques.

An interesting research, targeting seismic assessment of steel frames using braces, was provided by Qiao et al. (2016). This study has been focused on the seismic analysis of steel frame structures with brace configuration, using topology optimization based on truss-like material model. Zhou and Li (2006) have introduced such a method for continuum topology optimizations, which has been further investigated by Zhou and Chen (2014), by considering natural frequency constraints. In the present paper, the truss-like model has been applied by considering stress constraints and both earthquake and wind loads. Initial truss-like members were used to fill the

design domain for topology optimization, based on the original steel frame structure. The final layout of the least-weight structure was obtained by applying a fully-stress criterion and by considering as design variables, in the finite element analysis, both the density and orientation of the truss-like members. The optimized structure obtained by Zhou and Chang in 2014, referred to as a 10-storey 2D frame, has been repeated in order to see how the brace configuration could be improved in order not to have braces in the middle of columns but instead in the middle of beams. Thus, the new arrangement was created with diagonal braces or inverted "V" braces. The engineering requirements of the building function have been considered, further enhancing the optimal brace configuration. To reinforce the advantage of the proposed optimized structure, a comparison with two common optimized brace configurations under different earthquakes intensity was done. Common brace configurations were characterized by a “V” brace and a single bar brace that were placed vertically along the same bays.Results have shown that the first period of the optimized structure was reduced by 51.4% with respect the original frame without brace, while around 45% was the reduction of common brace configuration with respect the original one. Regarding the drift, an average reduction of 56.69 among the 10 storeys was obtained, in comparison of 50% average reduction of common braces.
An alternative lateral resisting solution to the common brace system is the Steel plate shear walls (SPSW) described in Bagherinejad and Haghollahi (2018). In recent decades, the efficacy of steel plate shear walls (SPSW) as lateral resistance solutions have been proved, even in comparison with brace systems or RC shear walls. In fact, they are characterized by large energy dissipation capability, and a stable hysteric behaviour along with considerably light and thin configurations, which ensure rapidity in the erection and suitability for seismic retrofitting. In this paper, topology optimization has been exploited to find a new configuration for the perforated steel plate shear wall (PSPSW) based on the maximization of reaction forces as the objective function. Finally, another application of topology optimization can be related to the optimal location of the connections inside the structure. This topic was treated by Baghdadi et al. (2021). The connection placement strategy, also known as the connections-placements approach(CAP), was the topic addressed by the article, which focuses on improving the position of connections in prefabricated buildings. Elements forces and connections properties were evaluated in order to define the optimum type and location of the connections.

Size and Topology In this section, all the studies that combined size and topology techniques for structural optimizations have been collected.
A first example was reported by Saka, in (1991b). The author presented an algorithm for the optimum design of steel frames, studied with both fixed or pinned supports, as well as with and without bracing systems. At first, a simple size optimization has been accounted for in the investigation of flexible support behaviours. Then, considering a specific condition, bracing configurations have been analysed in order to find the optimal arrangement. The objective function to be minimized was the weight of the structure, while at first the cross-sectional areas of members have been treated as design variables. In the process, the optimum value of the design parameter was chosen as the one related to the most severe between displacements constraints, combined stress constraints and minimum size constraints. The examples reported for simple portal frames, subjected to a distributed vertical load and a horizontal force, have shown that, with specific regard to pin supports in the static scheme, displacement limitations were dominant, while fixed-supported frames were governed by the combined stress constraints. Moreover, in the second case, the final design was lighter. Then, when the effect of bracing has been investigated in pin-ended portal frames, the resulting weight was further reduced. Also, pitched roof frame examples have been reported, where the structure subjected to distributed vertical loads has been studied with different support conditions, fixed and pinned ones, with and without bracing and, lastly, with the application of a horizontal force too. In the simple vertical load configuration, fixed supports showed lighter weights, but the best design was found with pinned supports and a bracing bar between the eaves. The same conclusions cannot be made with the second load configuration, where the best design was obtained with fixed supports and without bracing. In any case, the dominant constraint was the one regarding the combined stresses. Finally, also multi-storey and multi-bays frames have been analysed, which led to the conclusion that rigidly jointed frames yielded lighter designs if they were only subjected to vertical loads. However, in the presence of lateral loads too, frames with simple beam-column connections and bracing produced better designs.
Optimization under seismic loadings, addressing the topic of uniform distribution of certain structural properties, an application of such study has been conducted for simultaneous size and topology procedures by Hajirasouliha et al. (2011). They proposed an efficient method to design nonlinear truss-like structures, subjected to seismic load, in which the objective was to obtain a minimum weight truss by

shifting material from strong parts to weak parts until a uniform distribution of deformation demands was reached. In fact, during strong earthquakes, some structural elements' deformation requirements do not fully utilize the allowable level of seismic capacity; therefore, if the strength of these underused elements was reduced, a status of uniform deformation could be reached, maximizing the dissipation of seismic energy and fully utilizing the material capacity. Assuming that the cost of a member is proportional to its material weight, the least-cost design was interpreted as the least-weight design of the structure. Moreover, indirect considerations about the joints cost have been accounted by the fact that as the algorithm decreased the number of elements, the number of joints was minimized too, thus their overall expense. The minimum cost was achieved by considering as design variables the cross-section areas, specifically their material density and length, while constraints on element buckling and target ductility of each structural member had to be satisfied. The algorithm started from a ground structure with all possible connection members between nodes. Then nodes that were carrying external loads or that was needed to support the truss structure have been maintained in the design, while the ones used just for load sharing have been excluded. In the next step, based on the design load applied, the maximum ductility of each structural member has been computed and iterations proceeded until the maximum ductility demand of all truss elements reached the target ductility. Basically, if the calculated ductility demands were close enough to the target value, the optimization stopped, otherwise inefficient material was reduced. The assumption that the uniform deformation demand led to the full exploitation of material capacity has been previously demonstrated by other studies, such as Hajirasouliha I, Moghaddam H. Hajirasouliha and Moghaddam (2009) and Moghaddam H, Hajirasouliha I. Moghaddam and Hajirasouliha (2006). Based on the results of the presented study, the concept of uniform deformation can be used efficiently for topology optimization of nonlinear truss structures subjected to gravity loads and seismic excitations. It has been demonstrated that there is a unique optimum distribution of structural properties, which is independent of the initial cross-sectional area of the ground structure. Moreover, this method was dependent on the variation of target ductility demand, meaning that a fixed arrangement of truss members cannot be appropriate for different performance levels.

Additionally, it has shown that using conventional optimization methods based on elastic behaviour and equivalent static loads could lead to heavier design, up to an increase of 60% compared to the non-linear dynamic model. It was concluded

that the non-linear dynamic behaviour of truss structures should be considered in the optimum topology design of trusses subjected to seismic excitations. One year later, an application of size and topology optimization has been conducted to model braced frames in the lateral design of high-rise buildings, developed by Lauren L. Stromberg, Alessandro Beghini, William F. Baker, Glaucio H. Paulino in Stromberg et al. (2012b). Braced frames have been used in several noteworthy buildings like the John Hancock Center (Chicago, IL), Broadgate Tower (London, UK) and Bank of China Tower (Hong Kong), a picture of the building is reported in Figure.
The design of such systems is traditionally based on diagonal braces arranged at 45° to 60° angle. In this research, size and topology optimization have been combined to derive the optimal bracing layout of 2D high-rise frames. The energy method in conjunction with the principle of virtual work has been employed in size optimization. During the process, the cross-sectional area of the elements has been changed until the optimal configuration of beams and columns was found, while only gravitational loads were applied. Constraints on maximum allowable material that can be used and maximum stress in structural elements had to be properly checked among the iterations. The structural system was modelled using beam elements and quadrilateral elements(Q4); Q4 represent the region enclosed by two columns and two beams. Beam elements, used for beam and columns, consist of six degrees of freedom (two translation and rotational at each node). While four-node bilinear quadrilateral elements have eight degrees of freedom (two translations per node). To effectively connect the finite elements, the interaction between the rotational and translational degrees of freedom must be considered. Two types of design were explained, where in the first one, the beam consisted of simply connecting the beam ends to the extreme corners of the quadrilateral mesh. Thus, the end rotation of the beam had no influence on the quadrilateral finite elements because the rotational degree of freedom was decoupled and all the interior nodes along the length of the beam were free to move independently of the quadrilateral node translations. In the second design case, beams were discretized into beam elements with nodes coincident with the nodes of the quadrilateral mesh. Consequently, the translational degrees of freedom of both beam and quadrilateral elements were shared throughout the beam's length. Thus, the quadrilateral elements have been constrained to move jointly with the beam elements when the frame deformed.
An interesting observation that can be derived from the design example is that minimum compliance led to constant stresses, which was the condition of optimality.

Retrofitting and rehabilitation of the existing building are employed following a topology optimization approach in order to find optimal brace locations. Moreover in some studies also the cross-section of the braces is considered as a design variable, alongside brace positions, in order to reduce the amount of volume.
In the paper Tangaramvong and Tin-Loi (2015) Tangaramvong and F. Tin-Loi in 2015, presented a mathematical programming–based approach for optimal retrofitting of steel structures with braces, subjected to some system performance criteria. The aim was to ensure the safety of the post-retrofitted structures under applied forces and limited displacement conditions. In the present study, three distinct optimization cases have been addressed, in which the inclusion of non-linear elastoplastic constitutive behaviour of materials, considered a traditional complementary constraint, made the optimization problem nonconvex and non-smooth. For all three cases, the objective function was the minimum volume design of braces, while for the last analysis, also the minimization of the number of braces has been accounted. Displacement constraints were applied in all the analyses, whose value has been restricted within a limiting range. The authors started the optimization problem by considering a simple ground structure concept, in which all possible braces were first generated between direct neighbouring predefined nodes within a rehabilitation domain. Once the simple ground structure was known, brace members during the optimization procedure were then retained (non-zero brace areas) or eliminated (zero braces area). For all design cases, the structural performance of the repaired structures has been ensured and validated through comparisons with the corresponding exact elastoplastic responses. Specifically, the outcomes of the study have shown that the first practical example provided the least volume, which however resulted to be unpractical because a large number of sections were excessively small. Improvements in the design were obtained for the intermediate analysis, at the cost of larger computational time. Finally, the authors have considered the case with a limitation on the number of braces with the most realistic cost-effective design strategy because it has incorporated not only the material-related costs but also brace fabrication and erection expenses.
Finally, another contribution to retrofitting of existing frame structure was carried out by Apostolakis et al. (2020). The goal of this paper is to present an evolutionary computational framework that integrates hierarchical multiscale mega-bracing architecture for the seismic design of both regular and irregular three-dimensional multistory structures. Particularly, two steel three-dimensional buildings with moment-resisting

frames an 8-story irregular and a 14-story regular one are taken into consideration and retrofitted with friction dampers. Friction dampers are added to the structure to improve its seismic performance; in reality, by adding more damping, it absorbs some of the seismic energy that is induced in the building. The evaluation criteria used in this paper are based on story drifts and absolute accelerations on each floor. It is possible to build an objective function using relative or predetermined performance target levels. In the former, the objective function can be expressed in terms of the ratio of the story drift and absolute acceleration between the un-retrofitted structure and the structure retrofitted with damping devices. In the latter, the objective function can be expressed in terms of the ratio of the previous criteria between the retrofitted structures and prescribed performance target levels. By selecting the latter approach, the objective function of the structure is expressed as the ratio between the maximum and allowable floor displacement plus the same ratio but in terms of floor accelerations. Moreover, in the expression of the OF also a penalty is added, which takes into account the number of X-braces used. The value of the OF is then found for different earthquakes and the overall objective function value assigned to the structure is the minimum obtained. Design variables of the evolutionary framework are the parameters that characterize the friction dampers: multiscale configuration, or rather "V, inverted "V", "X" and diagonal braces, section area and slip force. For the design applications presented in this paper, the 25 ground motions with a 5% probability of exceedance in 50 years were used as the seismic environment. Three design scenarios were considered for practical applications, the difference was the brace configuration that was allowed to be used, varying from all possible choices to a limitation on X-brace configuration.

The ideal design for the 8-story irregular building has the maximum inter-story lateral stiffness and slip force values at the bottom levels and gradually decreasing values as you climb the stories. For the 14-story structure, the best designs for all scenarios, however, preferred a layered architecture with vacant stories first, followed by stories with fitted dampening devices.

Phan et al. (2012) explored the performance of combined size and topology optimization for a slightly different type of application. The case study presented is related to low-rise commercial, light industrial, and agricultural buildings made of cold-formed steel portal frames. This type of construction has been proven to be a competitive alternative to traditional hot-rolled steel portal frames for structures with moderate spans, up to 20 m. Cold-formed sections are lighter than hot-rolled ones,

making it possible for semi-skilled workers to bolt and erect the structural members on site without the use of a crane. As a result, the erection costs were significantly lowered if compared to those of hot-rolled steel portal frames, highlighting the importance of this research. Therefore, the authors proposed a combination of size and topology optimizations applied to cold-formed steel portal frame buildings through the use of areal-coded Genetic Algorithm (RC-GA). In place of earlier GAs, which were known for their slow convergence and lengthy computation times, RC-GA has been employed. A niching technique, that effectively increases the dissimilarity of the solutions in each generation, has been described in an effort to enhance the performance of the traditional GA. The objective of the overall design optimization, including the building topology and section sizes of members, was to determine the portal frame building having the minimum cost, whilst satisfying the design requirements. The design variables were related to some geometric characteristics of the frame, like the span length, height of eaves and the inclination of the pitch, as well as the member's cross-sections, which were chosen from a list containing 40 channel sections. It's important to highlight that the decision variables were both discrete and continuous. A case of a frame with a span of 20 meters and a column height of 4 meters has been analyzed in order to demonstrate the efficiency of the proposed method. The algorithm's computational effectiveness and robustness have also been proven and the computational time has been cut in half compared to standard GA.

Another study related to the validation of the application of a metaheuristic algorithm for size and topology optimization has been carried out by A.Kaveh, Mahdavi V.R. in Kaveh and Mahdavi (2015). In this paper, steel truss structures have been optimized using a meta-heuristic algorithm called Colliding Bodies Optimization (CBO). In the layout (simultaneous size and topology) optimization problem, two objectives have been taken into account: the best topology or shape for a ground structure and the best cross-sections of that topology. Therefore, the problem began with the ground structure, which was made up of all potential nodes and members. Then, the cross-sectional areas and node layout have been determined to gain the minimum cost. In particular, the cost of the entire structure has been calculated as the sum of the members expense, related to their masses, and of the nodes, evaluated by means of a constant mass value if the node was present. Design variables taken into account to obtain the outcomes included the cross-sectional areas (regarded as a continuous variable) and both the node and member positions. The constraints applied were

related to the upper and lower bound of stresses, buckling, displacements and natural frequencies requirements of the structure. The finite element model had to be revised and adjusted when members and nodes were eliminated, which was an important part of topology optimization that needs to be highlighted. This change resulted in a significant amount of useless computing work. Wang and Sun (Wang and Sun 1995) developed a technique in which the members suggested to be removed by the optimization, thus elements with zero cross-sectional value had to be associated instead with a very small value. The employment of such a technique was able to overcome the problem of having elements with the null area, which require the re-computation of the stiffness matrix. In this way, the computing effort has been reduced while maintaining the finite element model's integrity. Moreover, when a tiny cross-sectional area was chosen, the corresponding stress and local stability constraints were ignored. To compare the effectiveness of the CBO algorithm with other techniques, four numerical examples of various truss designs with increasing numbers of nodes and elements have been taken into consideration. In all the examples tested the cost of the optimized structure was minimum when using the proposed methodology. Moreover, while the majority of meta-heuristic algorithms had some parameters that needed to be carefully adjusted for various types of problems, CBO, being independent of settings, was easy to be implemented.

In another research, conducted by Kaveh, Ali Neda and Farhoudi Kaveh and Farhoudi (2015), topology and size optimizations have been exploited to find an economical solution for concentrically structural steel frames. Differential Evolution Algorithm (DE) and Dolphin Echolocation Optimization (DEO) have been applied for structural optimization, to find the best results in terms of minimum weight. Both placements of the bracings and size members have been considered as design variables, while the considered constrain were related to drift, deflection, compaction and strength of the structure.In particular, the structure taken into account was a steel braced frame with a dual building system, in which an essentially complete frame provided support for gravity loads, while resistance to lateral loads was provided by a specially detailedmoment-resisting frameand shear walls or braced frames. Three examples of 3 types of frames with different storey heights,have been illustrated to demonstrate that both DE and DEO have good performance in discrete structural topology optimization. Also, DEO leads to better results with less standard deviation in comparison to Genetic Algorithm (GA) and other metaheuristic algorithms.

The same authors in Kaveh and Farhoudi (2016), introduced another metaheuristic

algorithm, called Dolphin Monitoring (DM) for layout optimization of structures. Actually, the dolphin monitoring ability to control the convergence of the Dolphin Echolocation Optimization (DEO) algorithm has been demonstrated and it has also been applied to other metaheuristic algorithms, such as GA, PSO, BB-BC, CBO and their modified variants. More in detail, DM do not change the nature of the algorithms, but it is used only to set the convergence in a predefined number of loops. Specifically in this paper, the OF was the minimum weight of dual systems, characterized by the best placement of bracings and the best cross sections of the elements of both the moment frames and the X-bracings. The placement of bracings and the size of members have been considered simultaneously as optimization variables. The members had to satisfy constraints on the design storey drift, deflection, compaction (limiting width over thickness for compression members), strength, stability coefficients and slenderness ratio limits. The structures taken into account were subjected to both dead loads, as well as live loads and earthquake excitations. To evaluate the effectiveness of the suggested strategy, three numerical examples with 3-, 5-, and 10-story braced frames have been provided. The findings of applying DM to numerical examples of GA, ACO, PSO, BB-BC, and CBO demonstrated that DM enhances the minimum, maximum, mean, and standard deviation of the results of all these algorithms. Comparing the results of all the aforementioned algorithms to their modified versions, DM also produced better results in terms of minimum weight.

In the same year also Gholizadeh, S., Poorhoseini, H., performed a layout optimization, illustrated in Gholizadeh and Poorhoseini (2016b). Their interest was focused on the process of developing new structures or upgrading existing ones to fulfil specified performance objectives for likely future earthquakes, by applying the seismic performance-based design. Thus, the present paper exploited such a method on steel-braced frames subjected to earthquake loading. In the SPBD methodology, a nonlinear analysis tool was typically used to determine the seismic demands of structures at predetermined performance levels. According to FEMA-273 (1997), IO, LS, and CP performance levels have been considered in this study. The design variable of the optimization problem included the cross sections of all the structural members: beams, columns and X-bracing, as well as the optimal position of the latter ones. SPBLO process has been applied to five-bay steel braced frames with different numbers of storeys, with the aim of minimizing structural weight. To ensure that all potential solutions were workable, various design restrictions were examined, among

which serviceability and ultimate limit state constraints were considered. In detail, geometric and strength assessments were included in the serviceability restrictions. Geometric checks had to be completed in beam-column and column-column framing joints to meet practical requirements. Moreover, a hierarchy of the constraint has been considered, in fact, if the serviceability restrictions were not met the design was discarded. Otherwise, a nonlinear pushover analysis was carried out to assess the seismic response of the structure at the desired performance levels. Then, the design criteria and capacity demand levels have been presented in terms of displacements. The constraints of the optimization problem are handled by the exterior penalty function method (EPFM). An enhanced dolphin echolocation meta-heuristic method was suggested to carry out the optimization task. Additionally, as previously mentioned, nonlinear pushover analysis was carried out to analyze the structural responses at the performance levels, which can greatly increase the computing complexity of the layout optimization problem. The adoption of an effective optimization technique is required in order to search the vast design space of the SPBLO problem due to this important issue. An enhanced version of the Dolphin Echolocation (DE) Meta-heuristic was suggested in the current study to address this problem. By merging Chaos Theory (CT) and conventional DE, a novel meta-heuristic algorithm dubbed Improved Dolphin echolocation (IDE) is developed. Three examples including 6, 9 and 12 story SBFs were solved in the framework of SPBLO formulation. The numerical results of the SPBLO example revealed that in the framework of SPBSO the optimal solutions attained by IDE were respectively 3.61, 3.20, and 3.32% lighter than those obtained by DE.

So the results state that the computational performance of IDE was better than that of the DE in terms of optimal structural weight and convergence rate.

Going back to concentrically structural steel frames, an important aspect is related to the fact that braced steel structure's integrity may be compromised by the occurrence of some extremely serious events. This risk had driven researchers to create novel techniques for evaluating structural collapse, among which Jeriniaina Tantely and He in Tantely and He (2019) investigated such a topic. The introduction of incremental dynamic analysis (IDA), which allows for the creation of a collapse probability curve for the examined structure, was suggested as a technique to understand seismic events. Although the experts agree that the IDA is effective and reliable, they also believe that it is a long process. By using a few series of time history analyses(THA) to approximate the fragility curve, they were able to overcome these limits. It sig-

nificantly reduced the calculation time for the collapse assessment and provided a reliable approximation of the fragility curve. The use of the fragility curve was extended by proposing a collapse margin ratio (CMR), which become the primary parameter associated with the evaluation of structural safety. The scope of this work was to propose a design optimization of steel structures, using concentric braces, based on collapse safety assessment. Brace locations and sections were the variables of this investigation, while the objective was the maximization of the CMR of the structure. The higher the CMR value, the safer the structure. Constraints were the candidates' non-null vectors, meaning that each level of steel frame structure must have at least one brace. The idea of the designable matrix was presented in relation to the best placement for bracing in the structure and derived from the reality that, in actual projects, engineers are not always free to choose where to put the braces because of architectural constraints or owner preferences. So undesignable bay refers to the bay where bracing cannot be installed. An initial matrix describing the building's elevation was created in order to quickly count the number of designable and undesignable bays in a given structure. Sizing brace optimization of seismic steel frame structure aimed to reduce the total steel weight of the braces, which acted as a rough indicator of bracing construction cost. During the procedure, the optimal shape brace section at each story has been evaluated and then the optimal discrete brace section related to that story was identified. The authors advised utilizing a single section of brace for each story since employing several sections might imply the occurrence of weak braces, which would result in unequal lateral force dissipation at that story. Another reason was that premature damage of the structure's frame could be caused by the achievement of the strength limit by the weak brace before the other ones. The algorithm used a database of steel brace sections, selected from commercially available hot-rolled, wide-flange standard steel sections.The authors investigated four steel frame structures, in which the main difference was both the presence of undesignable bays on different sides of the structure and the number of storeys. From the interpretation of the results, the proposed methodology has been proved to be capable of a quick and practical estimation of the collapse margin of several structures in a short time, compared to the prior methods in this field.
Also the study of Hassanzadeh and Gholizadeh, illustrated in (2019) focused on the collapse-performance-aided optimization of steel concentrically braced frame (SCBF) structures. The interest of the authors had its roots in the evidence that the placement of braces directly affects the seismic performance of SCBF structures,

therefore finding an appropriate configuration had become increasingly important. In this analysis, both size and topology optimization have been performed in the framework of the performance-based design (PBD) methodology, using the collapse-margin-ratio (CMR) algorithm. In particular, CMR algorithm has been chosen for its ability to make an appropriate balance between exploration and exploitation. The proposed optimization was aimed at minimizing the structural weight, starting from a fully braced frame and gradually removing unnecessary bracing members. During the procedure, the design variables were representative of the discrete cross-sectional areas of columns, beams and braces, along with the placement of the brace members as topology variables. Moreover, due to practical requirements, symmetry in the structure was used to group the design variables. The applied constraints regarded practical geometric specifications about column-to-column and beam-to-column framing joints, strength requirements in terms of the elements demand-capacity ratios (DCR), according to LRFD-AISC code (Load and resistance factor design - American Institute of steel design), and PBD constraints as well. Actually, PBD constraints were not tested until the geometry and strength requirements were met in order to decrease the computational time. However, if PBD constraints were verified, a pushover analysis was performed at each performance level to assess the structural responses, i.e. the maximum inter-story drift and the maximum deformation of columns and braces, which had to be less than their permitted values. After the application of the PBD method, in order to evaluate the collapse potential of the structure, an incremental dynamic analysis (IDA) was carried out according to FEMA-P695 (Federal Emergency Management Agency – Quantification of building seismic performance factors). Consequently, the SCBFs were compared in terms of structural weight and seismic collapse capacity until the best optimal design was found. Three different frames have been analysed with the proposed methodology, which provided optimized structural solutions with simultaneously improved structural weight and collapse performance. The designs with the best bracing topologies were, respectively, 11.59%, 18.68%, and 16.0% lighter than the best SCBFs with fully braced frames in all examples of 5-, 10-, and 15-story SCBFs. Moreover, the best-optimized frame was the one with the largest safety factor, that does not necessarily imply heavier weight. Sotiropolous and Lagaros (2022) tried to identify the structural system's ideal layout and, more specifically, to determine the best lateral brace system configuration in tall buildings subjected to dynamic seismic loadings. Both topology and size optimization have been exploited to reach

a minimum value of the objective function (OF), that was tackled as the compliance of the structure. The minimization of the compliance of the structure means the maximization of the building stiffness and it was carried out by varying both the cross-section areas of the structural elements and the building topology. Standardized cross-sectional frame elements have been considered and specifically, the European HEA, IPE and CHS sections were used with the aid of regression analysis, while a number of possible brace configurations defined the design domain. Cross-sections were taken from a list, in which minimum and maximum values have been defined to avoid the singularity of the stiffness matrix. During the iterations, the final material volume used was restrained to a limiting value, while stress and strain constraints have been applied to the different frame elements. Two cases of dynamic loading have been examined: harmonic loading and earthquake ground motion excitation. The examples were focused on the optimization of tall structures, like High-rise buildings and Mega-braced frames.
Moreover, they can be divided into three groups, in which the first one addressed the maximization of a specific eigenfrequency while the structure was subjected to free vibration; in the second one, time history analysis has been employed and both concentrated harmonic load and ground motion seismic excitation were considered, leading to different formulations of the minimized OF, i.e. dynamic compliance for half-cycle sinusoidal concentrated load and roof deflection (using the sum root of sum squares), respectively; finally, in the third group the response spectrum of EC8 has been implemented for simulating the seismic load. Due to the different natures of the three cases tested, a great variety of observations can be made. More specifically, results from the first case showed how by giving more freedom to the initial ground structure, the optimization leads to larger and thus better OF. Then, in the first case of the second group of analyses, it has been observed that when the driving frequency was close to an eigenfrequency, more braces were developed to prevent resonance, while for high driving frequency, the structure had braces only in its upper half. Regarding the minimization of SRSS in which a real earthquake is applied, it has been noticed that the optimized structural system was derived from denser ground structures, more types of braces were produced and so the moment-resisting steel frame had smaller tip deflections. In conclusion, relative to the final depicted case, it has been noted that an important role has been played by the number of modes considered. In fact, by the comparison of two different moment-resisting frames,

the optimized structure had the best structural response if the first three eigenmodes were used for the evaluation of the sum of the compliance.

Size, Shape and Topology Optimization In the context of simultaneous size, shape and topology optimization was provided by Lagaros et Al (2008). In this paper, the authors have applied a combined size, shape and topology optimization in order to reach an optimum design of perforated I-section beams. Web openings in beams are suggested and the major advantages are: reducing the material volume without changing the strength properties of the structures, alleviating stresses in beam columns joints and finally also architectural limitations sometimes impose the necessity of web opening in the building. The considered design variables for size, shape and topology were respectively cross sections, coordinates of the open boundary and number of web openings. The Objective function of the problem was the weight minimization, however, the optimal design was obtained considering some design criteria like shear, bending and Vierendeel bending resistance as well as provision for local buckling and web buckling. The design constraints were mainly focused on the size of the openings. In fact, it need to be highlighted that any increase in size of the web openings will result in a lower global shear and the global moment resistances of the perforated sections. Due to that some geometric restrictions were implemented to control the size of the openings., in fact all web openings should be located along the centre line of the web, and the maximum diameter of the openings cannot exceed 0.75 times the total height of the beam and the distance between the edges of adjacent openings should not be less than the total height of the beam. Evolutionary Algorithms (EA) has been employed in order to run the optimization problem, practical example is related to a frame with different web opening diameters. Results have shown the efficiency of the considered structural system, in fact up to 20% in weight savings was achieved compared to the case with no openings. Another stimulating research has been proposed by Hasançebi, O., Doğan, E., (2011), where several truss bridges have been analyzed. In particular, a comparison based on the design weight efficiency of single-span steel truss bridge topologies, subjected to gravity load, has been employed. Through a combination of size, shape and topology optimization, nine distinct topological forms of truss bridges (namely, Pratt, Parker, Baltimore, Petit, K-Truss, Warren, Subdivided Warren, Quadrangular Warren and Whipple) have been designed for minimum weight.
It should be stressed that truss bridges are widely used, especially in the last years,

due to their advantages from both a structural and constructional point of views. Moreover, they allow to reach very large spans, using less amount of material. Specifically in this analysis, the bridges were first configured according to these topological forms and the resulting structures have been then optimized considering strength, stability and displacements provisions of ASD-AISC. In the optimum design process, both size (discrete) and shape (continuous) design variables have been employed. In this context, size variables have been used to choose appropriate dimensions for the bridge members, whereas the optimal height and/or shape of the bridge's upper chord have been explored with shape variables. In particular, the number of shape variables used in a model was dependent on the bridge topological form. For example, a single shape variable was used to define the height in bridge models with Pratt, Baltimore, Warren, Subdivided Warren, Quadrangular Warren, Whipple and K-truss forms, since they have a straight upper chord. Moreover, four different span lengths, namely 100, 200, 400 and 600 ft have been considered as separate case studies and for each of these span lengths nine bridges have been generated. In conclusion, it has been found that the topological form selected to create the structural system of a bridge significantly affects the weight of the bridge's final design. For span lengths of 100, 200, 400, and 600, respectively, the design weight disparities between the best (lightest) and worst (heaviest) models was 15%, 30%, 43%, and 55%. Consequently, the selection of economical topological form became more pronounced when span length of the bridge increased. The bridge's ideal forms, created using Petit and Parker trusses, lowered the height of the structure moving from the middle of the span to the ends, reducing the amount of material used in the design. The findings also suggest that, in order to maximize the weight efficiency of the final bridge, some bridge designs, such as Whipple and Pratt, should be avoided for all span lengths. Warren and Quadrangular Warren should also be avoided for relatively large span lengths. Baltimore, Subdivided Warren and K-truss topology led to similar design weights.

Finally, the work done by Ohsaki, M., Iwatsuki, O., Watanabe, H. in Ohsaki et al. (2014) gives a clear demonstration of the complexity and at the same time of the power of such procedures. In this research, a reverse rocking response was exploited to investigate the behaviour of a steel frame structure with a foundation modelled as a flexible base, with the objective to reduce roof displacements. Due to the foundation's flexibility, the frame had areverserocking when the base beam was rotating against the frame's drift to minimize the displacement of the roof. The

foundation beam, on the other hand, if above a stiff base, would be rotating slightly in the same direction as the frame. Topology, size and shape optimization have been carried out to find the best configuration of the base structure, modelled as a truss structure and the OF of the entire optimization was aimed at the reduction of the roof displacement. Running the analysis, unnecessary members have been removed, starting from the highly connected ground structure. Nodal locations have been also considered as variables to comply with shape optimization, while elements with square tube sections have been used as size discrete design variables. Constraints were mainly related to the maximum allowable displacements of the flexible base's elements, as well as to the upper and lower boundary of the node coordinates. A practical example of a frame, characterized by 10 meters of span and with a base made of rigidly-jointed frame with square tube sections, has been analyzed. The outputs have shown that the displacement as well as the acceleration of the roof of a frame under seismic ground motion can be effectively reduced using a flexible base structure, which exploits rocking of the base in the opposite direction to the drift of the upper frame. Such reverse rocking response is dominated by the 2nd mode rather than the 1st mode. Moreover, in the examples reported, the mean maximum roof displacement, computed using the SRSS method, was successfully minimized compared with the stiff model.

1.10.2 Cost impact-based optimization problems

Size and Topology optimization Without any doubt, coupled size and topology represent the most common optimization adopted by researchers due to their adaptability to different engineering problems. Specifically, this approach is chosen when the topology of the structures is changed by varying the properties connections at the level of each node. The most relevant and used a topological improvement to a simple size optimization was to consider the connection inside the original problem. In general, authors agreed to name with simply *connections* the joint between the columns and beams and *column base connections* the connection between the columns and the foundation.

Since the beginning, the authors noticed that traditional approaches to steel frame design ignore connection behaviour (see Chan et al. 2000). Although the theoretical pinned and totally rigid scheme was utilized to make analysis and design methods easier, the expected frame response could lead to no real results. In real-world

structures, most connections are designed in order to transfer moments and rotations, which can contribute significantly to the final stress and displacement distribution within the structure. The term semi-rigid is widely used to describe the intermediate behaviour of stiffness connections between extreme cases (i.e. double pinned, double fixed or pinned-fixed joints). In this way, a more reliable prediction of frame behaviour can be achieved by optimizing the mechanical properties of connections aiming to investigate how these changes affect the overall structural behaviour.

To involve economic consideration taking into account trivial details related to connections, Simoes et al.(1996) modelled the semi-rigid connections like springs with a certain stiffness. The objective function was composed of the members' weight and the cost of the connection which is the product between the fixity factor (usually chosen into the range $[0, 1]$ and representative of the stiffness grade of the connection) and a cost coefficient. In this way, the cost associated with a semi-rigid connection is evaluated as an extra cost to be summed to the base cost of a generic connection which is assumed to be equal to a pinned constraint scheme.
Further improvement in semi-rigid connection optimization was accomplished by Hayalioglu et al. (2005). In this study, the design of the connections was modelled with both Frye and Morris polynomial model and linear spring model for the standard connection and column base respectively. In particular, the cost function was given by the sum of the cost of the elements (that are simply the weight of the member multiplied by the cost for unit weight), the cost of the beam-column connection and the column base connection. At each iteration, either the connection cost and column base, are upgraded proportionally to the rigidity of the joint stiffness through some cost coefficients.
Moreover, another procedure in which the semi-rigid connection was included in the design was developed by Truong et al. (2017). The suggested approach for optimizing semi-rigid steel frames was built in such a way that the cost function considers both the steel frame weight and semi-rigid joints, while structural constraints such as member stresses and nodal displacements and/or inter-story drifts were adopted. When the stiffness values of the semi-rigid connections change, the sizing of each member was performed by choosing the optimal cross-sectional areas. If the percentage of the cost related to members (columns and beams) was simply assumed equal to the weight for the unitary cost, the complexity of the connection was evaluated by adopting a proportional trend between cost and the increasing level of the joint's rigidity.

Meanwhile, the previous work treats only connection cost related to well-known static constraints (pinned-pinned, fixed-pinned, etc.), Prendes et al. (2016) and Jarmai et al. (2004) tried to investigate the effect of welded and bolded connections into the global optimum solution. In this way, the optimization was able to include all the technical procedures required by each phase of the welding operations. In addition to the cost function previously described, the semi-rigid connection cost was obtained as a percentage of the element price multiplied by a suitable value of stiffness grade of joints, while the welding cost is simply the sum of the filler material, gas, machines and operation cost of the work. Joint stiffness and cross-sectional properties were chosen as design variables.

Basically, the same problem described above was solved by developing different optimization approaches in order to guarantee the effectiveness and robustness of the procedure and the simplicity of the implementation. (e.g. Rafiee et al. (2013), Hadidi and Rafiee (2014), Shallan et al. (2018)). Some authors added a specific constraint to guarantee the constructability of the connection (e.g. Hadidi and Rafiee (2015), Truong and Kim (2018)). The constructability constraints assure the feasibility of the connection between the beam and columns by checking the correct matching of the members (i.e. the web of the beam connected to the flange of the column should be shorter or equal to the flange length).

While so far only work challenged in associating connection cost with an optimized grade of joint's stiffness has been discussed, several authors focused on involving specific types of connections with a well-defined degree of constraints into the cost function.

For instance, Kaveh et al. in (2017) arranged an objective function which was a simple cost function composed of the cost of the structural members (computed as usual like weight by unit cost) and the cost of the connections assumed to vary between 0 (rigid) and 1 (pinned). While the latter is associated with a cost equal to 900$/connection, the former cost was assumed to be equal to zero based on the authors' practical evaluation. As a set of variables of Design Vector, all cross-sections (taken from the AISC steel construction guidebook) and beam-end connection types are chosen.

The effect of different types of static schemes for each connection was investigated by Laberdi et al. (2015). In this study, the connection can be either a pin or a moment connection. More in detail, the pin connection does not transmit a bending moment while the moment connection transmits a percentage of the moment. Combining

the information derived by coupling beam sizes and connection types, four types of beams were defined: fully moment-connected, fully pinned, left-end moment-connected and right-end moment-connected.
Other authors used a combined approach where only some specific connections typologies were taken into consideration by neglecting some useless values of the entire stiffness joint spectrum. One of these was Jarmai et al. (2006) which takes into account only four different connection types. The structure was subjected both to vertical and horizontal (seismic) loading. For the structural analysis of the building, the framework was decomposed into three parts and only the central part was analysed through a fish-bone model. For the columns and the beams was used a welded square box cross-section and a rolled universal beam I cross-section respectively and their dimensions were adopted as design variables of the optimization problem. Four types of assembled connections are considered and the most economical one was entered into the model. The cost function was evaluated as the single contribution of fabrication, connection and material cost.
Further developments in this field were done by Ali et al. (2009) who evaluated all the fabrication and erection phases by considering the most convenient connection typologies usually adopted by practitioners. A realistic optimization of frame design was performed by considering the effective costs of various phases of production activities, including manufacturing and erection, hence, a multi-stage production cost optimization was developed. The optimization problem considers the cross-sectional sizes of structural members, the type of beam-to-column connections and the type of column bases as design variables. The optimal size of the structural member was selected from available steel profiles, while the most adopted technical solutions by engineers of internal connections and column base connections were identified. If The material price was simply derived by using the unit price for different section types and different steel grades, the fabrication and erection cost was obtained by multiplying the unit cost per hour of workshop labour and machine power, respectively.

Up to now, topological optimization has been discussed with only connections in mind. Other applications rely into change the arrangement or the connectivity matrix of structural elements when size optimization is performed simultaneously. In this sense, steel portal frames result to be the most common case of interest for several optimization strategies.
In this regard, Phan et al. (2013) make a notable contribution in which several

optimization strategies and interesting real-world applications were proposed. The authors studied the rigid-jointed cold-formed steel portal frames largely chosen as a design solution for light industrial and agricultural buildings. One of the advantages is the competitive cost compared to the hot-rolled systems. The variables were taken into account where the spacing and pitch of the frame as continuous variables and the section size as discrete ones. The optimization of the minimum cost was performed with a real-coded genetic algorithm that minimizes a cost function considering the unit length cost multiplied by the member length and the frame spacing. The greater the spacing of the frames, the lower the total cost of the structure, hence, fewer steel portals are required. A few years later, the same author (Phan et al. (2017)) included also joint effects and secondary members. The cost function included in the portal frames' cost, variables representative of spacing and pitch of main beams, the secondary members (purlins) and the brackets used in the bolted joint. The analysis was performed by employing both rigid and semi-rigid joints .

Finally, in a third work (Phan et al. (2015)), he tried to reduce the cost of the industrial building consider the stressed skin action of the roof profiles with a beneficial effect on the global strength and economy of the design. The frame layout was fixed and 6 building configurations were investigated. The stressed-skin was considered in order to evaluate the additional rigidity to the overall structure thanks to the shear stiffness of these panels. This resulted in a global cost-saving of the structure thanks to stress limitation at the level of connections. The objective function was a cost function per square meter of floor area which takes into account the cost of the members and the cost of the angle brackets divided by the span length and the frame spacing. Moreover, grouping strategies were performed to minimize the length of the bolt connections which range in a continuum interval of 200 up to 2000 mm.

The beneficial effect of stressed skin action was taken into account by other authors like Wrzesien et al. (2016). In this work, the effect of stressed skin action on cost optimization of cold-formed portal frame buildings was studied by comparing different structures with a different number of bays. As in the previous case, the overall building shape was fixed and the objective function was expressed as the sum of the cost of members and angle brackets per unit floor area. The design variables representative of the columns and rafters were selected from the standard cross-section available in the UK, while the bolts' dimensions and position were assumed to range within a continuous domain. The optimization was performed by a real-coded Genetic Algorithm for a different number of bays. The comparative study

shows that the stressed skin action is relevant for buildings with few bays(threshold value found to be equal to 9), meanwhile, the effect can be considered almost negligible for more than 12 bays.

The seismic field was the research branch which receive the most benefit from the employing of optimization procedures.

Several applications have been recognized in literature and several works focused on optimizing specific aspects related to the seismic behaviour of structures.
For instance, bracing system design is usually an interesting case study chosen by researchers such as Braga et al. (2019). He developed an optimality procedure which allows the design of a bracing system by minimizing the intervention cost. The procedure leads to obtaining the minimum cost through a dimensional and topological optimization of the bracing. IDR (inter-story drift ratio) and braces displacement, derived by performing a linear modal analysis, were assumed as serviceability constraints of the problem. The independent variables of the problem are the ones required for a bracing design like the area of each steel truss, the yielding force and the yielding displacement. The objective function was the sum of material and works price for the realization of the intervention and was composed of the cost of steel elements, dissipative devices, masonry works (removal and reconstruction or drilling and traces of the infills) and foundation system improvement). The optimization aims to minimize the dimension of the global stiffness matrix of the consolidated system through an iterative algorithm. In this way, the optimal dimensions of the stiffness matrix correspond to the optimal retrofitted configuration with the optimal number of bracings.
Seismic device performance were investigated in Shin and Singh (2017) in which the yielding metallic devices are optimized. Yielding metallic devices are very useful to reduce inter-story drifts and contribute to ductile behaviour during seismic events. This article treats the cost optimization of a specific type of dissipator which is realized by assembling a determinate number of triangular plates whose thickness was assumed as design variables. The least cost is reached by performing a Genetic algorithm that minimizes the sum of the total failure cost and the cost of the devices including their replacement cost. The failure cost is linked to the story drift and floor acceleration responses computed by assigning to the devices a proper stiffness. The randomness of the seismic events with various probabilities of occurrence is included in the optimization by a seismic hazard curve.

Size, shape and Topology optimization The most effective and powerful approach to achieving the minimum cost of a structure is a combination of all three levels described above (size, shape, and topology). In this section, these three approaches are integrated simultaneously in the same procedure. The advantage of this type of technique is to achieve a design that is simultaneously well-compliant with all three design aspects.

Historically, the first studies that used combined optimization were performed by Lee et al. (1975b) and Thomas et al. (1977).

In the first paper, the minimum cost design of a steel portal framed building was achieved through the determination of the optimum shape and topology of the structure that is a function of material and fabrication cost only. The material costs were taken from the "British steel corporation home trade price list" which gives the unit weight cost and surface preparation cost meanwhile the fabrication costs were computed for the main construction procedures (welding, cutting and drilling) with the Standard Minute Value technique (SMV). To accomplish this goal, the design variables were formulated into primary variables, normally chosen at the beginning of the design process (building length, building width, number of bays, eaves height, roof pitch and frame spacing), and secondary variables like the length and size of the various elements (stanchion, rafter, wind braces, etc. . .).

On the other hand, Thomas Jr and Brown (1977) proposed an algorithm that allows a nonlinear optimization technique for the least cost-elastic design of roof systems composed of rigid steel trusses, web joists and steel roof decks. This procedure is used for various grades of steel and standard sections. In particular, it considers changes in the mechanical properties of the members, geometric variation and topology. The independent design variables are the cross-sectional area of each member, the plane coordinate of each joint and the number of trusses in the system. All variables are considered to be continuous due to the nature of the adopted optimization strategy. The criteria to evaluate the cost function is based on the overall material and fabrication cost computed by simply multiplying the area/weight of the element by the unit area/weight material and fabrication cost of the specific element. In this study, an important limitation was highlighted by the same authors related to the total absence of constructability constraints which would allow discarding unfeasible solutions. Lower and upper bound and/or adopted structural constraints can not guarantee that no realistic element sizing (negligible cross-section areas) and/or unfeasible connections between elements of the structure appear in the optimal

solution.
More recently, Kaveh et al. (2010) determined the cost optimization of a composite floor system, made-up of steel beams and a reinforced concrete slab. The cost function was determined by the minimum cost of the concrete, steel beams and shear studs (the connectors between the steel girder and the concrete slab). The design variables, that were assumed discrete, were the steel beam spacing, the beam size and the concrete slab thickness.

Since considering all the necessary design variables for each optimization level in a single objective function result in a heavy computational effort and in a lack of control of each parameter related to the single optimization strategies, many authors made use of parametric optimizations to tackle topology and/or shape optimal design.
In this regard, Kripka et al. (2018) developed a size and shape optimization by ranging between 7 common different topologies of steel trusses with parallel chords. The 7 truss typologies were analysed through a simple cost function composed of the total weight of the structure multiplied by the unit cost of the steel. Because the same profile was used for a group of pieces, the number of design variables drastically decreased in comparison to the total number of elements. Results show high variability in the final weight of the structure as the number of groups of elements increased. By including truss height in the set of design variables, significant additional cost savings were obtained. The authors found a significant difference between the height/span ratio recommendation provided by the technical guide and the one obtained with the proposed method.
Along this trail, Alhendi et al. (2021) implemented another parametric optimization regarding parallel chord trusses. The aim of this study was to investigate the performance and the cost-effectiveness of three parallel chord composite floor trusses (Prat, Howe and Warren) with 4 different composite floor panels and load intensities. The analysis was made by making 165 models with different spans between the trusses and different truss depths and panel typologies. In addition to that, a cost estimation function was implemented as the sum of the material cost, fabrication cost and painting cost dependent on the span range and span and depth ratio of the composite floor truss system. By observing the results pointed out by the optimization, the authors provided useful technical specifications for the composite tabular-floor trusses design.
The combined size, shape and topology approach lead to the resolution of very

sophisticated problems. In this sense, Cicconi et al. (Cicconi et al. (2020)) elaborated a special parametric procedure to accomplish a specific task. This paper proposes a sequential multi-objective procedure for the structural optimization of modular industrial towers such as the steel structure of the chimney used in oil and gas power plants. The optimization method is articulated in three stages of optimization: preliminary design, embodiment design and detail design. Objective functions focus on weight and cost reduction. The first optimization level uses a 1-D model (pole model), whereas the second uses a 3-D shell model. Finally, the third stage entails thorough design, which includes simulations and analysis based on 3-D solid models. Thanks to this approach, all the manufacturing, logistical and assembly cost aspects were investigated in different stages of optimization aiming to reduce the complexity of the entire problem into easier step-by-step sub-procedures.

1.10.3 Enviromental impact-based optimization problems

The study revealed that the topology optimization's literature is still in urgent need of refinement. Pure topology optimization examples are completely absent from the current study, but few examples from hybrid optimization categories are provided.

Size and Topology The emphasis recently placed on reducing operating energy consumption has made it more crucial than ever to take into account building's embodied carbon. The research of Ching and Carstensen (2022) offers a two-material truss topology optimization technique to lower the designed structure's Global Warming Potential (GWP). Optimization occurs gradually and step by step. The first one is a hybrid typology and size optimization, applying only structural restrictions to timber and steel individually. The result is the ideal outcome of a stiffer framework made of steel only. The second stage restricts the admissible stresses of wood only and the structure by the environmental parameter GWP, resulting in an ideal construction made entirely of wood. The optimization again leads to a building made entirely of steel in the following phase, which keeps the environmental constraints in force but this time takes into account realistic values for stresses. The GWP ultimately limits the issue, and the stresses are changed to make steel and wood operate in tension and compression, respectively. The latter scenario results in a mixed optimum structure that enables lower GWP levels. The stress conditions in the materials must therefore be suitably adjusted in order to see a minimum increase

in terms of environmental effect. The author recommends conducting the same analyses while taking into consideration a full LCA that also takes into account the transportation phases in order to balance the significant difference between structural (stiffness) and environmental (GWP) constraints.

Size, Shape and Topology In the study of Mensinger and Huang (2017) the preliminary structural design of a set of rectangular steel composite office buildings was done using a multi-objective optimization of costs and environmental impact. The cost is obtained by multiplying the weight of materials by their unit prices; while the second one is called Environmental Product Declaration (EPD) and it is computed as a weighted summation of the Global Warming Potential (GWP), the Ozone Depletion Potential (ODP), the Photochemical Ozone Creation Potential (POCP), the Acidification Potential (AP), the Eutrophication Potential (EP) and the Primary Energy, both non-renewable (PEne) and renewable (PEe). The data relating to these environmental criteria were taken from the Ökobaudat platform, which is a German standardized database for ecological evaluations of buildings. The outcomes of the optimization against the EPD value and the costs are the same or quite comparable.

1.11 tables of synthesis

Review table of the applications of optimization strategies for optimal structural performance

Ref.	Year	**S**tatic **D**ynamic	Size	Shape	Topology	**S**ingle/**M**ulti Objective	ID-OF	Design criteria	Design variables
Feng et al.	1977b	**D**	☑	☐	☐	**S**	Weight	Stresses Displacement Natural frequency Geom. bounds	Cross-sections
Haque et al.	1985b	**S**	☑	☑	☐	**S**	Weight	Geom. bounds AISC	Cross-sections Node's coordinates
Scholz et al.	1986b	**S**	☑	☐	☐	**S**	Failure load factor	Failure load factor range	Cross-sections
Machaly et al.	1986c	**S**	☑	☐	☐	**S**	Weight	Stresses Displacements Buckling Geom. bounds	Cross-section's parameters
Kapoor et al.	1987b	**D**	☑	☐	☐	**S**	Weight	Probability of failure Moment of inertia	Columns' moment of inertia

Cheng et al.	1989b	**S/D**	☑	☐	☐	**S**	Weight Cost	Stresses Displacement Natural frequency	Cross-sections
Saka et al.	1991b	**S**	☑	☐	☑	**S**	Weight	Stress Displacement	Cross-sections Brace locations
Saka et al.	1991	**S**	☑	☐	☐	**S**	Weight	Displacement Geom. bounds	Cross-sections
Balling et al.	1991b	**S**	☑	☐	☐	**S**	Weight	Stress Displacements	Cross-sections
Erbatur et al.	1992b	**S**	☑	☐	☐	**S**	Weight	Stresses Buckling Slenderness Geometric bound	Moment of inertia
Hayalioglu et al.	1992b	**S**	☑	☐	☐	**S**	Weight	Displacement Geom. bounds	Cross-section at one end of the beam and area ratio at its ends

Thevendran et al.	1992b	**S**	☑	☐	**S**	Weight	Stresses Displacements Buckling Geom. bounds	Cross-sections
Adeli et al.	1993	**S**	☑	☐	**S**	Weight	Stresses Displacements Geom. bounds	Cross-sections
Dhingra et al.	1994	**S/D**	☑	☐	**S/M**	Weight Displacement Frequency	Stresses Buckling Geom. bounds	Cross-sections
Al-Salloum and Almusallam	1995b	**S**	☑	☐	**S**	Volume	Stresses Displacements Geom. bounds	Moment of inertia
Memari et al.	1999b	**S/D**	☑	☐	**S**	Weight	Stresses Displacement Buckling Slenderness Geom. bounds	Cross-sections

Coello and Christiansen	2000b	**S**	☑	☐	☐	**M**	Weight Stress Displacement	Stresses Displacements	Cross-sections
Jakiela et al.	2000b	**S**	☐	☐	☑	**S**	Compliance	Stresses Displacement	Material distribution
Choi et al.	2002	**S**	☑	☐	☐	**S**	Weight	AISC-LRFD	Cross-sections
Saka et al.	2003	**S**	☑	☐	☐	**S**	Weight	BS 5950 Buckling	Cross-section's parameters
Moghaddam et al.	2005	**S/D**	☑	☐	☐	**S**	Uniform deformation	UBC FEMA365 SEAC2000	Cross-sections
Pan et al.	2006	**D**	☐	☐	☑	**S**	Weight	Frequency Displacement Acceleration	Bars arrangement
Safari et al.	2006	**S**	☐	☐	☑	**S**	Weight	Stresses Displacement Architectural limitations Max number of braced panels	Brace locations

Wang et al.	2006	**S/D**	☑	☐	☐	**S**	Uniform deformation	UBC FEMA365 SEAC2000	Cross-sections
Csebfalvi et al.	2007	**S**	☑	☐	☐	**S**	Weight	Stress Displacements	Cross-sections Connection flexibility
Lagaros et al.	2008	**S**	☑	☑	☑	**S**	Weight	Stress Geometric	Cross-sections Coordinates of web openings Number of web openings
Moghaddam et al.	2008	**S/D**	☑	☐	☐	**S**	Uniform deformation	UBC FEMA 365 SEAC2000	Cross-sections
Cheng et al.	2010	**S**	☑	☐	☐	**S**	Weight	Strenght Deflection	Cross-sections
Hasanccebi et al.	2011	**S**	☑	☑	☑	**S**	Weight	ASD-AISC	Cross-sections

Kaveh et al.	2011	**S**	☑	☐	☐	**S**	Weight	Strenght Deflection	Cross-sections
Hajirasouliha et al.	2011	**S**	☐	☐	☑	**S**	Weight	Strenght Deflection	Bars arrangement
Phan et al.	2012	**S**	☑	☐	☑	**S**	Weight	Stresses Displacements	Cross section Building topology
Stromberg et al.	2012b	**S**	☑	☐	☑	**S**	Compliance	Material used Stresses	Cross-sections Material distribution
Oskouei et al.	2012	**S/D**	☑	☐	☐	**S**	Weight	Stresses Displacement Plastic hinges	Cross-sections Connections flexibility
Choi et al.	2013	**S/D**	☑	☐	☐	**M**	(Weight Column-beam strengthratio	Strength Inter-story drift ratio Plastic hinges Geom. bounds	Cross-sections

Gandomi et al.	2013b	**S**	☑	☐	**S**	(Weight	Stresses Deflections Buckling Geom. bounds	Cross-sections
Kaveh et al.	2013	**S/D**	☑	☐	**M**	(Weight Inter-story drift Structural damage	Strength Slenderness Displacement Geom. bounds	Cross-sections
Camp et al.	2014b	**S**	☑	☐	**S**	Weight	Strength Displacement Geom. bounds	Cross-sections
Gholizadeh et al.	2014	**S/D**	☑	☐	**S**	Weight	Stresses Inter-story drift FEMA356	Cross-sections
Mohammadi et al.	2014	**S/D**	☑	☐	**S**	Weight	ASCE 41-06 Displacement Plastic hinges	Cross-sections

Ohsaki et al.	2014	**S/D**	☑	☑	☑	**S**	Roof displacements	Bounds on nodal coordinates Base displacement	Cross-sections Node's coordinates Members arrangements
Liu et al.	2015	**S**	☑	☐	☐	**D**	Weight	Stresses Geom. bounds	Cross-section parameters
mckinstray et al.	2015	**S**	☑	☐	☐	**S**	Weight	Stresses Displacements	Cross-section
Kaveh et al.	2015	**S**	☑	☐	☐	**S**	Weight	Strenght Displacements	Cross-sections
Tangaramvong et al.	2015	**S**	☑	☐	☑	**S**	Weight Min number of braces	Stresses Displacements	Cross-sections
Talatahari et al.	2015	**S**	☑	☐	☐	**S**	Weight	AISC	Cross-sections
Gholizadeh et al.	2015	**S**	☑	☐	☐	**D**	Weight	Strength Displacements	Cross-sections

Artar et al.	2015b	**S**	☑	☐	☐	**S**	Weight	AISC-ASD Geom. bounds	Cross-sections Connections rigidity
Artar et al.	2015c	**S**	☑	☐	☐	**S**	Weight	AISC-ASD Geom. bounds	Cross-sections Connections rigidity Beams material
Palizzolo et al.	2015	**S**	☑	☐	☐	**S/D**	Weight	Serviceability for static and seismic load	Cross-sections
Lv et al.	2015	**S**	☑	☐	☐	**D**	SPI	FEMA 356 FEMA-350	Cross-sections
Kaveh et al.	2015	**S**	☑	☐	☑	**D**	Weight	FEMA 356 FEMA-350	Cross-sections Brace locations
Kaveh et al.	2015	**S**	☑	☐	☑	**S/D**	Weight	Stresses Displacements Buckling Natural frequencies	Nodes and members arrangement

Artar et al.	2016	**S**	☑	☐	☐	**S**	Weight	AISC-ASD Displacements Cross-sections
Qiao et al.	2016	**S**	☐	☐	☑	**D**	Weight	Stresses Displacements Material distribution
Daloglu et al.	2016	**S**	☑	☐	☐	**D**	Weight	LRFD-AISC Cross-section
Gholizadeh et al.	2016b	**S**	☑	☐	☑	**D**	Weight	Geometric Strength Cross-section Brace locations
Gholizadeh et al.	2016	**D**	☑	☐	☐	**S**	Weight	Strength Displacements Performance objective Cross-sections Performance objectives
Kaveh et al.	2016	**D**	☑	☐	☑	**S**	Weight	Strength Displacements Stability Buckling Cross-sections Brace locations
Gholizadeh et al.	2017	**S**	☑	☐	☐	**S**	Weight	Stresses Displacements Geom. bounds Fabrication limits Cross-sections

Moradi et al.	2017	**M**	☑	☐	☐	**D**	Weight Ultimate drift Stiffness response	Stresses Geom. bounds	Cross-sections
Azad et al.	2018	**S**	☑	☑	☐	**S/D**	Weight	AISC-LRFD	Cross-sections Nodal Coordinates
Bagherinejad et al.	2018	**S**	☐	☐	☑	**S/D**	Reaction forces	Stresses	Material distribution
Xu et al.	2018	**M**	☑	☐	☐	**D**	Structural damage Energy Dissipation	Stresses Displacements	Cross-section
Korkmaz et al.	2018	**S**	☑	☐	☐	**S/D**	Weight	Stresses Displacements	Cross-section
Gholizadeh et al.	2018	**S**	☑	☐	☐	**S**	Weight	Stresses Displacements	Cross-sections

Dougan et al.	2018	**S**	☑	☐	☐	**S**	Weight	Strength Displacements Geom. bounds	Cross-sections
Hasanccebi et al.	2019	**S/D**	☑	☐	☐	**S**	Weight	Stress Displacements Slenderness Geom. bounds	Cross-sections
kaveh et al.	2019	**S**	☑	☐	☐	**S**	Weight	Stress Displacements	Cross-sections
kaveh et al.	2019	**M**	☑	☐	☐	**D**	Weight Std. deviation inter story drift	Stress Displacements	Cross-sections
karimi et al.	2019	**M**	☑	☐	☐	**D**	Weight Uniform distr. inter story drift	FEMA	Cross-sections
Fu et al.	2019	**S**	☑	☐	☐	**S**	Weight	Displacements	Cross-sections
Mansouri et al.	2019	**S**	☑	☐	☐	**D**	Weight	AISC-LRFD	Cross-sections

Dehghani et al.	2019	**M**	☑	☐	☐	**D**	Weight Inter story drift	Stresses Displacements Geom. Bounds	Cross-sections
Habibi et al.	2019	**S**	☑	☐	☐	**D**	Displacements	Base shear Lateral forces	Lateral forces
Hassanzadeh et al.	2019	**S**	☑	☐	☑	**D**	Weight	AISC-LRFD PBD	Cross-sections Brace locations
Tantely et al.	2019	**S**	☑	☐	☑	**S/D**	CMR	Designable matrix	Cross-sections Brace locations
Phan et al.	2020	**S**	☑	☑	☐	**S**	Weight	EC3	Cross-sections Elements' coordinate
Kaveh et al.	2020a	**S**	☑	☑	☐	**S**	Weight	ASCE	Cross-sections Elements coordinates

Apostolakis et al.	2020	**S**	☑	☐	☑	**D**	Displ.	Brace configuration	Cross-sections Brace locations Slip force
Elvin et al.	2021	**S**	☑	☐	☐	**S**	Weight	Strenght Deflection	Cross-sections
Baghdadi et al.	2021	**M**	☐	☐	☑	**S**	WIF	Constructability	Element forces
Ghasemof et al.	2021	**M**	☑	☐	☐	**S/D**	Weight IDR	Strenght Geoetric bubds Constructability	Cross-Section
Moghaddam et al.	2021	**S**	☑	☐	☐	**D**	Weight	Strenght Deformation Plastic rotations	Cross-Section
Mojtabaei et al.	2021	**M**	☑	☐	☐	**D**	Ductility Energy dissipation	Geom. bounds	Cross-Section
Kaveh et al.	2021	**S**	☑	☐	☐	**D**	Weight	Strenght Displacements	Cross-Section

Fathizadeh et al.	2021	**S**	☑	☐	☐	Weight	AISC-FEMA 365 Constructability	Cross-Section
Sotiropoulos et al.	2022	**S**	☑	☐	☑	**D**	Compliance	Stress Strain Max. material volume
						D		Cross-Section Brace locations

Review table of the application of optimization strategies for minimum cost of steel structures

Ref.	Year	**S**tatic **D**ynamic	Size	Shape	Topology	**S**ingle/**M**ulti Objective	ID-OF	Design criteria	Design Variables
Lee et al.	1975b	**S**	☑	☑	☑	**S**	Material cost Fabrication cost	Stresses Geometry boundaries	Cross-section Building geometry Elements' number
Thomas et al.	1977	**S/D**	☑	☑	☑	**S**	Material cost Fabrication cost	Stresses Buckling	Cross-section Elemnts' number Nodal coordinates
Gong et al.	1989	**S/D**	☑	☐	☐	**S**	Structural cost Inter-story drift	Geometry Inter-story drift	Cross-section
Chan et al.	1995b	**S/D**	☑	☐	☐	**S**	Weight	stresses Inter-story drift	Cross-section
Simoes	1996	**S**	☑	☐	☑	**S**	Weight Connection cost	stresses Serviceability constraints	cross-section Connection type

Jarmai et al.	1999	**S**	☑	☐	☐	**S**	Material cost Fabrication cost	Stresses Inter-story drift	Cross-section
Sarma and Adeli	2002b	**S/D**	☑	☐	☐	**S**	Initial cost Painting cost	Stresses	Cross-section
Foley and Schinler	2003	**S/D**	☑	☐	☑	**S**	Weight Connection cost	Stresses Serviceability constraints	Cross-section Connection type
Liu et al.	2004	**S/D**	☑	☐	☐	**M**	Material cost Construction cost Damage lifetime cost	Inter-story drift	Cross-section
Pavlovvcivc et al.	2004	**S**	☑	☐	☐	**S**	Material cost Manufacturing cost	Stresses	Cross-section
Hayalioglu et al.	2005	**S/D**	☑	☐	☑	**S**	Material cost Connection cost	Stresses Serviceability Geometrical boundaries	Cross-section Connection type

Jarmai et al.	2006	**S/D**	☑	☐	☑	**S**	Material cost Connection cost Fabrication cost	Stresses Inter-story drift	Cross-section Connection type
Xu et al.	2006	**S/D**	☑	☐	☐	**S**	Structural cost Uniform inter-story drift	Inter-story drift Geometrical boundaries	Cross-section
Ali et al.	2009	**S/D**	☑	☐	☑	**S**	Material cost Fabrication cost Erection cost Foundation cost	Stresses Buckling Serviceability	Cross-section Connection type
Farhat et al.	2009	**S/D**	☑	☐	☐	**S/M**	Material cost Damage level	Stresses Buckling Serviceability Seismic	Cross-section
kaveh et al.	2010	**S**	☑	☑	☑	**S**	Material cost	Stresses Serviceability	Cross-section Beam spacing Slab thickness
Li et al.	2012	**S/D**	☑	☐	☐	**S**	Initial cost Damage loss	Serviceability Interstory-drift	Cross-section

Kaveh et al.	2012	**S/D**	☑	☐	☐	**M**	Weight Life Cycle Cost	Stresses Serviceability	Cross-section
Cheng et al.	2013	**S**	☑	☑	☐	**S**	Structural cost	Stresses Serviceability	Cross-section Shape ratio
De Santana et al.	2013	**S/D**	☑	☑	☐	**S**	Life Cycle Cost	Stresses Serviceability Buckling	Cross-section Nodes' coordinates
Kaveh et al.	2013	**S**	☑	☐	☐	**S**	Weight	Stresses Serviceability	Cross-section
Liu et al.	2013	**S/D**	☑	☐	☐	**M**	Weight Mean value inter-story drift St. deviation inter-story drift	Stresses Serviceability Seismic	Cross-section
Phan et al.	2013	**S**	☑	☐	☑	**S**	Material cost	Stresses Serviceability	Cross-section
Rafiee et al.	2013	**S/D**	☑	☐	☑	**S**	Material cost	Stresses Serviceability Geometrical boundaries	Cross-section Connection type

Hadidi et al.	2014	**S/D**	☑	☐	☑	**S**	Material cost Connection cost	Stresses Serviceability	Cross-section Connection type
Alberdi et al.	2015	**S/D**	☑	☐	☑	**S**	Material cost Connection cost	Stresses Inter-story drift Constructability	Cross-section Connection type
Artar et al.	2015a	**S**	☑	☐	☑	**S/M**	Weight	Stresses Geometric boundary Buckling Serviceability	Cross-section Connection type
Aydin et al.	2015	**S**	☑	☑	☐	**S**	Material cost	Stresses Serviceability Buckling	Cross-section Truss height
Hadidi et al.	2015	**S/D**	☑	☐	☑	**S**	Material cost Connection cost	Stresses Serviceability Inter-story drift	Cross-section Connection stiffness

Phan et al.	2015	**S/D**	☑	☐	☑	**S**	Material cost Connection cost	Stresses Serviceability Cross-section Connection type Elements number
Mckinstray et al.	2016	**S**	☑	☑	☑	**S**	Weight	Stresses Serviceability Geometric boundaries Cross-section
Prendes et al.	2016	**S**	☑	☐	☑	**S**	Material cost Welding cost Connection cost	Stresses Serviceability Buckling Cross-section Connection stiffness
Saadat et al.	2016	**S/D**	☑	☐	☐	**M**	Weight Annual Damage loss	Stresses Serviceability Seismic Cross-section
Van Mellaert et al.	2016	**S/D**	☑	☐	☐	**S**	Structural cost	Stresses Serviceability Joint strength Cross-section Connection type

Wrzesien et al.	2016	**S/D**	☑	☐	☑	**S**	Material cost	Stresses Serviceability	Cross-section Connection type
Kaveh et al.	2017	**S**	☑	☐	☑	**S**	Material cost Connection cost	Stresses Serviceability	Cross-section Connection type
Jin et al.	2017	**S/D**	☑	☐	☐	**S/M**	Fabrication cost Welding cost (1) Structural performances	Stresses Drift angle Story stiffness Serviceability Constructability	Cross-section
Mensinger et al.	2017	**S**	☑	☑	☑	**M**	Material cost Environmental impact	Stresses Serviceability	Cross-section
Phan et al.	2017	**S**	☑	☐	☑	**S**	Material cost	Stresses Serviceability	Cross-section Connection type Elements' number
Shin et al.	2017	**S/D**	☑	☐	☑	**S**	Failure cost Replacement cost	Seismic	Dissipators' thickness number

Tiainen et al.	2017	S	☑	☑	☐	S	Weight Material cost Fabrication cost	Stresses Serviceability Buckling Geometrical boundaries	Truss height Joints location Cross-section
Truong et al.	2017	S/D	☑	☐	☑	S	Material cost Connection cost	Stresses Serviceability Inter-story drift	Cross-section Connection type
Kripka et al.	2018	S	☑	☑	☑	S	Material cost	Stresses Serviceability Buckling	cross-section Shape parameters Topology
Rezazadeh et al.	2018	S/D	☑	☐	☐	M	Structural cost Seismic energy	Seismic Inter-story drift	Cross-section
Shallan et al.	2018	S/D	☑	☐	☑	S	Material cost Connection cost	Stresses Serviceability Geometric boundaries	Cross-section Connection types

Truong et al.	2018	**S/D**	☑	☐	☑	**S**	Material cost Connection cost	Stresses Inter-story drift Constructability Cross-section Connection type
Braga et al.	2019	**S/D**	☑	☐	☑	**S**	Material cost Work price	Serviceability Inter-story drift Cross-section Yielding force Yielding displacement
Mavrokapnidis et al.	2019	**S**	☑	☐	☑	**S**	Material cost Work price	Stresses Serviceability Cross-section
Barg et al.	2020	**S**	☑	☐	☐	**M**	Material cost Displacement (DPF)	Stresses Serviceability Buckling Cross-section
Cicconi et al.	2020	**S**	☑	☑	☑	**M**	Weight Material cost	Stresses Serviceability
Gatheeshgar et al.	2020	**S**	☑	☐	☐	**S**	Weight Material cost	Stresses Serviceability Cross-section

Drewniok et al.	2020	**S/D**	☑	☐	☐	**S**	Lightest Beam	Stresses Serviceability Natural frequency	Cross-section
Rezazadeh et al.	2020	**S/D**	☑	☐	☐	**M**	Weight Seismic energy	seismic Inter-story drift	Cross-section
Tu et al.	2020	**S/D**	☑	☐	☐	**M**	Energy dissipation Material cost	Stresses Serviceability Inter-story drift	Cross-section
Xu et al.	2020	**S/D**	☑	☐	☐	**S**	Material cost	Serviceability Inter-story drift	Cross-section
Alhendi et al.	2021	**S**	☑	☑	☑	**S**	Material cost Fabrication cost Painting cost	Stresses Serviceability Constructability	Cross-section
Chen et al.	2021	**S**	☑	☐	☑	**S**	Weight	Stresses Buckling	Slenderness Element number
Cucuzza et al.	2021a	**S**	☑	☐	☐	**S**	Weight Global stiffness	Stresses Buckling	Cross-section

Ghaderi et al.	2021	**S/D**	☑	☐	☐	**S**	Weight Life Cycle Cost	Stresses Geometric boundaries Seismic Cross-section
Gholizadeh et al.	2021	**S/D**	☑	☐	☐	**M**	Initial cost Damage (ODI)	Stresses Geometric boundaries Seismic Cross-section
Kaveh et al.	2021	**S**	☑	☐	☐	**S**	Material cost Fabrication cost	Stresses Serviceability Geometric boundaries Cross-section Holes features Slab thickness
Saedi et al.	2021	**S/D**	☑	☐	☑	**S**	Weight	Stresses Serviceability Geometric boundaries Cross-section Wall arrangement
Sarcheshmeh et al.	2021	**S/D**	☑	☐	☐	**S**	Initial cost Life Cycle Cost	Stresses Serviceability Geometric boundaries Cross-section

						Stresses Serviceability Prestress losses Buckling	Material cost				Cross-section Truss height Prestressing eccentricity
Aydin et al.	2022	**S**	☑	☑	□		**S**				

Review table of the application of optimization strategies for minimum environmental cost of steel structures

Ref.	Year	**S**tatic **D**ynamic	Size	Shape	Topology	**S**ingle/**M**ulti Objective	ID-OF	Design criteria	Design Variables
Marks et al.	1997b	-	☑	☑	☐	**M**	Construction cost Annual heating cost	Geometric bounds	Building's form Wall geometry Window geometry
Caldas et al.	2002	**S**	☑	☐	☐	**S**	Annual energy consumption	Geometric bounds	Window geometry
Coley et al.	2002a	-	☑	☑	☑	**S**	Energy use	-	Wall geometry Roof geometry Window position Building form Building orientation
Caldas et al.	2003	-	☑	☑	☐	**S**	Annual energy consumption	Openings geometry	Window geometry Roof geometry
Caldas et al.	2003	-	☑	☑	☐	**M**	Materials cost Annual energy consumption	Layer's material	Window geometry Window position Building geometry

Wang et al.	2005a	-	☐	☑	☐	**M**	Life cycle cost Life cycle environmental impact Geometric bounds Glazing Window geometry Window type Building orientation Envelope
Wang et al.	2005b	**S**	☑	☑	☐	**M**	Life cycle cost Life cycle environmental impact Geometric bounds Layer's material Overhang depth Window type Building orientation Building shape Envelope
Wang et al.	2006	-	☐	☑	☐	**M**	Life cycle cost Life cycle environmental impact Geometric bounds Window type Window geometry Window type Building orientation Building shape Structural system Envelope Overhang depth
Flager et al.	2009	**S**	☑	☐	☐	**S/M**	Structural cost Energy cost Geometric bounds Daylight performance Cross-section Building orientation Building geometry Window-to-wall ratio

Paya Z. et al.	2009	**S**	☑	☐	☐	**S**	Materials cost Embedded CO_2 emissions	Cross-section Material type
Yi et al.	2009	-	☐	☑	☐	**S**	Geometric bounds Conduction, radiation, convection performance Heat flow indoor/outdoor	Building form
Magnier et al.	2010	-	☑	☐	☐	**M**	Geometric bounds Heating/cooling performance Thermal comfort Energy consumption	Envelope Window geometry HVAC system
Suga et al.	2010	-	☑	☐	☐	**M**	Glass cost Energy consumption Uniformity Draft performance Daylight performance Uniformity on desk surface	Window geometry Glass type

Tuhus et al.	2010	-	□	□	**S**	Annual total energy cost Life cycle cost Annual electricity use Annual gas use	Geometric bounds	Aspect ratio Orientation Building geometry	
			☑	☑					
Raphael	2011	-	☑	□	**M**	Cost Solar thermal load Lighting energy	Geometric bounds	Window geometry Shade dimensions	
			☑	☑					
Camp	2013	**S**	☑	□	**S**	Material cost CO_2 emissions	Geometric bounds Capacity checks Reinforcement ratio Deflection	Cross section Reinforcement area	
				□					

De Medeiros et al.	2014	**S**	☑	☐	☐	**S**	Cost CO_2 emissions Equivalent CO_2 emissions Global Warming Potential Eco indicator	Geometric bounds Reinforc. rate	Cross-section Reinforc. area
Antipova et al.	2014	**S**	☑	☐	☐	**M**	Total cost Total environmental impact	Type selection	Window type Solar panels type Envelope
Quaglia et al.	2014	**-**	☐	☑	☐	**S/M**	Deflection function Total thermal energy load	Geometric bounds	Wall geometry Roof geometry
Park et al.	2014	**S**	☑	☐	☐	**S**	Material cost CO_2 emissions	Geometric bounds Reinforcement ratio Capacity checks	Cross section Material strength Reinforcement diameter

Yeo et al.	2015	**S**	☑	☐	☐	**S**	Materials cost CO_2 footprint	Serviceability Strength	Cross-section Reinforcement area
Yepes et al.	2015	**S**	☑	☐	☐	**M**	Materials cost CO_2 footprint	Limit states	Cross-section Reinforcement area
Lu et al.	2015	**-**	☑	☐	☐	**S/M**	Total cost CO_2 emissions Grid interaction index	Geometric bounds Power performance	Renewable energy systems dimensions
Echenagucia et al.	2015	**-**	☑	☑	☐	**M**	Energy for heating, cooling, lighting	Geometric bounds	Window type, shape, position Glazing Wall thickness

Negendahl et al.	2015	-	☑	☑	□	**M**	Capital cost of the façade Energy use Thermal overheating Daylight	Geometric bounds	Façade geometry Plan geometry
Brunelli et al.	2016	**S**	☑	□	□	**M**	Net Present Value of investment Thermal energy consumption CO_2 emissions Comfort level	Power performance Energy performance	Building footprint Renewable system Electric system Installation variables
García-S. et al.	2016	**S**	☑	□	□	**M**	Materials cost CO_2 emissions	Limit states	Cross-section Material strength
Schwartz et al.	2016	**S**	☑	□	□	**M**	Life cycle cost Life cycle carbon footprint	Geometric bounds	Window type Envelope

Ascione et al.	2016	-	☑	☐	☐	**M**	Heating load Cooling load	Hours of discomfort	Window-to-wall ratio Glazing Envelope
Brown et al.	2016	-	☐	☑	☐	**M**	Embodied and operational energy	Geometric bounds	Roof geometry
Kaveh et al.	2017	**S**	☑	☐	☐	**S/M**	Materials cost CO_2 emissions	Geometric bounds Strength	Cross-section Material strength Reinforc. area
Mostavi et al.	2017	**S**	☑	☐	☐	**M**	Life cycle cost Life cycle emission Thermal comfort	Geometric bounds Material selection	Envelope Door type Glazing system

Li et al.	2017	**S**	☑	☐	☐	**M**	Life cycle cost Total percentage of cumulative time with discomfort Equivalent CO_2 emissions	Geometric bounds Material selection	Envelope Window geometry Building azimuth
Ascione et al.	2017	-	☑	☐	☐	**M**	Global cost Primary energy consumption Thermal discomfort hours	Geometric bounds Operative performance	Envelope HVAC system Building geometry

Gilles et al.	2017	-	☑	□	□	M	Life cycle cost Primary energy consumption CO_2 emissions Thermal comfort Compliance for hot water Boiler operating cycles Hours in solar collector	Geometric bounds Operative performance	Envelope Heating system
Mensinger et al.	2017	S	☑	☑	☑	S	Materials cost Environmental Product Declaration	Geometric bounds	Cross-section Slab thickness

Lagaros	2018b	S	☑	☐	S	Materials cost Equivalent CO_2 emissions Energy consumption	Geometric bounds	Cross-section Slab thickness
Brütting et al.	2018	S	☑	☐	S	Mass minimization Cut-off mass Embodied energy	Geometric bounds Buckling Stress capacity Deformation bounds Assignment of available stock elements	Cross-section
Penadés-P. et al.	2019	S	☑	☐	S	Embodied energy	Limit states Cracking Stress Vibration	Cross-section Slab and web geometry

Mavrokapnidis et al.	2019	**S**	☑	☐	**S**	Materials and construction cost CO_2 emissions	Eurocode requirements Geometric bounds	Cross-section
Ascione et al.	2019	-	☑	☑	**M**	Life cycle global cost Investment cost Equivalent CO_2 emissions Primary energy consumption	Geometric bounds Performance Type selection	Building geometry Envelope Energy systems
Gatheeshgar et al.	2020	**S**	☑	☐	**S**	-	Eurocode requir. Geometric bounds	Cross-section Moment capacity

Whitworth et al.	2020	**S**	☑	□	□	**M**	Structural optimizations Embodied energy	Limit states	Cross-section Shear and moment capacity
Drewniok et al.	2020	**S**	☑	□	□	**S**	-	Limit states Vibration Deflection	Cross-section Shear and moment capacity
Al-Saandi et al.	2020	-	☑	□	□	**S**	Life cycle cost Annual energy consumption	Regional guidelines Climate influence	Envelope Glazing Window-to-wall ratio
Santoro et al.	2020	**S**	☑	□	□	**S**	Material cost CO_2 emissions	Geometric bounds Brazilian standard checks	Cross section Reinf. area

Brütting et al.	2020a	**S**	☑	☐	☐	**S**	Mass minimization Cut-off mass GHG emissions	Geometric bounds Stress capacity Deformation bounds Assignment of available stock elements	Cross section
Brütting et al.	2020b	**S**	☑	☐	☐	**S**	Mass minimization Cut-off mass Environmental impact	Geometric bounds Stress capacity Deformation bounds Assignment of available stock elements	Cross section

									Building orientation
									Window-to-wall ratio
								Geometric bounds	Envelope
								Climate influence	Window type
									HVAC system
									Photovoltaic system
							Photovoltaic power generation		
							Embodied energy		
Ansah et al.	2021	-	☑	☑	□	**M**	Operational energy		
									Slab dimensions
									Formwork type
								Brazilian standard checks	Profile dimensions
Arpini et al.	2021	**S**	☑	□	□	**S**	CO_2 emissions		Degree of beam-slab interaction

Martínez-M. et al.	2022	S	☑	☐	☐	M	Materials cost CO_2 emissions	Limit states Eurocode requirements	Cross-section Material strength
Guimarães et al.	2022	S	☑	☐	☐	M	Materials cost CO_2 emissions	Brazilian standard checks	Cross-section Moment of inertia Plastic section modulus
Ching et al.	2022	S	☑	☐	☑	S	Compliance Global Warming Potential	Geometric bounds Stress	Cross-section
Van Cauteren et al.	2022	S	☑	☐	☐	M	Life cycle cost Environmental Life Cycle cost	Geometric bounds	Cross-section

1.12 Conclusion and summary vision

The review paper suggests the main trends in the structural optimization field. 446 papers were classified into categories and sub-categories by identifying the contributions with the same application fields and similar optimization strategies. Mainly, papers were distinguished in size, shape, topology and all the possible hybridizations among these three levels of optimization. Moreover, some sections were characterized by a further classification based on the type of application case study (i.e. buildings, bridges, etc.). Following, the results of the review will be summarized in order to emphasise eventual trends or significant outcomes pointed out by the candidate:

- As expected, most of the collected papers focused on size optimization independent of the type of adopted OFs (i.e. structural performance, cost and environmental impact). Size optimization, in fact, represents the first and less complex level of optimization which is already useful for preliminary design and first assessments of the structural cost savings.

- With specific regard to pure size optimization, classification based on thematic subjects or application cases was adopted. Specifically, structural optimization was employed in order to investigate the non-linear behaviour of multi-storeys multi-bays steel frames, under seismic action, the role of connection flexibility and the soil-structure interaction. The review revealed that the optimization process was largely used for the seismic analysis and dynamic identification of various steel structures (i.e. trusses, frames and bridges).

- The candidate observed little interest by researchers in pure shape optimization problems. The candidate believes this outcome derives from the common problems experienced in civil engineering. Normally, the geometrical layout of buildings or specific members of the structure is previously defined at the first stage of the design, hence, optimization can play a crucial role in optimal sizing only. However, a significant percentage of collected papers (5.6%) adopt algorithms when the size and geometric parameters are considered simultaneously.

- Topology optimization is the second most common approach chosen by authors. Mainly, they investigate the optimal position of bracing into the plane and

spacial frames. For this specific optimization, gradient-based algorithms were preferred over metaheuristic ones since the latter proved less efficient.

- Among the multi-level optimization approaches, simultaneous size and topology of steel structures is the most frequent one. The majority of the applications in this branch are entirely focused on detecting the minimum weight of the structure by varying the position of bracings and the cross-section properties.
- Since the computational effort required to perform size, shape and topology optimization, few papers were identified during the review process. Mainly, this level of complexity was experienced by adopting metaheuristic algorithms in order to face large-scale problems.

Once preliminary results of the review process are pointed out, a summary vision related to a lack of knowledge in specific branches of this subject or future trends can be found.

- A significant contribution still needs to be made in the area of multi-criteria or multi-objective problems. Due to the complexity of real civil engineering challenges, target functions with opposite trends must be simultaneously optimized. Moreover, a multi-level approach is fundamental for reducing the computational effort. For instance, structural performance and cost-based optimization could be treated by adopting a preliminary approach for the sizing of the structure and, then, by performing a detailed analysis taking into account design details such as performance and cost of the connections.
- No papers in which experimental campaigns were conducted in order to validate the results of the optimization have been recognized. This approach can be useful in order to check the goodness of the optimization process and realize more efficient prototypes like new connections' topology, retrofitting systems, etc.
- Especially for the branch related to the assessment of the optimal design of steel structures with variable connections' properties, the real challenge is to involve specific indexes entirely devoted to the assessment of the structural, economic and environmental cost since the production stage.
- Minimum weight is commonly confused with minimum cost. As demonstrated by the topics faced in the following Chapters, these two terms can even exhibit

opposite trends if practical issues related to constructability or design criteria at the initial stage of the construction are considered. In the future, more effort must be provided in order to make the field of structural optimization closer to real-engineering problems.

- It is worth noting that, among all the analyzed papers, a huge range of different structure typologies have been adopted by the authors as application case studies (i.e. buildings and tall buildings, bridges, turbines, etc.). However, few works have been recognized which investigate the optimal design of external retrofitting strategies like endo- or exoskeleton. In some countries, this specific consolidation system is attracting particular interest for its structural efficiency and versatility to improve the aesthetic aspect of old buildings. Interesting developments could result from the investigation of new efficient shapes of 2D (shear walls) and 3D (shell or plate) exoskeletons by varying their geometrical or topological features and type of connection with the existing structure.

  In conclusion, in the last decade, a significant effort was devoted to considering constructability issues in the structural optimization field. Specifically, in several papers, constructability constraints were introduced and refined analyses were adopted for the seismic analysis or, generally, the static and dynamic assessment of Civil structures. The implementation of accurate LCA analysis for the economic and environmental assessment of structures should be enriched through the realization of experimental campaigns in which the performance of innovative material could be validated through optimized numerical models. However, the crucial limit of the computational effort still nowadays represents the main obstacle to the spread of optimization techniques in real-world Civil Engineering Applications.
  Especially in these years, software houses are paying great attention to developing new power tools or open application programming interfaces into the Finite Element environment. In the future, principal efforts should be reserved to make the interoperability between FE software and optimization tools easier. On the other hand, the formulation of the optimization problem will always play a major role in the feasibility of the optimal design. The complexity derived by considering constructability issues at each construction stage or detailed design of specific components of the structures will only be faced if a reasonable decomposition in multi-step optimization procedures is implemented. In this way, the entire optimal design process, at each phase, will

be controlled and the computational effort reduced according to the industry needs and consistently with professional tasks.

Chapter 2

A machine learning approach for non-penalty constraint handling

2.1 Introduction

The majority of optimum design engineering problems can be modeled as continuous non-linear optimization problems, in which the original search space is reduced due to the existence of various constraints. In this introductory part of the present paper, firstly a general overview on evolutionary algorithm is presented with particular reference to swarm intelligent PSO algorithm. Then, a general constrained single-objective optimization problem over real domains is formed. Subsequently, existing methods for handling constraints in evolutionary computation are briefly described, with emphasis on the applications related to PSO algorithms.

Evolutionary algorithms (EAs) can be considered general and versatile tools for solving constrained optimization problems. The research interest for this class of optimizers is continuously increasing, mainly because objective functions (OF) and constraints are not required to be differentiable, continuous, or even explicit. In addition, no preliminary assumptions or a priori information are needed for solving constrained optimization problems by means of EAs. Moreover, EAs have a better global search ability compared to traditional numerical strategies (i.e., gradient-based algorithms) and a good starting design is not essential, since they operate on a population of individuals (coded candidate solutions of the optimization problem) which are efficiently handled during the evolutionary search. In contrast, EAs lack of well-

posed theories about their convergence and a large number of function evaluations and computational effort may be needed to converge. Within the framework of soft computing methodologies, a large number of non-conventional paradigms have been explored in order to create efficient and user-friendly optimizers. Nowadays, a wide variety of biological, social and physical metaphors has been analyzed and tested. In this study, the class of optimizers based on swarm intelligence, the so-called Particle Swarm Optimization (PSO) algorithms are considered, which have been proposed by Kennedy and Eberhart (1995a). To make some first comparisons with EAs we can refer to Quaranta (2020c). EAs are based on the simulation of natural Darwin's theory of evolution process with the survival of the fittest members, whereas swarm intelligence is based on collective behaviour in which each element move independently in search space. Thanks to somehow interaction among members of the community, the entire swarm shows intelligent global behaviour moving toward the optimal solution. This emerging class of optimizers is inspired by social behaviours observable in certain natural aggregations, such as bird flocking, fish schooling, or swarming of insects when they search for food, resources or protection. Every member of the population searches in its neighbourhood for the best outcome, learns from its own experience as well as from the other members' findings. Typically, if a member of the swarm discovers a desirable path to go, then the rest of the swarm will follow quickly. Thus, similar to other EAs, a PSO is a population-based optimizer and can solve complex non-convex optimization problems. PSO is based on the principle that social sharing of information among the individuals of the population can lead to optimum solutions. In fact, as affirmed in Plevris (2009b), every particle possesses a memory of the best position it has visited. Hence an appropriate combining of the self-experience of every particle with the global best position of the entire swarm, we can find a balance between exploration and exploitation. PSO is not complicated, resulting in an attractive tool for non-experts in the field of evolutionary computation. Several studies (e.g., Kennedy and Eberhart 2001) demonstrated that this optimizer has a good convergence rate. Based on the swarm intelligence theory, two different categories of PSO optimizers can be formalized:

- PSO algorithms in which it is assumed that a Newtonian dynamics regulates the movement of the particles.
- Quantum-behaved (Q-PSO) algorithms, in which the Newtonian hypothesis is rejected. In this case, the usual metaphors for PSO are replaced with physical

paradigms related to the movement of particles in the atomic or sub-atomic scale. Thus, the classical mechanic approach adopted for representing the dynamics in traditional PSO is replaced with the quantum mechanics process where the term "trajectory" is meaningless.

In this paper the first class of PSO optimizers is considered, in which according to Newton's theory, both position and velocity of the swarm can be determined simultaneously.

The use of evolutionary and swarm intelligence algorithms is constantly gaining popularity and many complex optimum design problems have been efficiently solved using nature-inspired memetic and meta-heuristic methods. In recent years, efficient optimizers based on swarm intelligence, namely, Particle Swarm Optimization (PSO) algorithms, proposed originally by Kennedy and Eberhart (1995a), have evolved. Several researchers have applied PSO algorithms to solve various types of structural optimization applications with continuous or discrete design variables, mainly for truss problems (Perez and Behdinan 2007; Li et al. 2009; Hasançebi et al. 2009; among others) and composite structures (Omkar et al. 2008; Bloomfield et al. 2010). Kaveh and Talatahari (2009) combined PSO with Ant Colony Optimization (ACO) and Harmony Search (HS) to obtain a hybrid scheme which has been implemented for the optimization of truss structures. Plevris and Papadrakakis (2011) combined PSO with an efficient mathematical programming method (Sequential Quadratic Programming (SQP)) to improve local convergence rate of PSO via gradient-based SQP and applied this hybrid scheme to optimize typical trusses. Rao and Sivasubramanian (2008) presented a computational system for the active vibration control of seismically excited buildings by combining a multi-objective PSO algorithm with a fuzzy logic controller. Ge et al. (2007) combined PSO with dynamic recurrent neural networks to perform speed control for ultrasonic motors. Begambre and Laier (2009) proposed a hybrid PSO that has been combined with a Simplex algorithm to deal with structural damage identification problems. Seyedpoor et al. (2009), implemented PSO for the optimum shape design of arch dams under earthquake loading using a fuzzy inference system and wavelet neural networks for the reduction of enormous computational cost. Under this perspective, Gholizadeh and Salajegheh (2009) performed optimal design of steel frames subjected to earthquake loading by swarm intelligence and advanced neural network metamodels. Similarly, Praveen and Duvigneau (2009) proposed the combination of PSO with radial basis

function approximations to solve demanding aerodynamic shape design problems. Furthermore, in order to reduce the computational cost Kalivarapu et al. (2009), presented the application of PSO in a parallel computing environment, in which digital pheromones have been used to coordinate swarms within the explored design spaces.

As one can find in Sengupta et al. (2018), in the last decades many hybrid algorithms were formulated in order to overcome the drawbacks of a single approach implementing different optimization strategies to find the optimal trade-off between exploration and exploitation, reducing computational efforts and avoiding the swarm to be entrapped into local sub-optimal solution. Both for constrained and unconstrained problems, there exist an integration with Genetic Algorithm operators named GA-PSO. These two approaches are referred to different contexts as one can check in Plevris (2009b): GA is the oldest approach and is referred to a biological context implementing genetic operators (selection, crossover, mutation) while PSO is based on a social context. These two strategies can be used both sequentially, where PSO allows to speed up global exploration whereas GA is mainly used in the exploitation phase and also to guarantee the diversity of members in the exploration phase, or using them in parallel. Other hybrid approaches integrate Differential Evolution Algorithm, DEA (by Storn and Price, 1997) with PSO. They are also known as SDEA (Swarm Differential Evolution Algorithm) or DEPSO. In this latter, at the origins, PSO and DEAs operators sequentially work alternating at odd and even iterations Das et al. (2010). In order to solve multi-objective problems an integration between PSO and Simulated Annealing (SA). Some approaches focused on implementing an adaptive updating of memory of particles' best solutions. Further hybridization was performed with Ant Colony Optimization (ACO) in order to find optimal solutions for highly non-convex problems. There are some other approaches based on Cuckoo Search (CS) which was inspired by behaviour of cuckoos integrated with Levy flight nature of birds. In these CSPSO approaches, cuckoos which reached a good solution communicate it to other members and then local exploitation of PSO is used. Later, another effort was done integrating CSPSO with DE. Always inspired by nature, researchers proposed Artificial Bee Colony (ABC) in parallel with PSO allowing exchanging information between swarm and bees and then many other developments. There was also an integration between PSO and other social metaheuristic approaches like Artificial Immune System (AIS), Bat Algorithm (BA), Firefly Algorithm (FA), Glow Worm Swarm Optimization (GSO). As explained in Sengupta et al. (2019),

using algorithms in parallel allows to improve each search mechanism thanks to information exchange between them. Mota et al. (2018) implement an hybrid PSO with Iterated Local Search (ILS) operator which is based on a deterministic hill climbing phase to improve local search around current gbest.

In order to solve constrained optimization problems with PSO several numerical techniques were incorporated for handling various types of constraints (e.g. Lagaros et al. 2023). It should be stressed that the selection of an appropriate technique for solving constrained optimization problems is a very important step because the performance of the optimizers strongly depends on the underlying mechanism for handling constraints. Motivated by this fact, various methodologies have been proposed in recent years and in this paper a new one is proposed. These methods have been classified by different authors into certain categories (see for instance the state-of-the-art review by Coello (2002), Koziel and Michalewicz (1999b); Michalewicz and Fogel (2013):

- penalty functions-based methods,
- methods based on special operators and representations,
- methods based on repair algorithms,
- methods based on the separation between OF and constraints,
- hybrid methods.

One of the most critical issues when searching multi-constrained non-convex design spaces is the preservation of the population diversity. The brutal elimination of the unfeasible solutions during the evolutionary search jeopardizes a complete exploration of the feasible domain. Therefore, it is crucial to maintain diversity in the population in order to keep track of the solutions inside and outside the feasible region as reported by Mezura and Coello (2002, 2005b). Moreover, it has been verified that several traditional penalty-based approaches may be not adequate to deal with highly complex search spaces, especially for problems in which several constraints are active in the optimum Runarsson et al. (2000). In these circumstances, unfeasible individuals may have very important information, thus, their role can be significant when looking for the global optimal solution.

An example of a very simple constraint handling approach in PSO consists in exploiting the randomness in velocity expression (2.4) and recalculate it until the new position of a particle becomes feasible. This simple approach is really time-consuming in particular for problems with a little feasible region. The penalty function approach allows to transform constrained problems into unconstrained ones (2015, 2016). Since its simplicity, the death penalty was the most widespread at the beginning. It introduced a strong penalty to unfeasible positions in order to consider only feasible ones. Later some authors proposed an adaptive penalty in order to evaluate the degree of violation of the unfeasible points. In fact, the optimum solution is often situated at the boundary between feasible and unfeasible region. Due to this fact, the degree of violation represents an extremely useful information in order to conduct the search along the boundary. Thanks to this latter information it is possible to implement a repairing operator which redirects the unfeasible point to the feasible region. It is important to set the velocity of redirected particles to zero in order to improve local boundary search, as illustrated in Plevris (2009b). As one can check also in Jordehi and Rezaee (2015), there also exist some approaches based on searching for feasibility operators. In Kohler et al. 2016 Kohler et al. (2016), a new variant called PSO+ based on preserving of feasibility is presented.

In the following, a review on classical formulation of PSO is illustrated and, after that, the new proposed approach is reported in detail. The main advantage of adopting a new non-penalty based constraint handling approach is related to the generality of the classification machine learning algorithm employed. As a matter of fact, the SVM depends only on the inner product of the data and it is able to generate predictive model. This latter represents substantially the boundary between the feasible positions of the swarm from the unfeasible ones. This predictive model is more adaptive than a typical penalty function approach because works fine both with discontinuous and non-linear constraints. In order to verify the convergence of the new code in terms of objective function, the proposed PSO-SVM algorithm is adopted in two numerical literature benchmark examples and it is compared with a PSO with penalty function code and with a genetic algorithm (GA) code. In the end part, the proposed PSO-SVM is adopted into the structural optimization field analyzing two examples. The first one is concerning the size optimization of a simply supported beam with constant rectangular cross section subjected to a constant load condition. The graphical obtained results highlight the generality of

the SVM to handle piecewise non-linear constraints with a good approximation in the neighbourhood of the optimal point and a roughly approximation elsewhere. The second example is regarding shape and size optimization of a warren truss plane beam which can be used in the design of a bridge. The PSO-SVM optimal results are compared in terms of total weight with the result obtained by Fiore et al. (2016b) where differential evolutionary algorithm (DEA) is adopted. The exact solution needs to be industrialized choosing a real existing profile dimensions both with a simple rounding-off of the optimal solution and with a more refined post-processing approach. Making a comparison between these latter industrial solutions the total weight of the structure does not change significantly and a simple rounding-off approach can be easily adopted by the designer without jeopardizing the entire optimization process.

2.2 Particle Swarm Optimization Algorithm

A typical single-objective optimization problem can be unconstrained or constrained. The mathematical form for an unconstrained one is

$$\min_{x\in\Omega}\{f(x)\} \tag{2.1}$$

whereas if the problem is constrained it is written as below

$$\begin{aligned} &\min_{x\in\Omega}\{f(x)\} \\ \text{s.t.}\quad &g_q(x)\leq 0 \quad \forall q=1,...,n_q \\ &h_r(x)=0 \quad \forall r=1,...,n_r \end{aligned} \tag{2.2}$$

in which $x=\{x_1,...,x_j,...,x_n\}$ is the design variable vector whose components are real numbers, $f(x)$ is the objective function (OF) to be minimized and Ω is a box-type search space. For instance, if $[x_j^l,x_j^u]$ is the admissible interval for the jth variable (x_j^l and x_j^u are its lower and the upper bounds, respectively), then

$$\Omega=[x_1^l,x_1^u]\times...\times[x_j^l,x_j^u]\times...\times[x_n^l,x_n^u] \tag{2.3}$$

where the symbol $\times$ denotes the Cartesian product between intervals. The constraints of the optimization problem defined by (5.4) can be inequalities $g_q(x)$ and/or equali-

ties $h_r(x)$. Without any loss of generality, all equalities can be easily converted into inequalities: therefore, only inequality constraints are considered in the following, e.g. $g_p(x) \leq 0$, for $p = 1,...,n_q,n_{q+1},...,n_p$, being $n_p = n_q + 2n_r$.

Evolutionary optimization algorithms were originally developed for solving unconstrained optimization problems, thus, they lacked mechanisms to handle the constraints of the problem at hand. Nonetheless, the unavoidable existence of several restrictions either from a mathematical and/or an engineering point-of-view leads to a huge contraction of the available design space, thus, reducing the number of the admissible solutions. It is obvious that the resolution of constrained optimization problems is much more complicated, especially when a large number of constraints are involved which can reduce the size and increase the complexity of the feasible domain dramatically. In these circumstances, both effectiveness and correctness of the evolutionary-based search can be jeopardized and the final results can be unsatisfactory. In fact, it is very probable to achieve an infeasible final solution if the search of the best objective function value does not take efficiently into account the imposed constraints. In contrast, the optimizer could be entrapped into a sub-optimal area if the exploration of the search space is conducted by taking into account feasible solutions only. Therefore, the implementation of effective constraint-handling mechanisms is considered a crucial issue for all biological inspired optimizers (Deb (2000b), Coello (2002), Wang et al. (2009), Mezura-Montes (2009b)). It is too evident that a competitive technique for handling constraints in evolutionary computation should be able to achieve the best possible compromise between conflicting requirements.

In the general formulation of PSO, the ith particle ($i = 1,...,N$, where N denotes the population size) at iteration k has two attributes, that are its velocity ${}^k\mathrm{v}_i = \{{}^k\mathrm{v}_{i1},...,{}^k\mathrm{v}_{ij},...,{}^k\mathrm{v}_{in}\}$ and position ${}^k x_i = \{{}^k x_{i1},...,{}^k x_{ij},...,{}^k x_{in}\}$. To protect the cohesion of the swarm, the velocity ${}^k\mathrm{v}_{ij}$ is forced to be (in absolute value) less than a maximum velocity $\mathrm{v}_j^{\max}$ with $\mathrm{v}^{\max} = \{\mathrm{v}_1^{\max},...,\mathrm{v}_j^{\max},...,\mathrm{v}_n^{\max}\}$. Typically, it is assumed that $\mathrm{v}^{\max} = \gamma(x^u - x^l)/\tau$, in which the time-related parameter $\tau = 1$ is introduced to assign a physical meaning to the formula and γ defines how far a particle can move starting from its current position Quaranta (2020c). Nevertheless, there is not sufficient degree of uniformity about the choice of γ whose numerical value can vary significantly, usually in the range $[0.1,1]$ and generally it is set to $\gamma = 0.50$. In addition, the initial values ${}^0 x_i$ for $i = 1,...,N$ are derived by generating pseudo-randomly the collection of N solutions within the assigned search space.

Moreover, ${}^{0}v_{ij}$ is pseudo-randomly generated using a uniform distribution between $-\mathrm{v}_j^{\max}$ and $+\mathrm{v}_j^{\max}$. For this purpose, the Latin Hypercube Sampling (LHS) technique has been iteratively used to generate the best initial population with minimum correlation between samples (see also Monti et al. (2010b). According to Plevris (2009b), making a comparison with EAs, it is possible to interpret the randomness in the setting of velocity particles as a "directional mutation operator". At iteration $k+1$ the velocity ${}^{(k+1)}\mathrm{v}_i$ and the position ${}^{(k+1)}x_i$ vectors are evaluated as follows

$$ {}^{(k+1)}\mathrm{v}_i = {}^{k}\mathrm{v}_i + c_1\,{}^{(k+1)}r_{1i} * \left[{}^{k}x_i^{Pb} - {}^{k}x_i\right] + c_2\,{}^{(k+1)}r_{2i} * \left[{}^{k}x_i^{Gb} - {}^{k}x_i\right], \tag{2.4} $$

$$ {}^{(k+1)}x_i = {}^{k}x_i + \tau\ {}^{(k+1)}\mathrm{v}_i \quad (\tau = 1). \tag{2.5} $$

where ${}^{k}x_i^{Pb}$ is the best previous position of the ith particle (also known as *pbest*)

$$ {}^{k}x_i^{Pb} = \begin{cases} {}^{k}x_i, & \text{if } f({}^{k}x_i) < f({}^{(k-1)}x_i^{Pb}), \\ {}^{(k-1)}x_i, & \text{otherwise.} \end{cases} \tag{2.6} $$

given that ${}^{0}x_i^{Pb} = {}^{0}x_i$. According to the adopted definition for ${}^{k}x^{Gb}$, one obtains two schemes of PSO. If ${}^{k}x^{Gb}$ denotes the best position among all the particles in the swarm (also known as *gbest*), then the swarm is designed to be fully informed or fully connected, thus, this approach is called global PSO. Conversely, if ${}^{k}x^{Gb}$ is evaluated for a smaller number of adjacent particles, then a "local-strategy" PSO is utilized by Chen et al. (2010). In (Quaranta 2020c), one can review which PSO originally has two topologies formulation: "*lBest PSO*" where multiple best particles influence only few neighbours and this limited information flow slow down convergence but increase the local search; "*gBest PSO*" where all particles influence each other in a fully connected net which bring to speed up convergence rate toward the global best particle position. The former approach is here used and all particles share information with each other about the best performer of the swarm, so that

$$ {}^{k}x^{Gb} = \arg\min_i \{f({}^{k}x_i^{Gb})\}. \tag{2.7} $$

The acceleration factors c_1 and c_2 in (2.4) (both positive scalars) are called *cognitive* and *social* parameters, respectively. Moreover, ${}^{(k+1)}r_{1i}$ and ${}^{(k+1)}r_{2i}$ are vectors whose terms are pseudo-random numbers uniformly distributed in the interval $[0,1]$, while the symbol $*$ denotes the term-by-term vector multiplication (Hadamard product

2009b). The superscripts on the left and the subscripts on the right denote that a different couple of pseudo-random vectors is needed for each particle at any iteration. It should be mentioned at this point that the formulation (2.4) is rather uncommon, in the sense that the majority of researchers in the field adopt a unique set of pseudo-random terms for any dimension of the search space. Nonetheless, Liang et al. (2006) pointed out that Eq. (2.4) yields better performance because of its problem-invariant property. The check on the maximum admissible velocity for any particle i is performed at iteration k in the following manner

$$ {}^{k}\mathrm{v}_{ij} = \begin{cases} \mathrm{sign}[{}^{k}\mathrm{v}_{ij}]\mathrm{v}_{j}^{\max}, & \text{if } {}^{k}\mathrm{v}_{ij} > {}^{k}\mathrm{v}_{j}^{max} \\ {}^{k}\mathrm{v}_{ij}, & \text{otherwise} \end{cases} \qquad \forall j = 1, \ldots, n. \tag{2.8} $$

where sign$[\cdot]$ is the sign operator. Another check is needed to verify that the particle is within the feasible search space

$$ \left({}^{k}x_{ij}, {}^{k}\mathrm{v}_{ij}\right) = \begin{cases} \left({}^{k}x_{ij}, {}^{k}\mathrm{v}_{ij}\right), & \text{if } x_j^l \leq {}^{k}x_{ij} \leq x_j^u \\ \left({}^{k}x_{ij} = x_j^l, {}^{k}\mathrm{v}_{ij} = 0\right), & \text{if } {}^{k}x_{ij} < x_j^l \\ \left({}^{k}x_{ij} = x_j^u, {}^{k}\mathrm{v}_{ij} = 0\right), & \text{otherwise} \end{cases} \tag{2.9} $$

The infeasible particles' velocity is fixed to zero in (2.9) for the next iteration to avoid considering any points outside the search space. Following iteratively this simple set of instructions, the swarm is expected to "fly" towards the global optimum of the problem. Since the required number of iterations L is not known *a priori* and therefore a stopping criterion is needed. In general, stopping criteria in PSO can be similar to those typically adopted for several EAs, see for instance Monti et al. (2010b) and its references. In this study, the search is terminated once a maximum number of iterations L is achieved. Although this strategy has the disadvantage to require some information about the problem or some preliminary runs, it appears to be useful when some parameters of the optimizer have to be iteratively tuned during the process. The interested reader is referred to the work by Li and Xiao (2007b) for a useful discussion on the selection of the number of iterations for PSO.

The performance of PSO strongly depends on choosing control parameter values, see Quaranta (2020c). Firstly, although it might seem better to choose swarm size N as bigger as possible it would lead to a very slow algorithm. Moreover, its choice should be based on the number of design variables n, but it has been experimentally

demonstrated which there is no substantial difference when N varies in the range $[20,100]$ for a maximum number of design variables $n_{\max} = 30$ (Quaranta 2020c). Furthermore version of PSO called micro-PSO (μPSO) which can work also with very small swarm size was also developed in years. Inertia weight and acceleration factors are also control parameter values which can affect the performances. The use of inertia weights in PSO has been proposed by Shi and Eberhart (1998), where the authors introduced this parameter in an effort to improve the convergence of the standard PSO. This concept is not new in soft computing community; actually, it is similar to the momentum term in a gradient descent artificial neural network training algorithm, or the temperature adjustment schedule for simulated annealing algorithms. Typical range of values for w was $[0.8,1.2]$. In a subsequent study by the same authors, a linearly decreasing inertia weight has been adopted **?**

$$ {}^{(k+1)}\mathrm{v}_i = {}^{k}w\,{}^{k}\mathrm{v}_i + c_1\,{}^{(k+1)}r_{1i} * \left[{}^{k}x_i^{Pb} - {}^{k}x_i\right] + c_2\,{}^{(k+1)}r_{2i} * \left[{}^{k}x_i^{Gb} - {}^{k}x_i\right], \tag{2.10} $$

with

$$ {}^{k}w = ({}^{0}w - {}^{L}w)\frac{L-k}{L} + {}^{L}w \tag{2.11} $$

in which ${}^{0}w$ and ${}^{L}w$ are the initial and the final values of the inertia weight, respectively. In principle, the inertia weight is a scaling factor of the previous velocity of the particle and its role is to control the exploration of the swarm: a large inertia weight will force larger velocity at the next generation and the swarm is expected to explore a larger region of the search space. In contrast, small inertia values have to be introduced to improve the local exploration. Some authors proposed also Non-Linear updating law for inertia weight e.g. in Plevris (2009b) define a three stages reduction of inertia weight using a cubic polynomial function in order to have fast reduction at initial stages and slower reduction at last iterations. One can check for further Non-Linear formulation about inertia weight in Sengupta et al. (2018). Concerning acceleration factors, some authors proposed varying models but usually they are assumed statically fixed to $c_1 = c_2 = 2$ (Quaranta 2020c). In another version of PSO, inertia weight is not considered and it is replaced with a constriction factor χ which multiply the whole second member of the velocity expression (2.4). The constriction factor expression is the following Quaranta (2020c)

$$ \chi = \frac{2}{2 - \varphi - \sqrt{\varphi^2 - 4\varphi}}, \quad \text{with } \varphi = c_1 + c_2 > 4. \tag{2.12} $$

According to Quaranta (2020c), typically $\varphi = 4.1$ which implies $\chi = 0.729$ by setting the same value to acceleration factor equal to $c_1 = c_2 = 2.05$. Although dynamic (deterministic and non-deterministic) models exist for social/cognitive factors and inertia weights, in this study it is assumed which all of them are constant values equal to $c_1 = c_2 = 2$, ${}^0w = 0.90$ and ${}^Lw = 0.40$ (Perez et a. 2007).

Additionally, a predetermined maximum number of iterations for each problem is not usually known in advance, therefore, one can refer to the suggestions of Li and Xiao (2007a) or conduct experimental trial and error tuning of the minimum k_{max}, which allows one to achieve the optimum, reducing the overall computational cost. Later on, for the sake of improving the exploration capacity of the swarm, Shi and Obaiahnahatti (1998) introduced an inertia weight term ${}^kw$ multiplied to the current kth velocity in the update rule (2.4). This parameter can be a constant or a variable with respect to the iterations flow, e.g., from an initial value ${}^0w$ to a final one ${}^Lw$ with a linearly decreasing law, but there are also many other variants in Sengupta et al. (2019). The performance of the algorithm is strongly affected by the choice of the parameters such as the swarm size N, usually set in a range of $[20, 100]$ with $n \leq 30$.

One of the most important aspects to enhance the PSO performances is to improve the way in which the information are exchanged among the particles. With efficient information sharing, the swarm can exhibit a better collective convergent behaviour. The information exchange is related to the structure of the neighbourhood of each particle, which is denoted as *neighbourhood topology*. This kind of implementation is also called a local PSO model or simply *lbest model* to differentiate it from the classical so-called global PSO model or simply *gbest model* Martí et al. (2018), Quaranta et al. (2020a), Sengupta et al. (2019). The classical gbest model approach can also be regarded as a neighbourhood strategy in which the neighbourhood is composed of the entire population. In this sense, the swarm is denoted as fully informed or fully connected. A schematic graphical representation of the swarm with the information flows is depicted in Figure 2.1a. The main negative aspect of this latter strategy is the greater inclination to premature convergence. If the global attractor gbest is entrapped in a local minimum, the entire swarm may probably fall down in the same local minimum without a sufficient exploration capability. The enhancement of the PSO was performed by a counter-intuitive approach which relies on slowing down the rapid convergence attitude of the PSO through channelling and limiting the information exchange, the neighbourhood con-

cept indeed Martí et al. (2018), Quaranta et al. (2020a), Sengupta et al. (2019). In the lbest models, it is necessary to define, firstly, the structure of the neighbourhood which controls the way in which the particles are interconnected and, secondly, the size of the neighbourhood which affects the influence of the swarm on each particle Martí et al. (2018). Considering the most popular time-invariant neighbourhood topologies, the ring topology is one of the easiest to be implemented, and it has also been adopted in the present study. As illustrated in Figure 2.1b,c, each particle in this topology forms a neighbourhood considering the nearest particles (nearest indices in a vector of positions), resulting in an ideal circular interconnection. The total number of the particles which belongs to the neighbourhood is denoted as radius R, as depicted in Figure 2.1b, in which $R = 2$, and (c), in which $R = 4$. These methods can be implemented considering that each particle in the numerical vector has a unique index, therefore, each particle can unequivocally be selected to enter in a neighbourhood through its index Medina et al. (2009), as schematically depicted in Figure 2.2. A very great number of different neighbourhood topologies were developed in the last decades as showed in Medina et al. (2009), Schmitt (2015). Some other implementations also involve a dynamic update of the neighbourhood size, which identifies new types of lbest models which are denoted as multi-populations or multi-swarm PSO, such as in Liang and Suganthan (2006).

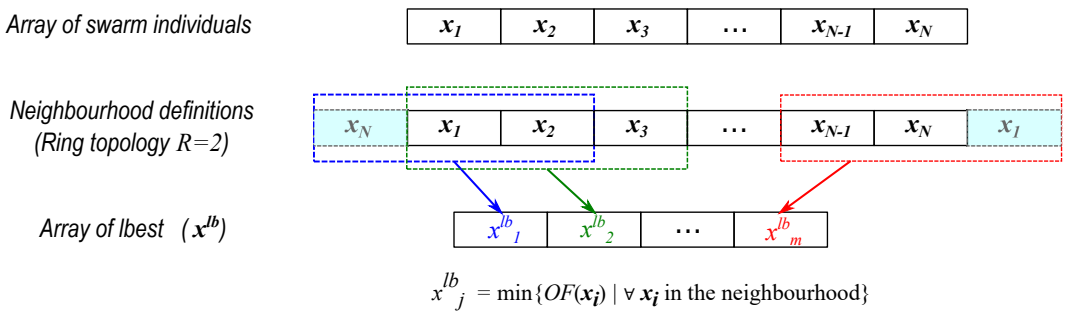

Fig. 2.2 Graphical schematization of the Ring topology implementation (R = 2).

2.3 Constraint Handling in the proposed framework

In this paper, a new non-penalty based constraint handling approach is implemented using the machine learning method SVM. This machine learning approach is based on statistical learning theory (Vapnik 1999). During the learning process, the ma-

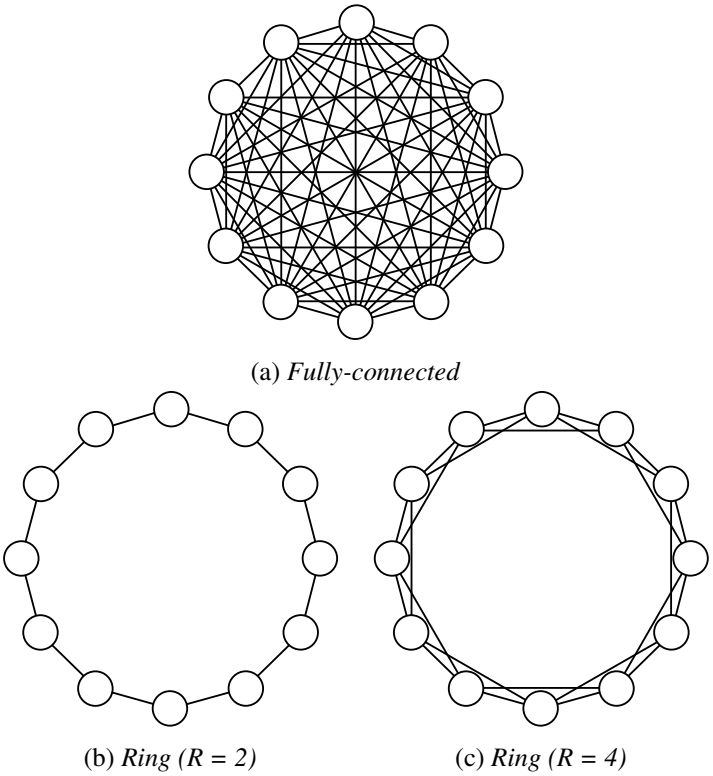

(a) *Fully-connected*

(b) *Ring (R = 2)* (c) *Ring (R = 4)*

Fig. 2.1 Some examples of PSO Neighborhood Topologies.

chine learns from examples contained in a known training data set which could be composed of both input and output data (supervised) or only input data (unsupervised) (Bishop 2006). The SVM is able to map the input data to another space (feature space) usually with higher dimension (Cristianini et al. 2002) where the data are linearly separable and it will search the optimal separating hyperplane according to the principle of the maximal margin Cortes et al. (1995). The transformation is performed by a Kernel Function which represents the inner product in the feature space (kernel trick) (Bishop 2006). Then, after the re-mapping the optimal separating hyperplane in the starting design space, the result of this process is the definition of a predictive model that could map the output of other new input data. If the output is a variable from a finite set which represents the class (or category or label) of the input data, the problem is called classification (or pattern recognition) problem (Bishop and Murphy 2006, 2012). After a training phase on the current positions of the swarm, the new trial positions are labeled as feasible or unfeasible using the trained predictive model. In this case, since the algorithm has to separate feasible positions from unfeasible ones, it is performing a binary classification problem

(Bishop 2006). The SVM is based on the inner product in feature space, so it is possible to avoid explicitly writing the transformation of training data into the feature space, but it is possible to directly operate defining a proper kernel function, as stated in Bishop and Nasrabadi (2006). This approach is called in Cristianini et al. 2002 as implicit mapping or implicit embedding. According to Li et al. (2006), typical widely spread kernel functions are polynomial kernels and Gaussian kernel (Bishop and Cristianini 2006, 2002) which is the isotropic form of the radial basis kernels, RBF (Murphy (2012)). In the proposed approach the Gaussian kernel is adopted. Multilayer perceptron kernels (MLP) or sigmoid kernels, typically used in Neural Networks, are examples of not Mercer kernel which are not representing the inner product in feature space, as reported in Murphy (2012). It can occur that training data are non-separable i.e. data which cannot be linearly divided without committing a certain error (Cortes et al. 1995). In this case, the SVM operates with a soft margin defining a hyperplane minimizing the error. This is governed by a penalty coefficient $C > 0$ also know as regularization parameter which controls the tolerance on training classification errors and the margin position related to the complexity of the model (Bishop and Nasrabadi (2006), Murphy (2012), Li et al. (2006)). For the proposed algorithm, it was found that a good trade-off between accuracy and computational effort is obtained using C between 100 and 1000.

2.4 Proposed PSO-SVM approach

In the proposed approach the aim is to integrate the classical PSO algorithm with SVM classification algorithm in order to separate feasible positions from the unfeasible ones. The main idea is to reduce the search space as also stated in Kohlet et al. (2016).

Starting from the initial random population, it is possible to classify feasible initial points than the unfeasible ones with respect to the constraints. In general, through the SVM, a hyperplane which linearly divides data is constructed in any higher-dimensional space (feature space) and it is possible to reconstruct a non-linear boundary in the starting design space. Indeed, this is a way to reduce the search space because after the learning phase (train the SVM model) it can predict which points are in the feasible design region described by the SVM model and which are in the unfeasible one. Obviously, to have a great result starting from the beginning,

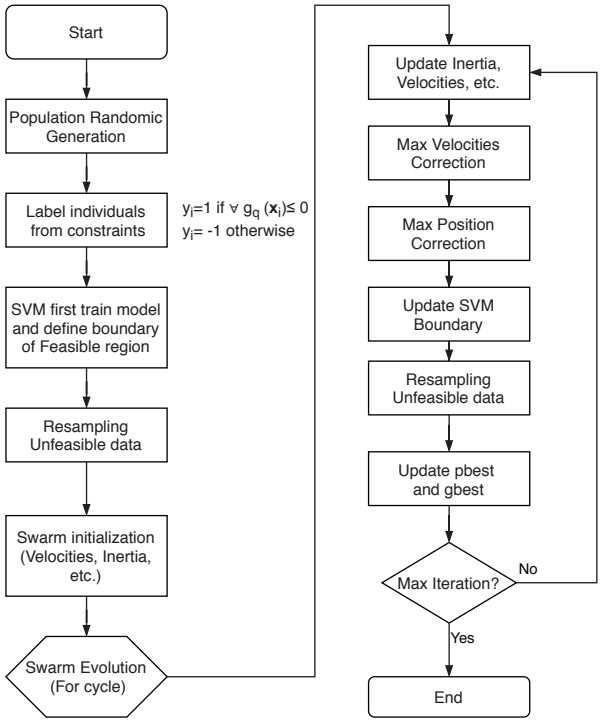

(a) *General Flowchart of the proposed algorithm*

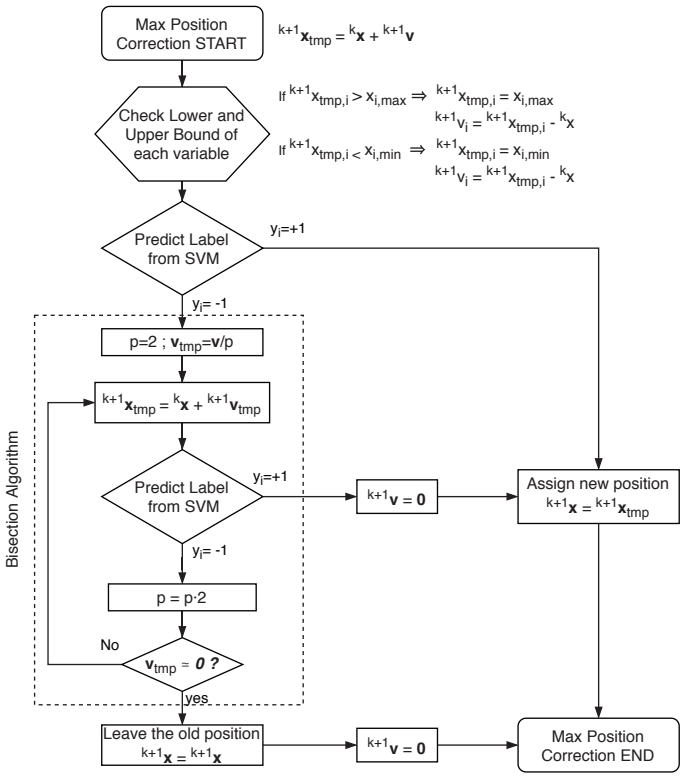

(b) *Flowchart of "Max Position Correction" block*

Fig. 2.3 Flowchart of the proposed PSO-SVM algorithm

it should need a massive initial population to construct a very accurate boundary which follows the theoretical one. In normal PSO, at every generation, the swarm from last generation move in a new position, hence new points are available to train a new better SVM model. With this incremental approach during the evolutionary stage of PSO, a new boundary is calculated at each generation adding the new swarm position to the previous ones. In general PSO constraint handling techniques do not work very well with equality constraints but they are more suitable for inequality constraint only. Therefore, the problem has to be expressed in the form of (5.4) without equality constraints. For a maximization problem with objective function $f(x)$, it is sufficient consider $-f(x)$ to transform it into a minimization problem. The proposed algorithm is implemented in Matlab® code.

In Figure 2.3 (a) the flowchart of the proposed algorithm is shown. At first, the initialization phase of the swarm adopts the LHS technique to generate the initial population with a minimum correlation between samples (see also Monti et al. Monti et al. (2010a)). Then this initial swarm is labelled into the design space regarding to the inequality constraints. Since these latter are defined as $g_q \leq 0$, if at least one of them is greater than zero the entire n-tuple (which is a single individual candidate solution) is labelled as unfeasible ($y_i = -1$) otherwise it is labelled as feasible ($y_i = +1$). In any case, for some problems with a very narrow search space, SVM really struggles to work properly. In fact, preserving only feasible points in wide unfeasible space and really narrow feasible region leads to instabilities and the algorithm probably fail to find the optimum. To improve the performance of the algorithm, a relax constraint function $\psi_i(k)$ is defined, wherein the subscript i refers to i-th constraint whereas the k refers to the current generation. This approach leads to enlarging the real feasible space to a fictitious wider one using relaxation of the constraints. This means that the real constraints are “moved" from their actual position to a fictitious one through a proper choice of $\psi_i(k)$ which is not trivial to generalize. This procedure acts as substituting the original inequality constraints with the following relaxed constraints:

$$g_{i,k}(x) \leq \psi_i(k) \qquad \Longrightarrow \qquad g_{i,k}(x) - \psi_i(k) \leq 0. \tag{2.13}$$

The $\psi_i(k)$ factor is tuned on the standard deviation $\sigma_{u,k}$ of the amount of all unfeasible points detected in all generations until the current one. This approach allows a better exploration in the first generations and then it could be forced to zero imple-

menting a decreasing function which directly depends on the current generation k and the number of maximum generations k_{max}. Defining a further reduction factor λ of the standard deviation directly chosen by the user, the following relaxation functions are implemented:

- Constant Relax:

$$\psi_i(k) = \lambda \sigma_{u,k};$$

- Piecewise Constant Relax:

$$\psi_i(k) = \begin{cases} \lambda \sigma_{u,k}, & \text{if } k \leq k_{max}/2 \\ 0, & \text{otherwise;} \end{cases}$$

- Linear decreasing Relax:

$$\psi_i(k) = \lambda \sigma_{u,k} - \frac{\lambda \sigma_{u,k}}{k_{max}} k;$$

- Piecewise Linear decreasing Relax:

$$\psi_i(k) = \begin{cases} \lambda \sigma_{u,k} - \frac{2\lambda \sigma_{u,k}}{k_{max}} k, & \text{if } k \leq k_{max}/2 \\ 0, & \text{otherwise;} \end{cases}$$

- Parabolic decreasing Relax:

$$\psi_i(k) = \lambda \sigma_{u,k} - \frac{\lambda \sigma_{u,k}}{k_{max}^2} k^2;$$

- Piecewise Parabolic decreasing Relax:

$$\psi_i(k) = \begin{cases} \lambda \sigma_{u,k} - \frac{4\lambda \sigma_{u,k}}{k_{max}^2} k^2, & \text{if } k \leq k_{max}/2 \\ 0, & \text{otherwise;} \end{cases}$$

The proposed algorithm implements SVM with soft margin with regularization parameter $C = 100$. Indeed, respect to a hard margin, to speed up the algorithm it is numerically convenient to adopt a high box-constraint value, e.g. between

100 and 1000, allowing a certain misclassification rate but assuring all the possible solutions lie in the feasible space boundary respecting the constraints with a certain engineering tolerance.

After the training phase, the unfeasible points of the initial population have to be re-sampled in the feasible region.So, the unfeasible points are randomly sampled with LHS technique in the entire design space and they are discarded and sampled again until their label becomes $y_i = +1$.

At this point, the initial velocity of the particles is randomly sampled always using LHS and then the evolutionary phase of the algorithm can begin. The velocity for the next generation is calculated as in equation (2.4) but it is necessary to check if it respect the allowable maximum velocity as in (2.8) (“Max Velocities Correction" block in Figure 2.3 (a)). The next block "Max Position Correction" is a fundamental step because it is the check of the feasibility of the position given by (2.5) and for the sake of clarity it is expanded in Figure 2.3 (b). A temporary position are computed with equation (2.5). Then, a first possibly corrections of the temporary positions can be performed in order to maintain the particles inside or at least on the edges of the hyper-rectangle design space Ω. If the temporary position label is $y_i = +1$ then the new temporary position lies in the feasible region and so it is accepted. Otherwise, if the label is negative a simply bisection approach is performed. The velocity vector which leads to the temporary position of a particle is firstly divided by $p = 2$ and a new temporary position is obtained. If the label of this new temporary position becomes positive, so this new position is accepted for the next generation. Otherwise, if it is still negative, the algorithm will increment p doubling it, getting a new temporary velocity vector and a new temporary position to label and so on. When all the elements of temporary velocity vector tend to zero, it is possible to leave the original position for the next generation. In this way the particle can move only if the destination position is into the feasible region, otherwise it does not move anywhere during the current generation.

At the end of the evolutionary stages, new positions are available to take into account in order to update the SVM boundary increasing the database of training set for the SVM model. As before, it is necessary to label the new points from the constraint expressions.After the training phase, a new boundary is defined but some of the points which were inside the previous boundary now may lie outside of the new region. In this case, it is necessary to re-sample these point before using LHS

until their label become positive. Despite this latter naive approach may slow the algorithm, it is beneficial for the diversity of the population, allowing new starting search positions. The update of the gbest is performed only on the real feasible points with respect to the original constraints and not the relaxed ones. This procedure ensures the algorithm performs good results also using a constant relax constraint function during the generations. In fact, at each generation, it will update the global optimum point (gbest) looking to the minimum objective function value only of those points which lie in the real feasible region. A further strategy to improve the behaviour of the PSO is reducing the maximum possible velocity range of the particles, governed by γ, updating this latter during generations. In the proposed algorithm it is set $\gamma/2$ starting from $k_{max}/3$ then it is set to a minimum value e.g. $\gamma = 0.1$ in the last generations from $2k_{max}/3$ to k_{max}, where k_{max} represent the max allowable generations. The stopping criterion of the algorithm is the achievement of a maximum number of iterations. It is possible that there exists an entire front of optimal solutions so one has always to check the convergent history of best solutions during the post-processing phase.

The proposed approach is firstly tested on some numerical mathematical literature problems which statements are reported in the Appendix. After that, two structural optimization problems are developed. To make some comparison of the results, in these last examples the objective function value is compared with the genetic algorithm of Matlab® and the PSO with penalty approach provided from the code proposed by Alam (2016b).

2.5 Numerical Example 1: Sickle Problem - Simionescu et al. (2004a)

The first numerical example (Simionescu et al. 2004a) is the benchmark test 1 stated in the Appendix also known as Sickle function. Since this optimization problem has two design variables, it can be depicted in a graphical representation in the bi-dimensional design space of the search process performed by PSO-SVM algorithm. In Figure 2.4 (a), the objective function and the constraints are graphically represented as a 3D graph and it is possible to notice that the objective function is

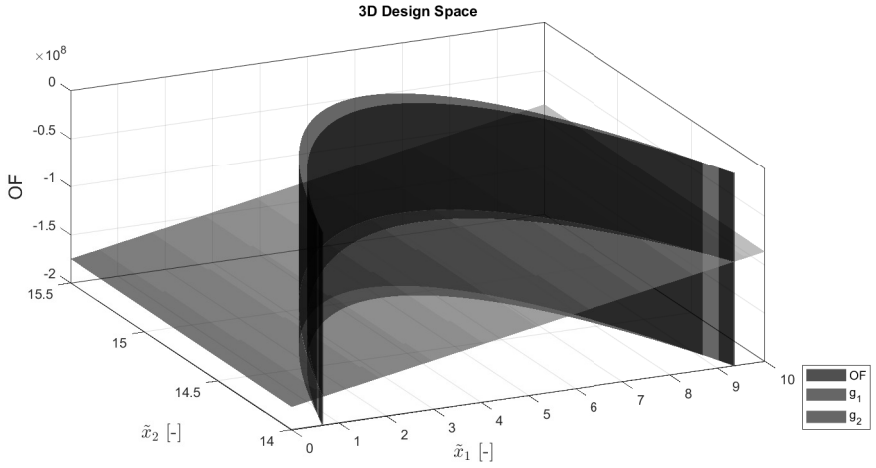

(a)

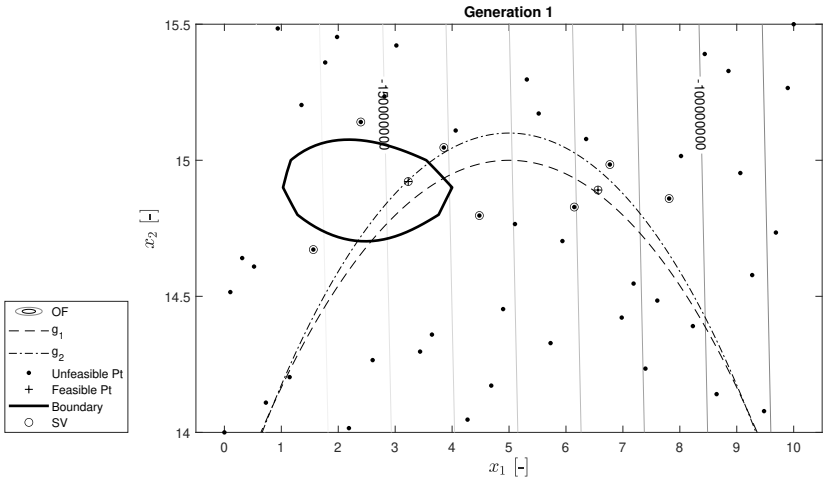

(b)

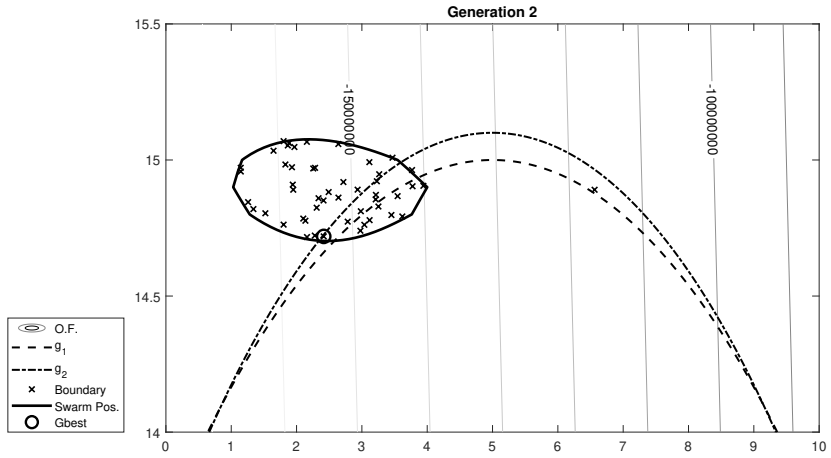

(c)

Fig. 2.4 Example 1 (Sickle Problem-Simionescu et al. 2004a), case No relax constraints function;
(a) 3D graph of Sickle problem design space; (b) Generation 1; (c) Generation 2

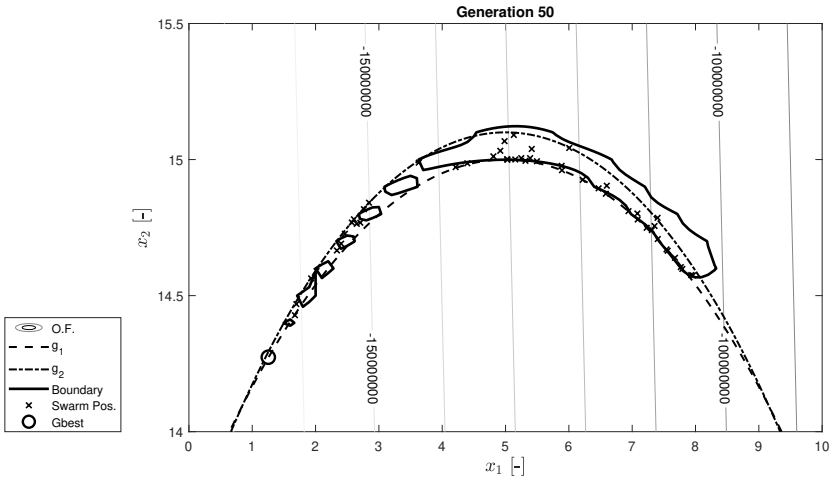

(a)

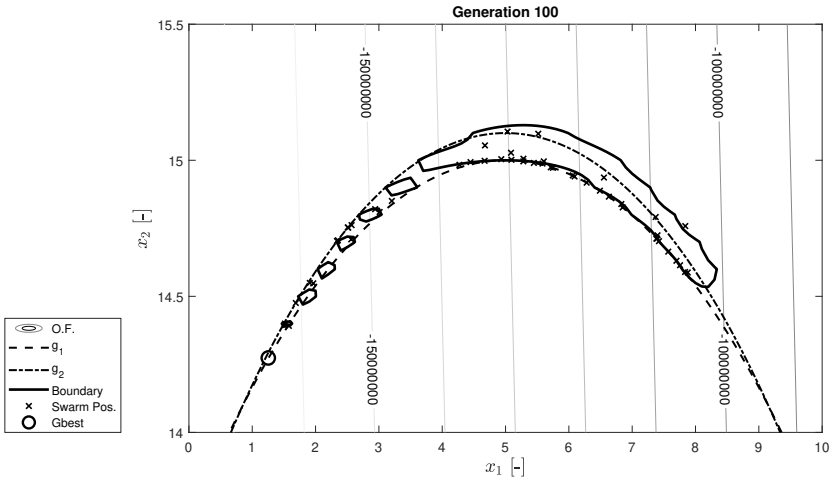

(b)

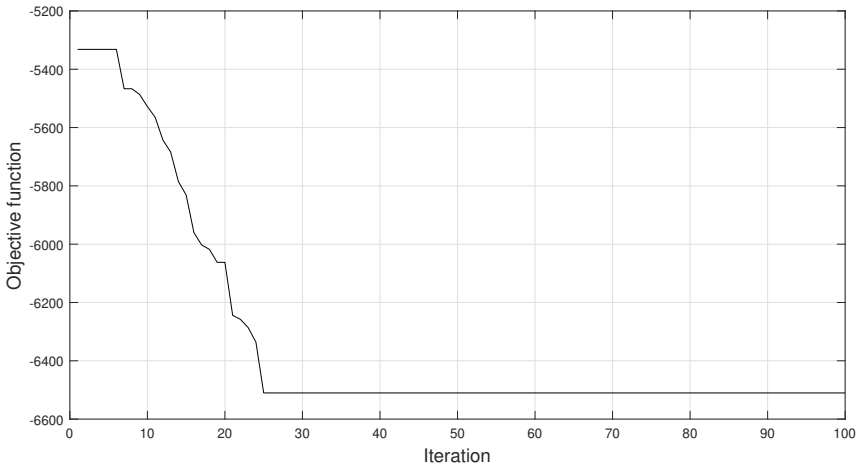

(c)

Fig. 2.5 Example 1 (Sickle Problem-Simionescu et al. 2004a), case No relax constraints function;
(a) Generation 50; (b) Generation 100; (c) Objective function history

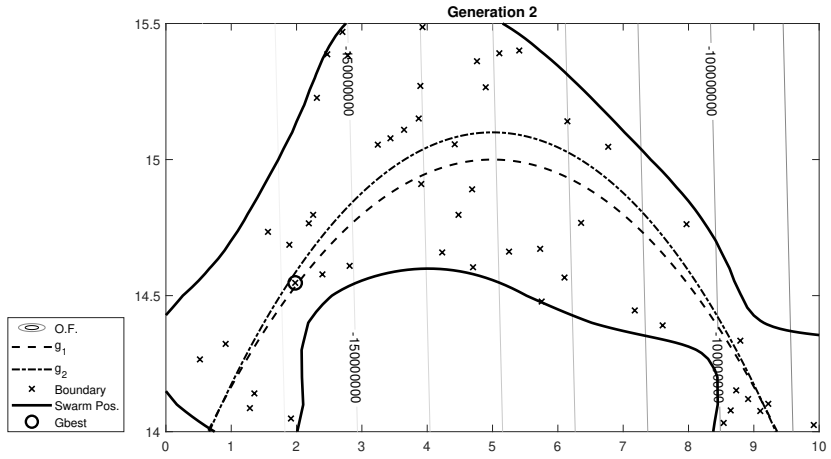

(a)

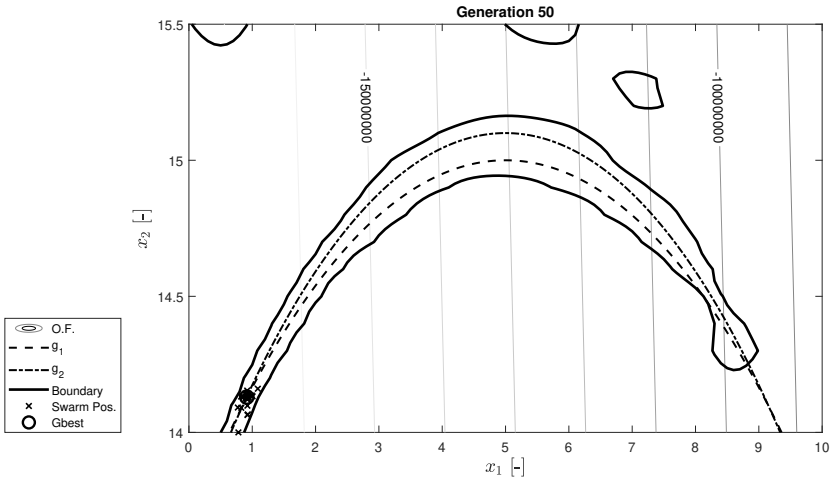

(b)

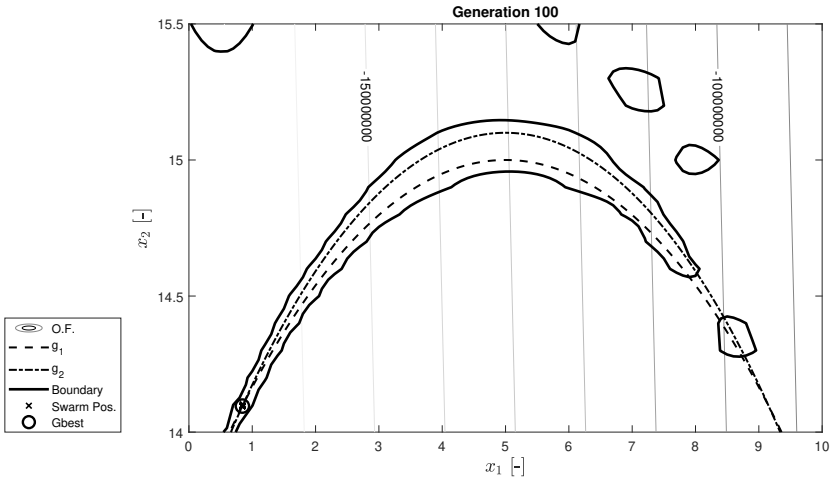

(c)

Fig. 2.6 Example 1 (Sickle Problem-Simionescu et al. 2004a), case constant relax constraints function;
(a) Generation 2; (b) Generation 50; (c) Generation 100

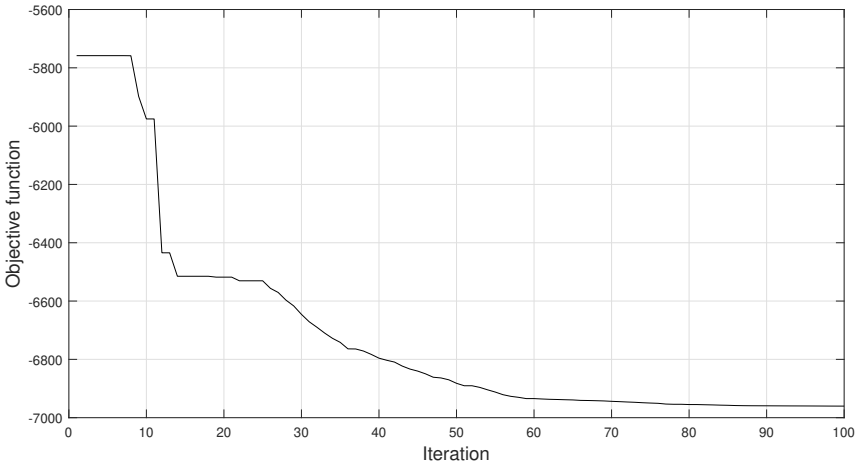

Fig. 2.7 Example 1 (Sickle Problem-Simionescu et al. 2004a), case constant relax constraints function, objective function history

substantially planar in the search space. The projection on the design variables plane of the feasible region is really narrow because it is formed by the space between the two constraints parabolas. For this problem, a population size of 50 individuals is set and in Figure 2.4 (b) the first random generation is shown and the support vectors are emphasized. After that, the unfeasible points are re-sampled until all the population falls inside the SVM-based boundary. At each generation, new points are added to the SVM training data and the boundary is improved. Since the search space is really narrow, running the algorithm with no relax constraint function it results in poor performance in defining the SVM boundary (black solid line) with respect to the actual one (dashed lines) as shown in Figure 2.5 (a) and (b). It is possible to improve the performance in terms of objective function decreasing history using the relax of constraints, as e.g. constant relax function shown in Figures 2.6 and 2.7. In this latter example, the reduction factor of standard deviation of the unfeasible point is chosen as $\lambda = 0.5$. The PSO-SVM performances using constant relax function is compared with other algorithms in Table 2.1. The comparison is done in terms of objective function value to the optimal solution after 50 runs with $k_{max} = 100$ each run and collecting mean value μ, standard deviations σ, best OF and worst OF. As one can check, the convergence of the new proposed method is satisfied as the objective function value is getting close to the global optimum with a little standard deviation as the other existing methods.

Table 2.1 Numerical Example 1 (Sickle Problem - Simionescu et al. (2004a)), comparison PSO-SVM, GA and PSO-penalty

	PSO-SVM	PSO-Penalty	GA
μ_{x_1}	0.8433	0.8721	0.8502
σ_{x_1}	0.0004	1.121e-15	0.0172
μ_{x_2}	14.0952	14.1091	14.0986
σ_{x_2}	0.0002	8.972e-15	0.0087
μ_{OF}	-6.9614e+03	-6.9291e+03	-6.9537e+03
σ_{OF}	0.4609	4.59e-12	19.2968
Best OF	-6.9595e+03	-6.93e+03	-6.9618e+03
Worst OF	-6.96e+03	-6.93e+03	-6.8547e+03

2.6 Numerical Example 2: five design variables optimization problem

The second numerical example statement reported in the Appendix is a literature benchmark test optimization problem with five design variables and six constraints. In this example, a comparison between different histories of the objective function

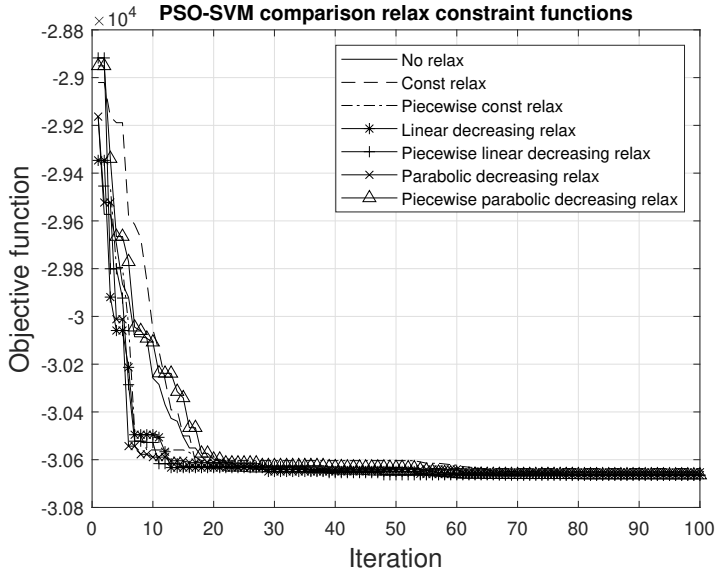

Fig. 2.8 Numerical Example 2: Objective value history comparison among different relax constraint functions for a single run

Table 2.2 Numerical Example 2, comparison among PSO-SVM with different relax constraint functions (check the Appendix and Runarsson and Yao (2005))

Comparison among Constraint Relax Functions in PSO-SVM							
Design Var.	No relax	Const. relax	Piecewise const.	Lin. relax	Piecewise lin.	Parabolic relax	Piecewise Par.
μ_{x_1}	78.0004	78.0086	78.0026	78.0009	78.0006	78.0027	78.0077
σ_{x_1}	0.0013	0.0243	0.0120	0.0038	0.0041	0.0100	0.0526
μ_{x_2}	33.0062	33.0040	33.0056	33.0104	33.0107	33.0740	33.0052
σ_{x_2}	0.0158	0.0183	0.0143	0.0438	0.0322	0.2274	0.0158
μ_{x_3}	30.0027	29.9985	30.0037	30.0009	30.0038	30.0366	30.0027
σ_{x_3}	0.0101	0.0105	0.0125	0.0235	0.0178	0.1217	0.0160
μ_{x_4}	44.6569	44.2360	44.3643	44.9858	44.8002	44.0814	44.6662
σ_{x_4}	1.5986	2.9630	2.0027	0.0617	1.0734	3.2862	1.3233
μ_{x_5}	36.8981	37.0755	37.0136	36.7671	36.8360	37.0446	36.8931
σ_{x_5}	0.6444	1.1956	0.8036	0.0652	0.4310	1.3843	0.5324
μ_{OF}	-3.0655e+04	-3.0644e+04	-3.0647e+04	-3.0664e+04	-3.0659e+04	-3.0634e+04	-3.0655e+04
σ_{OF}	43.0187	78.9205	53.7773	3.9918	28.9931	87.9967	36.2059
Best OF	-3.0666e+04	-3.0666e+04	-3.0666e+04	-3.0666e+04	-3.0666e+04	-3.0666e+04	-3.0666e+04
Worst OF	-3.0375e+04	-3.0185e+04	-3.0449e+04	-3.0643e+04	-3.0468e+04	-3.0186e+04	-3.0452e+04

using different relax constraint functions is performed. As shown in Figure 2.8, all the examples give a good result and tend to converge to the exact solution with different decreasing rate. In general, one can notice that in piecewise functions, the algorithm generally boosts the exploration instead of the exploitation that is usually performed in the second half with a zero relax coefficient. This feature is important because can affect the performance of the proposed algorithm with different kind of problems and the user need to try different relax functions in order to find the most suitable for this kind of problem. In Tables 2.2 and 2.3, a comparison with the GA and the PSO-Penalty is performed in terms of objective function value and optimal design points running the codes 50 times with $k_{max} = 100$ each run and collecting mean value μ, standard deviation σ, worst and best. Also with this more complex optimization problem, the convergence of the new proposed method is satisfied getting an objective function value close to the global optimum with a little standard deviation as the other existing methods.

2.7 Structural Example 1: simply supported beam

In Figure 2.9 it is considered an ideal simply supported beam of length L with a constant cross section $A = b \cdot h$ loaded with a distributed constant load q which is supposed to be much grater than the self weight for the sake of simplicity. The aim is to minimize the weight of this structure respecting the tensional constraints and maximum deflection constraint due to only the q load. The self weight is

Table 2.3 Numerical Example 2, results from PSO-SVM without relax constraints, PSO-Penalty and GA (check the Appendix and Runarsson and Yao (2005))

	PSO-SVM	PSO-Penalty	GA
μ_{x_1}	78.0004	78	78.0004
σ_{x_1}	0.0013	0	0.0024
μ_{x_2}	33.0062	33	34.2398
σ_{x_2}	0.0158	0	0.7052
μ_{x_3}	30.0027	29.9967	30.801
σ_{x_3}	0.0101	2.15E-14	0.378
μ_{x_4}	44.6569	45	45
σ_{x_4}	1.5986	0	0
μ_{x_5}	36.8981	36.7736	34.8023
σ_{x_5}	0.6444	0.00e+00	0.9057
μ_{OF}	-3.0655e+04	-3.0665e+04	-3.0531e+04
σ_{OF}	43.0187	1.47E-11	65.8031
Best OF	-3.0666e+04	-3.0665e+04	-3.0660e+04
Worst OF	-3.0375e+04	-3.0665e+04	-3.0378e+04

proportional to the volume V of the material as stated by **?**. The objective function is $f(d) = \rho V = \rho AL$, where d is the design vector and ρ is the material density which is supposed to be constant. In this case, only stress constraints on normal stress σ, tangential stress τ and on the maximum deflection $v(z)$ are considered. This is a typical sizing optimization problem. The design vector $d^T = \{d_1, d_2\}$ contains the design variables which are changed during the optimization process, i.e. in this case $d_1 = b$, $d_2 = h$. Since the cross section must be greater than zero as well as the cross sectional dimensions, it implies the presence of a new constraint to satisfy. Performing an elastic analysis, the maximum allowable stress is the yielding stress σ_y and it is possible to use the Navier Formula and the Jourawsky Formula for the normal and tangential stress respectively. The maximum moment

$$M_{Ed}(z = \frac{L}{2}) = \frac{qL^2}{8}$$

is in the middle span and the maximum shear force

$$V_{Ed} = \frac{qL}{2}$$

Fig. 2.9 Problem formulation: simply supported beam with constant cross section.

is in correspondence of the supports $z = 0$, $z = L$. Recalling the elastic resistance modulus for a rectangular section

$$W_{el} = \frac{bh^2}{6} = \frac{d_1 d_2^2}{6}$$

and using the Navier formula it is possible to write the maximum normal stress in the middle span as

$$\sigma\left(z = \frac{L}{2}\right) = \frac{M_{Ed}}{W_{el}} = \frac{3}{4}\frac{qL^2}{d_1 d_2^2}. \tag{2.14}$$

Using the Jourawsky formula, it is possible to write the maximum tangential stress in the middle of cross section $y = 0$ (parabolic tangential stress diagram on a rectangular section) as

$$\tau(z = 0, z = L) = \frac{V_{Ed} S_x^*(y = 0)}{I_x b} = \frac{3}{2}\frac{V_{Ed}}{bh} = \frac{3}{4}\frac{qL}{d_1 d_2}. \tag{2.15}$$

In order to take into account both normal and tangential stresses it is necessary to refer to a yield criterion. In this case, the Von Mises yield criterion is adopted:

$$\sqrt{\sigma^2(z) + 3\tau^2(z)} \leq \sigma_{id} \tag{2.16}$$

Substituting the (2.14) and the (2.15) into (2.16) respectively it is possible to obtain the two expression of the stress constraints in middle span $z = L/2$ (pure moment) and in $z = 0, L$ (pure shear):

$$\frac{3}{4}\frac{qL^2}{d_1 d_2^2} \leq \sigma_{id}, \tag{2.17}$$

$$\frac{3}{4}\frac{qL}{d_1 d_2} \leq \frac{\sigma_{id}}{\sqrt{3}}. \tag{2.18}$$

The maximum deflection $v(z = \frac{L}{2})$ can be calculated using the virtual work principle obtaining

$$v\left(z = \frac{L}{2}\right) = \frac{5}{384}\frac{qL^4}{EI_x} = \frac{5}{32}\frac{qL^4}{Ed_1 d_2^3}. \tag{2.19}$$

The complete statement of the optimization problem is the following:

$$\begin{aligned} \min \quad & f(d_1,d_2) = d_1 d_2, \\ \text{s.t.} \quad & d_1 > 0,\ d_2 > 0, \\ & \frac{3}{4}\frac{qL^2}{d_1 d_2^2} - \sigma_{id} \leq 0, \\ & \frac{3}{4}\frac{qL}{d_1 d_2} - \frac{\sigma_{id}}{\sqrt{3}} \leq 0, \\ & \frac{5}{32}\frac{qL^4}{E d_1 d_2^3} - v_{max} \leq 0, \end{aligned} \tag{2.20}$$

where the constant ρL is dropped by the objective function as stated in similar problems analyzed in **?**, σ_{id} is the ideal Von Mises normal stress and v_{max} is the maximum deflection admissible by reference design codes i.e. in this case it is fixed to $v_{max} = L/250$. It is possible to define the fixed variables vector $b^T = \{b_1, b_2, b_3, b_4, b_5\}$ which contains problem data which not change during the optimization process, i.e. in this case $b_1 = q$, $b_2 = L$, $b_3 = \sigma_{id}$, $b_4 = E$, $b_5 = v_{max}$. Since the amount of fixed parameters, it is more convenient work with a dimensionless form of the same problem. Posing $\tilde{d}_1 = b/L$ and $\tilde{d}_2 = h/L$, the new dimensionless objective function become

$$\tilde{f}(\tilde{d}_1, \tilde{d}_2) = f(d_1, d_2)/L^2 = \tilde{d}_1 \tilde{d}_2,$$

whilst the normal stress constraint (2.17), the shear constraint (2.18) and the deflection constraint (2.19) become respectively as

$$\frac{3}{4}\left(\frac{q}{L\sigma_{id}}\right)\frac{1}{\tilde{d}_1 \tilde{d}_2^2} \leq 1, \tag{2.21}$$

$$\frac{3\sqrt{3}}{4}\left(\frac{q}{L\sigma_{id}}\right)\frac{1}{\tilde{d}_1 \tilde{d}_2} \leq 1, \tag{2.22}$$

$$\frac{5 \cdot 125}{16}\left(\frac{q}{EL}\right)\frac{1}{\tilde{d}_1 \tilde{d}_2^3} \leq 1. \tag{2.23}$$

It is useful to define two dimensionless non-negative parameters, collected in $\tilde{b}$, which completely characterize the fixed variables of the problem:

$$\psi_\sigma = \frac{q}{L\sigma_{id}}, \tag{2.24}$$

$$\psi_E = \frac{q}{EL}. \tag{2.25}$$

Finally, the following dimensionless version of the problem is formulated (2.20)

$$\begin{aligned} \min \quad & \tilde{f}(\tilde{d}_1, \tilde{d}_2) = \tilde{d}_1 \tilde{d}_2, \\ \text{s.t.} \quad & \tilde{d}_1 > 0,\ \tilde{d}_2 > 0, \\ & \frac{3}{4}\psi_\sigma \frac{1}{\tilde{d}_1 \tilde{d}_2^2} \leq 1, \\ & \frac{3\sqrt{3}}{4}\psi_\sigma \frac{1}{\tilde{d}_1 \tilde{d}_2} \leq 1, \\ & \frac{5 \cdot 125}{16}\psi_E \frac{1}{\tilde{d}_1 \tilde{d}_2^3} \leq 1. \end{aligned} \tag{2.26}$$

To solve this problem, the PSO-SVM is adopted with the piecewise linear decreasing relax constraint function with a user coefficient λ for standard deviation of the unfeasible points fixed to $\lambda = 0.05$. For academic purposes, in order to graphically analyze the behaviour of the constraint handling, the dimensionless parameters are fixed as $\psi_\sigma = \psi_E = 0.2$, looking for a optimal solution in design domain for the dimensionless design variables as $0 \leq \tilde{d}_1 \leq 1.5$ and $0 \leq \tilde{d}_2 \leq 1$. In this way, with this particular choice of the dimensionless parameters the constraints intersect each other creating discontinuous non-linear boundary of the feasible region. The population size is always 50 individuals and the maximum iterations are 100. After 50 runs the results shown a quite great variability of the design variables but always at the same objective function value. This fact enlightens the presence of a front of possible optimal solutions. In fact, as showed in the graphical representations in Figures 2.10-2.11-2.12, for this specific choice of $\tilde{b}$, only two constraints are active and there exists a region of optimal solutions on the τ constraint boundary line. In the following, the comparison table with PSO-SVM, PSO-Penalty and GA shows the mean value and the standard deviation of the best objective function value obtained after 50 runs.

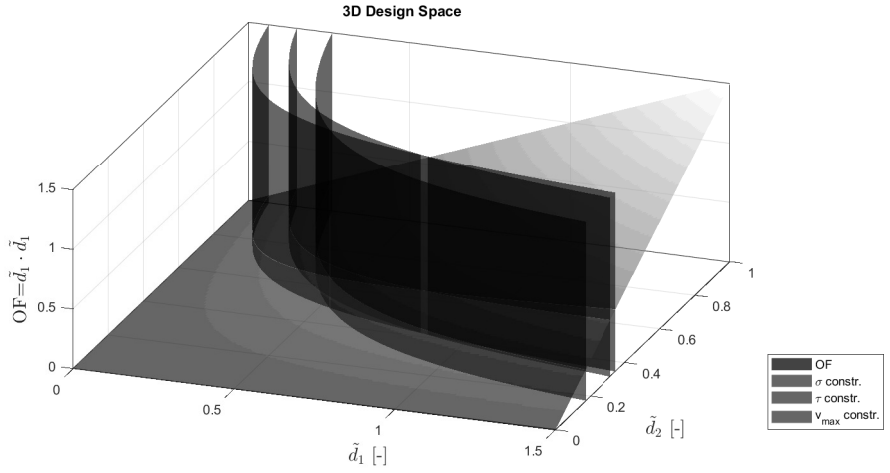

(a)

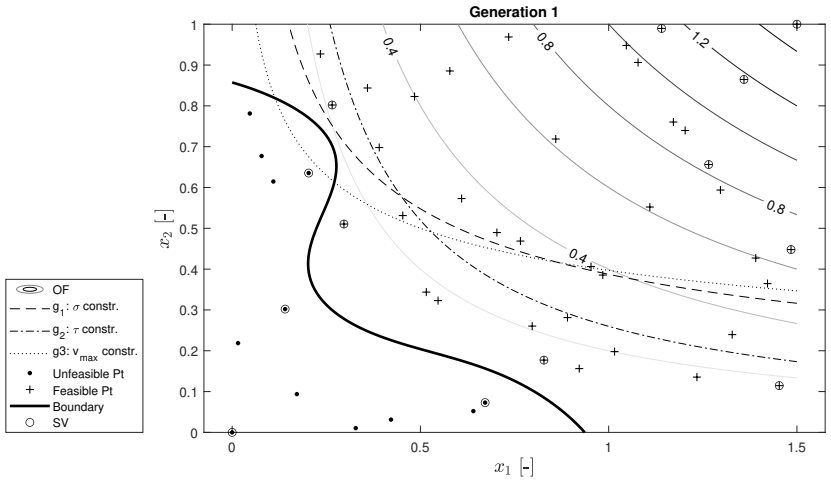

(b)

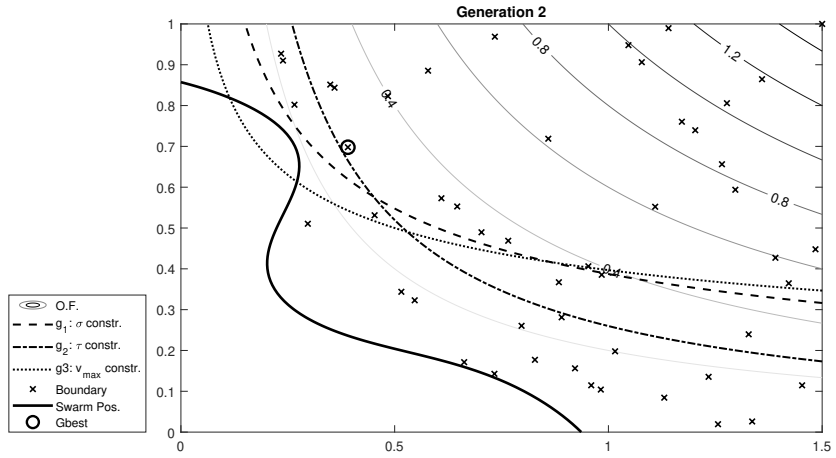

(c)

Fig. 2.10 Structural example 1: simply supported beam, case piecewise linear decreasing relax function;
(a) 3D graph of simply supported beam problem design space; (b) Generation 1; (c) Generation 2

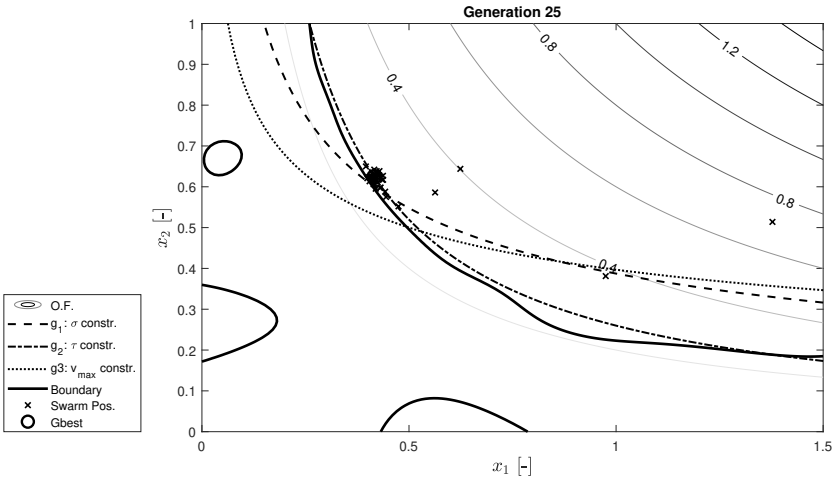

(a)

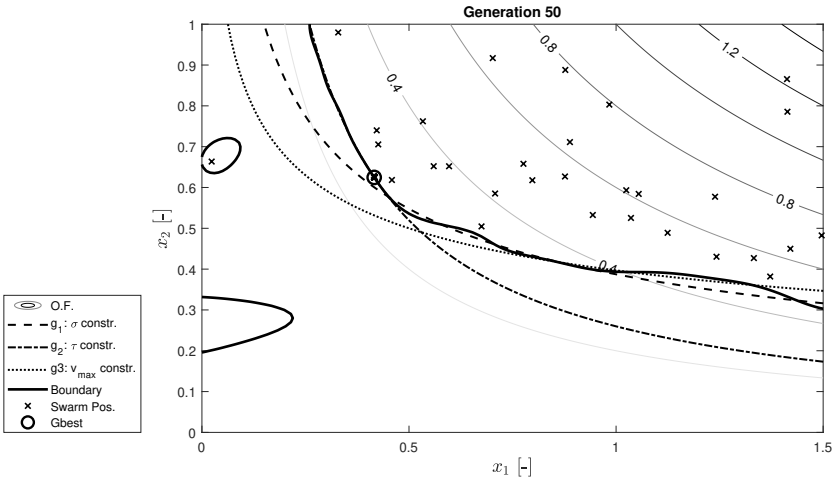

(b)

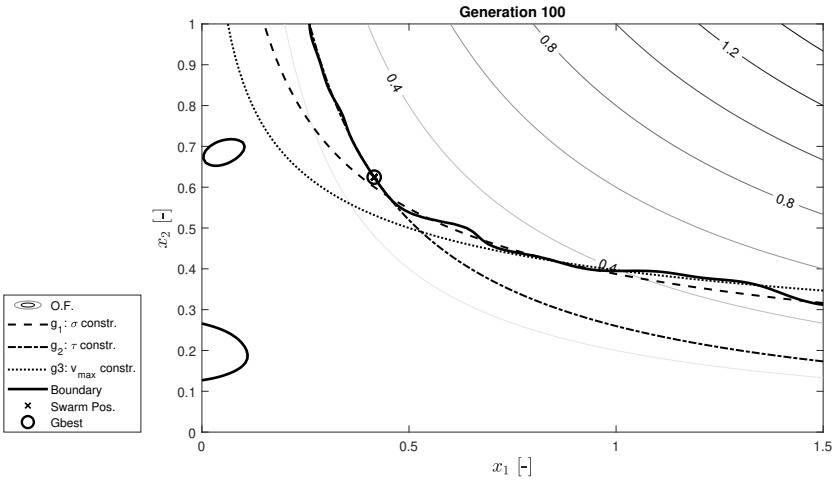

(c)

Fig. 2.11 Structural example 1: simply supported beam, case piecewise linear decreasing relax function;
(a) Generation 25; (b) Generation 50; (c) Generation 100

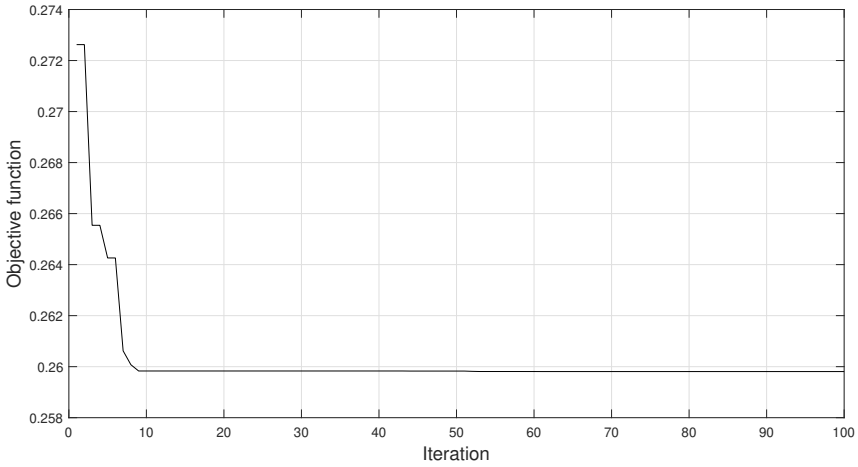

Fig. 2.12 Structural example 1: simply supported beam, case piecewise linear decreasing relax function; objective function history

Table 2.4 Structural Example 1, results from PSO-SVM piecewise linear decreasing relax constraints, PSO-Penalty and GA

	PSO-SVM	PSO-Penalty	GA
μ_{OF}	0.2598076	0.2598076	0.2610035
σ_{OF}	2.04e-09	5.61e-17	2.58e-03
Best OF	0.2598076	0.259808	0.2598076
Worst OF	0.2598076	0.259808	0.2664507

In order to find the entire front of the all optimal possible solutions for this specific problem, it is necessary to find the all the pairs $(\tilde{d}_{1,opt}, \tilde{d}_{2,opt})$ posing the objective function as $f(\tilde{d}_1, \tilde{d}_2) = \tilde{d}_1 \cdot \tilde{d}_2 \approx 0.2598$. As one can see in Figures 2.10-2.11-2.12, this optimal front corresponds to a part of the τ constraint (2.22) posed as an equality. Referring to the $\tilde{d}_1$ optimal possible values, the optimum front is upper bounded from the σ constraint (2.21) posed as an equality and lower bounded from the box search space limits. Then, to calculate the optimal upper bound $\tilde{d}_{1,\text{opt,UB}}$ it is

necessary to calculate the intersection between the two aforementioned constraints

$$\begin{aligned} &\frac{3}{4}\psi_\sigma \frac{1}{\tilde{d}_1 \tilde{d}_2^2} = 1, \\ &\frac{3\sqrt{3}}{4}\psi_\sigma \frac{1}{\tilde{d}_1 \tilde{d}_2} = 1, \\ &\sqrt{\frac{3}{4}\psi_\sigma \frac{1}{\tilde{d}_1}} = \frac{3\sqrt{3}}{4}\psi_\sigma \frac{1}{\tilde{d}_1} \end{aligned} \quad \Longrightarrow \quad \begin{aligned} &\tilde{d}_2 = \sqrt{\frac{3}{4}\psi_\sigma \frac{1}{\tilde{d}_1}}, \\ &\tilde{d}_2 = \frac{3\sqrt{3}}{4}\psi_\sigma \frac{1}{\tilde{d}_1}, \\ &\tilde{d}_{1,\text{opt,UB}} = \frac{9}{4}\psi_\sigma = 0.45. \end{aligned} \quad \Longrightarrow \quad (2.27)$$

As before, to calculate the optimal lower bound $\tilde{d}_{1,\text{opt,LB}}$ it is necessary to calculate the intersection between the equality τ constraint and the horizontal line $\tilde{d}_2 = 1$, obtaining

$$\begin{aligned} &\frac{3\sqrt{3}}{4}\psi_\sigma \frac{1}{\tilde{d}_1 \tilde{d}_2} = 1, \\ &\tilde{d}_2 = 1, \end{aligned} \quad \Longrightarrow \quad \tilde{d}_{1,\text{opt,LB}} = \frac{3\sqrt{3}}{4}\psi_\sigma = 0.2598. \quad (2.28)$$

Finally, considering (2.27) and (2.28), it is possible to obtain all the optimal pairs $(\tilde{d}_{1,opt}, \tilde{d}_{2,opt})$ using the following equation:

$$\tilde{d}_{2,\text{opt}} = \frac{0.2598}{\tilde{d}_{1,\text{opt}}}, \quad \text{with} \quad 0.2598 \leq \tilde{d}_{1,\text{opt}} \leq 0.45. \quad (2.29)$$

Since the algorithm works with dimensionless parameters, in order to find the physical dimensions of the optimized cross-section it is sufficient to multiply the obtained values $(\tilde{d}_{1,opt}, \tilde{d}_{2,opt})$ by L.

To show a technical possibly application coming from this simple example, a only concrete beam with span length $L = 3$ m is now considered. Disregarding for the moment the self-weight load, the q load set to 15 kN/m represents only a live load. The concrete modulus is set to $E = 25$ GPa and the Von Mises ideal stress is related to the tensile stress of concrete set to $\sigma_{id} = 3$ MPa. Considering the box search space as $0 \leq b \leq 40$ cm and $0 \leq h \leq 45$ cm, the algorithm found the minimum weight respecting the constraints with $b = 16.67$ cm and $h = 42$ cm. Rounding-off these values, the self-weight associated to a concrete beam with $b = 18$ cm and and

$h = 45$ cm is equal to:

$$G = \gamma_{concrete} \cdot b \cdot h = 24 \cdot 0.18 \cdot 0.45 = 1.944 \text{ kN/m}.$$

For sake of simplicity, adding G to q a new load equal to 16.944 kN/m which takes into account also the self-weight is defined. Launching again the algorithm, new optimal exact dimensions are now obtained: $b = 18.83$ cm and $h = 45$ cm. Rounding-up the exact solution, a new self-weight equal to $G = 2.16$ kN/m is coming from a section with $b = 20$ cm and $h = 45$ cm. Now the convergence is reached because the new optimal exact solution is $b = 19.07$ cm and $h = 45$ cm. Finally, the optimal cross-section for this concrete beam which minimize the self-weight is given by $b = 20$ cm and $h = 45$ cm.

2.8 Structural Example 2: Optimization of a Warren Truss Beam

The second structural example comes from Fiore et al. (2016c). In that work the weight optimization of an in-plane Warren truss simply supported beam, depicted in Figure 2.13, is performed with Differential Evolutionary Algorithm (DEA). The steel profile used for truss members is a square hollow core section, as shown in Figure 2.14. This kind of profile ensures good stability against buckling and it represents a good solution for this type of structure because of its high strength-to-weight ratio Fiore et al. (2016c). On the other hand, joint connections are usually welded and so, in order to reduce the total cost, it is important to reduce the size of sections to be welded. Regarding to the size optimization problem, as shown in Figure 2.14, this kind of sections are completely described by only two independent design variables: the outer dimension of the cross section B and the thickness of the webs s. In this problem the truss has m members belonging to four different type of cross sections as reported in Figure 2.13: lower chord (B_1, s_1), upper chord (B_2, s_2), internal webs (B_3, s_3) and external webs (B_4, s_4). To perform the shape optimization further two design variables are considered: vertical height of the external webs H_{min} and the

Fig. 2.13 Problem formulation: simply supported truss Warren beam.

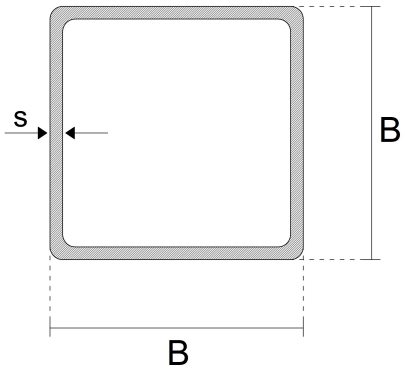

Fig. 2.14 Square hollow core tubular section design variables

maximum height H_{max}. The design vector is therefore defined as

$$x = (B_1, B_2, B_3, B_4, s_1, s_2, s_3, s_4, H_{min}, H_{max}), \tag{2.30}$$

and the box search space domain Ω is defined by:

$$\begin{aligned} 60 \leq & B_i \leq 360 \text{ mm}, \\ 4 \leq & s_i \leq 30 \text{ mm}, \\ 50 \leq & H \leq L \text{ mm}, \end{aligned} \tag{2.31}$$

where $i = 1, 2, 3$ and 4 and L is the total span lenght. Considering the maximum value of thickness $s_{max} = 30$ mm, the minimum value of dimension B cannot be assumed less than $2s_{max}$ due to geometric limits. The objective function is represented by the total weight of the structure (Marano et al., 2006):

$$W(x) = \sum_{i=1}^{m} \rho_i l_i A_i, \tag{2.32}$$

where $\rho_i = 7.85$ t$/m^3$ is the steel density supposed equal for all members, l_i is the length and A_i is the cross section of the i-th member. The structural steel used in this example is a S275 and the modulus of elasticity of the steel is 210 GPa.

Regarding topology optimization, in Fiore et al. (2016b) for fixed length $L =$ 20 m, the optimal number of bays in which divide the lower chord is 20. The external load is as a uniformly distributed load $q = 100$ kN/m applied on the lower chord acting as point loads in the nodes of the truss. The constrains are represented by the strength verifications about tensile stress (without any holes) (4.15), compression

stress (4.16) and buckling instability (4.17) according to Eurocode 3 (EN 1993-1 2005 and EN 1993-2 2006). Despite from the Eurocode $\gamma_{M0} = 1$ and $\gamma_{M1} = 1.1$ for bridges are recommended, to be more safe the partial safety factors are set both equal to $\gamma_{M_0} = \gamma_{M_1} = 1.1$.

$$\frac{N_{Ed}}{N_{t,Rd}} \leq 1, \text{ where } N_{t,Rd} = \frac{Af_y}{\gamma_{M_0}}, \tag{2.33}$$

$$\begin{aligned} \frac{N_{Ed}}{N_{c,Rd}} \leq 1, \text{ where for classes 1,2,3 } N_{c,Rd} &= \frac{Af_y}{\gamma_{M_0}}, \\ \text{while for class 4 } N_{c,Rd} &= \frac{A_{eff}f_y}{\gamma_{M_1}}, \end{aligned} \tag{2.34}$$

$$\begin{aligned} \frac{N_{Ed}}{N_{b,Rd}} \leq 1, \text{ where for classes 1,2,3 } N_{c,Rd} &= \chi\frac{Af_y}{\gamma_{M_1}}, \\ \text{while for class 4 } N_{c,Rd} &= \chi\frac{A_{eff}f_y}{\gamma_{M_1}}. \end{aligned} \tag{2.35}$$

Another constraint to satisfy is the maximum deflection which is usually set to $u_{lim} = L/500$ for bridges like that. In order to make a comparison with the results of Fiore et al. (2016c), for academic reasons, there is no distinction of the load combination for the strength verifications and for the deformability checks. The verification equations not need to deeper examination because this is beyond the scope of the present document. Therefore, the optimization problem statement is the following Fiore et al. (2016c): *Find* $x \in \Omega$ *such that*

$$\begin{aligned} \min \quad & f(x) = W(x), \\ \text{s.t.} \quad & \frac{N_{Ed}}{N_{t,Rd}} \leq 1, \\ & \frac{N_{Ed}}{N_{c,Rd}} \leq 1, \\ & \frac{N_{Ed}}{N_{b,Rd}} \leq 1, \\ & u_{max} \leq u_{lim}. \end{aligned} \tag{2.36}$$

In order to solve (2.36), the FEM structural analysis was performed in the Matlab® CALFEM and PSO-SVM was adopted for the optimization process. In the PSO-SVM a population size of 100 individuals is set with $k_{max} = 200$ iterations and

a constant relax function with user parameter $\lambda = 3$ applied to standard deviation of unfeasible points. It is performed 50 times runs and the best-obtained solutions are collected in Figure 2.15. As one can see in Figure 2.15, due to the complexity of the problem, sometimes the algorithm not reach the optimum and stack in a local minimum. As shown in the graph, the optimum solution is around 3.1 t, then it is possible to cut the graph considering only the 21 runs over the total 50 which are characterized by a best OF solution lower than 3.1 t (dashed line). In this way, the possible outliers are excluded and now it is possible to perform the post-processing searching for the real best solution.

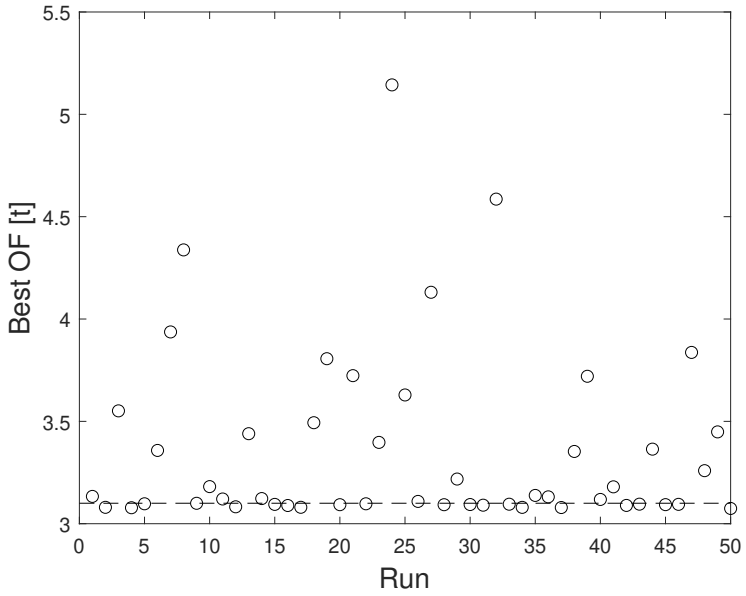

Fig. 2.15 Structural example 2: Warren Truss. Results from 50 times run PSO-SVM.

Considering the above-mentioned solutions, the obtained results showed in Table 2.5 has a quite large standard deviation in terms of design variables but very low in terms of objective function. This means that it is possible to find many combinations of design variables which is giving always the almost same objective function. The best design value of the 50 runs, also reported in table 2.5, is taken into consideration. It is possible to compare this latter objective function (3.074 t) with the optimal exact solution given by the original DEA code output (Fiore et al. 2016b). The DEA optimal solution was characterized by the weight of 2.95 t so this is in the right order of magnitude. The comparison of the design variables is based only on general observation in accordance with the literature, as affirmed in Fiore et al. 2016b. In

Table 2.5 Structural Example 2, Mean values μ and standard deviations σ of best results from 21 solution over 50 runs of PSO-SVM with OF less than 3.1 t; Last three columns: Best exact solution, Trivial rounded-up solution and Refined industrial solution.

[mm]	μ Exact Sol.	σ Exact Sol.	Best Sol.	Trivial Industrial Sol.	Best Industrial Sol.
B_1	72.5	15.7	94.2	95	95
B_2	190.2	70.2	128.1	130	105
B_3	128.9	1.4	128.8	130	130
B_4	211.7	107.9	132.1	135	110
s_1	6.0	1.5	4	4	4
s_2	14.7	7.4	18.8	20	26
s_3	4.0	0.03	4	4	4
s_4	14.0	8.4	14.7	15	19
H_{min}	399.4	21.5	410.5	410	410
H_{max}	4064.7	113.5	4145.0	4145	4145
OF [t]	3.0898	0.0071	3.074	3.189	3.092

fact, for instance, it is expected that, mainly due to instability problems, upper chord and external diagonals would be bigger than the lower chord and internal diagonals. Finally, the best exact solution may be trivially rounded-up to get an industrialized more realistic design. The new design variables are reported in 2.5 and as one can see this solution is more conservative and it leads to an increased total weight (3.189 t).

If one want to find a more accurate industrial solution it is necessary to perform a more accurate analysis of the obtained results. Since the topology optimization was already taken into account in Fiore et al. 2016b, one have to remember that in the design variables the algorithm is performing the size optimization and the shape optimization. This latter is regarding to the definition of the H_{min} and H_{max} values. Considering only the above-mentioned 21 solutions and the standard deviations of H_{min} and H_{max}, it is possible to assume that the rounded-up values of the best exact solution can represent a good result for shape optimal parameters values:

$$H_{min} \approx 410 \text{ mm},$$
$$H_{max} \approx 4145 \text{ mm}.$$

Table 2.6 Structural Example 2, Best exact solution cross section

$[\text{mm}, \text{mm}^2]$	$(B;s)_{exact}$	Requested Area	$(B;s)^{best}_{industrial}$	Provided Area
Lower Chord	(94.2 ; 4)	1442.46	(95 ; 4)	1456
Upper Chord	(128.1 ; 18.8)	8206.18	(105 ; 26)	8216
Internal Webs	(128.8 ; 4)	1996.81	(130 ; 4)	2016
External Webs	(132.1 ; 14.7)	6907.21	(110 ; 19)	6916

Once solved the shape optimization, regarding to the size optimization firstly the best exact solution as the optimal one. One have to remember that B_i and s_i were chosen as design parameters because of their independence, but in the optimization process, they are connected. In fact, in both objective function evaluation and constraints evaluation, these two parameters are combined into the resisting cross section value. It is possible to obtain almost the same value of cross section with different combinations of the design parameters. In particular, one can refer to the optimal exact solution in terms of resisting cross sections which represent the best solution in terms of both strength verification and minimization of the weight. As one can check, for the best exact solution, the section class of all members is 1, but other optimal solutions within the 21 considered are characterized by class 4 profile. In this case, to get the strength verification satisfied, it is necessary to refer to the resisting effective area. Usually in the design when it is possible it is preferred to avoid class 4 profiles and the best condition is to find an optimal solution with class 1 profile. Therefore, the best industrial solution which respects all the constraint is given by all the pairs (B_i, s_i) with $i = 1,2,3$ and 4 which gives class 1 profiles and which gives the minimum value of area greater or equal than the effective areas requested by the best solution in Table 2.6. This procedure allows us to find the best solution which respects the strength verification only. For the instability verification, it is necessary to take into account also the second moment of inertia which condition the Euler's critical load N_{cr} and consequently the dimensionless slenderness $\overline{\lambda}$ which influence the reduction factor χ. Fixing the thickness s_i to discrete values (rounded with 1 mm of precision), starting from the best-found solution and making an iterative discrete research to find the B_i (rounded with 5 mm of precision) respectful of our above-mentioned design rule, the best optimal industrial solution is found and reported in the last column of Table 2.5. As one can check, the minimum cross area of internal webs could be assured by the pair $(B_3, s_3) = (105\ ;\ 5)$ mm but, due

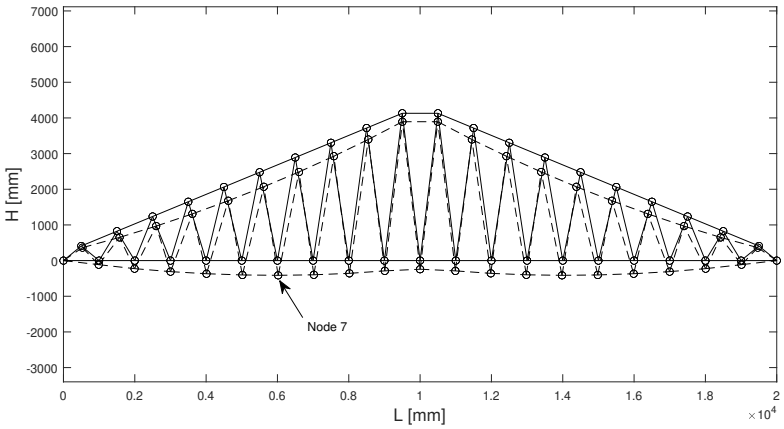

Fig. 2.16 Optimal Warren Truss. Solid Line: undeformed shape; Dashed Line: deformed shape

to instability problems, it is necessary to take into account the inertia and choose a profile that ensures both strength and instability verifications.
The best industrial structure is verified to all strength and instability constraints. Making a comparison between the two last columns of the Table 2.5, also the trivial rounded-up solution represents a good optimal solution in terms of objective function. In fact, minimizing the weight is important but the total cost is also affected by other aspects e.g welding and detailing, labour cost, etc. So, the solution obtained by trivial rounded-up the exact one it can be considered an acceptable optimal result. In Figure 2.16 the undeformed and the deformed shape are depicted. It is possible to appreciate which the node 7 and, due to symmetry, the node 15 are the nodes that undergo the most deflection $u_{max} = 39.8$ mm however it is respectfully of the service limit $L/500 = 40$ mm.

In order to assess the validity of the results of the optimization process, the warren truss beam is modelled with FEM professional software MIDAS Gen®. The assessment is made not only in terms of axial force for each member, but in particular in terms of performance ratio. This latter represents an efficiency percentage of the usage of the steel and is given by the strength ratio between the demand and the capacity. The simply supported warren truss is modelled through truss elements in order to guarantee pure axial behaviour of each member. The section properties of the trivial best industrial results from Table 2.5 are assigned to each element. The adopted steel is always a S275 and the uniformly distributed load $q = 100$ kN/m

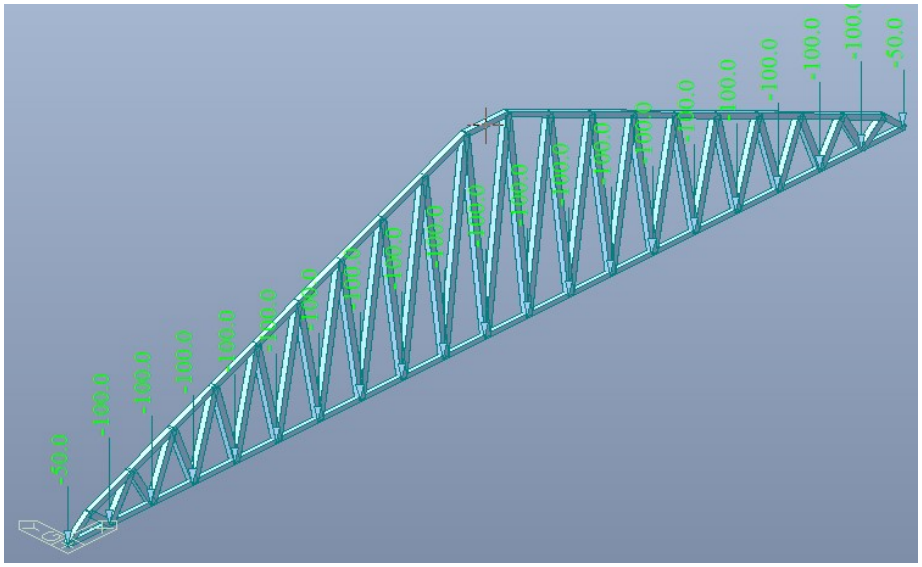

Fig. 2.17 Model of the warren truss beam on Midas Gen®

acting on the lower chord is reconducted as a hanged load directly applied at lower chord nodes acting as concentrated forces, as depicted in Figure 2.17. As already remarked, in order to get results which are directly comparable with the Matlab code and with DEA code from Fiore et al. (2016c) and for the sake of simplicity, none load combination is considered. The aim is to demonstrate that the proposed algorithm provides comparable results with DEA code which is used as a benchmark and not making a perfect design completely respectful of the current codes. In order to take into account this latter issue, it is sufficient to consider the correct the load combination at ULS for the strength verification and SLS for the maximum allowable displacement.

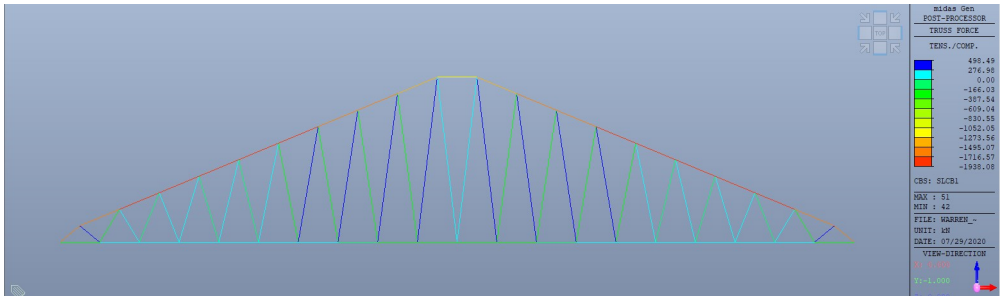

Fig. 2.18 Planar view of the warren truss beam on Midas Gen® with the axial force values

Table 2.7 Comparison between Midas model and Matlab axial force elements

Midas element	Matlab element	N_{Ed}	N_{Rd}	Midas element	Matlab element	N_{Ed}	N_{Rd}
1	1	350.47	364.00	23	41	150.24	504.00
2	2	166.18	364.00	25	42	20.80	504.00
3	3	255.42	364.00	27	43	66.77	504.00
4	4	238.70	364.00	29	44	139.27	504.00
5	5	179.70	364.00	31	45	204.59	504.00
6	6	99.54	364.00	33	46	265.90	504.00
7	7	7.27	364.00	35	47	324.76	504.00
8	8	92.60	364.00	37	48	382.00	504.00
9	9	197.58	364.00	39	49	50.75	504.00
10	10	306.16	364.00	68	50	482.83	504.00
11	11	306.16	364.00	66	51	425.57	504.00
12	12	197.58	364.00	64	52	366.75	504.00
13	13	92.60	364.00	62	53	305.56	504.00
14	14	7.27	364.00	60	54	240.59	504.00
15	15	99.54	364.00	58	55	169.06	504.00
16	16	179.70	364.00	56	56	84.69	504.00
17	17	238.70	364.00	54	57	30.40	504.00
18	18	255.42	364.00	52	58	252.62	504.00
19	19	166.18	364.00	22	59	252.62	504.00
80	20	350.47	364.00	24	60	30.40	504.00
40	21	1692.70	2200.00	26	61	84.69	504.00
41	22	1918.80	2200.00	28	62	169.06	504.00
42	23	1939.50	2200.00	30	63	240.59	504.00
43	24	1892.10	2200.00	32	64	305.56	504.00
44	25	1813.70	2200.00	34	65	366.75	504.00
45	26	1718.60	2200.00	36	66	425.57	504.00
46	27	1613.50	2200.00	38	67	482.83	504.00
47	28	1501.80	2200.00	69	68	50.75	504.00
48	29	1385.70	2200.00	67	69	382.00	504.00
49	30	1228.10	2200.00	65	70	324.76	504.00
78	31	1385.70	2200.00	63	71	265.90	504.00
77	32	1501.80	2200.00	61	72	204.59	504.00
76	33	1613.50	2200.00	59	73	139.27	504.00
75	34	1718.60	2200.00	57	74	66.77	504.00
74	35	1813.70	2200.00	55	75	20.80	504.00
73	36	1892.10	2200.00	53	76	150.24	504.00
72	37	1939.50	2200.00	51	77	498.81	504.00
71	38	1918.80	2200.00	20	78	1523.00	1800.00
70	39	1692.70	2200.00	50	79	1523.00	1800.00
21	40	498.81	504.00				

As reported in Figure 2.18 and in Table 2.7, the results obtained from the Matlab code are equal to the FEM software. The overall behaviour shows that the upper chord is entirely compressed whereas the lower chord is entirely tensed. The internal webs are alternatively compressed and tensed as usual for truss beam of this typology. Calculating the strength ratio, it is worth noting that a performance ratio between 75% to 98% is obtained for the members. These remarkable results show the importance of the optimization process during the design phase which can strongly support the decision process of the designer.

2.9 Conclusions

After an introductory part on PSO and the state of the art of constraint handling techniques, the paper presented a new valid alternative not-penalty method to solve constrained optimization problems. The main advantage with respect to the most used nowadays penalty approach is represented by the generality of the machine learning SVM algorithm. Since it depends intrinsically on the inner product of the data, it is more adaptive even with discontinuous and non-linear boundaries of the feasible region in the design space. In order to improve the behaviour of the proposed algorithm to deal with very sharp and narrow feasible regions, a relax constraint function was also implemented. Though a general set of parameters, which govern the PSO and SVM algorithm, did not lead to feasible results independently of the investigated problem statements, a well-calibrated relax constraint function contributes positively to the exploration capability of the algorithm. From the computational point of view, the trade-off was found in adopting a population size not too large and using an incremental boundary update. Although it is also possible sampling a huge initial random data and leave the boundary fixed during the generations, this does not conduct a good result in terms of the objective function. Finally, the two numerical benchmark examples demonstrated the convergence of the new method in comparison with another penalty approach and with a GA. The last two examples highlighted the adaptability of this new method even into the structural optimization field. In particular, in the warren truss beam problem, the optimization algorithm provided a numerical exact solution which can be easily industrialized by the designer with a trivial rounding-off without jeopardizing the optimization process. Although the warren truss beam example is performed under simplified

assumption in order to make comparisons with DEA code from Fiore et al. 2016b, from the technical point of view, the new optimization algorithm becomes a really useful and powerful support for the designer during the design and the decision process. It is important to stress that working with metaheuristic algorithm always involves the definition of the value of many arbitrary parameters. Starting from literature suggestions for these values, it is always strongly suggested to perform a fine-tuning of some of these parameters also with a trial-and-error approach for each specific problem in order to find the best optimal results in terms of objective function convergence, computational effort and elaboration time.

Appendix: Test Functions Constrained Problems

The following mathematical problems were tested for the proposed PSO-SVM algorithm.

1. The following problem is taken by Simionescu et al. (2004a) and it is called the Sickle function.

$$\begin{aligned} \min \quad & f(x) = (x_1 - 20)^3 + (x_2 - 10)^3 \\ \text{s.t.} \quad & g_1(x) = (x_1 - 5)^2 + (x_2 - 5)^2 - 100 \geq 0 \\ & g_2(x) = -(x_1 - 5)^2 - (x_2 - 5)^2 + 82.81 \geq 0, \end{aligned}$$

   where the search space is defined as $0 \leq x_1 \leq 10$ and $14 \leq x_2 \leq 15.5$. The global optimum is located at $x^* = [14.095, 0.84296]$ where $f(x) = -6961.8139$.

2. The following problem is taken from Runarsson et al. (2000) and it is a multi-variable problem with five design variables and six constraints.

$$\begin{aligned} \min \quad & f(x) = 5.3578547x_3^2 + 0.8356891x_1x_5 + 37.293239x_1 - 40792.141 \\ \text{s.t.} \quad & g_1(x) = 85.334407 + 0.0056858x_2x_5 + 0.0006262x_1x_4 - 0.0022053x_3x_5 - 92 \leq 0, \\ & g_2(x) = -85.334407 - 0.0056858x_2x_5 - 0.0006262x_1x_4 + 0.0022053x_3x_5 \leq 0, \\ & g_3(x) = 80.51249 + 0.0071317x_2x_5 + 0.0029955x_1x_2 + 0.0021813x_3^2 - 110 \leq 0, \\ & g_4(x) = -80.51249 - 0.0071317x_2x_5 - 0.0029955x_1x_2 - 0.0021813x_3^2 + 90 \leq 0, \\ & g_5(x) = 9.300961 + 0.0047026x_3x_5 + 0.0012547x_1x_3 + 0.0019085x_3x_4 - 25 \leq 0, \\ & g_6(x) = -9.300961 - 0.0047026x_3x_5 - 0.0012547x_1x_3 - 0.0019085x_3x_4 + 20 \leq 0, \end{aligned}$$

where the search space is defined as $78 \leq x_1 \leq 102$ and $33 \leq x_2 \leq 45$ and $27 \leq x_3, x_4, x_5 \leq 45$. The optimum is located at $x^* = [78, 33, 29.995256025682, 45, 36.775812905788]$ where $f(x) = -30,665.539$.

Chapter 3

Enhanced Multi-Strategy Particle Swarm Optimization

3.1 Introduction

In optimization problems, the aim is optimizing certain mathematical functions, called Objective Functions (OF) $f(x)$. These problems can be divided into single-objective or multi-objective problems, depending on the number of OFs, and a further subdivision for single-objective problems is based on the presence of constraints. Unconstrained problems are defined as:

$$\min_{x\in\Omega}\{f(x)\} \tag{3.1}$$

meanwhile, constrained problems are defined as:

$$\begin{aligned} & \min_{x\in\Omega}\{f(x)\} \\ \text{s.t.} \quad & g_q(x) \leq 0 \quad \forall q = 1,\ldots,n_q \\ & h_r(x) = 0 \quad \forall r = 1,\ldots,n_r \end{aligned} \tag{3.2}$$

where $x = \{x_1,\ldots,x_j,\ldots,x_n\}^T$ is the design vector whose terms are the parameters to be optimized. The search domain is a multidimensional space Ω based on the admissible intervals of values for each j-th variable, which are defined by its lower and upper bounds $[x_j^l, x_j^u]$. This detects a box-type hyper-rectangular search space

Ω, which is typically defined as the Cartesian product (denoted by the $\times$ symbol) among the admissible intervals:

$$\Omega = [x_1^l, x_1^u] \times \ldots \times [x_j^l, x_j^u] \times \ldots \times [x_n^l, x_n^u] \tag{3.3}$$

The constraints in (5.4) can belong to two different categories: inequality $g_q(x)$ and/or equality $h_r(x)$ constraints. Each equality constraint can be easily converted into a couple of inequality constraints; therefore, without any loss of generality, it is possible to consider only inequality constraints in (5.4), i.e., $g_p(x) \leq 0$, where $p = 1, \ldots, n_q, n_{q+1}, \ldots, n_p$, being $n_p = n_q + 2n_r$.

The adoption of evolutionary algorithms (EAs) has received much more attention in recent years because of their successful capability to handle complex optimization problems. This is addressed mainly to the fact that they do not require any first-order (gradient) or second-order (Hessian) information coming from the problem to be solved, which is conversely a prerogative of the traditional gradient-based mathematical search approaches. Furthermore, the quite simple implementation of EAs has determined their rapid spread, and they have immediately become an attractive tool among practitioners. Among the many alternatives available nowadays, the genetic algorithm (GA) proposed by J. Holland in the 1970s (Martí et al. (2018)) still represents one of the most popular population-based tools, which tries to simulate the biological evolutionary process of a set of candidates solutions mimicking the biological Darwinian Theory. This is realized by adopting specific pseudo-random-based operators such as crossover, mutation, and selection in order to reproduce the long-term process of evolution in a population with the survival of the fittest individuals (Lagaros 2002). In the last two decades, the adoption of metaheuristic algorithms in many engineering applications highlighted their successful capabilities to deal with real-world constrained problems (Marano et al. (2007), Pelliciari et al. (2018), Xue et al. (2018), Greco and Marano (2015), Di Trapani et al. (2022), Asso et al. (2021)), e.g., dealing with structural design De Domenico et al. (2020), De Tommasi et al. (2017), Sardone et al. (2021), Cucuzza et al. (2021b) and structural optimization tasks Cucuzza et al. (2021a), Fiore et al. (2016a), Aloisio et al. (2022), Marano et al. (2014).

In the framework of EAs, a more recent but already well-known approach is the particle swarm optimization (PSO) algorithm. It was mentioned by Kennedy and Eberhart (1995b) for the first time, and then it rapidly became widespread during

the following years. Contributions from the Scientific Community have not ended yet, and still nowadays there is active research about this topic to improve the search operators and the performances. The PSO is also a population-based algorithm which takes inspiration from the study of the behavioural models of birds flocking or fish schooling, whose individuals explore the natural environment in order to find and reach some source of food. Similarly, the algorithm tries to evolve a particle swarm of candidate solutions in the domain search space in order to find the optimum. The PSO was originally developed to face unconstrained problems, but it was later adapted to also solve constrained problems exploiting specific strategies.

The following section presents a brief review of the PSO mechanisms, and the main adopted strategies to solve constrained problems are mentioned. After that, the description of the proposed enhanced multi-strategy PSO method is illustrated. Finally, the authors try to merge several state-of-the-art concepts to obtain an improved PSO algorithm to successfully handle constrained problems with a non-penalty based approach. The novel contributions of this article can be summarized as follows:

- PSO implementation with the main state-of-art improvements, adopting a multi-strategy approach. In this way, the algorithm attempts to avoid wasting many iterations when the algorithm stalls or is trapped in local minima, etc.;
- A non-penalty approach for constraint handling which instead exploits information of swarm positions in terms of the objective function and the actual degree of constraint violation to guide the swarm evolution;
- A novel unfeasible local search operator is presented to help the PSO when it stalls in an unfeasible region quite close to the actual feasible one. This local search operator relies on the meta-heuristic, self-adaptive Evolutionary Strategy (ES) approach, which does not require any other further arbitrary parameter.

In a different recent contribution of the authors (Rosso et al. (2021b)), some further novel approaches to deal with constraints have been presented, considering a hybridization of the PSO with a machine learning support vector machine. However, the current paper presents a completely different approach based on handling constraints directly based on information which can be retrieved from the swarm positions in terms of objective function and constraints violations. Finally, the enhanced multi-strategy PSO is successfully tested on some benchmark constrained

mathematical problems from the literature compared with other PSO implementations that adopt more standard penalty-based constraint handling techniques. In conclusion, the proposed multi-strategy PSO has been validated on real-world case studies, considering some literature on three-dimensional truss design structural optimization problems.

3.2 State of the Art of Constraint Handling

In order to adapt EAs to deal with constrained problems, several strategies were developed by the scientific community. As a matter of fact, constraint handling is a big challenge because it is related to find the optimal point respecting all the constraints, and therefore, the algorithms may be able to deal with unfeasible solutions in an efficient way. Despite several studies (e.g., Kennedy and Eberhart (2001)) demonstrating that PSO has a good convergence rate, it was originally proposed to solve unconstrained optimization problems, such as many other Soft Computing techniques. The implementation of some effective constraint-handling mechanisms is a crucial issue for all biologically inspired optimizers Deb (2000a), Coello Coello (2002), Wang et al. (2008), Mezura-Montes (2009a). The several strategies developed have been classified by different authors into basically five main categories (see, for instance, the state-of-the-art review by Coello Coello (2002), Koziel and Michalewicz (1999a), Michalewicz and Fogel (2008)):

- Penalty-functions-based methods;
- Methods based on special operators and representations;
- Methods based on repair algorithms;
- Methods based on the separation between OFs and constraints;
- Hybrid methods.

The most adopted method due to its simplicity is the exterior penalty approach which allows to convert the problem in an unconstrained version rezaee jordehi (2015), Kohler et al. (2019). Many different approaches such as the death, static, dynamic, or adaptive penalty functions have been proposed in time, e.g., one can refer to rezaee jordehi (2015). A proper choice of the constraint-handling mechanism

affects the performance of the algorithm, and one of the critical issues to take into account is the preservation of the diversity of the population. The brutal elimination of the unfeasible particles, such as in the death penalty rule, can jeopardize the exploration performances due to a loss of information Coello Coello (2002), Mezura-Montes and Coello (2005a). In general, the penalty approach rely on the evaluation of a factor that applies a certain penalty to the OF, depending on the degree of violation and the number of violated constraints. Therefore, the constrained OF $f(x)$ is transformed into an analogous unconstrained OF $\phi(x)$:

$$\min_{x\in\Omega}\{\phi(x))\} = \min_{x\in\Omega}\{f(x)+H(x)\} \tag{3.4}$$

where $H(x)$ is the penalty function, whose specific definition depends on the strategy adopted. If the penalty is constant during the iterations, it is a *static penalty function*, while if it is changing at each iteration, it is addressed as a *dynamic penalty function*. These two techniques are the most popular tools in structural optimization, see, for instance, the papers by Hasançebi et al. Hasançebi et al. (2009) and Dimopoulos Dimopoulos (2007).

In the case of static-penalty-based techniques, the equivalent unconstrained problem is formulated with a static penalty factor $H_s(x)$ that is generally expressed as follows (see Parsopoulos and Vrahatis (2005), Coello (1999)):

$$H_s(x) = w_1 H_{NVC}(x) + w_2 H_{SVC}(x) \tag{3.5}$$

where H_{NVC} is the number of constraints that are violated by the particle x, H_{SVC} is the sum of all violated constraints, and $w1$ and $w2$ are static control parameters of the penalty scheme:

$$H_{SVC}(x) = \sum_{p=1}^{n_p} \max\{0, g_p(x)\} \tag{3.6}$$

The numerical values adopted by Parsopoulos and Vrahatis (2005) are $w_1 = w_2 = 100$. In the present research, some standard penalty PSO approaches are adopted for making comparisons with the enhanced PSO version, which is presented in the following section. For these PSOs with penalty approaches, $w_1 = 0$ and $1000 < w_2 < 10000$ have been assumed, depending on the analysed problem. Depending on the values of $w1$ and $w2$, it is possible to set the level of severity of the constraint violations: In case of extremely high control parameters, the penalty is called the

death penalty, and it tries to completely avoid any kind of research inside the unfeasible region, even if the number of violated constraints is rather limited.

The popularity of the penalty function technique is due to its simple implementation, and it strongly enhances the performance of an algorithm that is trying to solve constrained optimization problems. To improve the effectiveness of the penalty factor, a penalty function which changes the weight of the penalty during the iterations is also adopted in the current study. Indeed, it is possible to better control the search space of the particles with this latter dynamic approach, allowing a more relaxed constraint handling at the beginning and an increasing penalty value approaching the end of the available iterations. Firstly proposed by Parsopoulos and Vrahatis (2002), it has recently been adopted by Barakat and Altoubat (2009) for the optimum design of RC water tanks. To this end, the (5.6) is readily modified as follows:

$$\min_{x\in\Omega}\{f(x)+{}^{k}hH_d(x)\} \tag{3.7}$$

in which ${}^{k}h$ is a dynamic penalty whose numerical value was evaluated as (Parsopoulos and Vrahatis (2002), Barakat and Altoubat (2009)):

$${}^{k}h=\sqrt{k} \tag{3.8}$$

and $H_d(x)$ is the dynamic penalty factor:

$$H_d(x)=\sum_{p=1}^{n_p}\theta_p(x)[\max\{0,g_p(x)\}]^{\gamma_p(x)} \tag{3.9}$$

Typical assignments for the penalty parameters are (see, for instance, Parsopoulos and Vrahatis (2002), Barakat and Altoubat (2009)):

$$\theta_p(x)=\begin{cases}10 & \text{if } \max\{0,g_p(x)\}\le 0.001\\ 20 & \text{if } 0.001<\max\{0,g_p(x)\}\le 0.100\\ 100 & \text{if } 0.100<\max\{0,g_p(x)\}\le 1.000\\ 300 & \text{otherwise.}\end{cases} \tag{3.10}$$

$$\gamma_p(x)=\begin{cases}1 & \text{if } \max\{0,g_p(x)\}\le 1\\ 2 & \text{otherwise.}\end{cases} \tag{3.11}$$

It is evident that dynamic penalty methods require a larger number of control parameters in comparison to the static one. Considering ${}^{k}h$ as defined in (3.8), in the present paper, the dynamic penalty factor is assumed to have:

$$10 < H_d(x) < 1000 \tag{3.12}$$

The evaluation of a proper penalty is a fundamental passage to achieve a good solution of an optimization problem: Ideally, it should be set as low as possible to avoid high computational efforts and problems arising when the global optimum is close to the constraint. Indeed, if the optimum is at the boundary and the penalty is too high, the element which is attracted by that area is immediately pushed back when the boarder is crossed. This mechanism is avoided by adopting a low penalty that is not too severe in case of small violations and also allows a good investigation in such critical areas. However, if the penalty is too low and it does not contrast the constraint violation properly, a lot of effort will be spent in the unfeasible region, providing no useful information for the minimization purpose.

3.3 Enhanced PSO with a Multi-Strategy Implementation and Hybridisation with an ES-Based Operator

In the present section, starting from the standard Newtonian-dynamics-based PSO approach proposed by Kennedy and Eberhart (1995b), an enhanced PSO is implemented by adopting some of the most well-known available strategies in literature and adding a special operator in order to increase the search performance of the standard version. The various strategies are merged together, and the flowchart of the implemented algorithm is illustrated in Figure 3.1.

At first, the initial population is generated randomly in the hyper-rectangle search space, adopting the Latin Hypercube Sampling (LHS) to generate an initial population with the minimum correlation between samples Monti et al. (2010a). Thereafter, for each particle, the OF and the constraints are evaluated defining the level of violation of each constraint. Each particle is addressed to a specific aim according to their violation value. If none of the constraints are violated, this

particle is labelled as feasible, and it will be addressed to minimize the objective function. Otherwise, if it violates at least one constraint, it is labelled as unfeasible, and it will try to find the right path to minimize the constraint violation. If more than one constraint is violated, only the maximum violation is considered at that point. Therefore, it is possible to assume that each particle is able to see only the envelope of the maximum violations for all points in the solution space. For this reason, the current approach has been named as a *multi-strategy* PSO. In this way, it is not necessary to define some arbitrary violation penalty factor because the code directly relies on the envelope of the violation of the constraints in a particle position at a certain iteration number. After the first population is randomly sampled and evaluated, the role and the aim of each particle have been defined, and the swarm evolution cycle can start, as illustrated in Figure 3.1. The evolutionary phase of the PSO involves the Velocity update according to the before mentioned formulation (2.4) and the Position update according to Equation (2.5). After that, the cognitive memory (pbest) of each particle is updated if a better feasible position is reached with respect to the previous iterations, and the local best attractor (lbest) and the best position for the current generation (gbest) are also updated. The termination criterion is encountered when a predefined maximum number ($k_{\max}$) of iterations is reached.

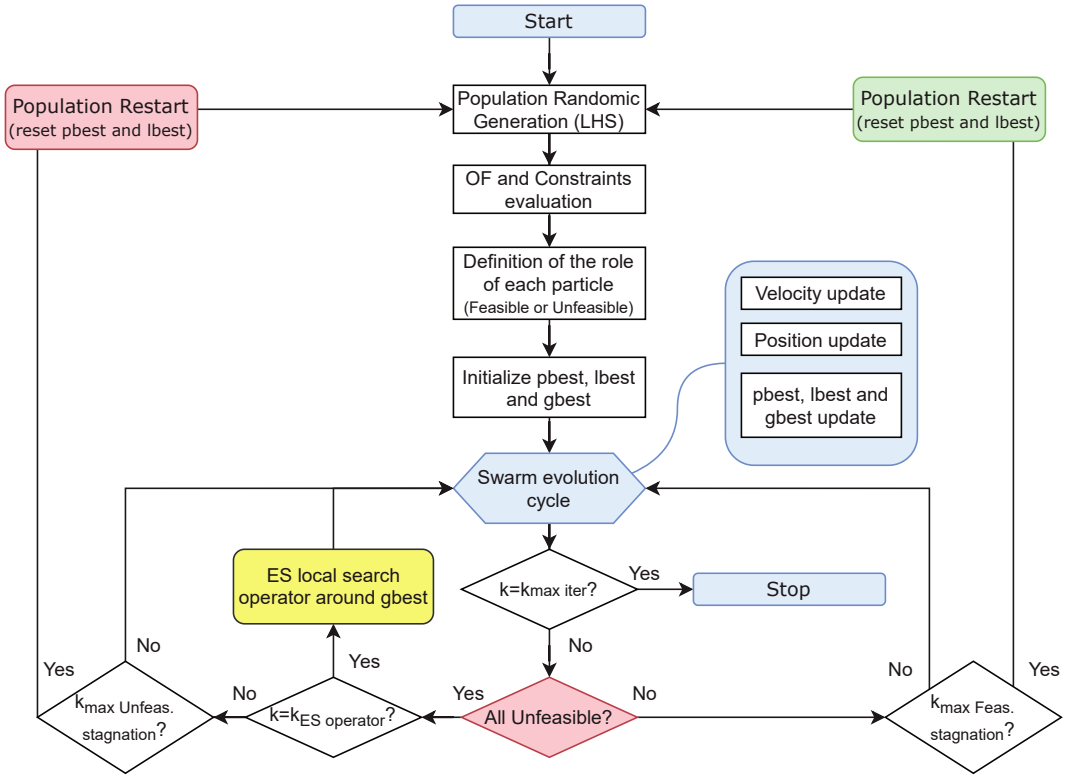

Fig. 3.1 Enhanced PSO multi-strategy flowchart.

It may happen that the feasible region is quite little and narrow with respect to the entire search space; therefore, after some iterations, the swarm also may not have found the feasible region yet. Since the swarm has so far minimized the constraint violation, the swam has probably converged to an unfeasible point with the minimum value of constraint violation, and the feasible region may be located relatively close to that point. This fact suggests that by enhancing the local exploration around the so far unfeasible gbest founded point, the algorithm could be able to identify the feasible search space. Therefore, if the swarm has stalled to an unfeasible point for a number $k = k_{\text{ES operator}}$ of iterations, a local search operator based on the Evolutionary Strategy approach is thus performed. The Evolutionary Strategy (ES) algorithm is another famous paradigm of the classical EAs based on Darwinian Selection and it was developed by Ingo Rechenberg and Hans-Paul Schwefel at the Technical University of Berlin around the 1960s Martí et al. (2018), Beyer and Schwefel (2002). Without entering deeper into the details of this algorithm, it is necessary to recall that this is a population-based method which relies on the survival

of the fittest members. Starting from a parent population, the best individuals have a greater chance to be selected and evolve, forming a certain number of offspring which are generated throughout a slight mutation in the genome of the selected parents. The degree of mutation is governed by a mutation step, which is usually drawn by a Gaussian normal distribution $N(0,\sigma)$, in which σ is also known as the *mutation step* size Beyer and Schwefel (2002), Eiben and Smith (2003). In formulae, it is possible to express that each gene of a selected parent x_i undergoes a mutation procedure which produces a new offspring's gene equal to $x_i + N(0,\sigma)$. Then, the parents and the offspring will compete for survival, and only the best individuals will survive to the next generation. The main advantage of ES is that it is based on a single parameter to be tuned, the mutation step σ. Many variants of ES were developed in recent decades as mentioned in Beyer and Schwefel (2002), but the self-adaptation strategy (also denoted as σSA-ES or simply SA-ES Beyer (1995), Fister jr and Fister (2015), Hansen (2006)) is taken into account in the current study. To perform an SA-ES, it is necessary to consider a new representation for the individuals. From a practical point of view, when the parent genome is slightly mutated, if the generated offspring is better in terms of OF evaluation, this offspring will probably survive to the next generation, and it will probably spread its improved genome in the next iterations. Based on this observation, the mutation step can also be added to the original genome of the parent chromosome, giving a new individual representation such as $(x_1,\ldots,x_n,\sigma)$. In this way, not only the genes but also the mutation step undergoes the mutation operator. Thus, if a better offspring is obtained, it will survive and spread its chromosome information, which now implicitly takes into account a new adaptive mutation step. Therefore, in an indirect manner, good individuals will also generate good mutation steps which will be adaptively tuned during the next generations. The above-mentioned approach is known in the literature as SA-ES with uncorrelated mutation with one step size Eiben and Smith (2003), Fister jr and Fister (2015). When a number of different mutation steps are considered, one for each gene in the chromosome ,such as $(x_1,\ldots,x_n,\sigma_1,\ldots,\sigma_n)$, the adaptive ES strategy is called SA-ES with uncorrelated mutation with n step size Eiben and Smith (2003), Fister jr and Fister (2015). It is now clear that the main advantage to introduce the ES local search operator to the current enhanced PSO implementation is due to the fact that it can be implemented without manually tuning other parameters because they are self-tuned by the algorithm itself. For example, in Miranda and Fonseca (2002), a hybridization of the PSO with ES

was performed to enhance the classical velocity update with an adaptive update of the inertia weight and the acceleration factors. For the sake of completeness, there are more sophisticated self-adaptive approaches which take into account also the correlations among the various step sizes associated with the various genes, which are named as SA-ES with correlated mutation Eiben and Smith (2003), Fister jr and Fister (2015) or covariance matrix adaptation CMA-ES Beyer (1995), Fister jr and Fister (2015), Kramer (2010). In the current study, the SA-ES with uncorrelated mutation with n step size operator is integrated with the PSO inside a local search operator in order to try to locate the feasible region if the swarm stalls to an unfeasible point for $k_{\text{ES operator}} = 10$ iterations. From the unfeasible gbest starting point $x^{Gb,\text{unfea}}$, a population of $N_p = 50$ parent points is sampled from a multivariate Gaussian mixture model in which each component has mean equal to the gbest's i-th component, $x_i^{Gb,\text{unfea}}$, and covariance equal to a first attempt mutation step σ_i. Each i-th mutation step is defined by:

$$\sigma_i = \tau \cdot N(0,1) \tag{3.13}$$

i.e., the absolute value of the product of a random number sampled from a normal standard distribution $N(0,1)$ multiplied to a learning rate parameter τ, which is suggested in Beyer (1995) to be assumed as $1/\sqrt{N_p}$. Then, a first population of $N_o = 100$ mutated offspring is generated by randomly selected parents adopting a mutation scheme in which the i-th new mutation step size component is updated as:

$$\sigma_{i,\text{off}} = \max\left(0, \sigma_i + N(0,1)\right). \tag{3.14}$$

Thereafter, a new offspring point is obtained by adding to the parent position the mutated vector sampled by the multivariate Gaussian mixture model with a mean equal to a zero array and covariance equal to the mutation step size vector updated as above. Subsequently, the mutated offspring are added to the parent population, and the best N_p individuals are selected to survive to the next iteration in terms of constraints violations (or in case of feasible points in term of OF). In the ES jargon, this approach is called the $\mu + \lambda$−ES strategy because the μ (N_p) parents will compete with both each other and also new λ (N_o) offspring, but finally, only μ individuals will survive, whereas the others will be discarded Beyer (1995). This mechanism resembles the steady-state approach of other EAs likewise in the genetic algorithm GA Martí et al. (2018). The ES operator could theoretically perform a maximum number of local iterations equal to $k_{\text{max,Local}} = 50$, but in the case that a

feasible point is found, the ES evolutionary cycle is interrupted. This new feasible point is thus set up as the gbest of the previous PSO swarm, which remained in a sort of standby state while the local ES operator was in action. In summary, the PSO cycle, which has entered in the ES operator due to the fact that it stalled for $k_{\text{ES operator}} = 10$ iterations on an unfeasible gbest point, can now restart again as usual with an improved knowledge provided by a new feasible posed gbest point found by the local search ES operator. The numerical example Problem g06, whose statement is in the Appendix 5.7 (Sickle Problem Simionescu et al. (2004b)), has been depicted in Figures 3.2 and 3.3 to graphically show the enhanced multi-strategy PSO procedure. Each swarm particle is able to see only the sub-figures (a), (c), and (e) of Figure 3.2 when its position is inside the feasible region (with the role to minimize the OF); otherwise, it is able to see only the landscape produced by the constraint envelope, subfigures (b), (d), and (f) of Figure 3.2. After 10 stagnations on the unfeasible gbest point (black cross in sub-figures (a), (b), (c), and (d) of Figure 3.2), the ES operator was performed. It generated a local population of points near the unfeasible gbest point, which are colored as purple if they are unfeasible or green if they are feasible. Then, this population evolves with the before explained SA-ES approach until at least one point falls inside the feasible region (which is the space between the two blue parabolas) or the maximum number of local iterations is reached. In that specific case, at the first local iteration, some feasible points were already found. Therefore, the best individuals in term of OFs was selected among the green points of Figure 3.2c,d, and then the PSO could continue its evolutionary cycles until the maximum number of iterations were reached ($k_{max} = 500$). The history of the optimal solution found during the PSO iterations is depicted in Figure 3.3.

For some very hard problems, it may also happen that after the action of the ES local search operator, the feasible region is not found. In that case, the PSO starts the evolution cycle again with the same unfeasible gbest point for some other iterations until the feasible region is found. Otherwise, when the iterations reach a total number of unfeasible stagnations $k_{\text{max Unfeas Stagn}} = 15$, the complete reset of the population is performed. In practise, the algorithm completely restarts again from the first point of the flowchart, as shown in Figure 3.1. Therefore, the hope is that a completely new random sampling of the initial swarm will generate a new initial configuration which may find this time the right path to the optimal solution of the optimization problem.

On the contrary, when the PSO normally finds the feasible region and it optimizes the solution until it reaches a gbest which stagnates for a certain number of iterations $k_{\text{max Feas Stagn}} = 50$, the population is restarted as well. This is due to the fact that the so far found optimal solution could be a local minimum. If there is a certain number of iterations left before reaching the maximum PSO available iterations, $k < k_{\max}$, the swarm is thus restarted again from the first step of the PSO flowchart. In that case, all the memories of the population are reset (pbests and lbests), but the so far found optimal solution (gbest) remains unchanged, unless a better solution in terms of OF is found from the new restarted-swarm exploration phase.

In the following section, the enhanced multi-strategy PSO has been tested on some constrained numerical benchmark literature problems, and the results are compared with two PSO implementations, which adopt a typical penalty approach.

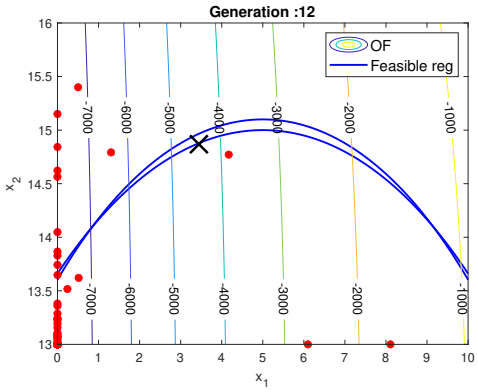

(a) *OF—Generation 12*

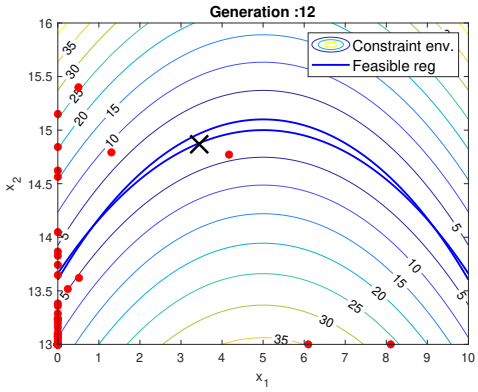

(b) *Constraints—Generation 12*

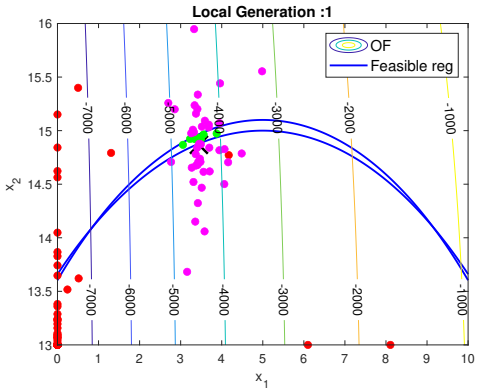

(c) *OF—ES operator Generation 1*

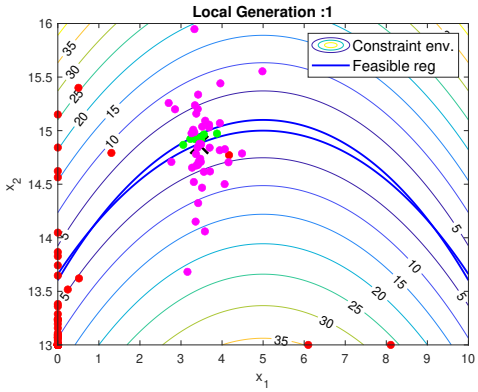

(d) *Constraints—ES operator Generation 1*

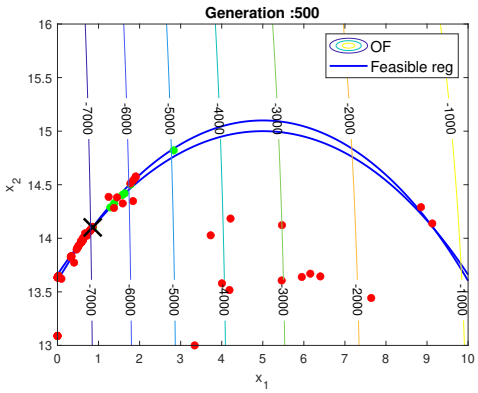

(e) *Generation 500*

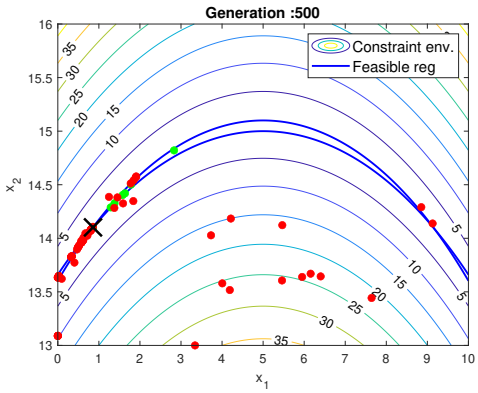

(f) *Generation 500*

Fig. 3.2 Example Problem g06, see the Appendix 5.7 (Sickle Problem Simionescu et al. (2004b)); (**a**,**b**) the OF and constraints envelope contour representations, respectively at generation 12. The black cross marker is the unfeasible gbest, the red dots are the swarm points. (**c**,**d**) After 10 unfeasible stagnations, the ES local search operator generate a local search population (purple dots) to find the feasible region (green dots). (**e**,**f**) the OF and constraints envelope contour representations, respectively, at the final generation 500. The black cross marker is the feasible gbest point, the red ones are the particles in a unfeasible region, and the green ones are the particle inside the feasible region.

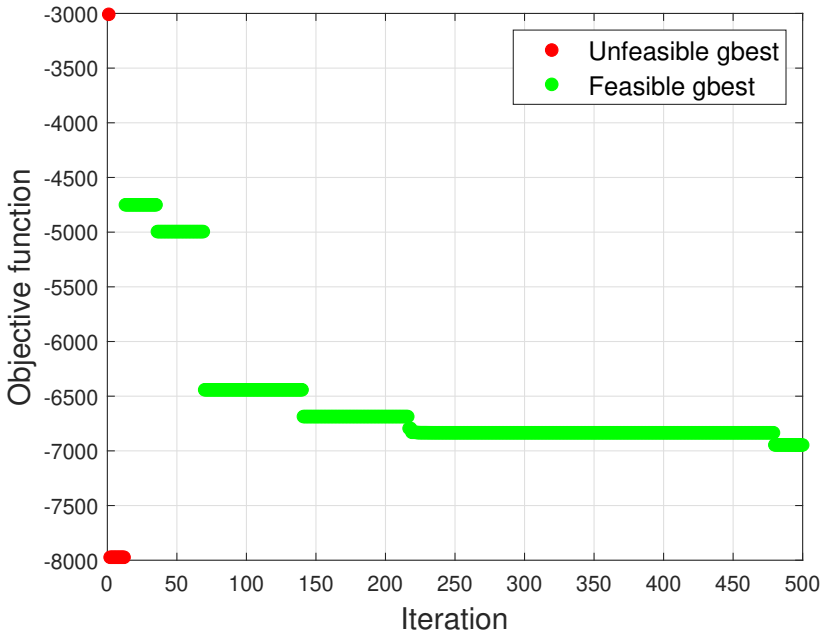

Fig. 3.3 Example Problem g06, see Appendix 5.7 (Sickle Problem Simionescu et al. (2004b)); Objective function history of the gbest (optimal solution).

3.4 Numerical Test and Comparisons

The new enhanced multi-strategy PSO illustrated in the previous section was implemented in a Matlab environment and some numerical constrained benchmark tests from the literature were analysed. In particular, the statements of the mathematical constrained problems were taken from Long et al. (2013), in which a total of 13 constrained problems are illustrated. In the current study, only some problems were considered, in particular, the problems with inequalities constraints only were analysed. As stated before, the PSO does not perform very well with equality constraints despite some strategies being proposed in literature to convert each equality constraint into a couple of equivalent inequality constraints. For the sake of completeness, the selected problem statements are also reported in the Appendix 5.7 of the present paper. In order to make some comparisons with the other more classical constraint handling approaches, the current enhanced multi-strategy PSO is compared with a more classic penalty approach. For this purpose, the PSO code proposed by Alam (2016a) was adopted and modified in order to take into consideration both

a static penalty approach as previously mentioned in (5.5) and also with a dynamic penalty as in (3.7). The penalty factors were properly tuned problem by problem in order to obtain the optimal results. The swarm size was set to $N = 100$, and the maximum allowable iterations were fixed to $k_{\max} = 500$ for all the PSOs considered. The comparisons shown in Table 3.1 are developed from the results obtained by 50 independent runs and making comparisons among best and worst results and the mean and standard deviation of the OF from the dataset of the 50 final results for the 3 different PSOs. The results in Table 3.1 produced by the enhanced multi-strategy PSO are satisfactory for the selected numerical problems, and they are generally consistent if compared with the theoretical results and with the other penalty-based PSO implementations. This proves the effectiveness of the current enhanced PSO implementation to deal with constrained optimization problems without the tedious calibration of too many arbitrary parameters. Because of these initial promising results, future works should therefore include some other numerical applications and some engineering practical optimization problems.

Table 3.1 Selected numerical benchmark examples taken from Long et al. (2013) and comparisons of the final results for 50 runs among the enhanced multi-strategy PSO (*PSO_MS*), the PSO with static penalty (*PSO_ST*), and the PSO with dynamic penalty (*PSO_DYN*).

Problem g01	*PSO_MS*	*PSO_ST*	*PSO_DYN*
optimum		−15.000	
best OF	−15.000	−15.000	−15.0
worst OF	−12.002	−12.000	−12.000
mean	−14.443	−13.938	−13.920
std	0.89478	1.4333	1.4546
Problem g02	*PSO_MS*	*PSO_ST*	*PSO_DYN*
optimum		0.803619	
best OF	0.80357	0.80146	0.79358
worst OF	0.60963	0.52013	0.38285
mean	0.75896	0.70105	0.66597
std	0.063604	0.07356	0.087006
Problem g04	*PSO_MS*	*PSO_ST*	*PSO_DYN*
optimum		−30,665.539	
best OF	−30,666.0	−30,666.0	−31,207.0
worst OF	−30,666.0	−30,665.0	−30,137.0
mean	−30,666.0	−30,665.0	−31,138.2
std	2.20e-05	0.86587	252.2036
Problem g06	*PSO_MS*	*PSO_ST*	*PSO_DYN*
optimum		−6961.81388	
best OF	−6961.8	−6973.0	−6963.0
worst OF	−6958.4	−6973.0	−6963.0
mean	−6960.7	−6973.0	−6963.0
std	0.97521	0.0000	0.0000
Problem g07	*PSO_MS*	*PSO_ST*	*PSO_DYN*
optimum		24.3062091	
best OF	24.426	25.034	24.477
worst OF	27.636	30.203	30.112
mean	25.4129	28.508	27.043
std	1.1209	1.4351	1.8821

Table 3.1 *Cont.*

Problem g08	*PSO_MS*	*PSO_ST*	*PSO_DYN*
optimum		0.095825	
best OF	0.095825	0.095825	0.095825
worst OF	0.095825	0.095825	0.095825
mean	0.095825	0.095825	0.095825
std	6.96e-17	6.77e-17	7.10e-17
Problem g09	*PSO_MS*	*PSO_ST*	*PSO_DYN*
optimum		680.6300573	
best OF	680.64	680.63	680.63
worst OF	680.98	680.72	680.73
mean	680.73	680.66	680.66
std	0.079365	0.017526	0.018915
Problem g12	*PSO_MS*	*PSO_ST*	*PSO_DYN*
optimum		1.0	
best OF	1.0	1.0	1.0
worst OF	1.0	1.0	1.0
mean	1.0	1.0	1.0
std	0.0000	2.12e-15	0.0000

3.5 Structural Optimization on Literature Benchmarks

In this final part, some well-acknowledged structural engineering optimization problems from the literature have been adopted for evaluating the performances of the proposed multi-strategy PSO algorithm with the unfeasible local search operator. In the analysed benchmarks, the multi-strategy PSO has been compared with other optimization strategies, i.e., the PSO with static and dynamic penalty inspired by the code of Alam (2016a) and with the GA from Matlab's built-in code functions. Structural optimization problems can be mainly grouped into three main categories Christensen and Klarbring (2008a): the *size optimization*, where the aim is to find

the optimal size of the structural elements; the *shape optimization*, in which the design variables govern the structural shape; the *topology optimization*, which is the more complex because it involves the modification of the structural typology and morphology. These problems could be tackled separately or even combined. Mainly focusing on the contribution of Camp and Farshchin (2014a), in the current study, three different truss design constrained size optimization problems have been analysed. The main goal of truss design problems is to minimize the total weight w of the structure, which is indirectly connected to the material consumption volume amount and thus to the cost of the structure Christensen and Klarbring (2008a). Indeed, adopting a certain material with unit weight ρ_i, the main goal results in seeking for the optimal cross-sectional areas A_i to be devoted to every structural element in the design domain. A first constraint is represented by the box-constraint related to the admissible range of cross section area values to be adopted $A_i \in [A_i^{\text{LB}}, A_i^{\text{UB}}]$. Thereafter, at least two other inequality constraints have to be considered. The first one is related to the respectfulness of the maximum allowable stress σ_{adm} in each truss member (resistance-side constraint) and the second one is referred to the respectfulness of a maximum displacement threshold δ_{adm} (deformation-side constraint). The general formulation of the truss design problem can be stated as follows:

$$\begin{aligned} \min_{x\in\Omega} \quad & f(x) = \sum_{i=1}^{N_e l} \rho_i L_i A_i \\ \text{s.t.} \quad & A_i^{\text{LB}} \leq A_i \leq A_i^{\text{UB}} \\ & \sigma_i \leq \sigma_{\text{adm}} \\ & \delta \leq \delta_{\text{adm}} \end{aligned} \tag{3.15}$$

where $N_e l$ is the total number of elements in the truss design domain and L_i is the actual length of each member. The material adopted in the current study is structural steel with unit weight of $\rho_i = \rho = 0.1$ lb/in^3 (1 lb/in^3 is equal to 0.0276799 kg/cm^3) and Young's modulus of 10^7 psi (1 psi is equal to 0.00689476 MPa).

3.5.1 Ten-Bar Truss Design Optimization

The first problem analysed is referred to as a 10 bar truss cantilever structure, as depicted in Figure 3.4. In the cantilever structure, each member has been labelled with a number from 1 to 10. The cantilever span is in total 720 inches (1 inch

is equal to 25.4 mm), and the depth is 360 in. The truss structure is loaded by 2 downward forces of 100 kips each (1 kips is equal to 4.4482 kN). The design vector considers cross-section areas as continuous variables belonging to the a close interval $[0.1, 35]$ in^2. The maximum allowable deflection both in horizontal and vertical direction for every node has been set to $\delta_{\text{adm}} = \pm 2$ in, whereas the maximum allowable stress is equal to $\sigma_{\text{adm}} = \pm 25$ ksi. In total, 100 independent executions have been performed, and the mean and standard deviation of the OFs have been calculated. A population size of 50 particles and a maximum iterations number of 500 have been set both for the multi-strategy PSO and the GA. For the PSO with penalty approaches, 500 particles have been set as the swarm size because of their very poor results when only 50 particles have been considered. The optimization results obtained are reported in Table 3.2, which compares the multi-strategy PSO with the PSO with static penalty (PSO-Static), with dynamic penalty (PSO-Dynamic), and with GA. It is worth noting that the penalty approaches fail dreadfully, in this case, to deal with real-life structural design problems, whereas the proposed multi-strategy PSO algorithm produces good results which are comparable with the GA and quite close to the actual unknown optimum solution.

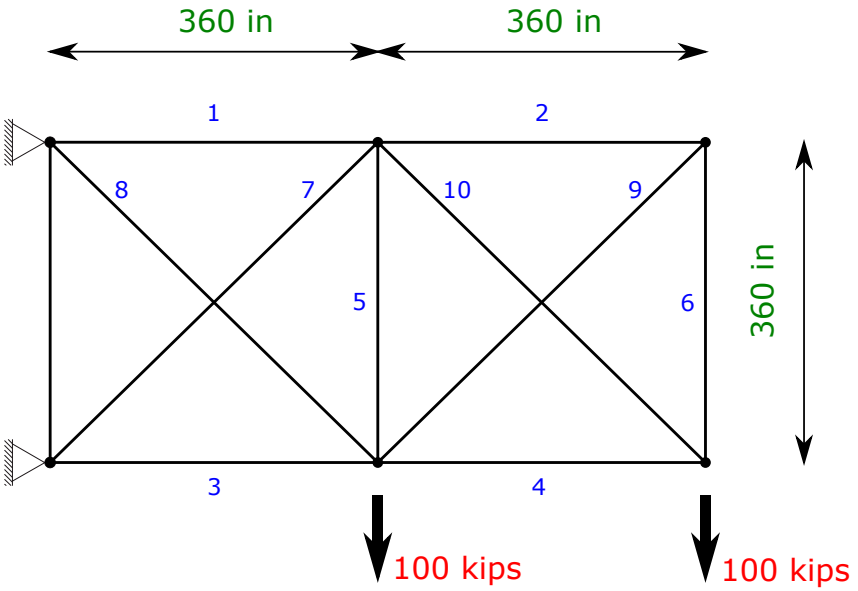

Fig. 3.4 Graphical representation of the 10 bar truss design optimization problem.

Table 3.2 Ten-bar truss design example: results comparisons for 100 runs among the enhanced multi-strategy PSO (*PSO-MS*), the PSO with static penalty (*PSO-Static*), and the PSO with dynamic penalty (*PSO-Dynamic*) and GA.

	Cross-Section [$\mathbf{in}^2$]				
Element	**Sol. from 2014a**	**PSO-Static**	**PSO-Dynamic**	**GA**	**PSO-MS**
1	28.920	29.6888	30.3092	30.145	30.372
2	0.100	18.3211	14.7464	0.100	0.110
3	24.070	19.9891	16.5717	22.466	23.644
4	13.960	18.2381	25.1945	15.112	15.391
5	0.100	2.3404	4.5489	0.101	0.101
6	0.560	20.8674	26.1207	0.543	0.496
7	21.950	21.1805	32.2698	21.667	20.984
8	7.690	16.0851	0.2168	7.577	7.410
9	0.100	6.0845	7.5871	0.100	0.103
10	22.090	25.5632	23.524	21.695	21.378
best OF [lb]	5076.310	6141.986	6333.035	5063.250	5063.328
worse OF [lb]	-	8415.134	8675.750	5144.148	5229.108
mean [lb]	-	7294.455	7501.395	5079.744	5076.473
std. dev. [lb]	-	516.7823	475.389	14.1194	24.867

3.5.2 Twenty-Five-Bar Truss Design Optimization with Multi-Load Cases Conditions

The second structural optimization problem analysed is referred to as the 25 bar three-dimensional truss tower structure, as depicted in Figure 3.5. In plan view, the tower footprint is a square of side 200 in, which tapers to 75 in at an elevation of 100 in, and finally reaches the maximum elevation at 200 in from the ground. The structural nodes have been labelled with a number from 1 to 10. The design vector considers the cross section areas of each member as continuous variables belonging to the close interval $[0.01, 3.40]$ in^2. The cross-sectional areas have been gathered into eight groups, as depicted in Figure 3.6, in order to reduce the dimensionality of the design vector. The maximum allowable displacement has been set to $\delta_{\text{adm}} = \pm 0.35$ in in every direction, whereas the maximum allowable stress of each member has been

to $\sigma_{adm} = \pm 40$ ksi. Furthermore, the current structural problem takes into account two different load cases during the optimization process, as shown in Figure 3.5. In total, 100 independent executions have been performed, and the mean and standard deviation of the OFs have been calculated. A population size of 50 particles and a maximum iterations number of 500 have been set both for the multi-strategy PSO and the GA. For the PSO with penalty approaches, 500 particles have been set as the swarm size because of their very poor results when only 50 particles have been considered. The optimization results obtained are reported in Table 3.3, which compares the multi-strategy PSO with the PSO with the static penalty (PSO-Static), with the dynamic penalty (PSO-Dynamic), and with the GA. It is worth noting that, even in this case, the penalty approaches dreadfully fail to deal with real-life structural design problems, whereas the proposed multi-strategy PSO algorithm produces good results which are comparable with the GA and quite close to the actual optimum solution.

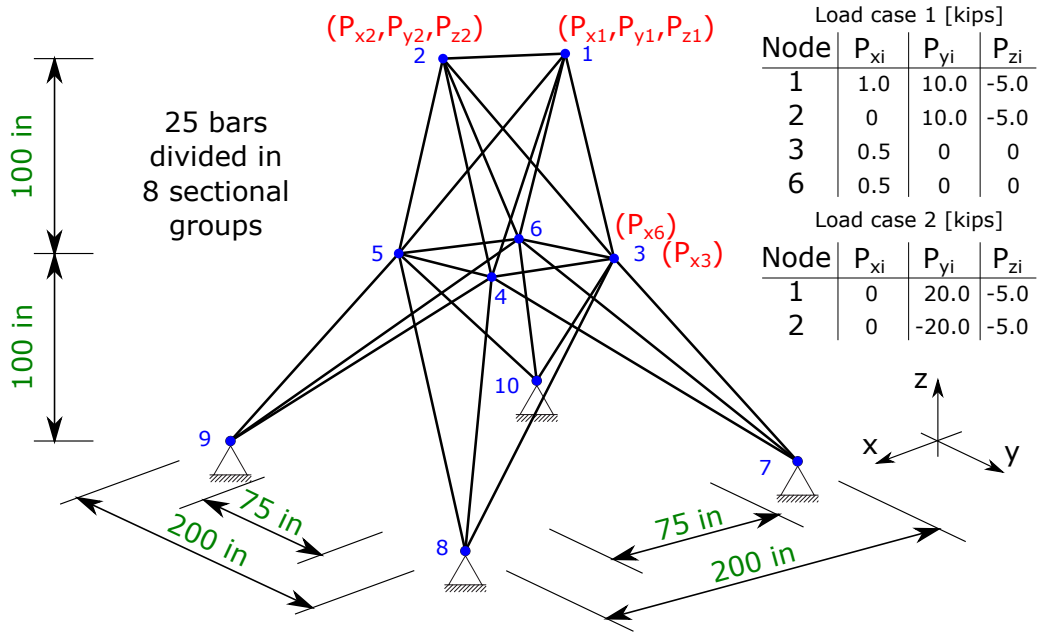

Fig. 3.5 Graphical representation of the 25 bar truss design optimization problem.

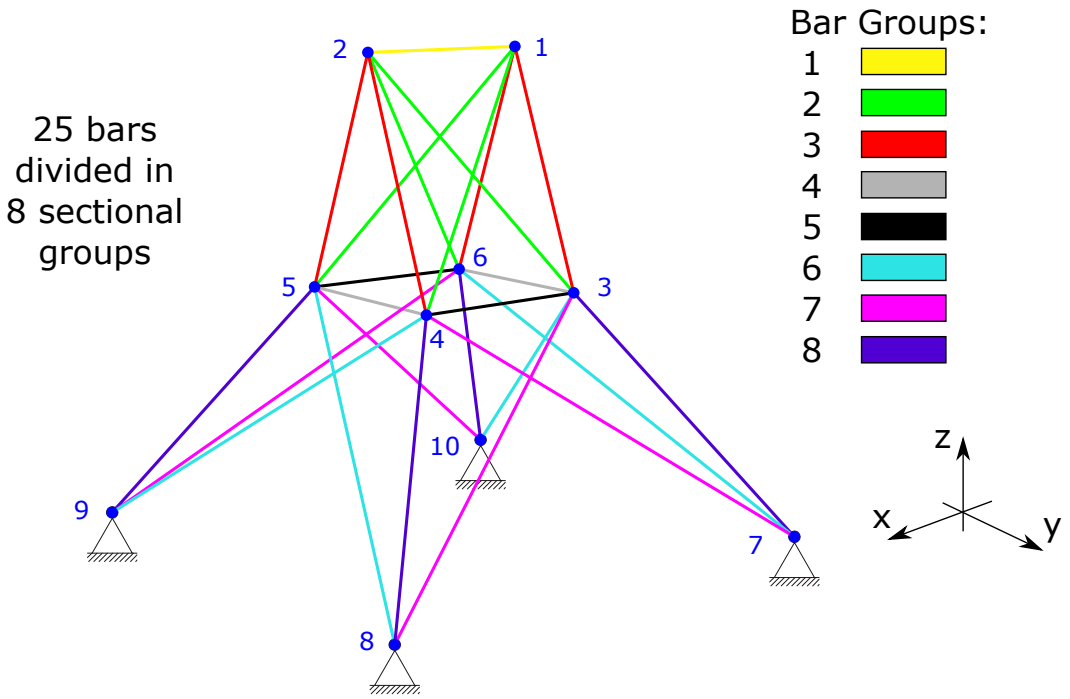

Fig. 3.6 Graphical representation of the 8 bar groups in which are collected all the members of the 25 bar truss design optimization problem.

Table 3.3 Twenty-five bar truss design example: results comparisons for 100 runs among the enhanced multi-strategy PSO (*PSO-MS*), the PSO with static penalty (*PSO-Static*), and the PSO with dynamic penalty (*PSO-Dynamic*) and GA.

	Cross-Section [$\mathbf{in}^2$]				
Bar Group	**Sol. from 2014a**	**PSO-Static**	**PSO-Dynamic**	**GA**	**PSO-MS**
1	0.100	2.054	1.116	0.010	0.011
2	1.800	2.675	2.670	2.023	1.976
3	2.300	1.402	1.942	2.941	2.989
4	0.200	3.388	0.166	0.010	0.010
5	0.100	0.204	0.342	0.010	0.011
6	0.800	0.453	1.985	0.671	0.690
7	1.800	1.274	1.976	1.673	1.689
8	3.000	0.048	2.345	2.694	2.654
best OF [lb]	546.010	568.186	596.058	545.236	545.249
worse OF [lb]	-	100,583.118	22,954.297	557.755	552.378
mean [lb]	-	1673.393	1122.518	547.828	546.003
std. dev. [lb]	-	9991.0201	3129.3192	2.0743	0.7879

3.5.3 Seventy-Two-Bar Truss Design Optimization with Multi-Load Cases Conditions

The last structural optimization problem analysed in the current study is referred to as a 72 bar three-dimensional truss tower structure, as depicted in Figure 3.7. In plan view, the tower footprint is a square of side 120 in, with 4 modular floors, each of them with a height of 60 in. The structural nodes have been labelled with a number from 1 to 20. The design vector considers the cross-sectional areas of each member as continuous variables belonging to the close interval $[0.1, 3.0]$ in^2. There are 18 bars inside each modular floor which can be grouped in 4 groups, as depicted in Figure 3.8. Therefore, since there are 4 floors, the cross-sectional areas have been parametrized into 16 groups in total in order to reduce the dimensionality of the design vector. The maximum allowable displacement has been set to $\delta_{\text{adm}} = \pm 0.25$ in in every direction, whereas the maximum allowable stress of each member has been set to $\sigma_{\text{adm}} = \pm 25$ ksi. Furthermore, the current structural problem takes into account two

different load cases during the optimization process, as shown in Figure 3.7. In total, 100 independent executions have been performed, and the mean and standard deviation of the OFs have been calculated. A population size of 50 particles and a maximum iterations number of 500 have been set both for the multi-strategy PSO and the GA. For the PSO with penalty approaches, 500 particles have been set as the swarm size because of their very poor results when only 50 particles have been considered. The optimization results obtained are reported in Table 3.4, which compares the multi-strategy PSO with the PSO with the static penalty (PSO-Static), with the dynamic penalty (PSO-Dynamic), and with the GA. Similarly to the previous cases, it is worth noting that the penalty approaches dreadfully fail to deal with real-life truss design structural optimization problems, whereas the proposed multi-strategy PSO algorithm produces good results which are comparable with the GA and quite close to the actual optimum solution. It is worth noting that the mean value and the best one are very close to the reference optimal solution from Camp and Farshchin (2014a). The final solution is even characterized by a low standard deviation among the 100 algorithm runs, demonstrating that the multi-strategy PSO is able to reach the optimal results in a more reliable way, reducing the uncertainties and scattering of the final results.

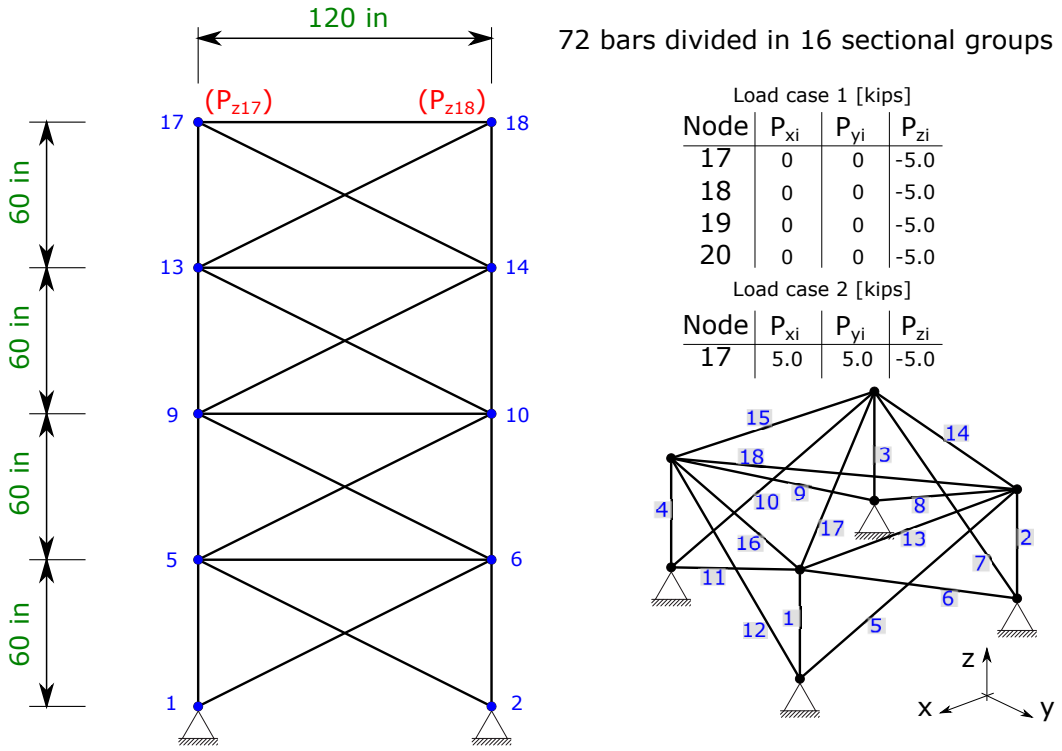

Fig. 3.7 Graphical representation of the seventy-two bars truss design optimization problem.

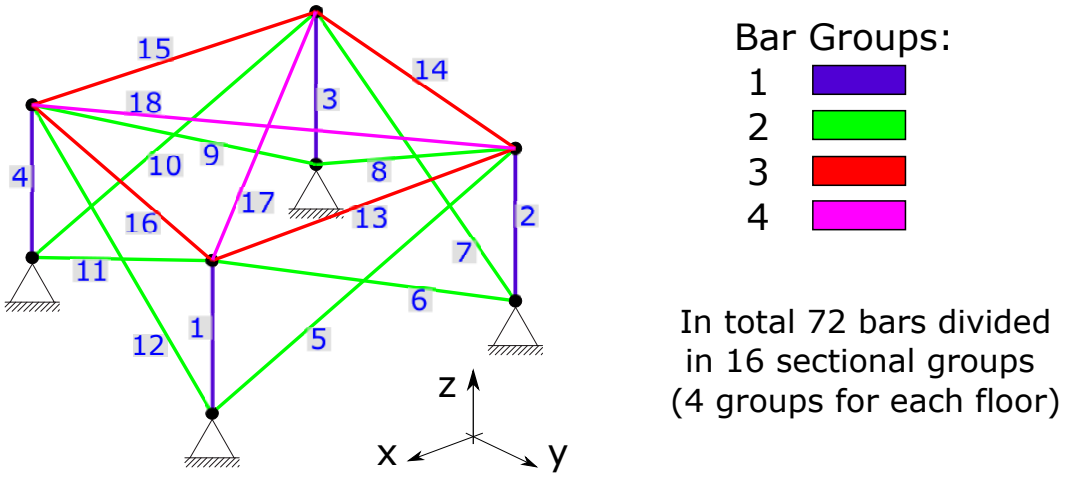

Fig. 3.8 Graphical representation of the four bar groups in which are collected the members inside one module of the seventy-two bars truss design optimization problem.

Table 3.4 Seventy-two bars truss design example: results comparisons for 100 runs among the enhanced multi-strategy PSO (*PSO-MS*), the PSO with static penalty (*PSO-Static*) and the PSO with dynamic penalty (*PSO-Dynamic*) and GA.

	Cross-Section [**in**^{2}]				
Bar Group	**Sol. from 2014a**	**PSO-Static**	**PSO-Dynamic**	**GA**	**PSO-MS**
1	2.026	2.176	0.746	1.801	1.856
2	0.533	0.661	0.539	0.545	0.523
3	0.100	2.686	0.523	0.100	0.100
4	0.100	1.771	2.660	0.100	0.100
5	1.157	1.662	2.316	1.311	1.301
6	0.569	0.276	1.051	0.511	0.519
7	0.100	0.158	0.642	0.100	0.100
8	0.100	0.986	2.370	0.100	0.100
9	0.514	0.271	0.757	0.531	0.539
10	0.479	1.240	0.793	0.520	0.507
11	0.100	0.517	0.453	0.100	0.100
12	0.100	0.378	1.754	0.107	0.101
13	0.158	0.119	2.236	0.157	0.157
14	0.550	0.794	1.677	0.534	0.540
15	0.345	1.363	0.824	0.386	0.403
16	0.498	1.190	0.830	0.561	0.564
best OF [lb]	379.310	629.108	662.148	380.150	379.753
worse OF [lb]	-	1054.764	1110.795	400.147	381.541
mean [lb]	-	874.024	854.233	383.377	380.150
std. dev. [lb]	-	88.8254	82.1187	3.7299	0.2766

3.6 Discussion

In the previous sections, it has been demonstrated that the proposed multi-strategy PSO algorithm provided quite interesting results. Foremost, focusing on numerical benchmark problems, the multi-strategy PSO technique has been compared with two other traditional PSO implementations which adopt the penalty function approaches to deal with constraints. The three algorithms have been executed 50 independent

times for each numerical problem stated in the Appendix 5.7, and the final results have been collected in Table 3.1. The optimization results have been presented in terms of the best solution, the worst solution, the mean of the OF values, and the standard deviation of the final results. These parameters evidence the scattering in the found solutions by the various algorithms. Specifically, the standard deviation parameter gives a direct insight into the degree of failure of the meta-heuristic algorithm to find the known benchmark solutions among the independent executions. In particular, the multi-strategy PSO presents in general lower values of a standard deviation compared with PSO-penalty methods, or at least the same order of magnitude. Furthermore, the multi-strategy PSO appears to be a more reliable algorithm because, focusing, e.g., on the problem g06, despite the standard deviation of the PSO-penalty being zero, they fail to reach the optimum solution. This fact highlights that, notwithstanding that the penalty functions method is very simple and easy to implemented, in general, it does not always represent the best approach to successfully deal with every kind of problem. Indeed, e.g., in problem g06, the nil value of the standard deviation actually points out how the penalty method provides a quite deterministic PSO algorithm which is trivially entrapped in the same local optimum among the independent runs, jeopardizing the potentialities of the stochastic search.

On the other hand, focusing on real-world engineering structural optimization problems, the multi-strategy PSO algorithm has revealed its powerful capabilities to deal with complex, combinatorially demanding, and highly non-linear optimization problems. For the sake of completeness, in these problems, a further comparison has been provided by the GA algorithm from the Matlab environment. This latter comparison is extremely relevant because it allows for performing a more objective evaluation which relies on a completely different implementation with respect to the PSO framework only. The optimization results of the 10 bar truss, 25 bar truss, and 72 bar truss problems have been reported in Tables 3.2–3.4, respectively. In all the analysed cases, the multi-strategy PSO provided very interesting results, which are really close or even better to the reference solution obtained from Camp and Farshchin (2014a). The penalty method revealed their weakness when dealing with these kinds of highly non-linear problems because they provided mean solutions quite far from the reference one and even more scattered when considering the standard deviation values. In conclusion, the proposed multi-strategy PSO algorithm provides an enhanced and more reliable implementation because it results in lower

standard deviation values than the GA ones, at least in the last two problems hereby analysed, which are the most complex and computationally demanding.

3.7 Conclusions

The research and developments in the EAs field to solve optimization problems are continuously increasing because of their lack of mathematical proofs and also because the perfect algorithm to solve any kind of problem does not exist. Therefore, in the present study, a new variant of the PSO has been implemented for the purpose of studying a different way to deal with constrained optimization problems. In fact, the standard version of the PSO Kennedy and Eberhart (1995b) lacked a proper mechanism to deal with constrained problems, and in literature Coello Coello (2002), Koziel and Michalewicz (1999a), Michalewicz and Fogel (2008), there are at least five main kinds of constraint-handling approaches. The so far most extensively used method in many different practical applications is the penalty function method. The main disadvantage of this technique is that it requires the user to tediously tune some arbitrary penalty factors, which is not always an easy task. In the current study, for the purpose of enhancing the performance of the standard version of the algorithm, the most important state-of-the-art improvements are also implemented, such as the inertia weight Shi and Obaiahnahatti (1998) and the neighbourhood topology Medina et al. (2009). Furthermore, in order to avoid a penalty-based approach, the violation degree of the constraints is directly exploited to define the aim of a particle which has to minimize this violation if it lies in the unfeasible region. Otherwise, if a particle lies in the feasible region, this particle is dedicated to minimize the OF. Another improvement is given by a local search self-adaptive ES operator, which takes action if the feasible region is not found by the PSO for a certain number of iterations. This allows the algorithm to spread the exploration around the so far unfeasible best solution found, which may be very close to the feasible region, if it is located in near this point. If the ES operator successfully finds the feasible region, this allows it to boost the PSO, giving it an important hint on where the feasible region is located, as demonstrated in Figure 3.2. If the local operator fails to identify the feasible region, the swarm has probably been entrapped in a local unfeasible minimum quite far from the feasible region. Consequently, only a new randomly resampled swarm may probably find the right path to the feasible region and thus to the real optimum.

This new enhanced PSO appears to be noticeably effective compared to other PSO algorithms which adopt a more traditional penalty-function-based method, as shown in Table 3.1. Outstanding results have been pointed out in the structural optimization benchmark analysed in the current study, which involves three truss design problems from the literature. The proposed PSO effectively dealt with real-life optimization problems, much better than traditional penalty approaches, and reached results comparable and competitive with other state-of-the-art implementations such as the GA.

Although the PSO algorithm already possesses two kinds of memories (cognitive and social), most of the information about the swarm visited positions is discarded, and a better exploitation of the past particles positions remains to be fully determined. In another recent work Rosso et al. (2021b), a first promising step in that direction has been already made. In Rosso et al. (2021b), the PSO has been hybridized with a machine learning algorithm, the support vector machine (SVM). The SVM has been trained on the dataset composed by all the visited swarm positions in order to build a predictive model which is able to learn where the feasible and the unfeasible regions are located in the search domain. The improvement in the managing information provided by the swarm positions during all the iterations allowed the algorithm to reduce the search space extension and considerably improve the PSO's performance.

Appendix: Test Functions Constrained Problems

In the following, the statements of the selected benchmark numerical problems, taken by Long et al. (2013), which were tested in the present work are exposed.

1. **Problem g01**
   Minimize:

$$f(x) = 5\sum_{i=1}^{4} x_i - 5\sum_{i=1}^{4} x_i^2 - \sum_{i=5}^{13} x_i$$

   Subject to:

$$
\begin{aligned}
g_1(x) &= 2x_1 + 2x_2 + x_{10} + x_{11} - 10 \leq 0 \\
g_2(x) &= 2x_1 + 2x_3 + x_{10} + x_{12} - 10 \leq 0 \\
g_3(x) &= 2x_2 + 2x_3 + x_{11} + x_{12} - 10 \leq 0 \\
g_4(x) &= -8x_1 + x_{10} \leq 0 \\
g_5(x) &= -8x_2 + x_{11} \leq 0 \\
g_6(x) &= -8x_3 + x_{12} \leq 0 \\
g_7(x) &= -2x_4 - x_5 + x_{10} \leq 0 \\
g_8(x) &= -2x_6 - x_7 + x_{11} \leq 0 \\
g_9(x) &= -2x_8 - x_9 + x_{12} \leq 0
\end{aligned}
$$

where the search space is defined as $0 \leq x_i \leq 1$ $(i = 1, \ldots, 9)$, $0 \leq x_i \leq 100$ $(i = 10, 11, 12)$, $0 \leq x_{13} \leq 1$. The optimum is located at $x^* = [1;1;1;1;1;1;1;1;1;3;3;3;1]$, where $f(x) = -15$.

2. **Problem g02**
   Maximize:

$$f(x) = \frac{\sum_{i=4}^{n} \cos^4(x_i) - 2\prod_{i=1}^{n} \cos^2(x_i)}{\sqrt{\sum_{i=1}^{n} i x_i^2}}$$

   Subject to:

$$
\begin{aligned}
g_1(x) &= 0.75 - \prod_{i=1}^{n} x_i \leq 0 \\
g_2(x) &= \sum_{i=1}^{n} x_i - 7.5n \leq 0
\end{aligned}
$$

   where $n = 20$ and the search space is defined as $0 \leq x_i \leq 10$ $(i = 1, \ldots, n)$. The optimum OF is $f(x) = 0.803619$.

3. **Problem g04**
   Minimize:

$$f(x) = 5.3578547x_3^2 + 0.8356891x_1x_5 + 37.293239x_1 - 40792.141$$

Subject to:

$$
\begin{aligned}
g_1(x) =& 85.334407 + 0.0056858x_2x_5 + 0.0006262x_1x_4 + 0.0022053x_3x_6 \leq 92,\\
g_2(x) =& -85.334407 - 0.0056858x_2x_5 - 0.0006262x_1x_4 + 0.0022053x_3x_6 \leq 0,\\
g_3(x) =& 80.51249 + 0.0071317x_2x_5 + 0.0029955x_1x_2 + 0.0021813x_3^2 - 110 \leq 0,\\
g_4(x) =& -80.51249 - 0.0071317x_2x_5 - 0.0029955x_1x_2 - 0.0021813x_3^2 + 90 \leq 0,\\
g_5(x) =& 9.300961 + 0.0047026x_3x_5 + 0.0012547x_1x_3 + 0.0019085x_3x_4 - 25 \leq 0,\\
g_6(x) =& -9.300961 - 0.0047026x_3x_5 - 0.0012547x_1x_3 - 0.0019085x_3x_4 + 20 \leq 0,
\end{aligned}
$$

where the search space is defined as $78 \leq x_1 \leq 102$ and $33 \leq x_2 \leq 45$ and $27 \leq x_3, x_4, x_5 \leq 45$. The optimum is located at $x^* = [78, 33, 29.995256025682, 45, 36.775812905788]$, where $f(x) = -30,665.539$.

4. **Problem g06**
   Minimize:

$$f(x) = (x_1 - 10)^3 + (x_2 - 20)^3$$

Subject to:

$$
\begin{aligned}
g_1(x) &= -(x_1 - 5)^2 - (x_2 - 5)^2 + 100 \leq 0\\
g_2(x) &= (x_1 - 6)^2 - (x_2 - 5)^2 - 82.81 \leq 0
\end{aligned}
$$

where the search space is defined as $13 \leq x_1 \leq 100$ and $0 \leq x_2 \leq 100$. The optimum is located at $x^* = [14.095; 0.84296]$, where $f(x^*) = -6961.81388$.

5. **Problem g07**
   Minimize:

$$
\begin{aligned}
f(x) =& x_1^2 + x_2^2 + x_1x_2 - 14x_1 - 16x_2 + (x_3 - 10)^2 + 4(x_4 - 5)^2 + (x_5 - 3)^2\\
&+ 2(x_6 - 1)^2 + 5x_7^2 + 7(x_8 - 11)^2 + 2(x_9 - 10)^2 + (x_{10} - 7)^2 + 45
\end{aligned}
$$

Subject to:

$$
\begin{aligned}
g_1(x) =& -105 + 4x_1 + 5x_2 - 3x_7 + 9x_8 \leq 0 \\
g_2(x) =& 10x_1 - 8x_2 - 17x_7 + 2x_8 \leq 0 \\
g_3(x) =& -8x_1 + 2x_2 + 5x_9 - 2x_{10} - 12 \leq 0 \\
g_4(x) =& 3(x_1-2)^2 + 4(x_2-3)^2 + 2x_3^2 - 7x_4 - 120 \leq 0 \\
g_5(x) =& 5x_1^2 + 8x_2 + (x_3-6)^2 - 2x_4 - 40 \leq 0 \\
g_6(x) =& x_1^2 + 2(x_2-2)^2 - 2x_1x_2 + 14x_5 - 6x_6 \leq 0 \\
g_7(x) =& 0.5(x_1-8)^2 + 2(x_2-4)^2 + 3x_5^2 - x_6 - 30 \leq 0 \\
g_8(x) =& -3x_1 + 6x_2 + 12(x_9-8)^2 - 7x_{10} \leq 0
\end{aligned}
$$

where the search space is defined as $-10 \leq x_i \leq 10$ $(i = 1, \ldots, 10)$. The optimum OF is $f(x^*) = 24.3062091$.

6. **Problem g08**
   Maximize:

$$f(x) = \frac{\sin^3(2\pi x_1)\sin 2\pi x_2}{x_1^3(x_1+x_2)}$$

   Subject to:

$$
\begin{aligned}
g_1(x) &= x_1^2 - x_2 + 1 \leq 0 \\
g_2(x) &= 1 - x_1 + (x_2-4)^2 \leq 0
\end{aligned}
$$

   where the search space is defined as $0 \leq x_1, x_2 \leq 10$. The optimum is located at $x^* = [1.2279713; 4.2453733]$, where $f(x^*) = -0.0958250414$.

7. **Problem g09**
   Minimize:

$$
\begin{aligned}
f(x) =& (x_1-10)^2 + 5(x_2-12)^2 + x_3^4 + 3(x_4-11)^2 \\
&+ 10x_5^6 + 7x_6^2 + x_7^4 - 4x_6x_7 - 10x_6 - 8x_7
\end{aligned}
$$

   Subject to:

$$
\begin{aligned}
g_1(x) &= -127 + 2x_1^2 + 3x_2^4 + +x_3 + 4x_4^2 + 5x_5 \leq 0 \\
g_2(x) &= -282 + 7x_1 + 3x_2 + 10x_3^2 + x_4 - x_5 \leq 0 \\
g_3(x) &= -196 + 23x_1 + x_2^2 + 6x_6^2 - 8x_7 \leq 0 \\
g_4(x) &= 4x_1^2 + x_2^2 - 3x_1x_2 + 2x_3^2 + 5x_6 - 11x_7 \leq 0
\end{aligned}
$$

where the search space is defined as $-10 \leq x_i \leq 10$ $(i = 1, \ldots, 7)$. The optimum OF is $f(x^*) = 680.6300573$.

8. **Problem g12**
   Maximize:

$$f(x) = \frac{100 - (x_1 - 5)^2 - (x_2 - 5)^2 - (x_3 - 5)^2}{100}$$

   Subject to:

$$g(x) = (x_1 - p)^2 + (x_2 - q)^2 + (x_3 - r)^2 - 0.0625 \leq 0$$

   where the search space is defined as $0 \leq x_i \leq 10$ $(i = 1, 2, 3)$ and $p, q, r = 1, 2, \ldots, 7$. The optimum OF is $f(x^*) = -1$.

Chapter 4

Optimal strengthening by steel truss arches in prestressed girder bridges

4.1 Introduction

Bridges can be considered the most important components of any road infrastructure. A state of complete or partial functionality loss of such structures generates significant issues on the whole transportation network Kashani et al. (2019). In this light, careful monitoring is of paramount importance with ordinary and extraordinary maintenance interventions in order to ensure an adequate level of functionality and safety over time. In Europe, as in the whole Western world, a considerable number of bridge structures were built between the '50s and '70s during the period of maximum development of road networks using the technology of pre-stressed reinforced concrete Di Ludovico et al. (2010). This technique, which has been established since the '50s, was relatively young, with the consequence that the technologies, materials, and construction process could not rely on consolidated experience. In addition, the structural design process was still mainly focused on the concept of strength, giving little importance to the durability requirement (Petrangeli et al. 2019, 1996). As a result, today, some decades after their construction and often at the end of their service life, many of these bridges show significant evidence of degradation with serious consequences on the safety levels and functionality. Direct evidence of such effects is provided by the different collapses that occurred in recent years in Italy, e.g. the collapse of the Fossano Viaduct in 2017 **?**, the Polcevera Viaduct in 2018

Domaneschi et al. (2020) and the Albiano Magra Bridge in 2020 **?**. Among the main reasons that can be identified, the loss of prestressing due to cable corrosion plays the major role Bazzucchi et al. (2018) Domaneschi et al. (2020) Morgese et al. (2020). In post-tensioned structures, one of the reasons that can facilitate this process is represented by the inadequacy of the ducts injection process during construction. Following several post-tensioned bridge collapses, the UK went so far as to prohibit the use of this technique between the years 1992 and 1996 Petrangeli et al. (2019). At the same time, traffic volumes and the number of heavy vehicles passing through reached levels that were not foreseen in the reference standards at the time of design, further contributing to the structural deterioration Morgese et al. (2020). A solution could be the complete replacement of the structure, but often it turns out to be the most expensive and impactful choice, not only for direct construction costs but also indirect ones such as traffic interruption, overloading of the alternative road system, etc. Park et al. (2005). The alternative choice consists, when possible, of reinforcement interventions that can extend the service life, restoring adequate levels of functionality and safety. The definition of the reinforcement system depends on the evaluations of the designer that is related to own experience and knowledge, identifying the critical conditions, and selecting the most effective solution from the technical, constructional and economic aspects. Each consolidation intervention has advantages and disadvantages: a relatively simple intervention from the point of view of implementation (commonly used materials, common labor, easy installation, etc.) may not be sufficiently efficient in restoring the required performance levels. On the contrary, an extremely efficient intervention from the structural point of view, but which foresees the use of advanced technologies (innovative solutions, highly specialized manpower and companies for the installation, etc.), could raise the costs and make the intervention uneconomic. Based on all of the above considerations, the introduction of new consolidation techniques for existing bridge structures is a topic of crucial interest.

The present work introduces an innovative solution for the reinforcement of a pre-stressed concrete (PRC) beam, which often constitutes a component of most existing bridge decks. With the proposed method the uncertainty related to the damage state of bridges and, consequently, the consolidation interventions were overcome. The new strengthening system leads to restore the safety level of the structure without any knowledge about the loss of prestressing due to cable corrosion. Moreover, the proposed retrofitting system represents a competitive alternative in terms of

installation complexity and even from an economical point of view. The objective is to propose a solution suitable for bridges with grid decks, i.e. composed of several longitudinal girder beams placed side by side and connected by stringers. The proposed solution consists of using two arch-shaped trusses coupled and connected to the existing beam to be consolidated, creating a parallel strengthening system to support part of the loads to which the existing deck is subjected. This kind of solution is analysed on PRC girder bridge which is the most widespread typology of existing heritage in Italy, but this strengthening system may virtually be applied even on composite girder bridges or concrete box girder bridges. Therefore, future works will address the applicability of the proposed retrofitting system to the above-mentioned bridge typologies and the relative case studies. The remaining parts of this paper are organized as follows: Section 2 deals with existing and the proposed consolidation solutions, Section 3 presents the case study with the performed finite element analysis, a parametric sensitivity analysis is the developed (Section 4) with an optimization procedure (Section 5) for the proposed consolidation technique. The remaining sections of the paper (Sections 6 and 7) are devoted to the presentation of the results with a preliminary cost comparison between the proposed solution and the traditional approach.

4.2 Prestressed bridge decks and consolidation solutions

Currently, most of the bridges that are built all over the world adopt pre-stressed reinforced concrete. The complete exploitation of concrete sections and of harmonic steel characteristics, the extensive use of prefabrication, the adoption of automated launching systems have made them very competitive for medium and large spans Arici et al. (2019). While very large spans are covered by cable-stayed and suspension solutions, smaller spans are overcome with truss, frame or arch solutions. In truss bridges, the main elements are beams, i.e. elements stressed mainly by bending and shear. The most commonly used solutions include grid or box girder decks. Focusing on the use of pre-stressed reinforced concrete as the constituent material of the beams or segments, the covered spans range from 30 to 50 m for the first type and up to about 150 m for the second. Grid decks are realized with side-by-side longitudinal beams connected by transversal elements and the slab, this latter usually

cast on-site. The longitudinal beams are generally prefabricated with I or V sections (box girder) pre-tensioned during the production process, post-tensioned on-site or adopting a mixed solution. The most frequent static scheme is the simply supported solution due to the rapidity of assembly. For this reason, such deck type was widely used in the post-second-world-war reconstruction period with the development of highway networks, from the '60s onwards. Due to their age, design and construction faults (inaccurate injection of sheaths, lack of or deterioration in the waterproofing of the deck), and poor maintenance, such bridge types have been increasingly found in critical situations Bazzucchi et al. (2018) Domaneschi et al. (2020) Morgese et al. (2020). Their origins can be divided into three categories: design defects, construction defects, maintenance deficiencies Godart (2015), while reinforcement corrosion is one of the central problems for prestressed concrete structures Recupero et al. (2018).

Given the age of many of the existing bridges, deterioration is certainly one of the factors for which reinforcement interventions are required. Corrosion of the reinforcements or of the prestressing systems, and deterioration of the concrete due to chemical attack, lead to a progressive reduction of the load-bearing capacity and therefore of the safety margins, which must be restored in some way. However, deterioration is not the only factor that makes reinforcement interventions of paramount importance. An increase in the traffic volume and of the axle loads, prestressed losses due to slow phenomena (concrete shrinkage and viscosity), design or executive errors require the infrastructure manager to adopt traffic restrictions or implement reinforcement interventions Daly and Witarnawan (1997).

The selection of the suitable reinforcement system needs to consider several factors (e.g. type of structure, capacity increase needed, cost of the intervention). The economic evaluation must also take into account future maintenance costs of the reinforced structure. It is important to evaluate the condition of the elements to be reinforced and other structural components, including the substructure (foundations, piers, abutments, etc.) Daly and Witarnawan (1997) agency. (1999). The inspection, knowledge and diagnosis phase of the structural condition and its components is fundamental. The reasons and origins that generated the functionality losses and safety levels reduction have to be identified (e.g. corrosion of reinforcement). Moreover, such performance reductions have to be quantified (e.g. decrease in load-bearing capacity) agency. (1999). Considerations of the interventions in terms of interference with traffic flow and also aesthetic evaluations are relevant in the choice of the

appropriate technology.
The following subsection presents a consolidation method widely used to remedy performance losses of existing bridges with prestressed grid decks, mainly related to corrosion degradation. Subsequently, the proposed solution, which is the subject of this paper, will be introduced.

4.2.1 Traditional consolidation systems for bridge decks: external prestressing cables

Adopting the external prestressing solution, the cables are external to the section and not adherent to the concrete bulk. As for traditional prestressing solutions, also in this case an axial load is applied in order to obtain a favorable pre-load, increasing the flexural capacity and improving the performance under service loads Daly and Witarnawan (1997). In general, the external prestressing solution can be considered as the coupling of two subsystems: the concrete beam and the external cables Pisani (1999). The prestressing force is not transmitted by adhesion but through a system of anchors and deflectors. Therefore, the profile of the external cables consists of straight paths.
The external cables transmit to the concrete beam, at the anchorages and the deviation points (deviators), concentrated forces whose intensity depends on the tensile forces in the cables and the shape of their path.
One of the main disadvantages has been identified in the increase of tensile forces in the reinforcement as the load increase depends on the overall elongation of the cable, which in turn is a function of the deformability of the entire structure and not just the section under consideration. The tensile increase is considerably lower than that which would occur in a structure with adherent cables and the calculation is not immediate. A further disadvantage is given by the reduction of the eccentricity of the cable as a result of deformation of the structure, especially if there are few points of deflection Alqam and Alkhairi (2019).
The addition of external prestressing as a technique for reinforcing existing bridges has seen significant adoption in recent years owing to several advantages Daly and Witarnawan (1997) Khudeira (2010). For example: (i) there is an increase in flexural capacity without significant increases in self-weight; (ii) the components are easy to inspect and any damage is easily detected; (iii) the process of installing the reinforcement system can be conducted without interrupting traffic; (iv) the in-service

behaviour can be corrected. However, the installation of the reinforcement system must be performed by expert labor in using this technique. Furthermore, the concrete material must be in good conditions to withstand the stresses deriving from additional prestressing.

4.2.2 Proposed consolidation system for bridge decks: steel arch trusses

In this work, a new consolidation system for bridge decks is proposed, which consists of two arch-shaped steel trusses linked to the beam to be consolidated. A FEM analysis was conducted in order to evaluate the load distribution between the arches and the beam and calculate the beneficial effects of the strengthening with suitable performance ratios. Although the external prestressing cables technique aims to restore the capacity and the structural efficiency of the damaged beam, the proposed consolidation technique is intended to reduce the external load carried by the existing PRC beam. The static behaviour of the arch offers several advantages respect to the straight barycentric axis beam one **?**. Referring to Figure 4.1, by comparing the static behaviour of a three hinged arch with the a straight beam with the same span, geometrical section and load pattern one obtains:

$$\begin{aligned} \sigma_a &= \frac{Pa}{Af}; \qquad \sigma_b = 6\left(\frac{Pa}{bh^2}\right) \\ \sigma_b &= \sigma_a\left(\frac{6f}{h}\right). \end{aligned} \tag{4.1}$$

where σ_a and σ_b indicate the stress at the midspan of the arch and the beam respectively. Hence, being that $f >> h$, the straight beam results significantly more stressed with respect the three hinged arch due to the fact, as depicted in Figure 4.1, for the first case, the external moment Pa is balanced by the internal moment Rf, while, in the second case, a higher balanced moment is guaranteed by Hf. For example, in the case of two hinged arch, the thrust H at external restraints generates internal actions of bending moment and shear that are opposite to the same load-induced by the external force. In the case study of interest, the effective stresses

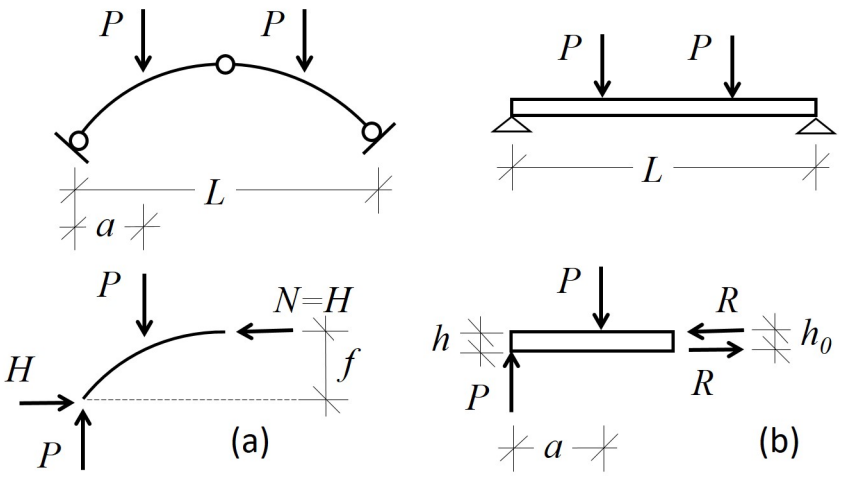

Fig. 4.1 Comparison between a three hinged arch beam and (a) a simply supported beam (b) under a symmetric load configuration.

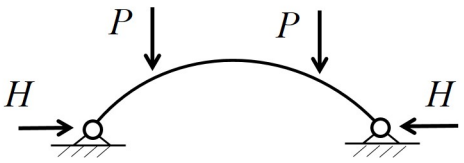

Fig. 4.2 Static scheme of a two hinged arch under symmetrical load configuration. The constraints avoid horizontal displacement at the level of the fixed hinges.

acting at the level of the arch have been calculated as follow:

$$\begin{aligned} &M = M_0 - Hy; \qquad V = V_0 - H\sin\theta; \\ &N = N_0 - H\cos\theta \end{aligned} \tag{4.2}$$

where y indicates the vertical distance between the fiber of the investigated section and the fixed hinges; θ is the angle between the tangent at the barycentric fiber of the considered arch section and the horizontal axis; M_0, V_0, N_0 indicate the bending moment, shear and tension stress respectively due to vertical external load or vertical reaction without taking into account any horizontal component (H).

Moreover, several advantages in terms of deformability are offered by an arch beam with respect to the straight beam simply supported. Comparing the vertical displacement due to a concentrated vertical force applied at the middle span of the straight beam (δ_t) with the, previously cited, parabolic arch static scheme (δ_a)

neglecting shear and axial deformability, one obtains:

$$\delta_b = \frac{Fl^3}{48E_bI_b}; \tag{4.3}$$

$$\delta_a = \frac{Fl^3}{2048E_aI_a} \tag{4.4}$$

where l indicates the beam span, E_b and E_a represents the elastic modulus of the beam and arch materials respectively, I_b and I_a are the beam and arch moments of inertia respectively.

Combining Equation 4.3 and 4.4 the following relation can be found:

$$\delta_a = \frac{3}{128}\delta_b \tag{4.5}$$

which demonstrates the higher stiffness of the arch solution despite to the straight beam one. Although the main differences in terms of structural behaviour between arches and straight beams are evident, the interaction between these two different structural elements and how they work together has not yet been fully investigated. With a preliminary study, the interaction between two hinged arches placed alongside the main simply supported beam, having the same span and under a symmetrical load condition, is herein investigated. The PRC beam and the lateral arches are bound together along their longitudinal length as a consequence that they are constrained to work together and thus sharing the external load according to their stiffness. The load distribution is carried by a structural system composed by two sub-systems that work in parallel. Therefore, the splitting percentage of the force F is a function of the stiffness elements and/or their different displacements. Simplifying the Equations 4.3 and 4.4, one obtains:

$$\delta_a = \frac{F_a}{K_a}; \tag{4.6}$$

$$\delta_b = \frac{F_b}{K_b} \tag{4.7}$$

where K_a and K_b represent respectively the arch and beam's stiffness while F_a and F_b indicate the percentage of the force F carried respectively by the arches and the beam. Due to the hypothesis of rigid connection, guaranteed by an anchoring system

Double T section	
E_t[Mpa]	$3,2836 * 10^4$
I_t [mm^4]	$1,806 * 10^1 1$
K_t [N/mm]	$6,102 * 10^3$

Table 4.1 Geometrical features of the concrete beam.

of the arch to the PRC beam, the following conditions must be satisfied:

$$\delta_a = \delta_b = \delta \tag{4.8}$$

Moreover, in order to respect the vertical translational equilibrium, the load distribution between arches and beam is defined as following:

$$F = F_b + 2F_a = (K_b + 2K_a)\delta = K\delta \tag{4.9}$$

where K represents the equivalent stiffness of the beam-arches assemblage and δ the global displacement system. In this way, it is possible calculate the load distribution between arches and beam as a function of their independent stiffness and also determine the equivalent one of the whole structural system.

$$F_a = K_a\delta = K_a\frac{F}{(K_t + 2K_A)}; \tag{4.10}$$

$$F_b = K_b\delta = K_b\frac{F}{(K_b + 2K_A)} \tag{4.11}$$

In order to achieve a major awareness about the efficiency of the proposed strengthening system, a numerical example has been conducted considering a simply supported beam of 36 m span consolidated with two double-hinged arches placed one on the left and on the right the main beam. The material and the geometrical features of the main beam and arches respectively are reported in Tables 4.1, 4.2 and depicted in Figure 4.3. With the aim to evaluate the distribution load between arches

Tubolar section 193x16 mm	
E_a[Mpa]	$2,100 * 10^5$
I_a [mm^4]	$3,554 * 10^7$
K_a [N/mm]	$3,276 * 10^2$

Table 4.2 Geometrical features of the steel arches.

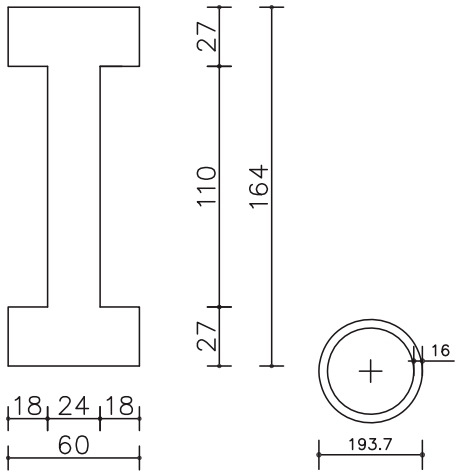

Fig. 4.3 Double-T-shaped section of the concrete beam (on the left). Dimensions are expressed in [cm]. Circular hollow section (CHS) of the steel arch beam (on the right). Dimensions are expressed in [mm].

and beam, in Table 4.3, the ratios K_a/K and K_b/K have been calculated considering the connection system previously described.

Load distribution of F	
$2K_a/K$	$0,10$
K_t/K	$0,90$

Table 4.3 Distribution load between beam and arches.

It is worth noting that, nevertheless the arch and beam's stiffness showed a gap of about one order of magnitude, the arches are able to carry a reasonable percentage of the external load F (evaluated almost the 10 % of the total force). In other words, the consolidated concrete beam has been relieved approximately of the 10 % with respect to the unconsolidated configuration.

Finally, the numerical example shows how, in order to retrofit a simply supported beam, the stiffness of the consolidation system plays a fundamental role in achieving the best structural performance and/or efficiency. Therefore, the strengthening system proposed in this work should perform according both to functionality and rigidity. This system results quite suitable to girder bridges composed of several spans sustained by different prestressed concrete beams with a maximum length of approximately $35-40$ m. The static scheme appears mostly as a simply supported beam for each span with variable height values between $1,2-2,5$ m. For these reasons the arches have the same height as the main beam and are stiffened by

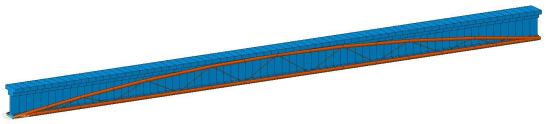

Fig. 4.4 Prospective view of the main beam with the strengthening system proposed

inclined trusses in order to reduce the deformability of the whole beam-arches assemblage as depicted in Figure 4.4. The consolidation system is suitably linked to both sides of the main beam with rigid anchoring beams with the aim to guarantee the transfer of stresses from the main element (PRC beam) to the secondary ones (trussed arches). Both beam and arches result equipped with different bearing devices placed at the top of the pillars (or abutments).

Although the two hinged arches provide the most stiffened static scheme, remarkable horizontal forces due to the thrust of the arch are absorbed by the restraints. To avoid this critical phenomenon, a tension tie lower chord was placed achieving a static scheme with arched thrust eliminated. In this way, a very stiffened tension chord tie rod provides a structural solution that performs similarly to the two-hinged arch beam instead of the more deformable solution with a lower structural efficiency.

4.3 Case study and modelling using MIDAS and OpenSees

In this section, the case study and FEM modelling are described. With the goal of providing a realistic scenario, a beam belonging to an existing girder bridge located in Piedmont in Turin province (Italy) has been investigated. The deck consists of 4 statically determined simply supported spans with variable lengths of 38 m, two consecutive spans of 31 m and the final one of 30 m respectively. Each beam is a post-tensioned PRC beam connected each other by transversal beams located at three points: two at the extremity of the main beam in correspondence of pillars or abutments and one intermediate at midspan of the main beam. Due to the critical length of the first span, this latter has been selected to focus the analysis. The deck consists of 8 longitudinal beams with a double-T-shaped section whereas the transversal ones exhibit a rectangular section. In particular, considering an hypothetical transversal section of the deck, in order to check the performances of the proposed strengthening system, the external main beam of first chosen span is

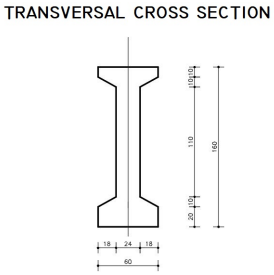

Fig. 4.5 Double T section of the investigated concrete beam.

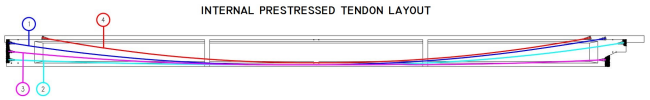

Fig. 4.6 Longitudinal section of the investigated concrete beam and tendon profile.

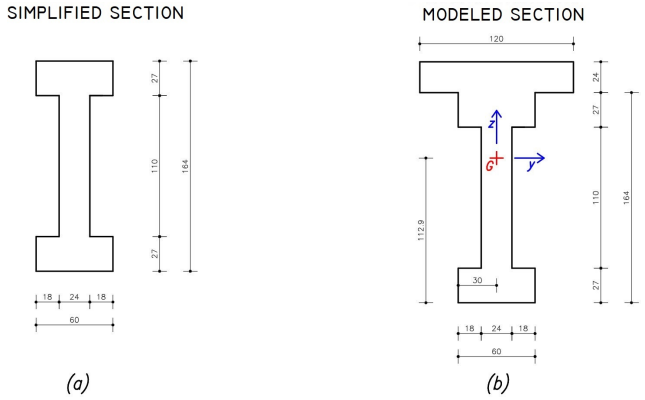

Fig. 4.7 (a) Geometrical section 4.5 after semplifications, (b) Geometrical section modeled taking into account the effective width of the concrete slab.

Concrete C30/37 **and steel** S355			
f_{ck} [Mpa]	f_{yk} [Mpa]	E_{cm} [Gpa]	E_s [Gpa]
30,0	355	32,8	210

Table 4.4 Concrete material characteristics of the main beam.

considered in the current work. Several technical drawings related to the selected concrete beam, reinforcement and prestressing internal reinforcement tendons have been consulted achieving a suited knowledge level of the existing structure. The main geometrical and material features of each structural element are reported in Figures 4.5, 4.6 and in Tables 4.4, 4.5.

Strand Y1860S7				
d [mm]	A [mm^2]	f_{pk} [Mpa]	$f_{p0,1k}$ [Mpa]	E_{cm} [Gpa]
15,2	139	1860	1640	196

Table 4.5 Steel material characteristics of strands.

4.3.1 Not consolidated beam model

FEM structural analyses, according to Italian Code and Eurocodes, have been conducted with the MidasGen© software, a "general purpose" numerical code. At first, a tapered beam was modeled adopting a simplified section as depicted in Figure 4.7. Later, tendon property and profile were assigned to the tapered beam with respect to the real coordinates provided by the technical drawings. All the geometrical and material features related to the concrete beam and prestressing cables, described previously, have been assigned to the element. All the long-short term prestressing losses were considered in the modelling. Each cable lied on the same vertical plane without any type of transversal offset.

The load pattern considered is composed by self-weight (SW) and uniformly distributed load Q equal to $10kN/m$ simulating live loads. In this preliminary phase, the value of live loads was chosen in an arbitrary manner in order to perform the efficiency of the proposed system. The effects of the internal forces due to the prestressing system were added to the external load configuration.

4.3.2 Strengthened system by steel trussed arches model

The proposed consolidation system consists of a steel structure with an arched with thrust eliminated static scheme. The compression and tension chords were stiffened by steel trusses as in the Nielsen truss structure (see Franciosi 1971). As described before, steel arches and the concrete beam work in parallel, hence the maximum height at the midspan coincides with the total height of the main beam without taking into account the thickness of the deck. Moreover, as the compression chord exhibits a parabolic shape profile with the arch axis, depicted with the red dashed line in Figure 4.8, it passes the midspan at the intermediate point of the upper flange thickness whereas the tension chord develops along the intermediate point of the lower flange thickness. The lower tie chord presents the same length span of the beam to be consolidated. The deck represents a natural obstacle that limits the height of the

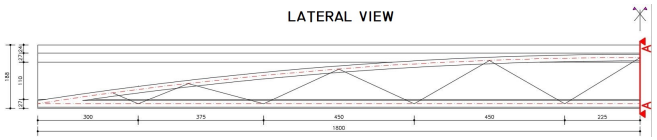

Fig. 4.8 Longitudinal view of half strenthening system with the concrete beam in the background

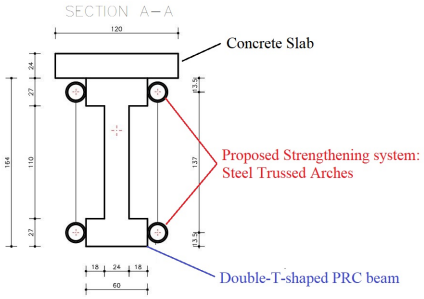

Fig. 4.9 Transversal section at midspan of both PRC beam and strengthening system. Dimensions are expressed in [cm].

Fig. 4.10 Plan view scheme of the external boundary assigned to each structural element.

crown. As shown in Figure 4.9, it appears clear how the slenderness of the arch strongly depends on the deck thickness: the ratio f/l, between the raise and the length span of the arch, plays a fundamental role in increasing the percentage of external load carried by the consolidation system. Higher slenderness ratio values allow taking advantage of benefits due to the arch shape behaviour. As a result that only vertical concentrated or distributed load are taken into account in the modelling, both main beam and arches were constrained with external boundary realized with fixed and sliding longitudinal supports (Figure 4.10). Due to the absence of transversal loads (as wind or earthquake) any boundaries that limit transversal displacements were modeled. Although the final properties of the proposed strengthening system are discussed in the next sections as a result of an Optimization process in order to maximize the efficiency of the system, in this preliminary design phase, a first attempt was conducted choosing several suited industrial solutions that respect the geometrical limits imposed by the problem. In Table 4.6, the material and geometrical features of the steel arches have been summarized.

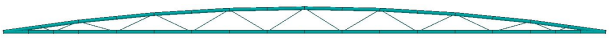

Fig. 4.11 Longitudinal view of the Strengthening system MidasGen© model.

Tubolar section type 193x16 mm	
A [mm^2]	I [mm^4]
$8,932x10^4$	$3,554x10^7$
Truss section type ϕ 22	
A [mm^2]	
$3,801 * 10^2$	

Table 4.6 Geometrical properties steel arch and truss section type.

With the aim to take into account the real behaviour of the compression and tension chords a *general beam/tapered beam* FEM element is used. *Truss* elements were used in order to carry normal stress and improve the flexural stiffness of the whole structure. Reducing the deformability of the whole system allows increasing the efficiency of the strengthening system due to a significant decrease of the concrete beam stress level.

4.3.3 Concrete beam connected to the strengthening system

After defining the modelling and assigned the preliminary properties to the model, the first analyses are performed. As described before, the PRC beam and steel arches work in parallel: the purpose of the consolidation system is to cooperate with the concrete beam when it is subjected to damaging phenomena or when unexpected live loads acting on the bridge. In order to achieve this goal, *rigid link* were provided allowing the load transfer thanks to the relative vertical displacement constraints between concrete beam and arches. In practice, these constraints could consist of transversal beam with the purpose to connect the two lower flanges of the double-T-shaped section with the arches. When a beam capacity reduction occurs due to a possible damage, the beam will exhibit an increasing vertical displacement that could be virtually limited by the connection of these supporting elements to the strengthening arches. Moreover, the stress transfer process between the main beam and the strengthening arches is further improved by including some other connections also at the level of the PRC beam web as depicted in Figure 4.12 where only the barycentric axis of each element are shown. The modelling and the position of these internal constraints have been investigated in the present work. It is worth noting that,

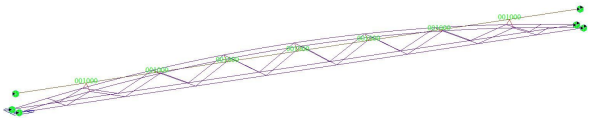

Fig. 4.12 Prospectical view of the Global MidasGen© model. In the Figure, the fixed and sliding boundaries are depicted with green-filled circles; red lines are used to indicate the *rigid links* as connections between beam and arches.

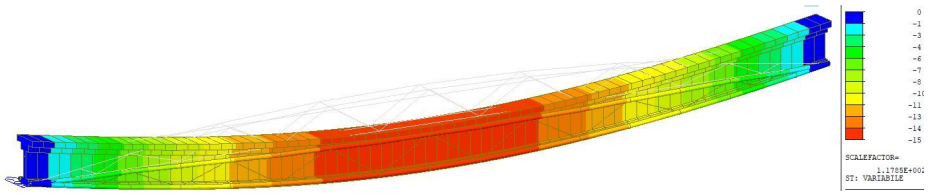

Fig. 4.13 MidasGen© plot of the vertical displacement of the Retrofitted beam under a preliminary uniform live load of 10 kN/m. Values are reported in [mm].

in a detailed design phase, a specific description and calculation of these connections is requested: the stress configuration under traffic loads, effects related to the load repartition and distribution among the different structural elements certainly could provide concentrations of actions and/or local instability issues. In this investigation phase, the focus of the study was mainly conducted on the global behavior of the PRC beam-arches without a detail model of the connections.

The application of a preliminary external load as uniform live load equal , with intensity equivalent to $10kN/m$, must be considered acting to the beam after the installation of the strengthening system. In this preliminary study, the effect of prestressing and self-weight has been neglected in order to evaluate the beneficial effect of the consolidation system under vertical load only, e.g. traffic loads, snow load, etc. Subsequently to the loading Assignment phase, stress and deformability effects induced by the variable loads are evaluated. As it could be expected, the beneficial effects of the strengthening system are verified (in particular, a decrease in the vertical displacement and bending moment at the midspan have been highlighted). In this way, the arches captured a quite significant percentage of the applied variable load. As shown in Table 4.7, a comparison between the two investigated configurations is conducted and the magnitude of the reduction of the vertical displacement and the bending moment in the critical section (midspan) is about 16% .

As shown in Figure 4.13, and summarized in Table 4.7, after the installation of the strengthening system, a partial reduction in terms of displacements and stresses

Comparison between Not consolidated and retrofitted beam configuration		
	Not consolidated beam	Retroffitted beam
$\delta_{(z,var)}(l/2)$ [mm]	-18	-15
$M_{(y,var)}(l/2)$ [kNm]	+1620	+1356
$R_{(z,1\ var)}$ [kN]	+180	+163
$R_{(z,2\ var)}$ [kN]	+180	+163

Table 4.7 Comparison between the unconsolidated and Retrofitted beam configurations.

of the main beam is recognised. Specifically, the compression and tension chords exhibit low symmetric values of bending moment despite the slenderness value imposed is not the optimal one whereas, on the contrary, important normal stresses are generated. Moreover, truss elements provided a more stiff behaviour to the whole system, respecting the theoretical previsions. It is worth noting that the performance ratio of each structural element resulted unsatisfactory due to the fact that the industrial solution implemented is not the optimal one. For this reason, A further optimization process will be necessary.

This preliminary results have shown that the idea of coupling the arch shape to the damaged beam could provide interesting developments. Unfortunately, the simplified hypothesis of external load acting simultaneously after the installation of the strengthening system does not comply with the real construction stage of the structure. The aim of the present work consists to propose a new type of consolidation technique as an alternative of the traditional external prestressing one. Therefore, the actual installation of a retrofitting system occurs only after an important loss of the capacity and/or serviceability. For this reason, a new construction stage is realized with the purpose to evaluate the efficiency of the strengthening system for an increasing value of the external loads by simulating a damage state that evolves over time.

In the software MidasGen© the *construction stage* procedure allows to define several *Elements, boundary and load groups* with the aim to take into account a certain effect due to a static scheme change, to the activation of additional load configuration or boundaries which act at a certain time or to material properties that are strongly time-dependent such as the prestressing cables. Generally, taking into consideration all these effects, it enables to consider and investigate the real stresses evolution which occurs in the structure during the damage evolution and after the strengthening system installation. For this reason, two main construction phase were defined:

Construction stage 1: at this phase, the main concrete beam was modeled without any strengthening system. Specifically all the external boundaries and load pattern, which consists into self-weight and prestressing cables, were activated at the same time as the starter point for further investigations.

Construction stage 2a: at this phase, the installation of the strengthening system was modeled. Both arches are supported by fixed and sliding supports, independent to the concrete beam external boundaries, which were assigned at the previous phase. During the installation stage, the concrete beam is loaded with the same load pattern already previously defined. On the contrary, arches were subjected to self-weight and still does not present any type of connection with the main structural beam element. At this stage the arches and the PRC beam are still non-connected and, therefore, act independently.

Construction stage 2b: the connection between the main PRC beam and the strengthening system was modeled. In this construction stage, *rigid links* were activated when the main structural element achieved a first stress and strain state. From this moment forwards, any load distribution changes is recognised: each load increment detected or any activation of new different load patterns will allow to evaluate the beneficial effect of the strengthening system. It is worth noting that, compared with the previous models in which concrete beam and arches were modeled simultaneously but act separately, in this phase the consolidation system acts when the main beam exhibit a certain stress and strain state and any future damage effect, e.g. the cables relaxing, will be detected.

Construction stage 2c: in this final step, the cooperation between the consolidation system and the main beam is investigated. Applying an uniform distributed load, the beneficial effect of the retrofitting system can be investigated. Moreover, potential prestressing losses, resulting in an unbounded configuration of one or more cables, can be studied by deactivating the cables and providing a comparison between the different previous configurations. In this way, deactivating some strands of a certain cable means that it will result in an unbounded situation for the the whole considered tendon profile.

A prestressing loss of cables 1 and 4, as reported in Figure 4.6, equivalent to the 43% of the normal stress at the midspan of the concrete beam for both the Not consolidated configuration and the retrofitted one is considered. The comparisons are summarized in Table 4.8 where beneficial effects of the consolidation system

Comparison between Not consolidated and retrofitted beam configuration		
	Not consolidated beam	Retroffitted beam
$F_{Z,1,SW+Prest}$ [kN]	$+394,2$	$+369,9(-6\%)$
$F_{Z,2,SW+Prest}$ [kN]	$+394,2$	$+374,0(-5\%)$
$M_{y,SW+Prest}(l/2)$ [kNm]	$+78,0$	$-263,0$

Table 4.8 Deactivating effect of cables 1 and 4 (-43%)

are described. In conclusion, the vertical reactions, obtained considering only self-weight and prestressing effect acting on the PRC beam, calculated at the edge of the main beam, receive a decrease of about the 6%, which is consistent with the conducted preliminary analysis.

4.4 Parametric and sensitivity analysis using OpenSees© and Matlab©

In the previous section, it was shown the beneficial effects of the proposed strengthening system without any specific considerations about the geometry, section properties and material assigned to each structural element. A *sensitivity analysis* is herein conducted with the purpose to investigate which are the variables that mainly affect the analysis. In this way, in the present section, the applicability field of the proposed system is discussed and, in particular, it is investigated what are the best industrial solution for a preliminary design. Since the proposed consolidation system appears to be suitable for girder bridges, the slenderness ratio plays a main role in the preliminary design. For this reason, a preliminary survey inherent the most usual slenderness ratios adopted for this kind of bridge was useful in order to define the lower and upper limit of this variable range. Summarily, the input variables that were taken into account in the sensitivity analysis are:

Beam length span (L): the investigation includes all the girder bridges with a value of beam span between the upper value of 42 m and the lower one of 28 m with successive increases of 1 meter step. In this way, the best representative range of Beam span was achieved. As discussed before, fixing the concrete beam span length, it consequently also set the length of the tie rod of the trussed arches.

Steel arch rise-length span ratio f/L: once defined the span length and the height of the concrete beam, automatically the arch slenderness ratio results well defined. In

order to conduct the study with the most representative values, the following values for the ratios are chosen: $0,04;0,05;0,06;0,07$.

Geometry and section of each element composing the strengthening system: compression and tension chord are chosen as input parameter of the problem due to the fact that, differently from trusses, they have the most influence on the global stiffness of the steel arches. Specifically, the external diameter of the tubular steel arch section varies between 150 mm up to 300 mm with successive increases of 50 mm each step.

External boundary of the trussed steel arches: Several static schemes are investigated providing also a double-pinned supports at the edges of the strengthening system simulating a two-hinged arch behaviour.

All the input parameters are summarized in Table 4.9:

Input parameter of the *sensitivity analysis*	
$f(h)/l$	$Area\ [mm^2]$
$0,04$	$\phi 150t.16 = 6732$
$0,05$	$\phi 200t.16 = 9249$
$0,06$	$\phi 250t.16 = 11762$
$0,07$	$\phi 300t.16 = 14275$

Table 4.9 Summary of input parameter of the sensitivity analysis.

4.4.1 Parametrization of the strengthening system

The parametrization of the geometrical model is conducted considering the span length (L) and the height (H) of the main beam as dominant parameters. When L is assigned, in fact, the coordinates of the external supports are defined, whereas setting the beam height automatically defines the position of the arch rise. Once the coordinates of these three points are identified, the parabolic profile of the steel arches can be drawn. Finally, a reference system is defined with the origin of axis placed at the intrados midspan of the main beam, with the X axis directed along the longitudinal direction of the beam whereas Y axis is vertical and perpendicular to the X direction. In Figure 4.14, the defined parametrization and the coordinates of each node of the structure have been illustrated.

In order to develop a suitable parametric model, it was adopted the object-oriented software framework open source *OpenSees*© developed by Berkeley University. The

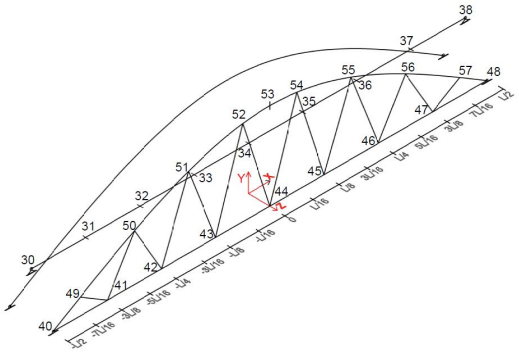

Fig. 4.14 Parametrization of the model adopted in OpenSees©.

connection realized between *Matlab*© and this FEM numerical code was extremely useful to post-process the *.tcl* output files, which stores the linear static analysis results. Furthermore, Matlab© allows to automatically manage and iterate many analysis characterized by different FEM models because they are function of the variable input parameters above-mentioned. Each constant value (geometrical section, material, etc...) and parametric variable defining the geometry of the structure have been implemented into the software. The loading pattern is associated to a time series in order to solve the structure at each step of the increasing of the uniform distributed load value.

In this paragraph, the results obtained by the conducted static analysis of the parametric model are discussed. The sensitivity analysis allows to understand which are the variables that mainly affect the solution and, in particular, which are the relationships among them. The efficiency of the system is evaluated considering a new index, which considers the percentage of the external load carried by arches. In this way, evaluating the *efficiency index* (*E.I.*) for each input parameter, it is possible to determine which variable will be dominant or negligible. This *efficiency index* is calculated as:

$$E.I. = \frac{\sum R_{y,arches}}{qL}, \tag{4.12}$$

where $\sum R_{y,arches}$ are the sum of the steel arches vertical reactions developed by the external supports, q is the intensity of the distributed load equivalent to 10 kN/m in these preliminary evaluations and L is the beam span length.

This performance parameter allows to evaluate two extreme scenarios: when its value is equal to zero, any external load is transferred from the main beam to the strengthening system, thus the consolidation system is completely inadequate to fulfill its role. On the contrary, when the value of the efficiency index is equal to 1 the whole external load is carried by the arches with a concrete beam that results in a zero stress and strain configuration. The trend of this performance parameter is investigated within the *sensitivity analysis*:

Dominance of the slenderness ratio f/l and the boundary condition: the trend of the efficiency index by varying length beam span and f/L are depicted in Figure 4.15. As said before, the slenderness ratio f/L of the arches respects the variable range of the slenderness ratio H/L of concrete beam which represents the widespread case studies in the field of the girder bridge. The diameter adopted to the compression and tension chords is 200 mm and it must be considered as a constant value for each iteration. A comparison between the static scheme including a sliding and a pinned support and the both double-pinned static scheme one is provided. As expected, results show that the double-pinned supports static scheme is the stiffest: the E.I. achieves the highest values rather than the static scheme with sliding and a pinned support. In the first configuration, the strengthening system is able to capture 32% of the entire external load acting to the concrete beam instead of only 20% detected in the second case. The E.I. shows a moderate dependence by the variable beam length and the slenderness ratio f/L. Specifically, with the increase of L, the efficiency index decreases about 6 or 4% respectively in the first and in the second investigated static scheme. Considering the reference case study of the present work, it is characterized by a ratio f/L equal to $0,04$ and the obtained efficiency index varies between 32% at 28 m up to 29% at 42 m of the beam span length. Since the strengthened structure works as a parallel system, this moderate variability depends on the stiffness ratio between beam and arches. Setting a constant value of the slenderness ratio f/L, when concrete beam span length L increases, it provides a higher stiffness and the arches will carry a bigger percentage of the external load compared to the situation when the arches results unloaded. In Figure 4.15, the steel arches slenderness ratio f/L can be studied. The efficiency index shows a low decreasing trend: when the f/L ratio is higher, the height of the beam increases in a non-proportional manner. Consequently, for a little increase of the arch stiffness, a bigger increase of the moment of Inertia of the concrete beam section occurs which

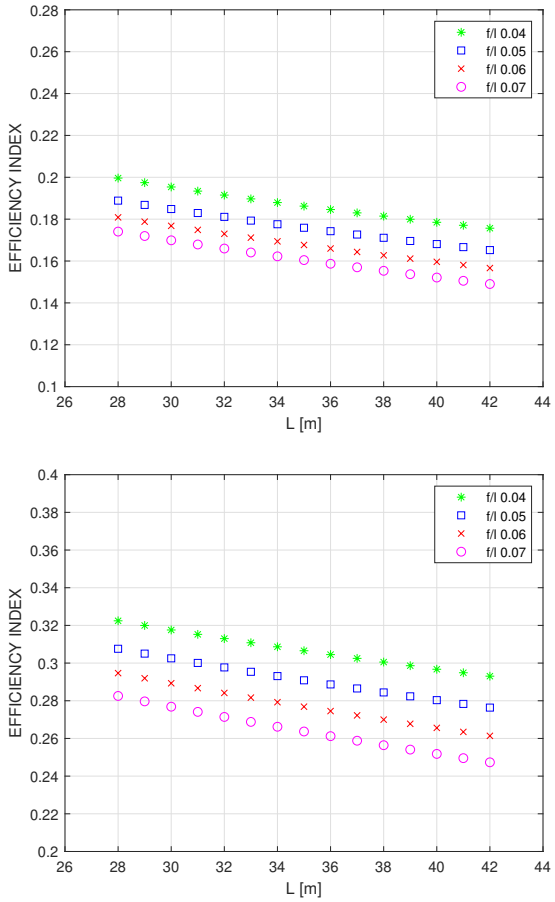

Fig. 4.15 Trend of the efficiency index with variable slenderness ratio (f/L) and beam length (L), constant value of the compression and tension chords equal to 200 mm and external load equal to 10 kN/m in the pin-roller static scheme (on the left) and double-pinned one (on the right).

explains the decreasing trend of the investigated parameter. A lower fraction of the entire external load is captured by the strengthening system.

Dominance of the geometrical arch section (A): the trend of the efficiency index by varying the sectional features of the compression and tension chord of the strengthening system has been investigated. Fixing the f/L ratio equal to $0,05$, the external diameter of the tubular section has been varied between a lower value of 150 mm to the upper one of 300 mm. Similarly to the previous case, the dependence of the solution by the restrained static scheme is analysed. As depicted in Figure 4.16, it is shown that with increasing value of the external diameter, the fraction of the entire external load captured by the arches increases. The increase of the external

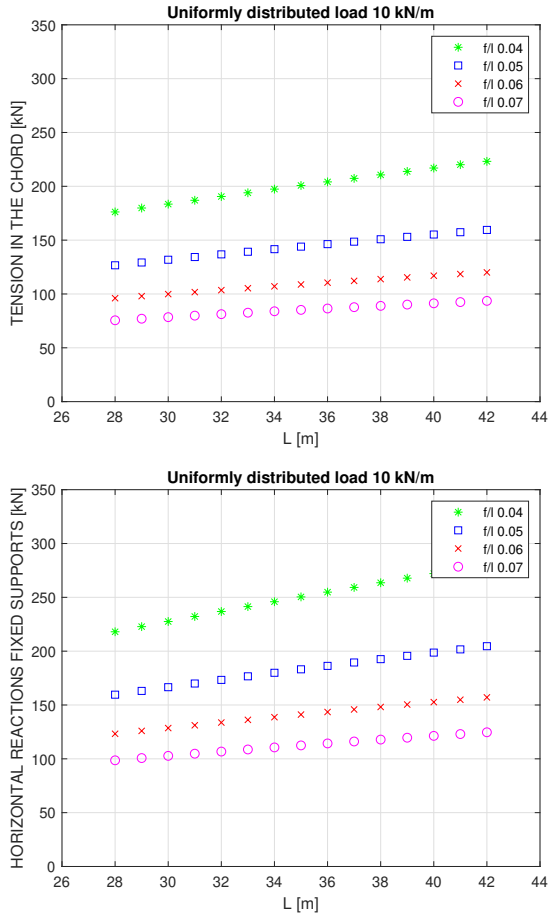

Fig. 4.16 Trend of the efficiency index with variable geometrical area and beam length (L), constant value of the slenderness ratio (f/l) equal to 0,05 and external load equal to 10 kN/m in the pin-roller static scheme (on the left) and double-pinned one (on the right).

diameter brings to more stiff arches due to an increment of the Moment of Inertia which justifies higher values of the efficiency index. As in the previous case, the double-pinned supports static scheme results the stiffest solution although the thrusts at the fixed support are higher. In the case of a beam span length of 28 m and a tubular section of arches equal to 300 mm, the fraction of the external load carried by the strengthening system is equal to 37% for a double-pinned supports static scheme than the second one in which is equal to 25%.

In conclusion, it is worth noting that the sectional features of the compression and tension chords represent the dominant parameters which mostly afflict the solution. A higher value of A means a higher value of the efficiency index, whereas a moderate influence on the efficiency index is performed by the slenderness ratio f/L or by

Simulated degradation levels

Degradation level	Resisting steel area reduction [%]
1	5%
2	10%
3	15%
4	20%

Table 4.10 Four simulated degradation levels.

external boundary. Obviously, the choice of the sectional features of each structural element composing arches must be defined as a function of the level of stresses recognised by the whole structure. In the further section, the preliminary design of the strengthening system will take into account not only the distribution load between concrete beam and arches but also the stress and strain check imposed by the Civil Codes and possible damaging conditions which affect the existing bridge heritage.

4.5 Degradation simulation and retrofitting with traditional intervention

Since the analyzed case study is referred to an existing structure, it is highly probable that this structure is affected to a certain ordinary level of degradation with respect to the original construction conditions. In order to take into account this fact in a simplified way, it is convenient to simulate the current damaged conditions referring to a reduction of the ultimate resisting moment M_{Rd}. Similarly to other studies about rebar losses due to corrosion, (e.g. Zhao et al. 2018), the resisting moment reduction is directly taken into account by a reduction of the actual resisting steel reinforcement area with respect to the original one. In this study, four different levels of degradation have been identified as reported in Table 4.10. Since the structural scheme is a simply supported PRC beam under a unique load condition for sake of simplicity (self weight and uniformly distributed load equal to 52 kN/m), the midspan section is the most stressed one. Therefore, the structural performance evaluation is reconducted to the analysis of the ratio M_{Sd}/M_{Rd} between the acting moment M_{Sd} and the resisting moment M_{Rd} in the midspan cross section. Due to the progressive increase of the deterioration level, when the performance ratio becomes greater than

Performance ratio for the unconsolidated situation

Degradation level	M_{Sd} [kNm]	M_{Rd} [kNm]	$\frac{M_{Sd}}{M_{Rd}}$
Undamaged	11'995	12'621	0,95
1	11'995	12'145	0,99
2	11'995	11'632	1,03
3	11'995	11'094	1,08
4	11'995	10'541	1,14

Table 4.11 Performance ratio for the unconsolidated situation for different degradation levels.

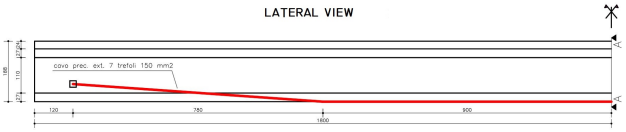

Fig. 4.17 External prestressed cables layout profile (red solid line) adopted as a traditional intervention proposal .

one, safety levels are no more satisfied a retrofitting intervention becomes strictly necessary in order to bring back the performance ratio below one. Referring to the original conditions (undamaged) and the simulated damaged induced situations, Table 4.11 illustrates the performance ratios for the unconsolidated PRC beam. As shown in the Table, the safety level is respected only for the undamaged condition and for the degradation level 1. Considering the damage level 3 as a reasonable ordinary damage level, it is possible to analyze an initial retrofitting intervention with the traditional technique of external prestressed cables in order to bring back the performance ratio of 1.08 to the initial undamaged value (0.95). The intervention proposal is depicted in Figure 4.17, where the symmetrical piecewise linear tendon layout profile is composed by two external tendons with 7 strands each of 0,6 inches. The prestressing force P_{ext} of each tendon at the anchorages is 550 kN. The deviators are placed at $L/4$ from the extremity of the beam. The effects of external cables intervention has been considered with the equivalent load method, thus as further external actions of axial force N_{ext} and bending moment M_{ext}. This latter is given by three contributions: $M_{\text{ext},1}$ is related to the eccentricity of the cable ($e_{\text{ext}} = M_{\text{ext}}/N_{\text{ext}}$), $M_{\text{ext},2}$ is given by the shear force induced at the anchorages whereas $M_{\text{ext},3}$ is given by the shear force produced in correspondence of the deviators. The traditional intervention with the above-mentioned characteristics, summarized in Table 4.12, has been identified to be able to bring back the performance ratio to its undamaged level as shown in Table 4.13. Considering always the same degradation level 3,

Summary of the traditional intervention

P_{ext}		$2 \cdot 550 = 1100$ kN	
Anchorages		Deviators	
N_{ext}	V_{ext}	N_{ext}	V_{ext}
1097	77	3	77
Barycenter elevation [m]		Eccentricity (Midspan sec.) [m]	
$y_{G,\text{midspan}}$	$y_{G,\text{cables,anchorages}}$	e_{ext}	
1.129	0.55	1.131	
$M_{\text{ext},1}$ [kNm]	$M_{\text{ext},2}$ [kNm]	$M_{\text{ext},3}$ [kNm]	M_{ext} [kNm]
635	1299	-693	1241

Table 4.12 Summary of the mechanical and geometrical properties of the external prestressed cable intervention.

Performance ratio for the post-intervention with external prestressed cables

M_{Sd} [kNm]	$M'_{Sd} = M_{Sd} - M_{\text{ext}}$ [kNm]	M_{Rd} [kNm]	$\frac{M'_{Sd}}{M_{Rd}}$
11'995	10'754	12'145	0,95

Table 4.13 Performance ratio evaluation for the post-intervention with external prestressed cables.

this traditional intervention is compared from a structural point of view with the strengthening method of steel trussed arches proposed in the current study. The characteristics of this latter intervention proposal is determined by an optimization procedure in order to define the most suitable solution for this kind of intervention. From the technical point of view, whereas the external prestressed cables intervention acts as externally induced actions and plays a role directly on increasing the resisting moment, the proposed steel trussed arches solution generates a reduction of the acting moment M_{Sd}. Since the arches work in parallel with the PRC beam, the acting loads on the whole strengthened system undergo a repartition process governed by the relative stiffness of the arches and the beam. With respect to the unconsolidated situation, this phenomenon leads to a decrease in the beam carried load without affecting in any way the beam midspan cross section ultimate resisting moment.

4.6 Selection of the Optimization strategy

In order to solve the problem stated in the previous section, a real-coded GA is adopted. This is a population-based stochastic optimization technique appropriate for

global optimization, which does not require direct evaluation of gradients. Introduced by John Holland (1992), it is inspired by Charles Darwin's theory of natural evolution. This algorithm reflects the process of natural selection where the fittest individuals, also called parents, are selected for reproduction in order to produce offspring of the next generation. At the end of the process, the best survival among all the fittest candidates found at each generation is selected as the best globally optimized solution. Although the native GA worked with binary values representing genes, encoded in string structures called chromosomes, in this paper the authors overcome the limits related to the decoding process by using a real-code GA in which genes and chromosomes represent directly the design variables and the solutions of the problem.

Since its pseudo-random roots, unfortunately, mathematical proofs of its convergence do not exist. However, numerical studies demonstrated that they are able to succeed also dealing with highly non-linear, non-convex and discontinuous domains. Conversely, to mathematical programming hard computing techniques which usually required information about the gradient, GA is considered a soft computing technique because it requires only the OF evaluation with a lower computational effort Plevris (2009a). For this reason, this paradigm can be ideally transposed to a numerical procedure which leads a population of trial solutions to evolve toward the global optimum of the optimization problem (OF) adapting to the environment which is represented by the feasible region reduced by the presence of the constraints. Substantially, these agents are competing for the resource and only the survival of the fittest to the environment will pass to the next generation Quaranta et al. (2020b). For further readings about the GA and in general meta-heuristic algorithms, one can refer to e.g. Martí et al. (2018). Actually, many applications of this optimization strategy can be found in the structural engineering field for steel, RC and masonry structures (e.g. Spiller et al. **?**). The versatility of Genetic programming for discrete or mixed-discrete optimization problems has been largely proved since the beginning Wu and Chow (1994), Qian et al. (1993), Stolpe (2016). Nevertheless, one crucial issue in applying GA has been premature convergence which causes trapping into local optima. Premature convergence is due to the loss of population diversity before optimal solutions have been found. The way for combating premature convergence is to maintain population diversity and prevent repeated selection of highly fit individuals. The more diverse the population, the more global the search. As with several metaheuristic algorithms, many researchers have noted, since GAs are character-

ized by their parameterized space which usually includes population size, crossover probability, mutation probability, etc. the choice of these parameters may result in different optimum solutions. It thus requires a lot of computational experiments to modify these adjustable parameters if we want to obtain acceptable solutions.

At each iteration, real-coded GA phases were adopted during the optimization as follows:

- **Initial population**: in this phase, individuals with a set of random genes (x_i) composing chromosomes (x) are created by observing lower and upper bounds defined as the first and last raw of the discrete standard section list. Gene represents, at each generation, the candidate value of a specific design variable involved in the identification procedure. A set of genes (vector form) represent a solution of the problem for the current generation. In this way, the best solution is selected and the optimal set of parameters which govern that specific law is detected.

- **Fitness function**: in this phase, the fitness of the candidate solutions is evaluated by calculating the OF introduced in the next setion.

- **Selection**: During this phase, a Roulette Wheel Selection was implemented in order to guarantee that the two fittest parents are selected for the next steps. Adopting this technique, a probability to each parent is assigned and the parents with higher fitness are more likely to be chosen for the next steps.

- **Crossover**: in this phase, a uniform random crossover was performed in which recombination of gene pool between parents is performed in a random way. Lower and upper bounds are imposed at this stage such that if only a gene of the new offspring is not ranged within the imposed interval (higher than the maximum value or lower than the minimum value of that specific parameter), it is forced to assume maximum or minimum value, respectively.

- **Mutation**: aiming to improve the exploration and exploitation ability of the algorithm, a mutation rate of 1% is assigned. In this way, new genes are introduced into the population by modifying the gene pools of parents in a random way.

- **Sort Function**: Aiming to maintain a certain level of diversity among the individuals, a dynamic amount of the best unfeasible solutions survive to the next iteration by substituting repeated selection of highly fit individuals.

4.7 Optimization process of the proposed consolidation system

The proposed steel arch strengthening system involves several issues and, in order to propose a reasonable solution from a practical point of view, an optimization process has been performed. Since the arch geometry is fixed because of the chosen typology of PRC beam, it is possible to perform only a size optimization process related to the steel members which compose the trussed arch structure. The main achievement is to optimize the intervention mainly in economic terms in comparison with other more traditional strengthening interventions, e.g. with external prestressed tendons as mentioned in Section 2. Structural optimization can be decomposed in three sub-problems: size optimization, shape optimization and topology optimization Christensen and Klarbring (2008c). In the size optimization process of steel truss structures, the reduction of the steel self-weight, and thus the adopted quantity of steel material, is usually indirectly connected to the reduction of the global cost of the steel structure Fiore et al. (2016c)Rosso et al. (2021a). The objective function (OF) in this case is equal to

$$f_1(x) = W(x) = \sum_{i=1}^{N_{el}} \rho_i V_i(x), \tag{4.13}$$

in which x is the design vector which defines the parameters referred to the tubular cross section (e.g. external diameter Φ_i and thickness t_i), ρ_i is the steel density ($7,86$ t/m^3), $V_i(x)$ is the volume of each steel member and N_{el} is the total number of elements. However, as mentioned in previous Sections, the strengthening system strongly affects the structural behaviour since it is working in parallel with the main structural beam element. Consequently, an effective optimization of the strengthening intervention has to take into account also an OF $f_2(x)$ related to the global stiffness K which is directly related to the level of the PRC beam load decrease and the global deformation of the structure δ. As a matter of fact, a trussed arch which satisfies

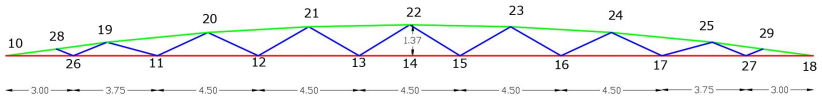

Fig. 4.18 Geometry view of the truss model and adopted node numbering (dimensions in meters).

completely $f_1(x)$ will result in an excessively slender solution which is useless in terms of structural performances, otherwise, an option which satisfies completely $f_2(x)$ will result in an excessive stiff solution which could be an extremely expensive solution.

These two stated aims point towards opposite directions and the best trade-off between the reduction of the steel weight and the increase of the trussed arch stiffness have to be found. Substantially, the optimization problem has to be formally stated as a multi-objective optimization problem. In reality, in Rao (2019b), the simplest approach to solve multi-objective optimization problems is to rewrite the OF to be minimize such as a single-objective optimization problem with a new OF given by a linear combination of the various OFs. In the present case, the single-objective OF becomes as

$$\begin{aligned} f(x) &= \alpha \cdot f_{1,\text{adim}} + (1-\alpha) \cdot f_{2,\text{adim}} \\ &= \alpha \cdot \frac{W(x)}{W_{\text{PRC beam}}} + (1-\alpha) \cdot \frac{u_{22}}{u_{\text{beam SW+Q}}} \end{aligned} \tag{4.14}$$

in which the two OFs have to be non-dimensionalized in order to be able to perform the combination. In particular, the f_1 is divided by the self weight of the PRC beam, $W_{\text{PRC beam}}$, whereas the f_2 is considered as the maximum deformation of the strengthened system monitored at the node 22, as depicted in Figure 4.18 which is normalized with respect to the mid-span deflection $u_{\text{beam SW+Q}}$ of the non-strengthened PRC beam under the self-weight (SW) and a uniformly distributed live load equal (Q) of 52 kN/m. The α coefficient is a user-defined parameter which allows controlling the relative weight of each OF in the optimization process in a simple and smart way. Since each OF is carrying information related to two opposite objectives, if α is set to 1, the classical single objective size optimization problem is performed but the final solution will be too much slender being useless as a strengthening system. Otherwise, on the other hand, when $\alpha = 0$ the OF will produce the most rigid solutions, very efficient but impracticable and incredibly expensive as a strengthening system. Moreover, in this latter case, the steel truss weight will be too much large also leading to an increase of reactions on piles and abutments. The trussed arch structure is

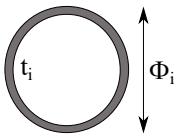

Fig. 4.19 Circular hollow cross section (CHS) profiles: a possible parametrization with two design parameters.

subjected to self-weight and nodal loads due to the connection with the PRC beam which are obtained by the OpenSees model. The OF is constrained because each steel member have to satisfy EN-1993-1-1 safety assessment at Ultimate Limit State in terms of Tensile Force, Compressive Force and Instability verifications as below:

$$\frac{N_{Ed}}{N_{t,Rd}} \leq 1, \text{ where } N_{t,Rd} = \frac{A_i f_y}{\gamma_{M_0}}, \tag{4.15}$$

$$\frac{N_{Ed}}{N_{c,Rd}} \leq 1, \text{ where } N_{c,Rd} = \frac{A_i f_y}{\gamma_{M_0}}, \tag{4.16}$$

$$\frac{N_{Ed}}{N_{b,Rd}} \leq 1, \text{ where } N_{c,Rd} = \chi \frac{A_i f_y}{\gamma_{M_1}}. \tag{4.17}$$

in which, for the sake of simplicity, class 4 section profiles were excluded. The adopted steel is S355 ($f_y = 355$ MPa). As depicted in Figure 4.18, the truss members are grouped in three categories of tubular section respectively, belonging to the upper arch (green members), diagonal elements (blue members) and lower tie elements (red members). A standard section list taken according to the European Normative EN 10219-2 has been adopted and 158 different profiles (excluding the class 4 section profiles) of steel tubes for circular hollow sections (CHS) have been considered. The design vector is thus completely defined by a vector of three integer numbers $x = [x_1, x_2, x_3]^T$, one for the type of truss steel member. Each integer number is referred to a specific row of the profile list which identifies all the specifications related to a certain CHS profile located at that corresponding row. This strategy produced a less computational cost with respect to optimising the two design variables (Φ_i, t_i) as depicted in Figure 4.19 for each element type as continuous variables. For the current study, a population size of 100 individuals was chosen with a stopping criterion referred to the achievement of a maximum number of prescribed iterations set to 100. The flowchart in Figure 4.20 describes, from a conceptual point of view, how the optimization was performed in Matlab environment and how the constrains have been managed.

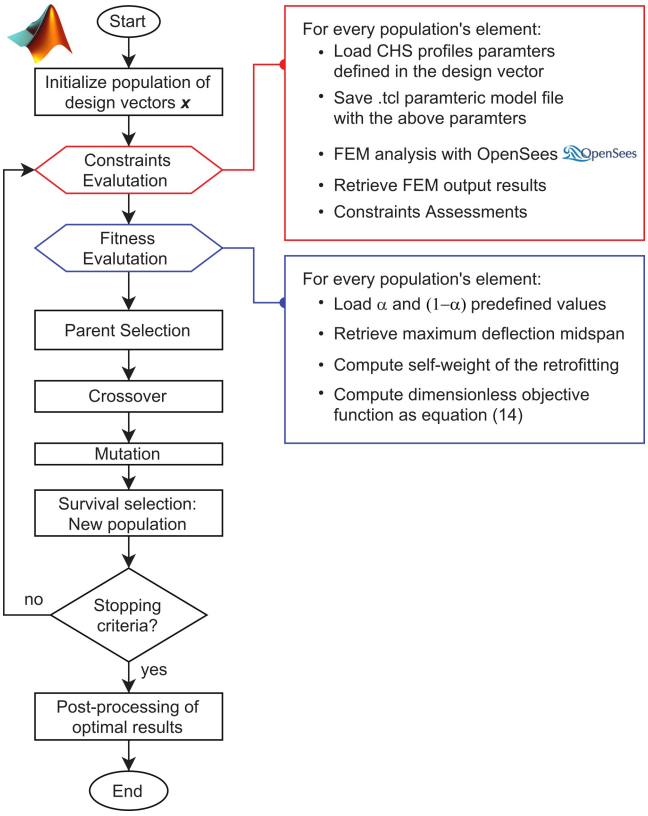

Fig. 4.20 Flowchart of the optimization process using Genetic Algorithm.

4.8 Results and Discussion

Solving the optimization problem presented in the previous Section, during each iteration of GA, a population of solutions' attempts is considered and, for each individual, Matlab will compile a OpenSees file to build the model with the characteristics defined by each individual. Thereafter, Matlab launches OpenSees analysis and finally it retrieves the FEM results in order to perform the final constraints verification and evaluate the fitness of each individual. Firstly, the two limit cases were analyzed with $\alpha = 1$ and $\alpha = 0$. As reported in Table 4.14, it is evident that none of the two limit case can be considered as an optimal trade-off between the two opposite OFs aims. As a matter of fact, with $\alpha = 1$ the trussed arch structure seems to be useless in terms of load reduction of the PRC beam; instead, on the opposite, with $\alpha = 0$ the self weight of the steel trussed arch is too much heavy. In the present study, it was found that values of α comprised between $0,6$ and $0,7$ allow solutions technically practicable, respectful of all the constraints verifications, with an optimal

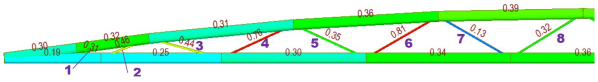

Fig. 4.21 Geometric lateral view of the optimal trussed arch system with annotations regarding to the performance ratio of each steel member.

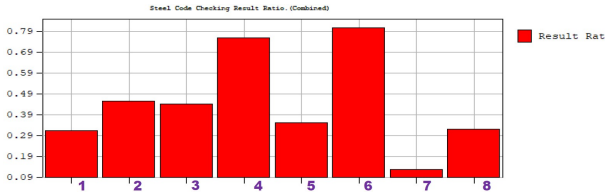

Fig. 4.22 Performance ratios of steel diagonals members obtained with MidasGen© software.

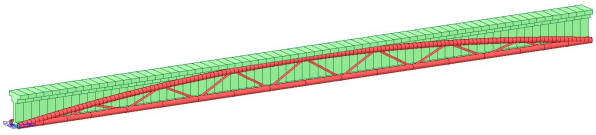

Fig. 4.23 Three-dimensional view of MidasGen© model of the optimal found solution.

balance between material consumption and the global stiffness of the strengthened beam. A value of $\alpha > 0,5$ means that a greater weight is associated to the size optimization OF, but always taking into account also a not negligible influence of the OF related to the global stiffness of the system. In Table 4.15, solutions obtained for $\alpha = 0,6$ and $\alpha = 0,7$ are illustrated where the structural efficiency is reported in terms of performance coefficient given by the ratio between the acting moment and resisting moment M_{Sd}/M_{Rd} after the strengthening intervention, always referred to the four degradation levels considered in the current study.

Results in Table 4.15 show promising strengthening solutions effectively able to deal with degradation levels 1, 2 and 3. Furthermore, the obtained CHS profiles are reasonable to perform this kind of intervention. Since with $\alpha = 0.6$ the OF is greater weighted towards maximization of global stiffness with respect to the minimization of the steel SW, it is reflected by the consistent increase of the total steel SW which almost redoubled with respect to the case $\alpha = 0.7$. Through the adoption of the tool design in MidasGen© software, the final results were assessed to be respectful of the stress and buckling constraints and the performance ratio of each element has been depicted in Figures 4.21 and 4.22. A three-dimensional view of MidasGen© model of the optimal found solution is illustrated in Figure 4.23. As shown in these figures, there is apparently a non-optimal distribution of the performance ratios. In reality, it

Effects of α coefficient

α	$1-\alpha$	PRC beam load decrease [%]	SW steel trussed arch [t]
0	1	0,1%	0,3
1	0	78%	58

Table 4.14 Effects of α coefficient

Results of optimal strengthened PRC beams.

α	CHS Arch [mm]	CHS Lower tie [mm]	CHS Diagonals [mm]	Steel SW [t]	Degradation level	$\frac{M_{Sd}}{M_{Rd}}$
0.7	$\phi 323,9$ $t.6$	$\phi 323,9$ $t.6$	$\phi 60,3$ $t.2,5$	3,54	1	0,89
					2	0,93
					3	0,98
					4	1,03
0.6	$\phi 323,9$ $t.12$	$\phi 323.9$ $t.12$	$\phi 114,3$ $t.3$	6,95	1	0,82
					2	0,86
					3	0,90
					4	0,95

Table 4.15 Results of optimal strengthened PRC beams for $\alpha = 0,6$ and $\alpha = 0,7$.

is necessary to recall that calibrating the α coefficient, it allows to optimize not only the minimization of the steel SW but also considering to reach a reasonable global stiffness to produce an actual effective strengthening system. In order to further push the optimization process in terms of performance ratio for each steel member, it would be virtually possible to also parametrize the diagonal elements with two different CHS profiles when they are in prevalent compression or tension under the current load configuration without compromise the overall global stiffness.

4.9 Preliminary cost comparison with traditional strengthening interventions

the proposed strengthening system evaluate also from an economic point of view , a preliminary comparison with the traditional external prestressing cables technique is performed. It is necessary to underline the preliminary level of this kind of evaluation, since some other technological aspects have to be fully investigated in the future, e.g. the connections design of the trussed arch element to the PRC

Preliminary economic comparison among consolidation interventions.

	Unitary cost	Quantity	Cost
Trussed arch $\alpha = 0.6$	2,59 €/kg	$2 \cdot 6.95 = 13,9$ t	36'000 €
Trussed arch $\alpha = 0.7$	2,59 €/kg	$2 \cdot 3.54 = 7,08$ t	18'337 €
Ext. prestr. with 2 cables	526 €/m	36 m	18'936 €
Ext. prestr. with 4 cables	878 €/m	36 m	31'608 €

Table 4.16 Preliminary economic comparison among traditional consolidation interventions with two or four external prestressed cables with the proposed optimal trussed arch strengthening system with $\alpha = 0,6$ and $\alpha = 0,7$.

beam. Furthermore, labour cost, technological aspects, etc. are considered in a very simplified manner taking into account unitary cost coming from some quoted works and Italian documents related to external tendons strengthening intervention and steel unitary cost. In a more refined economic analysis all of the previous aspects have to be deeper analysed.

In S.p.A. (2021), the steel unitary cost for truss beams with span length range 25-45 m can be considered as 2,59 €/kg which comprises materials cost and also launching operations. Instead, in Devitofranceschi (2018), in a simplified manner, four external prestressing cables can be considered an all-encompassing unitary cost (launching, anchorages, pretensioning operations) as 526 €/m for the intervention with two cables with 7 strands each, or 878 €/m for a solution with four external cables. In this case, two different solutions are considered in order to obtain a range of variability for the cost of external cable interventions in comparison with the two optimal trussed arch solutions obtained with $\alpha = 0,6$ or $0,7$. Based on the previous data, the overall global preliminary costs are reported in Table 4.16. Based on that preliminary estimations, it is possible to state that the steel trussed arch with $\alpha = 0,7$ is the most economic intervention because it is slightly lower than the external tendon solution with two cables. It is worth noting that, even considering different levels of degradation, the unitary cost for external prestressed cables solution does not change because, for different degradation levels, only the prestressing forces of the tendons vary and its unitary cost is mainly related to technological issues such as the design of anchorages, positioning hydraulic jacks, etc. On the other hand, the proposed trussed arch strengthening solution could virtually require cheaper truss structures,

more optimized, lighter and slender for lower levels of degradation. Instead, as shown in the previous Section, for higher levels of degradation, it is not reasonable to overcome $\alpha = 0,7$ because it may result in a structure excessively light and slender thus the percentage of PRC beam load decrease could be virtually almost negligible. Eventually, comparing the costs in Table 4.16 for $\alpha = 0,7$ and for a four tendons solution, these values appear to be higher than the two other solutions but they are always comparable at this preliminary stage, underlining once again the engineering relevance of the optimal found solution.

4.10 Conclusions

In this work, a new strengthening system, as an alternative to the traditional external prestressing cables method, has been proposed along with an efficiency index. This last includes both the economic impact and the structural performance.

A parametric modeling has been performed in order to investigate the variables that mainly affect the industrial solution considered as the target of this work. The double-pinned supports static scheme appears to be the stiffest solution despite several configurations investigated. The geometric and material features of the circular hollow sections (CHS) for each structural element, composing the proposed strengthening system, exhibit the greatest gyroscopic inertia in comparison with other cross section typologies with the same area. In this way, a maximum centrifugal mass effect is achieved in order to increase the efficiency of the strengthening system. Moreover, the sensitivity analysis shows how the proposed solution is strongly dependent on the dimensional characteristics of the compression and tension chords rather than truss diagonal elements: increasing the size of the arch and tie elements, a significant improvement in the efficiency of the system is recognized due to their main contribution to the centrifugal mass effect. For these reasons, structural optimization was performed in order to prefer this kind of structural characteristics. The optimization process allows to detect the best solution as the best trade-off in terms of stiffness and self-weight of the proposed solution. The multi-objective optimization problem has been reconducted to a single objective problem through an OF weight parameter α and its complementary $(1-\alpha)$ for the two counterposed OFs. The parameter α has been evaluated with the aim to identify the equilibrium solution which guarantees the lighter strengthening system with the highest stiffness.

In conclusion, the optimization model allows capturing, when 20% of the area loss occurs (degrade level 3), until to 40% of the total external distributed load. Finally, an economic estimation of the consolidation system installation has been presented comparing the total cost of the proposed retrofitting technique with the traditional external prestressing one. Although a significant cost saving is not found, it is worth noting that the proposed procedure allows the production of the beam-arch assemblage entirely on site without the need of skilled workers or specialist companies. Moreover, the proposed retrofitting technique does not need an estimation of the residual prestressing level, which could increase the compression stress configuration of the concrete beam without any beneficial effects.

Chapter 5

Size and Shape Optimization of a Guyed Mast Structure

5.1 Introduction

Guyed masts are extensively used in the telecommunications industry, and the size, shape, and topology optimization can significantly benefit their transportation and installation. The main loads acting on guyed mast structures arise from wind Law et al. (2006), Sparling and Wegner (2007), earthquakes Hensley and Plaut (2007), Amiri (2002), Liu et al. (2021), Sun et al. (2013), sudden rupture of guys Buchholdt et al. (1986), galloping of guys Ballaben et al. (2017), and sudden ice shedding from ice-laden guy wires Gerstoft and Davenport (1986).

Their optimization must fulfil several requirements under ultimate and service limit states de Souza et al. (2016). Specifically, service limit states are crucial for guyed mast structures due to high-amplitude oscillations caused by their high deformability. In some cases, these vibrations have led to a signal loss caused by excessive displacement and rotation of the antennas and, in other cases, have resulted in permanent deformation or failure. Therefore, size optimization of the guyed mast structure represents a challenging task since the increment of the performance ratio of the materials should be counterbalanced by an adequate lateral stiffness to reduce high-vibration drawbacks Saudi (2014).

Saxena Saxena et al. (1989) reported several happenings where heavy icing combined with moderate wind resulted in severe misalignment of towers and complete failure. Novak et al. Novak et al. (1978) showed that ice accumulation on some parts of the guy wires and moderate winds could lead to the guy galloping, resulting in unacceptable stress levels throughout the structure. The main topics investigated in the field of guyed structures can be summarized as follows:

- Structural design. Several researchers investigated the dynamic response of guyed mast structures through experimental tests and numerical modeling to derive design approaches and recommendations Wahba et al. (1997), Madugula et al. (1998), Luzardo et al. (2012). In particular, there are studies dealing with the dynamic identification and accurate estimate of the wind loads Davenport and Sparling (1992), Harikrishna et al. (2003), Gioffrè et al. (2004), Clobes and Peil (2011), Pezo and Bakić (2014).

- Nonlinear dynamics. The proneness to global and local instabilities challenged several scholars to estimate and predict the nonlinear behaviour of guyed masts Sparling (1995), Wahba et al. (1998), Madugula (2001), Orlando et al. (2013), Ballaben and Rosales (2018).

- Structural optimization. The need for guyed structures that are easy to install and transport challenged several scholars to optimize their shape in order to reduce the structural mass without reducing the lateral stiffness and prevent instability phenomena Belevičius et al. (2013).

- Structural control. There are some attempts of control methods to reduce vibrations in mast-like structures Gawronski et al. (1994), Fujino et al. (1993), Lacarbonara and Ballerini (2009). Among others, Blachowski Błachowski (2007) proposed the use of a hydraulic actuator to control cable forces in guyed masts using Kalman filtering.

This paper tackles the size and shape optimization of guyed mast structures. Since the first attempts by Bell and Brown Bell and Brown (1976), many engineers attempted to optimize guyed masts under wind loads using deterministic global optimization algorithms. However, as pointed out by Belevičius et al. (2013), this approach leads to local optimum points, since each design variable was considered separately. Thornton et al. Thornton et al. (1990) and Uys et al. Uys et al. (2007)

proposed general procedures for optimizing steel towers under dynamic loads. To the author's knowledge, Venanzi and Materazzi Venanzi and Materazzi (2007) were the first to implement a multi-objective optimization method for guyed mast structures under wind loads using the stochastic simulated annealing algorithm for size optimization. The objective function implemented by Venanzi and Materazzi (2007) included the sum of the squares of the nodal displacements and the in-plan width of the structure. Zhang and Li Zhang and Li (2011) attempted to achieve both shape and size optimization in a two-step procedure using the ant colony algorithm (ACA). Cucuzza et al. Cucuzza et al. (2021a) proposed an alternative approach in which the multi-objective optimization problem has been reduced to a single-objective problem through suitable parameters. Luh and Lin Luh and Lin (2011) were challenged in achieving the topology, size, and shape optimization of guyed masts using a modification of the binary particle swarm optimization (PSO) and the attractive and repulsive particle swarm optimization.

This paper discusses the size optimization of guyed masts using a genetic algorithm (GA) by considering different design scenarios (e.g., Cucuzza et al. **?** and Manuello et al. Bertetto and Marano (2022)). Kaveh and Talatahari Kaveh and Talatahari (2009) noticed that the particle swarm optimization (PSO) is more effective than ACA and the harmony search scheme for optimizing truss structures. However, Deng et al. Deng et al. (2012) and Guo and Li Guo and Li (2011) were successful in optimizing tapered masts and transmission towers using modifications of genetic algorithms (GA). Moreover, Belevivcius et al. Belevičius et al. (2013) attempted the topology-sizing optimization problem of the guyed mast as a single-level single-objective global optimization problem using GAs.

Therefore, given the numerous successful solutions of guyed masts using GAs, the authors chose to investigate the size optimization of a guyed mast structure using GAs. Following Venanzi and Materazzi (2007), this paper focuses on the size optimization by considering eight possible design scenarios. The purpose of the present paper is two-fold. Firstly, this work aims at achieving a size optimization on a real application case adopting structural verification according to Eurocode 3. During the load evaluation phase, detailed analyses have been conducted, including wind, ice, and seismic actions and the verifications against instabilities. Secondly, the computational intelligence procedure adopted by the authors allowed the investigation of several scenarios simultaneously. As a result, the parameters that mainly affected the design process have been detected to provide preliminary indications to

engineers in the practical design of similar structural typologies. Furthermore, the considered case study may represent a benchmark case for validating the reliability and accuracy of alternative numerical approaches. Therefore, the paper is organized as follows. After the case study description and the FE model, the authors introduce the first numerical results and the outcomes of the size and shape optimization.

5.2 Case Study

The considered structure is a guyed radio mast. It is a thin, slender, vertical structure sustained by tension cables fixed to the ground and typically arranged at 120° between each other.

The main body is a single central column made of tube profiles or truss systems when a high elevation must be reached, see Figure 5.1. More than one set of cables is placed at different elevations to prevent instability phenomena. Guyed towers are usually built for meteorological purposes or to support radio antennas, such as the one considered in this research. In particular, this structure can be used for a limited time during an event or maintenance of primary transmission towers. Therefore, it is also called a temporary base transceiver station (BTS), typically adopted to supply the immediate service. Sporting events, concerts, motor racing, military camps, and emergency events are typical examples of temporary BTS applications. The BTS is usually mounted on a moveable platform called the shelter.

The considered structure is located in Bassano Del Grappa, in the north of Italy, at a 129 m elevation from the sea level. The surrounding area is low-urbanized, with no relevant obstacles to the wind loads. The total height of the mast is 30.00 m. It is sustained by a central pole where 21 cables are fixed, see Figure 5.2. Other structural elements with rectangular cross-sections are used to create truss systems connecting cables and the central pole.

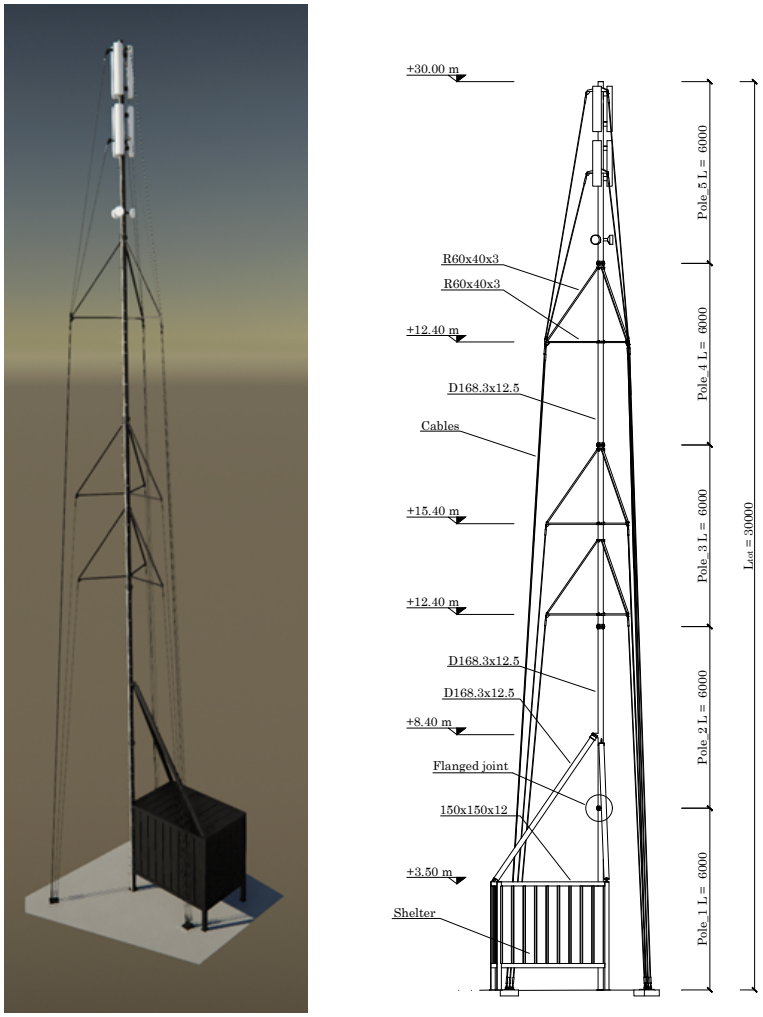

(a) (b)

Fig. 5.1 (**a**) Render model realized using Tekla Structures. (**b**). Technical drawing of the structure investigated with dimensions in mm.

The central pole consists of five circular hollow steel profiles with flanged joints and 6 m in length. All connections are bolted, as well as those connecting the cables to the pole.

The shelter is a steel box devoted to partially sustaining the structure and hosting electronic equipment. It is usually mounted on a moveable platform.

Fig. 5.2 Pictures and details of the considered structure.

5.3 Load Analysis

This section details the loads acting on the structures, from the dead to the variable loads. According to the Italian Standard Regulation NTC2018, the load combinations of the actions have been evaluated at the ultimate limit state (ULS) and, for seismic conditions, at the life safety (LS) limit state. In Appendix 5.7, Table **??** illustrates the most critical combinations for both static and dynamic configurations. Partial safety factors γ and combination coefficients ψ were adopted in order to consider maximization (positive sign) or minimization (negative sign) of effects both for vertical and horizontal actions.

5.3.1 Dead Loads

The structure is made of steel S355, whose mechanical stress-strain behaviour is depicted in Figure 5.3, and the characteristics are listed here: $f_{us} = 510$ MPa, $f_{ys} = 355$ MPa, E_s = 210,000 MPa, which are the ultimate and yielding stresses and Young's modulus, respectively.

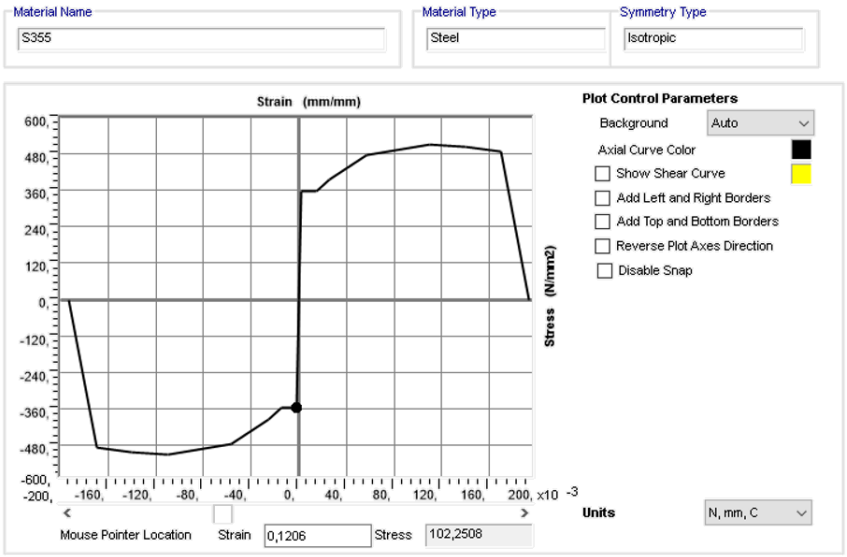

Fig. 5.3 Mechanical stress–strain behaviour of steel S355 implemented in SAP2000.

The cables are made of galvanized steel consisting of 6 strands (216 wires) with an independent metal core (49 wires). The main characteristics are illustrated in Table 5.1.

Table 5.1 Technical specifications of the steel ropes.

Steel Ropes (Cables)				
Model			$6 \times 36WS + IWRC/265$ wires	
Construction pattern			$6 \times (14 + (7 + 7) + 7 + 1) + (7 \times 7)$	
Winding direction			right cross	
Material			galvanized steel	
Resistance			1170 N/mm^2–180 kg/mm^2	
Cable diameter	Weight	Area	Wire diameter	Load to failure
[mm]	[kg/m]	[mm^2]	[mm]	[kN]
16	1.36	173.25	0.91	161
18	1.67	212.74	1.03	204
20	2.02	257.32	1.14	252
22	2.41	307.01	1.26	305

The structure investigated consists of a few types of elements, as indicated in Table 5.2. Dead loads are calculated from the weight per unit length of each member.

Table 5.2 Computation of the dead loads.

Computation of Dead Loads					
Profile [mm]		w [kg/m]	Length [m]	n°	Wtot [kg]
Circular	D168.3 × 12.5	48	6	5	1440
	D168.3 × 12.5	48	5.65	2	543
Rectangular	60 × 40 × 3	4.35	3.16	9	124
	60 × 40 × 3	4.35	1.8	9	71
	100 × 40 × 3	6.13	0.45	6	17
Rope	D16	1.3667	12.45	3	51
	D16	1.3667	15.44	3	63
	D16	1.3667	24.43	9	300
	D16	1.3667	5.76	3	24
	D16	1.3667	8.46	3	35
				2651 Kg	

The non-structural dead loads originate from the wiring weight and the steel ladder for inspection and maintenance. This load results in 0.3 kN/m. Antennas and parabolas represent the weight of the equipment. Two groups of three antennas are located at 26.00 and 29.25 m in height, with a 120° in mutual spacing. The first one is the model AOC4518R7v06 produced by Huawei®. The second one is the model 6888670N manufactured by Amphenol®. Finally, there are three parabolas located at 23.15 m height, spaced 120° apart from each other, 30 cm in diameter. Tables 5.3 and 5.4 detail the weight of the equipment and the non-structural dead loads.

Table 5.3 Weight of equipment, H, W, and D stand for height, width, and depth.

Typology	**Model**	**No**	**Elevation [m]**	**H×W×D [mm]**	**Self-Weight [kg]**
Antenna	AOC4518R7v06	3	29.25	1509 × 469 × 206	39.3
Antenna	6888670N	3	26	1997 × 305 × 163	32
Parabola	n.d	3	23.15	D = 300	15

Table 5.4 Non-structural dead loads.

Item	qk [kN/m]	Qk [kN]
Steel ladder, other	0.3	-
Antenna	-	1.53
Antenna	-	1.19
Parabolas	-	0.52

5.3.2 Variable Loads

In this section, the detailed load modeling phase, for each variable load considered, is described. With specific reference to the wind action evaluation, the drag and lift forces are calculated according to the CNR-DT 207 R1/2018 del (2009). The relationship between inertia and viscous forces, i.e., how wind load impacts to the surface, is taken into account with the Reynold's number R_e with the following expression:

$$R_e(z) = \frac{l \cdot v_m(z)}{\nu} \tag{5.1}$$

where z is the elevation, l is the characteristic length, v_m is the averaged wind speed, while ν is the kinematic viscosity of air ($\nu = 15 \times 10^{-6}$ m^2/s).

Maintenance and Repairing Loads

Following the Italian national recommendations Mordà and Mancini (2018), it is supposed that a typical situation of inspection or maintenance is performed by an operator working on the steel ladder. A concentrated load of 120 kg is applied at the top of the tower. Despite that, it is reasonable to believe that the operator could work by using a basket elevator, without loading the structure.

Wind Loads

The wind action was evaluated according to the Italian recommendations in del (2009). Firstly, the peak kinetic pressure (q_p) was evaluated as follows:

$$q_p = \frac{1}{2} \cdot \rho \cdot v_r^2 \cdot c_e(z) \tag{5.2}$$

where p is the kinetic pressure, while:

- ρ is the air density;
- v_r^2 is the reference wind velocity;
- c_e is the exposure coefficient, varying with the elevation z of the structure.

For this purpose, the equivalent longitudinal or drag forces, f_D, and transverse or lift force, f_L, are evaluated as follows:

$$f_{drag} = q_p(z) \cdot l \cdot c_{drag}; \qquad f_{lift} = q_p(z) \cdot b \cdot c_{lift} \tag{5.3}$$

where

- $q_p(z)$ is the *peak kinetic pressure* evaluated at height z;
- l is the characteristic element size;
- b is the reference transverse dimension of the section;
- c_{drag} and c_{lift} are the longitudinal and transverse dynamic coefficients.

Drag D and Lift L forces are reported in Tables **??** and **??**.

Ice Load

Ice and snow attached to the structural surface can significantly increase the variable loads in flexible and light structures. In particular, the radio mast is very sensitive to changes in the wind-exposed surface. In addition, the ice covering can increase the volume and the surface of the structural elements more than twice due to the low thickness of the central pole. The recommendations in del (2009) provide

several scenarios for ice coverings. In the absence of more detailed evaluations, it is customary to consider an ice sleeve formation that is 12.5 mm thick. After the estimate of the wind loads, the influence of the ice sleeve formation on the structure is considered by assuming an additional exposed surface equal to 15% of the original one.

Seismic Action

Seismic action is evaluated according to the Italian seismic hazard map Mordà and Mancini (2018). A linear dynamic analysis with seismic elastic response spectrum corresponding to the service limit state was carried out. Specifically, seismic actions are considered as acting independently in the X and Y plane directions.

The elastic response spectrum considered in the analysis was calculated by considering the topographic category of the site and geometry of the building (Figure 5.4). The first 33 vibration modes of the structure are included in the analysis, to reach 85% of the total participating mass according to the national regulations in Mordà and Mancini (2018). The mass participating ratios are listed in Appendix 5.7.

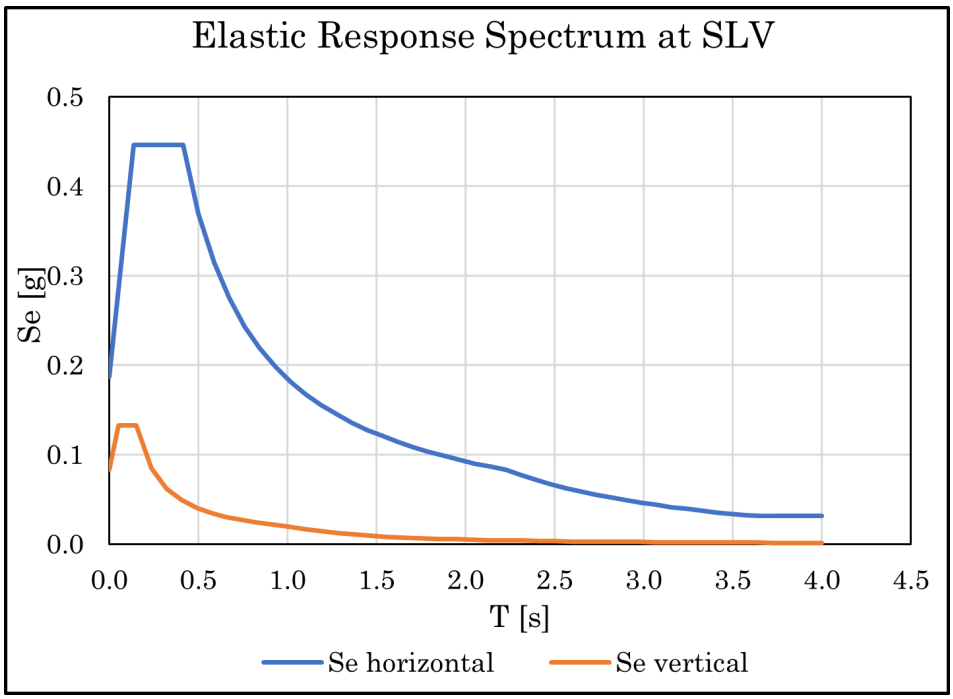

Fig. 5.4 Elastic response spectrum corresponding to the service limit state (SLV), where *Sa* is the spectral acceleration.

5.4 Finite Element Modeling

The structural model was developed using two different element types: beams and cables. Beam elements model the main pole and all structural elements except for the cables. They possess the geometric and material properties of structural elements. The beam elements are used to model the main pole and secondary elements. Moreover, except for the main pole, rotation releases are applied at the ends in order to consider no flexural rigidity, as occurring for trussed structures.

Cable elements are used to simulate the steel ropes. Cable elements undergo large displacements that give rise to geometric nonlinearities. Therefore, the equilibrium of the cables is considered in the deformed configuration using SAP2000. As a result, the structural behaviour of guyed towers can be highly nonlinear, especially for low pre-tension cables, which are prone to large displacements. On the contrary, the nonlinear behaviour becomes less pronounced by increasing the pre-tension, resulting in high compression levels and minor instability effects. This paper considers the envelope of the maximum and minimum responses associated with each load condition.

Figure 5.5 plots the three modes with a higher mass participation ratio. These are the 10th, 11th, and 12th modes obtained from the dynamic analysis of the mast structure with the dead loads. On the contrary, the first modes arising from the dynamic analysis have lower mass participation factors and are characterized by local deformation of the structural elements. The 10th, 11th, and 12th modes are the first modes exhibiting the global deformation of the mast structure.

X and Y identify the in-plane orthogonal directions. The 10th and 11th modes have an approximate 26% mass participation factor in the Y and X directions, respectively. The natural period is very low and at approximately 0.4 s. The 13th mode is mainly torsional with nearly a 7 and 4% mass participation factor in the X and Y directions.

Figure 5.6 shows the positive (in dark green and purple) and negative (in red and light green) maximum and minimum envelopes of the axial, shear forces, and bending moments acting on the structural elements. Figure 5.7 plots the performance ratios of all structural elements except for the cables. The performance ratio is the ratio between the maximum stress in the structural element and the yielding stress. The performance ratios are defined by the colour map next to Figure 5.7. The plots

highlight the presence of a structural element in the first half of the central pole with a high-performance ratio, depicted in yellow. The first section of the central pole has a low performance ratio, lower than 0.25. After the section with a performance ratio in the range 0.4–0.65, the following sections fall in the range 0.25–0.4 and are coloured in green. The top sections of the central pole are not significantly stressed, with a performance ratio of 0–0.25. The bracings have low stress, plotted in cyan, with performance ratios of 0–0.25.

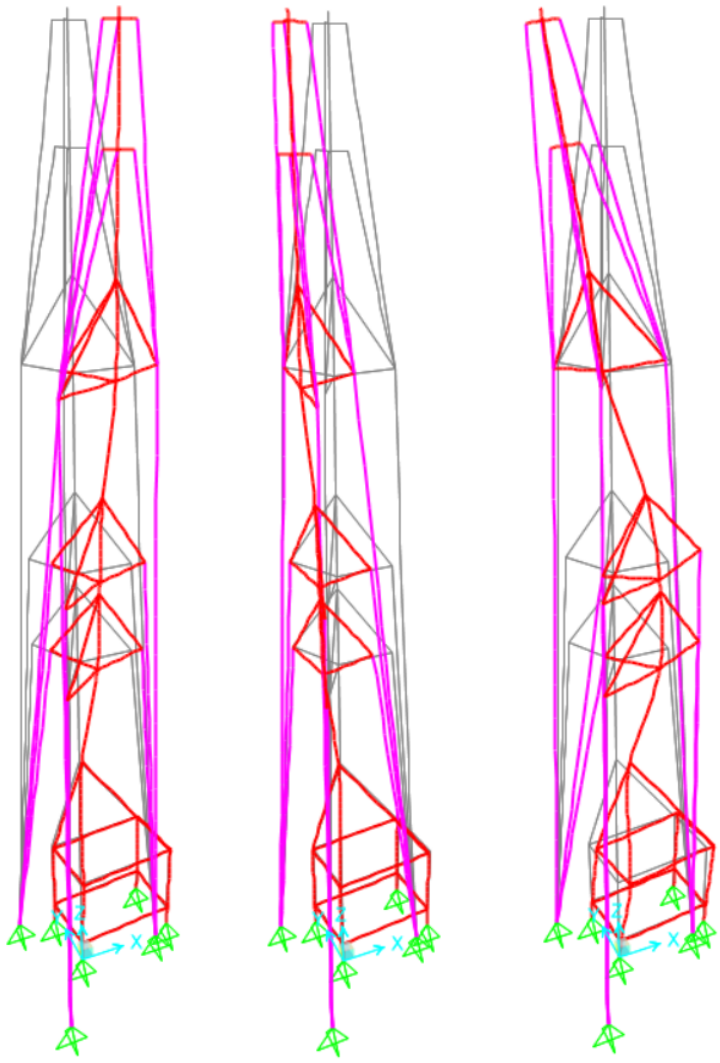

(a) (b) (c)

Fig. 5.5 (**a**) Mode 10th—Ts = 0.437 s—mass participation ratio X = 9.6%, Y = 26.2%; (**b**) Mode 11th—Ts = 0.434 s—mass participation ratio X = 26.4% Y = 9.2%; (**c**) Mode 12—Ts = 0.206 s—mass participation ratio X = 7.2% Y = 4.4%.

Figure 5.8 shows the maximum displacements in the X (u_1), Y (u_2) directions and their combination (u_t) at the service limit state. The maximum displacement is located at the top of the tower, in particular at joint 6 (z = 30.00 m), with a maximum displacement equal to u_t = 18.7 mm.

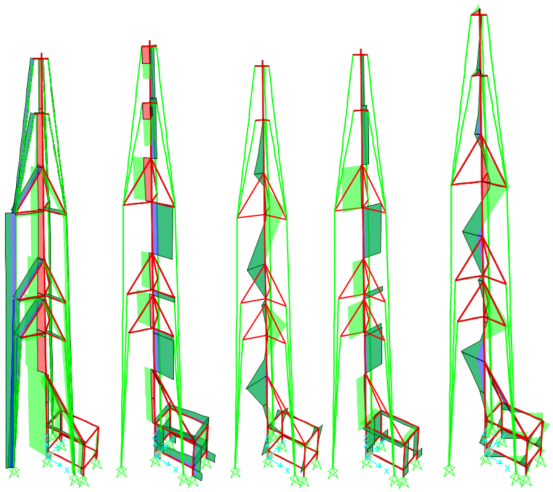

(a) (b) (c) (d) (e)

Fig. 5.6 (**a**) Axial force, (**b**) shear force (V_2), (**c**) bending moment (M_2), (**d**) shear force (V_3), (**e**) bending moment (M_3).

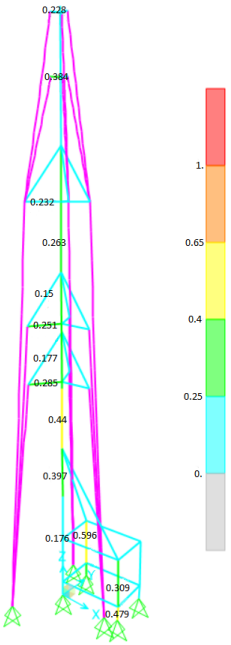

Fig. 5.7 Performance ratios of the pole before optimization. Cables are depicted with magenta colour because their performance ratios are not included in the current representation.

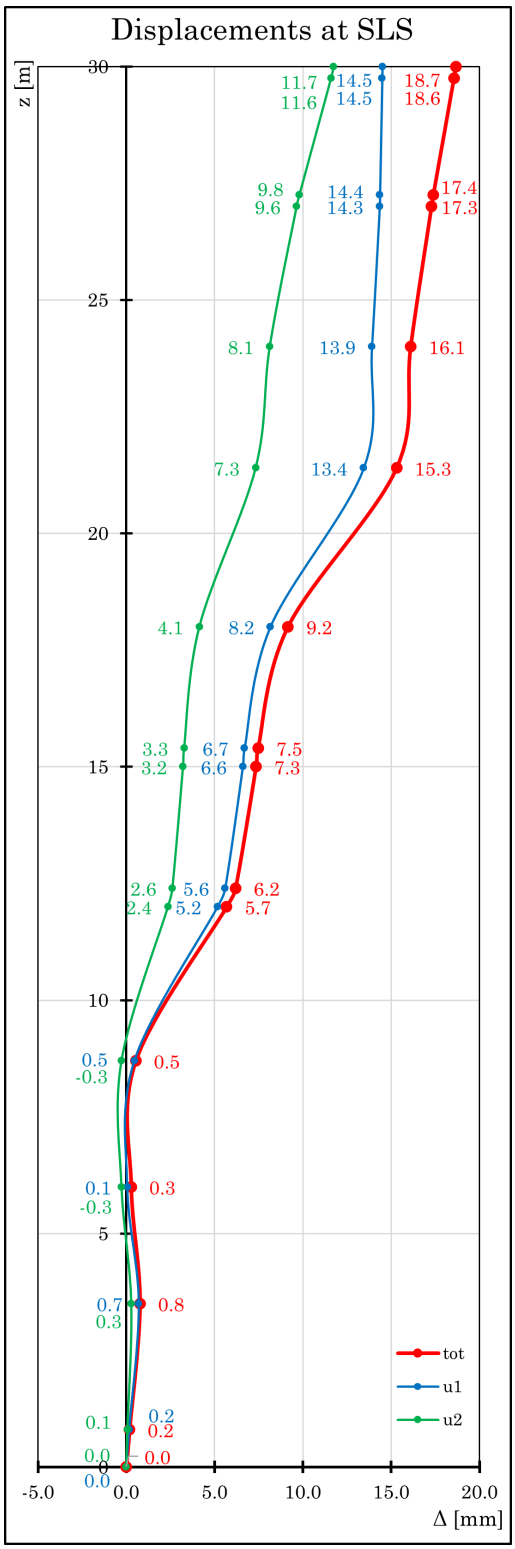

Fig. 5.8 Displacements vs. elevation at the service limit state in two in-plane orthogonal directions (u_1, u_2) and their combination (tot).

5.5 Structural Optimization

In optimization problems, the main goal is to find the best conditions in terms of the optimal set of design parameters collected in the design vector x, which minimizes an objective function (OF) $f(x)$ Melchiorre et al. (2021), Rosso et al. (2022, 2021c). These problems can be categorized into single-objective or multi-objective based on the number of OFs involved, and a further classification is based on the presence (or not) of constraints Rao (2019a), Aloisio et al. (2022), **?**. In the structural optimization field, it is common to deal with constrained optimization, whose general statement is Christensen and Klarbring (2008b):

$$\begin{aligned} & \min_{x\in\Omega}\{f(x)\} \\ \text{s.t.} \quad & g_q(x) \leq 0 \quad \forall q = 1,\ldots,n_q \\ & h_r(x) = 0 \quad \forall r = 1,\ldots,n_r \end{aligned} \tag{5.4}$$

where $x = \{x_1,\ldots,x_j,\ldots,x_n\}^T$ is the design vector to be optimized, whose terms are limited into a hyper-rectangular multidimensional box-type search space domain of interest denoted as Ω, given by the Cartesian product of the range of interest of each j-th of each design variable bounded in $[x_j^l, x_j^u]$, $\Omega = [x_1^l, x_1^u] \times \ldots \times [x_j^l, x_j^u] \times \ldots \times [x_n^l, x_n^u]$. The term $g_q(x)$ in (5.4) denotes inequality constraints whereas $h_r(x)$ are equality ones, which further reduce the feasible search space inside Ω. In structural optimization, it is typical to deal with inequality constraints, and a common goal is to minimize the global cost of the structure. Since this involves many terms, the main attempt is minimizing the self-weight of the structure, indirectly connected to material cost, i.e., material usage and natural resources consumption Christensen and Klarbring (2008b). Several strategies have been developed over the years to handle constraints Coello Coello (2002), Koziel and Michalewicz (1999a), Michalewicz and Fogel (2008). In the present work, the penalty function-based approach was implemented due to its simplicity, allowing converting the problem with OF $f(x)$ into a new unconstrained version $\phi(x)$:

$$\min_{x\in\Omega}\{\phi(x))\} = \min_{x\in\Omega}\{f(x) + H(x)\} \tag{5.5}$$

where $H(x)$ is the penalty function. Adopting a static-penalty strategy, $H(x)$, assume this form Parsopoulos and Vrahatis (2005), Coello (1999)

$$H_s(x) = w_1 H_{NVC}(x) + w_2 H_{SVC}(x) \tag{5.6}$$

where H_{NVC} is the number of violated constraints and H_{SVC} is the sum of all violations:

$$H_{SVC}(x) = \sum_{p=1}^{n_p} \max\{0, g_p(x)\} \tag{5.7}$$

w_1 and w_2 are the violation control parameters, whose numerical values are assumed equal to $w_1 = w_2 = 100$ following Parsopoulos and Vrahatis (2005).

In the current study, the authors carried out a parametric study on the design variables of the guyed mast. This fact has led to eight different scenarios, summarized in Table 5.5. In addition, the starting initial values of the design parameter are listed in Table 5.6, while the general optimization workflow is illustrated in Figure 5.9. To compare the results, the focus is related only to the performance ratios PR of the central pole of the guyed radio mast, being the pole the most stressed element. It consists of five segments 6.00 m long with the same cross-section. Thus, starting from the ground level:

1. Pole_1 (0.00 to 6.00 m);
2. Pole_2 (6.00 to 12.00 m);
3. Pole_3 (12.00 to 18.00 m);
4. Pole_4 (18.00 to 24.00 m);
5. Pole_5 (24.00 to 30.00 m).

Starting with a constant diameter of the cross-section for the pole, at the end of the optimization, it is advisable to find a tapered solution following a linear relationship with the height, as represented in Figure 5.10f. Accordingly, it is possible to shape the pole cross-section with two design variables described by the bottom Φ_i and top Φ_f diameters. In the following, the different scenarios obtained from the parametric study based on the design variables involved in the optimization problem are described:

- Scenario A: this scenario involves the diameter Φ, as a sole variable, in the attempt to reduce the material consumption with a constant pole cross-section diameter with the height, as illustrated in Figure 5.10a.
- Scenario B: this scenario attempts to refine the previous case by adopting a tapered solution for the pole, by using the bottom Φ_i and the top Φ_f diameters, as represented in Figure 5.10b.
- Scenario C: further improvements are considered concerning scenario B by adding the cable pre-stressing force F as a variable of the optimization, as represented in Figure 5.10c.
- Scenario D: further improvements are considered to scenario B by using a unique value for the pole thickness t of the tapered elements of the pole, as represented in Figure 5.10c.
- Scenario E: further improvements are considered with respect to scenario B by optimizing both cable pre-stressing force F with a unique value of thickness t for the tapered elements of the pole, as represented in Figure 5.10e.
- Scenario F: from the structural analysis of scenario E, it is possible to point out how the linear law for the tapering forces to use a larger section where it is not necessary. Elements 2 and 3 are the most stressed ones. Therefore it is possible to further refine scenario E by considering a thickness value for the intermediate pole elements t_{inter} and a different thickness for the other extremal pole elements $t_e nds$.
- Scenario G: in this scenario, the five different thickness values only have been governed for every pole element $\{t_1, t_2, t_3, t_4, t_5\}$ for a constant diameter solution with height, as depicted in Figure 5.10f.
- Scenario H: in this last scenario, a complete approach involves both the tapered solution by governing the initial bottom Φ_i and the final top Φ_f diameters, the five values of thickness for every pole element $\{t_1, t_2, t_3, t_4, t_5\}$, and even the cable pre-stressing force.

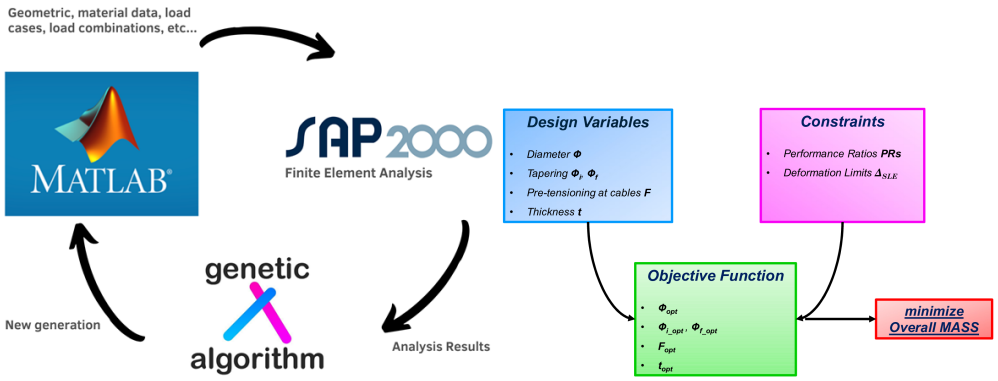

Fig. 5.9 Workflow of the optimization problem.

Table 5.5 Parametric study on the design variables involved and summary of the different scenarios.

Scenario	No. Parameters
A(Φ)	1
B(Φ_i, Φ_f)	2
C(Φ_i, Φ_f, F)	3
D(Φ_i, Φ_f, t)	3
E(Φ_i, Φ_f, t, F)	4
F($\Phi_i, \Phi_f, t_{ends}, t_{inter}, F$)	5
G(t_1, t_2, t_3, t_4, t_5)	5
H($\Phi_i, \Phi_f, t_1, t_2, t_3, t_4, t_5$)	8

Table 5.6 Total mass of the main pole.

Parameter	Measure	Value
Φ_0	[mm]	168.3
t_0	[mm]	12.5
L	[mm]	6000
Mass	[kg]	288
no elements	[-]	5
Total Mass	[kg]	1440

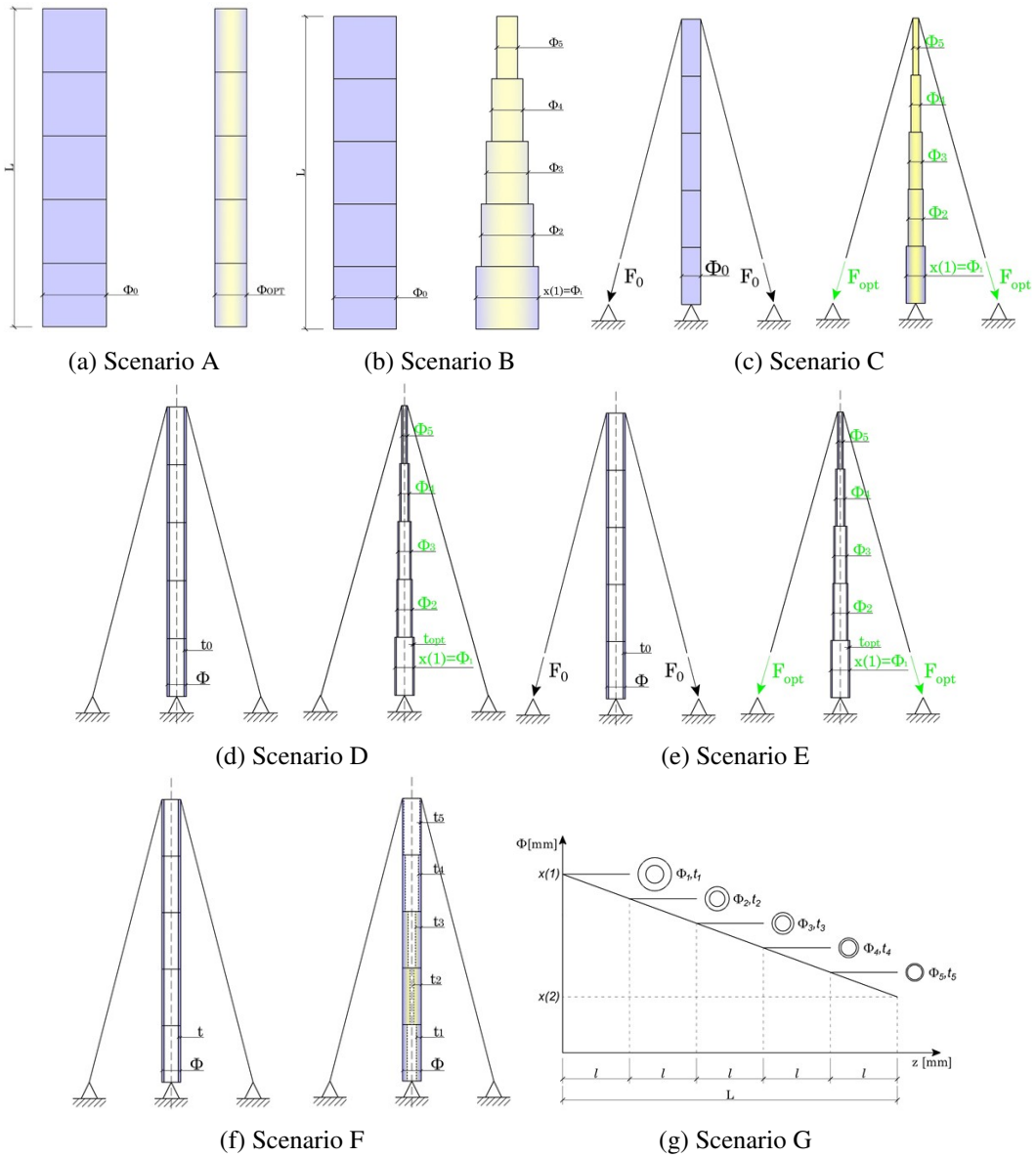

(a) Scenario A (b) Scenario B (c) Scenario C

(d) Scenario D (e) Scenario E

(f) Scenario F (g) Scenario G

Fig. 5.10 Parametric study on the design variables involved and representation of the different scenarios described in Tab.5.5.

Constraints Involved in the Structural Optimization Problem

The optimization problem statement is reported in (5.4) and the constraints were treated with the penalty-based approach illustrated in (5.5), by converting the constrained problem into an equivalent unconstrained one. The resolution of the optimization task considers the structural design assessment required by national and

international codes to ensure the safety of constructions. In particular, the structural verifications derive from Eurocode 3 (EN 1993-1-1: 2005) and are referred to the ultimate limit state (ULS). The design verifications include tensile, compression, and buckling verification, and a combined assessment, such as the interaction capacity according to Annex B of the Eurocode 3:

$$\frac{D}{C} = \frac{N_{Ed}}{\frac{\chi_y A f_{yk}}{\gamma_{M1}}} + k_{yy}\frac{M_{y,Ed}}{\frac{\chi_{LT} W_{pl,y} f_{yk}}{\gamma_{M1}}} + k_{yz}\frac{M_{z,Ed}}{\frac{W_{pl,z} f_{yk}}{\gamma_{M1}}} \leq 1 \tag{5.8}$$

$$\frac{D}{C} = \frac{N_{Ed}}{\frac{\chi_z A f_{yk}}{\gamma_{M1}}} + k_{zy}\frac{M_{y,Ed}}{\frac{\chi_{LT} W_{pl,y} f_{yk}}{\gamma_{M1}}} + k_{zz}\frac{M_{z,Ed}}{\frac{W_{pl,z} f_{yk}}{\gamma_{M1}}} \leq 1 \tag{5.9}$$

where D stands for the demand and C stands for the capacity of the structure. Specifically, N_{Ed} is the acting axial force, whereas $M_{y,Ed}$ and $M_{z,Ed}$ represent the acting bending moments in the two principal directions of a planar local reference system centered on the cross section center of gravity. A is the cross section area of the pole, $W_{pl,y}$ and $W_{pl,z}$ are the plastic section modulus in the two principal directions, f_{yk} is the yielding strength of the steel, whereas γ_{M1} is the partial safety factor for instability conditions, equal to 1.05 from the Italian National Annex. χ_{LT} is the reduction factor for lateral–torsional buckling, whereas kyy, kyz, kzy, and kzz are interaction factors whose values are derived according to two alternative approaches based on Annex A (method 1)and Annex B (method 2). The global structural deformation referred to the service limit state (SLS) has also been considered by verifying the top displacement of the mast. Specific recommendations for guyed mast structures are missing in national and international codes. Therefore, the authors adopted the suggestions defined in the Italian Technical Code NTC2018 (D.M.17/01/2018) reported in Chapter 4.2.4.2.2 Table 4.2.XIII related to limitations of lateral displacements of steel multi-storey frame structures. These limitations express a threshold condition in terms of the total height of the structure H:

$$\delta_{\text{SLS,top}} \leq \delta_{\text{SLS,top,lim}} = \frac{H}{500} = \frac{30000 \text{ mm}}{500} = 60 \text{ mm} \tag{5.10}$$

Since this condition is specific for steel multi-storey frame structures, the authors will assume this value as a reasonable choice to ensure service life assessment and preservation of working conditions of the telecommunication guyed mast tower. In the next section, a discussion on the results is carried out.

5.6 Results and Discussion

The paper compares the outcomes of the size and shape optimization in eight different scenarios, distinguished by different design variables. Scenario A is associated with the worst improvement of the structural performance since a single diameter is used for the central pole. Additionally, industrial steel profiles do not cover all possible ranges of the diameter. Improvements in the structural performance and weight reduction are achieved in the following scenarios when the search space becomes larger by increasing the number of design variables.

Scenario B introduces the tapering of the central pole with a linear variation from the bottom to the top. In this case, the optimal solution is affected by intermediate sections, which are more stressed. Consequently, the end cross-sections are over-estimated. In response to that, Scenario F introduces the linear tapering of the tube thickness t_{ends},t_{inter} to enhance the performance of the optimal solution. Parallelly, in Scenario G, five different thicknesses are adopted (t_1, t_2, t_3, t_4, t_5), and the results are analogue to case F. Therefore, the thickness of the steel members is a suitable optimization parameter. At the same time, the diameter alone is not capable of returning attractive solutions because a linear interpolation trend is used. In addition, lower and upper limits were imposed for d and t. In particular, for this kind of structure, a minimum diameter $d_{min} \geq 100$ mm and a minimum thickness $t_{min} \geq 3$ mm was imposed.

The cross-section area depends on the square of the thickness. Therefore, small changes in t significantly affect the resulting area. Conversely, if the diameter is the sole search space, despite being tapered linearly with height, even significant modifications may not produce notable improvements. Still, the increment of design variables involved in the structural optimization typically increases the computational efforts. However, the scenario with the highest number of variables was characterized by an average time iteration close to 18s, using a computer with average performance. The computational effort cost of the optimization procedure strongly depends on the machine performance, no convergence issues occur. Table 5.7 lists the average values of performance ratio obtained from the eight optimization scenarios. All scenarios were collected in terms of number of parameters involved during the analysis. Table 5.7 proves that the increment in the number of design variables is associated with higher performance ratios. The target of the optimization achieves the best weight reduction, fully exploiting the structural material, without exceeding the

ultimate and service limit states. Table 5.7 lists three sets of performance ratios: the initial one before optimization, the optimized, and the one obtained using commercial steel profiles, called the design performance ratio. The averaged performance ratio is equal to 28% before optimization. It significantly increases from scenario A, nearly 45%, to scenario G with 68%.

Table 5.7 Averaged performance ratios obtained in each optimization scenario.

No Parameters	PR Initial	PR Optimized	PR Design
	[%]	[%]	[%]
1	28.0	45.7	40.5
2		39.5	43.1
3		50.5	50.6
4		54.4	58
5		65.8	60.2
8		68	66

Essentially related to PR, mass reduction gives an idea about how much lighter (or heavier) the structure becomes due to the optimization process. It directly provides an estimate of cost savings.

Therefore, the results in Table 5.8 are consistent with the ones in terms of performance ratios, shown in Table 5.7.

Table 5.8 Mass values before/after optimization and after proper approximation (design) using commercial steel profiles.

No Parameters	Initial Mass [kg]	Optimized Mass [kg]	Design Mass [kg]
1	1440	1003	1176
2		1051	1111
3		803	818
4		574	588
5		403	453
8		385	408

Figure 5.11 shows the optimization results for the Scenario G, in term of the performance ratio obtained by averaging the performance ratios for each structural element. The results for all scenarios are reported in Appendix 5.7. Scenario

G, depicted below, exhibits higher values of the performance ratios. This fact becomes become more evident for poles 2, 3, and 4. In these cases, the performance ratios, associated with the design solutions, achieved values equal or greater than the optimized one due to the approximation of the design section adopted. In the post-processing phase, in fact, the optimized section chosen by the list of the FE software was manually edited since the structural constraint violation or the maximum performance ratio was not reached during to the optimization process. Moreover, in Table 5.9, the optimized design section for different independent iterations and the proposed industrial solutions according to product list, provided by the software, are listed. As expected, the mass reduction achieved during the optimization process results higher than the design solution due to the approximation issue. For the proposed scenario, the iteration (N_{trial}) that guarantees the best objective function is the second. In Appendix 5.7, the graphical (through histogram charts) and numerical representation (through tables) of the optimization result for each scenario are provided. In order to provide an overview of the objective function trend, the performance ratios and mass reduction for each scenario were collected into Figures 5.12 and 5.13. The mentioned values were obtained for each scenario, making an average of the results, before and after optimization, independently, for each steel profile composing the central pole.

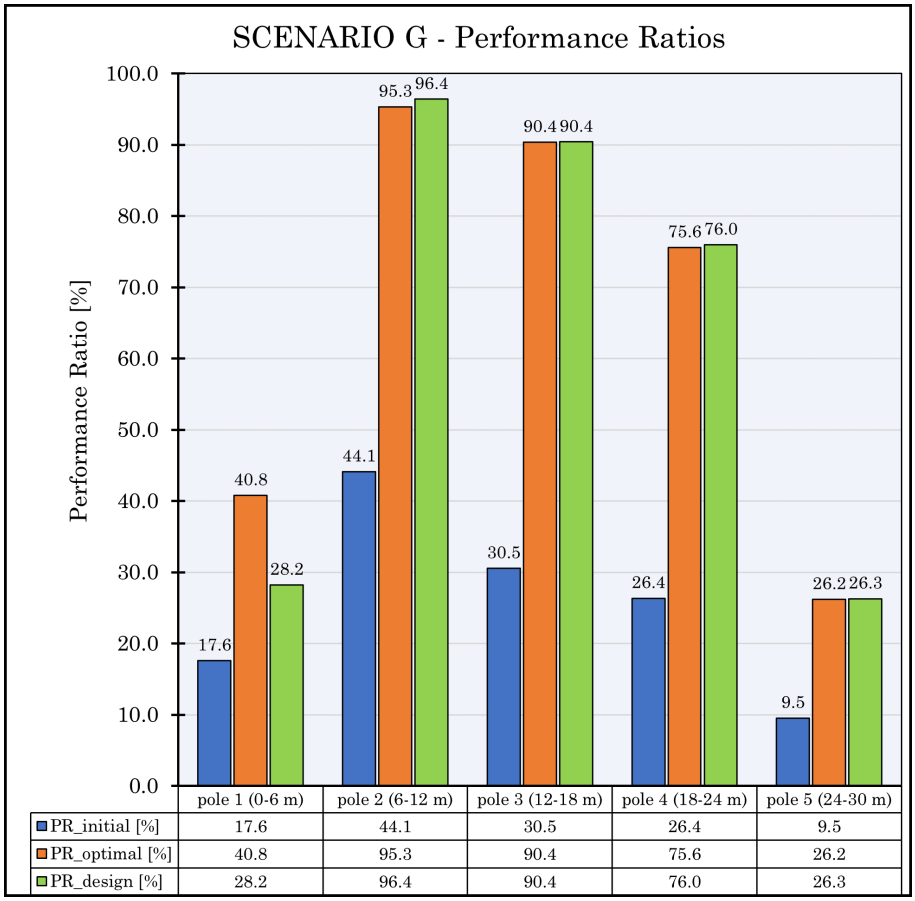

Fig. 5.11 *Scenario G.*—PRs trend. In blue—the performance ratios of each pole before optimization are illustrated, otherwise orange for the optimized solution. In green—PRs at a design configuration according to the product list.

Figure 5.12 highlights an almost monotone increment of the performance ratios to the number of design variables. Interestingly, for a number of variables $n \geq 5$, no significant improvements are achieved. Figure 5.13 emphasizes an important reduction of structural mass as the design variables increase. Once again, $n = 5$ represents trade-off. If the number of variables exceed 5, no significant improvements are observed.

Figures 5.12 and 5.13 show a comparison between each scenario in terms of the average performance ratio and mass reduction, respectively. Figure 5.12 highlights the difference with the initial state, which has an average performance ratio $PR_0 = 25.6\%$. An evident improvement is achieved for scenarios that include the thickness t as the design variable.

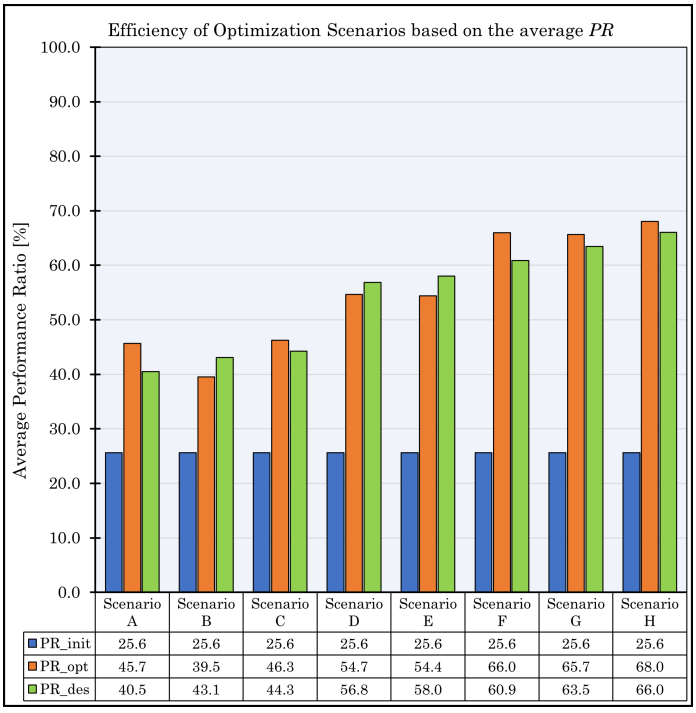

	Scenario A	Scenario B	Scenario C	Scenario D	Scenario E	Scenario F	Scenario G	Scenario H
PR_init	25.6	25.6	25.6	25.6	25.6	25.6	25.6	25.6
PR_opt	45.7	39.5	46.3	54.7	54.4	66.0	65.7	68.0
PR_des	40.5	43.1	44.3	56.8	58.0	60.9	63.5	66.0

Fig. 5.12 In blue, orange, and green, the average PRs at the initial condition, after optimization, and design solution, respectively.

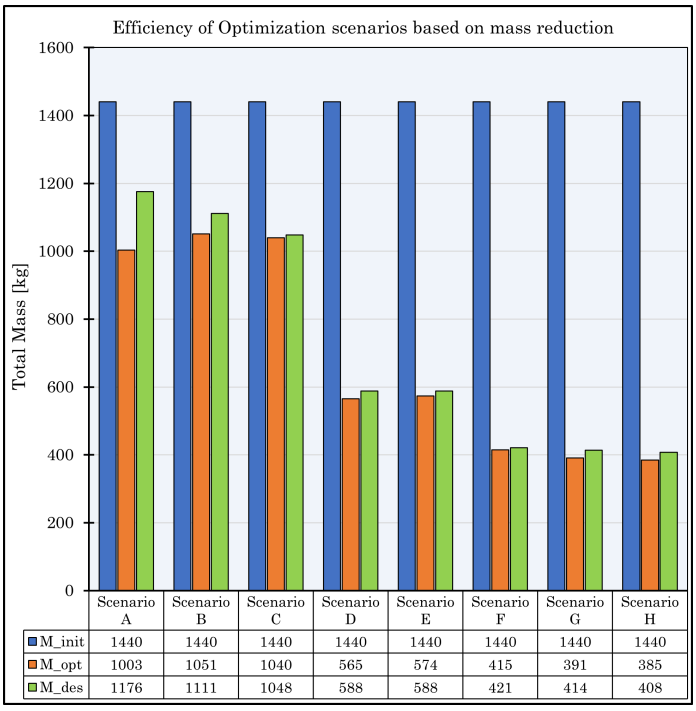

	Scenario A	Scenario B	Scenario C	Scenario D	Scenario E	Scenario F	Scenario G	Scenario H
M_init	1440	1440	1440	1440	1440	1440	1440	1440
M_opt	1003	1051	1040	565	574	415	391	385
M_des	1176	1111	1048	588	588	421	414	408

Fig. 5.13 Increasing the number of design variables, the final mass becomes gradually smaller, until 385 kg (scenario H).

Table 5.9 Scenario G results: optimized solutions for the different independent executions (Ntrial) and proposed industrial one, according to the product list.

SCENARIO G—Optimized Solution				
Element	d [mm]	t [mm]	L [mm]	Mass [Kg]
Pole 1 (0–6 m)	168.3	3	6000	73
Pole 2 (6–12 m)	168.3	4	6000	97
Pole 3 (12–18 m)	168.3	3	6000	73
Pole 4 (18–24 m)	168.3	3	6000	73
Pole 5 (24–30 m)	168.3	3	6000	73
	Total Mass [kg]		Σ	391
Mass variation [kg]	−1050	Mass variation [%]		−72.88
SCENARIO G—Design proposed according to the product list				
Element	d [mm]	t [mm]	L [mm]	Mass [Kg]
Pole 1 (0–6 m)	168.3	4	6000	97
Pole 2 (6–12 m)	168.3	4	6000	97
Pole 3 (12–18 m)	168.3	3	6000	73
Pole 4 (18–24 m)	168.3	3	6000	73
Pole 5 (24–30 m)	168.3	3	6000	73
	Total Mass [kg]		Σ	414
Mass variation [kg]	−1026	Mass variation [%]		−71.22
Ntrial = 3				
t_1 [mm]	t_2 [mm]	t_3 [mm]	t_4 [mm]	t_5 [mm]	OF [kN]
3	4	4	3	3	34.985
3	4	3	3	3	34.751
3	4	3	4	3	34.985

In particular, from Scenarios D, E, F, G, H, the average performance ratios exceed 50%, resulting in a more than 40% difference compared to the initial state. Figure 5.12 shows that the commercial profiles are sufficient to accommodate the optimized solution. An exception is noticeable in Scenario A because the optimiza-

tion is performed using just one diameter Φ, which is optimal for a few parts of the structure, while others are "over-fitted", resulting in a decrease of the performance ratios -28.4% and an increase of structural mass (+173 kg), as shown in Figure 5.13.

Similarly, a monotonic increment of the structural mass at the end of the optimization process is evident from Figure 5.13. In this case, the tonnage decreases with the increasing of the parameter's number. There is an overall mass reduction of about -67.5% (-972 kg) from scenario D to H. In scenarios A, B, and C, the thickness t of structural members is not considered. Therefore, the mass loss is not satisfactory, at about -28.4% (-409 kg). The choice of the best scenario should depend on one of the five situations described above (from D to H) related to the better PRs gain and mass loss.

5.7 Conclusions

In this paper, a guyed radio mast's size and shape optimization process was carried out to identify the equilibrium solution that guarantees the lighter optimized model, verifying strength, instability, and deformation requirements. The paper considers a detailed evaluation of the variable loads according to the Eurocodes recommendations. Furthermore, the OAPI was used to perform a structural analysis with the finite element software SAP2000 by considering the non-linearity of the cables. The optimization was carried out using a genetic optimization algorithm. Eight scenarios (labeled from A to H) were investigated, considering different arrangements of the geometric characteristics of the central pole and cables. The input parameters were increased from Scenario A to H to achieve the best fitness value of the self-weight. From Scenario A to H, the mass reduction index generally increased with the computational effort except in scenarios B and E, in which the input parameter did not represent the best vector design for the structural optimization. At this stage, the best design solution was evaluated from the database of cross-sections inside the finite element software. Though Scenario A provides the worst structural solution in terms of objective function, it represents the most convenient optimization strategy due to its low computational effort; on the contrary, Scenario H exhibits the best fitness value with the lowest self-weight, but it represents the most time-consuming solution. The best solution is achieved when the thickness values of each member, which, composed of the central pole, are included in the optimization process. An improvement

of the structural behaviour against instability is observed with increasing thickness. This verification is critical for this structure, mainly subjected to normal stresses resulting from self-weight and pre-stressing cable force. The entire optimization process seems to not be sensible to the pole diameter, chosen as the input parameter of the design vector. Although the final results of the FEM analyses are based on the Italian standards, other codes (e.g., Eurocodes, American code, etc.) can be selected from the SAP2000 settings. However, since no detailed analysis was carried out and many standards are based on the semi-probabilistic approach, the final results should be similar, even with different code formulations. Nevertheless, the partial safety factors involved in load combinations remain quite the same from the numerical point of view, regardless of the followed code.

In future developments, the authors will attempt to replace circular hollow sections with built-up steel solutions to achieve the best structural performance and assemblage procedures. Especially for higher structures, guyed radio masts generally consist of a truss skeleton. Another possible development could be a structural optimization for a cable-stayed radio antenna adopting other optimization strategies, such as particle swarm optimization, PSO, and the evolution differential algorithm (EDA), which could be less time-consuming. Finally, it could perform a typological optimization by managing the position of the cable connection, trying to find the best attachment points.

Appendix A

Fig. 5.14 Scenarios A, B.In blue, orange, and green, the average PRs, respectively, at the initial condition, after optimization, and the design solution.

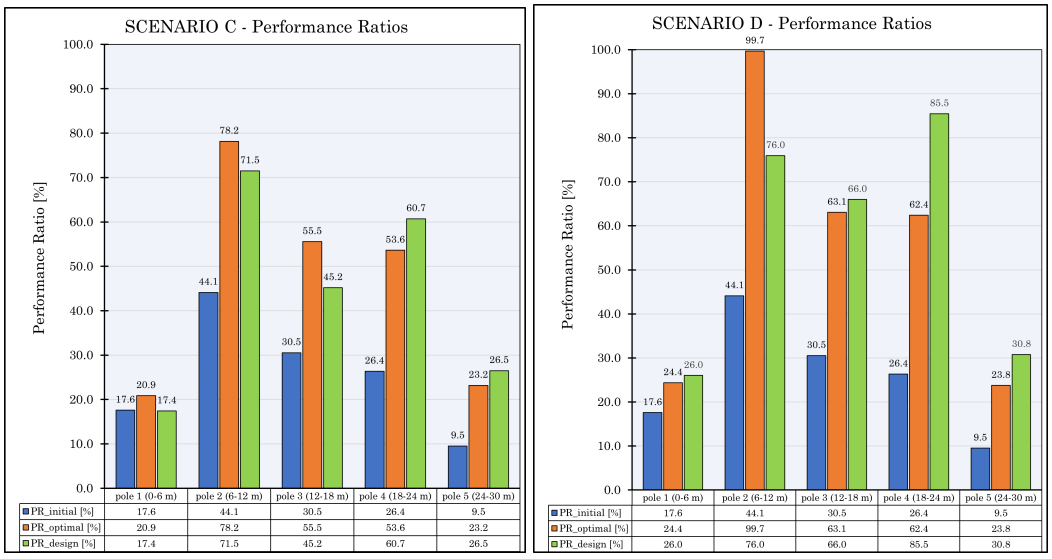

Fig. 5.15 Scenarios C, D.In blue, orange, and green, the average PRs, respectively, at the initial condition, after optimization, and the design solution.

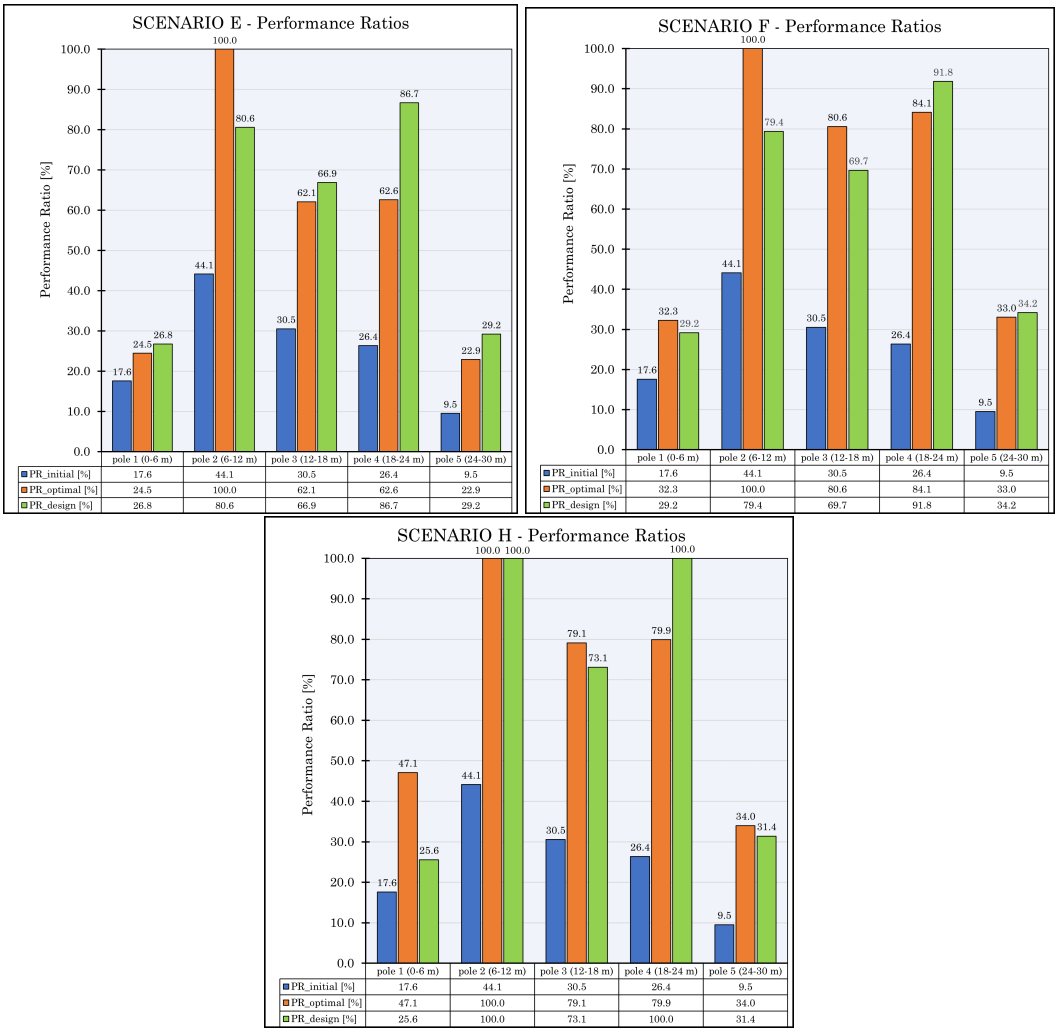

Fig. 5.16 Scenarios E, F, H.In blue, orange and green, the average PRs, respectively, at the initial condition, after optimization, and the design solution.

Table 5.10 Scenario A results: optimized solutions for the different independent executions (Ntrial) and the proposed industrial one, according to the product list.

SCENARIO A—Optimized Solution				
Element	d [mm]	t [mm]	L [mm]	Mass [Kg]
Pole 1 (0–6 m)	121	12.5	6000	201
Pole 2 (6–12 m)	121	12.5	6000	201
Pole 3 (12–18 m)	121	12.5	6000	201
Pole 4 (18–24 m)	121	12.5	6000	201
Pole 5 (24–30 m)	121	12.5	6000	201
		Total Mass [kg]	Σ	1003
Mass variation [kg]	−437	Mass variation [%]		−30.36
SCENARIO A—Design proposed according to the product list				
Element	d [mm]	t [mm]	L [mm]	Mass [Kg]
Pole 1 (0–6 m)	139.7	12.5	6000	235
Pole 2 (6–12 m)	139.7	12.5	6000	235
Pole 3 (12–18 m)	139.7	12.5	6000	235
Pole 4 (18–24 m)	139.7	12.5	6000	235
Pole 5 (24–30 m)	139.7	12.5	6000	235
		Total Mass [kg]	Σ	1176
Mass variation [kg]	−264	Mass variation [%]		−18.36
Ntrial = 5				
Φ_{opt} [mm]			OF [kN]	
121			40.758	
121			40.758	
121			40.758	
121			**40.758**	
122			40.849	

Table 5.11 Scenario B results: optimized solutions for the different independent executions (Ntrial) and the proposed industrial one according to the product list.

SCENARIO B—Optimized Solution				
Element	d [mm]	t [mm]	L [mm]	Mass [Kg]
Pole 1 (0–6 m)	149	12.5	6000	252
Pole 2 (6–12 m)	138	12.5	6000	231
Pole 3 (12–18 m)	126	12.5	6000	210
Pole 4 (18–24 m)	115	12.5	6000	189
Pole 5 (24–30 m)	103	12.5	6000	168
		Total Mass [kg]	Σ	1051
Mass variation [kg]	−389	Mass variation [%]		−27.02
SCENARIO B—Design proposed according to product list				
Element	d [mm]	t [mm]	L [mm]	Mass [Kg]
Pole 1 (0–6 m)	168.3	12.5	6000	288
Pole 2 (6–12 m)	139.7	12.5	6000	235
Pole 3 (12–18 m)	139.7	12.5	6000	235
Pole 4 (18–24 m)	114.3	12.5	6000	188
Pole 5 (24–30 m)	101.6	12.5	6000	165
		Total Mass [kg]	Σ	1111
Mass variation [kg]	−329	Mass variation [%]		−22.84
Ntrial = 5; best solutions				
Φ_i [mm]			Φ_f [mm]	OF [kN]
148			94	41.248
146			103	41.466
148			94	41.248
146			103	41.466
149			**92**	**41.230**

Table 5.12 Scenario C results: optimized solutions for the different independent executions (Ntrial) and the proposed industrial one according to the product list.

SCENARIO C—Optimized solution				
Element	d [mm]	t [mm]	L [mm]	Mass [Kg]
Pole 1 (0–6 m)	147	12.5	6000	249
Pole 2 (6–12 m)	136	12.5	6000	228
Pole 3 (12–18 m)	125	12.5	6000	208
Pole 4 (18–24 m)	114	12.5	6000	188
Pole 5 (24–30 m)	103	12.5	6000	167
		Total Mass [kg]	Σ	1040
Mass variation [kg]	−400	Mass variation [%]		−27.79
SCENARIO C—Design proposed according to the product list				
Element	d [mm]	t [mm]	L [mm]	Mass [Kg]
Pole 1 (0–6 m)	168.3	12.5	6000	288
Pole 2 (6–12 m)	139.7	12.5	6000	235
Pole 3 (12–18 m)	139.7	12.5	6000	235
Pole 4 (18–24 m)	114.3	10	6000	154
Pole 5 (24–30 m)	101.6	10	6000	135
		Total Mass [kg]	Σ	1048
Mass variation [kg]	−392	Mass variation [%]		−27.22
Ntrial = 5				
Φ_i [mm]		Φ_f [mm]	F [kN]	OF [kN]
152		92	1.8	41.393
151		92	1.4	41.339
149		92	1	41.230
156		92	2.4	41.610
147		**92**	**0.8**	**41.121**

Table 5.13 Scenario D results: optimized solutions for the different independent executions (Ntrial) and the proposed industrial one according to the product list.

SCENARIO D—Optimized solution				
Element	d [mm]	t [mm]	L [mm]	Mass [Kg]
Pole 1 (0–6 m)	161	6	6000	138
Pole 2 (6–12 m)	147	6	6000	125
Pole 3 (12–18 m)	133	6	6000	113
Pole 4 (18–24 m)	120	6	6000	101
Pole 5 (24–30 m)	106	6	6000	89
		Total Mass [kg]	Σ	565
Mass variation [kg]	−875	Mass variation [%]		−60.75
SCENARIO D—Design proposed according to the product list				
Element	d [mm]	t [mm]	L [mm]	Mass [Kg]
Pole 1 (0–6 m)	168.3	6	6000	144
Pole 2 (6–12 m)	168.3	6	6000	144
Pole 3 (12–18 m)	139.7	6	6000	119
Pole 4 (18–24 m)	114.3	6	6000	96
Pole 5 (24–30 m)	101.6	6	6000	85
		Total Mass [kg]	Σ	588
Mass variation [kg]	−853	Mass variation [%]		−59.20
Ntrial = 5				
Φ_i [mm]		Φ_f [mm]	t [mm]	OF [kN]
161		92	6	**36.465**
146		117	7	37.389
162		92	6	36.491
162		92	6	36.491
163		92	6	36.517

Table 5.14 Scenario E results: optimized solutions for the different independent executions (Ntrial) and the proposed industrial one according to the product list.

SCENARIO E—Optimized Solution				
Element	d [mm]	t [mm]	L [mm]	Mass [Kg]
Pole 1 (0–6 m)	165	6	6000	141
Pole 2 (6–12 m)	150	6	6000	128
Pole 3 (12–18 m)	135	6	6000	115
Pole 4 (18–24 m)	121	6	6000	102
Pole 5 (24–30 m)	106	6	6000	89
		Total Mass [kg]	Σ	574
Mass variation [kg]	−866	Mass variation [%]		−60.13
SCENARIO E—Design proposed according to the product list				
Element	d [mm]	t [mm]	L [mm]	Mass [Kg]
Pole 1 (0–6 m)	168.3	6	6000	144
Pole 2 (6–12 m)	168.3	6	6000	144
Pole 3 (12–18 m)	139.7	6	6000	119
Pole 4 (18–24 m)	114.3	6	6000	96
Pole 5 (24–30 m)	101.6	6	6000	85
		Total Mass [kg]	Σ	588
Mass variation [kg]	−853	Mass variation [%]		−59.20
Ntrial = 5; best solutions				
Φ_i [mm]	Φ_f [mm]	t [mm]	F [kN]	OF [kN]
150	97	7.8	1.3	37.766
153	112	6.4	1.6	36.964
165	91	6	2.3	36.552
160	91	7	1.3	37.287
139	104	8.8	1.3	38.337

Table 5.15 Scenario F results: optimized solutions for the different independent executions (Ntrial) and the proposed industrial one according to the product list.

SCENARIO F—Optimized Solution					
Element	d [mm]	t [mm]	L [mm]	Mass [Kg]	
Pole 1 (0–6 m)	157	4	6000	91	
Pole 2 (6–12 m)	144	6	6000	122	
Pole 3 (12–18 m)	131	4	6000	75	
Pole 4 (18–24 m)	118	4	6000	67	
Pole 5 (24–30 m)	105	4	6000	60	
		Total Mass [kg]	Σ	415	
Mass variation [kg]	−1025	Mass variation [%]		−71.16	
SCENARIO F—Design proposed according to the product list					
Element	d [mm]	t [mm]	L [mm]	Mass [Kg]	
Pole 1 (0–6 m)	168.3	4	6000	97	
Pole 2 (6–12 m)	168.3	5	6000	121	
Pole 3 (12–18 m)	139.7	4	6000	80	
Pole 4 (18–24 m)	114.3	4	6000	65	
Pole 5 (24–30 m)	101.6	4	6000	58	
		Total Mass [kg]	Σ	421	
Mass variation [kg]	−1019	Mass variation [%]		−70.75	
Ntrial = 3; best solutions					
Φ_i [mm]	Φ_f [mm]	t_{ends} [mm]	t_{inter} [mm]	F [kN]	OF [kN]
155	92	4	7	3.2	35.141
157	92	4	6	0.9	34.993
151	92	4	7	1.3	35.058

Table 5.16 Scenario H results: optimized solutions for the different independent executions (Ntrial) and the proposed industrial one according to the product list.

SCENARIO H—Optimized Solution				
Element	d [mm]	t [mm]	L [mm]	Mass [Kg]
Pole 1 (0–6 m)	158	3	6000	69
Pole 2 (6–12 m)	146	6	6000	124
Pole 3 (12–18 m)	133	4	6000	76
Pole 4 (18–24 m)	121	4	6000	69
Pole 5 (24–30 m)	108	3	6000	47
		Total Mass [kg]	Σ	385
Mass variation [kg]	−1055	Mass variation [%]		−73.27
SCENARIO H—Design proposed according to the product list				
Element	d [mm]	t [mm]	L [mm]	Mass [Kg]
Pole 1 (0–6 m)	168.3	5	6000	121
Pole 2 (6–12 m)	168.3	4	6000	97
Pole 3 (12–18 m)	139.7	4	6000	80
Pole 4 (18–24 m)	139.7	3	6000	61
Pole 5 (24–30 m)	114.3	3	6000	49

Table 5.16 *Cont.*

					Total Mass [kg]	Σ		408
	Mass variation [kg]				−1032	Mass variation [%]		−71.65
Ntrial = 3								
Φ_i [mm]	Φ_i [mm]	t_1 [mm]	t_2 [mm]	t_3 [mm]	t_4 [mm]	t_5 [mm]	F [kN]	OF [kN]
164	109	4	5	4	3	3	0.9	34.789
167	111	3	6	4	3	3	2	34.839
158	96	3	6	4	4	3	2	34.695

Chapter 6

Constructability in structural optimization

6.1 Introduction

In order to introduce properly this Chapter it should start with the definition of the term "constructability", which generally speaking is a crucial consideration in civil engineering that can greatly impact the success of a construction project. The Constructability Task Force of the Construction Industry Institute (CII), based at The University of Texas, in 1986, has defined constructability as *"the optimum use of construction knowledge and experience in planning, design, procurement and field operations to achieve overall project objectives"*. In the United Kingdom, the term "buildability" has been used to define *"the extent to which the design of the building facilitates ease of construction, subject to overall requirements for the completed building"*. Constructability has been defined also by Anderson et al. (1995) as *"the capability of being constructed"*. However, this section, it is mainly addressed the meaning of *"integration of construction knowledge, resources, technology and experience into the engineering and design of a project"*. Therefore, the key aspect one should have in mind is that information and experience gained throughout the construction phase must be accounted for and shared in the design in order to improve project objectives. Aimed at accomplishing this task, several considerations can be made, ranging from general management organization recommendations to more particular techniques.

O'Connor et al. (1987) started from the CII definition and explored seven concepts for improving constructability, stressing the importance of construction-driven schedules, simplified designs, standardization, preassembly work scoped in advance, easy accessibility, adverse weather facilitation and a careful review of specifications by owner, designer, and constructor personnel. Pulaski et al. (2005) proposed a model to organize constructability information for design, according to timing and levels of detail, with the intent to link constructability rules to different stages of building design in a step-by-step format. They concluded that "the key to accessing constructability is introducing the right information at the right time and in the right level of detail". Furthermore, also encouragement for innovations, learned lessons from past projects, availability of resources, as well as waste management may all enhance constructability as highlighted by Khan (2018).
Constructability considerations provide several important advantages, many of which are sometimes challenging to understand and evaluate. Russellet al. (1994) distinguished such benefits between qualitative and quantitative ones, as reported in 6.1, proposing a way for their estimation. The quantitative advantages are the ones that

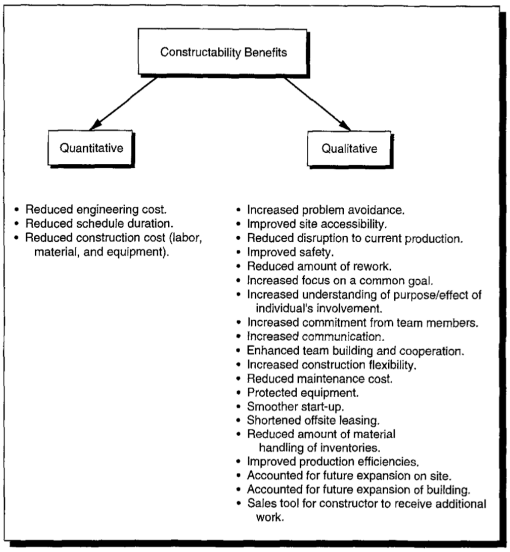

Fig. 6.1 Framework for determining constructability benefits Russell et al. (1994)

directly reduce cost and schedule duration; their effect can be measured by determining the impact of the change from that of standard practice. The utilization of fewer materials, fewer workers (i.e., reduced labour effort hours) and fewer fixed pieces of equipment during construction can all help to quantify cost abatement. Also the reduced schedule, in comparison with standard practice, can be translated into cost

savings. Instead, substantial qualitative advantages include the prevention of issues through improved collaboration, cooperation, and respect among participants. They also involved more site accessibility and safety, less rework, decreased maintenance costs, intensified focus on common goals, increased construction flexibility, etc. Since any construction project must be carried out by the planned completion date, to reduce issues like scheduling conflicts, delays and disagreements that may arise, Arditi et al. (2002) conducted a questionnaire survey of design companies about the adoption of constructability. The benefits, reported in 6.2, are in terms of creating better client and constructors relationships, being involved in fewer lawsuits, a better reputation, professional satisfaction and efficient design. In particular, they have been ranked from 0 to 3, with 0 being the least influential and 3 the most relevant.

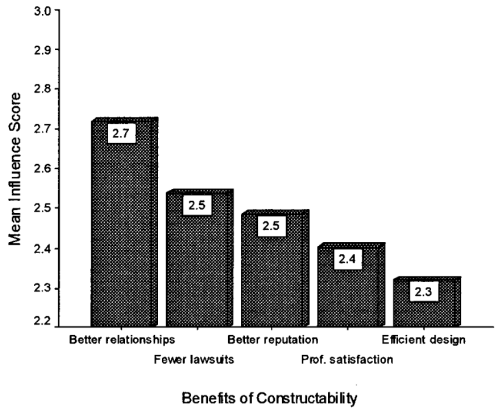

Fig. 6.2 Benefits of constructability highlighted by the survey in Arditi et al. (2002)

Another important aspect, emphasized in Ruby and David (2008) is the fact that constructability is a design philosophy that originates from the conceptual design stage, continues through design, and links project planning with design and construction. Therefore, constructability issues have to be identified and analysized during the design phase, not at the end once the construction phase starts. Integrating such considerations at the beginning will improve the overall project, and the efficiency of construction, as it allows for a more streamlined and cost-effective process. As stated in Khan et al. (2018), making use of construction knowledge from the earliest stages of a project, where the ability to influence cost is at its greatest, makes sense from both practical and financial viewpoints. Paulson (1976) described the interrelationships between engineering design, construction and operation costs for a facility, showing how the level of control on those costs decreases as the project evolves. In the reported figure 6.3, the idea of the author is exemplified. In the

lower portion, the life of a project, as a function of time, is distinguished into three phases, namely (1) Engineering and design, (2) Procurement and construction, (3) Utilization or operation; in the upper portion, instead, two curves are plotted, always as a function of project time, where the ascending one tracks the cumulative project expenditures, while the descending one shows the decreasing level of influence. In the early phases of design, when the expenditures are relatively small, the project team has the most opportunity to impact the overall cost of the facility. The decisions and commitments made during this period have an enormously greater impact on future costs; later on, when the cumulative cost of the project increases, the level of influence on such expense will go towards zero. Thus, the initial design phase is crucial and cooperation, together with a high level of detail, is required to incorporate basic constructability aspects.

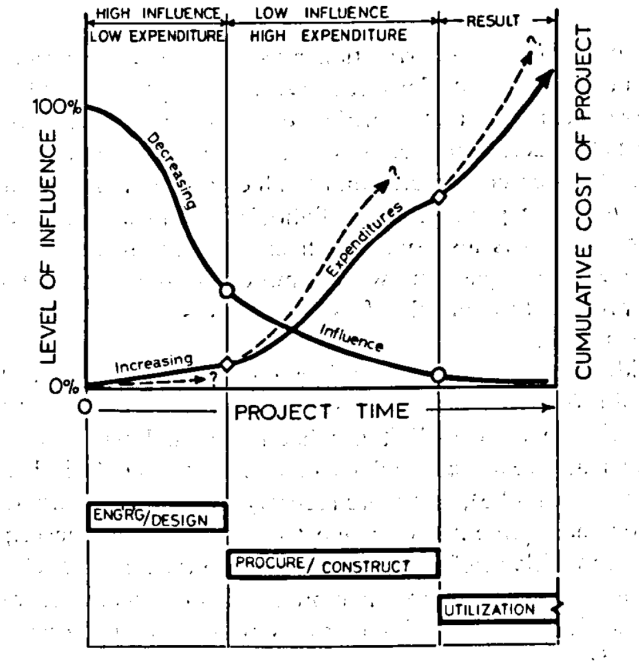

Fig. 6.3 Level of influence on project costs by Paulson in Paulson Jr (1976)

Therefore, constructability in structural optimization can be interpreted as the process of incorporating construction expertise and knowledge into the design and optimization phase. The difficulty of such a process is that there are many factors involved. Many of these influencing factors regard the management procedure, thus a good collaboration between all the team members, as well as the importance of having professional and qualified personnel, early involvement of the contractor in the

design and so on. However, in the present Thesis, we are more interested in looking at the constructability factors that can be integrated into the structural design choices, and more specifically in the optimization set-up. There are construction techniques that are just intended to simplify the overall production of necessary pieces for the given structure, to reduce the number of elements as well as connections typologies, to standardize sections, to encourage the employment of less diversity, to facilitate the assembly, but also the erection phase and so on. Always from the survey of Arditi et al. (2002), as reported in 6.4, eight factors impacting constructability have been listed and ranked, such as project complexity, design practices, project delivery, project size, project type, client type, project location, and design standards. In the same article, the authors also addressed the factors constraining constructability, as reported in 6.5. Faulty, ambiguous, or defective working drawings, incomplete specifications, and adversarial relationships were found to be the three major factors that cause constructability problems.

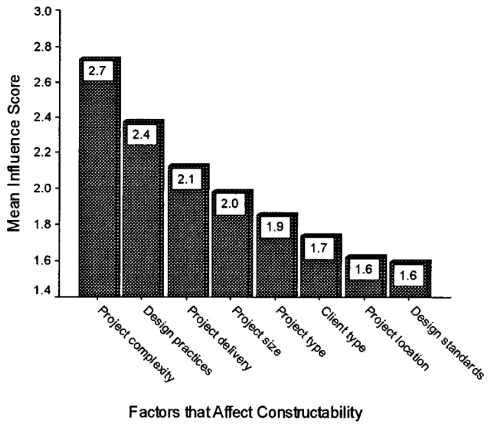

Fig. 6.4 Factors affecting constructability Arditi et al. (2002)

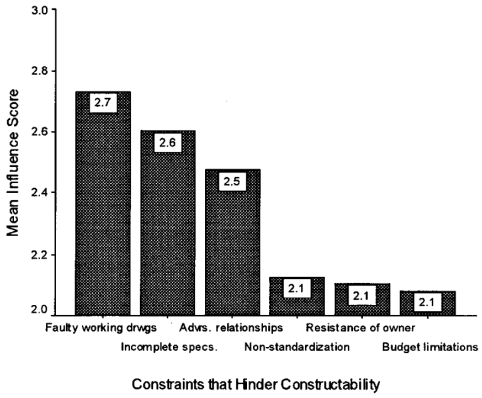

Fig. 6.5 Constraints on constructability Arditi et al. (2002)

Among them, non-standardization of design, which would have a detrimental impact, also plays a significant role. In general, using standardized components and systems can help improve constructability by reducing the need for custom fabrication and assembly. The idea of standardization has been defined, by Pasquire et al. (1999), as "the extensive use of components, methods or processes with regularity, repetition and a successful history". In Wong et al. (2006), also explained how standardization can be translated as the repetition of grids, sizes of components and connection details, stressing the benefits in terms of faster construction, reduced number of mould changes and enhanced productivity. In Khan et al. Khan (2018) it has been

emphasized the fact that it can be applied to various scenarios from building systems, materials types, construction details and so on, depending also on the economic analysis scale. The reduction in variety can lead to many benefits such as discounts on more pieces of the same material, simplified procedures and so on. Summarizing, standardization is a term that can include different meanings, from the employment of standard elements in the design of a structure, avoiding particular and unique shapes or sections, but also the repetition of members, connections, as well as procedures in the overall project. Furthermore, from a more general point of view, standardization is also paired with modularization and pre-assembly techniques. By looking at the design of a simple truss structure, the structural choices that can be made with a standardization-driven orientation regard the employment of the least amount of different cross-sections, but also the reduction in variation of the connections. In any case, we should always remember the verification of structural and geometric requirements. In Chapter 2 we have seen many examples of side constraints, mainly concerning the joints between beams and columns in frame structures.
An interesting research has been conducted by Abbigayle Horn (2015), where constructability has been defined as the standardization of primary structural elements to balance multi-objective design goals. In particular, the author has introduced non-subjective, quantifiable metrics to measure the standardization of structural components. The study focused on two-dimensional steel truss façade structures, subjected to lateral loading with a pinned base.

Shape optimization has been pursued by allowing node translations in the horizontal and vertical directions, while topology optimization has been completed via Boolean operators that turned diagonal elements on or off. Moreover, the number of vertical bays was also a variable in the study, exploring the possibility of having five or six vertical bays. Then, in the structural verification phase, member sizing has been determined based on the minimum area required to satisfy both stress and buckling criteria. The metrics that have been considered to quantify structural performance, which was later compared with constructability performance metrics, regarded the lateral deflection of the façade system at the top of the structure, strain energy and structural weight. The newly introduced constructability metrics, formulated to measure design characteristics from a constructability perspective, were:

1. Standardized Member Length (SL), using which, once calculated the average member length for each design iteration, each member has been penalized based on its difference from the mean;

2. Truck requirements (TR), accounting for length and weight restrictions that would lead to the acquisition of special permits for the shipping phase;

3. Field Connections, both bolted and welded, have been minimized to reduce the number of man-hours expended on site for labourers and crane operators;

4. Node Member Connectivity (NMC), aimed at minimizing the number of members framing into a single node;

5. Node Angle Connectivity (NAC), which imposed that each member framing into the node must have a minimum separation;

6. Cross Section Variation (CSV), aimed at reducing the number of sections used.

Regarding the first metric, it has been proposed a practical application of standardizing member length, in which members are grouped into sets of standard lengths in order to improve effective fabrication and erection procedures. Then, TR involved the application, at first, of length restrictions to the elements needed, leading to the cut of oversized members, and then of weight constraints, in order to count the number of trucks filled and eventually to obtain the minimum one. In this way, enhancing standard shipping, the timing of transportation could be better coordinated with on-site work, yielding construction cost savings and reducing site logistics associated with trucking and oversized load permitting. Depending on the number of splices required to satisfy shipping constraints and the total number of members in the structure, field connections have been evaluated, with the intent of reducing their number. Both NMC and NAC have been used to maximize the accessibility of the labourers to the cast node pads and minimize the number of infeasible connections. The final goal was to improve the speed of construction by reducing connection time in the fabrication and erection phases. Particularly interesting is the last metric developed, which discouraged high variation in member sizing, which would lead to more complex fabrication and erection processes, especially in the case of non-standard shapes. In an attempt to obtain the least amount of different cross-sectional areas, the author has assigned a value to each cross-section to determine the number of unique cross-sections. This has been obtained by multiplying the required

diameter, in inches, by ten and adding the member thickness in decimal inches. The final minimized metric was determined based on the percentage of all members that have unique cross sections, so the ratio between the number of unique cross sections divided by the total number of elements. From the output of the analysis, it has been found that the general trends observed implied that there are significant tradeoffs between constructability and structural performance. However, the impact of standardization on weight has to be carefully analysized. As the number of cross-sections in a given structure decreased, the overall weight of the structure increased, as expected, but this increase is relatively minor in comparison to the significant improvement in constructability. In the reported figure 6.6 it has been shown the case in which the number of different cross-sections in a structure was reduced by a factor of 10, while the structural weight increased by a factor of 2. This implies that remarkable labour and cost savings can be achieved by consolidating cross-sections, while the increase in the cost of material is marginal in comparison.

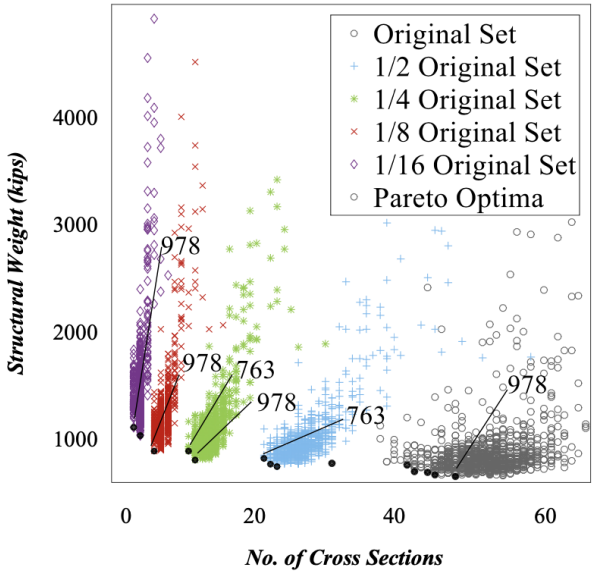

Figure 3.6: *Standardization of cross sections into consolidated sets compared with the structural performance metric, Structural Weight.*

Fig. 6.6 Impact of standardization on structural weight Horn (2015)

From the experience of the previous studies we can understand how constructability considerations integrated in the design phase will behave as competitive goals concerning the typical weight minimization one. We can think for example of the complex topic affecting truss structures, which involves the reduction of the number

of nodes and thus leads to longer members. In turn, these elements would have bigger sections to satisfy structural requirements, perhaps implying heavier designs. The same implication would follow the standardization technique, which encourages less diversity in the sections used. However, repetition of members' sizes at the cost of some added member weight can simplify detailing, fabrication and erection costs. Thus, using a simpler and standardized design, we can abate the overall cost, which is generally the most appealing target objective.

The entire chapter is entirely dedicated to the simultaneous size, shape and topology optimization of truss beams for industrial buildings at different levels. An objective function which takes into account constructability issues during the production and assembly phase has been adopted by considering the number of different cross-sections and the total number of employed pieces. Moreover, structural safety has been guaranteed and the feasible solution results verified with respect to compression, tension and buckling verifications. Then, the optimization conducted at the level of the trussed beam only has coupled with the size and layout optimization of a real industrial building. The optimal cross-section of all steel members composing the structure, span lengths and the number of horizontal or vertical bracings has been evaluated.

6.2 Case study 1: Truss beam only

After having discussed the basic structural optimization methodologies and constructability difficulties, the current section is going to describe the application case study of competence. Specifically, the simultaneous size, shape and topology optimization of steel truss structures has been performed by developing a novel objective function which takes into account constructability criteria. At first, the mechanical behaviour of different types of truss beams will be introduced and practical design recommendations will be discussed, as well as how they can be modelled following a parametric design; following, the problem definition and the design variables involved in the optimization will be introduced, along with the grouping strategy developed to improve the schematization of the problem. Subsequently, the model set-up and the definition of the Objective Function will be discussed, starting from the original hypothesis considered to the final formulation. Finally, by the comparison of the proposed method and the more common minimum-weight approach, it will be

highlighted the influence of the additional constructability criteria in the definition of the best individuals.

6.2.1 Problem overview

As stated before, the intent is to perform a simultaneous size, shape and topology optimization of a steel truss structure. Considering a total span length of 20 meters, the parametric model of the truss is realized, at first, by creating half of the geometry and then exploiting the symmetry with respect to the vertical axis in the middle.

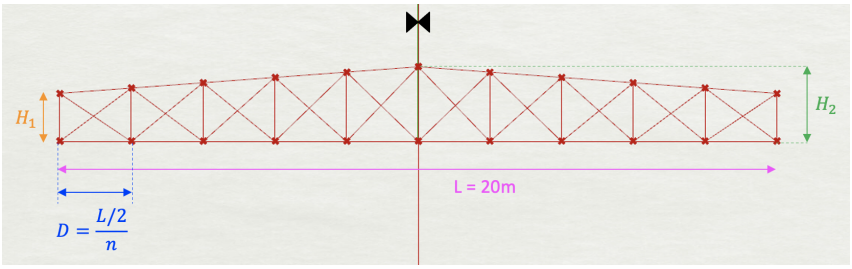

Fig. 6.7 Schematic representation of the truss

The shape optimization variables have been identified as the number of subdivisions of half the chords (n), along with the heights of the edges (H_1) and middle point (H_2) of the upper chord. Always considering half geometry, the range in which n can be varied is in between 3 and 10. The upper bound has been set considering a minimum distance between consecutive nodes of 1 meter, while the lower bound accounting for the grouping strategy, explained in the next paragraph 6.2.2. From a pre-dimensioning of the structure, we have set a range for the height at the edges H_1 in between a value of $L/15$ and $L/10$, while the central height H_2 ranges between the current value of H_1 and a maximum of $L/8$.
Anyways, each variable is dependent on the other because of geometrical considerations. In fact, the inclination of diagonal members is suggested to be in between 30° and 60° degrees (Marano et al. 2016b). Therefore, the relationship of $H1$ and $H2$ as a function of n, is recommended as following:

- Pre-dimensioning rules
  $\frac{L}{15} < H_1 < \frac{L}{10}$
  $H_1 < H_2 < \frac{L}{8}$

- Diagonals inclination in between 30° and 60°
  $D \cdot tan30° < H_i < D \cdot tan60°$, with D equal to the distance between consecutive nodes, computed as $\frac{L/2}{n}$

Depending whether the first of second condition is more stringent than the other, we would obtain a domain for H_1 and H_2 ranging from minimum and maximum values, according to the following relationships:

Domain of H_1	Domain of H_2
$H_{1,min}$=max($\frac{L}{15}$,$D \cdot tan30°$)	$H_{2,min}$ = max(H_1,$D \cdot tan30°$)
$H_{1,max}$=min($\frac{L}{10}$,$D \cdot tan60°$)	$H_{2,max}$=min($\frac{L}{8}$,$D \cdot tan60°$)

Table 6.1 Domains definition for H_1 and H_2 as $H_{i,min} < H_i < H_{i,max}$

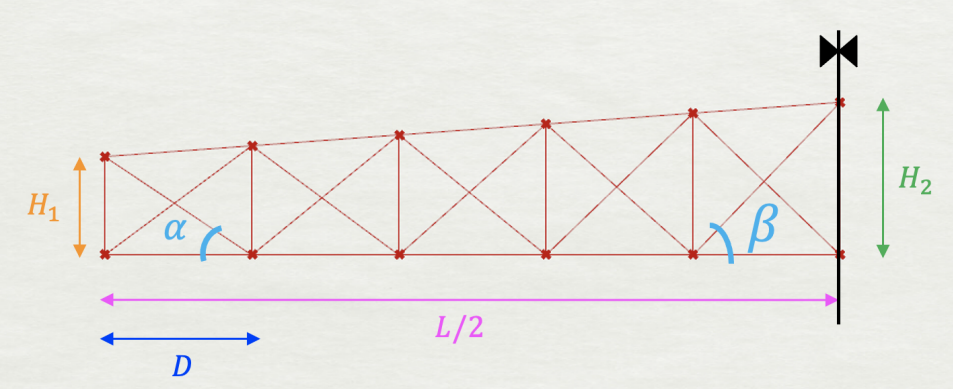

Fig. 6.8 Scheme for relationship between n and H1,H2, where α and β is assumed equal to at least 30°and maximum 60°, respectively.

Regarding the topology optimization, we have created in Grasshopper five different truss types, namely Vierendeel, Brown, Pratt, Howe and Warren ones. Here below, we have explained their main characteristics and real-life applications:

- **Vierendeel truss**
  This layout of structure was named after the Belgian engineer Arthur Vierendeel, who developed the design in 1896. It is characterized by the absence of diagonal members, without any triangular mesh inside. For this reason, to avoid the instability of the structure, the nodes have to be designed not as

pinned connections but fixed ones, in order to guarantee any relative rotation of the members. This is its primary characteristic that sets the Vierendeel apart from other truss layouts. Thus, its cross-sections would be thicker if compared to other typologies with the same span, resulting in heavier designs. Anyhow, it is widely employed in civil engineering structures, resulting in a more aesthetically pleasing harmonic configuration. For example, it is preferred in presence of windows or open doors, because the exterior envelope remains unobstructed.

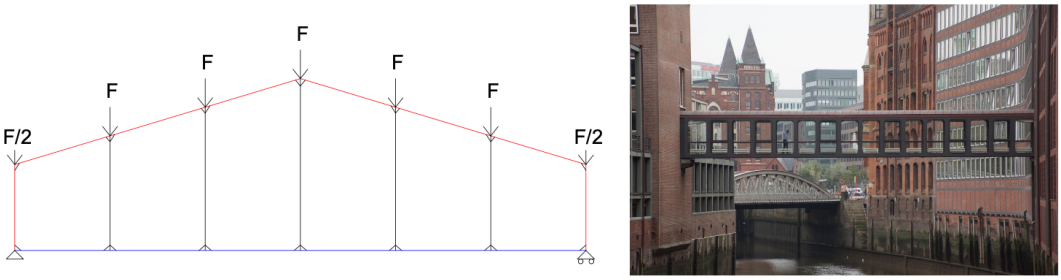

Fig. 6.9 Vierendeel truss scheme and application example: AMERON Hotel Speicherstadt footbridge

- **Pratt truss**
  Pratt truss, first proposed by Thomas Pratt and his son Caleb in 1844, nowadays is one of the most used, allowing long spans to be achieved, ranging from 20 to 100 meters. Also called N-shape, it is made up of vertical and diagonal members that form the 'N' pattern until the central point, where they are inverted. This type of truss is most appropriate for horizontal spans, where the force is predominantly in the vertical direction. Under gravity loads, the vertical members result to be in compression while the diagonals in tension. In this way, a more cost-effective design might be encouraged by giving the diagonal components smaller cross-sections. Besides, since they are in tension, they won't be affected by buckling problems.

- **Howe truss**
  The Howe truss was proposed by William Howe in 1840, four years before the Pratt one. Their configuration is similar, actually specular, because of the orientation of the diagonals. Therefore, under gravitational loads, they are in

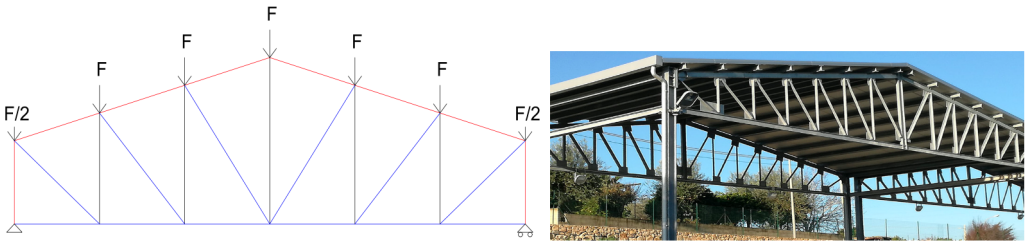

Fig. 6.10 Pratt truss scheme and application example (industrial building from "LA META costruzioni Vincenzo Cavallo")

compression, so buckling verification becomes an issue. Thus, Howe truss is better employed when uplift actions are predominant, which may be the case of open buildings such as aircraft hangers, so that the diagonals can be in tension.

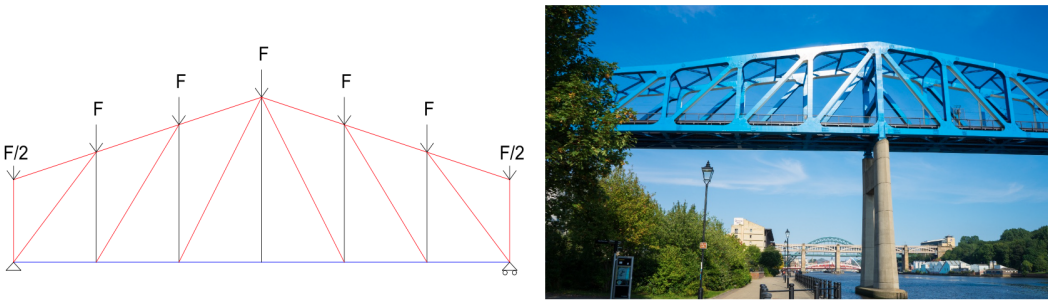

Fig. 6.11 Howe truss scheme and application example: Queen Elizabeth II Metro Bridge

- **Brown truss**
  The Brown truss has X-shaped diagonals. It is characterized by the fact that one leg of each X is always in tension. More in details, the double diagonals configuration is an hyperstatic truss scheme. This kind of truss is generally employed when we may have an inversion in sign of the actions, like in the case of wind loads or seismic excitations. Of course, this configuration will result in heavier designs even though the single diagonals can have smaller sections.

- **Warren truss**
  It is named after the British engineer James Warren, who patented it in 1848, together with Willoughby Theobald Monzani. Its original scheme had a configuration in which the truss members formed a series of equilateral triangles.

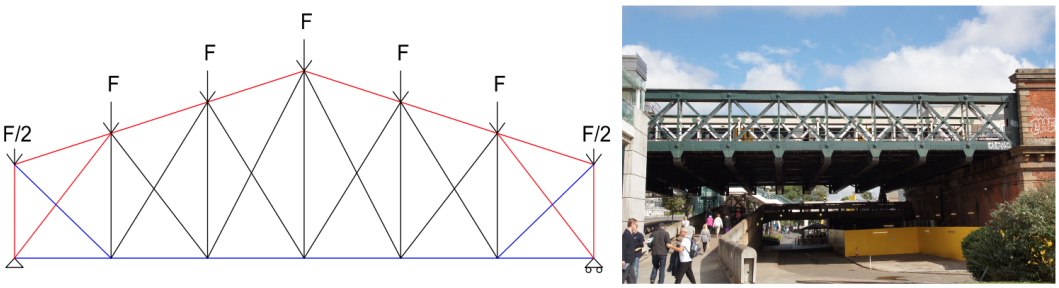

Fig. 6.12 Brown truss scheme and application example: Hungerford railway bridge

However, in our analysis, because we have an inclined upper chord, the triangles are not equilateral. There are different versions of the Warren truss type, with or without vertical elements, as well as with alternate verticals, with parallel chords or inclined upper chords, with equilateral or isosceles triangles. Looking at the scheme chosen for our investigation, reported in figure 6.13 we can observe that the upper chord is always in compression, while the lower chord is in tension. Then, the diagonals have to be distinguished into the descending ones, which are in tension, and ascending ones, which on the contrary are in compression; then once the middle is reached their solicitations are switched. Instead, the additional vertical elements present alternate stresses the even ones are in compression, while the odd ones are not stressed. The function of the even vertical elements is to help the distribution of compression actions when long spans are reached. This type of truss is largely employed in civil engineering applications thanks to its versatility. In particular, it is often used for steel railway bridges, thus the loads (dead and traffic load) are applied on the deck which distributes the load to the bottom chord.

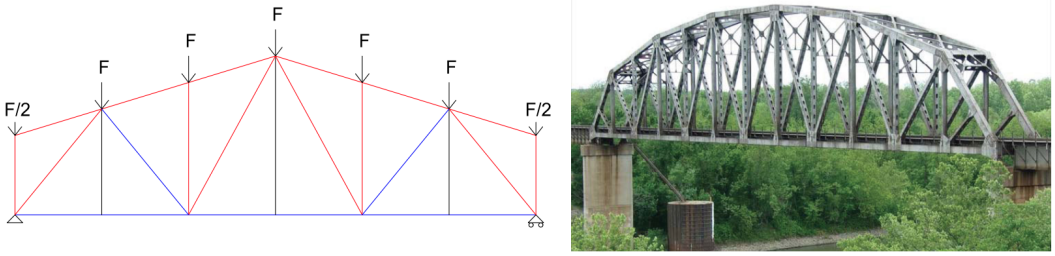

Fig. 6.13 Warren truss scheme and application example: BNSF Railroad over Verdigris River

In particular, to switch from one configuration to the other in our optimization, we have created a slider ranging from 0 to 4, in which each number represents a truss

type. For example, 0 stands for the Vierendeel one, thus if the topology design variable for the current individual is at 0 value, the configuration analyzed is the Vierendeel one.

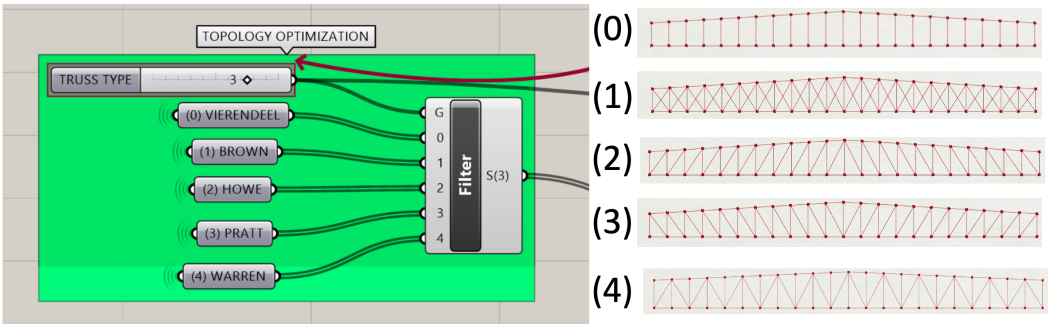

Fig. 6.14 Topology optimization design variable

Finally, the size optimization has been carried out by varying the cross-sections of the truss's members. Specifically, we have assigned CHS (circular hollow sections) profiles. In Karamba3D there is a pre-defined catalogue, which has been limited to the first 100 values to reduce the computational effort of the optimizer. This reduction has been computed by following the Eurocode 3 specification, in which the general formulation regarding the stability of the truss's members can be written as: $N_{Rd} = \frac{A \cdot f_y}{\gamma_m}$. It should be distinguished for tension or compression members, as well as for the different classes of cross-sections, but this was just a preliminary, rough and simplified evaluation.

6.2.2 Grouping strategy

In real-life, structures designed by employing a huge number of different sections lead to difficulties during the assembly and erection phases. Hence, if grouping strategies are adopted, the overall structural complexity is reduced and all the constructability issues can be simplified. The benefit derived from this approach is largely demonstrated by several authors such as Gholizadeh et al. (2017),Dehghani et al. (2019) and Hasançebi and Azad (2019). During the grouping strategy, the vertical symmetry of the investigated structures will be considered. First of all, we have distinguished five components of the truss (e.g. Marano et al. 2016b), namely:

1. Lower Chord

2. Upper Chord + External Vertical Structs
3. Internal Vertical Structs
4. Upward-Downward Diagonals
5. Downward-Upward Diagonals

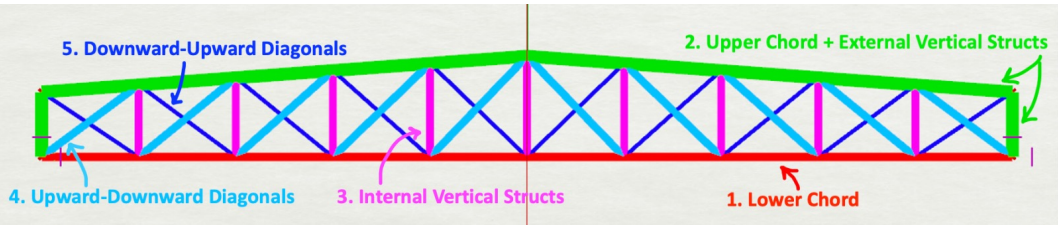

Fig. 6.15 Truss's components division

Each component has been in turn divided into three main regions, wherein each one of the solicitations can be assumed similar. Thus, the grouping strategy consisted of the creation of 3 groups for each component, to which a cross-section is assigned. In more detail, if we look at the lower chord's solicitation distribution, it can be highlighted that there are three main points at which the stress difference is more evident.

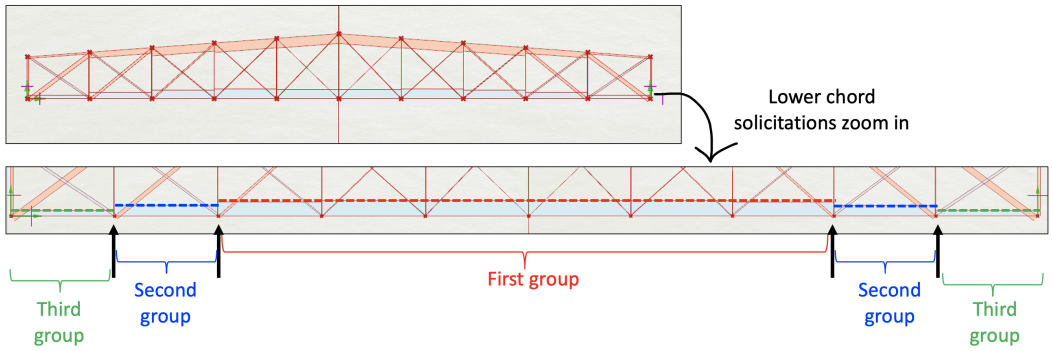

Fig. 6.16 Lower chord's solicitation distribution

Exploiting this observation, we have assigned three different cross-sections, one for each group. If we think to assign a single cross-section to the entire lower chord, it would require the largest one to sustain the highest stresses in the middle, increasing the overall weight of the structure. On the contrary, if we allow the optimizer to choose a different cross-section for each member, the overall structure would result

in the lowest weight possible, but with the highest complexity for its construction. Having a high number of different cross-sections increases the complexity of fabrication, assembly and erection phases, as well as the overall cost, thus it should not be encouraged. To make a first move towards a balance between the minimization of the cost and the number of different cross-sections used, we have developed the grouping strategy.

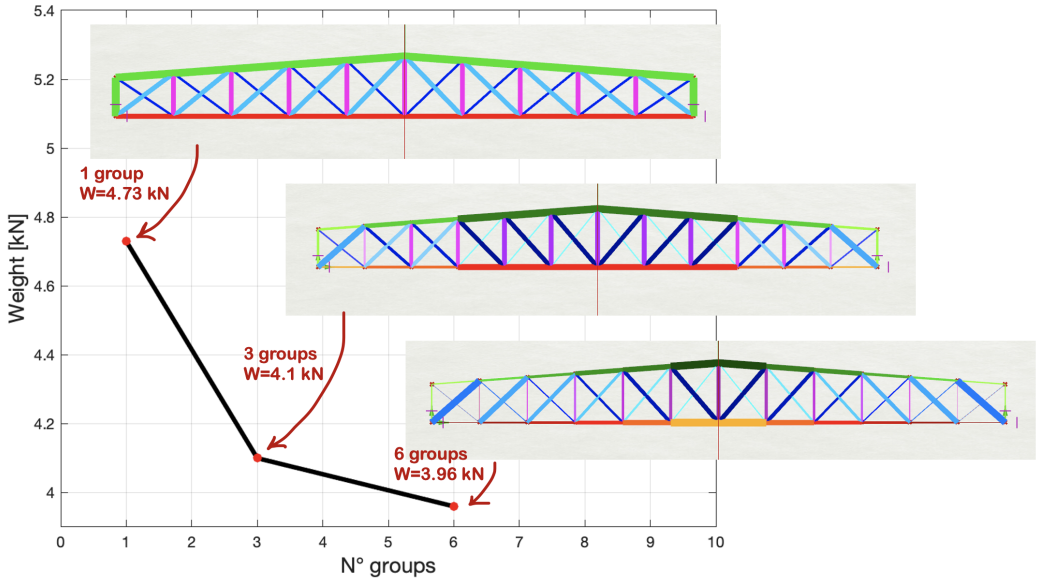

Fig. 6.17 Relationship between N°groups and corresponding weight [kN]

Furthermore, the grouping technique has been carried out dynamically. Specifically, the optimizer can manage the group division by changing the point at which we have the passage from one group to the other. To explain the developed approach, we can consider for the sake of simplicity only the lower chord. In particular, let's focus on the case of a truss with several subdivisions of the first half equal to 6. If we wanted, for example, to divide the lower chord into 2 groups we would have to identify n_1, which is the index of the node at which the lower chord will be divided. Then, in order to divide it into 2 groups, not having one of them with zero members, n_1 should be a number from 1 to $n-1=5$. From the reported figure 6.18 we have graphically illustrated the meaning of n_1.

Then, moving towards our case, if we want to divide the lower chord into 3 groups, we should identify two indexes, n_1 and n_2. In this case, n_1 would be a value in between 1 and $n-2=4$, while n_2 in between n_1+1 and $n-1=5$.

Looking at the figure 6.19, we can see that n_2 is establishing the ending node of the

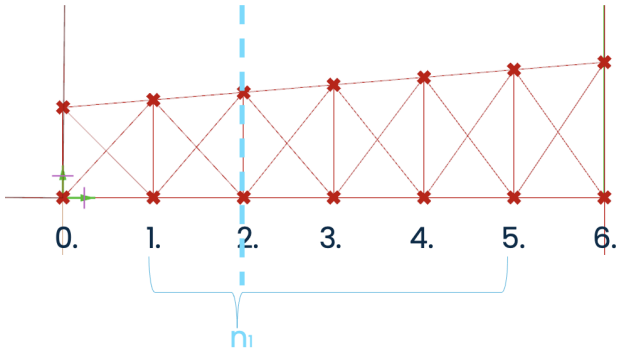

Fig. 6.18 Graphical representation of the meaning of n_1 variable

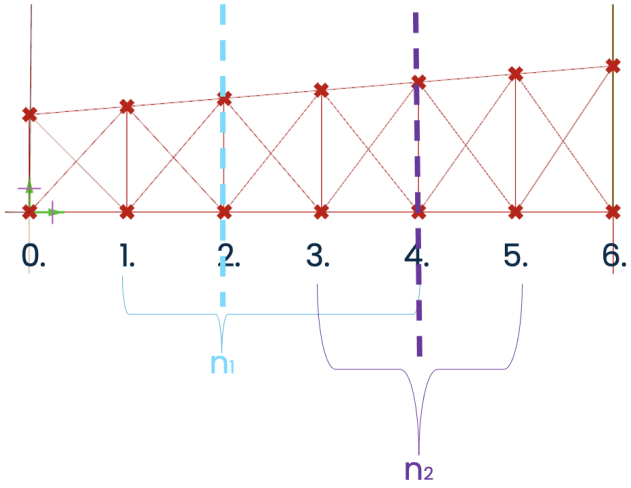

Fig. 6.19 Graphical representation of the dynamic grouping strategy with 3 groups

first group, while n_1 is the ending node of the second group.
Following this scheme, all the possible numbers of groups, N°groups, will be obtained by multiplying the N°subdivisions for n. However, because of the considerations previously made regarding the actual solicitation distributions and the reduction of the computation effort required for the optimization procedure, we have chosen to subdivide each component into three groups.

6.2.3 Problem formulation

In this section, the statement of the optimization problem is pointed out. Design variables, Objective function and constraints are clearly defined. The adopted formu-

lation allows performing an optimization not simply aimed at weight minimization, but both structural safety and constructability issues are accounted.

As stated before, we are going to perform an optimization not simply aimed at weight minimization, but we are accounting for both structural verifications and constructability issues. To properly formulate our problem, we should define the three main ingredients of the optimization, namely the objective function, the design variables and the constraints applied.
The formulation of our optimization can be expressed as:

$$min\, F(\mathbf{x}) = \rho \sum_{i=1}^{N} (A_i \cdot l_i) \cdot \phi_1(n_{un}) \cdot \phi_2(N_a) \cdot \phi_3(n) \tag{6.1}$$

subjected to

$$\frac{N_{Ed}}{N_{Rd}} \leq 1 \tag{6.2}$$

$$\mathbf{x}_{i,min} < \mathbf{x}_i < \mathbf{x}_{i,max} \tag{6.3}$$

Where:
N is the total number of elements in the truss and $\mathbf{x}$ is the vector of design variables while N_{Ed} and N_{Rd} represent the maximum solicitation selected between the tension, compression and buckling load at each member of the structure and the corresponding structural strength. Finally, $x_{i,min}$ and $x_{i,max}$ represent the maximum lower and upper value of the $i-th$ design variables.
In the previous sections, all the design variables, x_i, involved in the optimization have been introduced and they have been summarized in table 6.2 below. The four macro-categories of the design variables, i.e. Topology, Layout or Shape definition, Grouping division and Cross-sections assignment, have been distinguished by making use of different colours. Moreover, in the last column of table 6.2 have reported the lower and upper bound of each design variable, x_i. Their graphical representation has been reported in figure 6.20, where the Brown truss type has been chosen for clearness purposes.
In equation 6.1, the penalties are respectively:

$$\phi_1 = (1 + K_1 \cdot n_{un}) \tag{6.4}$$

$$\phi_2 = (1 + \Delta) - e^{-\beta \cdot (N_a - \frac{ln\Delta}{\beta})} \tag{6.5}$$

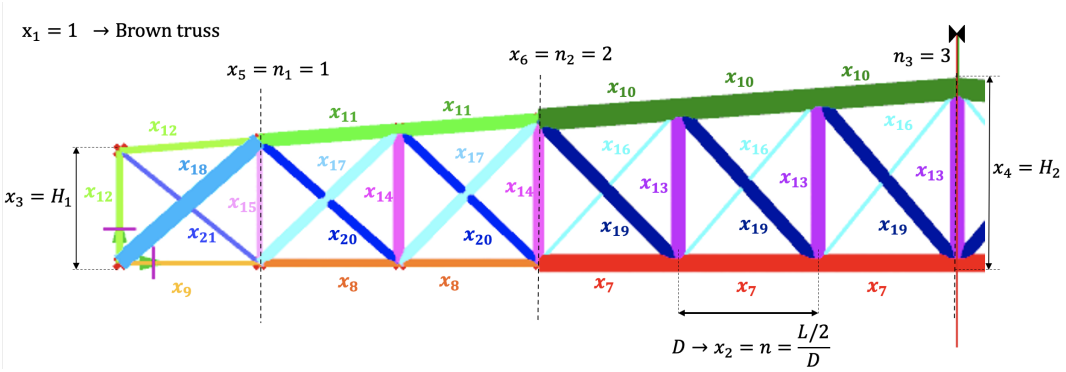

Fig. 6.20 Schematic representation of all the design variables

$$\phi_3 = (1+\gamma) - e^{-\alpha\cdot(n-\frac{ln\gamma}{\alpha})} \tag{6.6}$$

All the parameters related to the penalty functions have been calibrated using the analysis. For clearness and simplicity reason, all the optimal value for each curve's parameter is reported in table 6.3.
The first penalty 6.4, is assumed equal to the maximum violation, n_{un}, between compression, tension and buckling verification, and amplified by a coefficient K_1. Instead, ϕ_2 and ϕ_3, respectively 6.5 and 6.6, are representative of constructability criteria that, once more, encourage the optimization towards heavier designs. In particular, ϕ_2 is limiting the number of distinct cross-sections used to construct the entire truss (N_a). On the other hand, ϕ_3 tries to reduce the design complexity by lowering the number of subdivisions of the truss, thus the overall number of pieces to be assembled. Both ϕ_2 and ϕ_3 have an exponential form, as we can see in the graphical representations below, 6.21.

It should be highlighted the fact that, during the objective function evaluation, first, sizing of the structure was performed. Thus, the optimizer is allowed to vary only from x_7 to x_{21} design variables of table 6.2. Then, shape design variables are considered, i.e. x_2, x_3 and x_4, as well as the ones regarding the grouping strategy, which are x_5 and x_6. Once, all the penalties have been tested for the simultaneous size and shape optimization, finally, we included also the topology optimization, thus x_1 of 6.2. The reason behind this kind of step analysis is related to investigating the actual influence of the different design variables on the distinct penalty functions. For example, penalty Φ_1 about the structural verification is highly dependent on the size variables, while shape and topology ones are indirectly affecting such requirements. Analogously, Results showed that the optimal solution obtained by considering

Design variable	Description	Domain
x_1	Topology: (0) Vierendeel, (1) Brown, (2) Pratt, (3) Howe, (4) Warren	$0 \div 4$
$x_2 = n$	Number of subdivisions of half geometry	$3 \div 10$
$x_3 = H_1$	Heights of upper chord's edges	$H_{1,min} = max(\frac{L}{15}, D \cdot tan30)$ $H_{1,max} = min(\frac{L}{10}, D \cdot tan60)$
$x_4 = H_2$	Heights of upper chord's midpoint	$H_{2,min} = max(H_1, D \cdot tan30)$ $H_{2,max} = min(\frac{L}{8}, D \cdot tan60)$
$x_5 = n_1$	Index at which the third group ends	$1 \div n-2$
$x_6 = n_2$	Index at which the second group ends	$n_1+1 \div n-1$
x_7 x_8 x_9	3 sections for the lower chord elements	$0 \div 100$ CHS profiles' index from catalogue
x_{10} x_{11} x_{12}	3 sections for the upper chord + external vertical structs	$0 \div 100$ CHS profiles' index from catalogue
x_{13} x_{14} x_{15}	3 sections for the vertical internal structs	$0 \div 100$ CHS profiles' index from catalogue
x_{16} x_{17} x_{18}	3 sections for the upward-downward diagonals	$0 \div 100$ CHS profiles' index from catalogue
x_{19} x_{20} x_{21}	3 sections for the downward-upward diagonals	$0 \div 100$ CHS profiles' index from catalogue

Table 6.2 Design variables where the colours of the cells represent the different categories: blue - Topology; red - Layout definition; green - Grouping division; yellow - Cross-sections assignation.

constructability-based penalties seems to be not affected by topology variability. In Fig. 6.22, the procedure for the assessment is schematically shown.

Parameter	Value
K_1	10
Δ	2.70
β	0.1
γ	1.157
α	0.1

Table 6.3 Penalties parameters

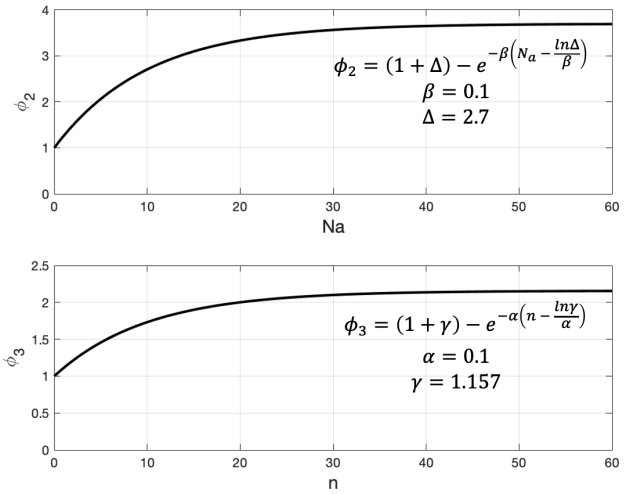

Fig. 6.21 ϕ_2 and ϕ_3, respectively 6.5 and 6.6

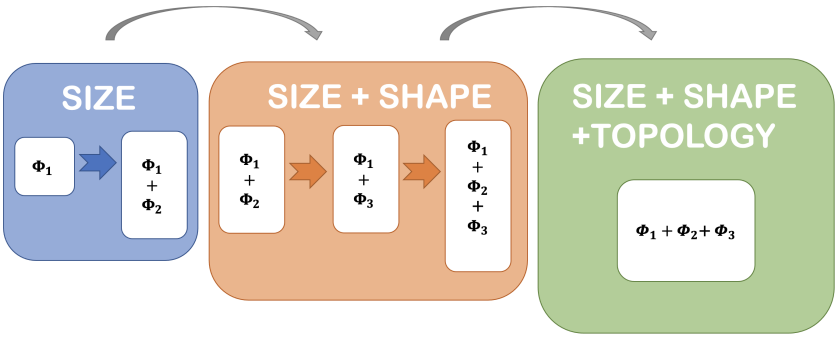

Fig. 6.22 Procedure for the assessment of each penalty

6.2.4 Modelling strategy and Software adopted

To fulfil the goal of the research, Rhinoceros 3D ©has been used to exploit the parametric design principles, which include Grasshopper 3D with Karamba 3D and Octopus plug-ins.

Fig. 6.23 Software and plug-ins adopted

- **Rhinoceros 3D**
  It is a 3D modelling tool, commonly used by architects and designers in the early design phase. The software have been developed by McNeel&Associates in 2008. It has been categorized in the CADs software, but it allows it to represent very complex forms and structures, making it more powerful concerning AutoCAD software, for example. Rhino uses non-uniform rational b-spline (NURBS), which are mathematical representations of a 3D geometry. NURBS allow us to accurately reproduce very complex geometries, from a simple 2D curve to the most challenging 3D shape. Rhino works in parallel with Grasshopper it allows us to visualize what we are designing in the Grasshopper environment.

- **Grasshopper 3D**
  Grasshopper3D is a visual modelling program, which can construct an iterative and interactive design process by modelling objects parametrically. The utility and efficiency of the program are enhanced by the plug-ins contained inside. Specifically, in this Thesis, Karamba3D and Octopus are the main ones used. Focusing on our case study, this software was very useful to run size, shape and topology optimizations. In fact, by changing the value of the slider component connected to the specific design variable, the software allows to re-create immediately and in a continuous way, several geometries by changing for example cross-sections, number of subdivisions, coordinates of the points, typology of the truss etc.

- **Karamba3D**
  Karamba 3D is a parametric structural analysis tool which is fully embedded into the visual programming environment Grasshopper. It can perform detailed Structural Finite Element Analysis (FEA) for spatial trusses, frames and shell structures. Specifically, in the present Thesis, this Rhino plug-in was used for the structural verification of the truss structure and in the following

one also for the industrial building. Although it could be less robust than commercial software, due to its fast interactivity with Grasshopper, it results more suitable than other FE programs, highly reducing the total amount of computational time. Data are instantly sent from the parametric model created in Grasshopper to the Karamba solver, which subsequently passes the analysis's outputs to the optimization. In particular, the elements created as simple geometry in Grasshopper are then converted into FEM components and assembled, by indicating the assigned cross-sections, material, joints, supports and loads applied. Using the "Utilization of elements" component, the structural verification towards buckling requirements can be implemented, according to EN 1993-1-1 included in Eurocode 3 (Design of steel structures - General rules and rules for buildings).

- **Octopus**
  In our Thesis we have not used the more common optimization Galapagos, but instead, we have employed Octopus, developed by Robert Vierlinger and his team, at the University of Applied Arts Vienna. It is a Grasshopper plug-in that enables the solving of a wide range of Multi-Objective Optimization (MOO) issues. To find Pareto-optimal solutions, Octopus offers two global metaheuristics methods:
  ⇒ SPEA2, which stands for "Strength Pareto Evolutionary Algorithm 2"
  ⇒ Hype Reduction, i.e. "Hypervolume Reduction Algorithm"
  Different parameters related to how the algorithm will search for the optimal solutions need to be set:

  - Elitism gives the percentage of new solutions that are bred out of the Elite instead of the entire pool; if high, more local optimization is performed.
  - Mut. Probability is the probability of each parameter /gene becoming mutated with the 'Mutation Rate'. A low Mutation Rate means little changes to the parameters' values, and a high rate means big changes.
  - Crossover Rate is the probability of two subsequently generated solutions to exchange parameter values.
  - Population Size is the number of solutions per generation. The Elite size is set accordingly, so a total of 2 x Population Size number of solutions are in each generation's pool. This size should be set according to the

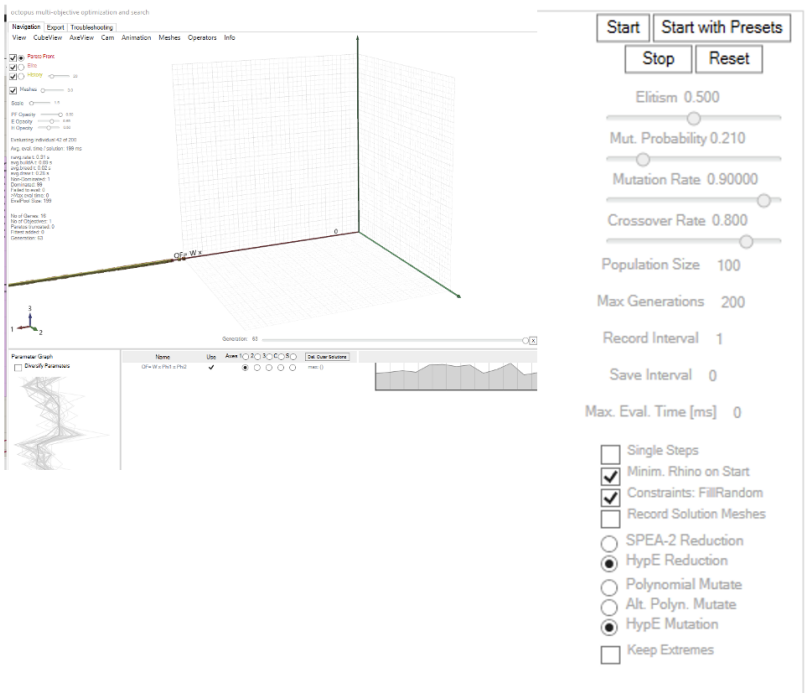

Fig. 6.24 Octopus interface

complexity of the problem since a lot of solutions at the same time can maintain a lot of different alternatives.

- Max. Generations are set to zero by default, meaning there is no end to the search. Otherwise, Octopus will stop after this number of generations.
- Record Interval is the interval of generations in which a history record is stored.
- Save Interval gives the interval of generations after which the Grasshopper file is saved to prevent data loss when Rhino crashes during the search for whatever reason.

More in detail, it is important to appropriately define the population size and maximum number of generations. Both of them are based on the complexity of the problem, in particular, a lot of solutions at the same time can maintain several alternatives leading to a more refined optimal solution. To start the optimization the algorithm needs to be connected to the different design variables previously defined and to the Objective Function that needs to be minimized.

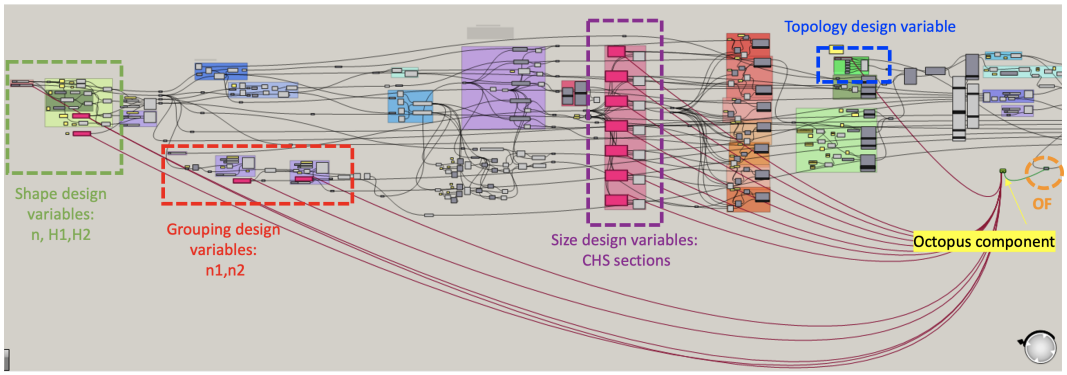

Fig. 6.25 Octopus component connected to all the design variables and the OF

Therefore, the geometry of our structure has been parametrically modelled in Grasshopper. Then, it has been traduced in the FEM elements using the Karamba3D components, assigning the cross-sections, loads and supports. Finally, the design variables and the objective function have been connected to the Octopus optimization.

6.2.5 Size, shape and topology optimization

In this section, we have directly performed the optimization comprehensive of all the design variables types (i.e. size, shape and topology). Among all the investigated case studies, it represents the most complex and the most representative of the goodness of the optimization procedure. However, results derived by the optimization procedure for each scenario will be shown in order to identify the level of influence of each design variable on the optimal solution.

Size, Shape & Topology: $\Phi_1(n_{un})+\Phi_2(N_a)+\Phi_3(n)$ The Objective Function is the same as the previous case, i.e

$$\rho \sum_{i=1}^{N} (A_i \cdot l_i) \cdot \phi_1 \cdot \phi_2 \cdot \phi_3$$

The resulting best individual found by Octopus is the following one:

From table 6.4 we can see the CHS cross-sections assigned to each element. Also in this case a balance between the complexity and weight of the truss structure has been

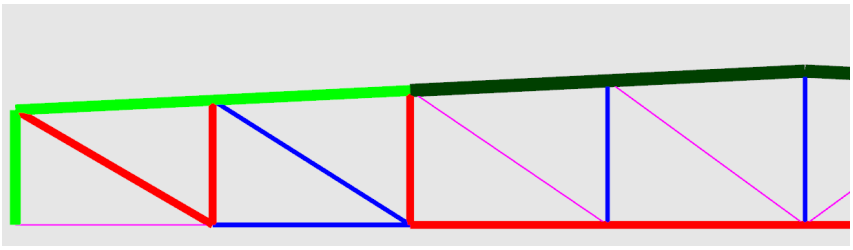

Fig. 6.26 Size, Shape & Topology: Configuration of the optimized truss

	CHS 1°group	**CHS 2°group**	**CHS 3°group**
Lower Chord	101.6x2	60.3x2	21.3x2
Upper Chord + Ext. Vert. Structs	168.3x3	139.7x3	139.7x3
Int. Vert. Structs	60.3x2	101.6x2	101.6x2
Downward-Upward Diagonals	21.3x2	60.3x2	101.6x2

Table 6.4 Size, Shape & Topology: Cross-sections of the optimized truss

Best OF	**Weight [kN]**	N_a	n	H_1	H_2	n_1	n_2	n_3
12.4295	4.3627	5	4	1.7	2.38	1	1	2

Table 6.5 Size, Shape & Topology: Main features of the optimized truss

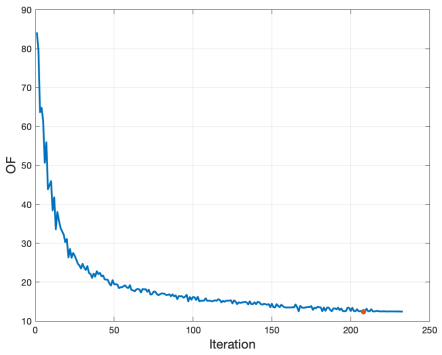

Fig. 6.27 Size, Shape & Topology: Best individual vs Iteration

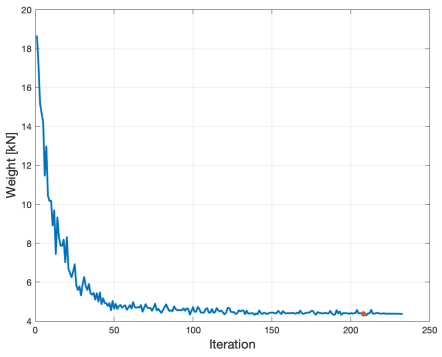

Fig. 6.28 Size, Shape & Topology: Weight of best individual vs iteration

found, as can be observed from table 6.5. However, the most important consideration that can be drawn from the results refers to the topology selected by the optimizer, which is Pratt one. As a matter of fact, it should be expected because we have considered only gravitational loadings. In Pratt trusses, as explained in the previous

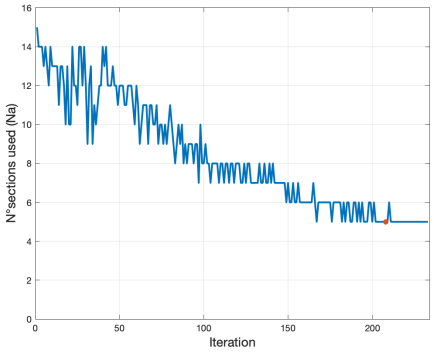

Fig. 6.29 Size, Shape & Topology: N_a of best individual vs iteration

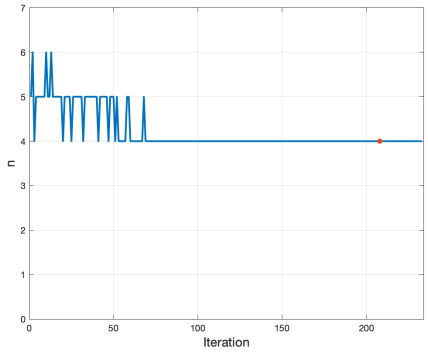

Fig. 6.30 Size, Shape & Topology: n of best individual vs iteration

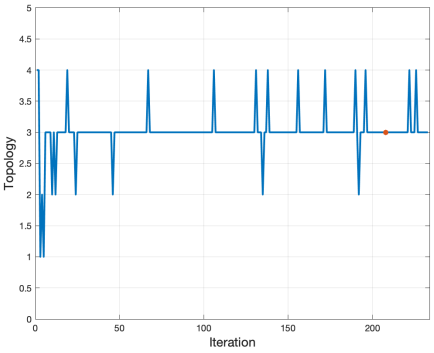

Fig. 6.31 Size, Shape & Topology: Topology of best individual vs iteration

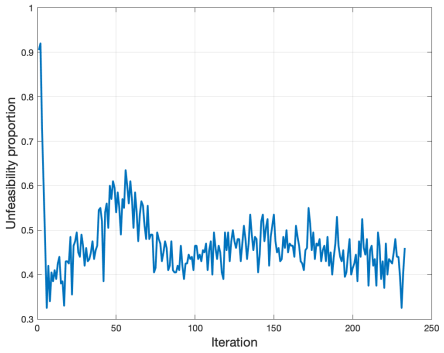

Fig. 6.32 Size, Shape & Topology: Unfeasibility proportion

chapter, the diagonal members, which are the longest ones, are in tension and not in compression, thus they won't require additional buckling instability verifications.

6.2.6 Discussion and final considerations

In the cases in which the Objective Function included all the penalties, i.e. $\phi 1$, $\phi 2$ and $\phi 3$, we have tested the robustness of the algorithm by performing the same analysis twenty times. At the end of this section, all the results obtained by each investigated scenario will be discussed. The author identified 4 scenarios (**A**, **B**, **C**, **D**) with different levels of penalties and different design variables involved in the process.

Results for 'Size, Shape & Topology: Φ_1+Φ_2+Φ_3' In table 6.6 the results of every optimization have been summarized and sorted from the smallest to the largest in terms of Best OF; while in table 6.7, Best (min), Worst (max), Mean and Standard Deviation have been reported.

Best OF	**Weight [kN]**	N_a	n	H_1	H_2	n_1	n_2	n_3	**Topology**
12.429	4.362	5	4	1.7	2.38	1	1	2	PRATT
12.435	4.143	5	5	1.53	1.96	1	1	3	PRATT
12.598	4.379	4	6	1.33	1.79	1	1	4	PRATT
12.604	4.424	5	4	1.97	2.39	1	1	2	PRATT
12.728	4.467	5	4	1.33	1.92	1	1	2	PRATT
12.776	4.644	4	5	1.55	1.85	1	1	3	HOWE
12.853	4.282	5	5	1.38	2.17	1	1	3	PRATT
12.876	4.202	6	4	1.57	2.24	1	1	2	PRATT
12.881	4.683	4	5	1.59	1.85	1	1	3	HOWE
13.069	4.587	5	4	1.33	1.86	1	1	2	PRATT
13.081	4.358	5	5	1.42	1.94	1	1	3	PRATT
13.144	4.613	5	4	1.34	2.06	1	1	2	WARREN
13.173	4.623	5	4	1.38	1.95	1	1	2	PRATT
13.182	4.392	5	5	1.37	1.85	1	1	3	PRATT
13.317	4.125	6	5	1.56	2.05	2	1	3	PRATT
13.389	4.699	5	4	1.46	1.68	1	1	2	PRATT
13.480	4.731	5	4	1.76	2.48	1	1	2	PRATT
13.777	4.590	5	5	1.33	1.84	1	1	3	HOWE
14.565	4.512	6	5	1.35	2.15	1	1	3	HOWE

Table 6.6 Results of the best individual of each optimization for 'Size, Shape & Topology: Φ_1+Φ_2+Φ_3'

Best	**Worst**	**Mean**	**Standard Deviation**
12.429	14.565	13.072	0.509

Table 6.7 Best, Worst, Mean and Standard deviation of the OF values'-'Size, Shape & Topology: Φ_1+Φ_2+Φ_3'

Analyzing the results of both cases there is a slight variability among the optimized individuals. To obtain more refined results, the same analysis should be performed at least 50 times.

Results of best individual for each case Following, the results obtained by each scenario with an increasing level of computational effort and complexity have been reported in table 6.8.

	Best OF	**W[kN]**	N_a	n	H_1	H_2	n_1	n_2	n_3
Size - case **A**: Φ_1	4.162	4.162	12	6	1.33	2.5	2	2	2
Size - case **B**: Φ_1+Φ_2	9.748	5.156	4	6	1.33	2.5	2	2	2
Size & Shape - Case **A**: Φ_1	4.399	4.399	10	7	1.33	1.59	1	1	5
Size & Shape - Case **B**: Φ_1+Φ_2	10.082	4.889	5	7	1.33	1.72	1	1	5
Size & Shape - Case **C**: Φ_1+Φ_3	6.148	4.224	11	5	1.33	1.81	1	1	3
Size & Shape - Case **D**: Φ_1+Φ_2+Φ_3	12.886	4.293	5	5	1.39	2.28	1	1	3
Size, Shape & Topology: Φ_1+Φ_2+Φ_3	12.429	4.363	5	4	1.7	2.38	1	1	2

Table 6.8 Results of the cases tested; in red the parameters fixed in the size analyses.

Because the objective function is not comparable with one another, except in the last two rows, we can analyze the resulting weights. The minimum value is obtained in the optimization denoted as 'Size - Case A: Φ_1'. It is interesting the fact that it is associated with the highest number of different cross-sections used. On the contrary, the heavier design has been found for the analysis denoted as 'Size - Case B: Φ_1+Φ_2', where the second penalty function has been integrated. Once again, we should underline the fact that it is the case in which the lowest number of sections used has been employed. Therefore, we can observe that the complexity in terms of N_a is the one that mainly influences the weight of the optimized structure. On the other hand, we can also state that the third penalty function, thus the complexity in terms of the number of subdivisions, is working fine when combined with the first two. In fact, from 'Size & Shape - Case C: Φ_1+Φ_3' and 'Size & Shape - Case D: Φ_1+Φ_2+Φ_3', n is stable at 5.

Another important observation is that, for the specific analysis considered with gravitational loads only, the optimized configuration is always characterized by $n_1 = n_2 = 1$. This means that the outer elements of each component have different sections, while the internal part is unified with the same cross-section.

For future development in this field, it would be interesting to employ a different grouping division, thus using two different indexes, for each component. For sure this would increase the computational effort because the design variables associated with the indexes are going to pass from 2 to $N^o of component \cdot 2$. However, it could be useful to discriminate among the different components and to refine the analysis, in order to see how the solicitation distribution would be optimized.

6.3 Case study 2: Industrial building

The analysis illustrated so far was limited to the level of the truss element, however, the scope of the research is to fit such theoretical procedure to a large-scale structure. Due to the great employment of truss structures in industrial buildings, it has decided to explore this type of construction. Thus, in the present Chapter, it is going to parametrically model and optimize the building under investigation, following the scheme adopted for the previous case study. The main differences and analogies between the analysis at the truss level and the current one will be discussed and the goodness of the procedures will be tested for a hard-computational problem.

6.3.1 Parametric modelling

Also for this instance, the power of parametric design to create the geometry of our structure using Grasshopper has been exploited. The design is composed of a repetition of specific modules at a distance s, which stands for spacing, which will be an indirect variable of the problem. Specifically, the number of modules has been optimized, which can be seen as the ratio of half the length and the spacing. Looking at the schematic representation of the overall geometry in figure 6.33, we can see that the modules consist of the truss system with two columns at the outer sides. In particular, the truss system is the same as the previous case study, while the height of the columns has been set equal to 5 meters. Actually, the external vertical structs of the truss are now removed and replaced by the column which rises to the upper chord nodes.
Therefore, once the structure footprint is fixed with a total span equal to 60 meters, modules can be denser or more widely spaced. Going into the details of the geometric modelling, it is started from the definition of the origin point in the middle of the

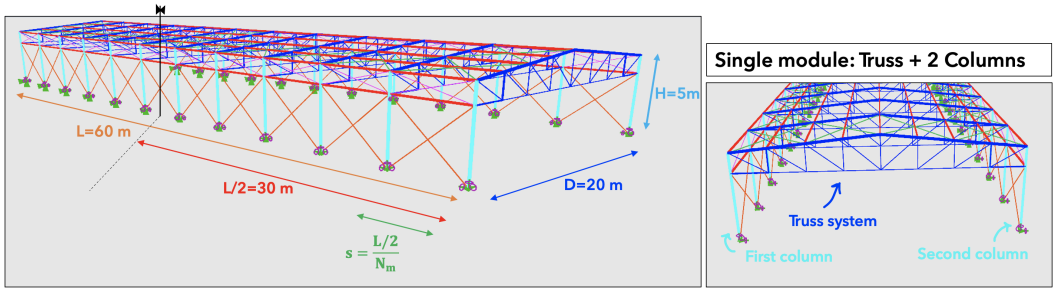

Fig. 6.33 Industrial building general scheme with modules

structure, in order to take advantage of the symmetry concerning the xz plane. Actually, yz plane symmetry is imposed, however, it cannot be exploited due to the presence of lateral load too. Hence, the geometry has been created in the first half, considering a half portion of the entire horizontal development of 60 meters on the y-axis. Then, it has been mirrored with respect to the xz plane. For this reason, the design variable related to the number of modules N_m is referred to as half geometry. Let's now focus on the actual model creation in Grasshopper. First of all, the main components of the industrial building must be defined:

- **Truss system**, distinguished in the five components seen in 6.2.2, i.e. Lower Chord, Upper Chord, Internal Vertical Structs, Upward-Downward Diagonals, Downward-Upward Diagonals;
- **Columns**;
- **Purlins or Secondary beams**;
- **Roof bracings**;
- **Vertical bracings type 1**, which are the upper ones;
- **Vertical bracings type 2**, the lower ones.

In the reported figure 6.34, each component group was identified by a different colour. Another important feature of the overall geometry is the presence of the symmetric scheme of the roof bracing systems, which are present at the edges of the structure and in the middle, regardless of the spacing used. Hence, the geometry definition was initialized by creating the first module, located at a distance of $s/2$ in the y-direction from the origin. Then, for obtaining a symmetric configuration of the

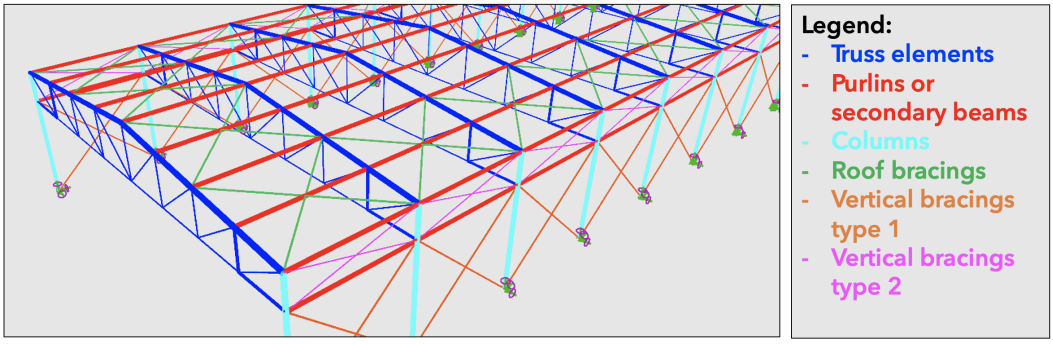

Fig. 6.34 Industrial building's components

roof bracings, it is imposed that in its half there will be at least two more modules. In this way, the lower bound of N_m equal to 3 was fixed, that in turn leads to a spacing value of 12 meters, according to the equations 6.7, 6.8 and 6.9. It has been found considering the following geometric relationships, represented graphically in figure 6.35.

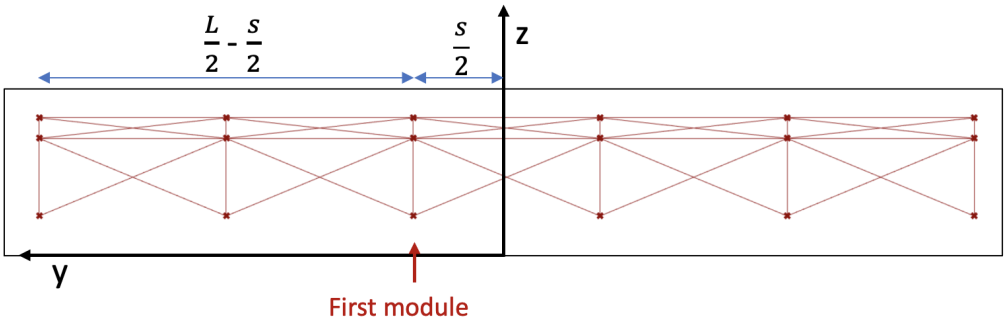

Fig. 6.35 Geometrical relationships for N_m domain definition

$$\frac{L}{2} - \frac{s}{2} = (N_m - 1) \cdot s \tag{6.7}$$

which leads to

$$N_m = \frac{\frac{L+s}{2}}{s} \tag{6.8}$$

and

$$s = \frac{\frac{L}{2}}{N_m - \frac{1}{2}} \tag{6.9}$$

Instead, the upper limit of N_m has been set by imposing a minimum spacing of 4 meters, thus obtaining $N_{m,max} = 8$. In the reported figure 6.36, it is evident how these extreme N_m values influence the overall configuration.

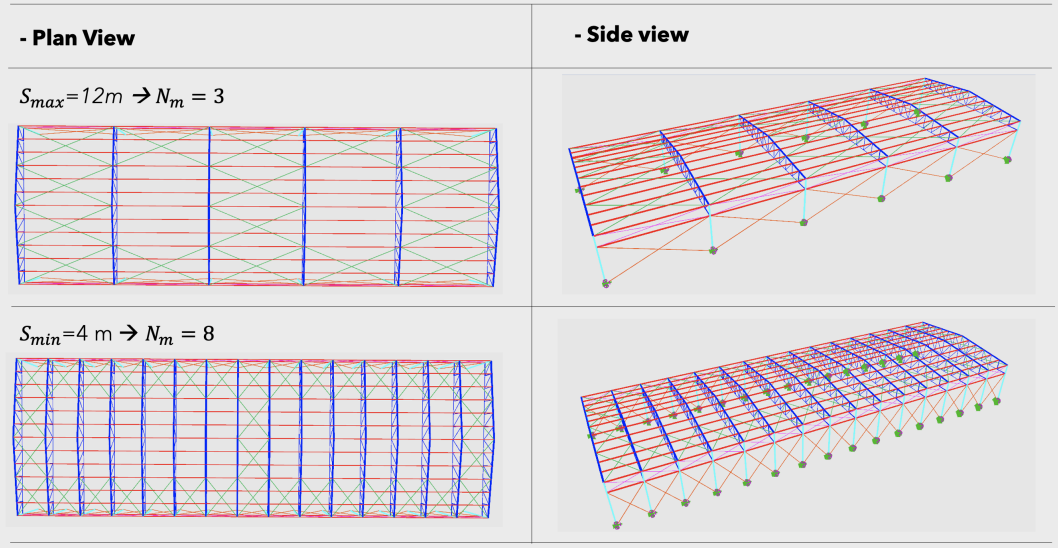

Fig. 6.36 N_m limiting configurations

The vertical bracings, both type 1 and 2, are covering the entire length in the y-direction. The roof bracing, instead, as said, is distributed symmetrically along the plan of the structure. However, it should be mentioned that looking at their distribution with respect to the upper chord nodes, they will cover a span length of one-quarter of the entire truss of 20 meters, no matter the value of n. It has been done to avoid the integration of the industrial building complexity, so their number will be fixed during the optimization. Then, for what regard the secondary beams, they are created by connecting the nodes of the upper chord from one module to the other. In this way, geometric modelling has been created.

6.3.2 Elements cross-section

The grouping and cross-section assignment of the truss system has been performed exactly as before. Instead, the other components have been simply assigned specific cross-section profiles, namely:

- **Columns** → HEA section, which stands for European wide flange beam section;

- **Purlins** → IPE section, i.e. European I-section beam with parallel flanges;
- **Bracings** → ROPE sections

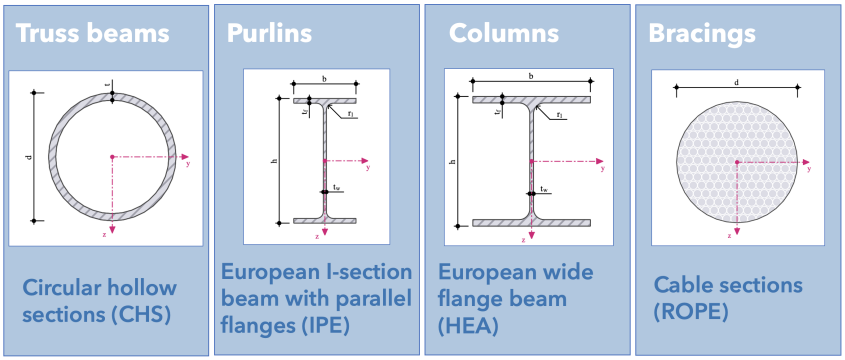

Fig. 6.37 Industrial building's elements sections

6.3.3 Loads

In this section the loads applied to the large span building are evaluated and properly described. As said in chapter **??**, Karamba 3D can consider only one combination of loads, therefore, also in this case, the Ultimate Limit State (ULS) analysis has been considered. In contrast to the case study at the truss level, where only gravity loads were applied to the structure, here both gravitational and horizontal loads were taken into consideration. Therefore, the following combination have been employed:

$$\gamma_{G1} \cdot G_1 + \gamma_{G2} \cdot G_2 + \gamma_P \cdot P + \gamma_{Q1} \cdot Q_{k1} + \gamma_{Q2} \cdot \psi_{02} \cdot Q_{k2} + \gamma_{Q3} \cdot \psi_{03} \cdot Q_{k3} + \ldots \quad (6.10)$$

- **Gravity loads**
  Regarding the gravitational loadings, the following ones have been evaluated:

  1. **Permanent Structural, or Dead, Load** (G_1)
     The Dead Load is simply the self-weight of all the components of the structure. In Karamba3D it is computed automatically, the coefficient of the load combination was simply applied.
  2. **Permanent Non-Structural Load** (G_2)
     The Permanent Non-Structural Load, i.e. G_2, is referred to the corrugated sheet, which is the material used to cover the roof of the building. In

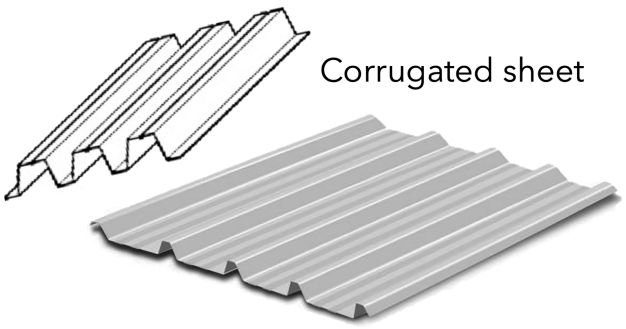

Fig. 6.38 Corrugated sheet

particular, it is useful to distribute loads on bottom purlins.
The standard load considered for the corrugated sheet is $0.05kN/m^2$, which has to be multiplied by the length of influence. The evaluation of the area of influence will be depicted at the end of this section.

3. **Maintenance Load (q_k)**
In order to define the value of q_k, we should refer to the indications provided by the Eurocode. In particular, the roof of our building, where the loads is going to be applied, belongs to the category H. Specifically, this category is referred to the covers accessible only for maintenance, which match with our case study. The value recommended by the Eurocode is $q_k = 0.4\frac{KN}{m^2}$, however, the Code specifies that it can be changed, according to the National Annex. Due to the fact that we are assuming the location of our building in Turin (Italy), the National Code we need to refer to is "Norme tecniche per le costruzioni" (NTC2018). Looking at the chapter 3.1 "Opere civili e industriali" and specifically the sub-section 3.1.4 "Sovraccarichi" from table 3.1.II in figure 6.39, the correct value is $q_k = 0.5\frac{KN}{m^2}$.

4. **Snow Load (q_s)**
Based on the building's position, the snow load is assessed and, as it was previously said, Turin's location has been taken into account. The general formulation for the snow pressure, according to the Eurocode, is:

$$q_s = q_{sk} \cdot \mu_i \cdot C_E \cdot C_T \tag{6.11}$$

Tabella 3.1.II – *Valori dei carichi d'esercizio per le diverse categorie di edifici*

Cat.	Ambienti	q_k [kN/m^2]	Q_k [kN]	H_k [kN/m]
A	**Ambienti ad uso residenziale**. Sono compresi in questa categoria i locali di abitazione e relativi servizi, gli alberghi. (ad esclusione delle aree suscettibili di affollamento)	2,00	2,00	1,00
B	**Uffici**.			
	Cat. B1 Uffici non aperti al pubblico	2,00	2,00	1,00
	Cat. B2 Uffici aperti al pubblico	3,00	2,00	1,00
C	**Ambienti suscettibili di affollamento**			
	Cat. C1 Ospedali, ristoranti, caffè, banche, scuole	3,00	2,00	1,00
	Cat. C2 Balconi, ballatoi e scale comuni, sale convegni, cinema, teatri, chiese, tribune con posti fissi	4,00	4,00	2,00
	Cat. C3 Ambienti privi di ostacoli per il libero movimento delle persone, quali musei, sale per esposizioni, stazioni ferroviarie, sale da ballo, palestre, tribune libere, edifici per eventi pubblici, sale da concerto, palazzetti per lo sport e relative tribune	5,00	5,00	3,00
D	**Ambienti ad uso commerciale**.			
	Cat. D1 Negozi	4,00	4,00	2,00
	Cat. D2 Centri commerciali, mercati, grandi magazzini, librerie…	5,00	5,00	2,00
E	**Biblioteche, archivi, magazzini e ambienti ad uso industriale**.			
	Cat. E1 Biblioteche, archivi, magazzini, depositi, laboratori manifatturieri	≥ 6,00	6,00	1,00*
	Cat. E2 Ambienti ad uso industriale, da valutarsi caso per caso	—	—	—
F-G	**Rimesse e parcheggi**.			
	Cat. F Rimesse e parcheggi per il transito di automezzi di peso a pieno carico fino a 30 kN	2,50	2 x 10,00	1,00**
	Cat. G Rimesse e parcheggi per transito di automezzi di peso a pieno carico superiore a 30 kN: da valutarsi caso per caso	—	—	—
H	**Coperture e sottotetti**			
	Cat. H1 Coperture e sottotetti accessibili per sola manutenzione	0,50	1,20	1,00
	Cat. H2 Coperture praticabili	secondo categoria di appartenenza		
	Cat. H3 Coperture speciali (impianti, eliporti, altri) da valutarsi caso per caso	—	—	—

Fig. 6.39 Table 3.1.II of NTC2018 to define the load q_k

Where:

- q_{sk} is the characteristic value of the snow load on the ground. In order to determine its value, we should refer to the Italian Standard code NTC2018. It depends on climate conditions and local exposure of the zone considered and it is correlated with the altitude. It can be computed according to the equation $q_{sk} = 1.39 \cdot (1 + (\frac{a_s}{728})^2)$, where a_s is the elevation above sea level. Specifically, Turin is at 239 meters above sea level, thus we obtain a value of $q_{sk} = 1.539 \frac{KN}{m^2}$.
- μ_i is a shape coefficient related to the inclination of the roof. It varies according to the reported table 6.9:

Shape coefficient	$0° \leq \alpha \leq 30°$	$30° \leq \alpha \leq 60°$	$\alpha \geq 60°$
μ_1	0.8	$0.8 \cdot \frac{(60-\alpha)}{30}$	0.0

Table 6.9 Values of shape coefficient μ_i based on the inclination of the roof

In our building the inclination of the roof is lower than 30°, therefore $\mu_i = 0.8$.

- C_E is the exposure coefficient and it is always related to the zone where the building is located. For our case, a value equal to 1 is assigned, due to the fact that there is not a significant removal of snow on buildings produced by the wind.
- C_T is the thermal coefficient and it is usually assumed equal to 1.

The final value of the snow load is: $q_s = 1.23 \frac{KN}{m^2}$

Before going into the details of the other class of actions considered, i.e. the lateral ones, we would like to explain how the mentioned-above vertical actions have been applied. With the exception of the Dead Load G_1, which is automatically considered by the software, for the other ones, the area of influence of such loads has to be identified. G_2, q_k, as well as q_s are applied on the purlins and their area of influence is a function of their relative distance. In the following figure 6.40, a schematic representation is reported.

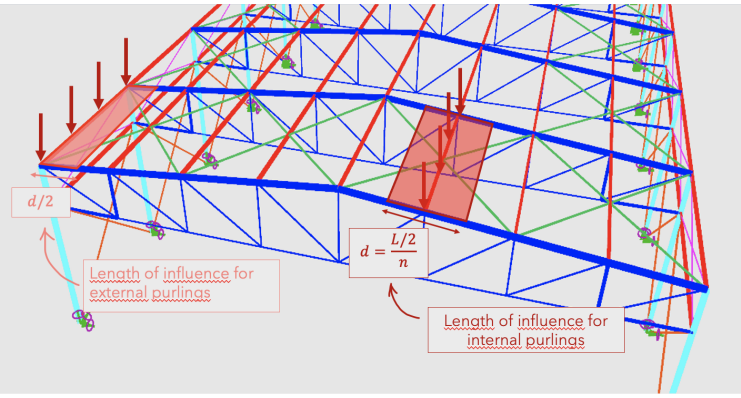

Fig. 6.40 Lenght of influence for internal and external purlins

As we can see, there is a difference between the length of influence for internal and external purlins, which are both functions of the distance between the upper chord's node. Specifically, the values considered in our analysis are a function of the design variable n. Finally, the unitary length loads to be applied on the purlins are computed as the just explained pressure values, multiplied by the length of influence, resulting in kN/m.

- **Lateral loads**

1. **Wind Load (p)**
   The wind is the movement of air masses characterised by a velocity field

that fluctuates randomly in time and space. It exerts aerodynamic actions on whole structures or on individual structural components. Wind load act as a lateral pressure on the external surface of the large-span building. As said for the other loads, Eurocode suggests referring to the National Annex to determine wind pressure.
Referring to Chapter 3.3 of NTC2018, the pressure exerted by the wind is:

$$p = q_b \cdot c_e \cdot c_p \cdot c_d \tag{6.12}$$

Where:

– q_b is the reference kinethic pressure evaluated as:

$$q_b = \frac{1}{2} \cdot \rho \cdot v_b^2 \tag{6.13}$$

Specifically, ρ is the air density equal to $1.25 \frac{kg}{m^3}$, while v_b is the wind velocity and it depends on the location of the building. NTC2018 in the section 3.3.1 provides the table illustrated in figure 6.41 with the values of v_b:

Zone	Description	$v_{b,0}$[m/s]	a_0[m]	k_a[1/s]
1	Valle d'Aosta, Piedmont, Lombardy, Trentino Alto Adige, Veneto, Friuli Venezia Giulia (excluding the province of Trieste)	25	1000	0.010
2	Emilia Romagna	25	750	0.015
3	Tuscany, Marche, Umbria, Lazio, Abruzzo, Molise, Puglia, Campania, Basilicata, Calabria, (excluding the province of Reggio Calabria)	27	500	0.020
4	Sicilia e provincia Reggio Calabria	28	500	0.020
5	Sardinia (east of the straight-line connecting Cape Teulada with the island of Maddalena)	28	750	0.015
6	Sardinia (area to the west of the straight-line connecting Cape Teulada with the island of Maddalena)	28	500	0.020
7	Liguria	28	1000	0.015
8	Province of Trieste	30	1500	0.010
9	Islands (with the exception of Sicily and Sardinia) and open sea	31	500	0.020

Fig. 6.41 Table 3.3.I of NTC2018 to define the v_b, a_0 and k_a

Turin is in zone 1 so the final value of q_b is $0.391 \frac{KN}{m^2}$ according to equation 6.13.

– C_e is the exposure coefficient, which has the following expression:

$$c_e(z) = k_r^2 \cdot c_t \cdot ln(\frac{z}{z_0}) \cdot [7 + c_t \cdot ln(\frac{z}{z_0})] \quad for \quad z \geq z_{min} \tag{6.14}$$

$$c_e(z) = c_e(z_{min}) \quad for \quad z < z_{min} \tag{6.15}$$

In particular, k_r is the class of roughness and we need to refer to Table 3.3.III of NTC2018 reported in figure 6.42.

Tab. 3.3.III - *Classi di rugosità del terreno*

Classe di rugosità del terreno	Descrizione
A	Aree urbane in cui almeno il 15% della superficie sia coperto da edifici la cui altezza media superi i 15 m
B	Aree urbane (non di classe A), suburbane, industriali e boschive
C	Aree con ostacoli diffusi (alberi, case, muri, recinzioni,....); aree con rugosità non riconducibile alle classi A, B, D
D	a) Mare e relativa fascia costiera (entro 2 km dalla costa); b) Lago (con larghezza massima pari ad almeno 1 km) e relativa fascia costiera (entro 1 km dalla costa) c) Aree prive di ostacoli o con al più rari ostacoli isolati (aperta campagna, aeroporti, aree agricole, pascoli, zone paludose o sabbiose, superfici innevate o ghiacciate, ...)

Fig. 6.42 Table 3.3.III of NTC2018 to define the class of roughness

Due to the fact that our structure is an industrial building, a class of roughness 'B' is assigned.
The next step concerns the definition of the exposure category, referring to the table shown in figure 6.43 provided by the National code.

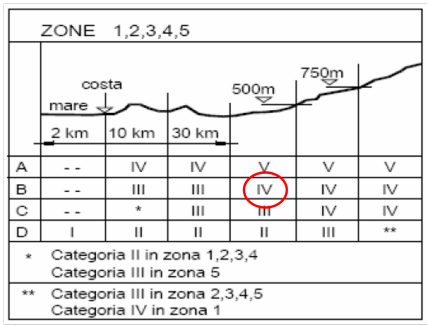

Fig. 6.43 Table 3.3.III of NTC2018 to define the exposure coefficient

For our case study the exposure coefficient is IV.
Finally, from table 3.3.II of NTC2018 6.44, based on the site exposure coefficient (IV) previosuly evaluated, all the terms contained in equation 6.14 can be determined.
The final value of c_e is 1.55 .

– c_p is the shape coefficient, which is related to the inclination of the roof α. The image below 6.45 illustrates how the coefficient should be considered in the evaluation of the wind pressure acting on the different structural elements, according to the Code.

Site exposure category	k_r	z_0 [m]	z_{min} [m]
I	0,17	0,01	2
II	0,19	0,05	4
III	0,20	0,10	5
IV	0,22	0,30	8
V	0,23	0,70	12

Fig. 6.44 Table 3.3.II of NTC2018 to define k_r, z_0 and z_{min}

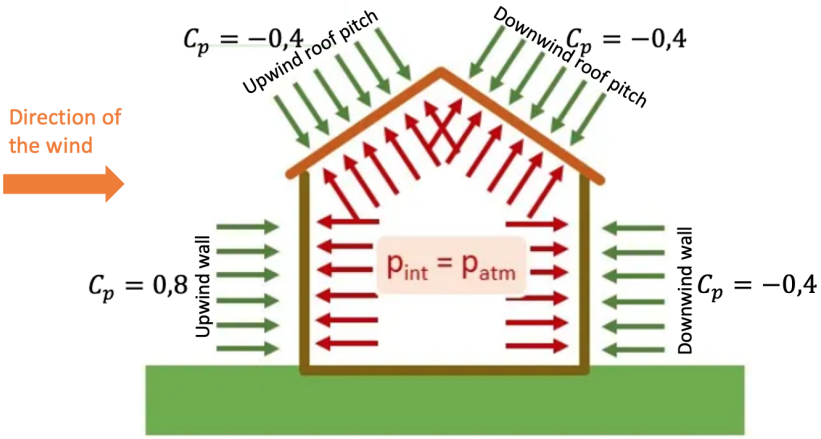

Fig. 6.45 Values of shape coefficient c_p

– c_d is the dynamic coefficient, which is generally set equal to 1 in buildings with an height lower than 80 meters.

Once v_b, c_t, c_p and c_e have been properly defined, the final wind pressure acting on the large span building is given. The following table 6.10 contains the values of the wind pressures p, evaluated according to the equation 6.12:

	c_p	$p[\frac{KN}{m^2}]$
Upwind wall	0.8	0.48
Downwind wall	-0.4	-0.24
Upwind roof pitch	-0.4	-0.24
Downwind roof pitch	-0.4	-0.24

Table 6.10 Wind pressure p values for the different c_pe

It's important to clarify that we have taken into account only the external pressure caused by the wind. This is due to the assumption that the building has no openings and it can be considered as an airtight construction, 'costruzione stagnant, according to NTC2018. Nevertheless, if we would like to consider any openings, it would be necessary to consider the coefficient c_{pi} referred to as internal pressure. Specifically, the value of c_{pi} will vary based on the area covered by the openings; for example if less than $1\backslash 3$ of the total area, a value of $c_{pi} = \pm 0.2$ should be considered. As illustrated in figure 6.45, the internal pressure is represented by the red arrows and is going to act oppositely with respect to the external one.
Regarding the application of the wind load, as already discussed for the vertical actions, a correct area of influence should be properly defined. Particularly, wind pressure has been applied only to purlins, normal to their development considering the same scheme shown in figure 6.40, while for columns, along the x-direction, as illustrated in the following figure 6.46:

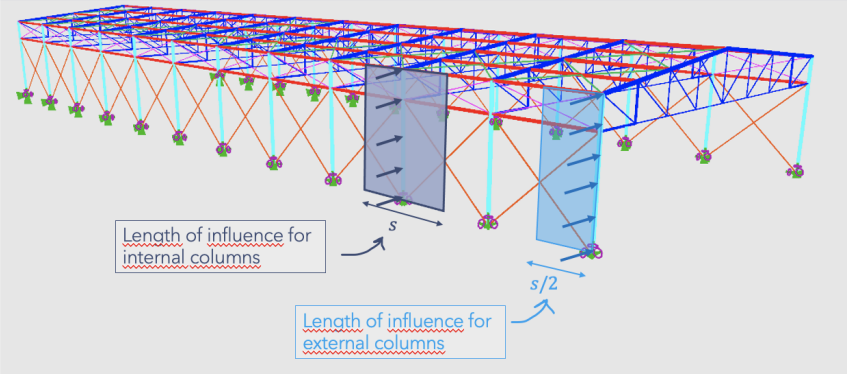

Fig. 6.46 Lenght of influence for internal and external columns

Once all the loads, both vertical and horizontal, are properly evaluated, the next step is to assign the coefficients of the load combination to each of them.
Unfortunately, there is only one load combination that can be defined in Karamba 3D, therefore we have considered the heaviest one. In particular, we have chosen as the dominant variable load the Maintenance Load q_k in order to be able to maximize the bending moment. In turn, the Snow load and the Wind action have been accounted as secondary variable loads with the proper ψ_{0j} coefficient. Referring to the ULS equation 6.10 and tables 2.5.I, 2.6. I of NTC2018 in figure 6.47 provided by the national annexe NTC2018, the following coefficients have been applied, as reported in table 6.11:

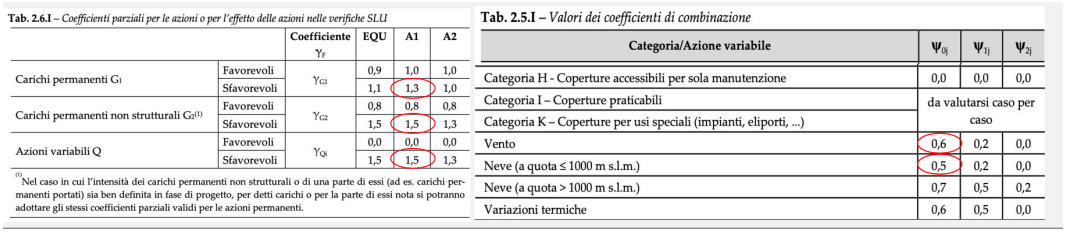

Tab. 2.6.I – *Coefficienti parziali per le azioni o per l'effetto delle azioni nelle verifiche SLU*

		Coefficiente γ_F	EQU	A1	A2
Carichi permanenti G_1	Favorevoli	γ_{G1}	0,9	1,0	1,0
	Sfavorevoli		1,1	1,3	1,0
Carichi permanenti non strutturali G_2[1]	Favorevoli	γ_{G2}	0,8	0,8	0,8
	Sfavorevoli		1,5	1,5	1,3
Azioni variabili Q	Favorevoli	γ_{Qi}	0,0	0,0	0,0
	Sfavorevoli		1,5	1,5	1,3

[1] Nel caso in cui l'intensità dei carichi permanenti non strutturali o di una parte di essi (ad es. carichi permanenti portati) sia ben definita in fase di progetto, per detti carichi o per la parte di essi nota si potranno adottare gli stessi coefficienti parziali validi per le azioni permanenti.

Tab. 2.5.I – *Valori dei coefficienti di combinazione*

Categoria/Azione variabile	ψ_{0j}	ψ_{1j}	ψ_{2j}
Categoria H - Coperture accessibili per sola manutenzione	0,0	0,0	0,0
Categoria I – Coperture praticabili	da valutarsi caso per caso		
Categoria K – Coperture per usi speciali (impianti, eliporti, ...)			
Vento	0,6	0,2	0,0
Neve (a quota ≤ 1000 m s.l.m.)	0,5	0,2	0,0
Neve (a quota > 1000 m s.l.m.)	0,7	0,5	0,2
Variazioni termiche	0,6	0,5	0,0

Fig. 6.47 Table 2.6.I and 2.5.I of NTC2018 to define the load's coefficient

Load Type	**Load Name**	**Load Value** $[\frac{KN}{m^2}]$	γ	ψ
Dead Load	G1	Structure weight	1.3	-
Perm. Non-struct. Load	G2	0.05	1.5	-
Maintenance Load	q_k	0.5	1.5	-
Snow Load	q_s	1.23	1.5	0.5
Wind Load	p	Depends on c_p	1.5	0.6

Table 6.11 Summary of loads applied to the building and their relative value and coefficient

6.3.4 Supports

Both internal and external constraints have been utilized for the large-span construction. Specifically, the base points of the columns were fixed to the ground, preventing any translational and rotational motions. Regarding the internal ones, Karamba 3D automatically applies rigid links between all the structural elements.

6.3.5 Objective Function Formulation

The optimization carried out for the industrial building application derives from the formulation of the simple truss, which has been slightly modified to better fit with this case study. First of all, we should start with the definition of the design variables involved. In fact, concerning the previous ones, reported in table 6.2, six additional design variables have been introduced. Specifically, the cross-sections of the structural members added, i.e. columns, purlins and bracings, distinguished into 1 roof bracing and 2 types of vertical ones, have been integrated with the former size variables of the truss. Moreover, a shape design variable related to the spatial configuration of the structure has been added, namely the number of modules of one half (N_m). The final number of design variables considered is 27 and the additional ones are summarized in table 6.12.

Design variable	Description	Domain
x_{22}	Numbers of modules in one half	$3 \div 8$
x_{23}	Column HEA cross-section	$0 \div 23$ profiles' index from catalogue
x_{24}	Purlin IPE cross-section	$0 \div 17$ profiles' index from catalogue
x_{25}	Roof bracing ROPE PV cross-section	$0 \div 24$ profiles' index from catalogue
x_{26}	Vertical bracing type 1 ROPE PV cross-section	$0 \div 24$ profiles' index from catalogue
x_{27}	Vertical bracing type 1 ROPE PV cross-section	$0 \div 24$ profiles' index from catalogue

Table 6.12 Design variables where the colours of the cells represent the different categories: purple - Global layout definition; orange - Additional size design variables

Once clarified all the parameters involved in the optimization, it can be easier to understand the aim of this analysis. The simultaneous size, shape and topology optimization of the truss, composing the modules of the industrial building, will be carried out, in parallel with the size and shape optimization at the larger scale. The cross-sections of the additional elements are going to be minimized, still satisfying the structural verification, while the spacing between the modules is going to be adjusted at each iteration. To be more clear, shape optimization at the industrial building level is going to be performed only by varying the number of modules present.

Focusing on the Objective Function formulation, it is the same as the one used for the analysis of the truss structure, explained in section 6.2.3 with the equation 6.1:

$$min\, F(\mathbf{x}) = \rho \sum_{i=1}^{N} (A_i \cdot l_i) \cdot \phi_1(n_{un}) \cdot \phi_2(N_a) \cdot \phi_3(n)$$

While the first penalty related to buckling instability verification is now enlarged to all the elements, the other two penalties regarding the design simplification are not working in the general framework. The constructability criteria embedded in ϕ_2 and ϕ_3 are going to act only on the truss components and, in particular, on the number of sections used (N_a) and the number of subdivisions of the chords (n), respectively.

In this way the complexity is going to be studied only at the truss level, making it possible to analyse the validity of the previous considerations. As a result, we can effectively appreciate the discoveries of the truss level optimization of Chapter **??**, in a more challenging scenario. In particular, this is the reason why we have fixed the number of roof bracings regardless of n, in order to avoid a higher complexity.

6.3.6 Results - Industrial building level

In this section, the results of the industrial building optimizations have been summarized. The analysis has been performed 15 times in order to obtain more refined results and to test how the algorithm works in this second case study. In the following table 6.13, the results are sorted from the smallest to the largest in terms of the best objective function.

Best OF	**Weight [kN]**	N_a	n	H_1	H_2	n_1	n_2	n_3	N_m	**Topology**
775,427	330,228	3	4	2	2,17	1	1	2	7	HOWE
790,020	336,442	3	4	2	2	1	1	2	7	HOWE
885,230	339,024	4	4	2	2	2	1	1	7	HOWE
888,228	340,172	4	4	1,99	2,07	1	1	1	7	HOWE
894,320	342,505	4	4	1,99	2,01	1	1	1	7	HOWE
940,256	350,687	4	4	1,67	1,75	1	2	1	6	HOWE
932,095	396,947	3	4	1,94	2,01	2	1	1	6	WARREN
937,174	399,110	3	4	2	2,43	1	1	1	6	HOWE
940,256	350,687	4	4	1,67	1,75	1	2	1	6	HOWE
941,401	400,910	3	4	1,46	1,57	1	2	1	6	HOWE
964,094	369,228	4	4	1,54	1,64	1	1	1	7	HOWE
967,429	370,505	4	4	1,67	1,67	2	1	1	6	HOWE
971,380	372,018	4	4	1,75	1,78	2	1	1	8	WARREN
974,337	341,988	5	4	2	2,1	2	1	1	7	HOWE
983,096	376,505	4	4	1,87	1,95	1	1	1	8	PRATT
991,875	378,404	4	4	1,87	1,95	1	1	1	8	HOWE
1014,911	356,229	5	4	1,68	1,87	1	2	1	8	HOWE
1023,262	391,888	4	4	2	2,31	1	2	1	7	WARREN
1036,499	396,957	4	4	2	2	1	2	1	7	PRATT
1042,326	399,189	4	4	1,96	2,16	1	1	1	6	PRATT

Table 6.13 Results of the best individual of each optimization for the Industrial building

Analyzing the results, several considerations can be drawn. First of all, focusing on

the last column 'Topology', the variability in the optimal solution can be highlighted. The Howe truss is the most chosen one, however, sometimes the optimizer prefers also Pratt and Warren. Due to that, we have distinguished the results for the different typologies, i.e. Howe 6.14, Warren 6.16 and Pratt 6.18. We should recall the fact that, because of the limit to only one load combination imposed by Karamba3D, we have been able to apply the wind action only from left to right. Therefore, this has influenced the final configuration of the truss systems.
Here below the results of the optimizations with the Howe truss as an optimal solution are reported in table 6.14.

Best OF	**Weight [kN]**	N_a	n	H_1	H_2	n_1	n_2	n_3	N_m	**Topology**
775,427	330,228	3	4	2	2,17	1	1	2	7	HOWE
790,02	336,442	3	4	2	2	1	1	2	7	HOWE
885,23	339,024	4	4	2	2	2	1	1	7	HOWE
888,228	340,172	4	4	1,99	2,07	1	1	2	7	HOWE
894,32	342,505	4	4	1,99	2,01	1	1	2	7	HOWE
937,174	399,11	3	4	2	2,43	1	1	2	6	HOWE
964,094	369,228	4	4	1,54	1,64	1	1	2	7	HOWE
967,429	370,505	4	4	1,67	1,67	2	1	1	6	HOWE
974,337	341,988	5	4	2	2,1	2	1	1	7	HOWE
1014,911	356,229	5	4	1,68	1,87	1	2	1	8	HOWE

Table 6.14 Results of the best individual for Industrial building with Howe truss

In the table below 6.15 also the Best, Worst and Mean values, as well as Standard Deviation of the OF are reported. Specifically, the best value is related to the minimum OF value, while the worst is to the maximum one.

Best	**Worst**	**Mean**	**Standard Deviation**
775.427	1014.911	942.425	77.05

Table 6.15 Best, Worst, Mean and Standard deviation related to the OF values of the optimized Industrial building with Howe truss

Focusing on the best-optimized individuals with Howe truss and referring to table 6.14, there is still some variability in the results and this is mainly due to the high number of design variables that the optimizer has to manage.
More in detail starting from the OF values the minimum one is obtained reducing the complexity at the truss level, as expected. Lowering the values of N_a and n the best individual is found. However, regarding N_a, looking at all the results, there

isn't a clear trend it varies from 3 to 5. On the contrary, the number of subdivisions n is stable at 4. About weight values of the optimized individuals, a narrow range of results can be observed it fluctuates between $330KN$ and $356KN$. With respect to case study 1, in which the weight increased when N_a and n decreased, here the total weight of the structure cannot be directly related to the complexity of the truss structure. Now many other structural elements contribute to the weight's final value. Moving to the column of the table referring to the values of N_m, the number of modules, and keeping in mind that it ranges between 3 and 8, we can state that the optimizer mainly prefers to work with more modules, from 6 to 8. This choice is justified by the fact that if the spacing is widened, resulting in a lower N_m value, heavier sections are necessary. Furthermore, the algorithm is not directly guided in the selection of N_m.
Regarding the geometric layout, i.e. H_1 and H_2 values, there is almost a clear trend. Specifically, fixing $n = 4$, the allowable ranges for the two parameters are $1.44 < H_1 < 2$ and $H_1 < H_2 < 2.5$. Looking at the results, we can see that the values assigned to the optimized structures vary in these limits: $1.54 < H_1 < 2$ and $1.64 < H_2 < 2.43$.
A final consideration can be made about the values assigned to the index n_i in the definition of the grouping. Index n_2 is almost fixed at 1, except for the last best individual which is also the worst in our set. Instead, n_1 and n_3 vary between 1 and 2. Perhaps if we could perform a higher number of analyses it would be possible to establish a more stable trend.
Here below are the tables summarizing the results of the remaining typologies, i.e. Warren and Pratt ones, which have been reported.

Best OF	**Weight [kN]**	N_a	n	H_1	H_2	n_1	n_2	n_3	N_m	**Topology**
932,095	396,947	3	4	1,94	2,01	2	1	1	6	WARREN
1023,262	391,888	4	4	2	2,31	1	2	1	7	WARREN

Table 6.16 Results of the best individual for Industrial building with Warren truss

Best	**Worst**	**Mean**	**Standard Deviation**
932,095	1023,262	932,095	63,008

Table 6.17 Best, Worst, Mean and Standard deviation related to the OF values of Industrial building with Warren truss

The Warren truss has been chosen only twice out of the 15 optimizations, therefore

we cannot make an analysis as detailed as the one referred to the Howe truss. However, looking at tables 6.16 and 6.17, first of all, we can say that the best objective function value is much higher than the best of the Howe configuration. It is interesting the fact that also in this case n is always stable at 4, proving that the penalty Φ_3 is guiding effectively the algorithm. All the other parameters are different in the two individuals, but recall a little bit the values of the Howe case.

Best OF	**Weight [kN]**	N_a	n	H_1	H_2	n_1	n_2	n_3	N_m	**Topology**
983,096	376,505	4	4	1,97	1,99	1	1	2	8	PRATT
1036,499	396,957	4	4	2	2	1	2	1	7	PRATT
1042,326	399,189	4	4	1,96	2,16	1	1	2	6	PRATT

Table 6.18 Results of the best individual for Industrial building with Pratt truss

Best	**Worst**	**Mean**	**Standard Deviation**
983,096	1042,326	1020,640	32,644

Table 6.19 Best, Worst, Mean and Standard deviation related to the OF values of Industrial building with Pratt truss

Looking at the Pratt optimized trusses, we have now three individuals out of the total 15 ones. The best OF is in between the two previously analyzed cases, however the difference with the Howe case is significant. In this case, both N_a and n are fixed at the same value in all the three optimized structures, while a variability in all the other parameter is visible.
Once all the outcomes have been introduced and examined, let's now focus on the best individual among the 15 analysis summarized in table 6.13.
The resulting best industrial building is characterized by truss systems belonging to the Howe category and the overall configuration is the following one:

Best OF	**Weight [kN]**	N_a	n	H_1	H_2	n_1	n_2	n_3	N_m
775.427	330.228065	3	4	2	2.17	1	1	2	7

Table 6.20 Best Individual of the optimized Industrial Building

The figure below 6.49 is showing the optimized truss and the groups subdivision of the different components:
In the tables 6.21 and 6.22 the cross-sections assigned to all the structural members are reported:

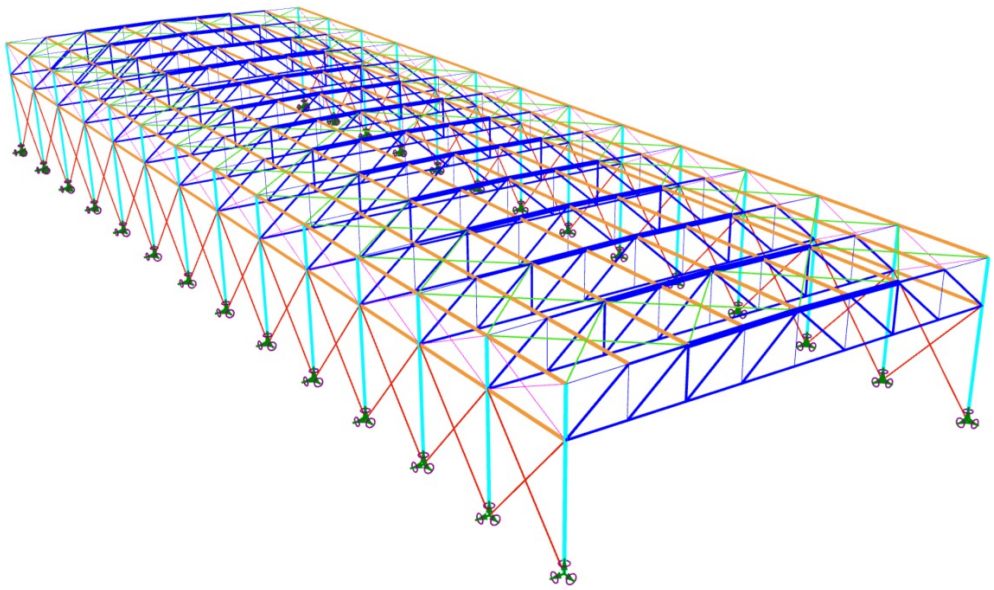

Fig. 6.48 Configuration of the optimized Industrial building

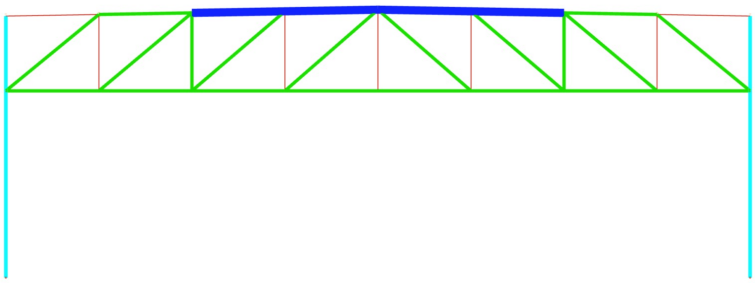

Fig. 6.49 Configuration of the Howe truss in the optimized Industrial building

	CHS 1°group	**CHS 2°group**	**CHS 3°group**
Lower Chord	88.9x2.5	88.9x2.5	88.9x2.5
Upper Chord	219.1x6	88.9x2.5	21.3x2
Int. Vert. Structs	21.3x2	88.9x2.5	21.3x2
Upward-Downward Diagonals	88.9x2.5	88.9x2.5	88.9x2.5

Table 6.21 Cross-sections of the optimized truss in the Industrial building

Now the charts about the main parameters of the best individual at each iteration have been reported.

From chart of 6.52 and 6.53 we can appreciate how the penalty $\phi 2$ and $\phi 3$ are

Structural Elements	**Cross Section Type**
Columns	HEA 100
Purlins	IPE 120
Roof Bracings	Rope PV 300
Vertical Bracings 1	Rope PV 40
Vertical Bracings 2	Rope PV 360

Table 6.22 Cross-sections of the structural elements in the Industrial building

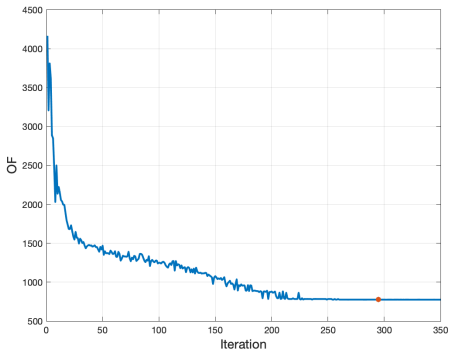

Fig. 6.50 Best individual vs iteration

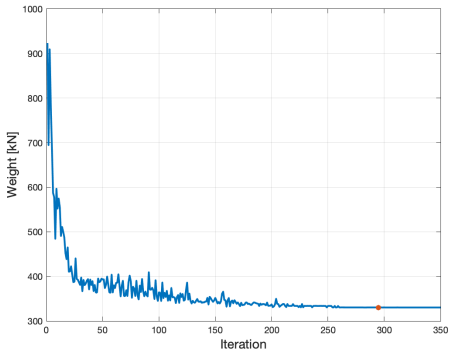

Fig. 6.51 Weight of best individual vs iteration

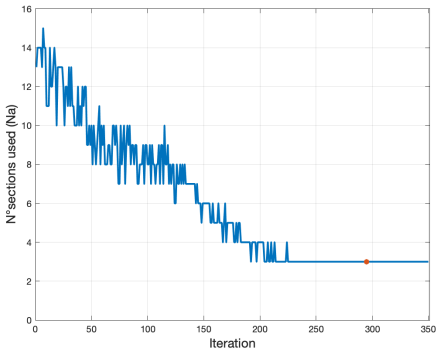

Fig. 6.52 N_a of best individual vs iteration

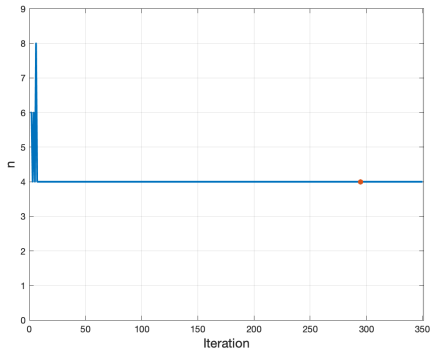

Fig. 6.53 n of best individual vs iteration

still working in the correct manner. Specifically, the complexity related to N_a has been further reduced the final value of different cross-sections used is 3. We can highlight the fact that with $\phi 2$ we are guiding the algorithm to refine the analysis and choose lower N_a values, as visible in 6.52. Instead, for the topology 6.54 as well as for N_m 6.56, with our objective function we have not led the optimization toward

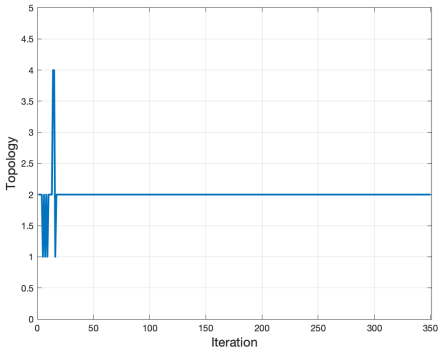

Fig. 6.54 Topology of the best individual vs iteration

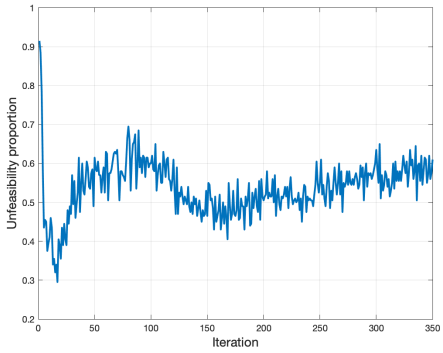

Fig. 6.55 Unfeasability proportion

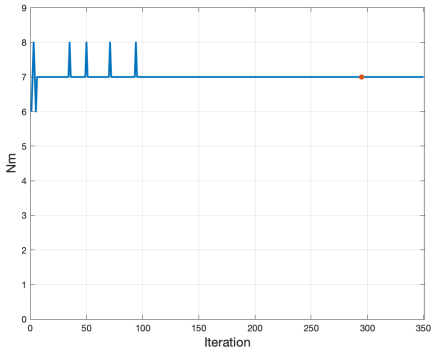

Fig. 6.56 N_m of the best individual vs iteration

a specific condition. The optimizer after a few iterations begins to stagnate in the same solution. This is due to the fact that is free to choose any solution because no penalty is influencing the optimal final value.

Let's see in detail the structural features of the optimized structure. In particular, in figure 6.57 it has been reported the axial force diagram of all structures. It is clearly visible that the Axial Stress is pronounced for the truss components and columns. In particular, in the Howe truss, Lower Chord and Vertical elements work in tension, while the beams of the Upper Chord and Diagonal are compressed, as well as the columns of the industrial building. Instead, in figure 6.58 it is visible that the bending moment diagrams affect the purlin elements.

In addition, in 6.59 the displacements of the different structural elements have been reported. We should highlight the fact that the analysis has been performed considering the Ultimate Limit States, therefore no restriction on the vertical displacements

has been imposed. In particular, the highest displacement affecting the central part of the structure is lower than 8 cm.

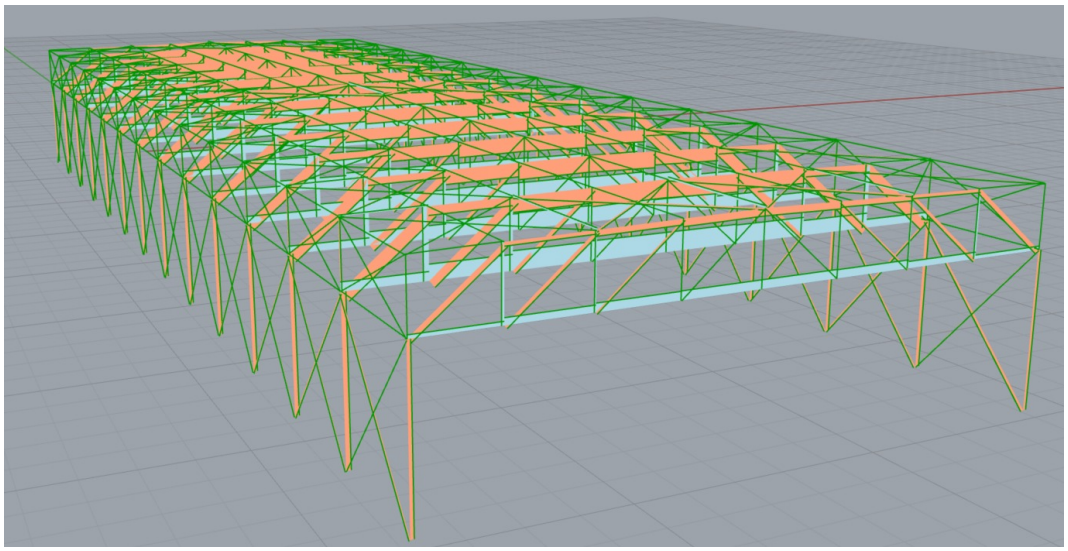

Fig. 6.57 Axial force diagram. In orange the compressed elements, in blue the tension one

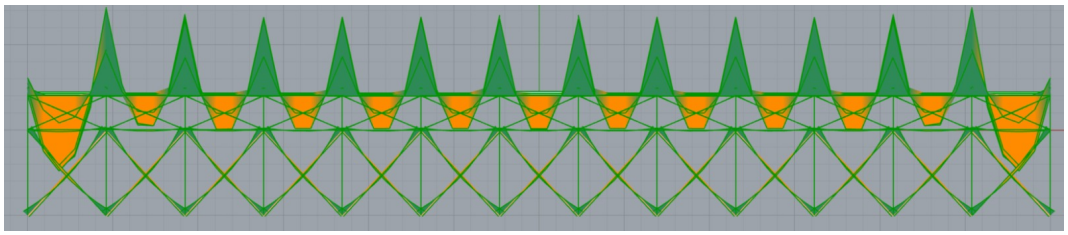

Fig. 6.58 Bending moment diagram. In orange the negative values, in green the positive ones

6.4 Conclusions

In this chapter, the applicability of the proposed objective function for simpler and more challenging truss structures was demonstrated. The importance of constructability issues with respect to a simple minimum weight approach was highlighted aiming to simplify the design and guarantee standardized procedures at the production phase of steel members. Ranging from a simple size optimization to a simultaneous size, shape and topology one, we have studied the single penalty functions introduced, how they work and how they can be calibrated according to specific needs. Starting

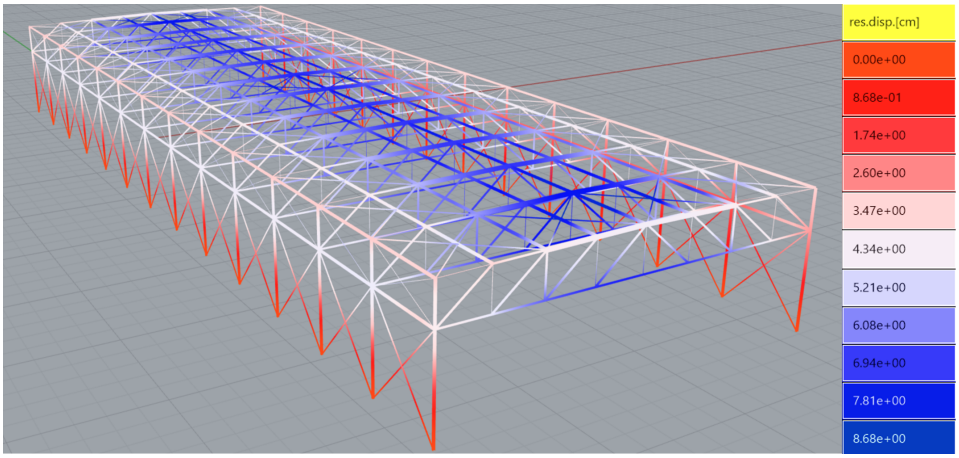

Fig. 6.59 Displacements and related legend of the Industrial building

from the truss level analysis (case study 1), the author originally expected to obtain higher weights for lower design complexity, in fact, the opposite trend was recognized for each scenario. Moreover, with specific regard to the scenario in which topology was investigated in addition to size and geometry, the Pratt configuration has been usually selected by the optimizer as the optimal solution. This was, once again, expected because, for gravitational loads only, in this type of truss the longer diagonal elements work in tension, thus avoiding critical verifications related to compression and buckling structural check. On the contrary, in the Howe truss, for example, the diagonals are in compression thus it was always excluded. The most challenging task was to understand the calibration of the parameters employed in each single penalty. Specific trends have been identified and recommendations on possible changes have been provided.

Regarding with the industrial building case study (case study 2), the most important modifications have been highlighted. In particular, the additional design variables were mainly related to the cross-sections employed for the new structural elements and the one linked to the spacing of the different modules. For this second case study, the objective function has been applied with a simple alteration regarding the buckling structural verification, which is now testing all the elements. Constructability considerations, instead, have not been enlarged to the global level, but remain at the truss one. This is evident, for example, in the variability of N_m in the optimized structures, visible in table 6.13. In fact, the algorithm is not encouraged towards a reduction of N_m, which in turn could lead to a decrease in the overall number of pieces and connections.

Chapter 7

Cutting Stock Problem in structural optimization

7.1 Introduction

In section 1, all the papers focused on cost-based optimal procedure were discussed and, specifically, the influence of material, fabrication and maintenance costs on the Objective function were analyzed. Specifically, materials cost minimization considers only those elements involved in the construction process.
As will be seen in the current chapter, a significant part of the expenses is also the waste of material from the cutting process. In other words, minimising the amount of material involved in the construction process without a carefully cutting design, which diminishes the waste, leads to inefficient cost optimization.
Construction and demolition wastes were expected to account for around 23% of the overall solid waste stream. This waste ratio equates to more than 100 million tonnes every year. Other nations' percentages corroborate the estimates from the United States. A percentage of the waste created by stock reduction is preventable, which means it is generated as a result of improper material utilisation. The quantity of superfluous acquired materials, needless workmanship, wastes and trucking and tipping fees required to discharge the garbage would be reduced if the supplies were used more efficiently (Khalifa et al. 2006).
Indeed, efficient resource use is not just in the interests of the industrialist, but also of the world at large. The disposal of trash from a stock-cutting operation may cause

pollution, and excessive wasting may deplete our planet's precious supplies (see Cheng et al. 1994).
Cutting losses is possibly the most major source of steel waste. Cutting losses arise when normal steel lengths are shortened to fit the project's required lengths. A significant amount of the created steel waste according to Adham et al. (2004) is related to cutting losses, which are mostly caused by:

- Dividing an order into separate, smaller orders typically results in more waste due to fewer cutting alternatives
- using inefficient cutting patterns in the cutting schedule results in the generation of avoidable waste that could be avoided through better stock-cutting planning
- using the optimum cutting patterns may result in unavoidable waste that is the minimum waste generated if the optimum cutting patterns are used

In order to minimise the waste the cutting stock problem (CSP) is a significant source of one-dimensional stock waste in the construction industry.
The following part of this chapter is organized into three subsections. The first section shows the state of art about cutting stock problems. Afterwards, the following section treats the cutting stock problem applied in the structural optimization of trusses. Lastly, a mathematical formulation of the cutting stock problem applied in the following chapters was developed.

7.2 State of art

Cutting and packing (C&P) problems of concrete and abstract objects appeared in the literature under various specifications (i.e. cutting problems, knapsack problems, container and vehicle loading problems, pallet loading, bin packing, assembly line balancing, capital budgeting, changing coins, etc.) within disciplines such as Management Science, Information and Computer Science, Engineering, Mathematics, and Operations Research. All of these problems have essentially the same logical structure (Belov (2003)).
The most famous of these problems is the bin packing problem (BPP) which determines how to pack as many items as possible into a container or, in other words,

minimize the number of containers (bins) used for the same stock of goods. Informally, the BPP can be stated as follows. There are given *n items*, each with an integer *weight* $w_j (j = 1...,n)$ and an infinite number of identical bins with integer *capacity* c. The goal is to load all the products into as few bins as possible so that the total weight packed in each bin does not exceed the limit. (Delorme et al. (2016))
Almost all the other C&P problems are variants (e.g. pallet loading problem) or generalizations (e.g. cutting stock problem) of the BPP.
In particular, in civil engineering, the most common problem of diminishing waste due to the steel element cutting process can be solved with the cutting stock problem. In summary, the cutting stock problem (CSP) tackles the practical question of cutting off needed pieces from stock material with the least trim loss. In more technical terms, the CSP can be defined starting from the BPP definition as follows. There are *m item* kinds, each with an integer *weight* w_j and an integer *demand* $d_j (j = 1,...,m)$, as well as a huge number of identical integer *capacity* c bins. In the CSP literature, the bins are typically referred to as rolls, a word derived from early implementations in the paper industry, and "cutting" is commonly used rather than "packing". The goal is to manufacture d_j copies of each item type j (i.e., cut/pack them) using the fewest number of bins possible while ensuring that the total weight in every bin does not exceed the capacity (Delorme et al. (2016)).
Moreover, the cutting stock problem can be classified as a one-dimensional and two-dimensional problem. A specified set of order lengths must be extracted from stock rods of a defined length in order to solve the one-dimensional cutting stock problem (1D-CSP). Usually, the goal is to use the fewest amount of rods possible (material input). The two-dimensional two-stage constrained cutting problem (2D-2CP) aims to select the most valuable group of rectangular objects from a single rectangular plate. Furthermore, the two-dimensional CSP can involve regular or irregular shapes, in the second case, the problem is called nesting and have a more difficult solution (Belov (2003))
These kinds of problems are complex combinatorial optimization, which in mathematical terms is a strongly NP-hard problem. For this reason, many linear programming, heuristic and metaheuristic approaches were proposed over the years.
The first approach to the C&P problems dates back to the '30s with Kantorovich (1960). Although his approach is poor and only handles small-scale cases, it aids in understanding the problem structure.
Numerous heuristic approaches (such as first solving the linear programming LP

problem and then converting the LP result to an integer solution) take advantage of this problem's linear programming (LP) relaxation.

This problem is often formulated as an integer programming (IP) problem, and its linear programming (LP) relaxation is exploited in many heuristic algorithms. In mathematics, the relaxation of a (mixed) integer linear program is the problem that arises by removing the integrality constraint of each variable and allows solving the integer programming (IP) problem as a linear programming one. This relaxing technique converts an NP-hard optimization issue (integer programming) into a similar problem that can be solved in polynomial time.
However, this method makes it impractical to take into account all cutting patterns that are practical and correspond to the columns in the LP formulation, especially when the length of a single item is much smaller than the roll length. By resolving the related knapsack issue, Gilmore and Gomory provided an inventive method to identify the cutting patterns required to enhance the LP solution.
Gilmore and Gomory (1961) proposed a column generation approach inspired by Dantzig and Wolfe (1960) for decreasing stock and bin packing concerns (BBP). Because enumerating all possible cutting patterns would take an inordinate amount of time, it reduces valid patterns repeatedly and adds them to the issue based on their contribution to the objective function. The column generation approach made large-scale cutting stock issues solvable in a reasonable amount of time.
In the following years, many algorithms were developed to solve the problem. While the most precise but computational and time consuming are the more rigorous procedure based on the integer linear programming, in more recent times several metaheuristic procedures have been implemented (e.g. Genetic Algorithm, Simulated annealing and Tabu search).

7.3 Use of cutting stock problem in truss solutions

In the previous section, it was seen the general formulation of the Cutting Stock problem. In recent years, the civil engineering sector has become increasingly interested in implementing the reuse of construction materials. The researcher notices that the cost and environmental optimization, by themselves, in not sufficient for reaching the best outcome. The building sector is a major contributor to material consumption, energy use, greenhouse gas emission, and waste production (Agency

(2011), Allwood et al. (2012)).
This problem can be solved basically in two ways: by minimizing the waste in the fabrication phase or by reusing stock materials from other structures. The first way wasn't so predicated and this was one of the aims of this thesis and the entire research. The second path was deeply explored by Brütting et al. in various publications that treated the reuse of the construction stock elements. In this section, it is possible to see the highlights of this specific topic.
The idea introduced by Brütting et al. (2019b) is to use the principle of circular economy in order to reduce the cost and the environmental impact of structures. In a circular economy, manufactured goods are kept in use as long as possible through closed loops, which consist of repair, reuse, and recycling. In particular, they were concerned about reuse because less energy is spent on reprocessing with respect to recycling.
A first way to approach the reuse optimization problem it can be seen in Brütting et al. (2019b). In this study, structural optimization with stock constraints was shown. For clarity, the term *member* is used for a position or bar in a reticulated structure and *member length* is the distance between nodes at this position. The term *element* is used for the individual component of a stock. The stock was reused materials which have different dimensions. In Figure 7.1 it is possible to see the two ways for approaching the problem: the 1-to-1 *assignment* of elements to positions in the truss (as in Stock A), and a *cutting stock approach*, where multiple members can be cut from individual elements(as in Stock B).

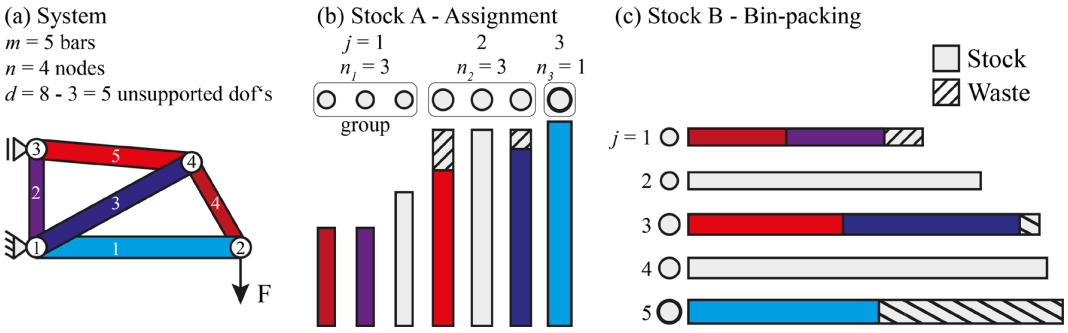

Fig. 7.1 (a) Cantilever truss, (b) stock A and assignment, (c) stock B and cutting stock configuration (image taken from Brütting et al. (2019b)

In the first case, which is the *assignment* problem, the objective of the optimization is to avoid waste by minimizing the long distance between members and stock elements. The second one is to find a cutting pattern which minimizes global waste.

Both cases were solved through a MILP (mixed-integer programming) procedure. Another problem addressed in the paper is that the lengths of the chosen elements may not correspond exactly to the lengths of the structure's members once both problems have been solved. For this reason, shape optimization is then used to reduce cut-off waste for the globally optimal assignment or bin-packing solutions by changing the placements of the structure nodes (coordinates).
Finally, Brütting et al. exposed also a procedure to optimize the configuration of a stock or kit-of-parts such that its elements can be reused in various structures. This last consideration allowed to spread of the stock of reusing items in many structures and the outcome is an ulterior minimization of the waste.
Ulterior amendments, only for the assignment problem, were done to this basic formulation in Brutting et al. (2019a) where the assignment was coupled with a topological optimization. After that, the truss was subjected to shape optimization. Is also noticeable the introduction of an absolute *buffer* that allows the allocation of also the very short items.
Moreover, the same authors (Brutting et al. 2020a) reported an entire structural optimization based on the principles set out above. In this work it is possible to see the simultaneous analysis and design approach, structural analysis is part of the optimization formulation by treating member end forces as well as nodal displacements and rotations as continuous state variables. Furthermore, designing a custom kit of parts (which is a group of discrete building parts that have been pre-engineered and are created to be put together in many ways to define a finished building) whose components are prepared to be combined in various structural configurations, serving diverse purposes, is an alternate approach to component reuse.
In one of the more recent papers, Brütting et al. (2021) use the assignment and CSP for creating a kit of parts used for three different construction types. The kit-of-parts bars are tubular components joined with bolts at spherical joints. The structures' original topology and geometry are provided as input. The process consists of two steps. To allow for the reuse of similar bars in different structures, the structural geometries and kit-of-parts bars' length and cross-section dimensions are optimised in the initial stage. The second stage optimises the hole pattern for the spherical joints' connection details, allowing each joint to be reused in many constructions.

7.4 Mathematical formulation of the problem

Now the following section analyzes the mathematical formulation of the cutting stock problem by using the column generation technique to reduce the problem's computational cost.

7.4.1 Bin Packing formulation

In order to understand how the cutting stock problem works it is necessary to exhibit the mathematical formulation of the one-dimensional bin packing problem. This problem aims to allocate a set of items into the minimum number of bins.
For initializing the problem are necessary the following parameters:

- I: set of items, indexed by i
- B: set of bins, indexed by b
- L_i: length of item i
- L: length of each bin
- $x_{i,b} \in \{0,1\}$: unitary if item i is allocated to bin k, 0 otherwise
- $y_b \in \{0,1\}$: unitary if bin b is used, 0 otherwise

The mathematical formulation of the problem is:

$$min \sum_{b \in B} y_b \tag{7.1}$$

Subjected to the following constraints:

$$\sum_{b \in B} x_{i,b} = 1 \quad \forall i \in I \tag{7.2}$$

$$\sum_{i \in I} L_i x_{i,b} \leq L y_b \quad \forall b \in B \tag{7.3}$$

$$x_{i,b} \leq y_b \quad \forall i \in I, \quad b \in B \tag{7.4}$$

$$x_{i,b} \in \{0,1\} \quad \forall i \in I, \quad b \in B \tag{7.5}$$

$$y_b \in \{0,1\} \quad \forall b \in B \tag{7.6}$$

The principal equation of the bin packing problem (7.1) simply minimizes the number of bins used to obtain the requested items. The mathematical equation was subjected to some constraints. In particular, the (7.2) equation means that each item must be assigned to a bin (i.e. each item should be cut from one of the paper rolls available). Additionally, the second condition (7.3) assures that the length of all items associated with a bin should not exceed the length of the bin and the third (7.4) entails that an item can be assigned to a bin if and only if that bin is used. Finally, the following two equation ((7.5), (7.6)) express the domains of the two decision variable $x_{i,b}$ and y_b.

7.4.2 Column generation

The bin packing problem is a very complex combinatorial problem. For simplifying this problem the Column Generation formulation is used in this thesis. In this formulation, the main element is no longer the bin, but the feasible cutting pattern, that is, the possible arrangement of items in a bin. Since enumerating all feasible cutting patterns is prohibitively time-consuming, it generates valid patterns iteratively and adds them to the problem according to their contribution to the objective function. The first step is to set up the restrained master problem (RMP).
The parameters involved into the column generation model are:

- I: set of unique items (subset of items with unique distinct lengths), indexed by i
- P: set of paths, indexed by p

- L_i: length of item i
- Q_i: quantity needed for item i
- L: length of each bin
- $M_{i,p}$: matrix whose element (i, p) defines the number of times item i is included in path p
- $x_p \in \mathbb{Z}$: number of times path p is chosen

The mathematical formulation is:

$$min \sum_{p \in P} x_p \tag{7.7}$$

Subjected to:

$$\sum_{p \in P} M_{i,p} x_p \geq Q_i \quad \forall i \in I \tag{7.8}$$

$$x_p \in \mathbb{Z} \tag{7.9}$$

The objective function of the RMP (7.7) is the minimization of the number of paths used which is strictly correlated with the minimization of the number of bins. The objective function is subjected to two constraints. First, it needs to select the number of paths in a way such that every unique item appears at least as many times as needed and this is what is done in (7.8). The second constraint defines the x_p domain.
The next step is to write the dual problem. The dual problem is a formulation correlated with the principal problem exposed above which is the primal. The dual problem is write in such a way that:

- A mostly horizontal constraint matrix becomes a mostly vertical constraint matrix
- A minimization problem (7.7) becomes a maximization problem (7.10)
- The objective value coefficients of the primal become constraint right hand side values of the dual

- The objective value coefficients of the dual are the dual values of the primal

In particular, the dual problem is:

$$max \sum_{i \in I} Q_i \lambda_i \tag{7.10}$$

Subjected to the following constraints:

$$\sum M_{p,i} \lambda_i \leq 1 \quad \forall p \in P \tag{7.11}$$

$$\lambda_i \in \mathbb{Z} \tag{7.12}$$

The λ_i is the dual value referred to a specific item constraint. Each dual value gives an indication of how profitable is to add the associate item to a new path. Moreover, to determine the best path to add it is necessary to set up the pricing problem where a new decision variable $y_i \quad \forall i \in I$ which represents how many times a certain item i appears in the new path. More in detail:

$$max \sum_{i \in I} \lambda_i y_i \tag{7.13}$$

Subjected to the following constraints:

$$\sum_{i \in I} L_i y_i \leq L \tag{7.14}$$

$$y_i \in \mathbb{Z} \tag{7.15}$$

Where the (7.14) ensures that the newly added path is feasible and the (7.15) imposes the y_i domain.
Forehead, to decide if a certain path should be added to the RMP it needs to verify the gain obtained by the addition of the new path with the following formula:

$$c - z \leq 0 \tag{7.16}$$

Where c is the original cost from the primal problem and z is the reduced cost computed in the pricing problem.
From the primal, it is possible to get $c = 1$ while from the pricing problem $z = \sum_{i \in I} \lambda_i y_i$. Finally by substituting:

$$1 - \sum_{i \in I} \lambda_i y_i \leq 0 \tag{7.17}$$

Which lastly becomes:

$$\sum_{i \in I} \lambda_i y_i \geq 1 \tag{7.18}$$

Until the previous condition is satisfied by the new generate path this one was added to the primal RMP and the procedure was iterated. To make more clear the overall process the algorithm is shown in the following:

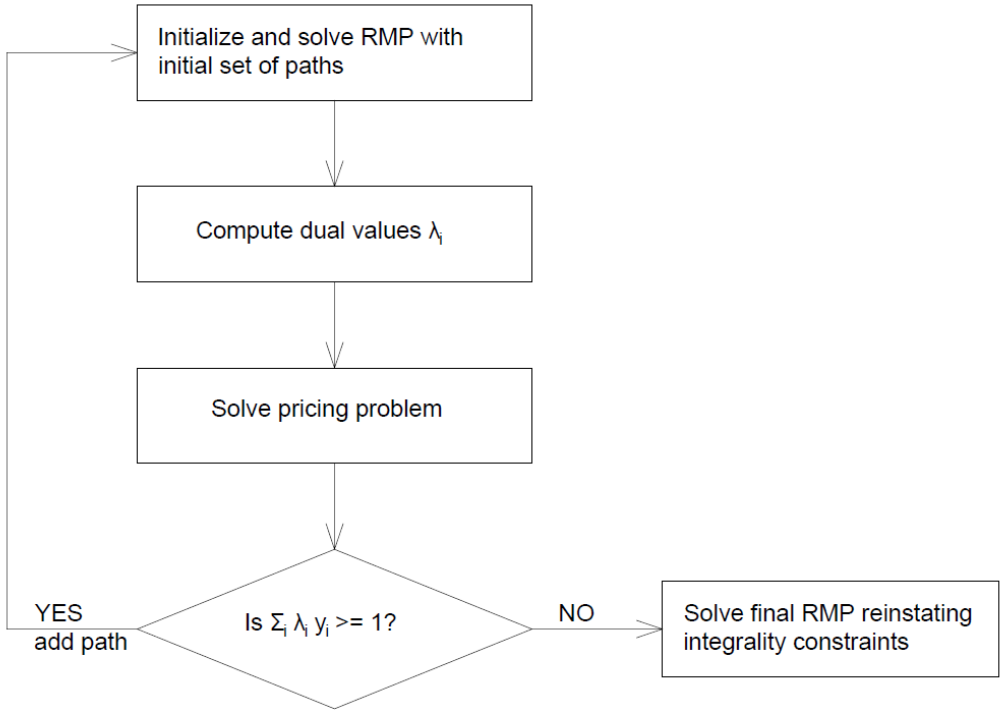

Fig. 7.2 Column Generation algorithm for the solution of Cutting Stock Problem

7.4.3 Numerical example

To a deeper understanding of the CSP functioning, in this section, a practical case study will be shown.
The input parameters are provided by the customer which gives the length and the number of items. In this case study it was assumed elements set which contained the items shown in the figure 7.3 (the lengths were assumed as adimensional for simplicity).

Fig. 7.3 Items requested by the customer

This data should be represented in two vectors:

$$I = \{2,3,4,5,6,7,8\} \tag{7.19}$$

$$Q = \{4,2,6,6,2,2,2\} \tag{7.20}$$

Where in the vector (7.19) are collected all the items' lengths and in (7.20) are collected the quantities for each item type.
Meanwhile, the producer provides the length of the bars available in the factory which becomes the bins of the CSP. In this example, the bin length was 9 $L_{bin} = 9$.

First, the matrix of the cutting pattern was initialized as an identity matrix:

$$M = \begin{bmatrix} 1 & 0 & 0 & 0 & 0 & 0 & 0 \\ 0 & 1 & 0 & 0 & 0 & 0 & 0 \\ 0 & 0 & 1 & 0 & 0 & 0 & 0 \\ 0 & 0 & 0 & 1 & 0 & 0 & 0 \\ 0 & 0 & 0 & 0 & 1 & 0 & 0 \\ 0 & 0 & 0 & 0 & 0 & 1 & 0 \\ 0 & 0 & 0 & 0 & 0 & 0 & 1 \end{bmatrix} \tag{7.21}$$

The matrix (7.21) simply contains all the pattern which contains only one item as shown in figure 7.4 for clarity: At this point, the initialization phase was over. After-

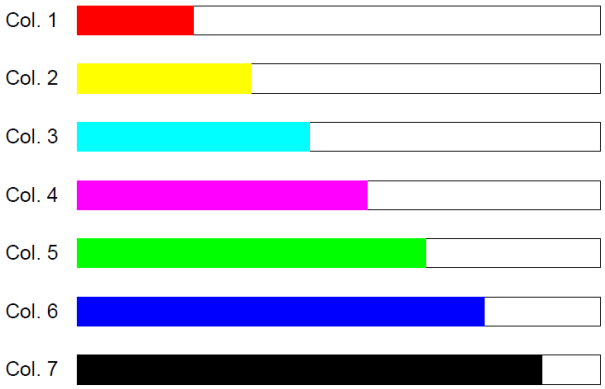

Fig. 7.4 Initial pattern at the iteration 0

wards, all the computation step exhibited in the previous subsection was performed. The entire process is iterated until the pricing problem returns a positive reduced cost. At each iteration, a new cutting pattern is added. In the following images, it is possible to see the pattern added for each cycle and the associated reduced cost.

Fig. 7.5 Iteration 1 where the reduced cost is -3.0000

Fig. 7.6 Iteration 2 where the reduced cost is -1.2500

Fig. 7.7 Iteration 3 where the reduced cost is -1.0000

Fig. 7.8 Iteration 4 where the reduced cost is -0.5000

Fig. 7.9 Iteration 5 where the reduced cost is -0.5000

Fig. 7.10 Iteration 6 where the reduced cost is -0.5000

Fig. 7.11 Iteration 7 where the reduced cost is -0.5000

Fig. 7.12 Iteration 8 where the reduced cost is -0.2500

Fig. 7.13 Iteration 9 where the reduced cost is -0.1250

At the end of the algorithm iterations the RMP is recomputed with all the new paths and it is possible to have the final results which are the number of bins ($N_{bins} = 13$) and the final cutting patterns related to each bin (shown in figure 7.14).

7.5 Cutting Stock Problem in truss beam optimization

In the last decades, the Scientific Community challenged on minimizing the structures' price by manipulating material, fabrication and maintenance costs. Specifically, in the structural optimization field, great attention was dedicated to materials cost minimization aiming to achieve a slender structure with optimal resource utilization. In this sense, the traditional approach adopted by researchers and practitioners is to optimize the design cost of structures while simultaneously satisfying safety recom-

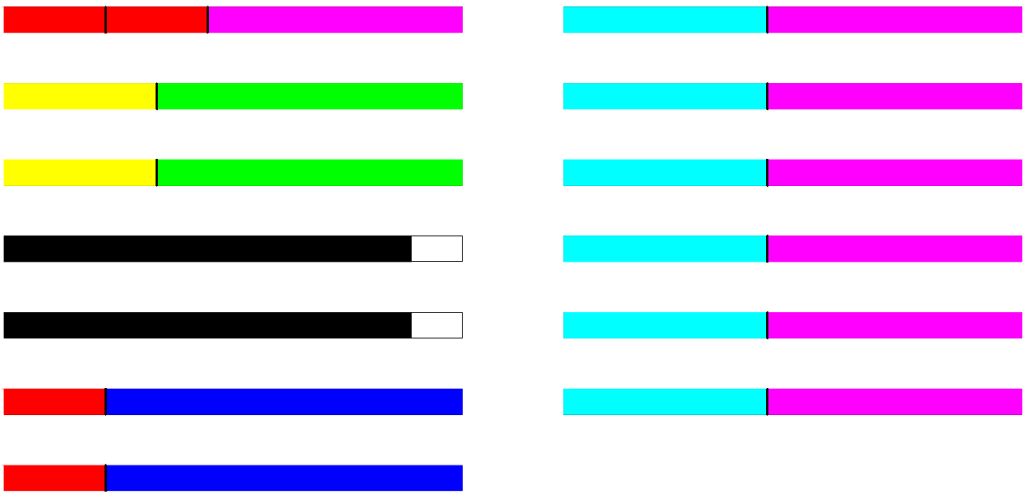

Fig. 7.14 Results from the CSP algorithm: bins and relative cutting patterns

mendations provided by specific standard regulations. Undoubtedly, this approach reduces the overall cost of the structure but does not take into account the effective quantity of steel involved in the process which is not only related to the material used in the structure but also to the factory waste resulting from the cutting process (an example of cutting machine in figure 7.15).
As demonstrated in the previous chapter, a significant part of the expenses is also the waste of material from the cutting process. In other words, minimizing the amount of material involved in the construction process without a carefully cutting design, for the minimization of waste, leads to inefficient cost optimization.
Hence, this thesis aims to create a structural optimization which not reduces the structural mass of the structure but the mass of the entire stock of rough bars involved in the construction. This ambitious goal was reached through the implementation of the Cutting Stock Problem (CSP) in the objective function of structural optimization.

In the initial chapters, it is possible to see the overall steps of structural optimization and how these steps work. Moreover, the previous chapters discuss how works the CSP and how this complex combinatorial problem was embedded in some reusing problems.
In the following, by combining the concepts exhibited in the first half of the thesis a new stock mass structural optimization was developed by the author and the respective supervisors of this dissertation.

Fig. 7.15 Beam cutting machine (image from www.asiacnc.com.tw)

When considering the cutting stock problem in the context of structural optimization, the goal is to design a structure that minimizes material usage while still meeting the required strength and stiffness criteria. This can be achieved by determining the optimal arrangement in the stock of items that make up the structure.

To solve this problem, mathematical models can be developed that represent the structural design and the material properties, as well as the constraints and objectives of the problem. These models can then be solved using optimization techniques such as linear programming, mixed-integer programming, or metaheuristic algorithms.

In addition to minimizing material waste, the cutting stock problem can also help reduce the overall cost and environmental impact of a structure. By optimizing the use of materials, the structure can be made lighter and more efficient, leading to savings in both production and operation costs, as well as reducing the carbon footprint of the project.

In a nutshell, the method exposed in the following is a weight minimization of the entire stock of factory bars where the truss members were cut. The problem was subjected to the serviceability and strength constraints and solved by a Genetic Algorithm with guided crossover.

The chapter is organized in order to have initially the mathematical formulation of the optimization than the overall algorithm with a detailed explanation of the CSP frow-chart implemented into the process. Afterwards, there is a section dedicated to the metaheuristic algorithm involved in the code and then the case studies and the relative setting parameters.

7.6 Mathematical formulation of the structural optimization

With respect to traditional optimization approaches (i.e Chan et al. (1995b), Van Mellaert et al. (2016), Kaveh and Bakhshpoori (2013), Hayalioglu and Saka (1992b)) in which the objective function represents the total weight of the structure as a sum of the mass of each element (structural mass), in this study the target function has been evaluated by computing the amount of steel requested during the production phase (stock mass). To achieve this goal, a real-coded guided-Genetic Algorithm (GA) has been developed by the author and the supervisors of the thesis. The design variables are the only discrete cross-sectional areas (taken from the cross-sectional commercial catalogue) of each element in case of a size optimization where is added the members' length in case of a combined size-shape optimization. CSP has been implemented within the optimization process and it has been independently solved for all groups of elements with the same cross-sectional properties. Finally, the solution obtained by the CSP for each group has been adopted for the evaluation of the objective function $W(x)$ expressed as follows:

$$W(x) = \phi_1 \rho \sum_{g=1}^{g=k} n_g A_g L_g \tag{7.22}$$

$W(x)$ is the optimization objective function and represents the total mass, more precisely the sum of the purchased bars' weight for each group g. Specifically, k represents the total number of groups of elements with the same cross-sectional areas. n_g, A_g and L_g are the cardinality, the cross-sectional area and the length of bins belonging to the same group g of elements with the same cross-sectional area A_g, respectively. ρ is material the mass density assumed to be equal for all members composing the structure (in this case the steel density).
The problem is constrained in order to guarantee structural conformity to the technical standards and these constraints are incorporated in the OF as a penalty coefficient ϕ_1. In figure 7.16 it is possible to see the general flowchart of the entire optimization.

STEP 1 Set the input assumption of the optimization problem. First, the model assumption as the features correlated with the geometry of the structure (number of elements and truss topology and eventual symmetry), the loading pattern

(position, values and eventual symmetry) and the material properties (Young modulus E and density ρ). Afterwards, set the algorithm's parameters (number of iterations, number of individuals N per population, mutation probability and probability for roulette wheel parents selection)

STEP 2 Generate a random initial population with N individuals (N different trusses having the same topology but different design variables). The design variables are size and eventually shape parameters. The algorithm works with discrete design variables taken from commercial standards.

STEP 3 Perform the structural analysis for the given load condition in order to find the structural behaviour and verify the structural conformity to the Eurocode 3 (EN 1993-12005 and EN 1993-2 2006). The structural analysis is performed by a FEM code which uses the Direct Stiffness Method (DSM).

STEP 4 Computation of the overall penalty ϕ_1 related to the violation of the optimization constraints. The penalties are coefficients that increment the objective function of the individuals which not satisfy the problem constraint in order to penalize the unfeasible solutions. Specifically, the penalties are computed for each violation by penalty functions. The results of the penalty functions are coefficients ϕ_i for each i violation (e.g. strength, deflection, etc...). The final penalty ϕ_1 is the sum of the single penalty ϕ_i.

STEP 5 Verify if at least 1% of the entire population is feasible. If this condition is not satisfied reinitialize the entire population (return to *STEP 2*) with a discrete design variable domain reduce by a certain number of cross-sections. These excluded cross-sections are the smaller ones in order to increase, in the next iteration, the probability to have a population which fits the feasibility request of this decision point.

STEP 6 To obtain the number of standard commercial bars purchased and the relative cutting patterns for each cross-sectional group g. The grouping on the elements is necessary because the items with the same cross-sectional area should be allocated in the same bar typology. The CSP allocates the various structural members into the standard factory bars in an optimal way in order to minimize waste. For more details see figure 7.17 and the relative explanation.

STEP 7 Evaluation of the objective function $W(x)$ which return the total mass of the purchased bars.The OF is simply the sum of the purchased bars' mass resulting

from the CSP for each cross-sectional group g multiplied for the overall penalty ϕ_1. The goal of the optimization is to reach the minimum $W(x)$.

STEP 8 Check of the stagnation condition. This step avoids the algorithm stuck in a local optimum while trying to search for a global optimum. Specifically, this condition verifies if the best solution is the same for a predetermined consecutive number of iterations. Whether the response is affirmative the optimization process re-initializes the population (return to *STEP 2*) in order to explore other solution spaces. Otherwise, the optimization process continues with the following steps.

STEP 9 This condition simply check if the imposed number of iteration is reached. Whether the number of the current iteration is lower the process comes to *STEP 3* otherwise continue with the plotting of the output results.

STEP 10 The outputs of the entire optimization process are final member properties, the overall mass of purchased steel, the number of bars for each cross-sectional class and the relative cutting pattern relative to the optimal individual.

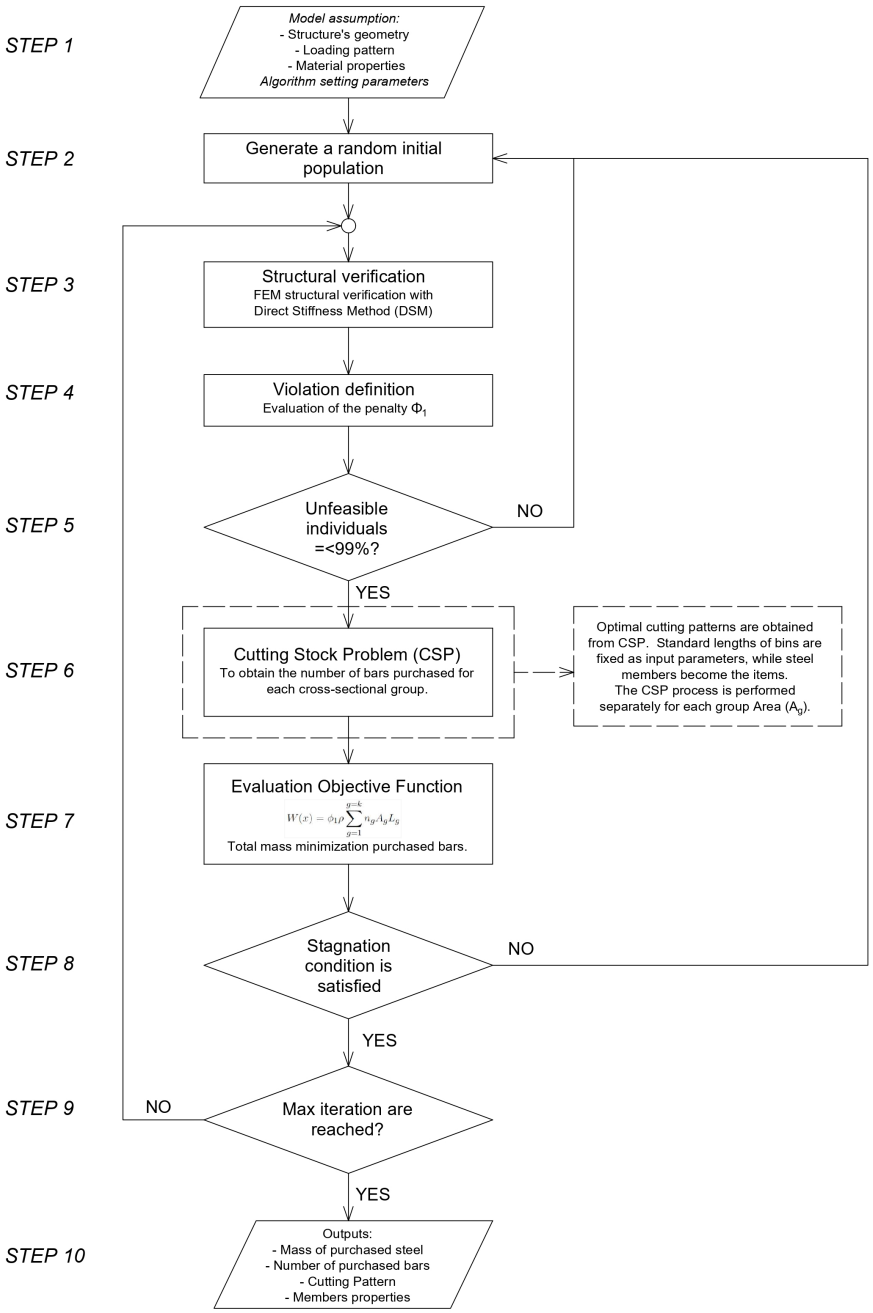

Fig. 7.16 Structural Optimization via CSP problem algorithm

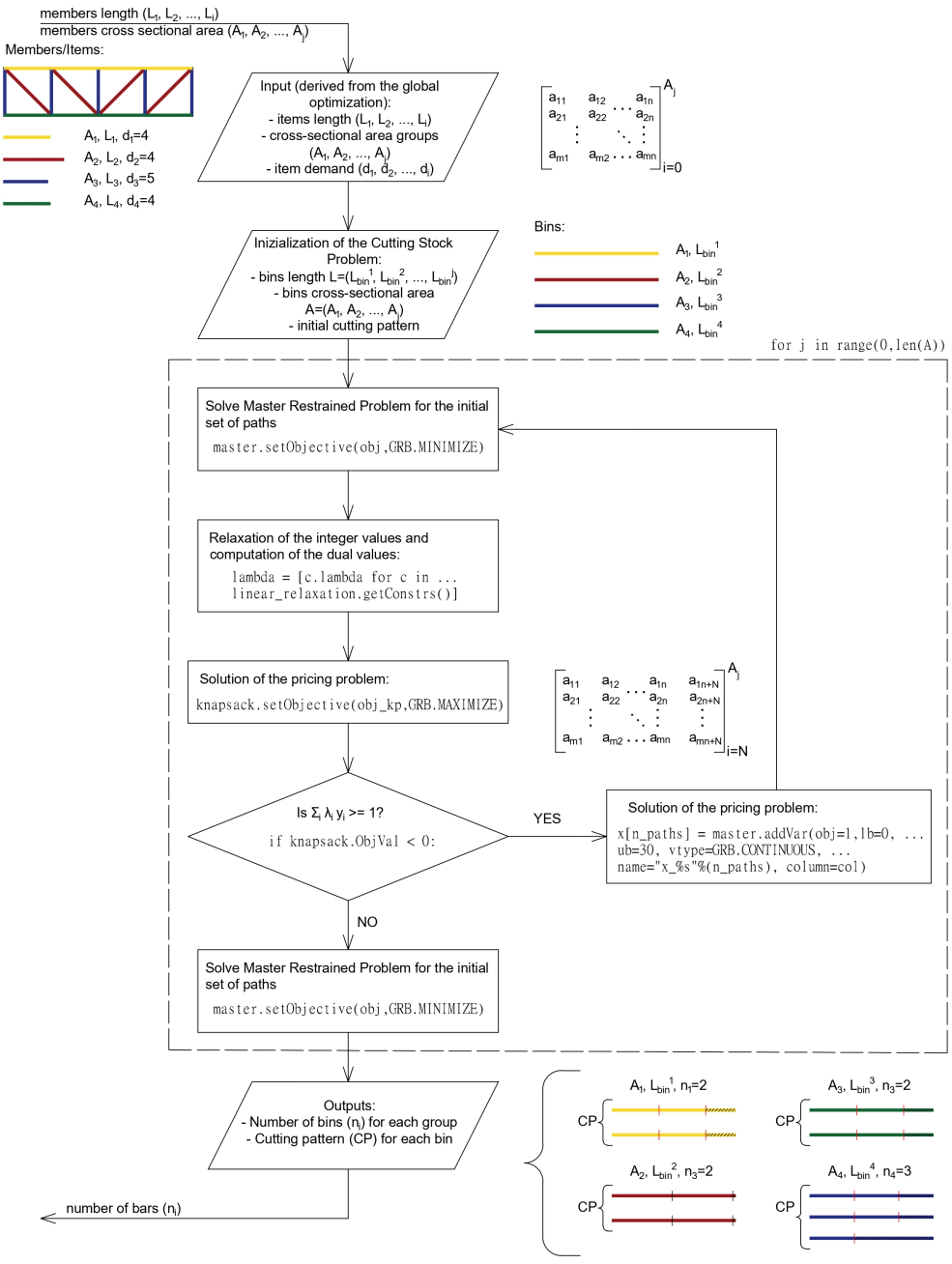

Fig. 7.17 Detailed CSP algorithm embedded in the structural optimization

7.7 GA with guided crossover

In order to solve the problem stated in previous section, a real-coded GA is adopted. This is a population-based stochastic optimization technique appropriate for global optimization, which does not require direct evaluation of gradients. Introduced by John Holland Holland (1992), it is inspired by Charles Darwin's theory of natural evolution. This algorithm reflects the process of natural selection where the fittest individuals, also called parents, are selected for reproduction in order to produce offspring of the next generation. At the end of the process, the best survival among all the fittest candidates found at each generation is selected as the best globally optimized solution. Although the native GA worked with binary values representing genes, encoded in string structures called chromosomes, in this paper the authors overcome the limits related to the decoding process by using a real-code GA in which genes and chromosomes represent directly the design variables and the solutions of the problem.

At each iteration, traditional GA phases were adopted during the optimization as following:

- **Initial population**: in this phase, individuals with a set of random genes (x_i) composing chromosomes (x) are created by observing lower and upper bounds reported in table. Gene represents, at each generation, the candidate value of a specific design variable involved in the identification procedure. A set of genes (vector form) represent a solution of the problem for the current generation. In this way, the best solution is selected and the optimal set of parameters which govern that specific law is detected.
- **Fitness function**: in this phase, the fitness of the candidate solutions is evaluated by calculating the OF introduced in the previous section.
- **Selection**: During this phase, a Roulette Wheel Selection was implemented in order to guarantee that the two fittest parents are selected for the next steps. Adopting this technique, a probability to each parent is assigned and the parents with higher fitness are more likely to be chosen for the next steps.
- **Crossover**: in this phase, a single point crossover was performed in which recombination of gene pool between parents occurs after a position selected in a random way fro each parent. Lower and upper bounds are imposed at this

stage such that if only a gene of the new offspring is not ranged within the imposed interval (higher than the maximum value or lower than the minimum value of that specific parameter), it is forced to assume maximum or minimum value, respectively.

- **Mutation**: aiming to improve the exploration and exploitation ability of the algorithm, a mutation rate of 1% is assigned. In this way, new genes are introduced into the population by modifying gene pools of parents in a random way.

At the end of these stages, a sorted function was implemented aiming to store survivors with the best fitness among the generated offspring, at each generation. The identification procedure can be considered ended when the stopping criteria of the algorithm are satisfied and the optimal set of parameters for each law is found. The entire procedure was run n times in order to check the reliability and robustness of the algorithm. Specifically, the authors observed that stagnation usually occurred for the algebraic models while no differential ones needed to use all the available 200 generations.

7.8 Case study 1: 10-bar truss

Within this section, it will be exhibited a simple application of CSP embedded in structural optimization. The structure under analysis in this section is a ten-bar truss benchmark coming from **?**. The case study is simple and the optimization assumptions are minimal just to check the results.
The section is divided into two subsections, the first show the model definition and the set of algorithm parameters and, afterwards, another subsection exposes and discusses the results.

7.8.1 Model definition and parameters' setting

As reported in Figure 7.18, the structure is a trussed isostatic cantilever composed of 10 steel bars and constrained by two pinned supports at nodes 5 and 6, respectively. A single-loading condition P_1 has been assumed and, specifically, two equal forces P_1 are applied at nodes 2 and 4.

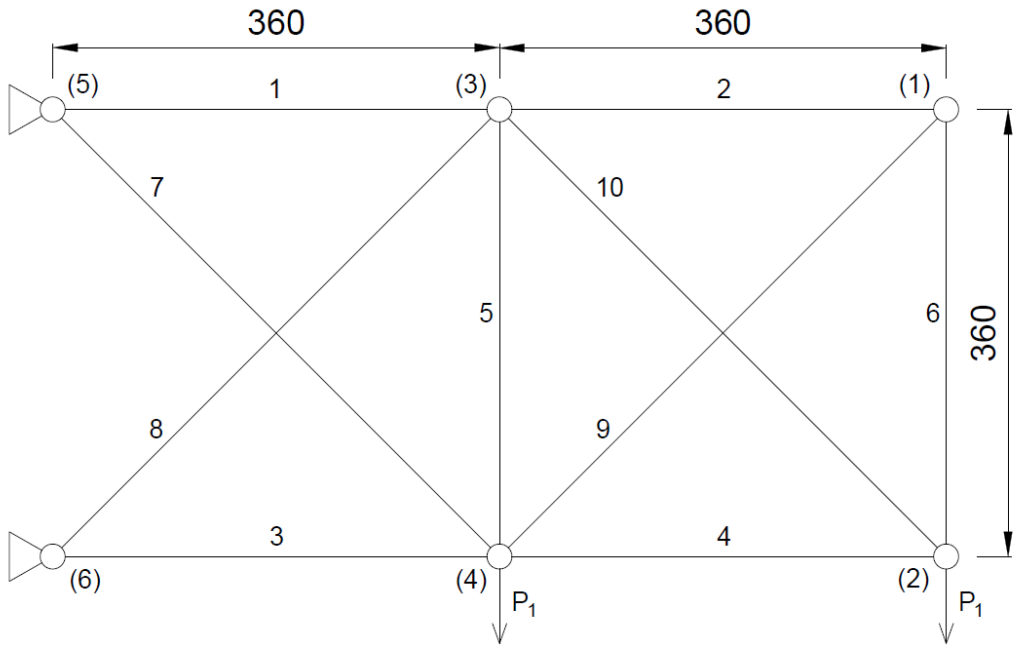

Fig. 7.18 Configuration of the in-plane 10-bar truss, measures are expressed in inches (in.)

For having a resume of numerical model assumption on the material and geometry of the truss the table 7.1 was created.

Parameter	**Value**
Modulus of elasticity of steel E	10000 ksi
Steel density ρ	0.10 lb/in^3
Loading P_1	100 $kips$
Length of purchased bars (bins) L_{bin}	1020 in
Number of design variables	10
Bounds of design variables (A_{min},A_{max})	[1.62, 33.5] in^2

Table 7.1 Model assumption relative to the 10 bar truss.

The design variables of the problem are simply the 10 cross-sectional areas of the truss components. The problem was solved by a GA algorithm which works with discrete values. This procedure allows taking into account only solutions with elements which have cross-sectional areas available in the commercial standards list. Therefore, a set of 42 discrete values (shown in table 7.2) have been used for the possible cross-sectional areas for each member. In this simplified optimization

it was not taken into account the elemental buckling and, for this reason, only the cross-sectional areas of the elements are sufficient as sectional properties.

Discrete cross-sectional areas A $[in^2]$						
1.62	1.8	1.99	2.13	2.38	2.62	2.63
2.88	2.93	3.09	3.13	3.38	3.47	3.55
3.63	3.84	3.87	3.88	4.18	4.22	4.49
4.59	4.8	4.97	5.12	5.74	7.22	7.97
11.5	13.5	13.9	14.2	15.5	16	16.9
18.8	19.9	22	22.9	26.5	30	33.5

Table 7.2 Discrete cross-sectional standard area within the design variables are chosen.

Now the assumptions related to the model are imposed. It is possible to proceed with the optimization statement.
The statement of the entire optimization process is the following:

$$\min f(x) = W(x) \tag{7.23}$$

$$\textbf{Subject to} \quad \frac{N_{ED}}{N_{t,RD}} \leq 1 \tag{7.24}$$

$$\frac{N_{ED}}{N_{c,RD}} \leq 1 \tag{7.25}$$

$$u_{max,x} \leq u_{lim,x} \tag{7.26}$$

$$u_{max,y} \leq u_{lim,y} \tag{7.27}$$

The goal of structural optimization is the minimization of the objective function $W(x)$ (see (7.22)) correlated to the stock mass.
Equations from (7.24) to (7.27) represent the structural constraints of the problem. In detail, strength verifications about tensile stress (without any holes) and compression stress according to Eurocode 3 (EN 1993-12005 and EN 1993-2 2006) are introduced by Equations (7.24) and (7.25) respectively. Other constraints to satisfy is the maximum deflection along x and y directions (represented by Equations (7.26)

and (7.27), respectively).
To apply the previously seen constraints to the optimization process a penalty coefficient ϕ_1 is multiplied by the stock mass. In this way, the unfeasible solutions are penalized with respect to the feasible ones.
The penalty applied to the SO is the sum of the single penalty related to the single violation:

$$\phi_1 = \phi_{Nc} + \phi_{Nt} + \phi_{ux} + \phi_{uy} \tag{7.28}$$

In particular, the violation functions are simply equal to the sum of the verification ratios

$$\phi_Q = \sum_{i}^{i=v} \frac{Q_{Ed}^{i}}{Q_{lim}} \tag{7.29}$$

Where Q is the constraint parameter (stress or deflections) for an element of the truss i which does not satisfy the constraint condition. The overall penalty related to a constraint ϕ_Q is the sum of the violation of all the violated items v. Particularly, the effective solicitation or deflection is at the numerator and the limit value is at the denominator. The displacements of the free nodes in both directions had to be less than ±2 in. and the allowable stress was set to ±25 ksi.
In this specific case study, two attempts were done with the implementation of an additional penalty ϕ_R related to the ripetitivity of the cross-section among the design variables.

$$\phi_R = kN_{single_A} \tag{7.30}$$

Where k is a proportional coefficient which set the impact of the ripetitivity penalty on the objective function. Conversely, N_{single_A} is the number of different areas present within the design variable. This penalty is added to the (7.22) but as it will exposes more in detail in the next paragraph the results are worse compared the original formulation.

The algorithm setting parameters are collected in table 7.3.

Parameter	Value
Maximum number of iterations	200
Number of individuals per population	200
Areas excluded if unfeasibility condition isn't satisfied	5 smaller DV
Mutations' probability	1%
Proportional children	1 child for each parent
Stagnation condition	10 iterations

Table 7.3 Optimization algorithm parameters set by the operator.

7.8.2 Results and discussion

In this section, the results of the structural optimization (SO) process with specific regard to the ten-bar case study are pointed out. Specifically, two optimization scenarios have been performed:

- Scenario (a): optimization by considering CSP (minimization of purchased steel bars).
- Scenario (b): optimization via traditional approach by minimizing the total weight of the structure without considering the CSP procedure.

In order to have a comparison between the two mentioned-above approaches, the CSP procedure has been performed at the end of (b) such that the total number of bins requested for the assemblage of the optimal weight structure has been evaluated. Afterwards, a case of the SO via CSP with the implementation of the ripetitivity penalty is exhibited.

Scenario (a) In scenario (a) 10 runs are performed through SO via CSP and the results are summarised in table 7.6 at the end of the section. Afterwards, from the data collected the best result and the mean value and standard deviation are collected in the following table 7.4.

The first observations concern the operation of the CSP in the SO. It can be seen that the results tend to have each bar with a different cross-section, containing 2 elements per bar (corresponding to the maximum number of elements that can be allocated in a bar). These two features allow for obtaining the best results because exploit at the maximum capacity the bars and simultaneously have a good degree of

	Stock Mass (OF) [lb]	Structural Mass [lb]	Waste Mass [lb]
Best	6825.84	5791.97	1033.87
μ	7320.13	6158.41	1161.73
σ	308.64	257.05	98.37

Table 7.4 Result of the optimization via CSP related to Scenario (a)

freedom in the size optimization of the elements.
In other words, the OS works on two levels: the correct choice of cutting pattern to maximise the utilisation of the bars and the selection of the minimum cross-sectional area for each bar.
Figure 7.19 gives a more clear view of the bars' exploitation in scenario (a).

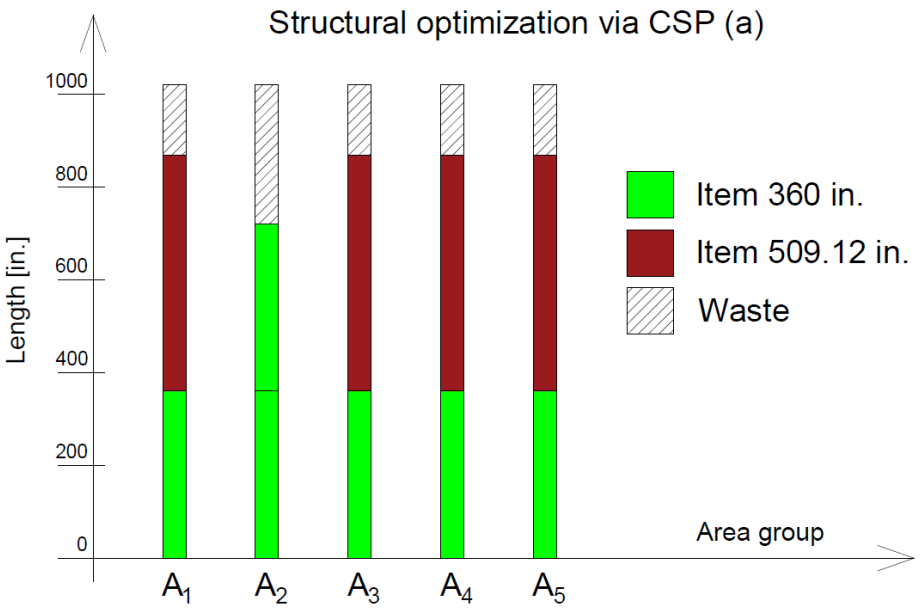

Fig. 7.19 Optimal cutting pattern derived by optimization scenario (a)

To show how the algorithm works in more detail, the plots of the best solution (Figure 7.20), the violation (Figure 7.21) and the unfeasibility (Figure 7.22) for each iteration are presented on following.

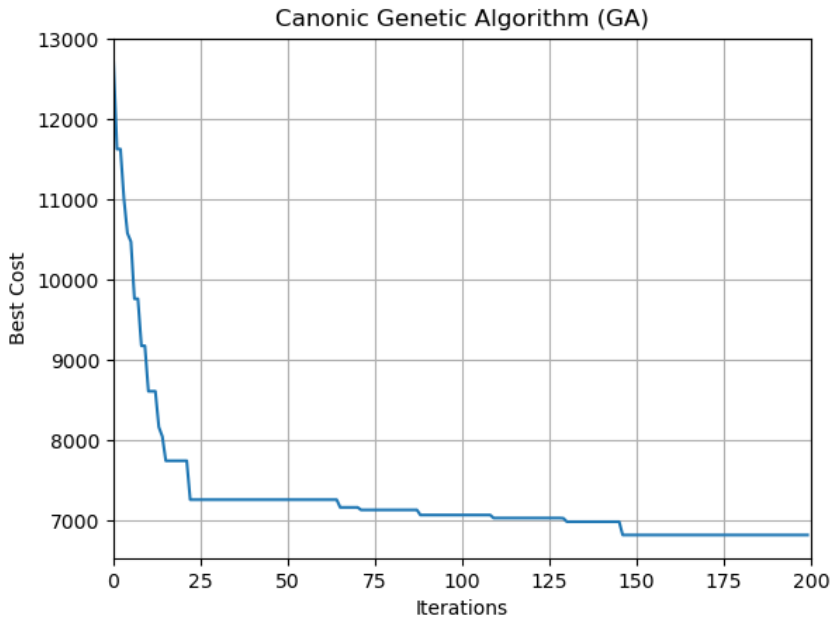

Fig. 7.20 OF best solution for each iteration related to Scenario (a)

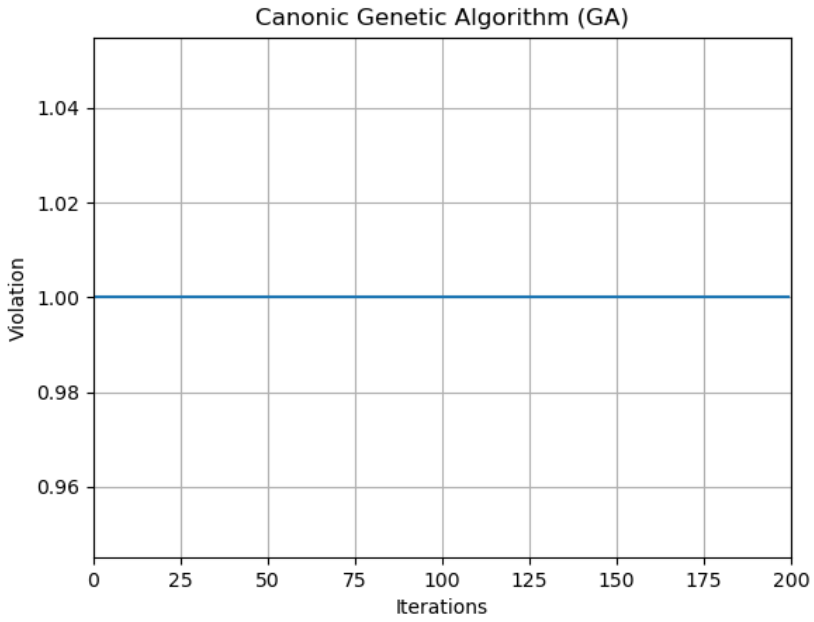

Fig. 7.21 OF violation for each iteration related to Scenario (a)

Scenario (b) Scenario (b) consists again of 10 runs performed with a traditional structural optimization which minimizes the total structural mass only. The mass

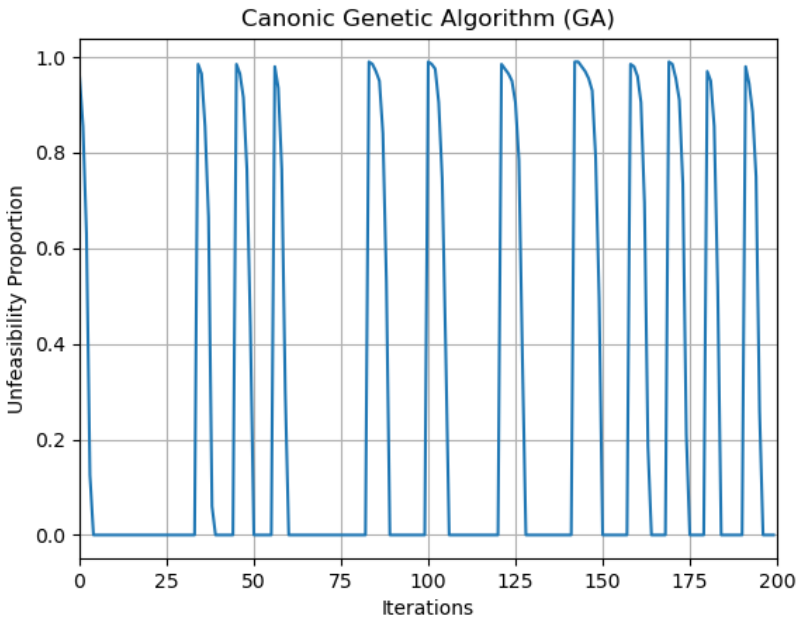

Fig. 7.22 OF unfeasibility for each iteration related to Scenario (a)

of the stock was obtained successively by applying the CSP to the cross sections obtained. The results of the 10 runs are summarised at the end of the section in table 7.7. The best solution, the average solution and the standard deviation are collected in the following table.

	Stock Mass (OF) [lb]	Structural Mass [lb]	Mass Waste [lb]
Best	10323.42	5580.42	4743.00
μ	12133.92	5632.88	6501.04
σ	1343.16	64.15	1348.10

Table 7.5 Result of the optimization via traditional approach (b)

On following the stock representation (Figure 7.23) and the plots of the best solution (Figure 7.24), the violation (Figure 7.25) and the unfeasibility (Figure 7.26) for each iteration.

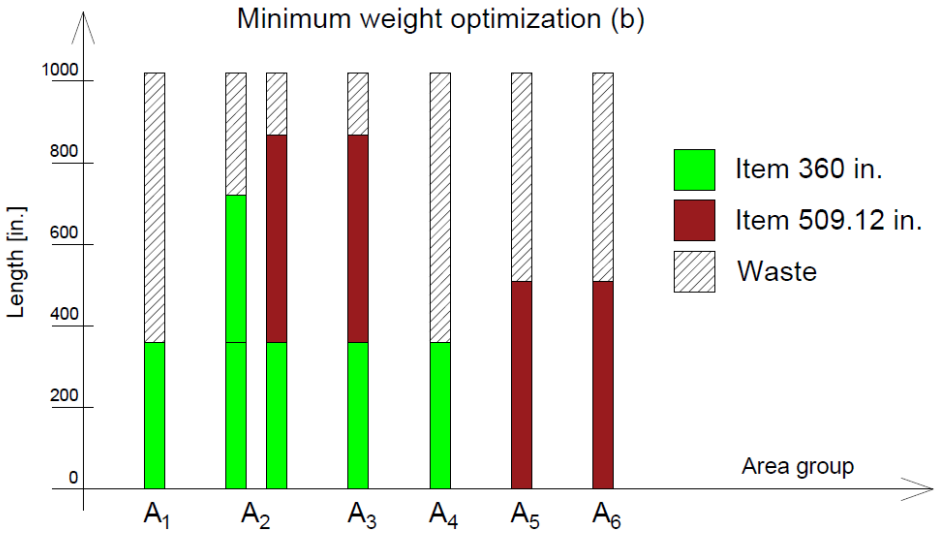

Fig. 7.23 Optimal cutting pattern derived by optimization scenario (b)

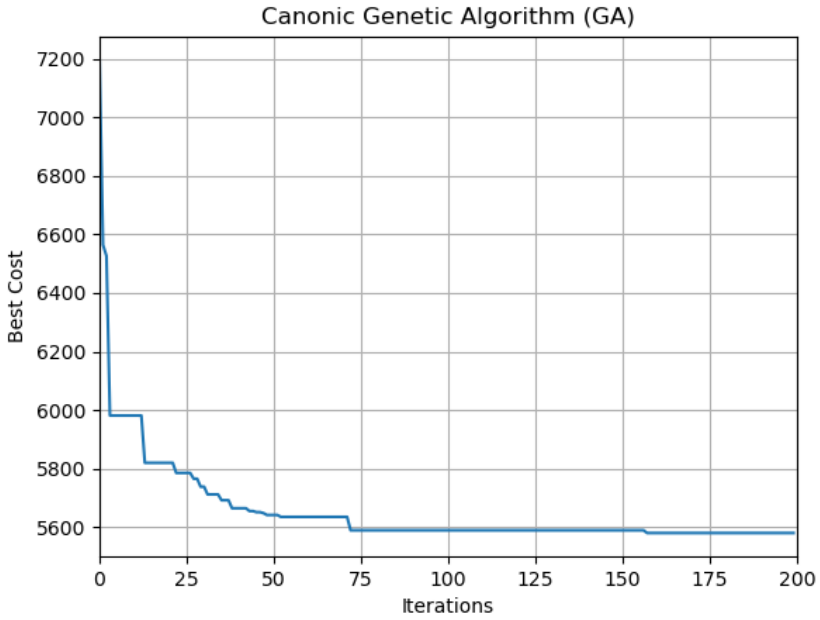

Fig. 7.24 OF best solution for each iteration related to Scenario (b)

Now it is possible to compare the results of the two optimizations (Scenario (a) and Scenario (b)). The first important result is that the stock mass is much lower in Scenario (a) versus a small increment of the structural mass which is very similar between the two scenarios. From these considerations, it is possible to deduce that the algorithm with embedded the CSP perform well because requests fewer

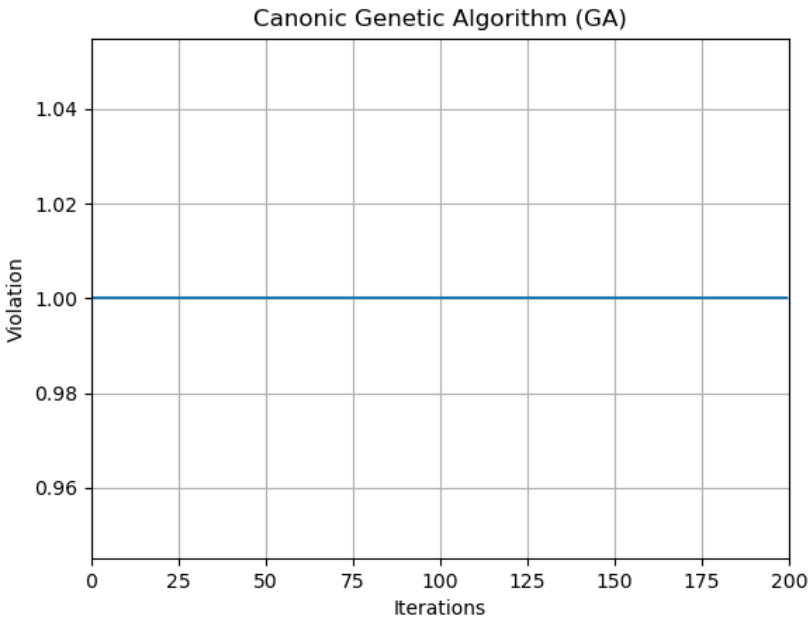

Fig. 7.25 OF violation for each iteration related to Scenario (b)

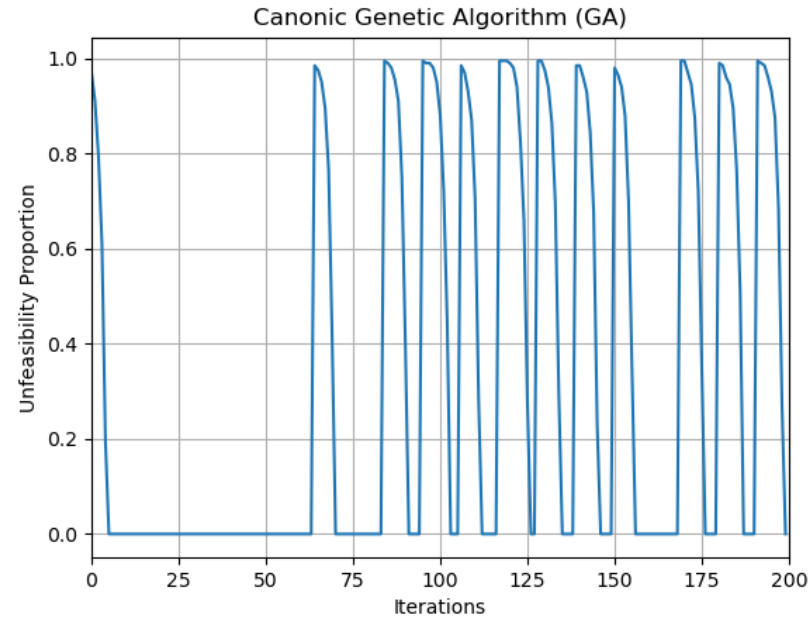

Fig. 7.26 OF unfeasibility for each iteration related to Scenario (b)

purchased bars with a small increment of the structural weight.
Another consideration is about the variability of the problem which presents better

results in terms of a stock mass standard deviation in scenario (a) and regarding the structural mass the standard deviation is lower in scenario (b). Moreover, the standard deviations' values of the relative OF (stock mass for (a) and structural mass for (b)) penalize scenario (a) because the variability of the cutting pattern does not allow to have a strong convergence of the results.

Attempt	Cross-sectional areas [in^2]	Number of bins	Structural Mass [lb]	Stock Mass [lb]	Waste Mass [lb]
1	[30.0 1.99 22.0 22.0 1.99 4.18 13.9 13.9 30.0 4.18]	[1, 1, 1, 1, 1]	6113.27	7351.14	1237.87
2	[18.8 4.22 26.5 18.8 1.8 1.8 26.5 22.0 22.0 4.22]	[1, 1, 1, 1, 1]	6393.24	7478.64	1085.40
3	[30.0 1.8 30.0 13.5 1.8 1.62 13.5 22.0 22.0 1.62]	[1, 1, 1, 1, 1]	5843.82	7029.84	1186.02
4	[22.0 1.62 22.0 22.0 1.99 1.62 22.9 22.0 22.9 1.99]	[2, 1, 1, 1]	6117.41	7192.02	1074.61
5	[30.0 1.99 30.0 13.5 1.99 1.99 13.5 22.0 22.0 1.99]	[1, 2, 1, 1]	5889.66	7086.96	1197.30
6	[30.0 1.62 22.0 11.5 1.62 1.8 11.5 22.0 30.0 1.8]	[1, 1, 1, 1, 1]	5791.97	6825.84	1033.87
7	[30.0 3.13 22.9 15.5 3.13 2.88 15.5 30.0 22.9 2.88]	[1, 1, 1, 1, 1]	6420.43	7589.82	1169.39
8	[26.5 4.49 26.5 13.9 4.49 15.5 15.5 16.9 16.9 13.9]	[1, 1, 1, 1, 1]	6507.30	7883.58	1376.28
9	[26.5 3.87 26.5 13.9 2.88 2.88 26.5 26.5 13.9 3.87]	[2, 1, 1, 1]	6358.10	7512.30	1154.20
10	[26.5 1.99 22.0 18.8 1.99 1.8 26.5 18.8 22.0 1.8]	[1, 1, 1, 1, 1]	6148.88	7251.18	1102.30

Table 7.6 Structural Optimization via CSP results of 10 runs. Scenario (a)

Attempt	Cross-sectional areas [in^2]	Number of bins	Structural Mass [lb]	Stock Mass [lb]	Waste Mass [lb]
1	[30. 1.8 26.5 14.2 1.62 1.62 13.5 18.8 22. 1.62]	[1 1 1 1 2 1 1 1]	5573.62	13264.08	7690.46
2	[30. 1.8 26.5 16. 1.62 1.62 11.5 18.8 22. 1.8]	[1 1 1 1 1 1 1 1]	5545.762334	13078.44	7532.68
3	[22.9 1.62 30. 13.9 1.62 1.62 15.5 22. 22.9 1.8]	[1 2 1 1 1 1 1]	5746.47	11152.68	5406.21
4	[30. 1.62 26.5 11.5 1.62 1.62 7.97 26.5 22. 1.62]	[1 2 1 1 1 1]	5580.42	10323.42	4743.00
5	[30. 3.38 26.5 13.5 1.62 1.8 15.5 16.9 22. 3.47]	[1 1 1 1 1 1 1 1 1 1]	5711.06	13736.34	8025.28
6	[26.5 1.62 22.9 15.5 1.62 1.62 13.5 22.9 22.9 1.62]	[1 2 2 1 1]	5612.90	10663.08	5050.18
7	[30. 1.62 26.5 13.9 1.62 1.62 13.5 22. 18.8 2.38]	[1 2 1 1 1 1 1 1]	5595.03	13292.64	7697.61
8	[26.5 1.8 30. 14.2 1.62 1.62 13.9 22.9 18.8 1.99]	[1 1 1 1 1 1 1 1 1]	5658.64	13434.42	7775.78
9	[30. 1.8 26.5 15.5 1.8 2.13 16. 18.8 18.8 2.88]	[1 1 1 1 1 1 1 1]	5673.77	11588.22	5914.45
10	[26.5 2.13 26.5 16. 1.62 1.8 14.2 18.8 22.9 1.99]	[1 1 1 1 1 1 1 1 1]	5631.08	10805.88	5174.80

Table 7.7 Traditional Structural Optimization (Structural mass only) results of 10 runs. Scenario (b)

Ripetitivity penalty With the idea of helping the algorithm find better results in terms of stock mass, a ripetitivity penalty was introduced that increases the OF value based on the number of different cross-sectional areas between the design variables. Therefore, greater is the number of cross-sectional different areas greater is the penalty.

$$\phi_R = kN_{single_A} \tag{7.31}$$

Where k and N_{single_A} are a coefficient which set the impact of the penalty on the OF and the number of different areas present within the design variable respectively. In the following pages in the tables 7.10 and 7.11 are presented the results of 10 runs (for k=0.1 and k=0.2 respectively). Meanwhile, in the following table the best solution, the average one and the standard deviation are collected (table 7.8 and 7.9)

	Stock Mass (OF) [lb]	Structural Mass [lb]	Mass Waste [lb]
Best	7127.76	6043.71	1084.05
μ	8128.38	6751.39	1376.99
σ	664.19	467.16	248.40

Table 7.8 Result of the optimization via CSP considering ripetitivity ($k = 0.1$)

	Stock Mass (OF) [lb]	Structural Mass [lb]	Mass Waste [lb]
Best	8051.88	6816.97	1234.91
μ	8768.23	7367.95	1400.28
σ	611.95	549.00	209.11

Table 7.9 Result of the optimization via CSP considering ripetitivity ($k = 0.2$)

The algorithms despite the low values of k do not work properly. The OF values are worse and the standard deviation too. These results show that considering the ripetitivity in this specific problem makes the algorithm more rigid because forces purchased bars to have the same cross-sectional areas. Therefore, a reduction of the degree of freedom in the problem has as a consequence less difference in item areas. Moreover, the reduction of the available area produces items with an overestimated cross-sectional area which increase both the structural and stock mass.

Attempt	Cross-sectional areas [in^2]	Number of bins	Structural Mass [lb]	Stock Mass [lb]	Waste Mass [lb]
1	[22.9 13.9 22.9 14.2 7.97 7.97 22. 22. 14.2 13.9]	[1, 1, 1, 1, 1]	6904.97	8258.94	1353.97
2	[26.5 4.97 26.5 13.9 4.97 13.9 13.9 26.5 13.9 26.5]	[2, 1, 2]	7380.30	8748.54	1368.24
3	[30. 4.49 22.9 22.9 1.99 1.99 30. 16. 16. 4.49]	[1, 1, 1, 1, 1]	6418.84	7688.76	1269.92
4	[30. 1.99 22. 13.9 1.99 1.99 13.9 30. 22. 1.99]	[1, 2, 1, 1]	6043.71	7127.76	1084.05
5	[26.5 14.2 26.5 14.2 16.9 3.47 16.9 26.5 26.5 3.47]	[2, 1, 1, 1]	7399.11	8932.14	1533.03
6	[30. 13.9 30. 13.5 13.5 13.5 13.5 13.9 16. 16.]	[1, 1, 2, 1]	7142.55	8863.80	1721.25
7	[22.9 4.8 22.9 15.5 4.8 7.97 15.5 30. 30. 4.8]	[1, 2, 1, 1, 1]	6927.53	8768.94	1841.41
8	[30. 4.18 30. 7.22 4.18 7.22 16. 18.8 16. 18.8]	[1, 1, 1, 1, 1]	6524.25	7772.40	1248.15
9	[26.5 3.87 22. 22. 2.38 2.38 26.5 18.8 18.8 3.87]	[1, 1, 1, 1, 1]	6309.15	7502.10	1192.95
10	[22. 1.99 30. 13.5 7.22 1.99 30. 13.5 22. 7.22]	[1, 1, 1, 1, 1]	6463.50	7620.42	1156.92

Table 7.10 Structural Optimization via CSP including ripetitivity (k=0.1) results of 10 runs

Attempt	Cross-sectional areas [in^2]	Number of bins	Structural Mass [lb]	Stock Mass [lb]	Waste Mass [lb]
1	[26.5 7.22 26.5 7.22 7.22 7.22 26.5 26.5 11.5 11.5]	[2, 2, 1]	6816.97	8051.88	1234.91
2	[30. 4.49 30. 4.59 4.49 4.59 30. 15.5 30. 15.5]	[2, 1, 1, 1]	7446.72	8627.16	1180.44
3	[26.5 22. 26.5 16.9 4.59 4.59 22. 11.5 16.9 11.5]	[1, 1, 1, 1, 1]	6790.31	8311.98	1521.67
4	[30. 4.8 16. 16.9 4.8 16.9 18.8 16. 30. 18.8]	[1, 1, 1, 1, 1]	7474.62	8823.00	1348.38
5	[26.5 4.49 26.5 16. 1.99 16. 16. 16. 16. 16.]	[1, 1, 3, 1]	6551.63	8259.96	1708.33
6	[30. 7.22 30. 7.22 2.38 2.38 30. 30. 13.9 13.9]	[2, 1, 1, 1]	7321.25	8517.00	1195.75
7	[22.9 26.5 26.5 16. 16. 7.97 26.5 7.97 26.5 22.9]	[1, 2, 1, 1]	8441.28	10186.74	1745.46
8	[22.9 26.5 26.5 7.97 7.22 7.22 26.5 22.9 26.5 7.97]	[1, 2, 1, 1]	7809.12	9291.18	1482.06
9	[30. 1.99 30. 7.97 7.97 1.99 30. 15.5 30. 15.5]	[2, 1, 1, 1]	7510.08	8716.92	1206.84
10	[30. 11.5 30. 11.5 4.22 4.22 30. 11.5 30. 11.5]	[2, 2, 1]	7517.51	8896.44	1378.93

Table 7.11 Structural Optimization via CSP including ripetitivity (k=0.2) results of 10 runs

7.9 Case study 2: Symmetric Warren truss

Within this section, a more complex application example is exhibited. The structure under analysis is a Warren truss with 23 members. The structure is subjected to symmetric loading and a symmetric geometry is assumed. This assumption approximately halves the design variables which becomes 12 cross-sectional areas. The section is divided into two subsections, the first show the model definition and the set of algorithm parameters and, afterwards, another subsection exposes and discusses the results.

7.9.1 Model definition and parameters' setting

This case study examines a single-support Warren truss with 23 elements that is being loaded uniformly in-plane on the lower chord. This decision was made in order to minimize production costs due to the Warren-type truss's reduced joint count as compared to other types (like the Pratt or Vierendeel types). The complete length L of the truss is likewise displayed in Figure 7.27, divided into 6 spans with a spacing of L/6.

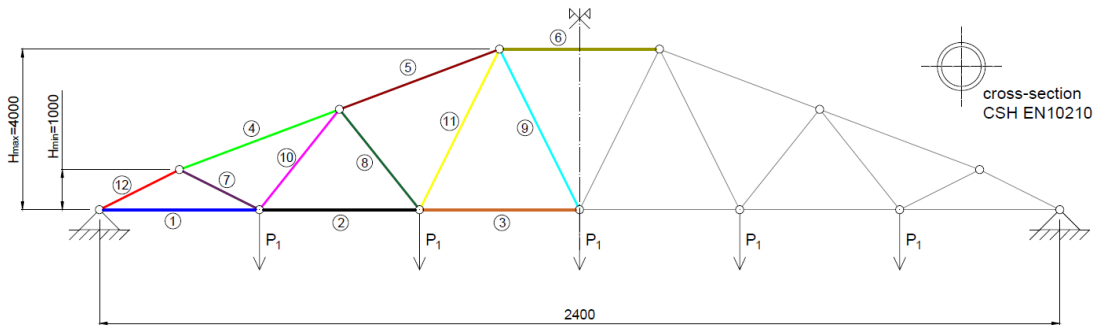

Fig. 7.27 Configuration of the Warren truss under analysis, the numbers indicate the design variables which are 12 because the symmetry is considered, measures are expressed in millimetres (mm)

The truss to be optimized is characterized by hollow members in particular in this truss typology Circular Hollow Sections (CHS) are used in particular a standard cross-sectional list from the standard code is used (EN 10210). In fact, hollow sections are particularly effective in compression as previously mentioned because

the material is far from the section axis, increasing the resistance to buckling. In some situations, hollow sections can also be more affordable than other profiles, such as when there are lower loads, cheaper steel prices, and higher hourly labour costs **?**. For reducing the computational effort and aiding the algorithm to search for the optimum symmetry of the truss is taken into account. This assumption almost halves the design variables which becomes 12 instead to 23 (the design variables of the problem are indicated in Figure 7.27.

The truss is loading symmetrically by considering a load due to the permanent non-structural load equal to 4 kN/m^2 a snow loading equal to 1.5 kN/m^2 and a maintenance loading of 0.5 kN/m^2. To obtain the in-plane loading of the truss, an influence area of 10 m is considered, which is the distance between two Warren trusses in a roof system. Afterwards, the uniform distributed load along the lower chord of the Warren truss is divided into 5 concentrated forces P_1 concentrated into the lower chord internal nodes. The self-weight of the structure is considered separately in the FEM code used for the structural analysis.

All the specifications regarding the material and the features of the model are reported in table 7.12.

Parameter	**Value**
Modulus of elasticity of steel E	210000 MPa
Steel density ρ	7.85 t/m^3
Loading lower chord nodes P_1	240 kN
Length of purchased bars (bins) L_{bin}	15 m
Number of design variables	12
Bounds of design variables (A_{min},A_{max})	[182, 24700] mm^2

Table 7.12 Model assumption relative to the symmetric Warren truss.

The statement of the entire optimization process is similar to Case Study 1 and is resumed in the following:

$$\min f(x) = W(x) \tag{7.32}$$

$$\textbf{Subject to} \quad \frac{N_{ED}}{N_{t,RD}} \leq 1 \tag{7.33}$$

$$\frac{N_{ED}}{N_{c,RD}} \leq 1 \tag{7.34}$$

$$\frac{N_{ED}}{N_{b,RD}} \leq 1 \tag{7.35}$$

$$u_{max,x} \leq u_{lim,x} \tag{7.36}$$

$$u_{max,y} \leq u_{lim,y} \tag{7.37}$$

An explanation of the constraints is available in the previous case study. The only noticeable difference is the equation (7.35) which assesses the buckling instability requirement according to Eurocode 3 (EN 1993-12005 and EN 1993-2 2006).
The violation comes from the constraint is computed as in the previous case study, the only difference is that the ϕ_1 used into the $W(x)$ is no more the sum between the various singular violations but the greater of them.

$$\phi_1 = max(\phi_{Nc}, \phi_{Nt}, \phi_{Nb}, \phi_{ux}, \phi_{uy}) \tag{7.38}$$

The settings of the algorithm are shown in the following table 7.13. Considering

Parameter	**Value**
Maximum number of iterations	200
Number of individuals per population	300
Areas excluded if unfeasibility condition isn't satisfied	5 smaller DV
Mutations' probability	5%
Proportional children	1 child for each parent
Stagnation condition	20 iterations

Table 7.13 Optimization algorithm parameters set by the operator.

that the complexity of the problem is grown with respect to the 10-bar-truss case study the number of individuals is increased to 300 and the stagnation is raised to 20 as well. A modification of the stagnation reinitialization is performed. The algorithm does not reinitialize all the individuals but stores the 10 best individuals in order to not lose the genetic pool.

7.9.2 Results and discussion

As in the previous case study, two optimization scenarios are investigated by performing 10 runs per scenario:

- Scenario (a): optimization by considering CSP (minimization of purchased steel bars).
- Scenario (b): optimization via traditional approach by minimizing the total weight of the structure without considering the CSP procedure.

Scenario (a) Regarding the first scenario (a) the results of the optimization are synthesised in the following table and figures referred to the best solution. For more detail about the ten runs see the table 7.16.

	Stock Mass (OF) [kg]	Structural Mass [kg]	Mass Waste [kg]
Best	4341.44	3006.42	1335.03
μ	5249.65	2952.80	2296.85
σ	391.43	292.55	391.10

Table 7.14 Result of the symmetric Warren optimization via CSP approach (a)

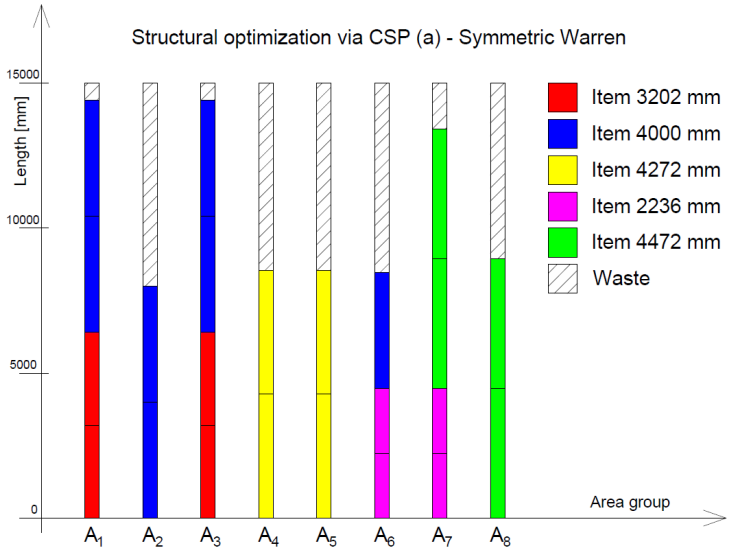

Fig. 7.28 Optimal cutting pattern derived by optimization via CSP scenario (a) - Symmetric Warren

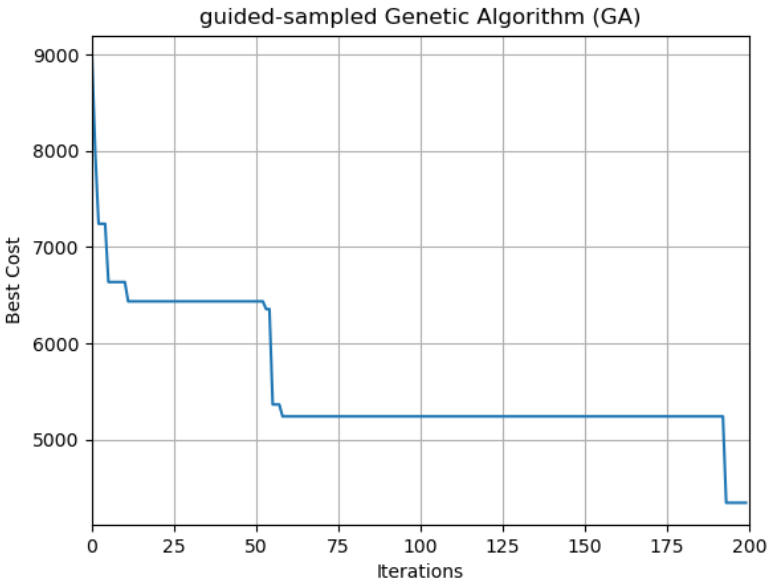

Fig. 7.29 OF best solution for each iteration related to Scenario (a) - Symmetric Warren

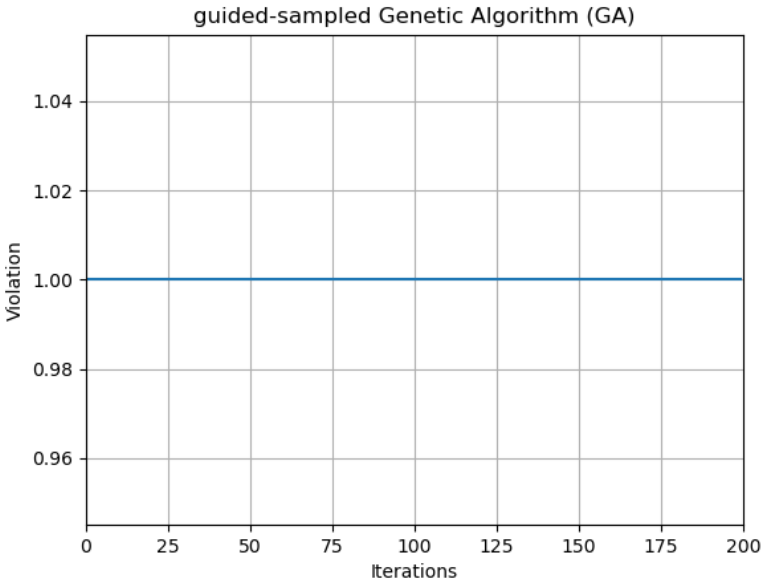

Fig. 7.30 OF violation for each iteration related to Scenario (a) - Symmetric Warren

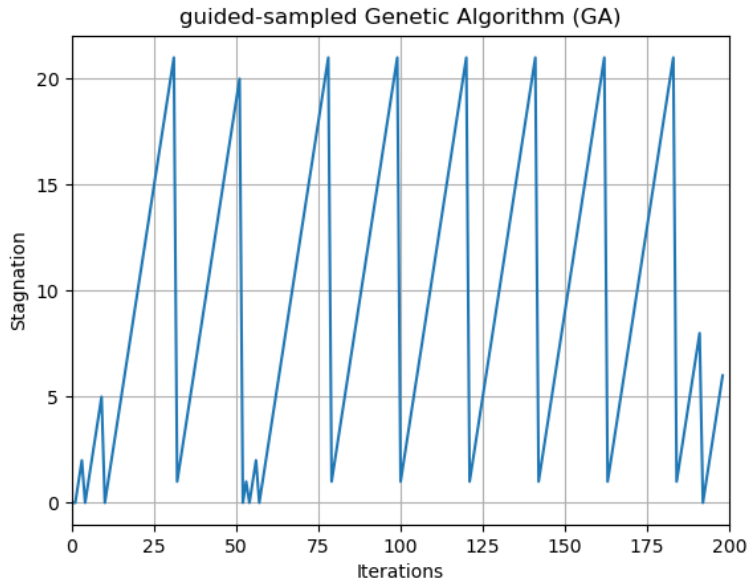

Fig. 7.31 OF stagnation for each iteration related to Scenario (a) - Symmetric Warren

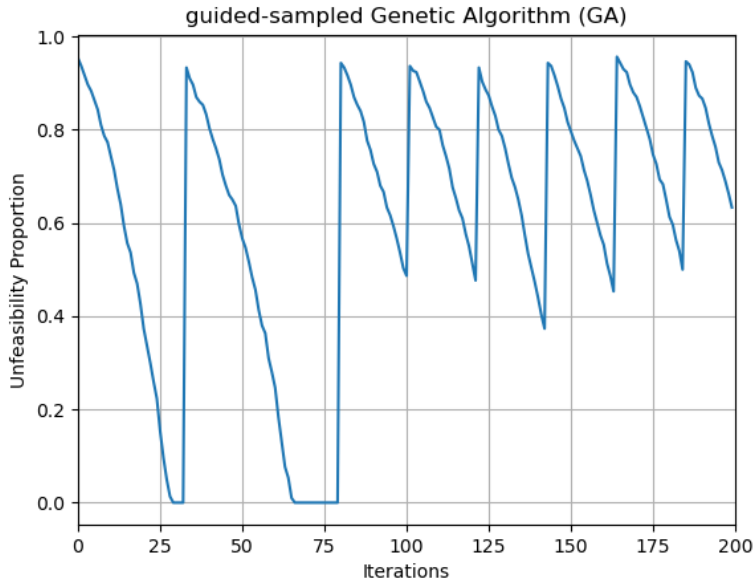

Fig. 7.32 OF unfeasibility for each iteration related to Scenario (a) - Symmetric Warren

The results of scenario (a) as it is possible to see in the stock representation (figure 7.28) are not optimal because the grouping of the areas does not reach the minimum in terms of the number of bars. For instance, it is possible to notice that the waste in the bars A_2, A_6, A_8 is greater than the length of each item. As it is possible to see in the best solution evolution through the 200 iterations plot (figure 7.29) achieving the best solution is more difficult and there are long stagnation points. The standard deviation of the stock mass is similar to the 10-bar truss case study and is related to the innate variability of the CSP problem.

Scenario (b) Now on following are exhibited the results and the plots related to scenario (b). More in detail the 10 runs results are shown in table 7.17.

	Stock Mass [kg]	Structural Mass (OF) [kg]	Mass Waste [kg]
Best	4610.62	2395.22	2215.40
μ	5832.42	2717.97	3114.45
σ	531.14	167.85	392.44

Table 7.15 Result of the symmetric Warren optimization via traditional approach (b)

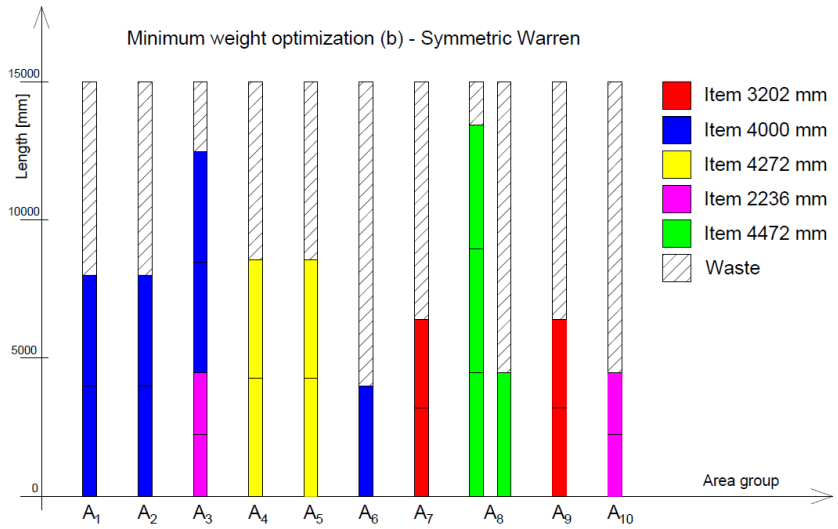

Fig. 7.33 Optimal cutting pattern derived by traditional optimization scenario (b) - Symmetric Warren

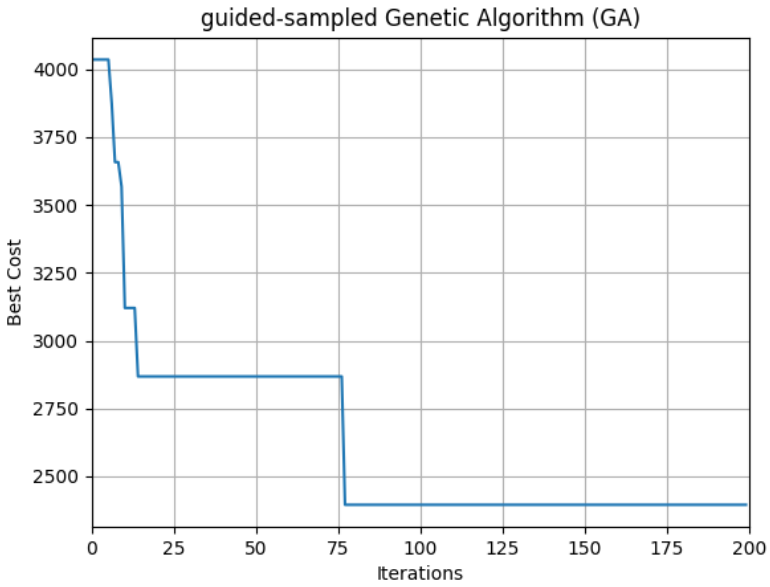

Fig. 7.34 OF best solution for each iteration related to Scenario (b) - Symmetric Warren

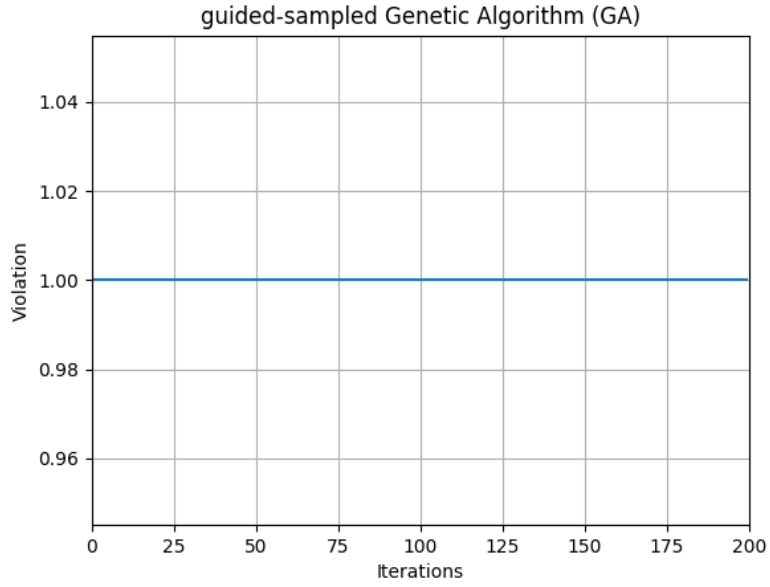

Fig. 7.35 OF violation for each iteration related to Scenario (b) - Symmetric Warren

The results derived from scenario (b) are much worse than the ones obtained from scenario (a). The assignation of the items to the beams in scenario (b) is only dependent on the optimum size for reducing the structural mass. Therefore, taking

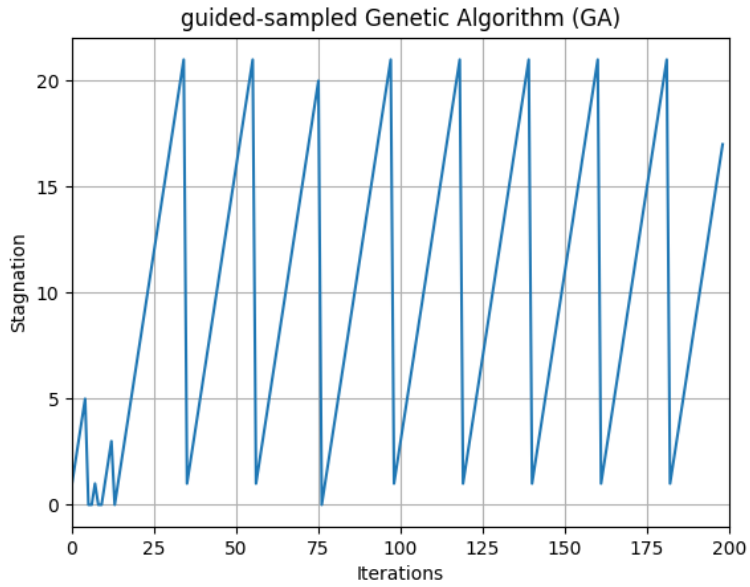

Fig. 7.36 OF stagnation for each iteration related to Scenario (b) - Symmetric Warren

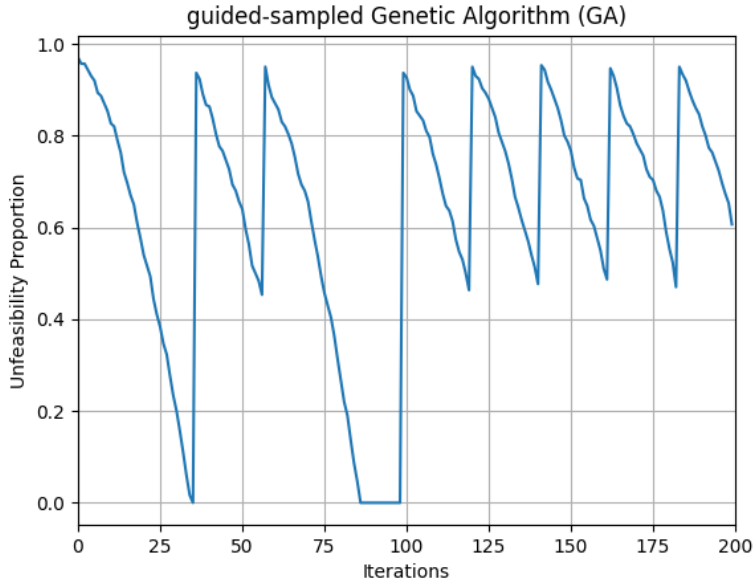

Fig. 7.37 OF unfeasibility for each iteration related to Scenario (b) - Symmetric Warren

into account only the structural mass optimization leads to great variability in terms of cross-sectional areas which means a raise in the number of bars. Moreover, a great number of bars results in a low exploitation rate which means a lot of waste material.

By comparing the two scenarios in (a) we have the use of 8 bars in the best results meanwhile in (b) the quantity raises to 11 bars. The scenario (a) best solution trend is more rigid (with more numerous and longer stagnation points) but is probably due to the higher complexity of the problem.
In terms of structural mass, the average value of scenario (a) is 234 kg much greater than scenario (b) which is an acceptable compromise because the gain in terms of average stock mass in scenario (a) is about 583 kg. The standard deviations of the results are a little high in both scenarios (less in terms of stock mass in scenario (a) and lower in structural mass in (b)) due to the high variability of the problem.
Unfortunately, the difference between the two scenarios is not high as in the previous case study and, for this reason, an ulterior simplification of the model is performed in the next case study.

Attempt	Cross-sectional areas [mm^2]	Number of bins	Structural Mass [kg]	Stock Mass [kg]	Waste Mass [kg]
1	[6910, 8740, 6570, 10000, 2640, 3760, 1560, 371, 810, 820, 5310, 3760]	[1, 1, 1, 1, 1, 1, 1, 1, 1, 1, 1]	2948.01	5592.07	2644.05
2	[4020, 4020, 2960, 5890, 8260, 5940, 689, 5940, 1050, 1120, 373, 9860]	[2, 1, 1, 1, 1, 1, 1, 1, 1, 1]	2666.38	5202.43	2536.05
3	[5890, 10200, 2960, 2640, 8740, 5990, 2040, 454, 1860, 5990, 1120, 4970]	[1, 1, 1, 1, 1, 1, 1, 1, 1, 1, 1]	3024.07	5518.24	2494.17
4	[8260, 7940, 4710, 5770, 7120, 5030, 679, 1660, 810, 1250, 454, 5030]	[1, 1, 1, 1, 1, 1, 1, 1, 1, 1, 1]	2786.95	5143.67	2356.73
5	[7120, 2520, 3760, 6570, 7370, 6850, 1120, 7120, 1560, 1120, 3760, 6850]	[1, 1, 1, 1, 1, 1, 1, 1]	3006.42	4341.44	1335.03
6	[4710, 3760, 8110, 4670, 8920, 3760, 574, 578, 4670, 5890, 4070, 5890]	[1, 1, 1, 2, 1, 1, 1, 1, 1]	3272.78	5410.85	2138.07
7	[5890, 10900, 9860, 4030, 4970, 8740, 540, 10900, 869, 1320, 540, 1560]	[1, 1, 1, 1, 1, 1, 1, 1, 1, 1]	3354.13	5731.95	2377.82
8	[3360, 3360, 6850, 9110, 3210, 3760, 1720, 2040, 3360, 1390, 182, 7120]	[2, 1, 1, 1, 1, 1, 1, 1, 1, 1]	2552.10	4957.51	2405.41
9	[5310, 6120, 8110, 5990, 6290, 8260, 1710, 289, 1320, 869, 439, 1710]	[1, 1, 1, 1, 1, 1, 1, 1, 1, 1, 1]	2620.45	5264.25	2643.80
10	[6290, 11300, 5030, 6910, 9860, 2520, 6910, 1120, 1120, 810, 340, 6290]	[1, 1, 1, 1, 1, 1, 2, 1, 1]	3296.73	5334.08	2037.34

Table 7.16 Structural Optimization via CSP results of 10 runs for symmetric Warren. Scenario (a)

Attempt	Cross-sectional areas [mm^2]	Number of bins	Structural Mass [kg]	Stock Mass [kg]	Waste Mass [kg]
1	[3710, 8110, 4710, 7370, 8770, 12500, 506, 2140, 360, 906, 1070, 1630]	[1 1 1 1 1 1 1 1 1 1 1 1]	2838.33	6097.33	3259.00
2	[4210, 7370, 3310, 6910, 4500, 6120, 1540, 5770, 1120, 1660, 360, 10000]	[1 1 1 1 1 1 1 1 1 1 1 1]	2800.97	6225.44	3424.47
3	[2640, 4030, 7940, 5010, 13000, 8110, 578, 820, 679, 1560, 906, 2960]	[1 1 1 1 1 1 1 1 1 1 1 1]	2748.27	5679.44	2931.17
4	[3310, 7120, 7810, 5010, 4020, 5770, 4500, 733, 707, 3210, 641, 5310]	[1 1 1 1 1 1 1 1 1 1 1 1]	2620.77	5668.60	3047.83
5	[2060, 5990, 4670, 7920, 8740, 15500, 965, 238, 454, 680, 574, 5890]	[1 1 1 1 1 1 1 1 1 1 1 1]	2764.00	6320.94	3556.94
6	[4210, 7370, 4210, 5030, 6290, 8110, 1120, 2040, 1320, 1320, 1540, 11300]	[2 1 1 1 1 1 1 2 1 1]	2806.83	6342.02	3535.18
7	[6660, 3360, 8260, 5010, 2960, 10200, 1710, 707, 1710, 5770, 483, 4500]	[1 1 1 1 1 1 1 1 1 1 1 1]	2805.83	5842.75	3036.93
8	[5280, 7370, 4020, 6570, 4210, 2060, 4020, 360, 965, 965, 506, 6850]	[1 1 1 1 1 1 1 2 1 1]	2395.22	4610.62	2215.40
9	[12500, 6910, 4500, 5310, 4070, 4030, 1070, 439, 540, 820, 6120, 5770]	[1 1 1 1 1 1 1 1 1 1 1 1]	2922.51	6132.30	3209.79
10	[5770, 7120, 3540, 5990, 3760, 9110, 1370, 1390, 1710, 1120, 810, 4210]	[1 1 1 1 1 1 1 1 1 1 1 1]	2476.97	5404.72	2927.75

Table 7.17 Traditional Structural Optimization results of 10 runs for symmetric Warren. Scenario (b)

7.10 Case study 3: 4 member types Warren truss

Within this section, a further reduction of the design variables regarding the previous model was implemented. The structure is the same as in case study 2 but all the members are grouped into 4 groups which have 4 different cross-sections. In this way, the design variables are only 4 and the computational effort is reduced.
The section is divided into two subsections, the first show the model definition and the set of algorithm parameters and, afterwards, another subsection exposes and discusses the results.

7.10.1 Model definition and parameters' setting

This case study is a simplification of the previous one. As it is possible to see in Figure 7.38 all the members are previously grouped into 4 cross-sectional classes based on the structural behaviour. The four classes are the lower chord, the upper chord the internal web and the external web. The only modification is this radical reduction of the design variable meanwhile the problem statement of the other model and optimization characteristics are equal to the one exposed in case study 2. The final aim of this assumption is to reduce the design variable and to force the grouping of the bars in order to exploit better the stock material.

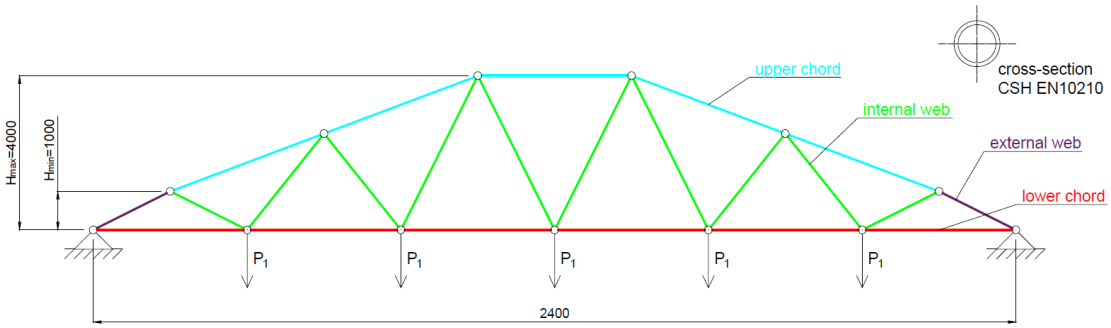

Fig. 7.38 Configuration of the Warren truss under analysis, the members are divided into 4 cross-sectional areas which are the 4 design variables, measures are expressed in millimetres (mm)

In the following tables (7.18, 7.19) are summarized the characteristics regarding the model properties in the first one and the setting parameters in the second table.

Parameter	Value
Modulus of elasticity of steel E	210000 MPa
Steel density ρ	7.85 t/m^3
Loading lower chord nodes P_1	240 kN
Length of purchased bars (bins) L_{bin}	15 m
Number of design variables	4
Bounds of design variables (A_{min}, A_{max})	[182, 24700] mm^2

Table 7.18 Model assumption relative to the symmetric Warren truss.

Parameter	Value
Maximum number of iterations	200
Number of individuals per population	300
Areas excluded if unfeasibility condition isn't satisfied	5 smaller DV
Mutations' probability	5%
Proportional children	1 child for each parent
Stagnation condition	20 iterations

Table 7.19 Optimization algorithm parameters set by the operator.

7.10.2 Results and discussion

As in the previous case study, two optimization scenarios are investigated by performing 10 runs per scenario (for more detail see case study one):

- Scenario (a): optimization by considering CSP (minimization of the stock).
- Scenario (b): optimization via traditional approach (minimization of the structural mass).

Scenario (a) On following the results of scenario (a) with 4 design variables are exposed. For more detail about the 10 runs see table 7.22.

	Stock Mass (OF) [kg]	Structural Mass [kg]	Mass Waste [kg]
Best	2656.44	2189.96	466.48
μ	2770.02	2265.11	504.91
σ	98.30	73.80	37.38

Table 7.20 Result of the 4 DV Warren optimization via CSP approach (a)

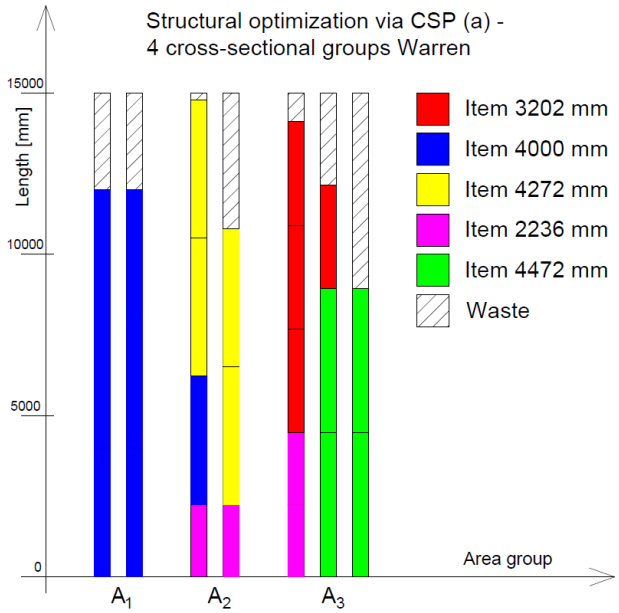

Fig. 7.39 Optimal cutting pattern derived by optimization via CSP scenario (a) - 4 DV Warren

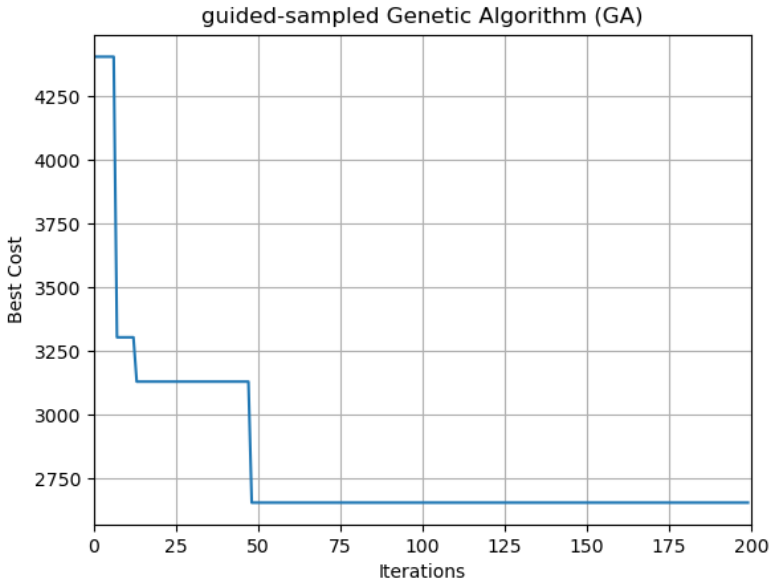

Fig. 7.40 OF best solution for each iteration related to Scenario (a) - 4 DV Warren

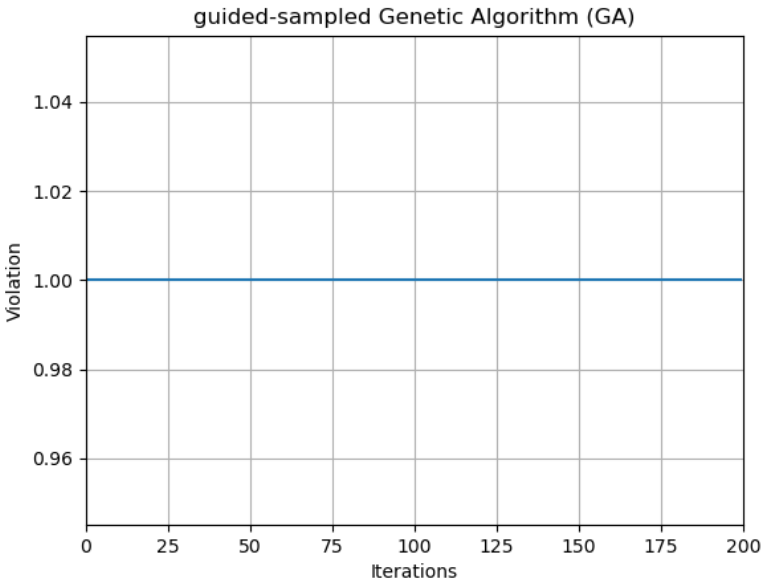

Fig. 7.41 OF violation for each iteration related to Scenario (a) - 4 DV Warren

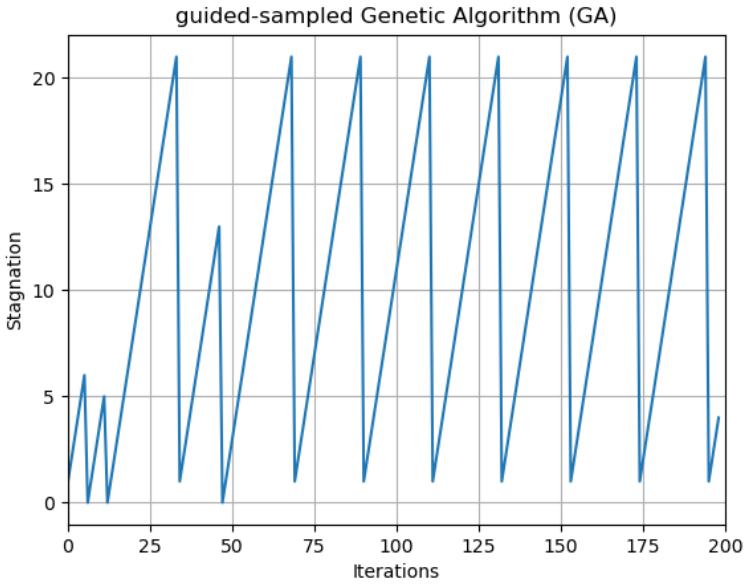

Fig. 7.42 OF stagnation for each iteration related to Scenario (a) - 4DV Warren

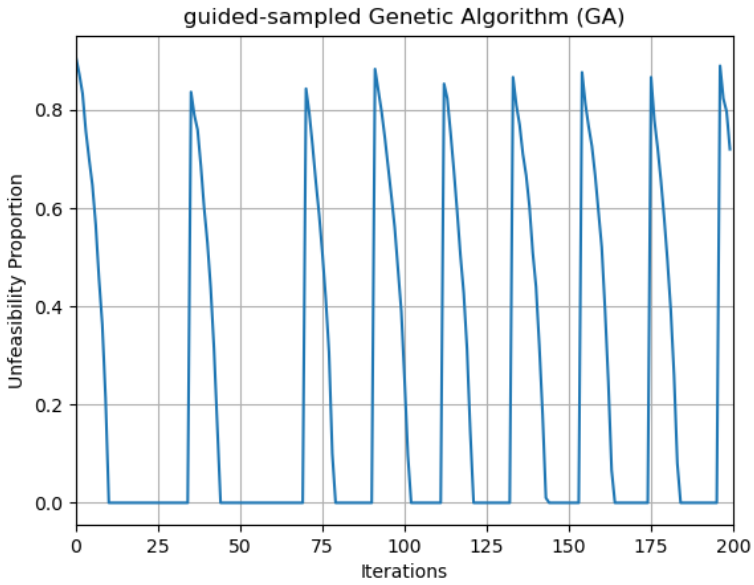

Fig. 7.43 OF unfeasibility for each iteration related to Scenario (a) - 4 DV Warren

In this case, the stock representation (Figure 7.39) shows that the rate of exploitation of the bars is the maximum that it is possible to attain. It is interesting to notice that all the 10 runs give as a result the grouping in three classes of areas because the two external webs are simply allocated in one of the other three existing bars. Another indicator of the algorithm's goodness is the decrease of the standard deviations both in stock and structural mass which means that the results tend to converge to similar results. Also, the waste mass is much lower than in the previous case study.

Scenario (b) On following the results of scenario (b) with 4 design variables are exposed. For more detail about the 10 runs see table 7.23.

	Stock Mass [kg]	Structural Mass (OF) [kg]	Mass Waste [kg]
Best	3109.78	2130.44	979.33
μ	3282.09	2146.42	1135.67
σ	222.82	26.38	215.64

Table 7.21 Result of the 4 DV Warren optimization via traditional approach (b)

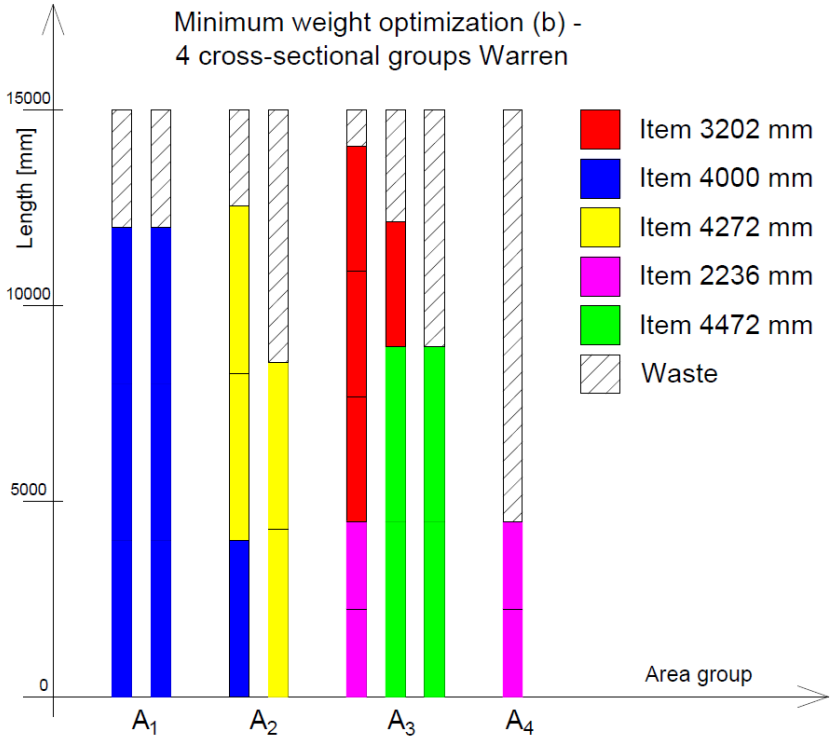

Fig. 7.44 Optimal cutting pattern derived by traditional optimization scenario (b) - 4 DV Warren

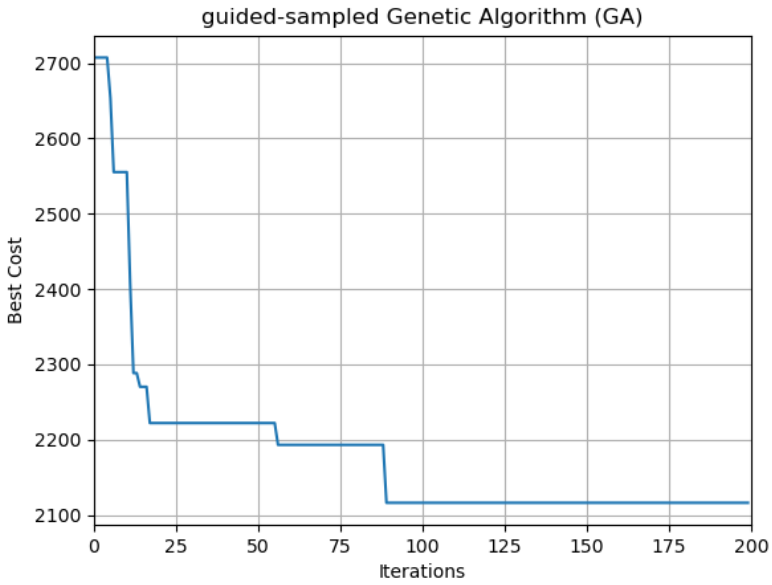

Fig. 7.45 OF best solution for each iteration related to Scenario (b) - 4 DV Warren

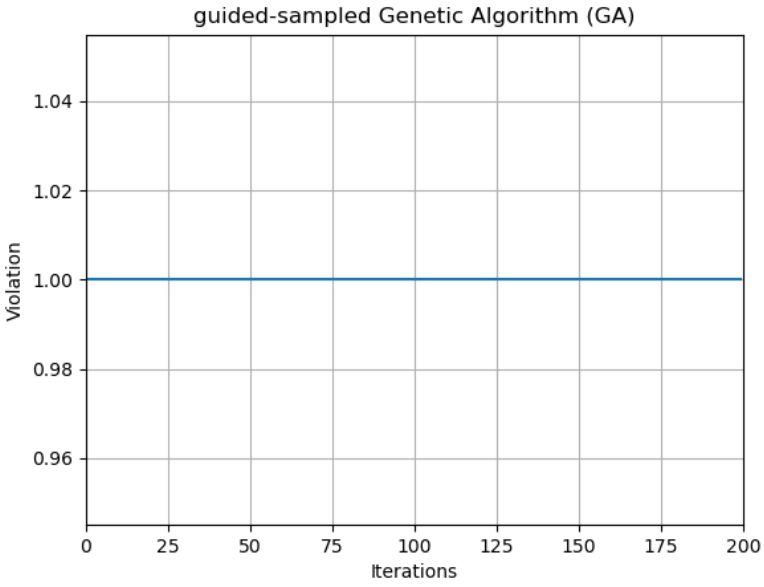

Fig. 7.46 OF violation for each iteration related to Scenario (b) - 4 DV Warren

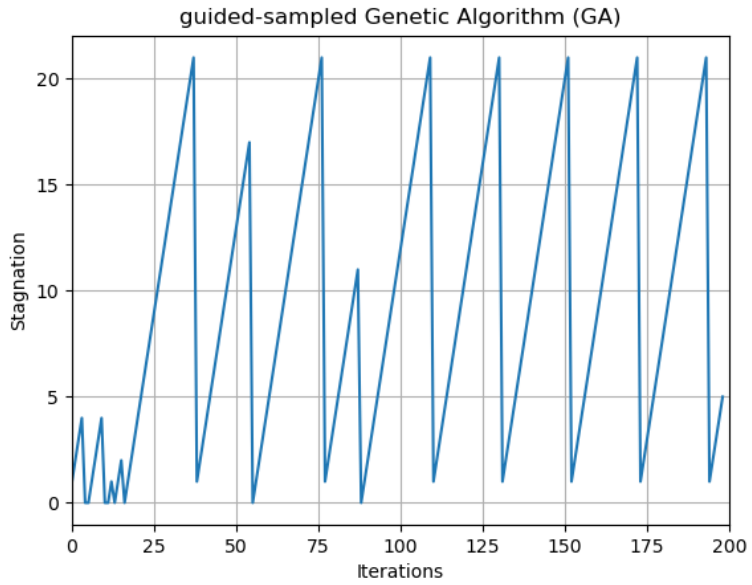

Fig. 7.47 OF stagnation for each iteration related to Scenario (b) - 4DV Warren

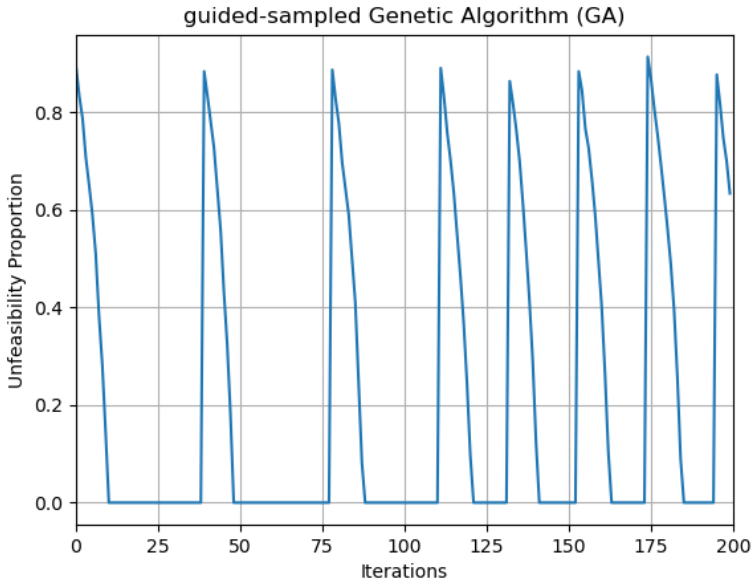

Fig. 7.48 OF unfeasibility for each iteration related to Scenario (b) - 4 DV Warren

In scenario (b) the results are a little bit worse than in (a). The increment is almost in all the runs of only one bar. These results are due to the fact that algorithm (b) uses the groups imposed from the operator without the merging of the external webs cross-sectional areal class with another of the three other classes.
The principal thought that comes from this outcome is that the traditional structural optimization itself works well and the impact of the CSP optimization, in this case, is minimum.
Therefore, the CSP algorithm in this case has more of a function of finding the best set of cutting patterns instead to group the items' areas which are similar to the one chosen by the traditional structural optimization (in fact the structural mass is very similar between the two scenarios). A noticeable value is the standard deviation which increases in scenario (b).

Attempt	Cross-sectional areas [mm^2]	Number of bins	Structural Mass [kg]	Stock Mass [kg]	Waste Mass [kg]
1	[4210, 5310, 1370, 5310]	[2, 2, 3]	2236.80	2725.91	489.11
2	[4970, 5280, 906, 4970]	[2, 2, 3]	2234.99	2733.92	498.93
3	[4210, 5940, 1120, 5940]	[2, 2, 3]	2294.20	2785.96	491.77
4	[4500, 4710, 2060, 4710]	[2, 2, 3]	2361.53	2896.65	535.12
5	[4030, 6120, 906, 4030]	[2, 2, 3]	2163.95	2710.37	546.42
6	[3710, 5890, 1120, 5890]	[2, 2, 3]	2189.96	2656.44	466.48
7	[4210, 6120, 680, 6120]	[2, 2, 3]	2208.85	2672.93	464.08
8	[4500, 5990, 1390, 4500]	[2, 2, 3]	2381.09	2961.41	580.32
9	[4020, 5890, 1120, 5890]	[2, 2, 3]	2248.37	2729.44	481.08
10	[5280, 4670, 1370, 5280]	[2, 2, 3]	2331.39	2827.18	495.79

Table 7.22 Structural Optimization via CSP results of 10 runs for 4 cross-sectional type Warren. Scenario (a)

Attempt	Cross-sectional areas [mm^2]	Number of bins	Structural Mass [kg]	Stock Mass [kg]	Waste Mass [kg]
1	[4030, 5990, 862, 4210]	[2 2 3 1]	2136.60	3159.94	1023.34
2	[5030, 4710, 965, 4070]	[2 2 3 1]	2136.63	3113.90	977.27
3	[5030, 5280, 869, 3360]	[2 2 3 1]	2179.56	3130.62	951.06
4	[4670, 5280, 641, 5890]	[2 2 3 1]	2137.61	3263.21	1125.59
5	[4500, 5030, 869, 5890]	[2 2 3 1]	2127.14	3244.84	1117.69
6	[4710, 4670, 810, 9110]	[2 2 3 1]	2203.87	3567.83	1363.96
7	[4210, 4970, 1050, 5990]	[2 2 3 1]	2116.05	3238.13	1122.07
8	[4970, 5010, 810, 4020]	[2 2 3 1]	2130.44	3109.78	979.33
9	[5280, 4710, 733, 5010]	[2 2 3 1]	2152.68	3201.50	1048.82
10	[5030, 5030, 679, 5010]	[5 3 1]	2143.65	3791.20	1647.55

Table 7.23 Traditional Structural Optimization results of 10 runs for 4 cross-sectional type Warren. Scenario (b)

7.11 Conclusion and future developments

In this chapter, a novel procedure for the optimization of steel truss structures has been introduced to evaluate the minimum number of bins (total mass of purchased steel bars) and the optimal cutting pattern of a stock of elements by solving the Cutting Stock Problem (CSP).
After an introductory part which gives an overview of the scientific literature concerned with Structural Optimization techniques which investigate the minimization of the cost related to the structure, the mathematical formulation of the Cutting Stock Problem in particular the Column Generation methodologies was explored in detail. Given the necessary prerequisites, the Structural Optimization via CSP developed by the author and supervisors of this thesis is exhibited. The new Structural Optimization aims to minimize the total mass of purchased steel bars by a GA-based size optimization algorithm. The number of bars requested by the objective function is obtained through a CSP column generation code which allocates all the items of the truss under analysis in an optimal way.
Thereafter, some application case studies are investigated for testing the goodness of the algorithm. To have effective feedback the Stock obtained by the Structural Optimization via CSP is compared with the stock obtained by a traditional Structural mass minimization.
In the first case study, which is a simple 10-bar truss used as a benchmark, the algorithm gives satisfactory results. The 10-bar truss under analysis is very simple and the bars have a capacity of a maximum of 2 items per bar. Nevertheless, the exploration of the domain of solution is very simple due to the standard cross-sectional list which has a small number of cross-sections, a small number of unfeasible solutions and a constant interval between two consecutive areas.
The two next case studies are a 23-bar Warren truss which is modelled in two different ways: as a symmetric truss that almost halves to 12 design variables and as a 4 cross-sectional areas truss (reduce the design variables to the upper chord, lower chord, external and internal web cross-sections). The problem, in this case, is more interesting because of the complexity of the problem that arises (i.e. the number of items per bar, more different items' lengths and a bigger solution domain) and hence the usefulness of the optimization. Due to the innate complexity of the question, the exploration capability of the algorithm is incremented. With respect to the 10-bar truss the solution of the symmetric Warren gives worse results. Probably

the principal cause is the solution domain correlated whit the standard cross-sectional list used for the Warren which has a greater number of areas with also a greater percentage of unfeasible solutions and a variable interval between two consecutive solutions. To reduce the variability of the algorithm the 4 cross-sectional areas truss model was created. As expected, forcing the grouping of the area more allows the collection of more items bars and has good results.
The limit of this work is a high variability of the solution due to the innate complexity of the problem, the request for a preventive grouping for more complex structures and the rigidity of the algorithm which have lots of stagnation point across the iterations.

Since the CSP is a problem strictly related to the length of the items and the bins it would be interesting in the future to add the lengths of the elements to the optimization design variables in order to obtain a size and shape optimization.
Another interesting aspect is to differentiate the length of the purchased bars in order to buy the bar typology which guarantees the minimum waste of material.
Moreover, this thesis treats only the weight as the objective function of the structural optimization, it would be useful to explore more the CSP utilization in cost minimization problem which takes into account more economic factors (i.e. fabrication cost, connection cost and maintenance).
A further development is to consider the environmental impact of the minimization of the stock bars by a life cycle assessment and/or an objective function which minimize the emission by implementing the optimization of the various environmental indexes.

Chapter 8

Conclusions and future developments

8.1 Original contribution of the thesis

The object of the present thesis is to develop algorithms with efficient clustering operators for the simultaneous optimal size, shape, and topology of steel trusses and show how constructability issues at different construction phases affect the optimal design. This is compared with other approaches used till now by the scientific community in which structural performance only has been optimized without considering those aspects. If in the former, the computational performance of new algorithms developed in this thesis and that one existed in literature were compared by testing on literature benchmarks and structural tests, the latter emphasized the role of structural optimization for real-engineering case studies.

Since the evident different nature of the problems coped in each Chapter, the original contribution of the thesis will be summarized with specific regard to two fundamental aspects: *improvement in computational* effort and reliability guaranteed by the proposed optimization strategies and *level of complexity* involved in the more realistic case studies investigated by the candidate.

Algorithm's improvement As covered extensively in chapters 2 and 3, PSO represents one of the most adopted metaheuristic algorithms for facing continuous design variables. Specifically, two approaches were developed in order to integrate new search strategies into the classical PSO:

- A novel no-penalty-based constraint handling approach using the machine learning method SVM was implemented (see Chapter 2) as a classification strategy aimed to separate efficiently feasible individuals from the unfeasible ones. The most common approaches that appeared in literature are entirely based on penalty functions or reduction of the original search space due to the existence of various constraints. Especially when evolutionary or swarm intelligence strategies are adopted, several efforts have been made by researchers for handling various types of constraints. However, none of the previous works focused on improving the clustering ability of the algorithm with a predictive method was recognized in the literature. In this sense, the new PSO-SVM proposes a viable alternative to improve the exploration capacity of the algorithm with respect to traditional approaches.

- An enhanced version of the standard Newtonian-dynamics-based PSO was proposed by the candidate in Chapter 3 when a multi-strategy approach was presented in order to avoid the definition of arbitrary violation penalty factor. An intelligent strategy for the identification of the most critical violation of constraints at each iteration was coupled with an enhancement of the local exploration capacity based on the Evolutionary Strategy. In this way, a new hybrid algorithm was introduced and computational performance was tested on numerical and structural problems.

Complexity in real applications In the previous Chapters, the concept of complexity was widely introduced and several aspects related to this topic were discussed. To achieve this goal, an original contribution was given by the candidate since real issues in design procedures were solved through optimization strategies.
With specific regard to the subject of competence of each Chapter, the original contribution relies on the following reasons:

- A new retrofitting system for prestressed bridges was proposed (see Chapter 4) as a viable alternative to traditional consolidation systems. Optimization has played a crucial role in the optimal design of the steel arch-trussed system and a multi-approach strategy was implemented. The challenge lies in the statement's formulation of the no-dimensional OF in which stiffness and the total weight of the system follow opposite trends. The advantages of adopting the proposed method were proved also from the economic point of view.

- Respect to traditional approaches in which minimum weight and structural cost, as well as maximization of structural performance, still represented the main goal of the research, in Chapter 6 and 7 the role of the optimization strategy was fundamental. Minimum weight does not always mean minimum cost. The real cost is a complex element to be evaluated, as it depends not only on material volume or weight. Other important aspects that deeply affect the cost are elements production, transport, assembly of elements as well as maintenance and durability. In many cases, the total material weight is only one term (maybe also not the more impactful) with respect to others. In this thesis, the aim has been to consider some determinant aspects in steel structures such as the number of elements and the production analysis. Reducing the number of steel pieces led to simple assembly procedures during the construction phase and an overall reduction of the structural complexity of the overall structures. Moreover, the identification of the optimal cutting pattern allows for the reduction of waste during the production phase and fulfilling the sustainability goals imposed by the guidelines.

The present thesis contributed to each one of the four points mentioned above, as will be demonstrated by the overall conclusion illustrated in detail in the next sections.

8.2 Overall conclusions

Apart from the conclusions discussed in detail in each Chapters of the thesis, the research work done for the thesis led to the following fundamental overall conclusions:

- A feasible strategy to improve PSO algorithms relies on adopting machine learning approaches aiming to improve the global performance of the algorithm at the level of both convergency rate during the exploration search and accuracy while the exploitation phase. Thanks to the capability of this machine learning approach to learn from examples contained in previous knowledge derived by training data set, it is able to reduce the search space because, after the learning phase, it can predict the feasible region in which new individuals are more likely to be close to the global optimum optimal.
- Algorithms' hybridization was confirmed to be useless as an effective strategy for improving the robustness of the algorithm. Specifically, Evolutionary

Strategies were successfully integrated into classic PSO for the local search to avoid being trapped in local minima.

- Considering design complexity as a parameter of the optimization leads to unexpected results if compared with the outcomes of the past. Reducing the number of different cross-sections employed in the structure or the number of pieces affects the optimal solution at each optimization level. This fact is quite evident by the results obtained by the size, shape and topology optimization conducted on industrial buildings. At each level of the optimization, the influence of constructability issues appears to be evident.
- Implementing the Cutting Stock Problem in size optimization of steel trusses, lead to a significant waste saving if compared with the minimum weight-only approach. This benefit was obtained with an acceptable increment of the structural mass.
- Generally, in most of the case studies investigated, the optimal solution obtained by adopting traditional approaches does not coincide or even seem to be in contrast with the one in which constructability issues and optimal production processes were considered. Minimum structural cost assures a slender solution but it represents, in most cases, the worst solution in terms of practicability, complexity and sustainability.

The ultimate research goal is to establish the use of these methods as state of the art in the near future and try to encourage practice towards that direction, away from the trial and error processes for the design of structural systems.

8.3 Future works

As in the previous sections, considerations about possible developments of the proposed optimization approaches will be summarized with respect to each topic. Moreover, further investigations aimed to expand the range of application cases in which the effect of structural optimization for solving practical design challenges is analyzed will be illustrated.

- The goodness of adopting the Machine learning approach SVM algorithm as a powerful tool to improve the local search ability of metaheuristic algorithms

could be tested on new benchmark tests. In this way, the global performance of the proposed method could be proved for an increasing computational level required to solve these numerical problems. Moreover, different metaheuristic algorithms could be selected for this purpose in which the adaptability of the method could be tested not only for evolutionary or swarm-based strategies but also for human and physics-based algorithms to detect the population's most compatible updating strategies.

- New attempts could be provided aiming to investigate the best match between different optimization strategies starting from the proposed one in this thesis to move toward hybridization with other evolution strategies like genetic approach, genetic programming and differential evolution. Moreover, another promising direction can be a hybridization with the estimation distribution algorithm (EDA) Pelikan et al. (2015), which relies on building and updating a complex probability distribution model of the search space domain, and therefore, it is potentially able to give considerably much more information about the fitness landscape with respect to a simple blind sampling inside the search space.

- As future developments, improvements in the proposed retrofitting systems could be achieved. It will be interesting to conduct a detailed design of the connections between the concrete beam and the strengthening system and provide a topological optimization with the aim to verify the optimal shape of the consolidation system. Furthermore, a complete analysis that will take into account realistic bridge actions (i.e. not only gravitational forces but also horizontal components of wind and earthquake) on the entire deck considering the global behaviour of the structure, will represent the final scope of the research.

- Structural complexity during the construction phase could be investigated with further considerations focused on realistic complexity cost function where trends related to the increase of the number of pieces and different cross-sections employed for the realization of the structure faithfully reflect the industrial market needs. Basically, complexity indexes could be obtained by suitable calibrations of the complexity cost function based on real-world scenarios.

- With specific regard to the case study 2 shown in Chapter 6, another future investigation could be the optimal sizing of each member composing the industrial building. In fact, it is well-known that for the truss elements, it could be convenient to employ I-shaped or H-shaped profiles, as well as UPN or single and double L-shaped ones. The choice could be guided by the type of feasible connection between the components that should be realized during the assembly phase. Moreover, the number of modules could be included as a parameter of the OF and not only as a parametric value. In this way, an answer to the following questions could be obtained: what is the optimal design which guarantees the minimum structural complexity? When all the members composing the structures contribute to the overall complexity and not only trusses' members, the optimizer will prefer solutions with a high number of modules resulting in more pieces in trusses or it will move toward design with a lower number of frames for reducing the global complexity of the structure?.
  Another significant finding from the analyses is that the algorithm is not sufficiently guided in the topology identification. In fact, during the optimization, Octopus was free to assign any possible type of configuration, without any penalty entirely dedicated to encouraging topologies with a minimum number of elements or optimal paths. However, this aspect was considered indirectly in the problem statement and a stable trend was recognized by observing the results of the analysis in terms of OF, violation plot and unfeasibility proportion at each iteration. Finally, new problem statements could include also seismic action in load combinations according to various standard regulations.

- Various improvements could be provided in the implementation of Bin Packing Problems into structural optimization. As discussed in the Chapter 7, The limit of solving the Cutting Stock Problem lies in the high variability of the solution due to the innate complexity of the problem, the request for a preventive grouping for more complex structures, and the rigidity of the algorithm which is characterized by several stagnation points across the iterations. Since the CSP is a problem strictly related to the length of the items and the bins it would be interesting in the future to consider the lengths of the elements as design variables of the problem in order to perform size and shape optimization simultaneously. Hence, optimal lengths of the purchased bars, according to transportability constraints, will be found and an improvement in the waste

saving could be recognized. With less effort, studies could be conducted on analyzing the effect of CSP in different 2D and 3D truss typologies by varying the number of subdivisions and, consequentially, the number of overall connection joints. In this way, a topology optimization will be performed. Moreover, since the proposed method treats only the weight as the objective function of the structural optimization, it would be useful to explore more CSP utilization in the cost minimization problem by considering other economic factors (i.e. fabrication cost, connection cost, and maintenance). Finally, in further developments, OF entirely based on environmental impact could be formulated by adopting a life cycle assessment method for the minimization of carbon emission or other environmental indexes.

References

Istruzioni per la valutazione delle azioni e degli effetti del vento sulle costruzioni. *CNR-DT*, 2009.

Word Steel Association. https://worldsteel.org/steel-topics/statistics/world-steel-in-figures/, 2021.

K. M. Abdalla and W.-F. Chen. Expanded database of semi-rigid steel connections. *Computers & Structures*, 56(4):553–564, 1995.

H. Abedini, S. R. H. Vaez, and A. Zarrineghbal. Optimum design of buckling-restrained braced frames. In *Structures*, volume 25, pages 99–112. Elsevier, 2020.

H. Adeli and N.-T. Cheng. Integrated genetic algorithm for optimization of space structures. *Journal of Aerospace Engineering*, 6(4):315–328, 1993.

E. E. Agency. *The European environment-state and outlook 2010: Assessment of Global Megatrends;[SOER 2010]*. Publications Office of the European Union, 2011.

H. agency. *Post-tensioned concrete bridges: Anglo-French liaison report*. Telford, 1999.

S. N. Al-Saadi and K. S. Al-Jabri. Optimization of envelope design for housing in hot climates using a genetic algorithm (ga) computational approach. *Journal of Building Engineering*, 32:101712, 2020.

Y. Al-Salloum and T. Almusallam. Optimality and safety of rigidly- and flexibly-jointed steel frames. *Journal of Constructional Steel Research*, 35(2): 189–215, 1995a. URL https://www.scopus.com/inward/record.uri?eid=2-s2.0-0029238016&doi=10.1016%2f0143-974X%2894%2900043-H&partnerID=40&md5=624243b338cb364e829aca2e9d299f08.

Y. Al-Salloum and T. Almusallam. Optimality and safety of rigidly-and flexibly-jointed steel frames. *Journal of Constructional Steel Research*, 35(2):189–215, 1995b.

M. Alam. Codes in matlab for particle swarm optimization. 03 2016a. doi: 10.13140/RG.2.1.1078.7608.

M. N. Alam. Codes in matlab for particle swarm optimization. *Research Gate Indian, Institute of Technology Roorkee*, 2016b.

R. Alberdi, P. Murren, and K. Khandelwal. Connection topology optimization of steel moment frames using metaheuristic algorithms. *Engineering structures*, 100: 276–292, 2015.

H. AlHendi, M. Mahmoud, and M. Celikag. Optimal depth selection of composite tubular-floor trusses based on cost estimation. *Advances in Structural Engineering*, 24(13):2912–2926, 2021.

N. B. H. Ali, M. Sellami, A.-F. Cutting-Decelle, and J.-C. Mangin. Multi-stage production cost optimization of semi-rigid steel frames using genetic algorithms. *Engineering Structures*, 31(11):2766–2778, 2009.

J. M. Allwood, J. M. Cullen, M. A. Carruth, D. R. Cooper, M. McBrien, R. L. Milford, M. C. Moynihan, and A. C. Patel. *Sustainable materials: with both eyes open*, volume 2012. UIT Cambridge Limited Cambridge, UK, 2012.

A. Aloisio, D. P. Pasca, L. Battista, M. M. Rosso, R. Cucuzza, G. Marano, and R. Alaggio. Indirect assessment of concrete resistance from fe model updating and young's modulus estimation of a multi-span psc viaduct: Experimental tests and validation. *Elsevier Structures*, 37:686–697, 01 2022. doi: 10.1016/j.istruc.2022.01.045.

M. Alqam and F. Alkhairi. Numerical and analytical behavior of beams prestressed with unbonded internal or external steel tendons: a state-of-the-art review. *Arabian journal for science and engineering*, 44(10):8149–8170, 2019.

Y. Al-Salloum. A pseudo-fully stressed design approach for optimum design of steel frames. *International Journal for Numerical Methods in Engineering*, 38 (20):3513–3527, 1995. URL https://www.scopus.com/inward/record.uri?eid=2-s2.0-0029394536&doi=10.1002%2fnme.1620382009&partnerID=40&md5=7504d783f56f149cbf42e2cb18acc8f2.

G. G. Amiri. Seismic sensitivity indicators for tall guyed telecommunication towers. *Computers & structures*, 80(3-4):349–364, 2002.

S. Anderson, D. Fisher, and V. Gupta. *Total Constructability Management: A Process-oriented Framework*. Project Management Institute, 1995. URL https://books.google.it/books?id=Ab6YoAEACAAJ.

M. K. Ansah, X. Chen, and H. Yang. Two-stage lifecycle energy optimization of mid-rise residential buildings with building-integrated photovoltaic and alternative composite façade materials. *Buildings*, 11(12):642, 2021.

E. Antipova, D. Boer, G. Guillén-Gosálbez, L. F. Cabeza, and L. Jiménez. Multi-objective optimization coupled with life cycle assessment for retrofitting buildings. *Energy and Buildings*, 82:92–99, 2014.

S. ANTONIOU and R. PINHO. Advantages and limitations of adaptive and non-adaptive force-based pushover procedures. *Journal of earthquake engineering*, 8 (04):497–522, 2004.

S. Antoniou and R. Pinho. Development and verification of a displacement-based adaptive pushover procedure. *Journal of earthquake engineering*, 8(05):643–661, 2004.

G. Apostolakis. Optimal evolutionary seismic design of three-dimensional multistory structures with damping devices. *Journal of Structural Engineering*, 146(10): 04020205, 2020.

D. Arditi, A. Elhassan, and Y. C. Toklu. Constructability analysis in the design firm. *Journal of construction engineering and management*, 128(2):117–126, 2002.

M. Arici, M. F. Granata, et al. Prevenzione del degrado dei ponti in cap con la precompressione bilanciata. il ponte funicolare. *Seminario Internazionale CIAS*, 2019.

J. Arora. *Introduction to optimum design*. Elsevier, 2004.

J. Arora and E. Haug Jr. Efficient optimal design of structures by generalized steepest descent programming. *International Journal for Numerical Methods in Engineering*, 10(4):747–766, 1976.

P. A. T. Arpini, M. C. Loureiro, B. D. Breda, A. F. Calenzani, and É. C. Alves. Optimum design of a composite floor system considering environmental and economic impacts. *Revista IBRACON de Estruturas e Materiais*, 15, 2021.

M. Artar. Optimum design of braced steel frames via teaching learning based optimization. *Steel and Composite Structures*, 22(4):733–744, 2016.

M. Artar and A. T. Daloglu. Optimum design of composite steel frames with semi-rigid connections and column bases via genetic algorithm. *Steel Compos. Struct*, 19(4):1035–1053, 2015a.

M. Artar and A. T. Daloglu. Optimum design of steel space frames with composite beams using genetic algorithm. *Steel and Composite Structures*, 19(2):503–519, 2015b.

M. Artar and A. T. Daloglu. Optimum design of steel frames with semi-rigid connections and composite beams. *Structural engineering and mechanics: An international journal*, 55(2):299–313, 2015c.

F. Ascione, R. F. De Masi, F. de Rossi, S. Ruggiero, and G. P. Vanoli. Optimization of building envelope design for nzebs in mediterranean climate: Performance analysis of residential case study. *Applied energy*, 183:938–957, 2016.

F. Ascione, N. Bianco, C. De Stasio, G. M. Mauro, and G. P. Vanoli. Casa, cost-optimal analysis by multi-objective optimisation and artificial neural networks: A new framework for the robust assessment of cost-optimal energy retrofit, feasible for any building. *Energy and Buildings*, 146:200–219, 2017.

F. Ascione, N. Bianco, G. M. Mauro, and G. P. Vanoli. A new comprehensive framework for the multi-objective optimization of building energy design: Harlequin. *Applied Energy*, 241:331–361, 2019.

R. Asso, R. Cucuzza, M. M. Rosso, D. Masera, and G. C. Marano. BRIDGES MONITORING: AN APPLICATION OF AI WITH GAUSSIAN PROCESSES. In *14th International Conference on Evolutionary and Deterministic Methods for Design, Optimization and Control*. Institute of Structural Analysis and Antiseismic Research National Technical University of Athens, 2021. doi: 10.7712/140121.7964.18426.

E. Atrek, R. H. GALLAGHER, K. Ragsdell, and O. C. ZIENKIEWICZ. New directions in optimum structural design. *Chichester, England and New York, Wiley-Interscience, 1984, 748*, 1984.

Z. Aydın. Size, layout and tendon profile optimization of prestressed steel trusses using jaya algorithm. In *Structures*, volume 40, pages 284–294. Elsevier, 2022.

Z. Aydın and E. Cakir. Cost minimization of prestressed steel trusses considering shape and size variables. *Steel and composite structures*, 19(1):43–58, 2015.

S. K. Azad, M. Bybordiani, S. K. Azad, and F. K. Jawad. Simultaneous size and geometry optimization of steel trusses under dynamic excitations. *Structural and Multidisciplinary Optimization*, 58:2545–2563, 2018.

A. Baghdadi, M. Heristchian, and H. Kloft. Connections placement optimization approach toward new prefabricated building systems. *Engineering Structures*, 233:111648, 2021.

M. H. Bagherinejad and A. Haghollahi. Topology optimization of steel plate shear walls in the moment frames. *Steel and Composite Structures*, 29(6):767–779, 2018.

R. Baker. Determination of the critical slip surface in slope stability computations. *International Journal for Numerical and Analytical Methods in Geomechanics*, 4 (4):333–359, 1980.

J. S. Ballaben and M. B. Rosales. Nonlinear dynamic analysis of a 3d guyed mast. *Nonlinear Dynamics*, 93:1395–1405, 2018.

J. S. Ballaben, A. M. Guzmán, and M. B. Rosales. Nonlinear dynamics of guyed masts under wind load: Sensitivity to structural parameters and load models. *Journal of Wind Engineering and Industrial Aerodynamics*, 169:128–138, 2017.

R. Balling. Optimal steel frame design by simulated annealing. *Journal of Structural Engineering (United States)*, 117(6):1780–1795, 1991a. URL https://www.scopus.com/inward/record.uri?eid=2-s2.0-0026173041&doi=10.1061%2f%28ASCE%290733-9445%281991%29117%3a6%281780%29&partnerID=40&md5=445f75d230f0dea8cb9a381c8c125fd4.

R. J. Balling. Optimal steel frame design by simulated annealing. *Journal of structural Engineering*, 117(6):1780–1795, 1991b.

R. J. Balling, L. J. Balling, and P. W. Richards. Design of buckling-restrained braced frames using nonlinear time history analysis and optimization. *Journal of structural engineering*, 135(5):461–468, 2009.

S. A. Barakat and S. Altoubat. Application of evolutionary global optimization techniques in the design of rc water tanks. *Engineering Structures*, 31(2):332–344, 2009. ISSN 0141-0296. doi: 10.1016/j.engstruct.2008.09.006.

S. Barg, F. Flager, and M. Fischer. A design-focused, cost-ranked, structural-frame sizing optimization. *Journal of Building Engineering*, 30:101269, 2020.

B. M. Basha and G. S. Babu. Target reliability based design optimization of anchored cantilever sheet pile walls. *Canadian Geotechnical Journal*, 45(4):535–548, 2008.

F. Bazzucchi, L. Restuccia, and G. A. Ferro. Considerations over the italian road bridge infrastructure safety after the polcevera viaduct collapse: past errors and future perspectives. *Frattura e Integrita Strutturale*, 12, 2018.

O. Begambre and J. E. Laier. A hybrid particle swarm optimization–simplex algorithm (psos) for structural damage identification. *Advances in Engineering Software*, 40(9):883–891, 2009.

L. L. Beghini, A. Beghini, N. Katz, W. F. Baker, and G. H. Paulino. Connecting architecture and engineering through structural topology optimization. *Engineering Structures*, 59:716–726, 2014.

A. D. Belegundu and T. R. Chandrupatla. *Optimization concepts and applications in engineering*. Cambridge University Press, 2019.

R. Belevičius, D. Jatulis, and D. Šešok. Optimization of tall guyed masts using genetic algorithms. *Engineering Structures*, 56:239–245, 2013.

L. C. Bell and D. M. Brown. Guyed tower optimization. *Computers & Structures*, 6 (6):447–450, 1976.

R. Bellman. Dynamic programming. *Science*, 153(3731):34–37, 1966.

G. Belov. Problems, models and algorithms in one-and two-dimensional cutting. 2003.

L. Berke. An efficient approach to the minimum weight design of deflection limited structures. *Rep. Air Force Flight Dynamics Lab*, 1970.

L. Berke and N. Khot. Structural optimization using optimality criteria. In *Computer aided optimal design: structural and mechanical systems*, pages 271–311. Springer, 1987.

A. M. Bertetto and G. Marano. Numerical and dimensionless analytical solutions for circular arch optimization. *Engineering Structures*, 253:113360, 2022.

H.-G. Beyer. Toward a theory of evolution strategies: Self-adaptation. *Evolutionary Computation*, 3(3):311–347, 1995. doi: 10.1162/evco.1995.3.3.311.

H.-G. Beyer and H.-P. Schwefel. Evolution strategies - a comprehensive introduction. *Natural Computing*, 1:3–52, 03 2002. doi: 10.1023/A:1015059928466.

C. M. Bishop and N. M. Nasrabadi. *Pattern recognition and machine learning*, volume 4. Springer, 2006.

B. Błachowski. Model based predictive control of guyed mast vibration. *Journal of Theoretical and Applied Mechanics*, 45(2):405–423, 2007.

M. W. Bloomfield, J. E. Herencia, and P. M. Weaver. Analysis and benchmarking of meta-heuristic techniques for lay-up optimization. *Computers & structures*, 88 (5-6):272–282, 2010.

R. M. Brach. Minimum dynamic response for a class of simply supported beam shapes. *International Journal of Mechanical Sciences*, 10(5):429–439, 1968.

F. Braga, R. Gigliotti, and R. Laguardia. Intervention cost optimization of bracing systems with multiperformance criteria. *Engineering Structures*, 182:185–197, 2019.

M. Brognoli, P. Gelfi, R. Zandonini, and M. Zanella. Optimal design of semi-rigid braced frames via knowledge-based approach. *Journal of Constructional Steel Research*, 46(1-3):365–366, 1998. URL https://www.scopus.com/inward/record.uri?eid=2-s2.0-0032036029&doi=10.1016%2fS0143-974X%2898%2980048-5&partnerID=40&md5=999888b6f850e406377ecdfaab8de3bf.

N. C. Brown and C. T. Mueller. Design for structural and energy performance of long span buildings using geometric multi-objective optimization. *Energy and Buildings*, 127:748–761, 2016.

C. Brunelli, F. Castellani, A. Garinei, L. Biondi, and M. Marconi. A procedure to perform multi-objective optimization for sustainable design of buildings. *Energies*, 9(11):915, 2016.

J. Brütting, G. Senatore, and C. Fivet. Optimization formulations for the design of low embodied energy structures made from reused elements. In *Advanced Computing Strategies for Engineering: 25th EG-ICE International Workshop 2018, Lausanne, Switzerland, June 10-13, 2018, Proceedings, Part I 25*, pages 139–163. Springer, 2018.

J. Brütting, J. Desruelle, G. Senatore, and C. Fivet. Design of truss structures through reuse. In *Structures*, volume 18, pages 128–137. Elsevier, 2019a.

J. Brütting, C. Fivet, and G. Senatore. Exploration of spatial structures made from reused elements and the design of optimal kits-of-parts. In *Structures and Architecture: Bridging the Gap and Crossing Borders*, pages 221–228. CRC Press, 2019b.

J. Brütting, G. Senatore, M. Schevenels, and C. Fivet. Optimum design of frame structures from a stock of reclaimed elements. *Frontiers in Built Environment*, 6: 57, 2020a.

J. Brütting, C. Vandervaeren, G. Senatore, N. De Temmerman, and C. Fivet. Environmental impact minimization of reticular structures made of reused and new elements through life cycle assessment and mixed-integer linear programming. *Energy and Buildings*, 215:109827, 2020b.

J. Brütting, G. Senatore, and C. Fivet. Design and fabrication of a reusable kit of parts for diverse structures. *Automation in Construction*, 125:103614, 2021.

H. Buchholdt, S. Moossavinejad, and A. Iannuzzi. Non-linear dynamic analysis of guyed masts subjected to wind and guy r uptures. *Proceedings of the Institution of Civil Engineers*, 81(3):353–395, 1986.

M. Bybordiani and S. Kazemzadeh Azad. Optimum design of steel braced frames considering dynamic soil-structure interaction. *Structural and Multidisciplinary Optimization*, 60:1123–1137, 2019.

L. Caldas, L. Norford, and J. Rocha. An evolutionary model for sustainable design. *Management of Environmental Quality: An International Journal*, 14(3):383–397, 2003.

L. G. Caldas and L. K. Norford. A design optimization tool based on a genetic algorithm. *Automation in construction*, 11(2):173–184, 2002.

L. G. Caldas and L. K. Norford. Genetic algorithms for optimization of building envelopes and the design and control of hvac systems. *J. Sol. Energy Eng.*, 125(3): 343–351, 2003.

C. Camp and M. Farshchin. Design of space trusses using modified teaching-learning based optimization. *Engineering Structures*, 62-63:87–97, 2014a. URL https://www.scopus.com/inward/record.uri?eid=2-s2.0-84893775759&doi=10.1016%2fj.engstruct.2014.01.020&partnerID=40&md5=4a2992c3ca6aaee0a85d907cb3ad18c9.

C. V. Camp and M. Farshchin. Design of space trusses using modified teaching–learning based optimization. *Engineering Structures*, 62:87–97, 2014b.

C. V. Camp and F. Huq. Co2 and cost optimization of reinforced concrete frames using a big bang-big crunch algorithm. *Engineering Structures*, 48:363–372, 2013.

C. W. Carroll. The created response surface technique for optimizing nonlinear, restrained systems. *Operations research*, 9(2):169–184, 1961.

C.-M. Chan, A. Sherbourne, and D. Grierson. Stiffness optimization technique for 3d tall steel building frameworks under multiple lateral loadings. *Engineering Structures*, 16(8):570–576, 1994. URL https://www.scopus.com/inward/record.uri?eid=2-s2.0-0028542032&doi=10.1016%2f0141-0296%2894%2990042-6&partnerID=40&md5=24cc4294ac576a8dfdf7e9a5ebefa9d4.

C.-M. Chan, D. Grierson, and A. Sherbourne. Automatic optimal design of tall steel building frameworks. *Journal of Structural Engineering (United States)*, 121(5):838–847, 1995a. URL https://www.scopus.com/inward/record.uri?eid=2-s2.0-0029310358&doi=10.1061%2f%28ASCE%290733-9445%281995%29121%3a5%28838%29&partnerID=40&md5=95a3f3a2da55b4ed8febfc76e4e72264.

C.-M. Chan, D. E. Grierson, and A. N. Sherbourne. Automatic optimal design of tall steel building frameworks. *Journal of Structural Engineering*, 121(5):838–847, 1995b.

S.-L. Chan and P.-T. Chui. *Non-linear static and cyclic analysis of steel frames with semi-rigid connections*. Elsevier, 2000.

D. Chen. *Least weight design of 2-D and 3-D geometrically nonlinear framed structures using a genetic algorithm*. The University of Memphis, 1997.

J. Chen, Y. Wang, and X. Zhan. Topology optimization of steel structure for waste incineration steam generator based on de and pso. *International Journal of Steel Structures*, 21(4):1210–1227, 2021.

T.-Y. Chen and T.-M. Chi. On the improvements of the particle swarm optimization algorithm. *Advances in Engineering Software*, 41(2):229–239, 2010.

W.-F. Chen and N. Kishi. Semirigid steel beam-to-column connections: Data base and modeling. *Journal of Structural Engineering*, 115(1):105–119, 1989.

W.-F. Chen, Y. Goto, and J. R. Liew. *Stability design of semi-rigid frames*. John Wiley & Sons, 1995.

W.-K. Chen. *Stability design of steel frames*. CRC press, 2018.

B. Cheng, Q. Qian, and H. Sun. Steel truss bridges with welded box-section members and bowknot integral joints, part ii: Minimum weight optimization. *Journal of Constructional Steel Research*, 80:475–482, 2013.

C. Cheng, B. Feiring, and T. Cheng. The cutting stock problem—a survey. *International Journal of Production Economics*, 36(3):291–305, 1994.

F. Cheng and D. Juang. Recursive optimization for seismic steel frames. *Journal of Structural Engineering (United States)*, 115(2):445–466, 1989a. URL https://www.scopus.com/inward/record.uri?eid=2-s2.0-0024607497&doi=10.1061%2f%28ASCE%290733-9445%281989%29115%3a2%28445%29&partnerID=40&md5=4495c5844b7d271f9330ae2fce001615.

F. Y. Cheng and D. Juang. Recursive optimization for seismic steel frames. *Journal of Structural Engineering*, 115(2):445–466, 1989b.

J. Cheng. Optimum design of steel truss arch bridges using a hybrid genetic algorithm. *Journal of Constructional Steel Research*, 66(8-9):1011–1017, 2010.

Y. M. Cheng. Global optimization analysis of slope stability by simulated annealing with dynamic bounds and dirac function. *Engineering Optimization*, 39(1):17–32, 2007.

Y. M. Cheng, L. Li, and S. Chi. Performance studies on six heuristic global optimization methods in the location of critical slip surface. *Computers and Geotechnics*, 34(6):462–484, 2007.

E. Ching and J. V. Carstensen. Truss topology optimization of timber–steel structures for reduced embodied carbon design. *Engineering Structures*, 252:113540, 2022.

S.-H. Choi and S.-E. Kim. Optimal design of steel frame using practical nonlinear inelastic analysis. *Engineering Structures*, 24(9):1189–1201, 2002.

S. W. Choi, Y. Kim, J. Lee, K. Hong, and H. S. Park. Minimum column-to-beam strength ratios for beam–hinge mechanisms based on multi-objective seismic design. *Journal of Constructional Steel Research*, 88:53–62, 2013.

P. Christensen and A. Klarbring. *An Introduction to Structural Optimization*, volume 153. 01 2008a. ISBN 978-1-4020-8665-6. doi: 10.1007/978-1-4020-8666-3.

P. W. Christensen and A. Klarbring. *An introduction to structural optimization*, volume 153. Springer Science & Business Media, 2008b.

P. W. Christensen and A. Klarbring. *An introduction to structural optimization*, volume 153. Springer Science & Business Media, 2008c.

P. Cicconi, V. Castorani, M. Germani, M. Mandolini, and A. Vita. A multi-objective sequential method for manufacturing cost and structural optimization of modular steel towers. *Engineering with Computers*, 36(2):475–497, 2020.

M. Clobes and U. Peil. Unsteady buffeting wind loads in the time domain and their effect on the life-cycle prediction of guyed masts. *Structure and Infrastructure Engineering*, 7(1-2):187–196, 2011.

C. Coello. Self-adaptive penalties for ga-based optimization. In *Proceedings of the 1999 Congress on Evolutionary Computation-CEC99 (Cat. No. 99TH8406)*, volume 1, pages 573–580 Vol. 1, 1999. doi: 10.1109/CEC.1999.781984.

C. Coello and A. Christiansen. Multiobjective optimization of trusses using genetic algorithms. *Computers and Structures*, 75(6):647–660, 2000a. URL https://www.scopus.com/inward/record.uri?eid=2-s2.0-0033873684&doi=10.1016%2fS0045-7949%2899%2900110-8&partnerID=40&md5=bc560dea4fb33141bdf753ed5105a1d8.

C. Coello and A. D. Christiansen. Multiobjective optimization of trusses using genetic algorithms. *Computers & Structures*, 75(6):647–660, 2000b.

C. A. C. Coello. Theoretical and numerical constraint-handling techniques used with evolutionary algorithms: a survey of the state of the art. *Computer methods in applied mechanics and engineering*, 191(11-12):1245–1287, 2002.

C. A. Coello Coello. Theoretical and numerical constraint-handling techniques used with evolutionary algorithms: a survey of the state of the art. *Computer Methods in Applied Mechanics and Engineering*, 191(11):1245–1287, 2002. ISSN 0045-7825. doi: 10.1016/S0045-7825(01)00323-1.

D. A. Coley and S. Schukat. Low-energy design: combining computer-based optimisation and human judgement. *Building and Environment*, 37(12):1241–1247, 2002a.

D. A. Coley and S. Schukat. Low-energy design: combining computer-based optimisation and human judgement. *Building and Environment*, 37(12):1241–1247, 2002b.

C. Cortes and V. Vapnik. Support-vector networks. *Machine learning*, 20:273–297, 1995.

R. Costa, P. Providencia, and M. Ferreira. Influence of joint modelling on the pushover analysis of a rc frame. *Structural Engineering and Mechanics, An Int'l Journal*, 64(5):641–652, 2017.

A. Crawford and W. Jenkins. Optimum design of some steel roof structures. *Structural Engineer*, 58 A(10):317–325, 1980. URL https://www.scopus.com/inward/record.uri?eid=2-s2.0-0019069684&partnerID=40&md5=d2335d3133db60add53bb606154e0712.

N. Cristianini and B. Scholkopf. Support vector machines and kernel methods: the new generation of learning machines. *Ai Magazine*, 23(3):31–31, 2002.

A. Csébfalvi. Optimal design of frame structures with semi-rigid joints. *Periodica Polytechnica Civil Engineering*, 51(1):9–15, 2007.

R. Cucuzza, C. Costi, M. M. Rosso, M. Domaneschi, G. C. Marano, and D. Masera. Optimal strengthening by steel truss arches in prestressed girder bridges. In *Proceedings of the Institution of Civil Engineers-Bridge Engineering*, pages 1–21. Thomas Telford Ltd, 2021a.

R. Cucuzza, M. M. Rosso, and G. Marano. Optimal preliminary design of variable section beams criterion. *SN Applied Sciences*, 3, 08 2021b. doi: 10.1007/s42452-021-04702-5.

R. Cucuzza, M. M. Rosso, A. Aloisio, J. Melchiorre, M. L. Giudice, and G. C. Marano. Size and shape optimization of a guyed mast structure under wind, ice and seismic loading. *Applied Sciences*, 12(10):4875, 2022.

J. Da Silva, L. De Lima, P. d. S. Vellasco, S. De Andrade, and R. De Castro. Nonlinear dynamic analysis of steel portal frames with semi-rigid connections. *Engineering Structures*, 30(9):2566–2579, 2008.

A. T. Daloglu, M. Artar, K. Özgan, and A. İ. Karakas. Optimum design of steel space frames including soil-structure interaction. *Structural and Multidisciplinary Optimization*, 54(1):117–131, 2016.

A. Daly and W. Witarnawan. Strengthening of bridges using external post-tensioning. In *Conference of eastern Asia society for transportation studies, Seoul, Korea*, 1997.

G. B. Dantzig and P. Wolfe. Decomposition principle for linear programs. *Operations research*, 8(1):101–111, 1960.

S. Das and P. N. Suganthan. Differential evolution: A survey of the state-of-the-art. *IEEE transactions on evolutionary computation*, 15(1):4–31, 2010.

A. Davenport and B. Sparling. Dynamic gust response factors for guyed towers. *Journal of Wind Engineering and Industrial Aerodynamics*, 43(1-3):2237–2248, 1992.

D. De Domenico, H. Qiao, Q. Wang, Z. Zhu, and G. Marano. Optimal design and seismic performance of multi-tuned mass damper inerter (mtmdi) applied to adjacent high-rise buildings. *The Structural Design of Tall and Special Buildings*, 29(14):e1781, 2020. doi: https://doi.org/10.1002/tal.1781.

G. F. de Medeiros and M. Kripka. Optimization of reinforced concrete columns according to different environmental impact assessment parameters. *Engineering Structures*, 59:185–194, 2014.

W. J. de Santana Gomes and A. T. Beck. Global structural optimization considering expected consequences of failure and using ann surrogates. *Computers & Structures*, 126:56–68, 2013.

R. R. de Souza, L. F. F. Miguel, R. H. Lopez, L. F. F. Miguel, and A. J. Torii. A procedure for the size, shape and topology optimization of transmission line tower structures. *Engineering Structures*, 111:162–184, 2016.

D. De Tommasi, G. Marano, G. Puglisi, and F. Trentadue. Morphological optimization of tensegrity-type metamaterials. *Composites Part B: Engineering*, 115: 182–187, 2017. doi: 10.1016/j.compositesb.2016.10.017.

K. Deb. An efficient constraint handling method for genetic algorithms. *Comput. Method Appl. M.*, 186:311–338, 01 2000a.

K. Deb. An efficient constraint handling method for genetic algorithms. *Computer methods in applied mechanics and engineering*, 186(2-4):311–338, 2000b.

S. Degertekin, M. Hayalioglu, and H. Gorgun. Optimum design of geometrically nonlinear steel frames with semi-rigid connections using a harmony search algorithm. *Steel and Composite Structures, An International Journal*, 9(6):535–555, 2009.

S. Dehghani, A. Vosoughi, and M. R. Banan. The effects of rehabilitation objectives on near optimal trade-off relation between minimum weight and maximum drift of 2d steel x-braced frames considering soil-structure interaction using a cluster-based nsga ii. *Structural and Multidisciplinary Optimization*, 59:1703–1722, 2019.

M. Delorme, M. Iori, and S. Martello. Bin packing and cutting stock problems: Mathematical models and exact algorithms. *European Journal of Operational Research*, 255(1):1–20, 2016.

Z. Q. Deng, Y. Zhang, H. L. Huang, and B. Li. Parametric optimization for a tapered deployable mast in an integrated design environment. In *Advanced Materials Research*, volume 346, pages 426–432. Trans Tech Publ, 2012.

A. Devitofranceschi. Riparazione di viadotti stradali in precompresso: tecniche di intervento ed analisi costi benefici. *Italian Concrete Days-AICAP*, 2018.

B. S. Dhillon and J. W. O'Malley III. Interactive design of semirigid steel frames. *Journal of Structural Engineering*, 125(5):556–564, 1999.

A. K. Dhingra and B. Lee. A genetic algorithm approach to single and multiobjective structural optimization with discrete–continuous variables. *International Journal for Numerical Methods in Engineering*, 37(23):4059–4080, 1994.

M. Di Ludovico, A. Prota, G. Manfredi, and E. Cosenza. Frp strengthening of full-scale pc girders. *Journal of Composites for Construction*, 14(5):510–520, 2010.

F. Di Trapani, G. Tomaselli, A. P. Sberna, M. M. Rosso, G. C. Marano, L. Cavaleri, and G. Bertagnoli. Dynamic response of infilled frames subject to accidental column losses. In C. Pellegrino, F. Faleschini, M. A. Zanini, J. C. Matos, J. R. Casas, and A. Strauss, editors, *Proceedings of the 1st Conference of the European Association on Quality Control of Bridges and Structures*, pages 1100–1107, Cham, 2022. Springer International Publishing. ISBN 978-3-030-91877-4.

C. Diakaki, E. Grigoroudis, N. Kabelis, D. Kolokotsa, K. Kalaitzakis, and G. Stavrakakis. A multi-objective decision model for the improvement of energy efficiency in buildings. *Energy*, 35(12):5483–5496, 2010.

G. G. Dimopoulos. Mixed-variable engineering optimization based on evolutionary and social metaphors. *Computer Methods in Applied Mechanics and Engineering*, 196(4):803–817, 2007. ISSN 0045-7825. doi: 10.1016/j.cma.2006.06.010.

E. Doğan, S. Şeker, and M. P. S. andCelalettin Kozanoğlu. Investigating the effect of joint behavior on the optimum design of steel frames via hunting search algorithm. *Advanced Steel Construction*, 14(2):166–183, 2018.

M. Domaneschi, C. Pellecchia, E. De Iuliis, G. Cimellaro, M. Morgese, A. Khalil, and F. Ansari. Collapse analysis of the polcevera viaduct by the applied element method. *Engineering Structures*, 214:110659, 2020.

M. P. Drewniok, J. Campbell, and J. Orr. The lightest beam method–a methodology to find ultimate steel savings and reduce embodied carbon in steel framed buildings. In *Structures*, volume 27, pages 687–701. Elsevier, 2020.

R. C. Eberhart, Y. Shi, and J. Kennedy. *Swarm intelligence*. Elsevier, 2001.

T. M. Echenagucia, A. Capozzoli, Y. Cascone, and M. Sassone. The early design stage of a building envelope: Multi-objective search through heating, cooling and lighting energy performance analysis. *Applied energy*, 154:577–591, 2015.

A. Eiben and J. Smith. *Introduction To Evolutionary Computing*, volume 45. 01 2003. ISBN 978-3-642-07285-7. doi: 10.1007/978-3-662-05094-1.

A. Elvin and J. Strydom. Optimizing structures with semi-rigid connections using the principle of virtual work. *International Journal of Steel Structures*, 18:1006–1017, 2018.

A. Elvin and J. Strydom. Optimizing the design of tall buildings using the principle of virtual work: The effect of semi rigid connections. *International Journal of Steel Structures*, 21:1–21, 2021.

F. Erbatur and M. Al-Hussainy. Optimum design of frames. *Computers and Structures*, 45(5-6):887–891, 1992a. URL https://www.scopus.com/inward/record.uri?eid=2-s2.0-0027111099&doi=10.1016%2f0045-7949%2892%2990047-4&partnerID=40&md5=44ab1e69804fb2ebcf03ea71872a1177.

F. Erbatur and M. Al-Hussainy. Optimum design of frames. *Computers & structures*, 45(5-6):887–891, 1992b.

F. Erbatur, O. Hasançebi, I. Tütüncü, and H. Kılıç. Optimal design of planar and space structures with genetic algorithms. *Computers and Structures*, 75(2): 209–224, 2000. URL https://www.scopus.com/inward/record.uri?eid=2-s2.0-0342647286&doi=10.1016%2fS0045-7949%2899%2900084-X&partnerID=40&md5=786f5f777403689f4fe7d25447204fb4.

Z. Fan, X. Liu, X. Fan, C. Hu, T. Hu, X. Wu, and Y. Yu. Design and research of large-span steel structure for the national stadium. *Jianzhu Jiegou Xuebao/Journal of Building Structures*, 28(2): 1–16, 2007. URL https://www.scopus.com/inward/record.uri?eid=2-s2.0-34249860637&partnerID=40&md5=821f3581bdccb774547efefff488c989.

F. Farhat, S. Nakamura, and K. Takahashi. Application of genetic algorithm to optimization of buckling restrained braces for seismic upgrading of existing structures. *Computers & structures*, 87(1-2):110–119, 2009.

M. Farshchin, M. Maniat, C. V. Camp, and S. Pezeshk. School based optimization algorithm for design of steel frames. *Engineering Structures*, 171:326–335, 2018.

M. A. Fathali and S. R. H. Vaez. Optimum performance-based design of eccentrically braced frames. *Engineering Structures*, 202:109857, 2020.

S. Fathizadeh, A. Vosoughi, and M. R. Banan. Considering soil–structure interaction effects on performance-based design optimization of moment-resisting steel frames by an engineered cluster-based genetic algorithm. *Engineering Optimization*, 53(3):440–460, 2021.

T. Feng, J. Arora, and J. Haug, E.J. Optimal structural design under dynamic loads. *International Journal for Numerical Methods in Engineering*, 11(1): 39–52, 1977a. URL https://www.scopus.com/inward/record.uri?eid=2-s2.0-0017417628&doi=10.1002%2fnme.1620110106&partnerID=40&md5=45506be25bb6b18c8426770ea2d6ed20.

T.-T. Feng, J. Arora, and E. Haug Jr. Optimal structural design under dynamic loads. *International Journal for Numerical Methods in Engineering*, 11(1):39–52, 1977b.

A. V. Fiacco and G. P. McCormick. *Nonlinear programming: sequential unconstrained minimization techniques*. SIAM, 1990.

A. Fiore, G. Marano, R. Greco, and E. Mastromarino. Structural optimization of hollow-section steel trusses by differential evolution algorithm. *International Journal of Steel Structures*, 16(2):411–423, 2016a. URL https://www.scopus.com/inward/record.uri?eid=2-s2.0-84978256862&doi=10.1007%2fs13296-016-6013-1&partnerID=40&md5=f53f0173104cd5811f052b456130b92f.

A. Fiore, G. C. Marano, R. Greco, and E. Mastromarino. Structural optimization of hollow-section steel trusses by differential evolution algorithm. *International journal of steel Structures*, 16:411–423, 2016b.

A. Fiore, G. C. Marano, R. Greco, and E. Mastromarino. Structural optimization of hollow-section steel trusses by differential evolution algorithm. *International journal of steel Structures*, 16:411–423, 2016c.

I. Fister jr and I. Fister. *On the Mutation Operators in Evolution Strategies*, volume 18, pages 69–89. 01 2015. doi: 10.1007/978-3-319-14400-9_3.

F. Flager, B. Welle, P. Bansal, G. Soremekun, and J. Haymaker. Multidisciplinary process integration and design optimization of a classroom building. *Journal of Information Technology in Construction (ITcon)*, 14(38):595–612, 2009.

C. Foley, S. Pezeshk, and A. Alimoradi. Probabilistic performance-based optimal design of steel moment-resisting frames. i: Formulation. *Journal of Structural Engineering*, 133(6):757–766, 2007. URL https://www.scopus.com/inward/record.uri?eid=2-s2.0-34248592926&doi=10.1061%2f%28ASCE%290733-9445%282007%29133%3a6%28757%29&partnerID=40&md5=f8581a13a0e55c7d3c63c95f493db358.

C. M. Foley and D. Schinler. Automated design of steel frames using advanced analysis and object-oriented evolutionary computation. *Journal of Structural Engineering*, 129(5):648–660, 2003.

R. L. FOX and M. P. KAPOOR. Structural optimization in the dynamics response regime-a computational approach. *AIAA Journal*, 8(10):1798–1804, 1970.

M. Fragiadakis, N. D. Lagaros, and M. Papadrakakis. Performance-based multiobjective optimum design of steel structures considering life-cycle cost. *Structural and Multidisciplinary Optimization*, 32:1–11, 2006.

V. Franciosi. Archi. *Scienza delle costruzioni*, 3(2):208–209, 1971.

D. Frangopol and K. Maute. Life-cycle reliability-based optimization of civil and aerospace structures. *Computers and Structures*, 81(7):397–410, 2003. URL https://www.scopus.com/inward/record.uri?eid=2-s2.0-0037400057&doi=10.1016%2fS0045-7949%2803%2900020-8&partnerID=40&md5=95585389c5a7768f1c779f48711d86cd.

J. Fu, J. Wu, C. Dong, A. Xu, and Y.-L. Pi. Optimization design of large span portal-rigid steel frame with tapered sections under wind-induced drift constraint. *Engineering Structures*, 194:396–405, 2019.

Y. Fujino, P. Warnitchai, and B. Pacheco. Active stiffness control of cable vibration. 1993.

A. Gandomi, X.-S. Yang, S. Talatahari, and A. Alavi. *Metaheuristic Algorithms in Modeling and Optimization*. 2013a. doi: 10.1016/B978-0-12-398364-0.00001-2. URL https://www.scopus.com/inward/record.uri?eid=2-s2.0-84882701685&doi=10.1016%2fB978-0-12-398364-0.00001-2&partnerID=40&md5=45b15539896d7277462abe1aec0efaa2. cited By 146.

A. H. Gandomi. Interior search algorithm (isa): a novel approach for global optimization. *ISA transactions*, 53(4):1168–1183, 2014.

A. H. Gandomi, S. Talatahari, X.-S. Yang, and S. Deb. Design optimization of truss structures using cuckoo search algorithm. *The structural design of tall and special buildings*, 22(17):1330–1349, 2013b.

A. H. Gandomi, A. R. Kashani, M. Mousavi, and M. Jalalvandi. Slope stability analyzing using recent swarm intelligence techniques. *International Journal for Numerical and Analytical Methods in Geomechanics*, 39(3):295–309, 2015.

T. García-Segura and V. Yepes. Multiobjective optimization of post-tensioned concrete box-girder road bridges considering cost, co2 emissions, and safety. *Engineering Structures*, 125:325–336, 2016.

P. Gatheeshgar, K. Poologanathan, S. Gunalan, K. D. Tsavdaridis, B. Nagaratnam, and E. Iacovidou. Optimised cold-formed steel beams in modular building applications. *Journal of Building Engineering*, 32:101607, 2020.

W. Gawronski, B. Bienkiewicz, and R. Hill. Wind-induced dynamics of a deep space network antenna. *Journal of sound and vibration*, 178(1):67–77, 1994.

H.-W. Ge, Y.-C. Liang, and M. Marchese. A modified particle swarm optimization-based dynamic recurrent neural network for identifying and controlling nonlinear systems. *Computers & Structures*, 85(21-22):1611–1622, 2007.

Z. W. Geem, J. H. Kim, and G. V. Loganathan. A new heuristic optimization algorithm: harmony search. *simulation*, 76(2):60–68, 2001.

P. Gerstoft and A. Davenport. A simplified method for dynamic analysis of a guyed mast. *Journal of Wind Engineering and Industrial Aerodynamics*, 23:487–499, 1986.

M. Ghaderi and S. Gholizadeh. Mainshock–aftershock low-cycle fatigue damage evaluation of performance-based optimally designed steel moment frames. *Engineering Structures*, 237:112207, 2021.

A. Ghasemof, M. Mirtaheri, and R. K. Mohammadi. A new swift algorithm for bi-objective optimum design of steel moment frames. *Journal of Building Engineering*, 39:102162, 2021.

S. Gholizadeh and F. Fattahi. Optimum design of steel structures for earthquake loading by grey wolf algorithm. 2015.

S. Gholizadeh and F. Fattahi. Multi-objective design optimization of steel moment frames considering seismic collapse safety. *Engineering with Computers*, 37(2): 1315–1328, 2021.

S. Gholizadeh and A. Milani. Optimal performance-based design of steel frames using advanced metaheuristics. 2016.

S. Gholizadeh and A. Milany. An improved fireworks algorithm for discrete sizing optimization of steel skeletal structures. *Engineering Optimization*, 50(11):1829–1849, 2018.

S. Gholizadeh and R. K. Moghadas. Performance-based optimum design of steel frames by an improved quantum particle swarm optimization. *Advances in Structural Engineering*, 17(2):143–156, 2014.

S. Gholizadeh and H. Poorhoseini. Performance-based optimum seismic design of steel dual braced frames by bat algorithm. *Metaheuristics and optimization in civil engineering*, pages 95–114, 2016a.

S. Gholizadeh and H. Poorhoseini. Seismic layout optimization of steel braced frames by an improved dolphin echolocation algorithm. *Structural and Multidisciplinary Optimization*, 54:1011–1029, 2016b.

S. Gholizadeh and E. Salajegheh. Optimal design of structures subjected to time history loading by swarm intelligence and an advanced metamodel. *Computer Methods in Applied Mechanics and Engineering*, 198(37-40):2936–2949, 2009.

S. Gholizadeh, H. Davoudi, and F. Fattahi. Design of steel frames by an enhanced moth-flame optimization algorithm. *Steel Compos Struct*, 24(1):129–140, 2017.

S. Gholizadeh, A. Hassanzadeh, A. Milany, and H. F. Ghatte. On the seismic collapse capacity of optimally designed steel braced frames. *Engineering with Computers*, pages 1–13, 2022.

L. Gil and A. Andreu. Shape and cross-section optimization of a truss structure. *Computers and Structures*, 79(7):681–689, 2001. URL https://www.scopus.com/inward/record.uri?eid=2-s2.0-0035283353&doi=10.1016%2fS0045-7949%2800%2900182-6&partnerID=40&md5=0609466f84ca6013aa5bfbfd7e44f569.

F. Gilles, S. Bernard, A. Ioannis, and R. Simon. Decision-making based on network visualization applied to building life cycle optimization. *Sustainable cities and society*, 35:565–573, 2017.

P. C. Gilmore and R. E. Gomory. A linear programming approach to the cutting-stock problem. *Operations research*, 9(6):849–859, 1961.

M. Gioffrè, V. Gusella, A. Materazzi, and I. Venanzi. Removable guyed mast for mobile phone networks: wind load modeling and structural response. *Journal of wind engineering and industrial aerodynamics*, 92(6):463–475, 2004.

K. M. Gisvold and J. Moe. A method for nonlinear mixed-integer programming and its application to design problems. 1972.

B. Godart. Pathology, appraisal, repair and management of old prestressed concrete beam and slab bridges. *Structure and Infrastructure Engineering*, 11(4):501–518, 2015.

Y. Gong. Design optimization of steel moment frames under extreme earthquake loading. *ISSN 1816-112X*, 115(1):485, 1989.

H. Gorgun and S. Yilmaz. Geometrically nonlinear analysis of plane frames with semi-rigid connections accounting for shear deformations. *Structural Engineering and Mechanics, An Int'l Journal*, 44(4):539–569, 2012.

R. Grandhi. Structural optimization with frequency constraints - a review. American Institute of Aeronautics and Astronautics Inc, AIAA, 1992. URL https://www.scopus.com/inward/record.uri?eid=2-s2.0-84990964684&doi=10.2514%2f6.1992-4813&partnerID=40&md5=ea198e6610d8d617aca941b523391be5.

R. Greco and G. Marano. Identification of parameters of maxwell and kelvin-voigt generalized models for fluid viscous dampers. *JVC/Journal of Vibration and Control*, 21(2):260–274, 2015. doi: 10.1177/1077546313487937.

D. Griersoni and T. Chiu. Optimal synthesis of frameworks under multilevel performance constraints. *Computers and Structures*, 18(5):889–898, 1984. URL https://www.scopus.com/inward/record.uri?eid=2-s2.0-0021158087&doi=10.1016%2f0045-7949%2884%2990034-8&partnerID=40&md5=3c51f0d1d447bbd6d6f0c51061bbd14a.

R. E. Griffith and R. Stewart. A nonlinear programming technique for the optimization of continuous processing systems. *Management science*, 7(4):379–392, 1961.

S. A. Guimarães, D. Klein, A. F. G. Calenzani, and É. C. Alves. Optimum design of steel columns filled with concrete via genetic algorithm: environmental impact and cost analysis. *REM-International Engineering Journal*, 75:117–128, 2022.

H. Guo and Z. Li. Structural topology optimization of high-voltage transmission tower with discrete variables. *Structural and Multidisciplinary Optimization*, 43: 851–861, 2011.

B. Gupta and S. K. Kunnath. Adaptive spectra-based pushover procedure for seismic evaluation of structures. *Earthquake spectra*, 16(2):367–391, 2000.

J. Haapio. Feature-based costing method for skeletal steel structures based on the process approach. 2012.

A. Habibi, H. Saffari, and M. Izadpanah. Optimal lateral load pattern for pushover analysis of building structures. *Steel Compos Struct*, 32(1):67–77, 2019.

A. Hadidi and A. Rafiee. Harmony search based, improved particle swarm optimizer for minimum cost design of semi-rigid steel frames. *Structural engineering and mechanics: An international journal*, 50(3):323–347, 2014.

A. Hadidi and A. Rafiee. A new hybrid algorithm for simultaneous size and semi-rigid connection type optimization of steel frames. *International Journal of Steel Structures*, 15(1):89–102, 2015.

I. Hajirasouliha and H. Moghaddam. New lateral force distribution for seismic design of structures. *Journal of Structural Engineering*, 135(8):906–915, 2009.

I. Hajirasouliha, K. Pilakoutas, and H. Moghaddam. Topology optimization for the seismic design of truss-like structures. *Computers & structures*, 89(7-8):702–711, 2011.

S. K. Hall, G. E. Cameron, and D. E. Grierson. Least-weight design of steel frameworks accounting for p-δ effects. *Journal of Structural Engineering*, 115(6): 1463–1475, 1989.

N. Hansen. An analysis of mutative σ-self-adaptation on linear fitness functions. *Evolutionary computation*, 14(3):255–275, 2006.

M. Haque. Optimal design of plane frames by the complex method. *Computers and Structures*, 20(1-3):451–456, 1985a. URL https://www.scopus.com/inward/record.uri?eid=2-s2.0-0021586996&doi=10.1016%2f0045-7949%2885%2990093-8&partnerID=40&md5=a802b80e23875008fddde47b071c5cf2.

M. Haque. Optimal design of plane frames by the complex method. In *Advances and Trends in Structures and Dynamics*, pages 451–456. Elsevier, 1985b.

P. Harikrishna, A. Annadurai, S. Gomathinayagam, and N. Lakshmanan. Full scale measurements of the structural response of a 50 m guyed mast under wind loading. *Engineering Structures*, 25(7):859–867, 2003.

O. Hasançebi and S. K. Azad. Discrete sizing of steel frames using adaptive dimensional search algorithm. *Periodica Polytechnica Civil Engineering*, 63(4): 1062–1079, 2019.

O. Hasançebi and E. DOGANB. Evaluation of topological forms for weight effective optimum design of single-span steel truss bridges. 2011.

O. Hasançebi, S. Çarbaş, E. Doğan, F. Erdal, and M. Saka. Performance evaluation of metaheuristic search techniques in the optimum design of real size pin jointed structures. *Computers & Structures*, 87(5-6):284–302, 2009.

O. Hasançebi, S. Çarbaş, E. Doğan, F. Erdal, and M. Saka. Performance evaluation of metaheuristic search techniques in the optimum design of real size pin jointed structures. *Computers & Structures*, 87(5):284–302, 2009. ISSN 0045-7949. doi: 10.1016/j.compstruc.2009.01.002.

A. Hassanzadeh and S. Gholizadeh. Collapse-performance-aided design optimization of steel concentrically braced frames. *Engineering Structures*, 197:109411, 2019.

M. Hayalioglu and S. Degertekin. Design of non-linear steel frames for stress and displacement constraints with semi-rigid connections via genetic optimization. *Structural and Multidisciplinary Optimization*, 27:259–271, 2004a.

M. Hayalioglu and S. Degertekin. Genetic algorithm based optimum design of non-linear steel frames with semi-rigid connections. *Steel and Composite Structures, An International Journal*, 4(6):453–469, 2004b.

M. Hayalioglu and S. Degertekin. Minimum cost design of steel frames with semi-rigid connections and column bases via genetic optimization. *Computers & structures*, 83(21-22):1849–1863, 2005.

M. Hayalioglu and M. Saka. Optimum design of geometrically nonlinear elastic-plastic steel frames with tapered members. *Computers and Structures*, 44 (4):915–924, 1992a. URL https://www.scopus.com/inward/record.uri?eid=2-s2.0-0027110747&doi=10.1016%2f0045-7949%2892%2990479-J&partnerID=40&md5=b3ca6aa73f75f5d871e1623cc0a57c18.

M. Hayalioglu and M. Saka. Optimum design of geometrically nonlinear elastic-plastic steel frames with tapered members. *Computers & structures*, 44(4):915–924, 1992b.

G. M. Hensley and R. H. Plaut. Three-dimensional analysis of the seismic response of guyed masts. *Engineering structures*, 29(9):2254–2261, 2007.

S. Hernández. Optimum design of steel structures. *Journal of Constructional Steel Research*, 46(1-3):374–378, 1998. URL https://www.scopus.com/inward/record.uri?eid=2-s2.0-0032036044&doi=10.1016%2fS0143-974X%2898%2980049-7&partnerID=40&md5=c9eff72d2b68afbe1ff5c5544b419096.

J. H. Holland. Genetic algorithms. *Scientific american*, 267(1):66–73, 1992.

Y.-S. Hong and E. Yu. Capacity design of eccentrically braced frame using multiobjective optimization technique. *Journal of the Computational Structural Engineering Institute of Korea*, 33(6):419–426, 2020.

A. Horn. *Integrating constructability into conceptual structural design and optimization*. PhD thesis, Massachusetts Institute of Technology, 2015.

S.-H. Hsieh and G. Deierlein. Nonlinear analysis of three-dimensional steel frames with semi-rigid connections. *Computers & structures*, 41(5):995–1009, 1991.

Y.-L. Hsu. A review of structural shape optimization. *Computers in Industry*, 25 (1):3–13, 1994a. URL https://www.scopus.com/inward/record.uri?eid=2-s2.0-0028550984&doi=10.1016%2f0166-3615%2894%2990028-0&partnerID=40&md5=84cd08de0cb68e9a696790cc0b067de4.

Y.-L. Hsu. A review of structural shape optimization. *Computers in Industry*, 25(1): 3–13, 1994b.

N. Hung. Aspects of analysis and optimization of structures under proportional and variable loadings. *Engineering Optimization*, 7(1):35–57, 1983. URL https://www.scopus.com/inward/record.uri?eid=2-s2.0-0020950533&doi=10.1080%2f03052158308960627&partnerID=40&md5=3926269297cb0d183a0578c9649c69b4.

L. J. Icerman. Optimal structural design for given dynamic deflection. *International Journal of Solids and Structures*, 5(5):473–490, 1969.

N. Ishikawa, A. Miura, S. Katsuki, and N. Satoh. A reliability analysis based on elastic-plastic displacement using an optimization technique. *Engineering Optimization*, 22(2):123–136, 1993. URL https://www.scopus.com/inward/record.uri?eid=2-s2.0-84947884590&doi=10.1080%2f03052159308941329&partnerID=40&md5=b9b56c1118f099c50ba0b172f91853e8.

M. Izadpanah and A. Habibi. Evaluating the spread plasticity model of idarc for inelastic analysis of reinforced concrete frames. *Struct. Eng. Mech*, 56(2):169–188, 2015.

M. Izadpanah and A. R. Habibi. New spread plasticity model for reinforced concrete structural elements accounting for both gravity and lateral load effects. *Journal of Structural Engineering*, 144(5):04018028, 2018.

M. Jakiela, C. Chapman, J. Duda, A. Adewuya, and K. Saitou. Continuum structural topology design with genetic algorithms. *Computer Methods in Applied Mechanics and Engineering*, 186(2-4):339–356, 2000a. URL https://www.scopus.com/inward/record.uri?eid=2-s2.0-0033746608&doi=10.1016%2fS0045-7825%2899%2900390-4&partnerID=40&md5=5101c57a00a627eedadf8a81d5c10d88.

M. J. Jakiela, C. Chapman, J. Duda, A. Adewuya, and K. Saitou. Continuum structural topology design with genetic algorithms. *Computer Methods in Applied Mechanics and Engineering*, 186(2-4):339–356, 2000b.

T. S. Jan, M. W. Liu, and Y. C. Kao. An upper-bound pushover analysis procedure for estimating the seismic demands of high-rise buildings. *Engineering structures*, 26(1):117–128, 2004.

K. Jármai and J. Farkas. Cost calculation and optimisation of welded steel structures. *Journal of Constructional Steel Research*, 50(2):115–135, 1999.

K. Jármai, J. Farkas, and P. Uys. Optimum design and cost calculation of a simple frame with welded or bolted corner joints. *Welding in the World*, 48:42–49, 2004.

K. Jármai, J. Farkas, and Y. Kurobane. Optimum seismic design of a multi-storey steel frame. *Engineering Structures*, 28(7):1038–1048, 2006.

S.-W. Jin, H. Ohmori, and S.-J. Lee. Optimal design of steel structures considering welding cost and constructability of beam-column connections. *Journal of Constructional Steel Research*, 135:292–301, 2017.

D. Johnson and D. M. Brotton. Optimum elastic design of redundant trusses. *Journal of the Structural Division*, 95(12):2589–2610, 1969.

A. R. Jordehi. A review on constraint handling strategies in particle swarm optimisation. *Neural Computing and Applications*, 26:1265–1275, 2015.

V. Kalivarapu, J.-L. Foo, and E. Winer. Synchronous parallelization of particle swarm optimization with digital pheromones. *Advances in Engineering Software*, 40(10):975–985, 2009.

E. Kameshki and M. Saka. Optimum design of nonlinear steel frames with semi-rigid connections using a genetic algorithm. *Computers and Structures*, 79 (17):1593–1604, 2001. URL https://www.scopus.com/inward/record.uri?eid=2-s2.0-0035388343&doi=10.1016%2fS0045-7949%2801%2900035-9&partnerID=40&md5=adf7515444113170b6b6619110616744.

E. Kameshki and M. Saka. Genetic algorithm based optimum design of nonlinear planar steel frames with various semi-rigid connections. *Journal of Constructional Steel Research*, 59(1):109–134, 2003.

E. Kameshki and M. Saka. Optimum geometry design of nonlinear braced domes using genetic algorithm. *Computers & structures*, 85(1-2):71–79, 2007.

L. V. Kantorovich. Mathematical methods of organizing and planning production. *Management science*, 6(4):366–422, 1960.

M. Kapoor and J. Rao. Optimum aseismic design of multistorey steel frames. *Engineering Optimization*, 11(3-4):339–353, 1987a. URL https://www.scopus.com/inward/record.uri?eid=2-s2.0-0007198299&doi=10.1080%2f03052158708941056&partnerID=40&md5=44262f7673ff2e96813d5978f08485bd.

M. Kapoor and J. Rao. Optimum aseismic design of multistorey steel frames. *Engineering optimization*, 11(3-4):339–353, 1987b.

F. Karimi and S. R. H. Vaez. Two-stage optimal seismic design of steel moment frames using the lrfd-pbd method. *Journal of Constructional Steel Research*, 155: 77–89, 2019.

A. Kashani, C. Camp, M. Rostamian, K. Azizi, and A. Gandomi. Population-based optimization in structural engineering: a review. *Artificial Intelligence Review*, 55 (1):345–452, 2022. URL https://www.scopus.com/inward/record.uri?eid=2-s2.0-85109279334&doi=10.1007%2fs10462-021-10036-w&partnerID=40&md5=2a209aaf7f244a02c324334d6215d1f0.

M. M. Kashani, J. Maddocks, and E. A. Dizaj. Residual capacity of corroded reinforced concrete bridge components: State-of-the-art review. *Journal of Bridge Engineering*, 24(7):03119001, 2019.

A. Kaveh. *Advances in metaheuristic algorithms for optimal design of structures*, volume 9783319055497. Springer International Publishing, 2014. URL https://www.scopus.com/inward/record.uri?eid=2-s2.0-84930805146&doi=10.1007%2f978-3-319-05549-7&partnerID=40&md5=58fb3806f48ef8558ae8170a2eb1fc55.

A. Kaveh and A. S. M. Abadi. Cost optimization of a composite floor system using an improved harmony search algorithm. *Journal of Constructional Steel Research*, 66(5):664–669, 2010.

A. Kaveh and H. Abbasgholiha. Optimum design of steel sway frames using big bangbig crunch algorithm. 2011.

A. Kaveh and T. Bakhshpoori. Optimum design of steel frames using cuckoo search algorithm with lévy flights. *The Structural Design of Tall and Special Buildings*, 22(13):1023–1036, 2013.

A. Kaveh and A. Fakoor. Cost optimization of steel-concrete composite floor systems with castellated steel beams. *Periodica Polytechnica Civil Engineering*, 65(2): 353–375, 2021.

A. Kaveh and M. Farhadmanesh. Optimal seismic design of steel plate shear walls using metaheuristic algorithms. *Periodica Polytechnica Civil Engineering*, 63(1): 1–17, 2019.

A. Kaveh and N. Farhoudi. Layout optimization of braced frames using differential evolution algorithm and dolphin echolocation optimization. *Periodica Polytechnica Civil Engineering*, 59(3):441–449, 2015.

A. Kaveh and N. Farhoudi. Dolphin monitoring for enhancing metaheuristic algorithms: Layout optimization of braced frames. *Computers & Structures*, 165:1–9, 2016.

A. Kaveh and M. I. Ghazaan. A comparative study of cbo and ecbo for optimal design of skeletal structures. *Computers & Structures*, 153:137–147, 2015.

A. Kaveh and A. Kaveh. Cost and co 2 emission optimization of reinforced concrete frames using enhanced colliding bodies optimization algorithm. *Applications of Metaheuristic Optimization Algorithms in Civil Engineering*, pages 319–350, 2017.

A. Kaveh and V. Mahdavi. Colliding bodies optimization for size and topology optimization of truss structures. *Structural Engineering and Mechanics*, 53(5): 847–865, 2015.

A. Kaveh and H. Moez. Minimal cycle bases for analysis of frames with semi-rigid joints. *Computers & structures*, 86(6):503–510, 2008.

A. Kaveh and S. Talatahari. Particle swarm optimizer, ant colony strategy and harmony search scheme hybridized for optimization of truss structures. *Computers & Structures*, 87(5-6):267–283, 2009.

A. Kaveh and S. Talatahari. A novel heuristic optimization method: charged system search. *Acta mechanica*, 213(3-4):267–289, 2010.

A. Kaveh, K. Laknejadi, and B. Alinejad. Performance-based multi-objective optimization of large steel structures. *Acta Mechanica*, 223(2):355–369, 2012.

A. Kaveh, I. Shojaei, Y. Gholipour, and H. Rahami. Seismic design of steel frames using multi-objective optimization. *Structural Engineering and Mechanics*, 45(2): 211–232, 2013.

A. Kaveh, M. Ghafari, and Y. Gholipour. Optimum seismic design of steel frames considering the connection types. *Journal of Constructional Steel Research*, 130: 79–87, 2017.

A. Kaveh, M. Z. Kabir, and M. Bohlool. Optimal design of multi-span pitched roof frames with tapered members. *Periodica Polytechnica Civil Engineering*, 63(1): 77–86, 2019.

A. Kaveh, K. B. Hamedani, S. M. Hosseini, and T. Bakhshpoori. Optimal design of planar steel frame structures utilizing meta-heuristic optimization algorithms. In *Structures*, volume 25, pages 335–346. Elsevier, 2020a.

A. Kaveh, S. Hoseini Vaez, P. Hosseini, and H. Abedini. Weight minimization and energy dissipation maximization of braced frames using evps algorithm. *Int J Optim Civil Eng*, 10(3):513–29, 2020b.

A. Kaveh, R. Mahdipour Moghanni, and S. Javadi. Chaotic optimization algorithm for performance-based optimization design of composite moment frames. *Engineering with Computers*, pages 1–13, 2021.

D. Kavlie and J. Moe. Automated design of frame structures. *Journal of the Structural Division*, 97(1):33–62, 1971.

J. Kennedy and R. Eberhart. Particle swarm optimization. In *Proceedings of ICNN'95-international conference on neural networks*, volume 4, pages 1942–1948. IEEE, 1995a.

J. Kennedy and R. Eberhart. Particle swarm optimization. In *Proceedings of ICNN'95 - International Conference on Neural Networks*, volume 4, pages 1942–1948 vol.4, 1995b. doi: https://www.doi.org/10.1109/ICNN.1995.488968.

J. Kennedy and R. C. Eberhart. *Swarm Intelligence*. Morgan Kaufmann Publishers Inc., San Francisco, CA, USA, 2001. ISBN 1558605959.

Y. Khalifa, O. Salem, and A. Shahin. Cutting stock waste reduction using genetic algorithms. In *Proceedings of the 8th annual conference on Genetic and evolutionary computation*, pages 1675–1680, 2006.

S. Khan. *Constructability: A Tool for Project Management*. CRC Press, 2018.

N. Khot. Algorithms based on optimality criteria to design minimum weight structures. *Engineering Optimization*, 5(2):73–90, 1981a.

N. Khot. Optimal design of a structure for system stability for a specified eigenvalue distribution. Technical report, AIR FORCE WRIGHT AERONAUTICAL LABS WRIGHT-PATTERSON AFB OH FLIGHT DYNAMICS LAB, 1981b.

N. Khot, L. Berke, and V. Venkayya. Comparison of optimality criteria algorithms for minimum weight design of structures. *AIAA Journal*, 17(2):182–190, 1979.

S. Khudeira. Strengthening of deteriorated concrete bridge girders using an external posttensioning system. *Practice Periodical on Structural Design and Construction*, 15(4):242–247, 2010.

R. Kicinger, T. Arciszewski, and K. De Jong. Evolutionary computation and structural design: A survey of the state-of-the-art. *Computers and Structures*, 83(23-24):1943–1978, 2005. doi: 10.1016/j.compstruc.2005.03.002. URL https://www.scopus.com/inward/record.uri?eid=2-s2.0-21444447611&doi=10.1016%2fj.compstruc.2005.03.002&partnerID=40&md5=85d263689e6f2f90853b0a0c6f2ef4b3. cited By 288.

U. Kirsch. *Structural optimization: fundamentals and applications*. Springer Science & Business Media, 2012.

M. Kohler, L. Forero, M. Vellasco, R. Tanscheit, and M. A. Pacheco. Pso+: A non-linear constraints-handling particle swarm optimization. In *2016 IEEE Congress on Evolutionary Computation (CEC)*, pages 2518–2523. IEEE, 2016.

M. Kohler, M. M. Vellasco, and R. Tanscheit. Pso+: A new particle swarm optimization algorithm for constrained problems. *Applied Soft Computing*, 85:105865, 2019. ISSN 1568-4946. doi: 10.1016/j.asoc.2019.105865.

K. Korkmaz and M. El-Gafy. Structural optimization assessment for steel structures. *J Steel Struct Constr*, 4(147):2472–0437, 2018.

S. Koziel and Z. Michalewicz. Evolutionary algorithms, homomorphous mappings, and constrained parameter optimization. *Evolutionary computation*, 7:19–44, 02 1999a. doi: 10.1162/evco.1999.7.1.19.

S. Koziel and Z. Michalewicz. Evolutionary algorithms, homomorphous mappings, and constrained parameter optimization. *Evolutionary computation*, 7(1):19–44, 1999b.

O. Kramer. Evolutionary self-adaptation: a survey of operators and strategy parameters. *Evolutionary Intelligence*, 3(2):51–65, 2010.

M. Kripka and G. Drehmer. Geometric optimization of steel trusses with parallel chords. *Journal of Construction Engineering*, 1(3):129–138, 2018.

C. Krishnamoorthy. Structural optimization in practice: potential applications of genetic algorithms. *Structural Engineering and Mechanics*, 11(2): 151–170, 2001. URL https://www.scopus.com/inward/record.uri?eid=2-s2.0-0035252159&doi=10.12989%2fsem.2001.11.2.151&partnerID=40&md5=5f3ba9b0b0a4dbb4dab265b86f4be126.

W. Lacarbonara and S. Ballerini. Vibration mitigation of guyed masts via tuned pendulum dampers. *Structural Engineering and Mechanics, An Int'l Journal*, 32 (4):517–529, 2009.

A. Lacey, W. Chen, H. Hao, and K. Bi. Review of bolted inter-module connections in modular steel buildings. *Journal of Building Engineering*, 23: 207–219, 2019. URL https://www.scopus.com/inward/record.uri?eid=2-s2.0-85061031098&doi=10.1016%2fj.jobe.2019.01.035&partnerID=40&md5=a0de6c84de940202f0570364b732b036.

N. Lagaros. The environmental and economic impact of structural optimization. *Structural and Multidisciplinary Optimization*, 58(4):1751–1768, 2018a. URL https://www.scopus.com/inward/record.uri?eid=2-s2.0-85046775995&doi=10.1007%2fs00158-018-1998-z&partnerID=40&md5=5a7194671aca3c2cfc6695f66549e756.

N. D. Lagaros. The environmental and economic impact of structural optimization. *Structural and Multidisciplinary Optimization*, 58(4):1751–1768, 2018b.

N. D. Lagaros and M. G. Karlaftis. Life-cycle cost structural design optimization of steel wind towers. *Computers & Structures*, 174:122–132, 2016.

N. D. Lagaros and E. Magoula. Life-cycle cost assessment of mid-rise and high-rise steel and steel–reinforced concrete composite minimum cost building designs. *The Structural Design of Tall and Special Buildings*, 22(12):954–974, 2013.

N. D. Lagaros, M. Papadrakakis, and G. Kokossalakis. Structural optimization using evolutionary algorithms. *Computers & Structures*, 80(7):571–589, 2002. ISSN 0045-7949. doi: 10.1016/S0045-7949(02)00027-5.

N. D. Lagaros, L. D. Psarras, M. Papadrakakis, and G. Panagiotou. Optimum design of steel structures with web openings. *Engineering structures*, 30(9):2528–2537, 2008.

N. D. Lagaros, M. Kournoutos, N. A. Kallioras, and A. N. Nordas. Constraint handling techniques for metaheuristics: a state-of-the-art review and new variants. *Optimization and Engineering*, pages 1–48, 2023.

S. Law, J. Bu, X. Zhu, and S. L. Chan. Wind characteristics of typhoon dujuan as measured at a 50m guyed mast. *Wind & structures*, 9(5):387–396, 2006.

R. Lawson, R. Ogden, and R. Bergin. Application of modular construction in high-rise buildings. *Journal of Architectural Engineering*, 18(2):148–154, 2012. URL https://www.scopus.com/inward/record.uri?eid=2-s2.0-84862557157&doi=10.1061%2f%28ASCE%29AE.1943-5568.0000057&partnerID=40&md5=725be4d7740199cad4df69c1bb8b3550.

B. Lee and J. Knapton. Optimum cost design of a steel-framed building. *Engineering Optimization*, 1(3):139–153, 1975a. URL https://www.scopus.com/inward/record.uri?eid=2-s2.0-0016595684&doi=10.1080%2f03052157508960583&partnerID=40&md5=ba696b776437180c93678fb06bf18730.

B. Lee and J. Knapton. Optimum cost design of a steel-framed building. *Engineering Optimization*, 1(3):139–153, 1975b.

Y. F. Leung, A. Klar, and K. Soga. Theoretical study on pile length optimization of pile groups and piled rafts. *Journal of geotechnical and geoenvironmental engineering*, 136(2):319–330, 2010.

B. Li and R. Xiao. The particle swarm optimization algorithm: How to select the number of iteration. pages 191 – 196, 12 2007a. ISBN 978-0-7695-2994-1. doi: 10.1109/IIH-MSP.2007.298.

B. Li and R.-Y. Xiao. The particle swarm optimization algorithm: How to select the number of iteration. In *Third International Conference on Intelligent Information Hiding and Multimedia Signal Processing (IIH-MSP 2007)*, volume 2, pages 191–196. IEEE, 2007b.

G. Li, R.-G. Zhou, L. Duan, and W.-F. Chen. Multiobjective and multilevel optimization for steel frames. *Engineering Structures*, 21(6):519–529, 1999. URL https://www.scopus.com/inward/record.uri?eid=2-s2.0-0033150380&doi=10.1016%2fS0141-0296%2897%2900226-5&partnerID=40&md5=c100b26c0f20688c427e1ecd5aa56e93.

G. Li, Y. Jiang, and D. Yang. Modified-modal-pushover-based seismic optimum design for steel structures considering life-cycle cost. *Structural and Multidisciplinary Optimization*, 45(6):861–874, 2012.

H.-s. Li, Z.-z. Lü, and Z.-f. Yue. Support vector machine for structural reliability analysis. *Applied Mathematics and Mechanics*, 27(10):1295–1303, 2006.

K. Li, L. Pan, W. Xue, H. Jiang, and H. Mao. Multi-objective optimization for energy performance improvement of residential buildings: A comparative study. *Energies*, 10(2):245, 2017.

L. Li, Z. Huang, and F. Liu. A heuristic particle swarm optimization method for truss structures with discrete variables. *Computers & structures*, 87(7-8):435–443, 2009.

Z. Li, Y. Lv, L. Xu, and Y. Ding. Advances in failure mode optimization and damage control for highrise steel frames during earthquakes. *Jianzhu Jiegou Xuebao/Journal of Building Structures*, 32(12):62–70, 2011. URL https://www.scopus.com/inward/record.uri?eid=2-s2.0-84155181844&partnerID=40&md5=38327f852dbda12b1b45d4098021cdc3.

J. Liang and P. Suganthan. Dynamic multi-swarm particle swarm optimizer with a novel constraint-handling mechanism. In *2006 IEEE International Conference on Evolutionary Computation*, pages 9–16, 2006. doi: 10.1109/CEC.2006.1688284.

J. J. Liang, A. K. Qin, P. N. Suganthan, and S. Baskar. Comprehensive learning particle swarm optimizer for global optimization of multimodal functions. *IEEE transactions on evolutionary computation*, 10(3):281–295, 2006.

J. Liew, Y. Chua, and Z. Dai. Steel concrete composite systems for modular construction of high-rise buildings. *Structures*, 21:135–149, 2019. URL https://www.scopus.com/inward/record.uri?eid=2-s2.0-85061768420&doi=10.1016%2fj.istruc.2019.02.010&partnerID=40&md5=5de49037d762728d48319b310d0212d4.

C.-Y. Lin and P. Hajela. Design optimization with advanced genetic search strategies. *Advances in Engineering Software*, 21(3):179–189, 1994. doi: 10.1016/0965-9978(94)90020-5. URL https://www.scopus.com/inward/record.uri?eid=2-s2.0-0028738992&doi=10.1016%2f0965-9978%2894%2990020-5&partnerID=40&md5=c6cbd4a86e8107c868e1e6097d42f67e. cited By 13.

C. Liu, D. Fang, and L. Zhao. Reflection on earthquake damage of buildings in 2015 nepal earthquake and seismic measures for post-earthquake reconstruction. In *Structures*, volume 30, pages 647–658. Elsevier, 2021.

M. Liu, Y. Wen, and S. A. Burns. Life cycle cost oriented seismic design optimization of steel moment frame structures with risk-taking preference. *Engineering Structures*, 26(10):1407–1421, 2004.

Q. Liu and J. Paavola. An optimization procedure for seismic design of steel frames for multi-performance and multi-hazard levels. *Advances in Structural Engineering*, 18(1):59–74, 2015.

Z. Liu, S. Atamturktur, and C. H. Juang. Performance based robust design optimization of steel moment resisting frames. *Journal of Constructional Steel Research*, 89:165–174, 2013.

W. Long, X. Liang, Y. Huang, and Y. Chen. A hybrid differential evolution augmented lagrangian method for constrained numerical and engineering optimization. *Computer-Aided Design*, 45(12):1562–1574, 2013.

Y. Lu, S. Wang, Y. Zhao, and C. Yan. Renewable energy system optimization of low/zero energy buildings using single-objective and multi-objective optimization methods. *Energy and Buildings*, 89:61–75, 2015.

G.-C. Luh and C.-Y. Lin. Optimal design of truss-structures using particle swarm optimization. *Computers & structures*, 89(23-24):2221–2232, 2011.

A. C. Luzardo, V. E. Parnás, and P. M. Rodríguez. Guy tension influence on the structural behavior of a guyed mast. *Journal of the International Association for Shell and Spatial Structures*, 53(2):111–116, 2012.

Y. Lv, Z.-X. Li, L.-H. Xu, and Y. Ding. Equivalent seismic performance optimization of steel structures based on nonlinear damage analysis. *Advances in Structural Engineering*, 18(7):941–958, 2015.

V. Machairas, A. Tsangrassoulis, and K. Axarli. Algorithms for optimization of building design: A review. *Renewable and Sustainable Energy Reviews*, 31:101–112, 2014. URL https://www.scopus.com/inward/record.uri?eid=2-s2.0-84890263545&doi=10.1016%2fj.rser.2013.11.036&partnerID=40&md5=40284f0069df5ae4712d81943f117ea0.

E. Machaly. Optimum weight analysis of steel frames with semirigid connections. *Computers and Structures*, 23(4):461–474, 1986a. URL https://www.scopus.com/inward/record.uri?eid=2-s2.0-0022604259&doi=10.1016%2f0045-7949%2886%2990089-1&partnerID=40&md5=69610bd39aefdffdf33c88be254318d5.

E. Machaly. Optimum weight analysis of steel grid bridges. *Computers and Structures*, 23(5):575–586, 1986b. URL https://www.scopus.com/inward/record.uri?eid=2-s2.0-46149134810&doi=10.1016%2f0045-7949%2886%2990068-4&partnerID=40&md5=7382f24f4ddafbc5d99275ad282fd6e0.

E. Machaly. Optimum weight analysis of steel frames with semirigid connections. *Computers & structures*, 23(4):461–474, 1986c.

M. K. Madugula. *Dynamic response of lattice towers and guyed masts*. ASCE Publications, 2001.

M. K. Madugula, Y. M. Wahba, and G. R. Monforton. Dynamic response of guyed masts. *Engineering Structures*, 20(12):1097–1101, 1998.

L. Magnier and F. Haghighat. Multiobjective optimization of building design using trnsys simulations, genetic algorithm, and artificial neural network. *Building and Environment*, 45(3):739–746, 2010.

K. I. Majid. Optimum design of structures. Technical report, 1974.

K. Mam, C. Douthe, R. Le Roy, and F. Consigny. Shape optimization of braced frames for tall timber buildings: Influence of semi-rigid connections on design and optimization process. *Engineering Structures*, 216:110692, 2020.

S. F. Mansouri and M. R. Maheri. Performance-based seismic design of steel frames using constraint control method. *Advances in Structural Engineering*, 22(12): 2648–2661, 2019.

G. Marano, F. Trentadue, and R. Greco. Stochastic optimum design criterion of added viscous dampers for buildings seismic protection. *Structural Engineering and Mechanics*, 25(1):21–37, 2007. doi: 10.12989/sem.2007.25.1.021.

G. Marano, F. Trentadue, and F. Petrone. Optimal arch shape solution under static vertical loads. *Acta Mechanica*, 225(3):679–686, 2014. doi: 10.1007/s00707-013-0985-0.

W. Marks. Multicriteria optimisation of shape of energy-saving buildings. *Building and Environment*, 32(4):331–339, 1997a. URL https://www.scopus.com/inward/record.uri?eid=2-s2.0-0031185502&doi=10.1016%2fS0360-1323%2896%2900065-0&partnerID=40&md5=31105e52dc6bfb8a61f961f6d1bb2c61.

W. Marks. Multicriteria optimisation of shape of energy-saving buildings. *Building and environment*, 32(4):331–339, 1997b.

R. Marler and J. Arora. Survey of multi-objective optimization methods for engineering. *Structural and Multidisciplinary Optimization*, 26(6):369–395, 2004. URL https://www.scopus.com/inward/record.uri?eid=2-s2.0-2442535151&doi=10.1007%2fs00158-003-0368-6&partnerID=40&md5=4139f4adec0a24676ea2d2762299e751.

D. Martínez-Muñoz, J. García, J. Martí, and V. Yepes. Discrete swarm intelligence optimization algorithms applied to steel–concrete composite bridges. *Engineering Structures*, 266:114607, 2022.

R. Martí, P. M. Pardalos, and M. G. C. Resende. *Handbook of Heuristics*. Springer Publishing Company, Incorporated, 1st edition, 2018. ISBN 3319071254. doi: 10.1007/978-3-319-07124-4.

D. Mavrokapnidis, C. C. Mitropoulou, and N. D. Lagaros. Environmental assessment of cost optimized structural systems in tall buildings. *Journal of Building Engineering*, 24:100730, 2019.

R. McKinstray, J. B. Lim, T. T. Tanyimboh, D. T. Phan, and W. Sha. Optimal design of long-span steel portal frames using fabricated beams. *Journal of Constructional Steel Research*, 104:104–114, 2015.

R. McKinstray, J. B. Lim, T. T. Tanyimboh, D. T. Phan, and W. Sha. Comparison of optimal designs of steel portal frames including topological asymmetry considering rolled, fabricated and tapered sections. *Engineering Structures*, 111:505–524, 2016.

A. Medina, G. Toscano Pulido, and J. Ramírez-Torres. A comparative study of neighborhood topologies for particle swarm optimizers. pages 152–159, 01 2009.

J. Melchiorre, A. M. Bertetto, and G. C. Marano. Application of a machine learning algorithm for the structural optimization of circular arches with different cross-sections. *Journal of Applied Mathematics and Physics*, 9(5):1159–1170, 2021.

A. Memari and M. Madhkhan. Optimal design of steel frames subject to gravity and seismic codes' prescribed lateral forces. *Structural Optimization*, 18 (1):56–66, 1999a. URL https://www.scopus.com/inward/record.uri?eid=2-s2.0-0033169396&doi=10.1007%2fs001580050068&partnerID=40&md5=74e502b8aa4ba8f25f1a67b54c9f4a2f.

A. Memari and M. Madhkhan. Optimal design of steel frames subject to gravity and seismic codes' prescribed lateral forces. *Structural optimization*, 18(1):56–66, 1999b.

M. Mensinger and L. Huang. Optimized preliminary structural design of steel composite buildings using the sustainable office designer: Comparing optimizations to satisfy different objectives. *Steel Construction*, 10(1):17–22, 2017.

E. Mezura-Montes. *Constraint-Handling in Evolutionary Optimization*, volume 198. 01 2009a. ISBN 978-3-642-00618-0. doi: 10.1007/978-3-642-00619-7.

E. Mezura-Montes. Constraint-handling in evolutionary optimization efrén mezura-montes (editor) springer, studies in computational intelligence series vol. 198, 2009 isbn: 978-3-642-00618-0. *Journal of Computer Science and Technology*, 9 (01):34–35, 2009b.

E. Mezura-Montes and C. Coello. A simple multimembered evolution strategy to solve constrained optimization problems. *IEEE Transactions on Evolutionary Computation*, 9(1):1–17, 2005a. doi: 10.1109/TEVC.2004.836819.

E. Mezura-Montes and C. A. C. Coello. A simple multimembered evolution strategy to solve constrained optimization problems. *IEEE Transactions on Evolutionary computation*, 9(1):1–17, 2005b.

Z. Michalewicz and D. Fogel. *How to Solve It: Modern Heuristics*. 01 2008. ISBN 978-3-662-04133-8. doi: 10.1007/978-3-662-04131-4.

Z. Michalewicz and D. B. Fogel. *How to solve it: modern heuristics*. Springer Science & Business Media, 2013.

V. Miranda and N. Fonseca. Epso-evolutionary particle swarm optimization, a new algorithm with applications in power systems. In *IEEE/PES Transmission and Distribution Conference and Exhibition*, volume 2, pages 745–750. IEEE, 2002.

H. Moghaddam and I. Hajirasouliha. A new approach for optimum design of structures under dynamic exciation. 2004.

H. Moghaddam and I. Hajirasouliha. Fundamentals of optimum performance-based design for dynamic excitations. 2005.

H. Moghaddam and I. Hajirasouliha. Toward more rational criteria for determination of design earthquake forces. *International Journal of Solids and Structures*, 43(9): 2631–2645, 2006.

H. Moghaddam and I. Hajirasouliha. Optimum strength distribution for seismic design of tall buildings. *The Structural Design of Tall and Special Buildings*, 17 (2):331–349, 2008.

H. Moghaddam, I. Hajirasouliha, and A. Doostan. Optimum seismic design of concentrically braced steel frames: concepts and design procedures. *Journal of Constructional Steel Research*, 61(2):151–166, 2005.

H. Moghaddam, I. Hajirasouliha, and S. M. H. Gelekolai. Performance-based seismic design of moment resisting steel frames: Adaptive optimisation framework and optimum design load pattern. In *Structures*, volume 33, pages 1690–1704. Elsevier, 2021.

R. K. Mohammadi and A. H. Sharghi. On the optimum performance-based design of eccentrically braced frames. *Steel Compos. Struct*, 16(4):357–374, 2014.

R. K. Mohammadi, M. El Naggar, and H. Moghaddam. Optimum strength distribution for seismic resistant shear buildings. *International Journal of Solids and Structures*, 41(22-23):6597–6612, 2004.

S. M. Mojtabaei, I. Hajirasouliha, and J. Ye. Optimisation of cold-formed steel beams for best seismic performance in bolted moment connections. *Journal of Constructional Steel Research*, 181:106621, 2021.

G. Monti, G. Quaranta, and G. Marano. Genetic-algorithm-based strategies for dynamic identification of nonlinear systems with noise-corrupted response. *Journal of Computing in Civil Engineering - J COMPUT CIVIL ENG*, 24, 03 2010a. doi: 10.1061/(ASCE)CP.1943-5487.0000024.

G. Monti, G. Quaranta, and G. C. Marano. Genetic-algorithm-based strategies for dynamic identification of nonlinear systems with noise-corrupted response. *Journal of Computing in Civil Engineering*, 24(2):173–187, 2010b.

S. Moradi and M. S. Alam. Multi-criteria optimization of lateral load-drift response of posttensioned steel beam-column connections. *Engineering structures*, 130: 180–197, 2017.

N. Mordà and A. Mancini. Norme tecniche per le costruzioni (ntc 2018) d. min. infrastrutture e trasporti 17 gennaio 2018, 2018.

M. Morgese, F. Ansari, M. Domaneschi, and G. P. Cimellaro. Post-collapse analysis of morandi's polcevera viaduct in genoa italy. *Journal of Civil Structural Health Monitoring*, 10:69–85, 2020.

A. Morris. Structural optimization by geometric programming. *International Journal of Solids and Structures*, 8(7):847–864, 1972.

E. Mostavi, S. Asadi, and D. Boussaa. Development of a new methodology to optimize building life cycle cost, environmental impacts, and occupant satisfaction. *Energy*, 121:606–615, 2017.

F. Mota, V. Almeida, E. F. Wanner, and G. Moreira. Hybrid pso algorithm with iterated local search operator for equality constraints problems. In *2018 IEEE Congress on Evolutionary Computation (CEC)*, pages 1–6. IEEE, 2018.

K. P. Murphy. *Machine learning: a probabilistic perspective*. MIT press, 2012.

K. Negendahl and T. R. Nielsen. Building energy optimization in the early design stages: A simplified method. *Energy and Buildings*, 105:88–99, 2015.

D. Nethercot. *Steel beam to column connections-a review of tests data*. CIRIA, Construction Industry Research and Information Assoc., 1985.

M. Novak, H. Tanaka, and A. G. Davenport. Vibration of towers due to galloping of iced cables. *Journal of the Engineering Mechanics Division*, 104(2):457–473, 1978.

E. O'Brien and A. Dixon. Optimal plastic design of pitched roof frames for multiple loading. *Computers and Structures*, 64(1-4):737–740, 1997. URL https://www.scopus.com/inward/record.uri?eid=2-s2.0-0031190448&doi=10.1016%2fS0045-7949%2896%2900428-2&partnerID=40&md5=1f461ebe1b0e60dcce13b08c88fabf23.

J. T. O'Connor, S. E. Rusch, and M. J. Schulz. Constructability concepts for engineering and procurement. *Journal of Construction Engineering and Management*, 113(2):235–248, 1987.

M. Ohsaki and T. Nakajima. Optimization of link member of eccentrically braced frames for maximum energy dissipation. *Journal of Constructional Steel Research*, 75:38–44, 2012.

M. Ohsaki, O. Iwatsuki, and H. Watanabe. Seismic response of building frames with flexible base optimized for reverse rocking response. *Engineering structures*, 74: 170–179, 2014.

S. Omkar, D. Mudigere, G. N. Naik, and S. Gopalakrishnan. Vector evaluated particle swarm optimization (vepso) for multi-objective design optimization of composite structures. *Computers & structures*, 86(1-2):1–14, 2008.

D. Orlando, P. B. Gonçalves, G. Rega, and S. Lenci. Nonlinear dynamics and instability as important design concerns for a guyed mast. In *IUTAM Symposium on Nonlinear Dynamics for Advanced Technologies and Engineering Design: Proceedings of the IUTAM Symposium on Nonlinear Dynamics for Advanced Technologies and Engineering Design, held Aberdeen, UK, 27-30 July 2010*, pages 223–234. Springer, 2013.

A. V. Oskouei, S. S. Fard, and O. Aksogan. Using genetic algorithm for the optimization of seismic behavior of steel planar frames with semi-rigid connections. *Structural and multidisciplinary optimization*, 45:287–302, 2012.

I. Osman and G. Laporte. Metaheuristics: A bibliography. *Annals of Operations Research*, 63:513–623, 1996. URL https://www.scopus.com/inward/record.uri?eid=2-s2.0-27844568382&doi=10.1007%2fbf02125421&partnerID=40&md5=1758201a8ce34d78794b84022fcb2b8a.

M. Ozgenoglu and Y. Arıcı. Comparison of asce/sei standard and modal pushover-based ground motion scaling procedures for pre-tensioned concrete bridges. *Structure and Infrastructure Engineering*, 13(12):1609–1623, 2017.

S. Palizi and A. Saedi Daryan. Plastic analysis of braced frames by application of metaheuristic optimization algorithms. *International Journal of Steel Structures*, 20:1135–1150, 2020.

L. Palizzolo, S. Benfratello, and P. Tabbuso. Discrete variable design of frames subjected to seismic actions accounting for element slenderness. *Computers & Structures*, 147:147–158, 2015.

J. Pan and D.-y. Wang. Topology optimization of truss structure with fundamental frequency and frequency domain dynamic response constraints. *Acta Mechanica Solida Sinica*, 19:231–240, 2006.

G. S. Papavasileiou, D. C. Charmpis, and N. D. Lagaros. Optimized seismic retrofit of steel-concrete composite buildings. *Engineering Structures*, 213:110573, 2020.

H. Park and H. Adeli. A neural dynamics model for structural optimization-application to plastic design of structures. *Computers and Structures*, 57(3): 391–399, 1995. URL https://www.scopus.com/inward/record.uri?eid=2-s2.0-0029634818&doi=10.1016%2f0045-7949%2895%2900047-K&partnerID=40&md5=2e1b9e61f144fec63a9f64bb01c16bb0.

H. S. Park, H. Lee, Y. Kim, T. Hong, and S. W. Choi. Evaluation of the influence of design factors on the co2 emissions and costs of reinforced concrete columns. *Energy and Buildings*, 82:378–384, 2014.

Y. H. Park, C. Park, and Y. G. Park. The behavior of an in-service plate girder bridge strengthened with external prestressing tendons. *Engineering structures*, 27(3): 379–386, 2005.

K. Parsopoulos and M. Vrahatis. *Particle Swarm Optimization Method for Constrained Optimization Problem*, volume 76, pages 214–220. 01 2002. ISBN 1-58603-256-9.

K. Parsopoulos and M. Vrahatis. Unified particle swarm optimization for solving constrained engineering optimization problems. volume 3612, pages 582–591, 08 2005. ISBN 978-3-540-28320-1. doi: 10.1007/11539902_71.

C. Pasquire and A. Gibb. Considerations for assessing the benefits of standardisation and pre-assembly in construction (the findings of a pilot study). In *report to CIBSE Seminar on Standardisation in the Design and Construction of Building Services Installations*, volume 26, 1999.

B. Paulson Jr. Designing to reduce construction costs. *Journal of the Construction Division*, 102(C04), 1976.

L. Pavlovčič, A. Krajnc, and D. Beg. Cost function analysis in the structural optimization of steel frames. *Structural and Multidisciplinary Optimization*, 28 (4):286–295, 2004.

I. Paya-Zaforteza, V. Yepes, A. Hospitaler, and F. Gonzalez-Vidosa. Co2-optimization of reinforced concrete frames by simulated annealing. *Engineering Structures*, 31(7):1501–1508, 2009.

M. Pelikan, M. W. Hauschild, and F. G. Lobo. Estimation of distribution algorithms. pages 899–928, 2015. doi: 10.1007/978-3-662-43505-2_45.

M. Pelliciari, G. Marano, T. Cuoghi, B. Briseghella, D. Lavorato, and A. Tarantino. Parameter identification of degrading and pinched hysteretic systems using a modified bouc–wen model. *Structure and Infrastructure Engineering*, 14(12): 1573–1585, 2018. doi: 10.1080/15732479.2018.1469652.

V. Penadés-Plà, T. García-Segura, and V. Yepes. Accelerated optimization method for low-embodied energy concrete box-girder bridge design. *Engineering Structures*, 179:556–565, 2019.

R. E. Perez and K. Behdinan. Particle swarm approach for structural design optimization. *Computers & Structures*, 85(19-20):1579–1588, 2007.

M. Petrangeli, L. Fieno, and R. Orlandi. Valutazione della sicurezza in esercizio dei ponti esistenti con impalcati in cap, 2019.

M. P. Petrangeli. *Progettazione e costruzione di ponti: con cenni di patologia e diagnostica delle opere esistenti*. Masson, 1996.

S. Pezeshk and C. Camp. *State of the art on the use of genetic algorithms in design of steel structures*. 2002. URL https://www.scopus.com/inward/record.uri?eid=2-s2.0-0036397173&partnerID=40&md5=cf71ecbb9b1341ddd215b411b639f5ef. cited By 23.

S. Pezeshk, C. Camp, and D. Chen. Design of nonlinear framed structures using genetic optimization. *Journal of structural engineering*, 126(3):382–388, 2000.

M. L. Pezo and V. V. Bakić. Numerical determination of drag coefficient for guyed mast exposed to wind action. *Engineering structures*, 62:98–104, 2014.

D. T. Phan, J. B. Lim, T. T. Tanyimboh, and W. Sha. An efficient genetic algorithm for the design optimization of cold-formed steel portal frame buildings. 2012.

D. T. Phan, J. B. Lim, W. Sha, C. Y. Siew, T. T. Tanyimboh, H. K. Issa, and F. A. Mohammad. Design optimization of cold-formed steel portal frames taking into account the effect of building topology. *Engineering Optimization*, 45(4):415–433, 2013.

D. T. Phan, J. B. Lim, T. T. Tanyimboh, A. Wrzesien, W. Sha, and R. Lawson. Optimal design of cold-formed steel portal frames for stressed-skin action using genetic algorithm. *Engineering Structures*, 93:36–49, 2015.

D. T. Phan, J. B. Lim, T. T. Tanyimboh, and W. Sha. Optimum design of cold-formed steel portal frame buildings including joint effects and secondary members. *International Journal of Steel Structures*, 17(2):427–442, 2017.

D. T. Phan, S. M. Mojtabaei, I. Hajirasouliha, J. Ye, and J. B. Lim. Coupled element and structural level optimisation framework for cold-formed steel frames. *Journal of Constructional Steel Research*, 168:105867, 2020.

B. L. Pierson. A survey of optimal structural design under dynamic constraints. *International Journal for Numerical Methods in Engineering*, 4(4):491–499, 1972.

M. A. Pisani. Strengthening by means of external prestressing. *Journal of Bridge Engineering*, 4(2):131–135, 1999.

G. Platt, X.-S. Yang, and A. Silva Neto. *Computational intelligence, optimization and inverse problems with applications in engineering*. 2018a. doi: 10.1007/978-3-319-96433-1. URL https://www.scopus.com/inward/record.uri?eid=2-s2.0-85063363067&doi=10.1007%2f978-3-319-96433-1&partnerID=40&md5=4d9e37dff628761afb8eb1ffe9c160da. cited By 3.

G. M. Platt, X.-S. Yang, and A. J. S. Neto. *Computational Intelligence, Optimization and Inverse Problems With Applications in Engineering*. Springer, 2018b.

V. Plevris. *Innovative Computational Techniques for the Optimum Structural Design Considering Uncertainties*. PhD thesis, Institute of Structural Analysis and Seismic Research, School of Civil Engineering, National Technical University of Athens (NTUA), 2009a.

V. Plevris. *Innovative computational techniques for the optimum structural design considering uncertainties*. PhD thesis, Εθνικό Μετσόβιο Πολυτεχνείο (ΕΜΠ). Σχολή Πολιτικών Μηχανικών. Τομέας ..., 2009b.

V. Plevris and M. Papadrakakis. A hybrid particle swarm—gradient algorithm for global structural optimization. *Computer-Aided Civil and Infrastructure Engineering*, 26(1):48–68, 2011.

W. Prager. Optimality criteria in structural design. *Proceedings of the National Academy of Sciences*, 61(3):794–796, 1968.

W. Prager. *Introduction to structural optimization*. Number 212. Springer, 1974.

C. Praveen and R. Duvigneau. Low cost pso using metamodels and inexact pre-evaluation: Application to aerodynamic shape design. *Computer Methods in Applied Mechanics and Engineering*, 198(9-12):1087–1096, 2009.

M.-B. Prendes-Gero, M.-I. Álvarez-Fernández, F. López-Gayarre, J.-M. Drouet, and J. R.-V. Junco. Cost optimization of structures using a genetic algorithm with eugenic evolutionary theory. *Structural and multidisciplinary optimization*, 54(2): 199–213, 2016.

M. H. Pulaski and M. J. Horman. Organizing constructability knowledge for design. *Journal of construction engineering and management*, 131(8):911–919, 2005.

Z. Qian, J. Yu, and J. Zhou. A genetic algorithm for solving mixed discrete optimization problems. In *International Design Engineering Technical Conferences and Computers and Information in Engineering Conference*, volume 11818, pages 499–504. American Society of Mechanical Engineers, 1993.

S. Qiao, X. Han, K. Zhou, and J. Ji. Seismic analysis of steel structure with brace configuration using topology optimization. *Steel and Composite Structures*, 21(3): 501–515, 2016.

C. Quaglia, N. Yu, A. Thrall, and S. Paolucci. Balancing energy efficiency and structural performance through multi-objective shape optimization: Case study of a rapidly deployable origami-inspired shelter. *Energy and Buildings*, 82:733–745, 2014.

G. Quaranta, W. Lacarbonara, and S. Masri. A review on computational intelligence for identification of nonlinear dynamical systems. *Nonlinear Dynamics*, 99, 01 2020a. doi: 10.1007/s11071-019-05430-7.

G. Quaranta, W. Lacarbonara, and S. F. Masri. A review on computational intelligence for identification of nonlinear dynamical systems. *Nonlinear Dynamics*, 99 (2):1709–1761, 2020b.

G. Quaranta, W. Lacarbonara, and S. F. Masri. A review on computational intelligence for identification of nonlinear dynamical systems. *Nonlinear Dynamics*, 99 (2):1709–1761, 2020c.

A. Rafiee, S. Talatahari, and A. Hadidi. Optimum design of steel frames with semi-rigid connections using big bang-big crunch method. *Steel and Composite Structures, An International Journal*, 14(5):431–451, 2013.

S. N. Rahane and S. Nalawade. A review on optimization of industrial trusses. *International Journal of Research in Engineering, Science and Management*, 5(1): 237–242, 2022.

G. Ramaswamy and M. Eekhout. *Analysis, design and construction of steel space frames*. Thomas Telford, 2002.

A. R. M. Rao and K. Sivasubramanian. Multi-objective optimal design of fuzzy logic controller using a self configurable swarm intelligence algorithm. *Computers & structures*, 86(23-24):2141–2154, 2008.

R. V. Rao, V. J. Savsani, and D. Vakharia. Teaching–learning-based optimization: a novel method for constrained mechanical design optimization problems. *Computer-aided design*, 43(3):303–315, 2011.

S. S. Rao. *Engineering optimization: theory and practice*. John Wiley & Sons, 2019a.

S. S. Rao. *Engineering optimization: theory and practice*. John Wiley & Sons, 2019b.

B. Raphael. Multi-criteria decision making for collaborative design optimization of buildings. *Built Environment Project and Asset Management*, 1(2):122–136, 2011.

E. Rashedi, H. Nezamabadi-Pour, and S. Saryazdi. Gsa: a gravitational search algorithm. *Information sciences*, 179(13):2232–2248, 2009.

A. Recupero, N. Spinella, and F. Tondolo. A model for the analysis of ultimate capacity of rc and pc corroded beams. *Advances in civil engineering*, 2018, 2018.

K. F. Reinschmidt, C. A. Cornell, and J. F. Brotchie. Iterative design and structural optimization. *Journal of the Structural Division*, 92(6):281–318, 1966.

A. rezaee jordehi. A review on constraint handling strategies in particle swarm optimisation. *Neural Computing and Applications*, 26, 01 2015. doi: 10.1007/s00521-014-1808-5.

F. Rezazadeh and S. Talatahari. Seismic energy-based design of brb frames using multi-objective vibrating particles system optimization. In *Structures*, volume 24, pages 227–239. Elsevier, 2020.

F. Rezazadeh, R. Mirghaderi, A. Hosseini, and S. Talatahari. Optimum energy-based design of brb frames using nonlinear response history analysis. *Structural and Multidisciplinary Optimization*, 57(3):1005–1019, 2018.

J. B. Rosen. The gradient projection method for nonlinear programming. part i. linear constraints. *Journal of the society for industrial and applied mathematics*, 8(1):181–217, 1960.

M. M. Rosso, R. Cucuzza, F. Di Trapani, and G. C. Marano. Nonpenalty machine learning constraint handling using pso-svm for structural optimization. *Advances in Civil Engineering*, 2021:1–17, 2021a.

M. M. Rosso, R. Cucuzza, F. Di Trapani, and G. C. Marano. Nonpenalty machine learning constraint handling using pso-svm for structural optimization. *Advances in Civil Engineering*, 2021, 2021b.

M. M. Rosso, R. Cucuzza, F. Di Trapani, and G. C. Marano. Nonpenalty machine learning constraint handling using pso-svm for structural optimization. *Advances in Civil Engineering*, 2021:1–17, 2021c.

M. M. Rosso, R. Cucuzza, A. Aloisio, and G. C. Marano. Enhanced multi-strategy particle swarm optimization for constrained problems with an evolutionary-strategies-based unfeasible local search operator. *Applied Sciences*, 12(5):2285, 2022.

G. Rozvany. Stress ratio and compliance based methods in topology optimization–a critical review. *Structural and Multidisciplinary Optimization*, 21:109–119, 2001.

G. Rozvany, M. Bendsoe, and U. Kirsch. Layout optimization of structures. 1995.

G. I. Rozvany. A critical review of established methods of structural topology optimization. *Structural and multidisciplinary optimization*, 37:217–237, 2009.

D. I. Ruby. *Constructability of structural steel buildings*. American Institute of Steel Construction, 2008.

T. P. Runarsson and X. Yao. Stochastic ranking for constrained evolutionary optimization. *IEEE Transactions on evolutionary computation*, 4(3):284–294, 2000.

T. P. Runarsson and X. Yao. Search biases in constrained evolutionary optimization. *IEEE Transactions on Systems, Man, and Cybernetics, Part C (Applications and Reviews)*, 35(2):233–243, 2005.

J. S. Russell, K. E. Swiggum, J. M. Shapiro, and A. F. Alaydrus. Constructability related to tqm, value engineering, and cost/benefits. *Journal of performance of constructed facilities*, 8(1):31–45, 1994.

S. Saadat, C. V. Camp, and S. Pezeshk. Probabilistic seismic loss analysis for the design of steel structures: Optimizing for multiple-objective functions. *Earthquake Spectra*, 32(3):1587–1605, 2016.

A. Saedi Daryan and S. Palizi. New plastic analysis procedure for collapse prediction of braced frames by means of genetic algorithm. *Journal of Structural Engineering*, 146(1):04019168, 2020.

A. Saedi Daryan, M. Salari, N. Farhoudi, and S. Palizi. Seismic design optimization of steel frames with steel shear wall system using modified dolphin algorithm. *International Journal of Steel Structures*, 21(3):771–786, 2021.

D. Safari and M. R. Maheri. Genetic algorithm search for optimal brace positions in steel frames. *J Adv Conc Des*, 2(4):400–415, 2006.

M. Saka. Optimum design of rigidly jointed frames. *Computers & Structures*, 11(5): 411–419, 1980.

M. Saka. Optimum design of steel frames with stability constraints. *Computers and Structures*, 41(6):1365–1377, 1991a. URL https://www.scopus.com/inward/record.uri?eid=2-s2.0-0026393395&doi=10.1016%2f0045-7949%2891%2990274-P&partnerID=40&md5=5f4f2df2c04b0fddd057fb145f731e26.

M. Saka. Optimum design of steel frames with stability constraints. *Computers & structures*, 41(6):1365–1377, 1991b.

M. Saka. Optimum design of pitched roof steel frames with haunched rafters by genetic algorithm. *Computers & structures*, 81(18-19):1967–1978, 2003.

M. Saka and M. Hayalioglu. Optimum design of geometrically nonlinear elastic-plastic steel frames. *Computers & structures*, 38(3):329–344, 1991.

M. P. Saka and Z. W. Geem. Mathematical and metaheuristic applications in design optimization of steel frame structures: an extensive review. *Mathematical problems in engineering*, 2013, 2013.

J. F. Santoro and M. Kripka. Minimizing environmental impact from optimized sizing of reinforced concrete elements. *Computers and Concrete*, 25(2):111, 2020.

M. Sarcheshmehpour and H. Estekanchi. Life cycle cost optimization of earthquake-resistant steel framed tube tall buildings. In *Structures*, volume 30, pages 585–601. Elsevier, 2021.

L. Sardone, M. M. Rosso, R. Cucuzza, R. Greco, and G. C. Marano. COMPUTATIONAL DESIGN OF COMPARATIVE MODELS AND GEOMETRICALLY CONSTRAINED OPTIMIZATION OF a MULTI DOMAIN VARIABLE SECTION BEAM BASED ON TIMOSHENKO MODEL. In *14th International Conference on Evolutionary and Deterministic Methods for Design, Optimization and Control*. Institute of Structural Analysis and Antiseismic Research National Technical University of Athens, 2021. doi: 10.7712/140121.7961.18535.

K. Sarma and H. Adeli. Life-cycle cost optimization of steel structures. *International Journal for Numerical Methods in Engineering*, 55(12):1451–1462, 2002a. URL https://www.scopus.com/inward/record.uri?eid=2-s2.0-0037203053&doi=10.1002%2fnme.549&partnerID=40&md5=c3b1248cd76e2d7adc8678e2f0f61aca.

K. C. Sarma and H. Adeli. Cost optimization of steel structures. *Engineering Optimization+ A35*, 32(6):777–802, 2000.

K. C. Sarma and H. Adeli. Life-cycle cost optimization of steel structures. *International Journal for Numerical Methods in Engineering*, 55(12):1451–1462, 2002b.

G. Saudi. Structural assessment of a guyed mast through measurement of natural frequencies. *Engineering Structures*, 59:104–112, 2014.

R. Saxena, N. Popplewell, P. Trainor, and A. Shah. Vibrations of complex guyed towers. In *12th Biennial Conference on Mechanical Vibration and Noise Control, Montreal, Canada*, 1989.

L. A. Schmit. Structural design by systematic synthesis. In *Proceedings of the Second National Conference on Electronic Computation, ASCE, Sept., 1960*, 1960.

L. A. Schmit Jr and H. Miura. Approximation concepts for efficient structural synthesis. Technical report, NASA, 1976.

B. I. Schmitt. *Convergence Analysis for Particle Swarm Optimization*. PhD thesis, FAU University Press, Erlangen, Nürnberg, Germany, 01 2015.

H. Scholz and G. Faller. A micro-computer program for the elastic-plastic analysis and optimum design of plane frames. *Computers and Structures*, 24(6): 941–947, 1986a. URL https://www.scopus.com/inward/record.uri?eid=2-s2.0-0022866026&doi=10.1016%2f0045-7949%2886%2990302-0&partnerID=40&md5=9f2b2c99be8d1f54ea1841178654cee8.

H. Scholz and G. Faller. A micro-computer program for the elastic-plastic analysis and optimum design of plane frames. *Computers & structures*, 24(6):941–947, 1986b.

Y. Schwartz, R. Raslan, and D. Mumovic. Implementing multi objective genetic algorithm for life cycle carbon footprint and life cycle cost minimisation: A building refurbishment case study. *Energy*, 97:58–68, 2016.

S. Sengupta, S. Basak, and R. A. Peters. Particle swarm optimization: A survey of historical and recent developments with hybridization perspectives. *Machine Learning and Knowledge Extraction*, 1(1):157–191, 2018.

S. Sengupta, S. Basak, and R. A. Peters. Particle swarm optimization: A survey of historical and recent developments with hybridization perspectives. *Machine Learning and Knowledge Extraction*, 1(1):157–191, 2019. ISSN 2504-4990. doi: 10.3390/make1010010.

S. Seyedpoor, J. Salajegheh, E. Salajegheh, and S. Gholizadeh. Optimum shape design of arch dams for earthquake loading using a fuzzy inference system and wavelet neural networks. *Engineering optimization*, 41(5):473–493, 2009.

A. A. Shahin and O. M. Salem. Using genetic algorithms in solving the one-dimensional cutting stock problem in the construction industry. *Canadian journal of civil engineering*, 31(2):321–332, 2004.

O. Shallan, H. M. Maaly, and O. Hamdy. A developed design optimization model for semi-rigid steel frames using teaching-learning-based optimization and genetic algorithms. *Structural engineering and mechanics: An international journal*, 66 (2):173–183, 2018.

D. J. Sheppard and A. C. Palmer. Optimal design of transmission towers by dynamic programming. *Computers & Structures*, 2(4):455–468, 1972.

Y. Shi and R. Eberhart. A modified particle swarm optimizer. In *1998 IEEE international conference on evolutionary computation proceedings. IEEE world congress on computational intelligence (Cat. No. 98TH8360)*, pages 69–73. IEEE, 1998.

Y. Shi and B. Obaiahnahatti. A modified particle swarm optimizer. volume 6, pages 69 – 73, 06 1998. ISBN 0-7803-4869-9. doi: 10.1109/ICEC.1998.699146.

H. Shin and M. Singh. Minimum life-cycle cost-based optimal design of yielding metallic devices for seismic loads. *Engineering Structures*, 144:174–184, 2017.

O. Sigmund. On the usefulness of non-gradient approaches in topology optimization. *Structural and Multidisciplinary Optimization*, 43:589–596, 2011.

P.-A. Simionescu, D. Beale, and G. V. Dozier. Constrained optimization problem solving using estimation of distribution algorithms. In *Proceedings of the 2004 Congress on Evolutionary Computation (IEEE Cat. No. 04TH8753)*, volume 1, pages 296–302. IEEE, 2004a.

P.-A. Simionescu, D. Beale, and G. V. Dozier. Constrained optimization problem solving using estimation of distribution algorithms. In *Proceedings of the 2004 Congress on Evolutionary Computation (IEEE Cat. No. 04TH8753)*, volume 1, pages 296–302. IEEE, 2004b.

L. Simoes. Optimization of frames with semi-rigid connections. *Computers & structures*, 60(4):531–539, 1996.

L. Simões. Optimization of frames with semi-rigid connections. *Computers and Structures*, 60(4):531–539, 1996. URL https://www.scopus.com/inward/record.uri?eid=2-s2.0-0030169693&doi=10.1016%2f0045-7949%2895%2900427-0&partnerID=40&md5=38c956739bf89eae38c590c984f5ecb5.

R. Soegiarso and H. Adeli. Optimum load and resistance factor design of steel space-frame structures. *Journal of Structural Engineering*, 123(2):184–192, 1997. URL https://www.scopus.com/inward/record.uri?eid=2-s2.0-0031077851&doi=10.1061%2f%28ASCE%290733-9445%281997%29123%3a2%28184%29&partnerID=40&md5=aba8267389de9810e5b4d9893fc2651a.

S. Sotiropoulos and N. D. Lagaros. Optimum topological bracing design of tall steel frames subjected to dynamic loading. *Computers & Structures*, 259:106705, 2022.

A. S.p.A. Elenco prezzi 2021 - nuove costruzioni e manutenzione straordinaria. , *Direzione Ingegneria e Verifiche*, 2021.

B. Sparling and L. Wegner. Estimating peak wind load effects in guyed masts. *Wind & structures*, 10(4):347–366, 2007.

B. F. Sparling. The dynamic behavior of guys and guyed masts in turbulent winds. 1995.

K. Stasa. Optimum design procedure for steel trusses. *Journal of Constructional Steel Research*, 46(1-3):114, 1998. URL https://www.scopus.com/inward/record.uri?eid=2-s2.0-0032035779&doi=10.1016%2fS0143-974X%2898%2900192-8&partnerID=40&md5=b94736b2de970e5d9f7cc3f74ecb3c05.

G. N. . W. K. Steenhuis, M. Pre-design of semi-rigid joints in steel frames. In *Proceedings of the Second State of the Art Workshop on Semi-Rigid Behaviour of Civil Engineering Structural Connections*, 1994.

M. Stewart and R. Melchers. Optimization of structural design checking. *Journal of Structural Engineering (United States)*, 115(10):2448–2460, 1989. URL https://www.scopus.com/inward/record.uri?eid=2-s2.0-0024740270&doi=10.1061%2f%28ASCE%290733-9445%281989%29115%3a10%282448%29&partnerID=40&md5=9d0f77cac7128a3aa6decfc4156e247c.

M. Stolpe. Truss optimization with discrete design variables: a critical review. *Structural and Multidisciplinary Optimization*, 53:349–374, 2016.

L. Stromberg, A. Beghini, W. F. Baker, and G. H. Paulino. Design of structural braced frames using group optimization. In *20th analysis and computation specialty conference*, pages 267–277, 2012a.

L. L. Stromberg, A. Beghini, W. F. Baker, and G. H. Paulino. Topology optimization for braced frames: combining continuum and beam/column elements. *Engineering Structures*, 37:106–124, 2012b.

K. Suga, S. Kato, and K. Hiyama. Structural analysis of pareto-optimal solution sets for multi-objective optimization: An application to outer window design problems using multiple objective genetic algorithms. *Building and Environment*, 45(5): 1144–1152, 2010.

X. Sun, X. Tao, S. Duan, and C. Liu. Kappa (k) derived from accelerograms recorded in the 2008 wenchuan mainshock, sichuan, china. *Journal of Asian Earth Sciences*, 73:306–316, 2013.

E. I. Tabak and P. M. Wright. Optimality criteria method for building frames. *Journal of the Structural Division*, 107(7):1327–1342, 1981.

I. Takewaki, J. Conte, S. Mahin, and K. Pister. Probabilistic multi-objective optimal design of seismic-resistant braced steel frames using arma models. *Computers and Structures*, 41(4):687–707, 1991. URL https://www.scopus.com/inward/record.uri?eid=2-s2.0-0026367156&doi=10.1016%2f0045-7949%2891%2990180-T&partnerID=40&md5=ef3f74a4dac0c47d7ec8f3d3c8ed5c10.

S. Talatahari, A. H. Gandomi, X.-S. Yang, and S. Deb. Optimum design of frame structures using the eagle strategy with differential evolution. *Engineering Structures*, 91:16–25, 2015.

S. Tangaramvong and F. Tin-Loi. Optimal performance-based rehabilitation of steel frames using braces. *Journal of Structural Engineering*, 141(10):04015015, 2015.

J. S. Tantely and Z. He. Collapse safety margin-based design optimization of steel structures with concentrically braced frames. *Adv. Steel Constr.*, 15(2):137–144, 2019.

V. Thevendran, N. Gupta, and G. Tan. Minimum weight design of multi-bay multi-storey steel frames. *Computers and Structures*, 43(3):495–503, 1992a. URL https://www.scopus.com/inward/record.uri?eid=2-s2.0-0027110454&doi=10.1016%2f0045-7949%2892%2990283-6&partnerID=40&md5=490c8c9ff9afe27ea319e94acfcfb981.

V. Thevendran, N. D. Gupta, and G. Tan. Minimum weight design of multi-bay multi-storey steel frames. *Computers & structures*, 43(3):495–503, 1992b.

H. Thomas Jr. and D. Brown. Optimum least-cost design of a truss roof system. *Computers and Structures*, 7(1):13–22, 1977. URL https://www.scopus.com/inward/record.uri?eid=2-s2.0-0017454012&doi=10.1016%2f0045-7949%2877%2990056-6&partnerID=40&md5=ea5fd4bd8a5b558bc352d6326c8e0244.

H. R. Thomas Jr and D. M. Brown. Optimum least-cost design of a truss roof system. *Computers & Structures*, 7(1):13–22, 1977.

C. H. Thornton, L. Joseph, and T. Scarangello. Optimization of tall structures for wind loading. *Journal of Wind Engineering and Industrial Aerodynamics*, 36: 235–244, 1990.

T. Tiainen, K. Mela, T. Jokinen, and M. Heinisuo. The effect of steel grade on weight and cost of warren-type welded tubular trusses. *Proceedings of the Institution of Civil Engineers-Structures and Buildings*, 170(11):854–872, 2017.

L. Tian and C. Qiu. Modal pushover analysis of self-centering concentrically braced frames. *Structural engineering and mechanics: An international journal*, 65(3): 251–261, 2018.

B. Topping. Shape optimization of skeletal structures: A review. *Journal of Structural Engineering (United States)*, 109(8):1933–1951, 1983. URL https://www.scopus.com/inward/record.uri?eid=2-s2.0-0020799721&doi=10.1061%2f%28ASCE%290733-9445%281983%29109%3a8%281933%29&partnerID=40&md5=e7141e899579cd19bf1b85cbfe6df0ec.

V.-H. Truong and S.-E. Kim. A robust method for optimization of semi-rigid steel frames subject to seismic loading. *Journal of Constructional Steel Research*, 145: 184–195, 2018.

V.-H. Truong, P.-C. Nguyen, and S.-E. Kim. An efficient method for optimizing space steel frames with semi-rigid joints using practical advanced analysis and the micro-genetic algorithm. *Journal of Constructional steel research*, 128:416–427, 2017.

X. Tu, Z. He, and G. Huang. Performance-based multi-objective collaborative optimization of steel frames with fuse-oriented buckling-restrained braces. *Structural and Multidisciplinary Optimization*, 61(1):365–379, 2020.

D. Tuhus-Dubrow and M. Krarti. Genetic-algorithm based approach to optimize building envelope design for residential buildings. *Building and environment*, 45 (7):1574–1581, 2010.

M. Ülker. Optimum design of space trusses with buckling constraints by means of spreadsheets. *Turkish Journal of Engineering and Environmental Sciences*, 25(4): 355–367, 2001.

P. Uys, J. Farkas, K. Jarmai, and F. Van Tonder. Optimisation of a steel tower for a wind turbine structure. *Engineering structures*, 29(7):1337–1342, 2007.

D. Van Cauteren, D. Ramon, J. Stroeckx, K. Allacker, and M. Schevenels. Design optimization of hybrid steel/timber structures for minimal environmental impact and financial cost: A case study. *Energy and Buildings*, 254:111600, 2022.

P. J. Van Laarhoven, E. H. Aarts, P. J. van Laarhoven, and E. H. Aarts. *Simulated annealing*. Springer, 1987.

R. Van Mellaert, G. Lombaert, and M. Schevenels. Global size optimization of statically determinate trusses considering displacement, member, and joint constraints. *Journal of Structural Engineering*, 142(2), 2016.

V. N. Vapnik. An overview of statistical learning theory. *IEEE transactions on neural networks*, 10(5):988–999, 1999.

I. Venanzi and A. Materazzi. Multi-objective optimization of wind-excited structures. *Engineering Structures*, 29(6):983–990, 2007.

V. Venkayya. Application of optimality criteria approaches to automated design of large practical structures, agard-cpp-123. In *Second Symposium on Structural Optimization*, 1973.

V. Venkayya. Optimality criteria: a basis for multidisciplinary design optimization. *Computational mechanics*, 5(1):1–21, 1989.

V. Venkayya, N. Khot, and V. Reddy. Energy distribution in an optimum structural design. Technical report, AIR FORCE FLIGHT DYNAMICS LAB WRIGHT-PATTERSON AFB OHIO, 1969.

V. B. Venkayya. Structural optimization: a review and some recommendations. *International Journal for Numerical Methods in Engineering*, 13(2):203–228, 1978.

Y. Wahba, M. Madugula, and G. Monforton. Evaluation of non-linear analysis of guyed antenna towers. *Computers & Structures*, 68(1-3):207–212, 1998.

Y. M. Wahba, M. K. Madugula, and G. R. Monforton. Shake table for dynamic testing of guyed towers. In *Building to Last*, pages 353–357. ASCE, 1997.

F. Wang and S. L. Chan. Optimization and sensitivity analysis of space frames allowing for large deflection. *Engineering structures*, 28(10):1395–1406, 2006.

J.-y. Wang. *Nonlinear behaviour of semi-rigid composite joints under lateral loading: experimental and theoretical study*. PhD thesis, Hong Kong Polytechnic University (Hong Kong), 1999.

W. Wang, R. Zmeureanu, and H. Rivard. Applying multi-objective genetic algorithms in green building design optimization. *Building and environment*, 40(11):1512–1525, 2005a.

W. Wang, R. Zmeureanu, and H. Rivard. Two-phase application of multi-objective genetic algorithms in green building design. *Proceedings of IBPSA-2005, Montreal*, 2005b.

W. Wang, H. Rivard, and R. Zmeureanu. Floor shape optimization for green building design. *Advanced Engineering Informatics*, 20(4):363–378, 2006.

Y. Wang, Z. Cai, Y. Zhou, and Z. Fan. Constrained optimization based on hybrid evolutionary algorithm and adaptive constraint-handling technique. *Structural and Multidisciplinary Optimization*, 37:395–413, 01 2008. doi: 10.1007/s00158-008-0238-3.

Y. Wang, Z. Cai, Y. Zhou, and Z. Fan. Constrained optimization based on hybrid evolutionary algorithm and adaptive constraint-handling technique. *Structural and Multidisciplinary Optimization*, 37:395–413, 2009.

K. Weynand, J.-P. Jaspart, and M. Steenhuis. Economy studies of steel building frames with semi-rigid joints. In *Second World Conference on Constructional Steel Design*, 1998.

A. H. Whitworth and K. D. Tsavdaridis. Genetic algorithm for embodied energy optimisation of steel-concrete composite beams. *Sustainability*, 12(8):3102, 2020.

F. W. Wong, P. T. Lam, E. H. Chan, and F. K. Wong. Factors affecting buildability of building designs. *Canadian Journal of Civil Engineering*, 33(7):795–806, 2006.

A. M. Wrzesien, D. T. Phan, J. B. Lim, H.-H. Lau, I. Hajirasouliha, and C. S. Tan. Effect of stressed-skin action on optimal design of cold-formed steel square and rectangular-shaped portal frame buildings. *International Journal of Steel Structures*, 16(2):299–307, 2016.

S.-J. Wu and P.-T. Chow. Genetic algorithms for solving mixed-discrete optimization problems. *Journal of the Franklin Institute*, 331(4):381–401, 1994.

A. Xu and R. Zhao. Wind-resistant structural optimization of a supertall building with complex structural system. *Structural and Multidisciplinary Optimization*, 62(6):3493–3506, 2020.

L. Xu. *Optimal design of steel frameworks with semi-rigid connections.* University of Waterloo, 1994.

L. Xu. On the minimum-maximum bending moment and the least-weight design of semi-rigid beams. *Structural and Multidisciplinary Optimization*, 21:316–321, 2001.

L. Xu and D. Grierson. Computer-automated design of semirigid steel frameworks. *Journal of Structural Engineering (United States)*, 119(6):1740–1760, 1993a. URL https://www.scopus.com/inward/record.uri?eid=2-s2.0-0027606501&doi=10.1061%2f%28ASCE%290733-9445%281993%29119%3a6%281740%29&partnerID=40&md5=7322d37406af754b74180d28b911c07f.

L. Xu and D. E. Grierson. Computer-automated design of semirigid steel frameworks. *Journal of Structural Engineering*, 119(6):1740–1760, 1993b.

L. Xu, Y. Gong, and D. E. Grierson. Seismic design optimization of steel building frameworks. *Journal of Structural Engineering*, 132(2):277–286, 2006.

L.-H. Xu, S.-J. Xiao, Y.-W. Wu, and Z.-X. Li. Seismic failure mode identification and multi-objective optimization for steel frame structure. *Advances in Structural Engineering*, 21(13):2005–2017, 2018.

J. Xue, D. Lavorato, A. Bergami, C. Nuti, B. Briseghella, G. Marano, T. Ji, I. Vanzi, A. Tarantino, and S. Santini. Severely damaged reinforced concrete circular columns repaired by turned steel rebar and high-performance concrete jacketing with steel or polymer fibers. *Applied Sciences (Switzerland)*, 8(9), 2018. doi: 10.3390/app8091671.

X.-S. Yang. *Engineering optimization: an introduction with metaheuristic applications*. John Wiley & Sons, 2010a.

X.-S. Yang. *Nature-inspired metaheuristic algorithms*. Luniver press, 2010b.

W. Yau. Optimal design of simply supported beams for minimum upper bound of dynamic response. 1974.

D. Yeo and F. A. Potra. Sustainable design of reinforced concrete structures through co 2 emission optimization. *Journal of structural engineering*, 141(3):B4014002, 2015.

V. Yepes, J. V. Martí, and T. García-Segura. Cost and co2 emission optimization of precast–prestressed concrete u-beam road bridges by a hybrid glowworm swarm algorithm. *Automation in Construction*, 49:123–134, 2015.

Y. K. Yi and A. M. Malkawi. Optimizing building form for energy performance based on hierarchical geometry relation. *Automation in Construction*, 18(6):825–833, 2009.

Z. Q. Zhang and H. N. Li. Two-level optimization method of transmission tower structure based on ant colony algorithm. In *Advanced Materials Research*, volume 243, pages 5849–5853. Trans Tech Publ, 2011.

G. Zhao, J. Xu, Y. Li, and M. Zhang. Numerical analysis of the degradation characteristics of bearing capacity of a corroded reinforced concrete beam. *Advances in Civil Engineering*, 2018, 2018.

K. Zhou and C. Chen. Topology optimization of frame bracing system for natural frequency. *The Open Civil Engineering Journal*, 8(1), 2014.

K.-m. Zhou and X. Li. Topology optimization of structures under multiple load cases using a fiber-reinforced composite material model. *Computational Mechanics*, 38: 163–170, 2006.

M. Zhou. Difficulties in truss topology optimization with stress and local buckling constraints. *Structural Optimization*, 11(2):134–136, 1996. URL https://www.scopus.com/inward/record.uri?eid=2-s2.0-0030128305&doi=10.1007%2fBF01376857&partnerID=40&md5=f639935bc31bd055e76e62b287ec6268.

G. Zoutendijk. Methods of feasible directions. *1960*, 1960.